THE UNIVERSITY
of EDINBURGH

Intramolecular Direct Arylation

THE UNIVERSITY *of* EDINBURGH

Tom Corrie

Doctor of Philosophy

University of Edinburgh

2017

Declaration

I declare that the work in this thesis was carried out principally by me, with collaborators specifically acknowledged, under the supervision of Prof. Guy Lloyd-Jones FRS and is in accordance with the requirements of the University of Edinburgh. This work is original, except where indicated by special reference in the text, and no part of the thesis has been previously submitted for any other academic award.

Signed 

Date 18/06/17

Publications

Sections of work presented in Chapters 2, 3 and 4 have been communicated:

T. J. A. Corrie, L. T. Ball, G. C. Lloyd-Jones, C. A. Russell, *J. Am. Chem. Soc*. **2017**, *139*, 245 and T. J. A. Corrie, G. C. Lloyd-Jones, *Topics in Catalysis*, **2017**, *60*, 570.

Abstract

The research conducted for this thesis has led to the development of an intramolecular gold-catalysed direct arylation protocol whereby tethered arenes and aryltrimethylsilanes are coupled (Scheme 1). In Chapter 1, the key synthetic and mechanistic studies that have ultimately led to the conception of this project are introduced. In Chapter 2, the substrate scope of intramolecular direct arylation is assessed. The reaction tolerates a wide range of substrates with tether lengths between one and five units (containing C, N and O) generating 5- to 9-membered rings. Substrates that lead to 5-membered rings (**1** → **2**) can tolerate a broad electronic range of substituents and proceed under the mildest reaction conditions (≤ 1 mol% catalyst, room temperature) and with excellent yields. A smaller collection of examples is demonstrated for the cyclisation to 6- and 7- membered rings (**3** → **4**, **5** → **6**), but no heating is required and good yields are maintained throughout the series. The synthetically challenging synthesis of 8- and 9- membered rings (**7** → **8**, **9** → **10**) is successful, albeit with slightly more forcing conditions (4 mol%, up to 50 °C). The methodology was subsequently applied in the successful 10-step synthesis of natural product allocolchicine **11**.

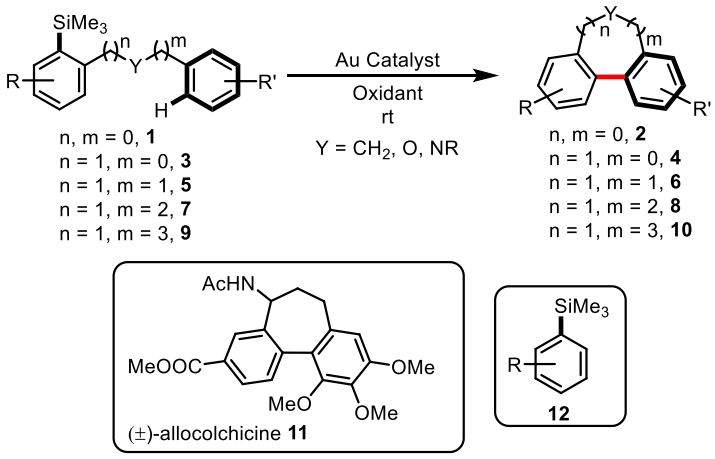

Scheme 1. Intramolecular gold-catalysed direct arylation.

In Chapter 3, the operative reaction mechanism is elucidated. Reaction monitoring techniques allowed for the detailed study of linear free energy relationships (LFERs) and kinetic isotope effects (KIEs), which in turn allowed for deduction of the reaction turnover-limiting step (TLS) and thus the first quantitative experimental data on the effects of aryl electron demand and conformational freedom on the rate of reductive elimination from diarylgold(III) species. The mechanistic investigation led to the observation of complex kinetic profiles for specific substrates. The origin of these unusual effects is the focus of Chapter 4. By combining

experiment with kinetic simulation, an off-cycle catalyst inhibition pathway was identified and the understanding of this process allowed for a re-optimisation of reaction conditions.

In Chapter 5, the general kinetic parameters that could govern any domino reaction combining inter- and intramolecular direct arylation are deduced through kinetic analysis and simulation of hypothetical systems. The results of the kinetic analysis were proved experimentally through the successful combination of intra- and intermolecular gold-catalysed direct arylation. The products of intramolecular cyclisation **2**, generated *in-situ*, are demonstrated to couple with intermolecular aryltrimethylsilanes **12**, resulting in a rapid increase in molecular complexity from simple substrates in one pot.

Lay Summary

Despite the long-held belief that gold is unreactive, gold complexes which arise from the oxidation of elemental gold possess unique and potent reactivity. Indeed, over the past 2 decades, synthetic chemists across the globe have demonstrated numerous applications of gold as a catalyst to construct complex and useful molecules. Catalysts are molecules added to a reaction, to either speed it up, or to allow the reaction to occur in the first place, and remain unchanged at the end of the reaction. Catalysis is of enormous industrial significance, particularly in a day and age where consideration of environmental impact is of fundamental importance. One of the most significant classes of catalytic reactions used in chemistry is cross-coupling, which allows for the facile and rapid construction of very important molecular scaffolds. However, traditional cross-coupling reactions have a fundamental flaw, and that is significant waste is generated.

Previous research in the Lloyd-Jones research group has described a gold-catalysed approach to cross-coupling, rivalling traditional approaches through a reduced environmental impact resulting from minimised waste, as well as milder operative reaction conditions. This research was primarily on the intermolecular reaction, which is the formation of a single molecule from two components. This thesis primarily describes the development of the intramolecular variant, which is the transformation of one molecule to another. Rendering the reaction intramolecular has led to fundamental new insights, not only with respect to novel reactivity which was exploited in the synthesis of a biologically active natural product, but also through a greater understanding of the reaction mechanism. The mechanistic investigation was of central importance and has led to key new developments.

Acknowledgments

My PhD has been a challenging, but ultimately rewarding experience, in no small part thanks to the people who I have had the pleasure of working with over the past 4 years. First and foremost, I would like to thank Professor Guy Lloyd-Jones, for his continued support and guidance. I am incredibly grateful to have been a part of this group and have valued every minute of time spent in meetings discussing this project.

Many people have come and gone during my PhD, and a huge thanks goes to all of you who have made it such a supportive and enjoyable time: Alistair Lennox, Tomas Racys, Louise Evans, Liam Ball, Carl Poree, Ruth Dooley, Rob Cox, Nick Taylor, Joe Tate, Jorge Gonzaléz, Paul Cox, Alex Cresswell, Marc Reid, Matt Robinson, Katherine Geogheghan, Eric Keske, Alba Collado, Ariana Jones, Eduardo Nieto, Magdalene Teh, Alex Pagett, Craig Johnston, Tom West and Chris Nottingham. Special thanks to Liam who I inherited this project from and who has been a great mentor over the past few years.

Thanks to all the people that keep the department running, in particular Alan Taylor in the MS department, Juraj Bella and Lorna Murray in the NMR facility, and Gary Nichol in the X-ray department. In addition, I thank the University of Edinburgh and the European Research Council for financial support.

Finally, I would like to thank my family, who have always provided love, support and encouragement, and my new in-laws who have given me a home away from home. Above all, the biggest thanks goes to my wife, Emily, the most selfless and caring person I know.

Contents

Abbreviations

Å	ångström
ρ	Hammett reaction constant
σ	Hammett substituent constant
σBM	σ-bond metathesis
μL	microlitre
1,2-DCE	1,2-dichloroethane
Ac	acetyl
Ar	aryl substituent
BINAP	2,2'-bis(diphenylphosphino)-1,1'-binaphthyl
Bn	benzyl
Bu	butyl
CI	chemical ionisation
CMD	concerted metalation-deprotonation
CSA	camphorsulfonic acid
Cy	cyclohexyl
DDQ	2,3-dichloro-5,6-dicyano-1,4-benzoquinone
DMA	*N*,*N*-dimethylacetamide
DMAP	4-(dimethylamino)pyridine
DMF	*N*,*N*-dimethylformamide
DMSO	dimethyl sulfoxide
d.r.	diastereomeric ratio
E, E^+	electrophile
EI	electron impact ionisation

equiv.	molar equivalents
ESI-MS	electrospray ionisation mass spectrometry
er	enantiomeric ratio
Et	ethyl
g	gram
Gly	glycine
HCIB	[hydroxy(camphorsulfonyloxy)iodo]benzene
HFIP	hexafluoro*iso*propanol
HTIB	[hydroxy(tosyloxy)iodo]benzene
IBDA	iodobenzene diacetate
KIE	kinetic isotope effect
k	rate constant
L	neutral ligand
LFER	linear free energy relationship
*m*CPBA	*meta*-chloroperbenzoic acid
M	molar
Me	methyl
mg	milligram
MHz	megahertz
mL	millilitre
mmol	millimole
mol%	mole percent
m.p.	melting point
MS	molecular sieve

m/z	mass-to-charge ratio
NBS	*N*-bromosuccinimide
NFSI	*N*-fluorosuccinimide
NMR	nuclear magnetic resonance
Nu, Nu^-	nucleophile
OA	oxidative addition
Ph	phenyl
PhDave-Phos	2′-(diphenylphosphino)-N,N′-dimethyl-(1,1′-biphenyl)-2-amine
ppm	parts per million
Pin	Pinacol
Pr	propyl
Pv	pivalyl, trimethylacetyl
R	alkyl, aryl or heteroatomic substituent
RSM	recovered starting material
rr	regioisomeric ratio
rt	room temperature
S_EAr	electrophilic aromatic substitution
TBA	tetrabutylammonium
TBHP	*tert*-butyl hydroperoxide
Tf	trifluoromethanesulfonyl
TFA	trifluoroacetic acid
tfe	2,2,2-trifluoroethanol
THF	tetrahydrofuran
tht	tetrahydrothiophene

TLC	thin-layer chromatography
TM	transition metal
WI	Wheland intermediate
X	(halogen) substituent, or anionic ligand
Xantphos	4,5-bis(diphenylphosphino)-9,9-dimethylxanthene
XPhos	2-dicyclohexylphosphino-2′,4′,6′-tri*iso*propylbiphenyl

1. Introduction

1.1 Biaryl Synthesis *via* Transition-Metal Catalysed Cross-Coupling

Organic chemistry revolves around the synthesis of carbon based compounds, the building blocks of all known life. Often inspired by nature, the role of the synthetic organic chemist is to construct molecules through the breaking and forming of new chemical bonds. Synthetic chemistry has undoubtedly shaped modern society, leading to a thriving pharmaceutical industry tackling the challenges of modern medicine, and through to advances in agrochemicals in the fight to ensure food security.[1] The bioactive molecules upon which these industries rely can vary significantly in structure, they can be simple or complex, derived from nature or entirely synthetic, but one common feature that many of these molecules possess is the presence of an aromatic moiety. In drug development and medicinal chemistry, aromatic groups are "by far the most essential pharmacophores", and greater than 75% of recent phase III or marketed pharmaceuticals contain at least one aromatic group.[2] It is therefore unsurprising that significant efforts have gone into the development of strategies to functionalise aromatic molecules, and, in particular, to form new carbon-carbon bonds. A landmark development in the synthesis of C-C bonds in aromatic molecules was the advent of transition-metal catalysed coupling reactions. In a relatively short time-frame, methodologies developed from simple homocoupling protocols under forcing conditions, to cross-coupling procedures with near perfect selectivity and minimal catalyst loadings.[3] Although other metals such as Cu,[4] Ni[5–10] and Fe[11–14] are competent catalysts in certain cross-coupling reactions, it is palladium that transcends the field.[15] The pioneering scientists who led the advance of palladium-catalysed cross couplings in organic synthesis, Negishi, Heck and Suzuki, were rewarded for their efforts in the award of the 2010 Nobel prize for chemistry.[3]

One of the key structural motifs constructed through transition-metal-catalysed cross-coupling is the biaryl, which is ubiquitous in nature and industry. It is found in many bioactive molecules suitable for agrochemical and medicinal purposes, as well as being the key structural motif in state-of-the-art technological developments such as OLED devices (Figure 1.1).[16]

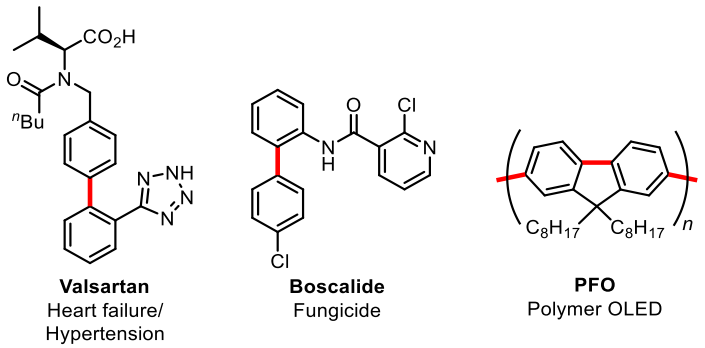

Figure 1.1. Industrially important biaryl containing molecules.

The basic strategy to synthesise biaryls using palladium catalysis involves the coupling of an aryl (pseudo)halide with an aryl organometallic reagent, with the identity of the organometallic reagent distinguishing between the myriad available protocols.[5,9,10,17,18] The general mechanism involves the oxidative addition of the aryl (pseudo)halide to the Pd(0) species, followed by transmetalation of the organometallic coupling partner yielding a (diaryl)Pd(II) complex which can reductively eliminate to give the desired biaryl and regenerate the Pd(0) species completing the cycle (Scheme 1.1).

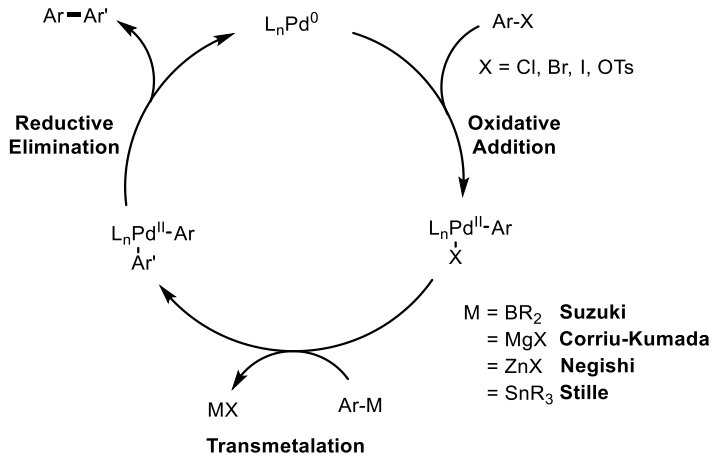

Scheme 1.1. General palladium-catalysed cross-coupling catalytic cycle.

1.1.1 Direct Arylation

Whilst traditional cross-coupling methods are widely employed and continuously studied, a new phase of development has begun, where there is equal emphasis on efficiency, particularly with regards to step economy and streamlined synthesis. Traditional cross-coupling methods are inherently wasteful as both coupling partners require pre-functionalisation, which may require multiple tedious steps, only for these activated functional groups to ultimately form stoichiometric wasteful by-products. Therefore, emphasis has been placed on avoiding pre-

functionalisation and instead considering the aryl C-H bond as a functional group (Scheme 1.2).[19–21] The ultimate strategy would be the ability to cross-couple two unactivated arenes in a formal dehydrogenative coupling reaction. This is a formidable challenge, however, as discrimination between multiple C-H bonds is non-trivial and the possibility for poor regioselectivity is high. Although some notable approaches have been developed, they currently lack generality.[22] An alternative approach which has gained much traction in recent years is that of direct arylation, where one of the pre-functionalised coupling partners is replaced with a simple arene, thus significantly improving the likelihood for acceptable regioselectivity. There are two approaches, one were the organometallic is replaced and a catalytic cycle resembling Scheme 1.1 will occur with Ar-M replaced with Ar-H, or the other where the halide can be replaced, and in this case an external oxidant will be required to complete the catalytic cycle.

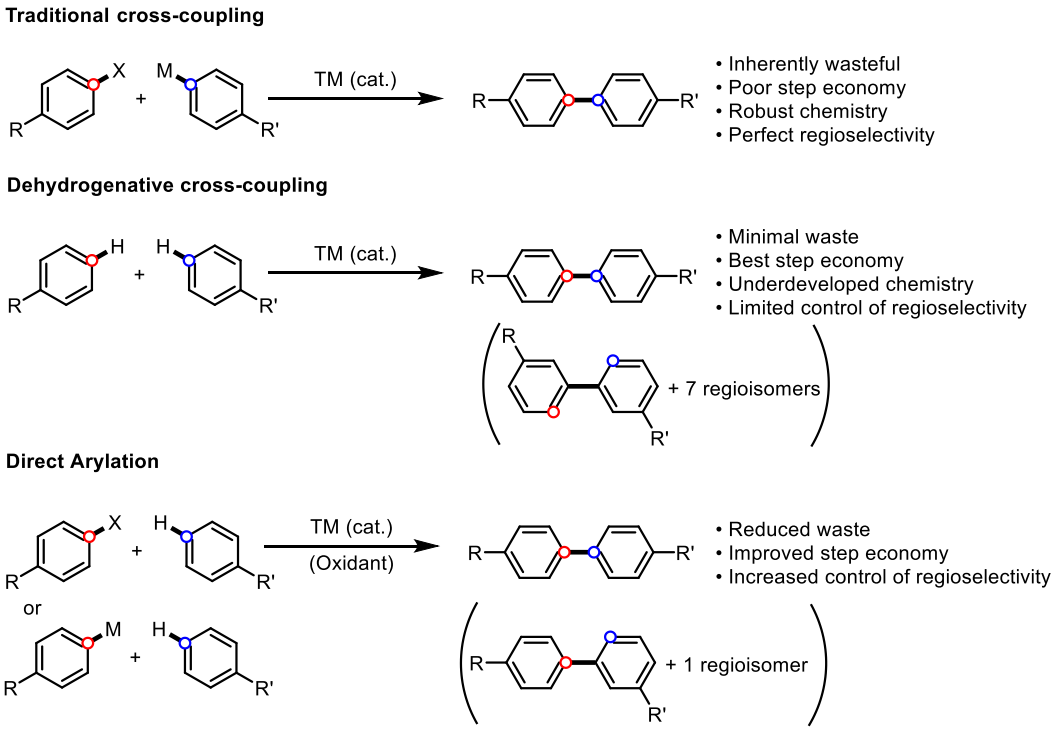

Scheme 1.2. Comparison between traditional cross-coupling and C-H functionalisation methods.

1.1.2 Mechanism of C-H Metalation

A major driving force in the development and optimisation of novel methodologies is mechanistic understanding. This is certainly true in the field of direct arylation where seminal mechanistic studies have led to the developments of processes previously envisioned to be

impossible.[23] One of the key questions in a direct arylation reaction is the mechanism by which the C-H bond is replaced with a carbon-metal bond , which is commonly referred to as the C-H activation step. The most common modes of C-H activation postulated in direct arylation reactions are, oxidative addition, sigma-bond metathesis (σBM), electrophilic metalation (electrophilic aromatic substitution- S_EAr), and concerted metalation-deprotonation (CMD), Scheme 1.3.[24]

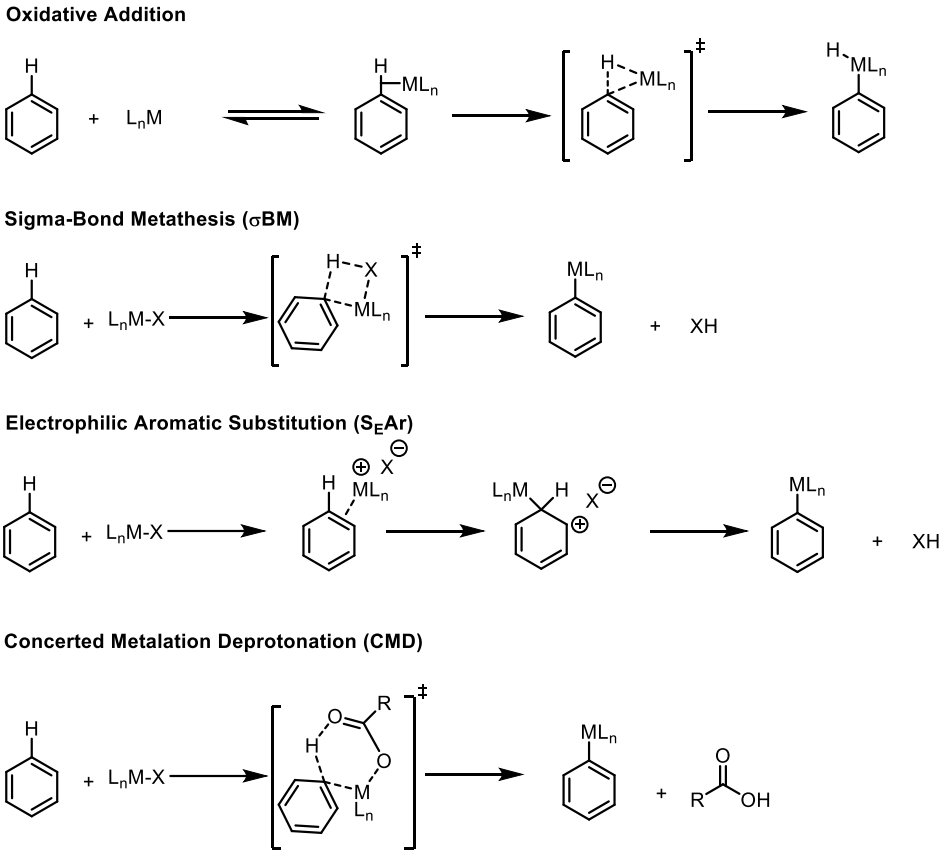

Scheme 1.3. Mechanisms for C-H bond metalation.[25]

Oxidative Addition

Oxidative addition is typical for electron-rich, low-valent complexes of the late transition metals.[26] For example, rhodium complexes were one of the first shown to be capable of oxidative addition across both arene and alkane C-H bonds. A thorough mechanistic investigation across several research groups unveiled the mechanism of C-H bond metalation of benzene from **13** (Scheme 1.4). Irradiation of **13** results in the elimination of dihydrogen and formation of an unstable, coordinatively unsaturated 16-electron complex **14**. Rapid π-complexation leading to η^2-arene species **15** precedes a reversible C-H oxidative addition to **16**.[27–33]

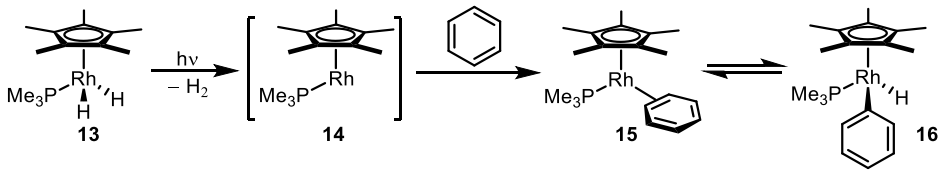

Scheme 1.4. Mechanism of oxidative for low-valent ruthenium complex.

Despite a thorough understanding of oxidative addition across C-H bonds, aside from limited examples, it is not normally the mechanism of C-H bond activation in catalytic direct arylation reactions.

Sigma-Bond Metathesis

In contrast, σBM is typically restricted to low valent early transition metals and is characterised by a 4-membered transition state. In particular, it is a mechanistic pathway for metals that cannot undergo oxidative addition.[26] Whilst σBM has been invoked in certain catalytic direct arylation reactions of late transition metals, evidence is low and other processes (such as CMD, *vide infra*) are proposed preferentially.

Electrophilic Metalation

Electrophilic metalation is one of the most commonly invoked mechanisms for arene metalation and is typically the proposed mechanism in the reaction of electron-rich arenes with late transition- and main-group metals in high oxidation states. The reaction pathway consists of a π-complexation of the arene to the metal, followed by formation of a Wheland intermediate (WI), which upon rearomatisation forms the aryl-metal species. Depending on the kinetically significant step during metalation, Hammett linear free energy relationships (LFER) correlate against σ or σ^+ and typically the reaction constants (ρ/ρ^+) are large and negative. Additionally, regioselectivity is predictable with *ortho*/*para* selectivity for arenes bearing EDGs or halogens and *meta* selectivity for those bearing EWGs. The presence of a $^1H/^2H$ kinetic isotope effect is entirely dependent on the rate-limiting event in stoichiometric studies of metalation. If it is the π-complexation, a significant KIE is not expected as there is no change in hybridisation nor is a C-H bond broken during this step. If Wheland intermediate formation is rate-limiting, then an inverse secondary KIE may be expected due to the change in hybridisation from sp^2 to sp^3 at the reacting carbon. If rearomatisation is found to be rate-limiting, a primary KIE can be expected.

An example of electrophilic metalation is the reaction of arenes with cationic, highly electrophilic Rh(III) species. Cationic octaethylporphyrinatorhodium(III) complex **18**, which is generated through halide abstraction from **17**, readily reacts with a range of arenes (Scheme

1.5). A reaction constant of ρ = −5.43 was obtained, alongside no measurable kinetic isotope effect. Regioselectivity was high for the *para* isomer for the reaction of anisole, toluene and chlorobenzene, whereas methyl benzoate was *meta* selective. The authors concluded that these results were consistent with an electrophilic metalation, with a rate limiting π-complexation.[34]

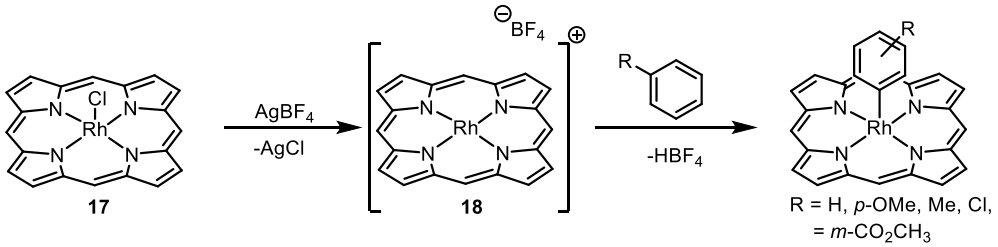

Scheme 1.5. Electrophilic metalation by a Rh(III) complex.

Concerted Metalation Deprotonation

For many years, catalysed direct arylation reactions were primarily proposed to proceed *via* S_EAr type mechanisms, particularly with palladium, which has a significant history of catalysing direct arylation reactions. Indeed, pioneering examples of direct arylation involved the coupling of electron-rich heteroarenes and aryl halides using palladium.[35] It was intuitive to assume that the nucleophilicity of the arene was of importance as it was replacing the organometallic coupling partner required in more conventional cross-coupling, and therefore that electrophilic metalation was occurring.

However, in the mid-2000s, mechanistic work in several research groups began to uncover an alternative mode of metalation where a Wheland intermediate is not formed, and the C-H bond cleavage occurs by simultaneous metalation and intramolecular deprotonation. Initially referred to as internal electrophilic substitution (IES) or ambiphilic metal-ligand activation (AMLA), the mechanism is most commonly known as concerted metalation deprotonation (CMD).[36]

Crucial to the development of this new theory was the use of intramolecular reactions to probe the reaction mechanism. The first compelling evidence of an alternative mechanism to S_EAr in catalytic direct arylation was through intramolecular competition experiments advanced in separate studies by the research groups of Fagnou[37,38] and Echavarren.[39] In a study of intramolecular direct arylation by Fagnou, the regioselectivity of several substrates was measured when the coupling arene was unsymmetrical. Although *ortho* coupling was possible, *para* selectivity was primarily observed (Table 1.1). This selectivity was explained on steric

grounds, with the *ortho*-site being sterically inaccessible. However, when the substituent was fluorine, the major observed isomer was the *ortho* product (Entry 7, Table 1.1).

Table 1.1. Regioselectivity in Pd-catalysed intramolecular direct arylation

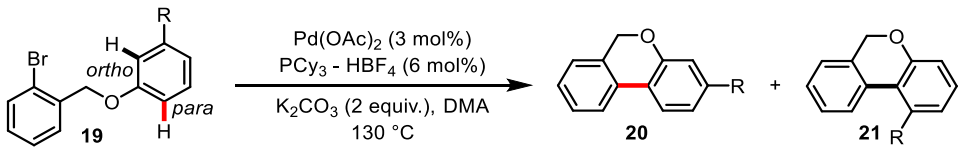

Entry	Subsituent	Ratio **20**:**21**
1	OMe	10:1
2	Me	15:1
3	*i*-Pr	>30:1
4	CF_3	>30:1
5	NO_2	>30:1
6	Cl	3.2:1
7	**F**	**1:4.3**

This is inconsistent with an S_EAr mechanism as the *ortho* position is significantly less nucleophilic than the *para* site due to inductive effects. Additionally, cyclisation of naphthyl substrate **22**, led to both regioisomeric products, **23** and **24**, in near equal proportions (Scheme 1.6). However, electrophilic additions to naphthalenes are well known to favour the 1-position.[40] This lack of selectivity was another indication that the reaction may not be occurring *via* an S_EAr mechanism.[37,38]

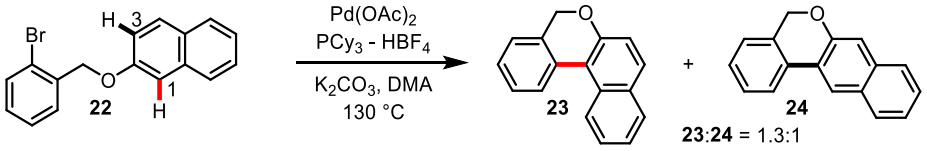

Scheme 1.6. Regioselectivity in Pd-catalysed intramolecular direct arylation.

A more systematic investigation into the effect of aryl electronics on palladium-catalysed intramolecular direct arylation was performed in the research group of Echavarren.[39] A series of substituted bromobenzyldiarylmethanes were subjected to direct arylation reaction conditions, followed by DDQ oxidation to aid product analysis (Scheme 1.7). The regioselectivity pattern of arylation was analysed in combination with computational studies. In each example, arylation took place preferentially on the less electron-rich aromatic, with regioselectivities of up to 25:1 when multiple fluorine substituents are employed.

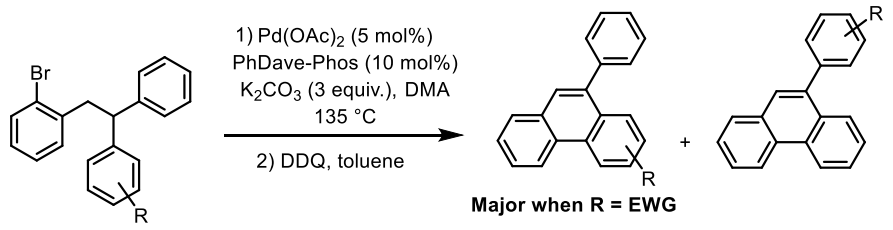

Scheme 1.7. Intramolecular competition reaction of electronically biased arenes.

Once again, the results were incompatible with an S_EAr mechanism which would result in arylation of the more electron-rich ring. Three mechanisms were theorised, and subjected to computational analysis. The potential mechanisms envisioned were; 1) an unassisted, σBM type process, 2) an intramolecular base-assisted and 3) and intermolecular base-assisted mechanism (Scheme 1.8). The energy barrier to the unassisted process was at least 20 kcal mol^{-1} higher than both assisted processes. Discrimination between the intra- and intermolecular mechanism was difficult as similar energy barriers were obtained with a small bias toward the intermolecular process.

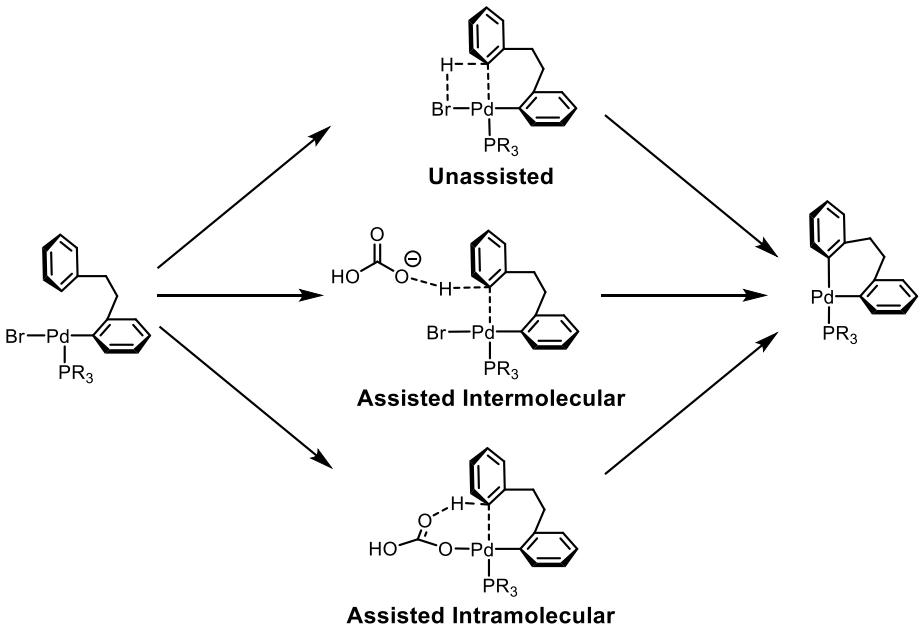

Scheme 1.8. Proposed Mechanisms of C-H bond activation.

Therefore, in reactions that proceed *via* a CMD mechanism, the acidity of the C-H bonds, rather than the nucleophilicity of the aromatic is of importance. CMD mechanisms are commonly invoked in the arylation of electron-neutral or electron-deficient arenes, however recently it has also been proposed for electron-rich heteroarenes.[41] Typically, large KIE

values are obtained in CMD mechanisms, however to uncover the mechanism of C-H activation a comprehensive mechanistic investigation is required.

1.1.3 Directing Group-Assisted Direct Arylation

As previously stated, control of regioselectivity is one of the biggest challenges of direct arylation chemistry. A common strategy used to control regioselectivity is through directed C-H bond activation (Scheme 1.9). A directing-group can be employed to hold the catalyst in a specific position so that it can react with the desired C-H bond. Not only does this strategy lead to the control of regiochemistry, but fundamentally, the direct arylation becomes intramolecular and ultimately a more facile process. Significant advances have been gained in the field of *ortho*-functionalisation and numerous strategies are available across several metals.[19–21] Directing groups bear an available lone pair of electrons that can coordinate to the transition-metal, and the direct arylation can typically proceed *via* a 5- or 6-membered metallacycle.

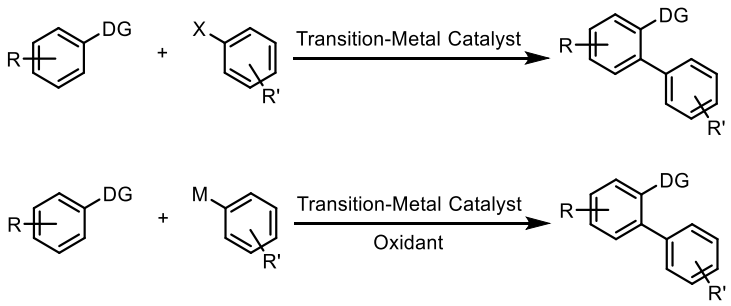

Scheme 1.9. Directing group strategy for regiocontrol in direct arylation.

Once again, numerous examples are available using palladium catalysis, with several oxidative examples involving organometallic coupling partners, as well as numerous examples involving aryl halides too. The list of available functional groups implemented as directing groups is ever increasing and has been comprehensively reviewed.[19–21] For example, Sanford and co-workers have demonstrated the versatility of directing groups in the direct arylation with diaryliodonium salts (Scheme 1.10).[42]

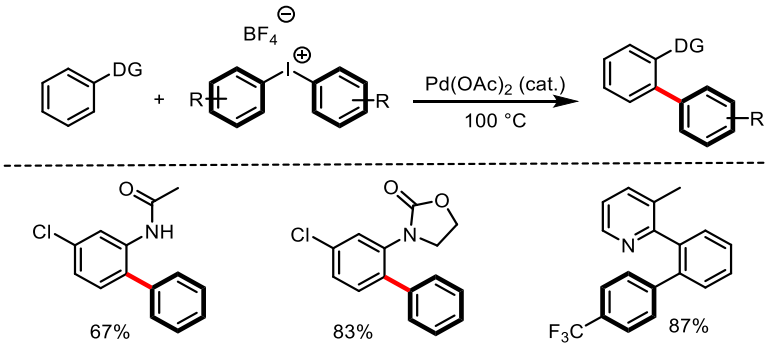

Scheme 1.10. Representative examples of directing groups used in Pd catalysed direct arylation.

A notable example of *ortho*-functionalisation by Kakiuchi *et al.*[43,44] using ruthenium catalysis is a direct arylation of arylboronates with aromatic ketone **25**, employing a carbonyl as the directing group (Scheme 1.11).

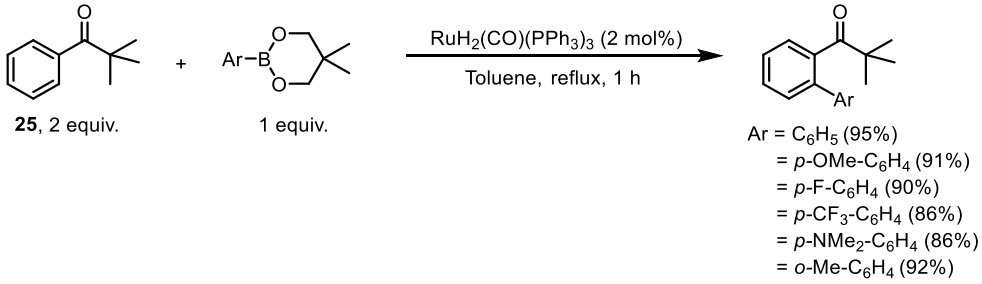

Scheme 1.11. Ruthenium catalysed direct arylation employing a ketone directing group.

However, the substrate scope was rather limited with respect to the ketone, as the *tert*-butyl group was key in preventing diarylation, which is a common problem when directing groups are employed. When replacing the *tert*-butyl group with methyl or *iso*-propyl groups, diarylation products were obtained in 60% and 76% respectively, with only minor amounts of monoarylation product isolated. The proposed origin of the improved selectivity when the *tert*-butyl group is employed is through steric repulsion of the newly introduced phenyl group and the *tert*-butyl group, thus blocking access to the second position for metalation. Through a combination of inter- and intramolecular competition experiments, a plausible mechanism was proposed which involved: 1) an irreversible pre-coordination of the ruthenium to the ketone; 2) a regioselective oxidative addition yielding a ruthenium hydride species; 3) a second equivalent of **25** inserts into the [Ru]-H bond; 4) transmetalation of the boronate; and 5) reductive elimination to the desired product (Scheme 1.12).

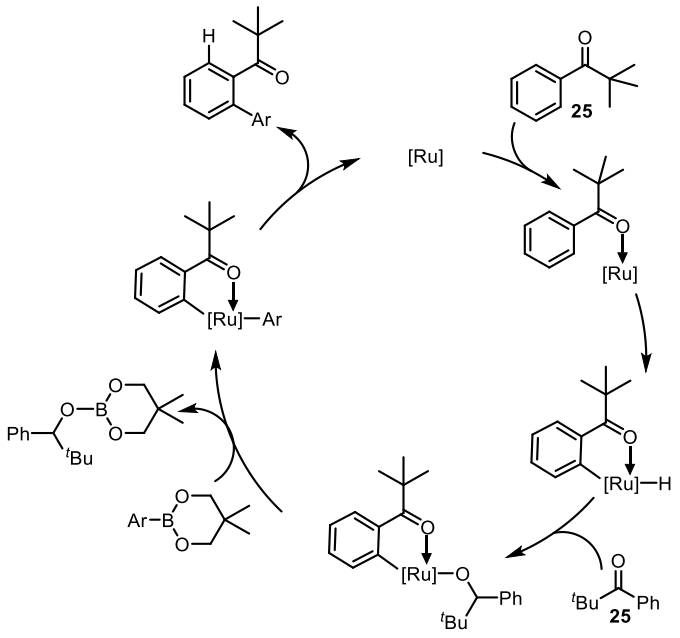

Scheme 1.12. Proposed mechanism of Ru-catalysed direct arylation. [43,44]

Whilst *ortho*-functionalisation is well established, the use of directing groups to facilitate *meta*-functionalisation is significantly underdeveloped. This is due to the difficulty in accessing these remote positions, and ingenious methods have been required to advance the field.

Since the seminal work by the research group of Yu demonstrating the *meta*-olefination of aromatic molecules using a "template-assisted *meta*-selective C-H activation" strategy in 2012,[45] there has been increased interest in developing the strategy.[46–49] Further developments by Yu *et al*. extended their methodology to a direct arylation strategy with an extended nitrile directing group, which made the *meta*-position accessible (Scheme 1.13).[50]

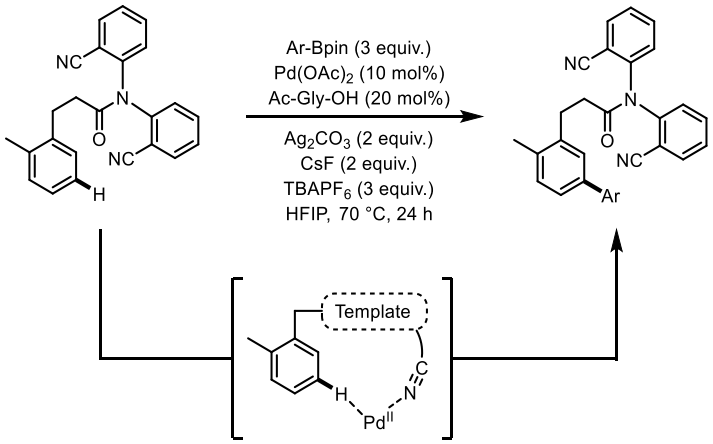

Scheme 1.13. *Meta*-directed C-H arylation.

The nitrile template could be removed post arylation by hydrolysis under mild conditions yielding the desired carboxylic acid, with the template also being recovered.

1.1.4 Direct Arylation in the Absence of a Directing Group

Although significant traction has been gained with the use of directing groups, the general applicability is somewhat limited as the directing group may be undesired in the final product, and therefore this strategy could be considered as another form of "pre-functionalisation". In the absence of directing-groups, the control of regiochemistry becomes significantly more difficult and relies on an understanding of the inherent reactivity of the catalyst employed towards specific C-H bonds. Whilst direct arylation of heteroarenes with aryl halides has shown to be relatively facile, as the inherent electron bias of the heteroarene can be sufficient to control the selectivity arylation, electron-neutral and poor arenes provide a significantly greater challenge.[19] It is therefore the mechanism of C-H activation that will dictate the regiochemistry, with different products expected depending on an S_EAr or CMD type mechanism.[24]

Ye and co-workers recently reported a palladium-catalysed direct arylation of arylboronic acids with monosubstituted arenes (Scheme 1.14).[51] The regioselectivity was highly *para*-selective, consistent with an S_EAr mechanism. However, the reaction conditions were forcing as 10 mol% of catalyst is required with solvent quantities of arene (≈ 100 equiv.). This clearly demonstrates the difficulty of direct arylation of simple aromatics in the absence of directing groups.

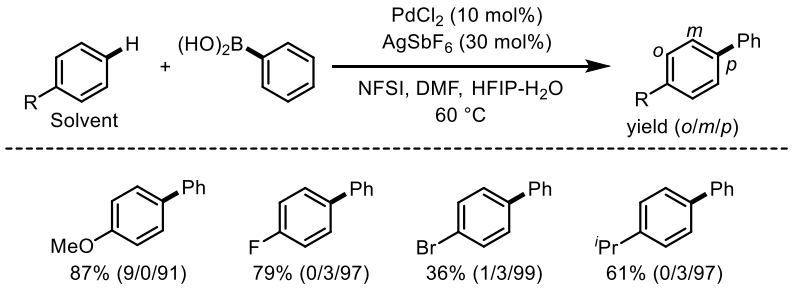

Scheme 1.14. Palladium-catalysed direct arylation (S_EAr mechanism).

An unprecedented arylation procedure was reported by Fagnou in 2006[23] where electron-deficient arenes are coupled with aryl halides. Prior to this study, the most commonly invoked mechanism for direct arylation was *via* an S_EAr type pathway. The authors recognised that this pathway was ultimately limiting to substrate scope as many aromatic compounds would not be nucleophilic enough. However, through the mechanistic rationalisation that the recently proposed CMD mechanism may operate and allow such reactivity, they attempted the direct

arylation of perfluorobenzenes and aryl halides. For example, pentafluorobenzene **26** reacts with 4-bromotoluene **27** to furnish biaryl **28** in near quantitative yields (Scheme 1.15). Fundamentally, a large excess of either coupling partner was not required and almost equal stoichiometries of both coupling partners were used.

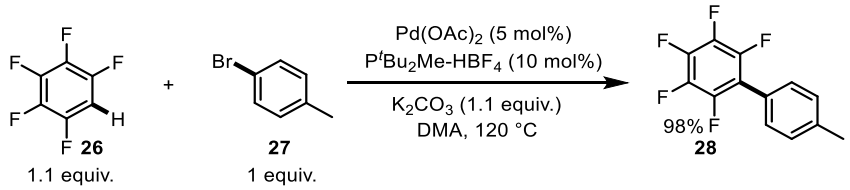

Scheme 1.15. Representative example of palladium-catalysed direct arylation (CMD mechanism).

Competition experiments between different perfluoroarenes demonstrated that the relative reactivity of the arenes are predicted by their relative acidities. Therefore, in general the more electron-deficient arene react preferentially, which is the opposite reactivity trend to that predicted by an S_EAr mechanism, and wholly consistent with a CMD mechanism.

Whilst notable examples of direct arylation with other transition metals have been shown, palladium is by far the most widely used catalyst. This versatile metal has been so widely studied and this has led to a multitude of ligands to ensure effective optimisation of several processes. However, there are still some flaws in palladium-catalysed direct arylation protocols. Significantly, high temperatures are consistently used to ensure efficient transformation of starting materials to product. Therefore, the search for new, milder conditions, with different catalyst species is of the upmost importance.

1.2. Gold-Catalysed Aryl Cross-Coupling

Gold, regarded to be the noblest of all the metals,[52] is probably the most widely known element across the globe.[53] This rare metal - which is resistant to corrosion and oxidation, whilst remaining easy to mould - has accompanied mankind throughout history as a measure of currency and, to this day, remains a symbol of wealth.[53] In addition the aesthetic properties of gold and corresponding use in jewellery, the inertness of elemental gold has resulted in applications in dentistry, electronic connectors, space technology, and even as a food additive.[54] However, the resistance of elemental gold to react has resulted in gold being one of the most overlooked metals in the periodic table with regard to chemical reactivity. Indeed, gold in its zero-oxidation state is generally unreactive, but when exposed to strongly oxidising conditions, the resulting complexes possesses unique and unprecedented reactivity. Over the

past 20 years, the growth in interest into gold as a catalyst for a plethora of chemical transformations has been substantial.

By far the most common use for gold as a catalyst has been to facilitate the nucleophilic attack upon C-C π-bonds through Lewis acid activation in its gold(I) oxidation state.[53,55–60] The ability of gold to act as a mild, carbophilic Lewis acid has been exploited in numerous applications. For example, the use of gold in cycloisomerisations of enynes has been demonstrated to be one of the most important and versatile methods to rapidly construct complex cyclic structures from simple acyclic substrates. An early demonstration of the synthetic utility of gold(I) catalysed cycloisomerisations by Toste and co-workers was the reaction of 1,5-enynes to bicyclo[3.1.0]hexenes (Scheme 1.16). The reactions were conducted at room temperature with 1-3 mol% of catalyst and were high yielding (> 82%). A notable demonstration of this reaction was the conversion of enantio-enriched **29** to **30** with excellent transfer of chirality as well as a high diastereomeric ratio.[61]

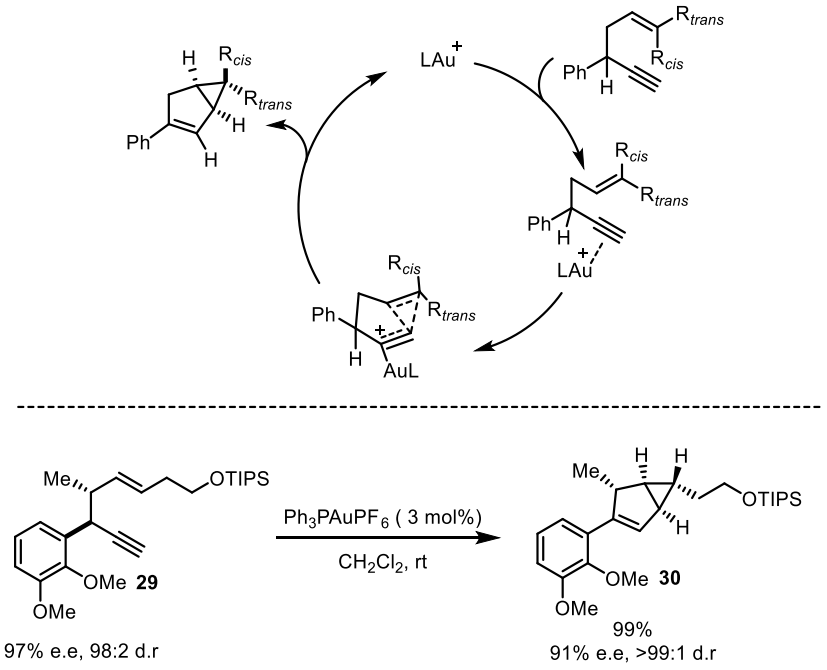

Scheme 1.16. Catalytic cycle (Top), and example (bottom) of gold(I) catalysed cycloisomerisation of 1,5-enynes.[61]

Gold(I) complexes are often found to show greater reactivity than other electrophilic salts such as Pt(II) and are unique in that they are highly reactive and selective for π-bonds.[56] The high π-acidity is attributed to relativistic effects, which are at a maximum with gold.[62] Of particular interest is the reaction conditions with which many gold-catalysed processes operate; they

often require a simple experimental set up due to air and moisture tolerance, low catalyst loadings are prevalent, and regularly reactions require no additional heating.[56]

Whilst significant transformations are available with the use of gold(I) as a catalyst, the use of gold as a catalyst for synthesis of the highly prized biaryl motif is a formidable challenge. The use of gold as a catalyst in cross-coupling to generate biaryls is highly sought after due to the unique properties of gold outlined; it has good functional group tolerance, reactions are often mild and tolerate air, moisture and often operate at room temperature. However, for such a reaction to operate, a gold(I/III) redox cycle must operate. A hypothetical catalytic cycle of a traditional cross-coupling reaction with a gold-catalyst can serve to illustrate some of the potential issues of designing a gold-catalysed cross-coupling procedure (Scheme 1.17).

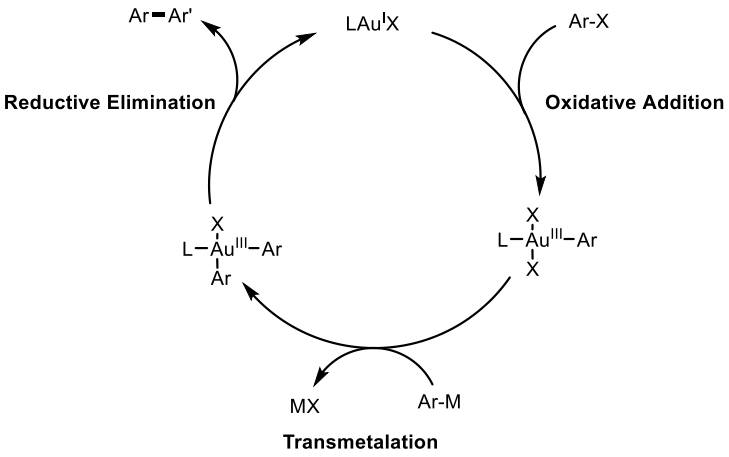

Scheme 1.17. Hypothetical gold-catalysed cross-coupling reaction.

Whilst the fundamental steps of oxidative addition, transmetalation, and reductive elimination have been well studied in many other transition metals, the overall mechanistic understanding of homogeneous gold catalysis remains less well developed. However, in recent years, stoichiometric studies have shed new light on the mechanistic pathways of these processes.

1.2.1 Oxidative Addition

The major hurdle in the replacement of palladium with gold in a traditional cross-coupling reaction is the oxidative addition. Indeed, the high redox potential of gold(I) to gold(III) have previously led researchers to believe that the oxidative addition of, for example, an aryl halide to gold(I) was impossible.[63] This consensus has been reversed as recent key stoichiometric studies have demonstrated that oxidative addition of C_{Ar}-X bonds to gold(I) is indeed possible. The first direct evidence of oxidative addition of C(sp^2)-X bonds to a mononuclear gold(I) centre was demonstrated by Amgoune, Bourissou *et al.*[64] To facilitate the oxidative addition, 8-halo naphthyl phosphines were employed so that pre-coordination of the gold(I) centre to

the phosphine placed the metal in close proximity to the C_{Ar}-X bond to allow for an intramolecular oxidative addition (Scheme 1.18). Indeed, for compound **31**, coordination of the phosphine to gold(I) occurred rapidly forming **32**, which decayed in a first-order fashion to the Au(III) complex **33**, consistent with an intramolecular unimolecular oxidative addition.

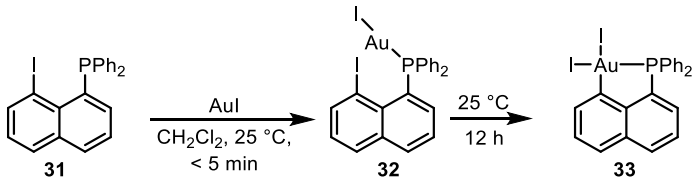

Scheme 1.18. Intramolecular oxidative addition to gold(I).

Whilst oxidative addition into the analogous C_{Ar}-Br bond was demonstrated, significantly higher temperatures were required (130 °C). No oxidative addition into the C_{Ar}-Cl bond, even at elevated temperatures for several hours, was observed. The barrier to oxidative addition of C_{Ar}-Br bonds to gold(I) could be reduced, and therefore milder conditions employed, when diphosphine ligands were used. Au(III) pincer complex **35** was formed from aryl bromide **34** at a reduced temperature of 60 °C, demonstrating the importance of a second phosphine arm (Scheme 1.19). DFT calculations suggested that bidentate coordination of the phosphine ligands to gold facilitates a more facile oxidative addition than the 8-bromo naphthyl counterpart.[64]

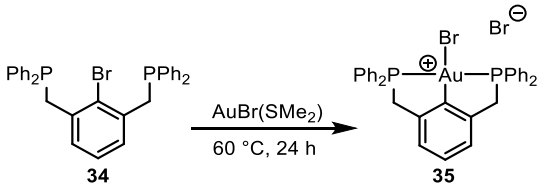

Scheme 1.19. Synthesis of pincer gold(III) complex through oxidative addition.

Although oxidative addition into C_{Ar}-X bonds has been shown to be experimentally possible, its use in general cross-coupling has yet to be demonstrated as the high redox potential necessitates specific ligand environments which limits the general applicability in catalytic reactions.

1.2.2 Transmetalation

Unlike many oxidative addition processes, transmetalation of aryl groups to gold is a significantly more facile process. There are numerous examples of transmetalation to both Au(I)/(III) from reagents such as boron (including, aryl borates,[65] boronic acids[66] and boranes[67]), silicon,[68,69] tin,[70] lithium, Grignard and mercury reagents.[71]

Historical studies into the transmetalation at gold focused on the use of lithium and Grignard reagents, however due to the limit this placed on functional group tolerance, recent studies have focused on more mild transmetalating agents. Arylboronic acids have been shown to transmetalate to both gold(I) and gold(III) under mildly basic conditions. For example, Nolan *et al.* studied the reaction of $ArB(OH)_2$ with AuCl(IPr) in detail and demonstrated that the identity of the base was crucial. Indeed, replacing Cs_2CO_3 with KOH allowed for significantly milder reaction conditions, from 70 °C over 24 h with Cs_2CO_3, to room temperature for 1 h using KOH. A gold(I) hydroxide was proposed to be the key intermediate to which transmetalation occurs (Scheme 1.20).[72]

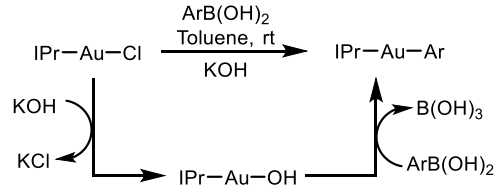

Scheme 1.20. KOH promoted transmetalation of boron-to-gold(I)

Bochmann was subsequently able to demonstrate direct transmetalation of arylboronic acids with a gold(III) hydroxide pincer complex **36** (Scheme 1.21). Both electron-rich and electron deficient boronic acids were successful in transmetalating.[73]

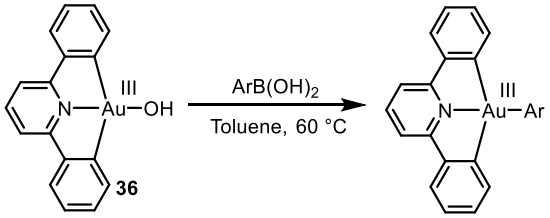

Scheme 1.21. Transmetalation of boron-to-gold(III) hydroxide species.

Although the presence of base favours transmetalation of arylboronic acids, it is not a requirement. Nevado *et al.* were able to demonstrate a gold(III)-boron transmetalation in the absence of base, albeit under forcing conditions. However, only very electron-deficient boronic acids could transmetalate, with electron-rich examples completely unreactive. The mechanism of transmetalation proposed to explain this reactivity trend was a rate-determining chloride abstraction from **37** by the highly electrophilic boron species **38**, followed by coordination of the hydroxy group to form intermediate **39**, which upon migration of the aryl group yields **40** (Scheme 1.22). The proposed chloride abstraction would be disfavoured for electron-rich boronic acids, thus explaining the reactivity.[74]

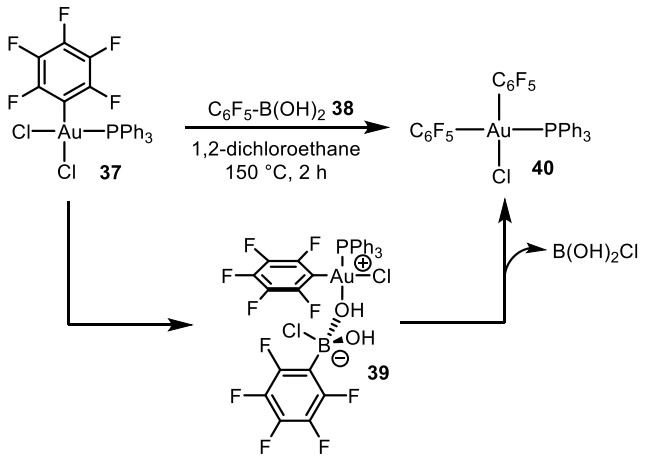

Scheme 1.22. Direct transmetalation of electron-deficient boronic acids to Au(III) in the absence of base.

1.2.3 Reductive Elimination

Despite advances in the understanding of oxidative addition and transmetalation, the parameters that govern reductive elimination from diarylgold(III) complexes remains understudied. Seminal studies into reductive elimination from trialkyl and dialkylgold(III) phosphine complexes were performed by Kochi. It was proposed that dissociation of the phosphine was required for reductive elimination, this occurring *via* a high-energy T-shaped species. Indeed, added phosphine retarded the rate of reaction which implied a dissociative pre-equilibrium prior to reductive elimination (Scheme 1.23).[75]

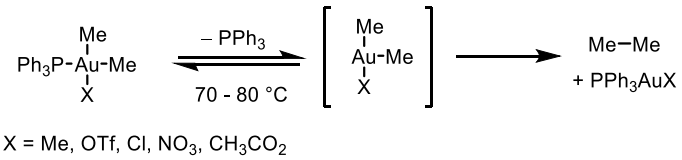

Scheme 1.23. Proposed mechanism of reductive elimination from di/trialkyl gold(III) complexes.

In one of the few studies into reductive elimination of biaryls from diarylgold(III) complexes, Vicente *et al.* first demonstrated that the dissociative pre-equilibrium with the phosphine ligand seen in dialkylgold(III) complexes may not be required. In fact, for reductive elimination to occur from the complexes synthesised, added phosphine was necessary (Scheme 1.24).[76]

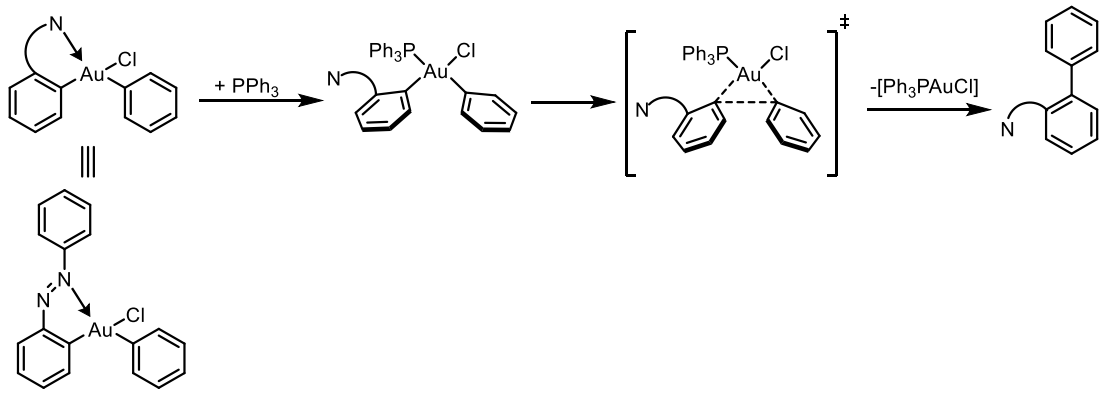

Scheme 1.24. Proposed mechanism of reductive elimination from diarylgold(III) complexes.

These results were corroborated by Toste *et al*. who studied the mechanism of reductive elimination from non-chelating diarylgold(III) complex **41** by measuring the rate of reductive elimination to biaryl **43**. It was concluded that reductive elimination could indeed occur *via* a four-coordinate species, and that two pathways were possible (Scheme 1.25), one where reductive elimination occurred from neutral complex **41**, and the other where added phosphine increased the rate of reductive elimination through the formation of cationic intermediate **42** (where $k_2 > 1000k_1$). In fact, reductive elimination from **42** was determined to be "among the fastest C–C bond-forming reductive eliminations (between −50 and −10 °C) reported for any transition metal complex."[77]

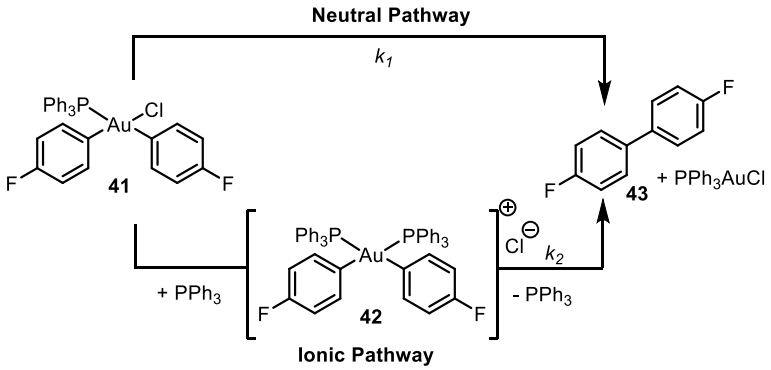

Scheme 1.25. Neutral and ionic mechanisms for reductive elimination from diarylgold(III) complexes.

In contrast, when Nevado *et al.* prepared similar diarylgold(III) phosphine complex **40**,[74] reductive elimination was slow, and forcing conditions were required, thus suggesting that aryl electronics have a large effect on the rates of reductive elimination from diarylgold(III) complexes (Scheme 1.26).

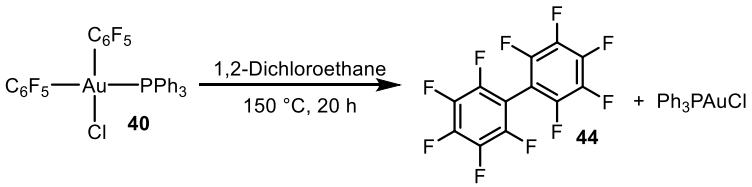

Scheme 1.26. Slow reductive elimination of electron-deficient biaryl.

1.2.4 Gold-Catalysed Direct Arylation

Transmetalation and reductive elimination, two of the three major transformations in a general gold-catalysed cross-coupling reaction to generate a biaryl, have been demonstrated to be relatively facile processes. The major obstacle is therefore the oxidative addition which has only been demonstrated in highly designed systems. A strategy which has been implemented in recent years, and has been demonstrated in three distinct studies, is the replacement of the aryl halide with an arene and the concomitant use of an external oxidant for an oxidative gold-catalysed direct arylation reaction (Scheme 1.27).

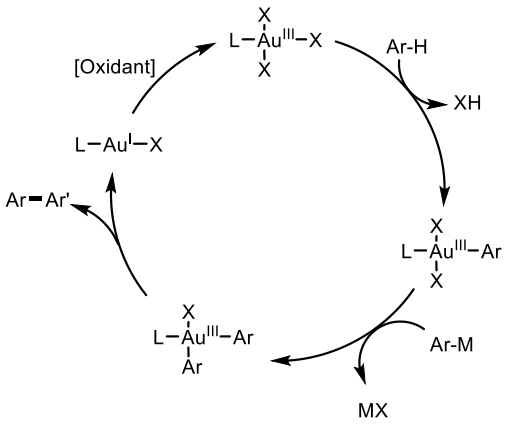

Scheme 1.27. General gold-catalysed direct arylation mechanism. N.B. Exact order of steps may vary depending on conditions.

The ability of gold(III) to selectively react with arenes under mild conditions to generate arylgold(III) complexes is well-established, and is widely understood to proceed *via* an S_EAr type mechanism.[78] The first example of direct auration of aromatic molecules and gold(III) complexes was demonstrated over 80 years ago by Kharasch and Isbell in the auration of benzene using anhydrous $AuCl_3$.[79] However, it was not until 2008 when the first example of a gold-catalysed C-C coupling reaction to generate biaryls was demonstrated by Tse *et al*.[80] The protocol, which generated a series of homocoupled arenes, was studied at 2 mol% gold(III) in the presence of iodobenzene diacetate (IBDA) as the external oxidant (Scheme 1.28).

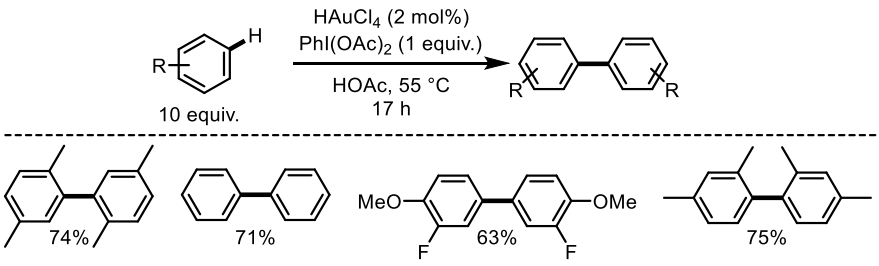

Scheme 1.28. Oxidative gold-catalysed biaryl homocoupling.

The first account of the use of oxidative gold-catalysis in a *cross-coupling* reaction to generate biaryls was jointly demonstrated in 2012 by the research groups of Lloyd-Jones and Russell.[81] Inspired by the oxidative coupling of arenes reported by Tse, and the recent observation of homocoupling of aryltrimethylsilanes in their recently reported oxidative gold-catalysed oxyarylation of alkenes,[69] the direct arylation of arenes by aryltrimethyl silanes was reported (Scheme 1.29).

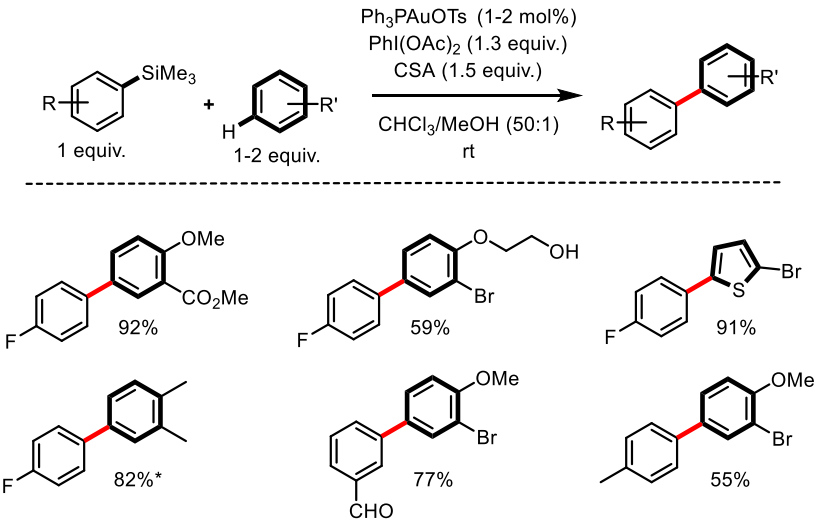

Scheme 1.29. Representative scope of gold-catalysed direct arylation with aryltrimethylsilanes. * = 87% Site selectivity

In contrast to many previous direct arylation procedures, the reaction conditions are remarkably mild; the reaction does not require a large excess of either coupling partner, it operates at room temperature, under air, and with low catalyst loadings (1-2 mol%), and was demonstrated to tolerate moisture. Fundamentally, the reaction required no directing groups and regioselectivity was high and based on S_EAr reactivity. The substrate scope incorporated a number of mildly electron-rich arenes, electron-rich and electron-deficient silanes, and also exhibited a broad functional group tolerance, with esters, aldehydes, and alcohols remaining

intact despite the oxidative nature of the reaction. In addition, recent developments have shown a number of heterocycles to be efficient arene coupling partners.[82]

The reaction was subsequently subjected to a substantial mechanistic study which outlined the steps in the catalytic cycle (Scheme 1.30) and resulted in identification of an improved precatalyst, thtAuBr$_3$, with a significantly reduced induction period.[83] The turnover-limiting step in the cycle was found to be π-complexation of the arene to the arylgold(III) complex.

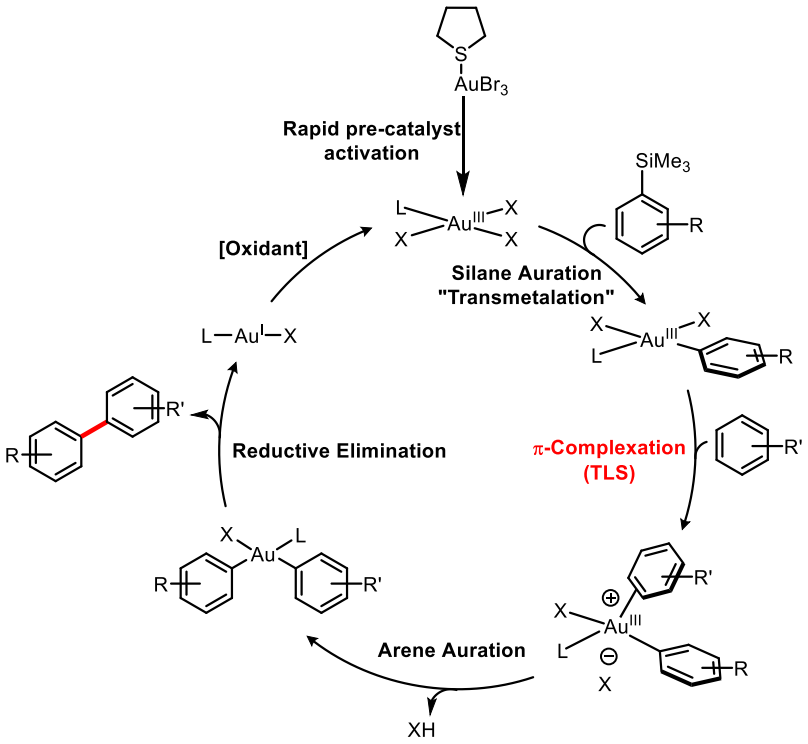

Scheme 1.30. Simplified catalytic cycle for gold-catalysed direct arylation.

Once again, the use of intramolecular direct arylation was key in elucidating the reaction mechanism. The ordering of catalytic events (i.e. transmetalation *vs* arene auration as the first step) was identified through the successful cyclisation of **1a**, with **2a** as the sole product (Scheme 1.31, Top). Excellent selectivity for the C-3 position would be required for C-H auration if this was the first step, however this was dismissed as the C-5 position was independently shown to be the most reactive to S_EAr through the iodination of **45** to **46** (Scheme 1.31, bottom). Reversible C-H auration could explain the observed selectivity, however this was discounted as no isotopic incorporation was observed when conducting the reaction in deuterated solvent.

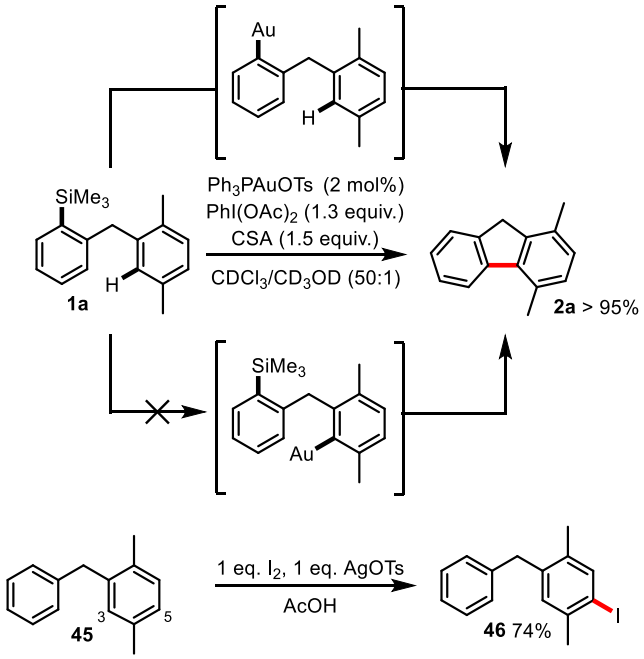

Scheme 1.31. Intramolecular direct arylation as a mechanistic tool.

In 2016, Nevado and co-workers developed a similar approach with boronic esters (either pinacol (Bpin) or 2,3-pentanediol (Bpen) esters) as transmetalating agents instead of arylsilanes. The scope was found to be complimentary to the reaction developed by Ball, Lloyd-Jones and Russell, as only extremely electron-deficient boronic acids were competent in the reaction (Scheme 1.32). Whilst this restricts the substrate scope, it allows for the synthesis of arenes that have not been shown to be possible with the use of arylsilanes.[84]

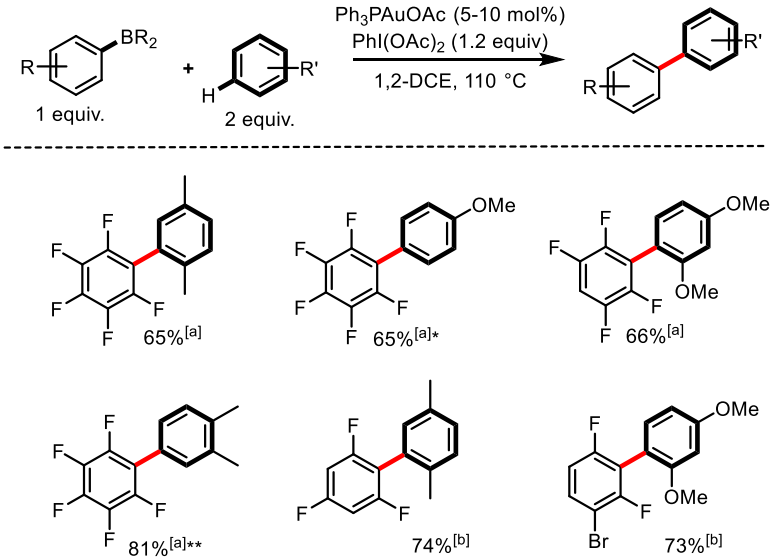

Scheme 1.32. Representative scope of gold-catalysed direct arylation with boronic esters. [a] With Bpin; [b] with Bpent. * = 66% Site selectivity. ** = 79% Site selectivity.

Whilst for many decades gold(III) has been known to react with arenes *via* an S_EAr type mechanism, and that electron-rich substrates are more reactive, it has been recently shown that gold(I) has the opposite reactivity and that electron-deficient arenes react preferentially, consistent with a CMD type mechanism (Scheme 1.33).[85]

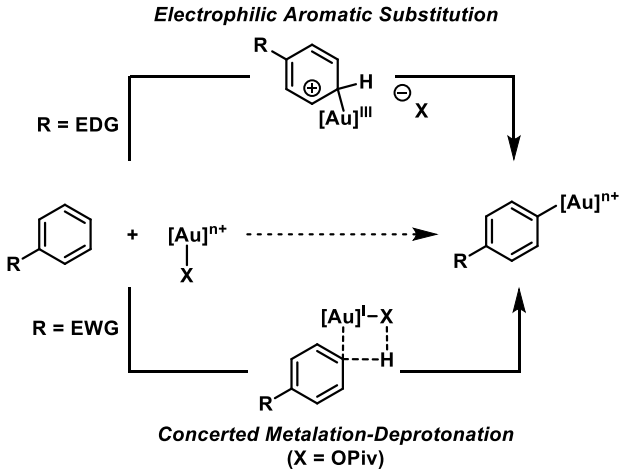

Scheme 1.33. Dependence of the mechanism of C-H bond metalation on gold oxidation state.

The marked difference between gold(III) and gold(I) towards C-H bond activation was recently discovered by the research group of Larrosa.[85] In their study, solely electron-deficient arenes were shown to react with the Au(I) complex at the most electron-deficient C-H bond (Scheme 1.34). The reactions were performed with a mild base and at 50 °C; however, a silver additive was crucial for reactivity. The exact role of the silver is yet to be determined but C-H activation by silver followed by transmetalation to gold was ruled out through control experiments.

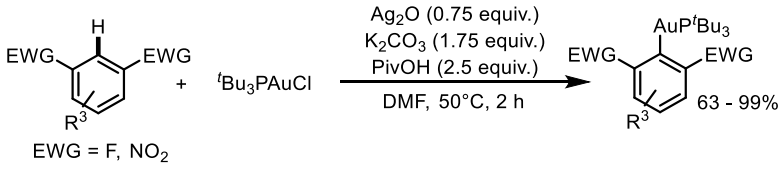

Scheme 1.34. C-H bond metalation of electron-deficient arenes by Au(I).

The reactivity difference between Au(I) and Au(III) was exploited by the same research group in a catalytic cross-dehydrogenative protocol coupling electron-rich with electron-deficient arenes (Scheme 1.35).[86]

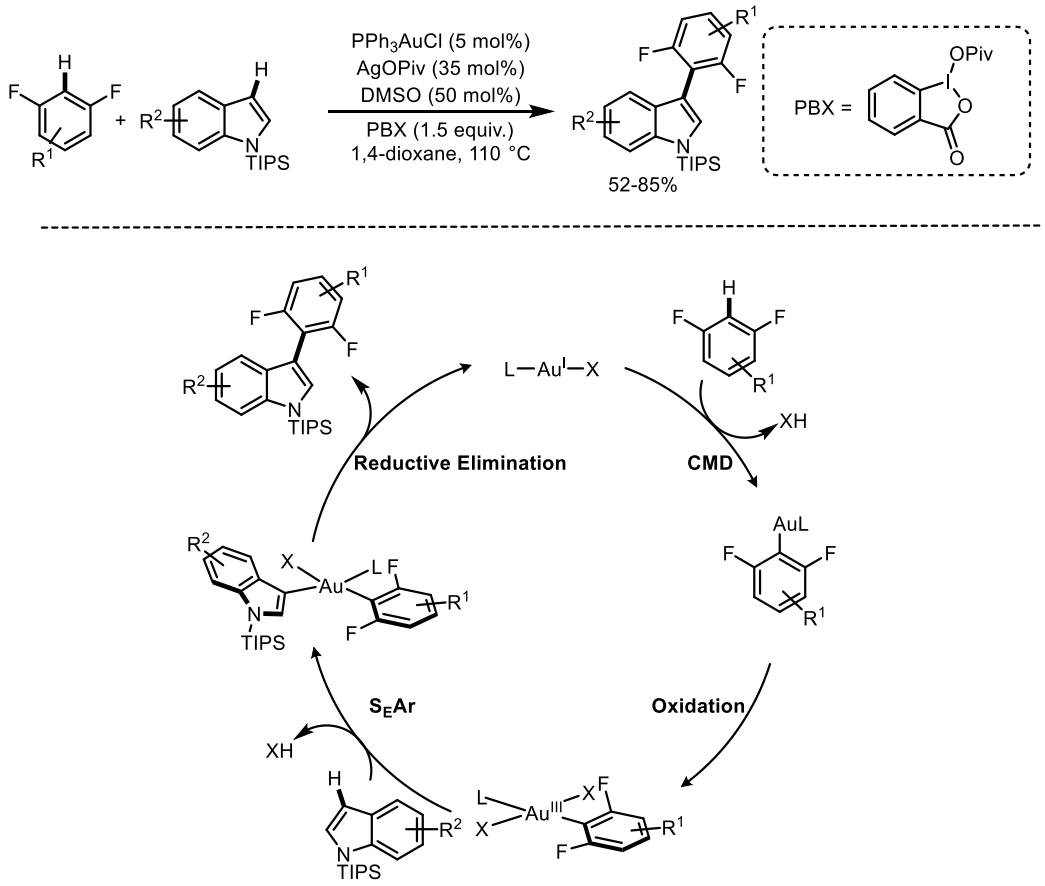

Scheme 1.35. Gold-catalysed double C-H activation of arenes (Top) and proposed catalytic cycle (bottom).

1.3 Summary and Project Aims

Biaryl molecules are fundamentally important across the chemical industry. Whilst the cross-coupling of aryl halides and organometallic reagents is the most popular route to these structures, direct arylation procedures where aromatic C-H bonds are functionalised is an increasingly popular alternative. Direct arylation catalysed by palladium has received the most attention, but recently, gold-catalysed approaches have been developed. The direct arylation of arenes by aryltrimethylsilanes developed in this research group[81,83] was a significant breakthrough, and compared with typical palladium-catalysed conditions, the reaction proceeds under remarkably mild conditions.

Whilst intermolecular gold-catalysed direct arylations have been advanced, at the time this project was started,[87] there were no such methodologies available to synthesise cyclic biaryls through intramolecular direct arylation. Whilst **1a** (Scheme 1.31) was demonstrated to cyclise successfully, the reaction was not optimised, nor was the scope of the reaction assessed. However, the success of this reaction indicated that an intramolecular methodology could be

established. The aim of this project was to develop the intramolecular gold-catalysed direct arylation, from both a synthetic and mechanistic aspect. Not only are the products of intramolecular direct arylation of high synthetic value, but as seen in several instances in this Chapter, intramolecular reactions have been key in elucidating fundamental new mechanistic insights.

2. Intramolecular Direct Arylation: Substrate Scope and Formal Synthesis of (±)-Allocolchicine

ABSTRACT: Chapter 2

The use of aryltrimethylsilanes in intramolecular gold-catalysed direct arylation is demonstrated. Utilising the conditions developed for intermolecular coupling, 31 examples are shown, spanning 5- to 9- membered rings. In the most electron-rich examples, significant diaryliodonium salt is formed from the reaction of the cyclised product with the hypervalent iodine oxidant, resulting in moderate to poor yields. The use of [bis(trifluoroacetoxy)iodo]benzene (PIFA), which is not competent in intermolecular coupling, largely eliminates this deleterious process and allows for the implementation of previously unexplored molecular architectures. This is demonstrated through the formal synthesis of natural product allocolchicine, which bears a highly electron-rich trimethoxy-arene moiety.

Substrates **2a**, **c-e**, **i**, **q-s**, **u**, **w**, **3a**, **e**, and **5b-d** were prepared and characterised by Dr. Liam Ball. The results presented in this Chapter have been communicated: T. J. A. Corrie, L. T. Ball, G. C. Lloyd-Jones, C. A. Russell, *J. Am. Chem. Soc*. **2017**, *139*, 245 and T. J. A. Corrie, G. C. Lloyd-Jones, *Topics in Catalysis*, **2017**, *60*, 570.

2.1 Introduction

Tricyclic biaryls (Scheme 2.1) are an extremely broad class of compound with innumerable applications across organic chemistry, materials science and pharmaceutical chemistry, as well as being a common motif in several natural products, including the antibiotic vancomycin which is on the World Health Organisation's List of Essential Medicines.[88]

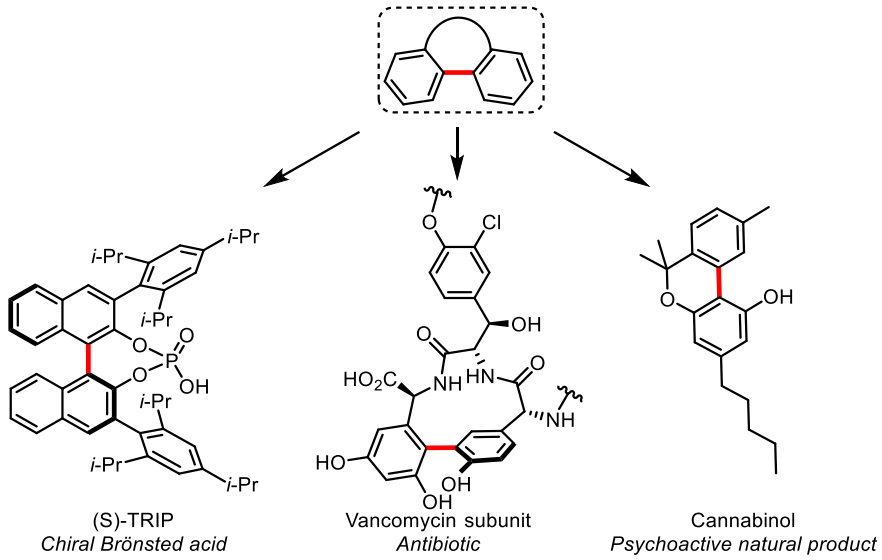

Scheme 2.1 Tricyclic biaryl motif in natural and synthetic compounds.

Due to the importance of the cyclic biaryl, countless strategies are available to synthesise this moiety, with many methodologies dedicated to the synthesis of just a single class of this diverse structure. For example, synthesis of one of the simplest tricyclic biaryls, fluorene, is still subject to intense research despite numerous strategies available for its synthesis.[89] Modern methods tend to utilise C-H activation as a strategy, with functionalisation of both C(sp^2)-H and C(sp^3)-H bonds employed in recent syntheses of fluorene (Scheme 2.2).

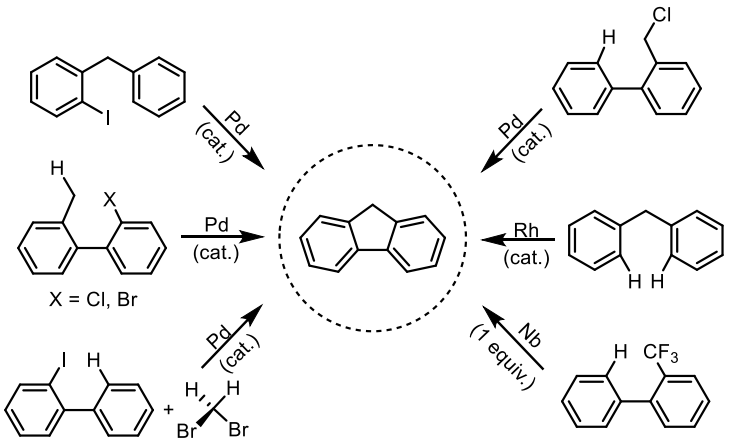

Scheme 2.2. Select C-H activation methods for synthesis of fluorene.[90–96]

In recent years, intramolecular direct arylation has become a successful strategy in the synthesis of tricyclic biaryls.[19–21] Unlike intermolecular direct arylation, where poor regioselectivity can be obtained in the absence of directing groups, regioselectivity in intramolecular direct arylation is restricted through the conformational bias the tether enforces (Scheme 2.3).

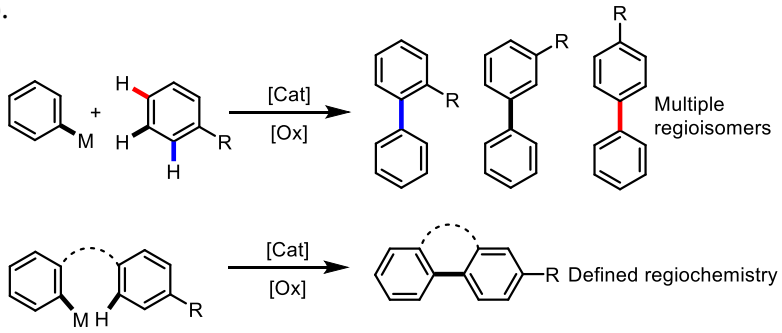

Scheme 2.3. Regioselectivity in inter- and intramolecular direct arylation.

2.1.1 Direct Arylation Strategies to construct 5- and 6-Membered Rings

The synthesis of 5- and 6-membered rings is easily accessible through direct arylation, with higher ring sizes providing a more significant challenge. Over the past 40 years, research into intramolecular direct arylation has gained much attention. Palladium has been at the heart of the research, and many classes of 5- and 6- membered rings can be synthesised *via* direct arylation employing palladium as a catalyst.

A seminal study into palladium-catalysed intramolecular direct arylation was by Ames and Opalko in 1983.[97] In their report, a series of functionalised dibenzofurans were synthesised from the corresponding 2-bromophenyl phenyl ethers. A large electronic range was tolerated, but harsh conditions were required with catalyst loadings up to 10 mol% and temperatures of at least 150 °C (scheme 2.4).

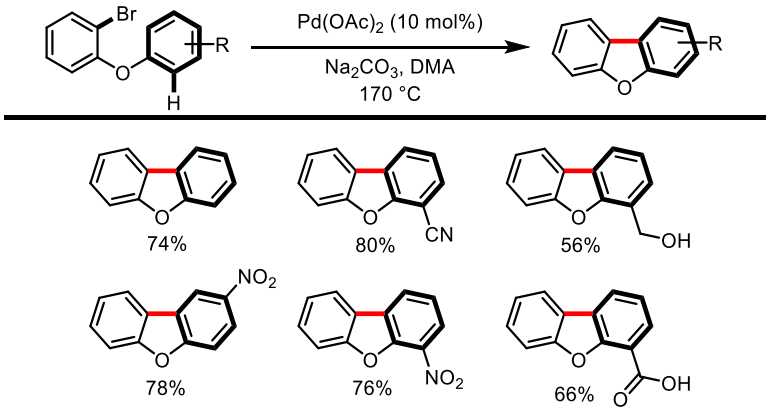

Scheme 2.4. Early example of palladium-catalysed direct arylation of ethers

Some of the most important studies into palladium-catalysed intramolecular direct arylation from both a mechanistic and preparative aspect were from the research group of Fagnou. Whilst previous studies were only successful for specific substrate classes, and relied upon high catalyst loadings, the reaction conditions developed by Fagnou led to an extensive substrate scope, with a myriad of 5- and 6- membered rings synthesised from aryl bromides, chlorides and iodides. A selection of the broad substrate scope is shown in scheme 2.5.[37,38]

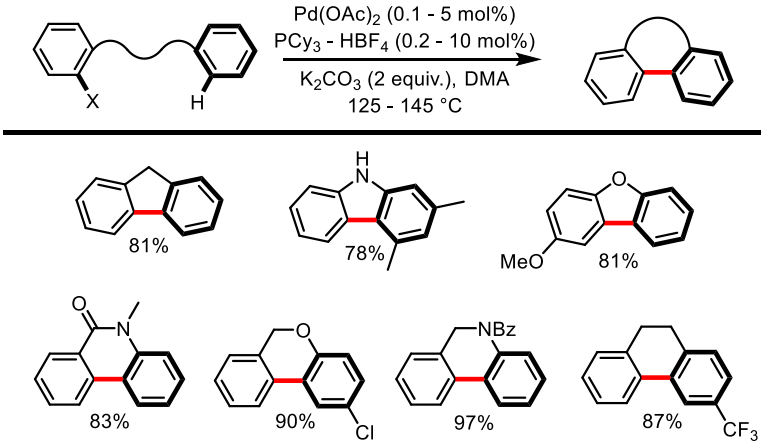

Scheme 2.5. Representative scope of modern Pd-catalysed direct arylation.

Whilst impressively low catalyst loadings were demonstrated, high temperatures were required in these reactions. Further developments by Fagnou, inspired by improved

understanding of the CMD mechanism, led to a reduction in temperature to 50 °C when pivalic acid was used as an additive (Scheme 2.6). The pivalic acid formed potassium pivalate *in-situ*, which was found to be a superior base, in part due to increased solubility compared to K_2CO_3.

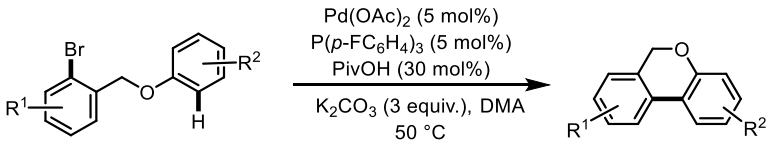

Scheme 2.6. PivOH as an additive in mild direct arylation.

2.1.2 Synthesis of 7+ Membered Rings

Whilst the synthesis of 5- and 6-membered rings *via* intramolecular direct arylation is relatively facile, the opposite is found with larger ring systems. Examples of the synthesis of 7+ membered rings are rare, and often relatively electron-rich arene coupling partners are required to react with the electrophilic metal centre. The difficulty in synthesising such structures arises from a large entropic cost in forming the metallocycle as well as transannular strain.[98,99] Once again, the research of Fagnou reported an early example of the synthesis of 7-membered ring **27** under palladium-catalysed conditions (Scheme 2.7). Successful ligand design facilitated the reaction, as modification of PhDave-Phos, which was employed in the synthesis of smaller rings, to the more electron-deficient **28**, resulted in a more electrophilic catalyst and increased reactivity.[100] This example is noteworthy for the low catalyst loading required, however high temperatures are still needed.

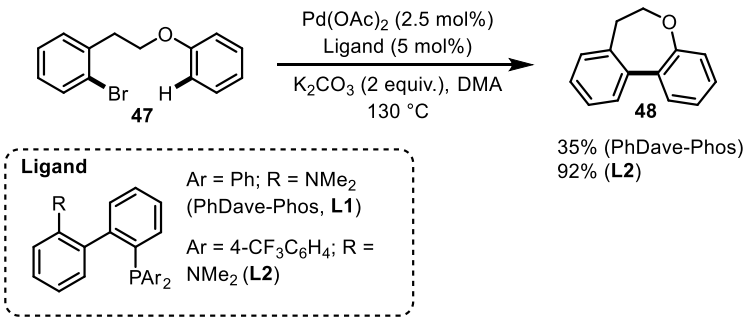

Scheme 2.7. Synthesis of 7-membered ring by Pd-catalysed direct arylation.

A notable example of 7-membered ring synthesis *via* a palladium-catalysed direct arylation was reported by Saget and Cramer in their enantioselective syntheses of chiral dibenzazepinones with quaternary stereogenic centres (Scheme 2.8).[101] The reactions proceeded under relatively mild conditions of 80 °C with 5 mol% Pd compared to the harsh conditions typically required (up to 130 °C, 10 mol% Pd) and represented the first example of direct enantioselective arylation to form seven-membered rings. Notably, this is a rare example

of the synthesis of a larger ring system when the reactive arene can be a simple phenyl group (R^4 = H), and therefore not significantly activated for either S_EAr or CMD-type mechanisms.

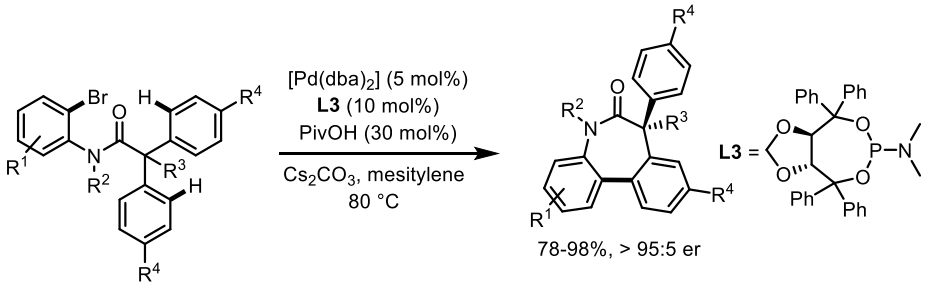

Scheme 2.8. Representative example of enantioselective direct arylation.

The research group of Greaney demonstrated the synthesis of 7- and 8- membered rings containing biaryls through palladium-catalysed dehydrogenative coupling (Scheme 2.9).[102] The substrate scope of the 7- membered rings was wide as both electron-donating and withdrawing phenyl substituents were tolerated, as were tethers both with and without heteroatoms (N, O). Intriguingly, the success of the 8-membered ring reaction relied on the inclusion of a nitrogen in the tether as in its absence, no reaction occurred. This was attributed to coordination of the nitrogen to palladium, reducing transannular strain and stabilising the catalyst (Scheme 2.9, bottom).

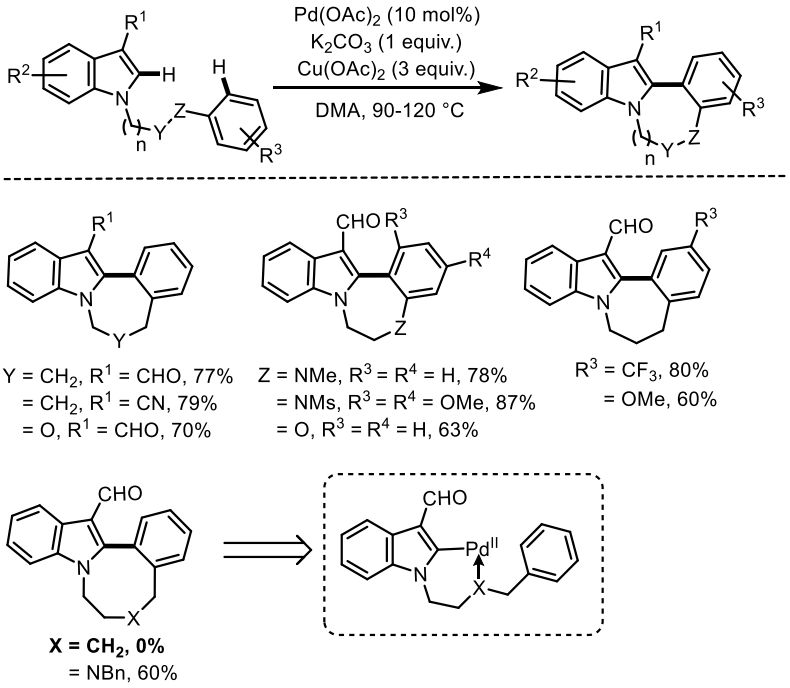

Scheme 2.9. Oxidative biaryl coupling for medium ring synthesis.

An additional insight into the mechanism of the reaction was through the regioselectivity of cyclisation of **49** where *ortho*-arylation generates **50**, consistent with a CMD-type mechanism (Scheme 2.10).

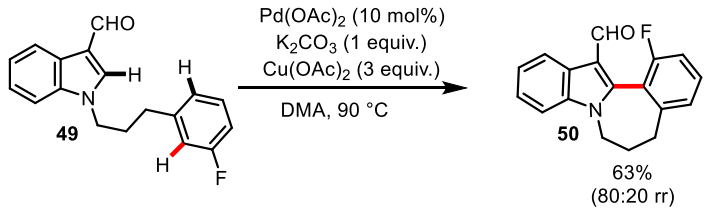

Scheme 2.10. Mechanistic insight into arylation mechanism.

One of the few examples of the synthesis of 9-membered rings *via* direct arylation was reported by the research group of Beccalli in 2006 (Scheme 2.11).[103] Seven-, eight- and nine-membered indole-based biaryls were synthesised under palladium-catalysed conditions, however significantly reduced yields were reported for the 9-membered examples.

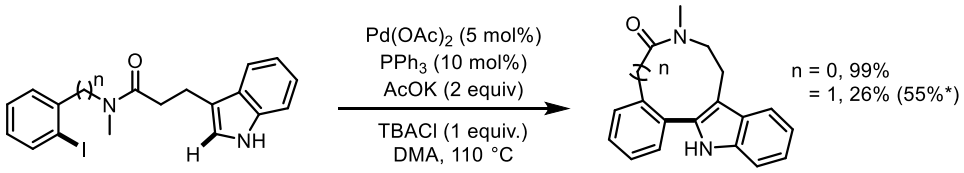

Scheme 2.11. Synthesis of 8- and 9- membered rings *via* direct arylation. * = microwave heating at 160 °C.

2.1.3 Synthesis of Natural Products

Despite the rich library of cyclic biaryl natural products,[104] applications of intramolecular direct arylation in natural product synthesis are relatively rare. Whilst the application of a methodology to model substrates (*vide supra*) can give an indication of synthetic value, implementation of a strategy in complex molecule synthesis can be a true test of robustness. Natural product synthesis can highlight the deficiencies of certain processes and expose problems in catalyst chemo-, regio- (and perhaps stereo-) selectivity, as well as other critical aspects relating to catalyst stability, efficiency, activity and functional group compatibility. It is therefore unsurprising that despite the enormous advances in the field of direct arylation, applications to complex molecules are uncommon.

Pioneering studies by Bringmann *et al.*[105,106] led to the advancement of 2-haloaryl esters in intramolecular direct arylation to synthesise natural product biaryl frameworks (Scheme 2.12).

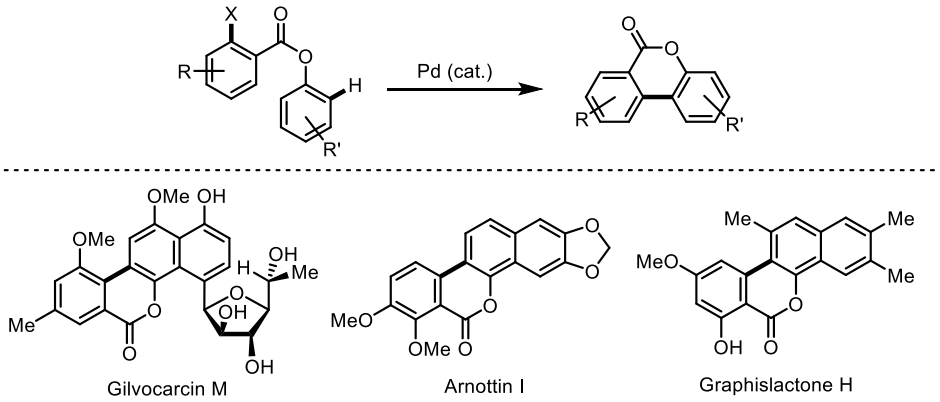

Scheme 2.12. Examples of natural products synthesised where the biaryl is formed through direct arylation.[107–109]

The strategy was only successful for 6-membered cyclic lactones however, and efforts to synthesise larger ring sizes have failed. For example, in the formal synthesis of (−)-steganone **51** by Abe and Harayama, attempts to form a 7-membered biaryl lactone **53** from aryl iodide **52** *via* direct arylation were unsuccessful and only protodehalogenation was observed (Scheme 2.13).[110]

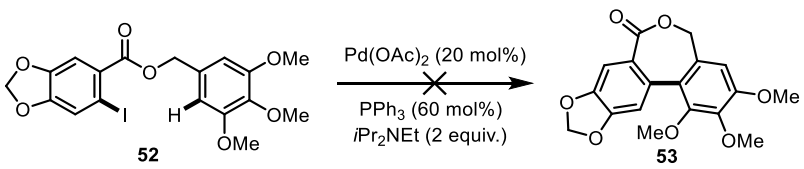

Scheme 2.13. Failure of direct arylation of 2-haloaryl ester in synthesis of 7-membered ring

The authors had to alter their synthetic strategy such that the direct arylation of **54** yielded 6-membered cyclic lactone **55** which could be ring opened atropselectively to yield **56**, which can be further functionalised[111,112] to complete the synthesis of **51** (Scheme 2.14).

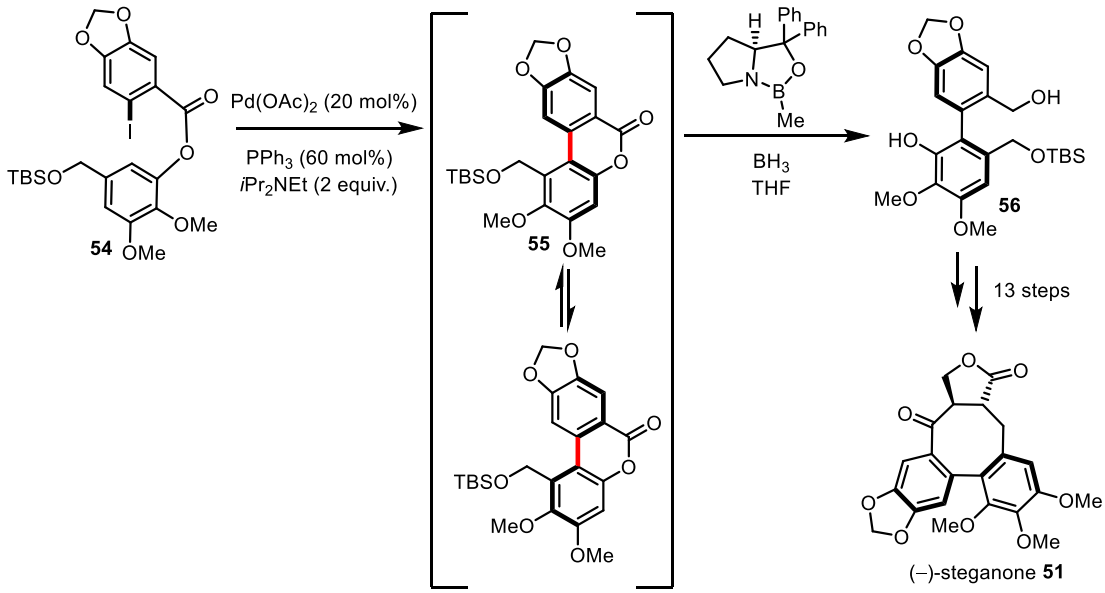

Scheme 2.14. Total synthesis of (−)-steganone *via* direct arylation

The atropselective ring opening strategy was pioneered in the research group of Bringmann. This dynamic kinetic resolution relies on the two atropisomers rapidly equilibrating, and one being selectively reduced by the chiral reducing agent whilst the other restores the equilibrium with the consumed atropisomer.[106]

Although many natural products synthesised *via* direct arylation are derived from ester linkages, several other linkages have also been employed including, ketones, amides and amines.[104] As previously mentioned, the synthesis of larger rings *via* direct arylation is synthetically challenging and there are only a limited number of examples in general. It is therefore unsurprising that despite numerous available targets, only a handful of examples exist. Two notable examples are the synthesis of allocolchicine **11**, a 7-membered cyclic biaryl, by Fagnou and Leblanc,[113] and the synthesis of (±)-rhazinilam **61** by Trauner *et al*.,[114] employing an unprecedented nine-membered ring synthesis (Scheme 2.15). The reaction conditions developed by Fagnou were found to be optimal for the synthesis of rhazinilam after an extensive ligand screen. The high temperature and catalyst loading required for these cyclisations emphasises the challenge such structures pose.

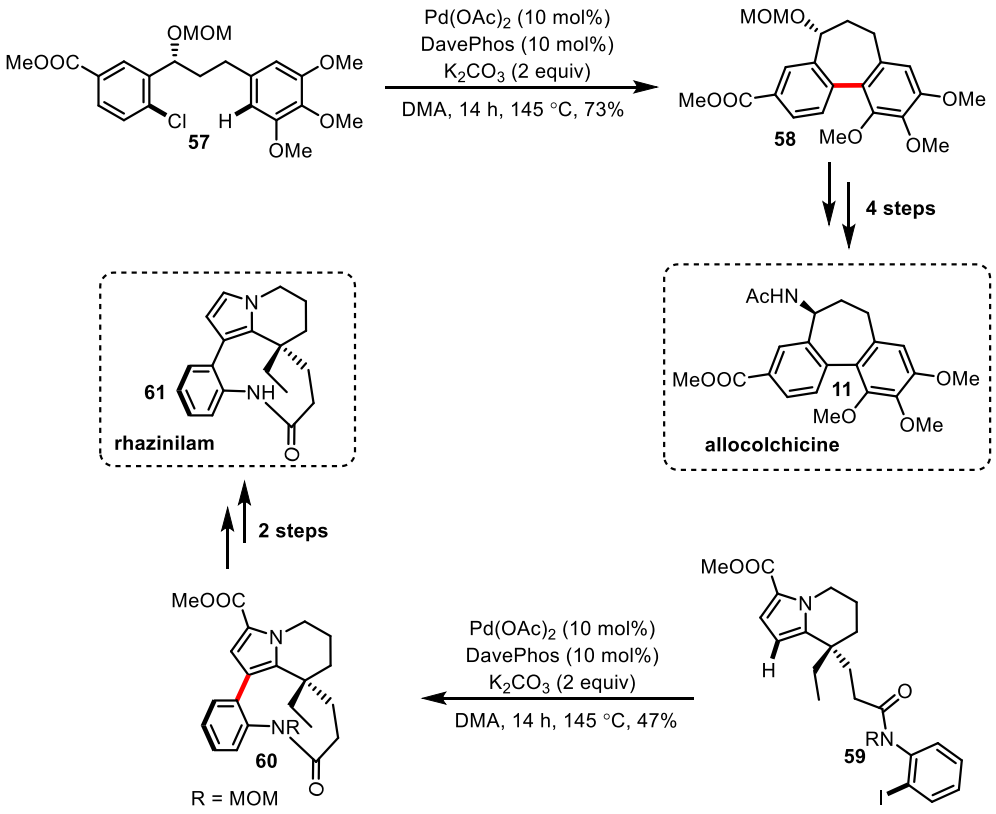

Scheme 2.15. Intramolecular direct arylation in natural product synthesis.

2.1.4 Chapter Aims

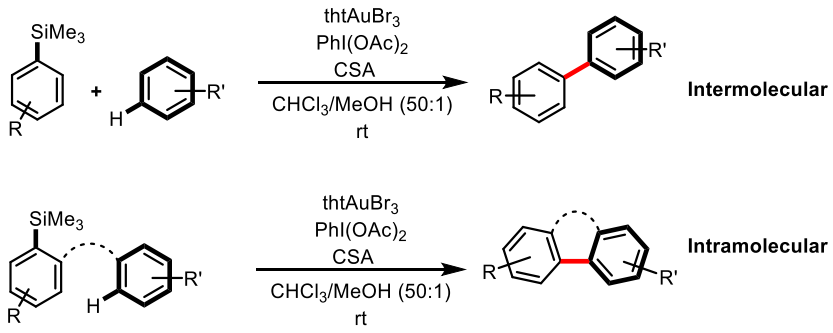

Scheme 2.16. Gold-catalysed inter- and intramolecular direct arylation.

Significant developments into intramolecular direct arylation have led to a myriad of synthetic applications. Typically, palladium is the catalyst of choice to facilitate this transformation, however, high temperatures are invariably required, and strategies to synthesise ring sizes greater than 6-membered are limited. Therefore, a gold-catalysed approach is highly desired as the characteristic qualities of gold-catalysis (e.g. low temperatures, excellent functional group tolerance, air and moisture sensitivity, short reaction times) are lacking in current state-of-the-art methods. In addition, gold-catalysis is orthogonal to Pd(0) cross-coupling as aryl

halides are tolerated, thus the use of gold in intramolecular direct arylation could increase the scope of post-cyclisation derivatisation. The aim of this project was to develop the synthetic methodology of a gold-catalysed intramolecular direct arylation, based on the previous intermolecular direct arylation of arenes by aryltrimethylsilanes (Scheme 2.16). Preliminary studies demonstrated the success of a single, electronically activated substrate leading to a 5-membered ring (Chapter 1, Scheme 1.31). The full electronic range of substituents was to be explored, followed by an investigation into the limits of ring size. The final aim was to utilise the methodology in the synthesis of a natural product to demonstrate the full synthetic value of the reaction.

2.2 Substrate Scope

2.2.1 Synthesis of 5-membered rings

The previously reported reaction conditions for the coupling of aryltrimethylsilanes and arenes were optimised for intermolecular reactions, where 1-2 mol% of catalyst was successful for a range of coupling reactions (Scheme 2.17).

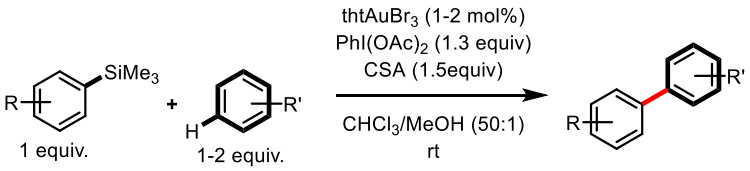

Scheme 2.17. Standard reaction conditions for intermolecular coupling.

It was therefore necessary to assess whether these were ideal conditions for intramolecular coupling, or if further optimisation was necessary. Each component of the reaction has at least one key role in the intermolecular coupling which were determined in prior mechanistic studies,[83] and these roles were assessed in the context of an intramolecular reaction when considering additional optimisation. The methanol has several roles, it solubilises all the reaction components resulting in a visibly homogenous mixture, key for *in-situ* NMR monitoring of the reaction, as well as likely being responsible for cleavage of the TMS group (Scheme 2.18).

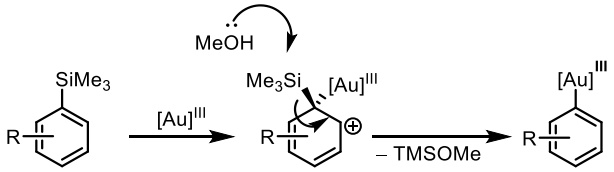

Scheme 2.18. Removal of TMS group by methanol in reaction mechanism.

However, methanol also acts as an inhibitor preventing effective π-complexation, which is the turnover-limiting step in intermolecular coupling, and the CSA is necessary to displace the methanol, resulting in a more active catalyst (Scheme 2.19).

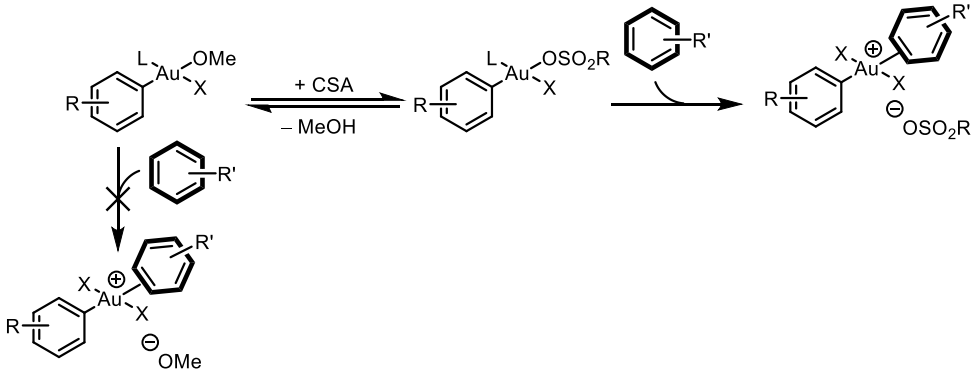

Scheme 2.19. Role of CSA in the π-complexation of the arene.

The CSA also reacts with iodobenzene diacetate (IBDA/PhI(OAc)$_2$) to form the *in-situ* oxidant, which is presumably a mixture of HCIB **62** (R = H) and MCIB **63** (R = Me) depending on the presence of water (Scheme 2.20). From this point forward, the term "IBDA/CSA" will be used to refer to the mixture of IBDA and CSA as a method of preparing the presumed *in-situ* oxidants **62**/**63**, and the term "HCIB, **62**" will be used when this compound is independently synthesised and used instead of the IBDA/CSA mixture. Due to the necessity of CSA in the pre-equilibrium to π-complexation, it is a requirement in intermolecular coupling that: [CSA] ≥ [IBDA], and if this is not the case, all CSA is sequestered as the oxidant.

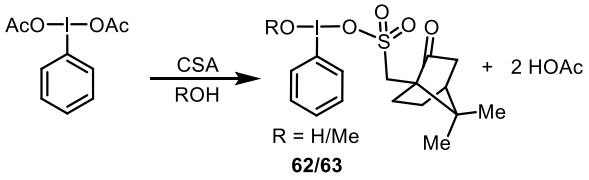

Scheme 2.20. Identity of the *in-situ* oxidants.

The oxidant is also responsible for the rapid activation of the precatalyst thtAuBr$_3$. During precatalyst activation, five equivalents of oxidant relative to the catalyst are consumed, and two of the three bromide ligands are taken up by either the arene or silane coupling partner following oxidation. The tetrahydrothiophene (tht) ligand is oxidised to the sulfoxide, and an unidentified acyclic compound. The fate of the final bromide is currently unknown (Scheme 2.21).

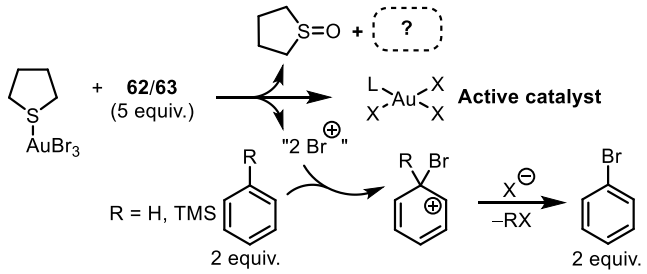

Scheme 2.21. Proposed catalyst activation mechanism.

The use of hypervalent iodine oxidants is a strict requirement for the coupling to operate, and the use of other oxidants does not lead to any turnover of catalyst. The origin of this is currently unclear; although rapid redox of the Au(I) to Au(III) is required to inhibit disproportionation.

By rendering the reaction intramolecular, the effective molarity of the arene moiety will be raised significantly. As the TLS in the intermolecular coupling is π-complexation, it was expected that this increase in molarity could lead to an increase in rate such that substantial changes in reaction conditions with regard to catalyst loading, and possibly the need for CSA if direct displacement of methanol could be tolerated (Scheme 2.19). Initial optimisation was performed with substrate **1b**. Employing the reaction conditions developed for the intermolecular coupling to the cyclisation of **1b** to fluorene, **2b**, led to a successful reaction, and a short (40 min.) reaction time, significantly shorter than all intermolecular examples (> 5 hours). This is informative as it gives a measure of the impact the short tether has on reactivity, especially as the most electronically-similar intermolecular example, 4-fluorophenylsilane **12a** with toluene **64**, required 45 hours to go to completion (Scheme 2.22).

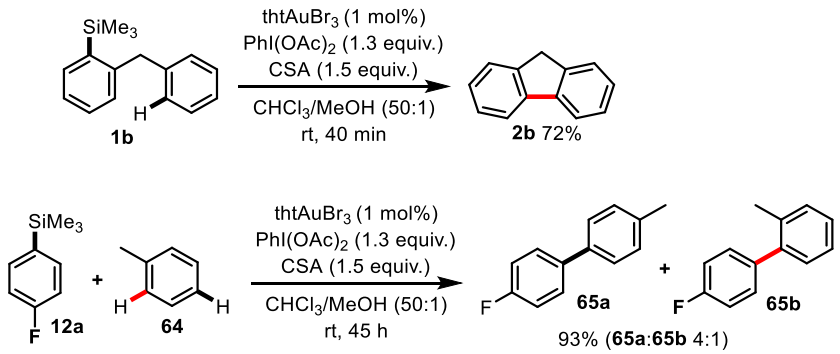

Scheme 2.22. Comparison of inter- and intramolecular direct arylation of electronically similar arenes

Whilst the ratio of IBDA:CSA used in the intermolecular coupling (1.3:1.5) was successful for **1b**, at the end of the reaction 0.2 equivalents of oxidant remained. This excess oxidant slowly consumed the product due to diaryliodonium salt formation, presumably *via* an S_EAr

mechanism.[115] Hypervalent iodine oxidants are very electrophilic at iodine and therefore prone to react with electron-rich arenes, such as fluorene (Scheme 2.23).[115]

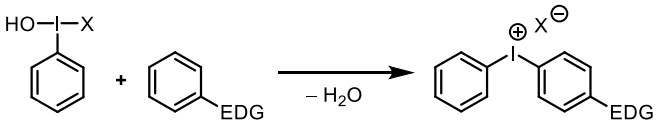

Scheme 2.23. Diaryliodonium salt formation.

To reduce the impact of this, the ratio of IBDA:CSA was reduced to the minimum necessary, 1.1:1.3. With these conditions in hand, the effect of catalyst concentration was analysed (Table 2.1). Pleasingly, high yields were maintained for loadings as low as 0.1 mol%.

Table 2.1 Effect on catalyst loading on yield of cyclisation of **1b**.

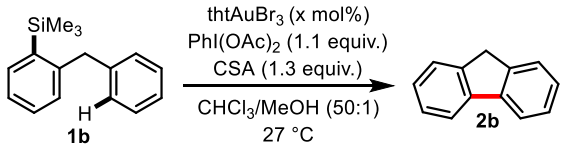

Entry	Catalyst Loading (mol%)	Yield (%)*	Time (min)
1	2	92%	15
2	1	98%	25
3	0.5	97%	60
4	0.1	99%	540

Substrate (0.05 mmol), thtAuBr$_3$ (1 mol%), PhI(OAc)$_2$ (0.055 mmol), CSA (0.065 mmol) in $CDCl_3/CD_3OD$ (50:1, 0.1 M). *Yield by NMR spectroscopy.

Due to the presence of bromodesilylation during the activation of the catalyst (Scheme 2.21), higher yields were obtained with lower catalyst loadings as less of the substrate was consumed during the activation of the catalyst

Whilst the success of the reaction at 0.1 mol% was impressive, the duration of the reaction was much less convenient than at 0.5 mol%. Therefore, the optimum conditions for substrate **1b** were 0.5 mol% catalyst, 1.1 equivalents of IBDA and 1.3 equivalents of CSA. The next step was to assess the generality of these conditions against other substrates. **1c** and **1d** were chosen due to the large electronic range in which they span. Unfortunately, 0.5 mol% was not a suitable catalyst loading for either substrate but for different reasons. Cyclisation of **1d** proved impractically slow, with only 5% of product formed after 5 hours, whereas with **1c**, total consumption of the oxidant occurred within a few hours, but with only a 17% yield of product. Raising the catalyst loading to 1 mol% led to a significant improvement for **1d** and a

92% yield was obtained after 16 hours. However, only minor improvements were gained with **1c**, where a 33% NMR yield was obtained (Scheme 2.24).

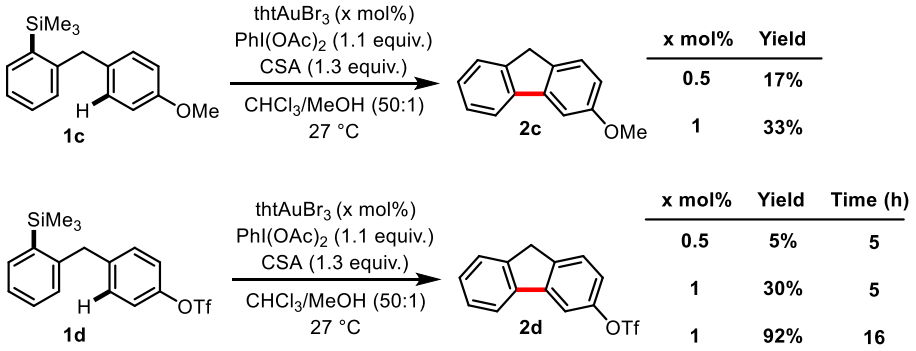

Scheme 2.24. Effect of catalyst loading on electronically-biased substrates

The origin of the reduced yield for the reaction of **1c** was rapid decomposition of the product to its diaryliodonium salt, which outcompeted cyclisation. Recognising that this could be severely detrimental to the methodology and substrate scope; alternative oxidants were sought.

Table 2.2. Oxidant screen on cyclisation of **1b**.

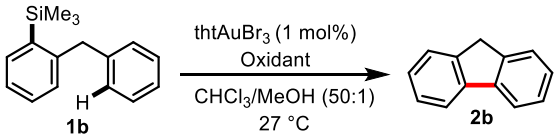

Entry	Oxidant	Additive	Yield
1	IBDA	CSA (1.3 equiv.)	98%
2	IBDA		Trace
3	IBDA		95% (55 °C)
4	PIFA, **66**		80%
5	Oxone	CSA (1.3 equiv.)	0%
6	*m*CPBA*	CSA (1.3 equiv.)	0%
7	TBHP**		0%

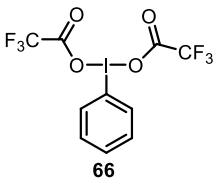

* *meta*-chloroperbenzoic acid **tert*-Butyl hydroperoxide.

Unfortunately, as seen in the intermolecular reaction, no product was observed for oxidants other than those based on hypervalent iodine (See Chapter 6 for further discussion). However, trace amounts of product was observed by ^{1}H NMR spectroscopy when IBDA was used in the absence of CSA. Heating this reaction to 55 °C led to full conversion of starting material. This is a clear difference with the intermolecular reaction where successful turnover depended on having CSA in excess ([CSA] ≥ [IBDA]) (scheme 2.19, *vide supra*). This disconnection

between the intra- and intermolecular reaction suggests that for π-complexation to occur, camphorsulfonic acid may not be necessary and that the acetic acid generated from IBDA forms an active enough catalyst when the arene is closely tethered (Scheme 2.25).

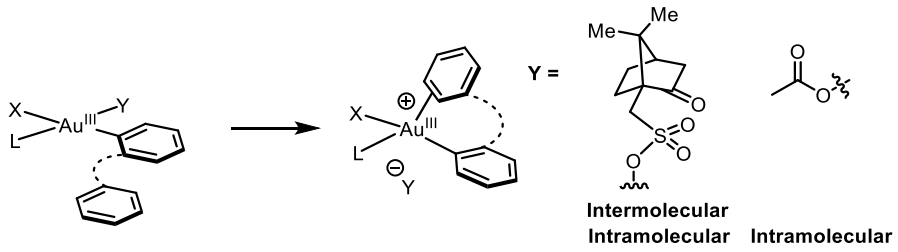

Scheme 2.25. Proposed mechanism of π-complexation in inter- and intramolecular direct arylation.

With this result in hand, the use of bis(trifluoroacetoxy)iodobenzene (PIFA, **66**), a commercially available hypervalent iodine oxidant, which introduces a stronger acid than IBDA (trifluoracetic acid-TFA- *vs* acetic acid) was attempted. Pleasingly PIFA was competent as an oxidant at room temperature, with similar reaction times and a comparable yield to the IBDA/CSA system.

Importantly, the use of PIFA led to a significant improvement in yield of substrate **1c** which suffers from significant diaryliodonium salt formation with IBDA/CSA (Table 2.3).

Table 2.3. Effect of oxidant on the cyclisation of **23c**.

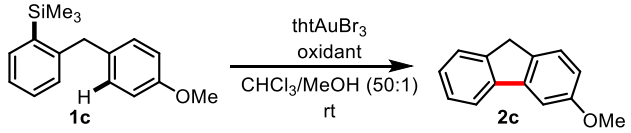

thtAuBr$_3$ (mol%)	Yield of **1c** to **2c** (%)	
	IBDA/CSA [a]	PIFA (**66**)[b]
0.25	11	85
0.5	17	90
1	33	88
2	42	90

[a] IBDA (1.1 equiv), CSA (1.3 equiv). [b] 1.1 equiv. Yield by ^{1}H NMR spectroscopy using internal standard (CH_2Br_2).

When PIFA is used, catalyst loadings could be reduced without an adverse effect on yield. This is in stark contrast to IBDA/CSA, where lowering of catalyst loading led to extremely poor yields due to competitive diaryliodonium formation. This result demonstrates the relative resistance of PIFA toward diaryliodonium salt formation compared to IBDA/CSA.

Unfortunately, PIFA was not suitable for the cyclisation of **1d**, suggesting that trifluoroacetate is insufficiently labile to be used in combination with deactivated arenes. With standard conditions in-hand, and either IBDA/CSA or PIFA as the oxidant species, the substrate scope was assessed. Table 2.4 shows the full substrate scope of 5-membered rings, using either PIFA or IBDA/CSA.

Although the use of 1 mol% of catalyst was a convenient standard condition, significantly lower loadings could be used. For example, cyclisation of **1a** (Table 2.4, entry 3) was complete in under 2 min using 1 mol% Au (95% yield), and with 0.06 mol% Au, the reaction proceeded to 80% conversion, with a formal turnover number of 1330. The range of reaction times was dependent on the electronics of the arene moiety, with electron-deficient examples requiring the longest reaction times. However, the reaction timescales were still convenient, with the most sluggish examples (**1d**, **h**, **m**, **n**) going to completion overnight.

Of particular note is the large electronic range tolerated on the arene moiety in the synthesis of substituted fluorenes, with high yields maintained throughout the series. Whilst the arene substrate in the intermolecular reaction is required to be relatively electron-rich, the intramolecular reaction can even tolerate CF_3 substituents (**1h**, **1m**).

In the cases where substituents are *meta*- to the methylene linker, and therefore two regioisomeric products are possible, high regioselectivity is observed in favour of the product resulting from arylation *para* to the substituent (Scheme 2.26).

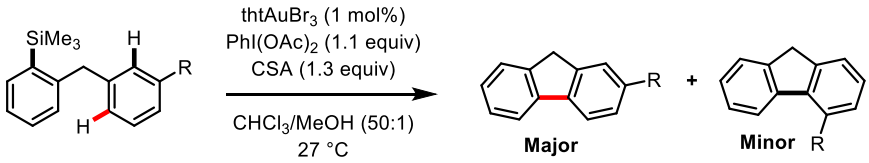

Scheme 2.26. Regioselectivity in intramolecular direct arylation

This ratio improved with electron-withdrawing ability as the inductive effects reduce the reactivity of the *ortho* greater than the *para* site, consistent with an S_EAr type mechanism.

Table 2.4. Substrate scope of intramolecular direct arylation for 5-membered rings.

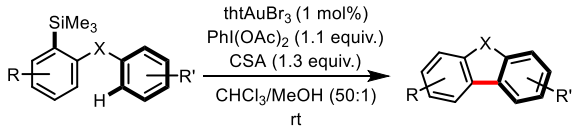

Entry	Substrate	Product (Yield, Time)			
1	1b-h	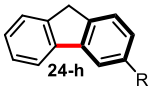	R = H	(94%, 1 h)	2b
			OMe	(88%, 2 h)[c]	2c
			OTf	(92%, 16 h)[b]	2d
			t-Bu	(81%, 1 h)	2e
			Cl	(90%, 4 h)	2f
			OPiv	(81%, 6 h)	2g
			CF_3	(80%, 15 h)	2h
2[e]	1i-n		R = Me	(95%, 1 h)	2i
			OMe	(80%, 1 h)[c]	2j
			F	(85%, 2 h)	2k
			Cl	(90%, 3 h)	2l
			CF_3	(88%, 16 h)[d]	2m
			OTf	(78%, 15 h)	2n
3	1a,o,p	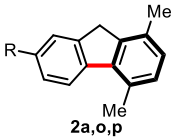	R = H	(95%, 10 min)	2a
			F	(89%, 15 min)	2o
			Cl	(91%, 1 h)[b]	2p
4	1q	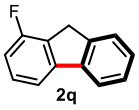	(87%, 16 h)		
5	1r	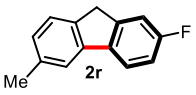	(89%, 5 h)		
6	1s	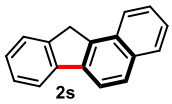	(80%, 1 h)[c]		
7	1t		(76%, 1 h)		
8[e]	1u	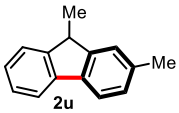	(79%, 1 h)[b,c]		
9	1v	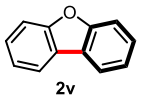	(87%, 30 min)		
10	1w	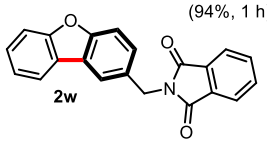	(94%, 1 h)		

[a]Unless otherwise stated, all reactions were performed under the following conditions: Substrate (0.50 mmol), thtAuBr$_3$ (1 mol%), PhI(OAc)$_2$ (0.55 mmol), CSA (0.65 mmol) in CHCl$_3$/MeOH (50:1, 0.1 M).[b] thtAuBr$_3$ (2 mol%).[c]PhI(OCOCF$_3$)$_2$ [0.55 mmol replaces PhI(OAc)$_2$ and CSA]. [d]CSA (1.0 mmol.). [e]Ratio of regioisomers of 2-/4- substituted fluorenes: **2i** (95:5), **2j** (88:12),**2k** (97:3), **2u** (95:5).

2.2.2 Synthesis of 6+ Membered Rings

To demonstrate the general applicability of the reaction conditions across a wide range of examples, the methodology was applied to larger ring systems (Table 2.5). In the synthesis of the 6-membered ring systems, once again using the minimum excess of oxidant possible (1.1 equivalents) was necessary to avoid over oxidation of product, which in the case of 9,10-dihydrophenanthrene **4a**, included oxidation to phenanthrene when excess oxidant was used. Under the standard conditions, benzo[c]chromene examples **4d-f** (Table 2.5, entry 2 and 3) suffered from the formation of several unidentified minor side products, derived from oxidation, which complicated purification. Unfortunately, the implementation of PIFA as an oxidant did not lead to product formation in these examples, suggesting that the presumed

gold-TFA complex **67** is not reactive enough to facilitate rapid π-complexation of the arene moiety in longer tethers.

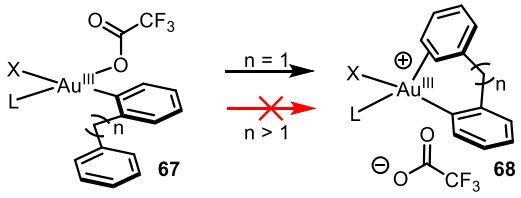

Scheme 2.27. Effect of increase in tether length on π-complexation with a TFA ligand.

Diluting the reaction with respect to the substrate and oxidant, whilst maintaining the same catalyst concentration as the standard conditions significantly reduced side product formation, and facilitated purification.

Table 2.5. Substrate scope of intramolecular direct arylation for 6- and 7-membered rings.

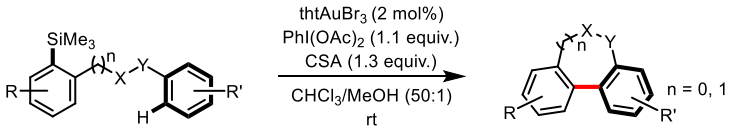

Entry	Substrate	Product (Yield, Time)	Entry	Substrate	Product (Yield, Time)
1	**3a-c**	 R = H (72%, 1 h)[b] **4a**; Cl (91%, 1 h) **4b**; CF_3 (82%, 16 h) **4c**	5	**5b**	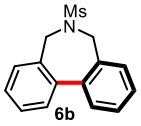 (73%, 16 h)[b]
2	**3d-e**	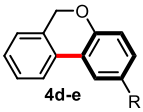 R = H (86%, 2 h)[d] **4d**; *t*-Bu (60%, 1 h)[d] **4e**	6	**5c**	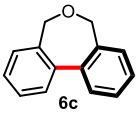 (76%, 16 h)[c]
3[g]	**3f**	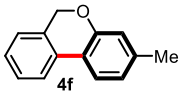 (86%, 1 h)[d]	7	**5d**	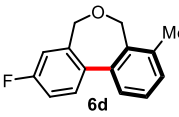 (82%, 15 h)
4	**5a**	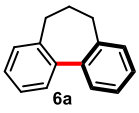 (85%, 15 h)[b]			

[a]Unless otherwise stated, all reactions were performed under the following conditions: Substrate (0.50 mmol), $thtAuBr_3$ (2 mol%), $PhI(OAc)_2$ (0.55 mmol), CSA (0.65 mmol) in $CHCl_3$/MeOH (50:1, 0.1 M).[b] $thtAuBr_3$ (1 mol%).[c] CSA (1.0 mmol.).[d] $thtAuBr_3$ (2 mol%), $CHCl_3$/MeOH (50:1, 0.05 M). [g]Ratio of regioisomers of 3-/1- substituted chromene: **4f** (88:12).

As mentioned previously, methodologies to prepare greater than 6-membered rings through direct arylation are exceedingly rare, especially when unactivated arenes are used. The

formation of the desired metallocycle is often proposed as the difficult step, and the increase in tether length reduces the effective molarity of the incoming arene, making the formation of the metallocycle less entropically favoured. In addition, transannular and torsional strain make this process even more difficult. Somewhat surprisingly, the synthesis of 7-membered rings did not require significantly modified or harsher conditions. (Table 2.5, entries 4 – 7). Although longer reaction times were required, the reaction conditions were still mild, with reactions proceeding at room temperature at catalyst loadings of 2 mol%. Additionally, the linker could be entirely methylene based, or contain both N or O as the central atom.

Given the ease in which 7-membered rings could be synthesised, the next goal was to attempt to construct even larger ring sizes and discover the limit of the ring size that could be formed. It was anticipated that at some point, as with many macrocyclisations, intermolecular coupling would begin to outcompete intramolecular cyclisation. The synthesis of 8-, 9- and 10-membered rings was attempted by subjecting **7**, **9** and **69** to the arylation conditions (Scheme 2.28). The cyclisation of **7** proceeded smoothly with an excellent yield of 75% after 16 h at room temperature, albeit with a slightly higher catalyst loading of 4 mol% compared to other ring sizes. Pleasingly, 9-membered ring **10** could be isolated with a good yield of 52%. However, more forcing conditions were needed as in addition to the 4 mol% catalyst required, 2 equivalents of CSA and a temperature of 50 °C were necessary. Unfortunately, the synthesis of 10-membered **70** was not successful and subjecting **69** to the same reaction conditions as **9** led to a complex mixture. This was indicative of an oligomerisation reaction due to competing intermolecular reactions. Nevertheless, the synthesis of 8- and 9-membered rings was a significant achievement, and although the conditions were more forceful than those used in the other substrates, they are remarkably mild compared with literature syntheses of these ring sizes. Both **8** and **10** were solids at room temperature and single crystals suitable for X-ray crystallography were grown, and crystallographic analysis confirmed the structures.

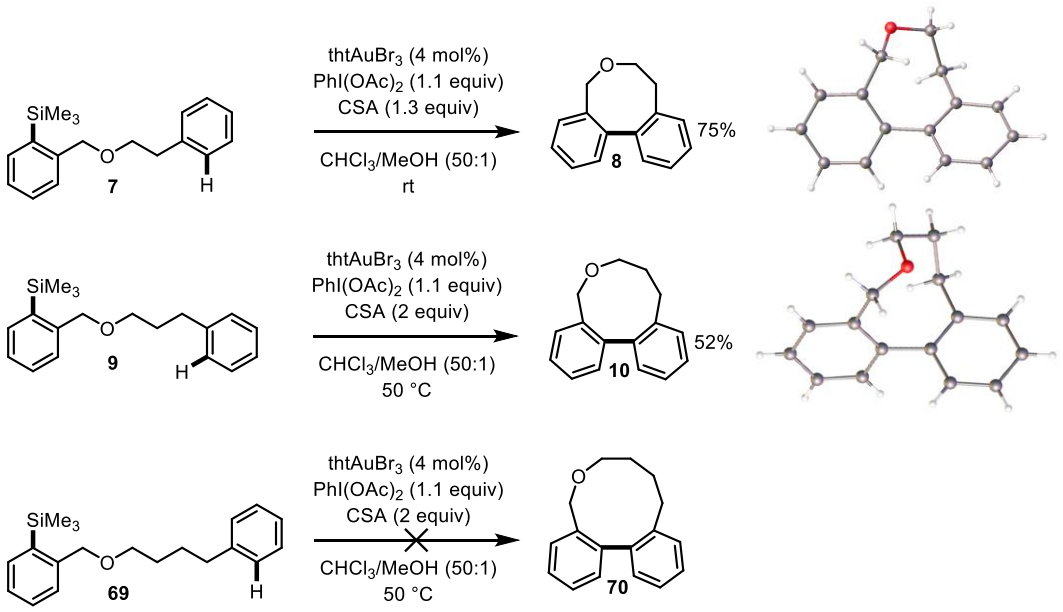

Scheme 2.28. Synthesis of 8- and 9- membered rings, with X-ray crystal structures of **8** and **10** (8- and 9- membered rings).

The reaction conditions developed herein for intramolecular direct arylation represent a breakthrough with regards to the breadth of substrate scope, operational simplicity and mild reaction conditions. A single set of conditions is suitable for the synthesis of ring sizes varying from 5- to 9-membered, with a large range of substituents, and with most reactions occurring at room temperature. Additionally, external ligands are not required, eliminating the requirement for laborious screening. However, there were limitations to the scope as substrates containing a basic nitrogen were not tolerated, and therefore substrate classes such as carbazoles were not accessed. This is potentially due to binding to and deactivation of the catalyst, or through reaction with the CSA. However, employing protecting groups such as the mesyl functional group allows access to nitrogen containing heterocycles. Given the ease in which 7-membered rings are synthesised, the final goal was to apply this methodology toward the formal synthesis of allocolchicine **11**, which had previously been synthesised by Fagnou and Leblanc who employed a palladium-catalysed direct arylation. It was anticipated that a gold-catalysed approach could lead to significant improvements, particularly with respect to reaction temperature. Additionally, whilst the substrate scope demonstrated thus far encompasses a wide variety of functional groups, the application of the methodology toward a natural product would demonstrate the applicability of the chemistry, as well as potentially expose deficiencies that could be fundamental to future development.

2.3 Formal Synthesis of (±)-Allocolchicine

2.3.1 Background

Isolated from *Colchicum autumnale*, allocolchicine **11** is the first discovered natural allocolchinoid. For over a millennium, plant extracts from *C. autumnale* have been used in medicine, initially for rheumatism and swelling, and subsequently gout.[116] The major alkaloid produced by *C. autumnale*, and the source of the biological effects, is colchicine **71**, which was first isolated in 1820 by Pelletier and Caventou. As well as having anti-inflammatory effects, colchicine also has antimitotic effects.

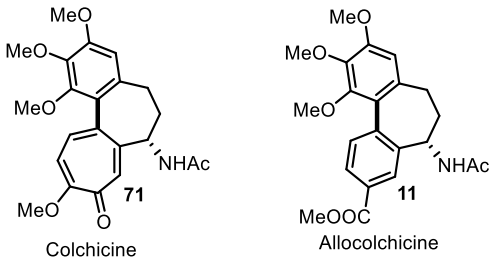

Scheme 2.29. Structures of natural products colchicine and allocolchicine.

The mechanism of action of colchicine that leads to antimitotic effects is to bind to the protein tubulin and by doing so inhibit microtubule polymerisation. Since tubulin availability is fundamental to cell division, colchicine can act to disrupt mitosis and behave as "mitotic poison." Mitotic poisons, also known as spindle poisons, can help to stop the spread of tumours, however the toxicity of colchicine means it is not applicable as an anti-cancer agent. Allocolchicine and its analogues, however, are also known to bind tubulin but have significantly lower toxicity thresholds and are therefore promising drug targets.[117]

The first stereoselective total synthesis of (−)-allocolchicine was performed by Wulff *et al.* in 2003 and is a 14 step synthesis with a 7% overall yield (Scheme 2.30) starting from commercially available ketone **72**.[118] The key bond forming step was a regioselective Diels-Alder reaction of **73** with methyl propiolate **74**, which after aromatisation yielded the allocolchinoid skeleton **75**. Deprotection of the TBDMS ether and oxidation of the resultant alcohol gave **76**, which could be reduced enantioselectively using $LiBH_4$ and TarB-NO_2,[119] a chiral Lewis acid to **77**. Mitsunobu conditions were subsequently used to invert the stereochemistry using Zn(N_3)-2Py, forming azide **78**. Reduction of the azide, followed by acetylation of the resulting amine afforded (−)-(7*S*)-allocolchicine **11**.

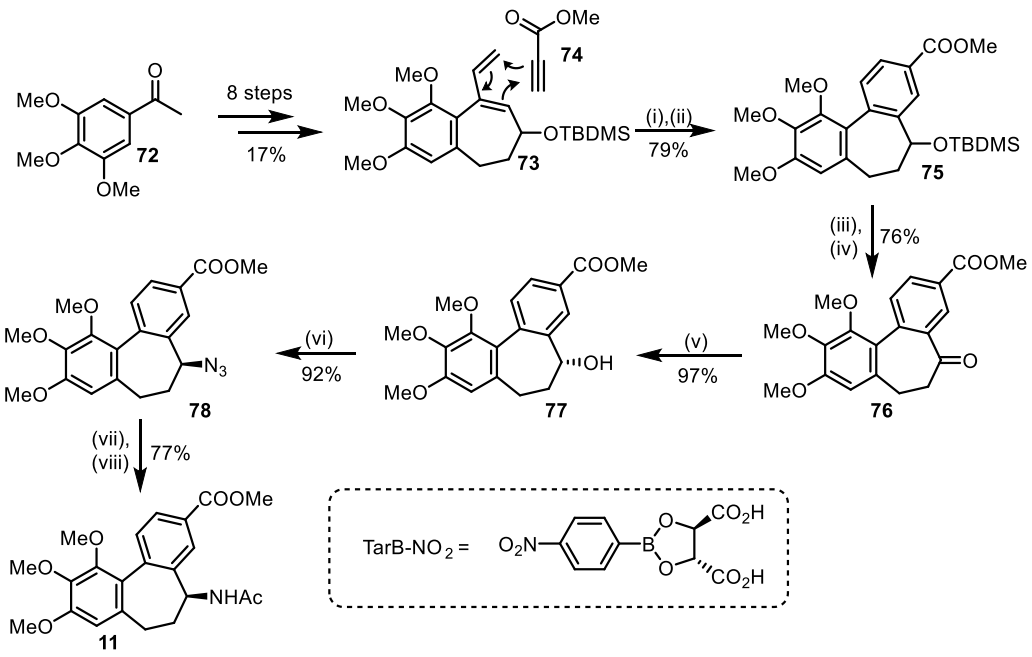

Scheme 2.30. Total synthesis of allocolchicine. (i) Methyl propiolate, toluene, 110 °C; (ii) DDQ, CH_2Cl_2, rt; (iii) TBAF-3H_2O, THF, rt; (iv) NMO-H_2O, 5% TPAP, 4 Å MS, CH_2Cl_2, rt; (v) TarB-NO_2, $LiBH_4$, (vi) Ph_3P, DIAD, $Zn(N_3)$2-2Py, toluene, rt; (vii) H_2, 5% Pd/$CaCO_3$/3.5% Pb, EtOH, rt; (vii) Ac_2O, pyridine, CH_2Cl_2, rt.

Two years after the synthesis of (−)-allocolchicine by Wulff *et al.*, Fagnou and Leblanc reported their enantioselective formal synthesis of allocolchicine (Scheme 2.31). This route cut 4 steps off the synthetic route of Wulff and had an impressive overall yield of 26%. The key step in the synthesis was an intramolecular direct arylation reaction catalysed by palladium.

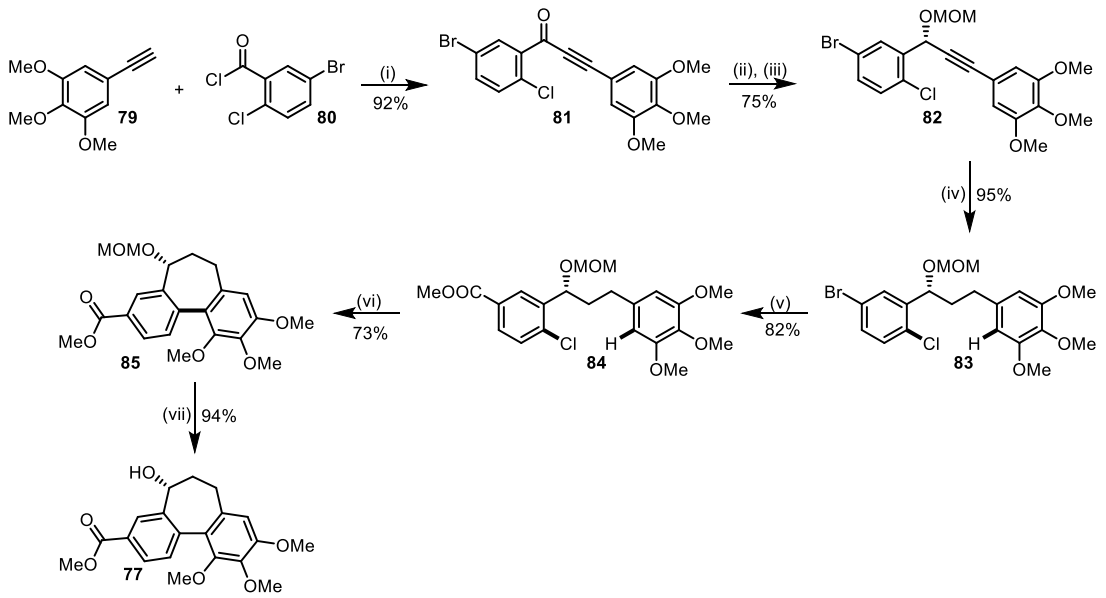

Scheme 2.31. Formal synthesis of allocolchicine. (i) $PdCl_2(PPh_3)_2$ (1 mol%), CuI (3 mol %), Et_3N, THF, rt; (ii) 1. (*S*)-pinene, 9-BBN, THF, reflux 2. **81** 3. NaOH, H_2O_2; (iii) NaH, CH_3OCH_2Br, THF, 0 °C to rt. (iv) $NH_2NHSO_2C_6H_4CH_3$, AcONa, DME/H_2O, reflux. (v) $PdCl_2(PPh_3)_2$ (5 mol%), K_2CO_3 (3 equiv), MeOH (15 equiv), DMF, CO (5 atm), 95 °C; (vi) $Pd(OAc)_2$ (10 mol%), DavePhos (10 mol%), K_2CO_3 (2 equiv.) DMA, 145 °C; (vii) MeOH, HCl, reflux.

Although a direct arylation approach to the total synthesis of allocolchicine has been shown, the reaction conditions for the cyclisation are notably harsh with high temperatures and catalyst loadings. Despite the harsh conditions, this is the state-of-the-art approach, as Fagnou's conditions continue to be used successfully to this day. An alternative, gold-catalysed approach, is therefore desirable as milder reactions conditions as well as different functional group tolerance to palladium is possible. In addition, the possibility to directly compare the methodologies could serve to highlight both the advantages and deficiencies of the gold-catalysed direct arylation chemistry.

2.3.2 Retrosynthesis of Allocolchicine

Retrosynthetic analysis (Scheme 2.32) was initiated from **76**, which is an intermediate along the reaction pathway of Wulff and co-workers. The first disconnection was at the methyl ester back to aryl chloride **6e**. A key point in the synthetic strategy was to demonstrate the orthogonality of the gold-catalysed direct arylation methodology to palladium(0) cross-coupling. This goal could be realised with a palladium-catalysed carbonylation of the aryl chloride to the ester. This strategy would be of high synthetic value as rapid access to analogues would also be available using the rich chemistry of palladium-catalysed cross-

coupling, and in fact it has been shown that some of the largest biological differences between allocolchinoids has been due to alteration of this ring. The next disconnection was at the biaryl linker, leading to compound **5e**. The silane could theoretically be placed on either side of the molecule, but it was desirable for the arene to be the trimethoxy moiety as it is significantly more activated for electrophilic metalation than the aryl chloride. The final disconnection was between the two methylene groups in the linker between the aromatics. This disconnection went back to silyl enol ether **87**, which could be prepared from ketone **86**, and benzyl bromide **88.**

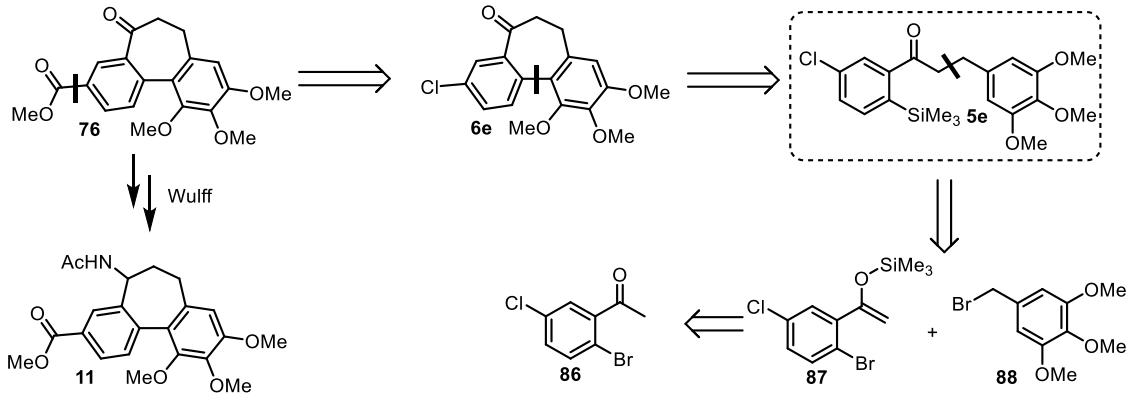

Scheme 2.32. Retrosynthesis of allocolchicine.

2.3.3 Model Studies: Formal Synthesis of Allocolchicine Analogue

Prior to any synthetic studies, the tolerance of the trimethoxy-arene moiety to the reaction conditions had to be assessed. As previously demonstrated, electron-rich arenes are prone to diaryliodonium salt formation, and this was to be the most electron-rich example attempted. Trimethoxytoluene **89** was used as a proxy to measure the effect of oxidant on the starting material (Scheme 2.33). Subjecting trimethoxytoluene to the standard reaction conditions (without the gold catalyst) led its rapid degradation, with all of the arene converted, within seconds, to the diaryliodonium salt **90**.

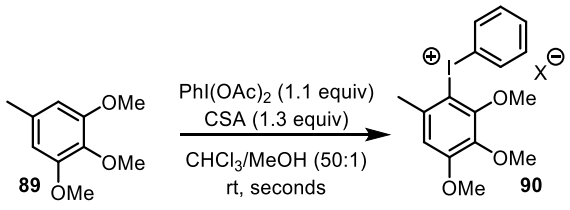

Scheme 2.33. Effect of IBDA/CSA on trimethyl toluene.

This immediately removed the possibility of employing the IBDA/CSA conditions in the natural product synthesis. It was therefore proposed that PIFA could be a candidate to facilitate

the reaction. Subjecting trimethoxytoluene to PIFA under the reaction solvent conditions demonstrated a good stability toward the oxidant, with only minimal degradation to the diaryliodonium salt after several hours. Although PIFA was shown to be ineffective in the Au-catalysed synthesis of ring sizes greater than five membered, it was of interest to understand if the increase in tether length could be offset by the very activated arene.

Due to the relative expense of ketone **86** and the availability of 2'-bromoacetophenone **91**, the synthetic route was first optimised for allocolchicine analogue **92**. This analogue had also been prepared by the research group of Fagnou.

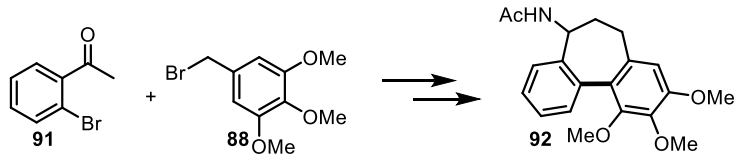

Scheme 2.34. Allocolchicine analogue for model studies.

The synthesis of key intermediate **5f** was achieved in just two steps (Scheme 2.35). The first step was conversion of the ketone to silyl enol ether **93**, which after lithium-halogen exchange using ^{n}BuLi, resulted in a retro-Brook rearrangement forming lithium enolate **94**. This was then alkylated by trimethoxy benzylbromide **87** to afford *ortho*-silyl arylketone **5f**. Unfortunately, only moderate yields of **5f** were obtained due to competing double alkylation by the lithium enolate of **5f**, to generate **95**. Despite the moderate yield, in just two steps all of the carbons required to complete the formal synthesis of the allocolchicine analogue were in place.

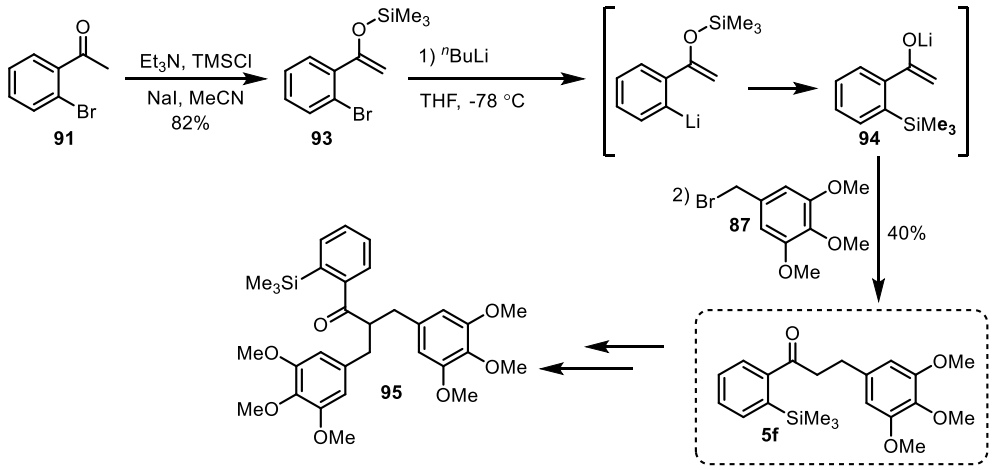

Scheme 2.35. Route to key intermediate **5f** in the synthesis of allocolchicine analogue.

With **5f** synthesised, the gold-catalysed direct arylation protocol could be attempted (Scheme 2.36). Unfortunately, no product was observed over the course of several hours. Despite this, it was promising that no significant degradation of the starting material was observed, confirming the stability of **6f** toward PIFA as the oxidant.

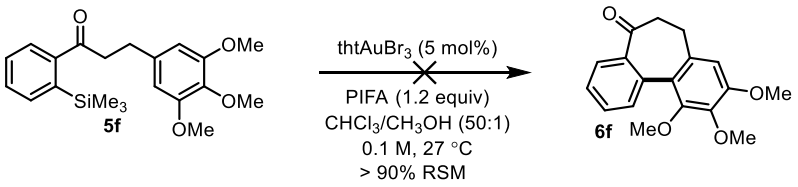

Scheme 2.36. Attempted cyclisation of **5f**.

It was proposed that that the presence of the benzylic ketone may be the cause of the lack of reactivity. Indeed, in palladium-catalysed direct arylation, 2-haloaryl esters (*vide supra*) only cyclised when the products formed were 6-membered, and not larger (Scheme 2.13). The rigidity that the ketone might install on the carbon skeleton could restrict the configuration of the incoming arene, and therefore prevent successful π-complexation. Thus, it was anticipated that the ketone could be modified to a functional group that the cyclisation could tolerate. To explore the impact of the identity of the benzylic substituent on the reactivity towards arylation, a number of analogues were prepared from ketone **5f**, *via* alcohol **5g** (Scheme 2.37).

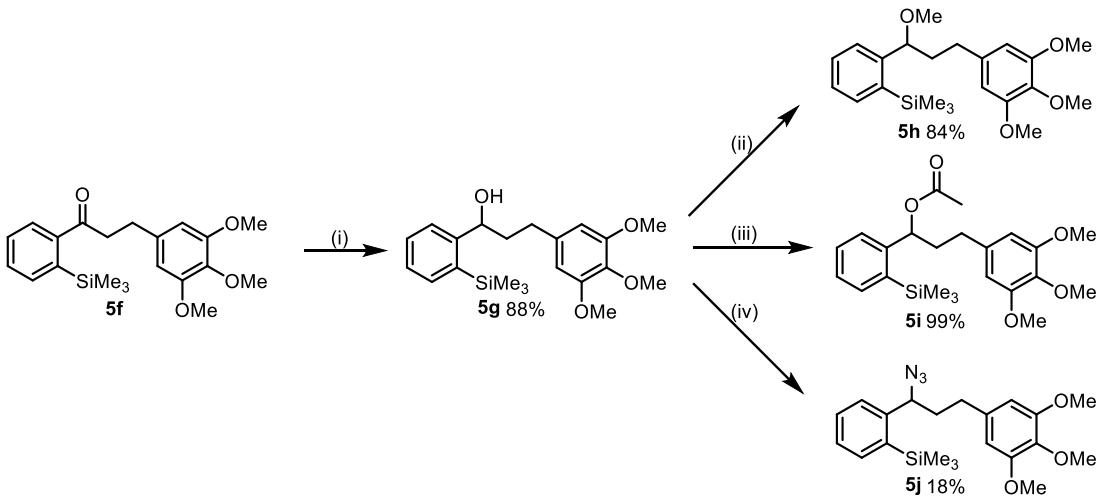

Scheme 2.37. Synthesis of analogues to test cyclisation. (i) $NaBH_4$, MeOH, 0 °C - rt; (ii) Me_3OBF_4, Proton-Sponge®, 0 °C - rt; (iii) Ac_2O, DMAP, pyridine, 0 °C - rt; (iv) $(PhO)_2P(O)N_3$, DBU, toluene, 0 °C - rt.

The impact of the benzylic substituent on the success of the reaction is clearly demonstrated in Scheme 2.38.

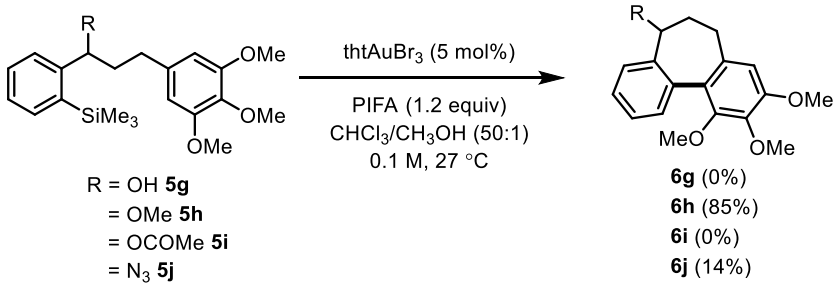

Scheme 2.38. Effect of benzylic substituents on synthesis of the allocolchinoid skeleton.

Whilst alcohol **5g** and ester **5i** did not form any cyclised product, both methyl ether **5h** and azide **5j** did lead to productive catalysis. Pleasingly, the cyclisation of methyl ether **5h** was an efficient process, yielding 85% of the desired product in under 2 h at room temperature. Control experiments demonstrated the reaction is indeed gold-catalysed, and not PIFA mediated, as previous studies have demonstrated PIFA can facilitate oxidative biaryl coupling of the allocolchinoid skeleton in the presence of $BF_3.OEt_2$.[120] The cyclisation of azide **5j** to **6j** is a step economic route as it directly intercepts the synthetic pathway of Fagnou, however the poor yield and difficulty preparing the starting material excluded its use. Although methyl ether **5h** was successful in cyclising, the inability to selectively deprotect the methyl group to form alcohol **6g** and enter the desired synthetic pathway precluded the use of **5h** in the formal synthesis, and therefore other, more readily deprotected ethers were considered.

In the synthetic pathway of Fagnou and Leblanc, a MOM protecting group was employed, and therefore the use of a MOM protecting group in this study would lead to a direct comparison of methodologies. Additionally, it was of interest to discover if MOM protecting groups would withstand the acidic nature of the reaction. The MOM protection was achieved with MOMBr in the presence of DIPEA. The cyclisation of MOM protected **5k** was successful, with the MOM protecting group remaining intact during the reaction timescale. The reaction compared favourably to the palladium-catalysed conditions developed by Fagnou, with higher isolated yields, lower temperature and shorter reaction times (Scheme 2.39).

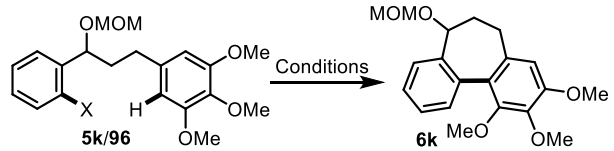

Scheme 2.39. Au *vs* Pd-catalysed direct arylation in synthesis of allocolchicine skeleton.

2.3.4 Formal Synthesis of Allocolchicine

With an effective synthetic route established, the formal synthesis of allocolchicine was attempted. Comparable yields to the model study were obtained for the steps leading up to the direct arylation, however, crucially, the cyclisation itself took significantly longer, with a poorer yield, than the model study (5 h *vs* 2.5 h and 56 *vs* 75%). Efforts to improve the yield through change in temperature, reaction concentration and solvent ratio were unsuccessful (see Chapter 4 for analysis of kinetics). Nevertheless, the formal synthesis of allocolchicine was completed by subjecting **5m** to the palladium-catalysed methoxycarbonylation conditions developed by Buchwald,[121] to afford **85**, which intercepts the synthetic pathway of Fagnou.

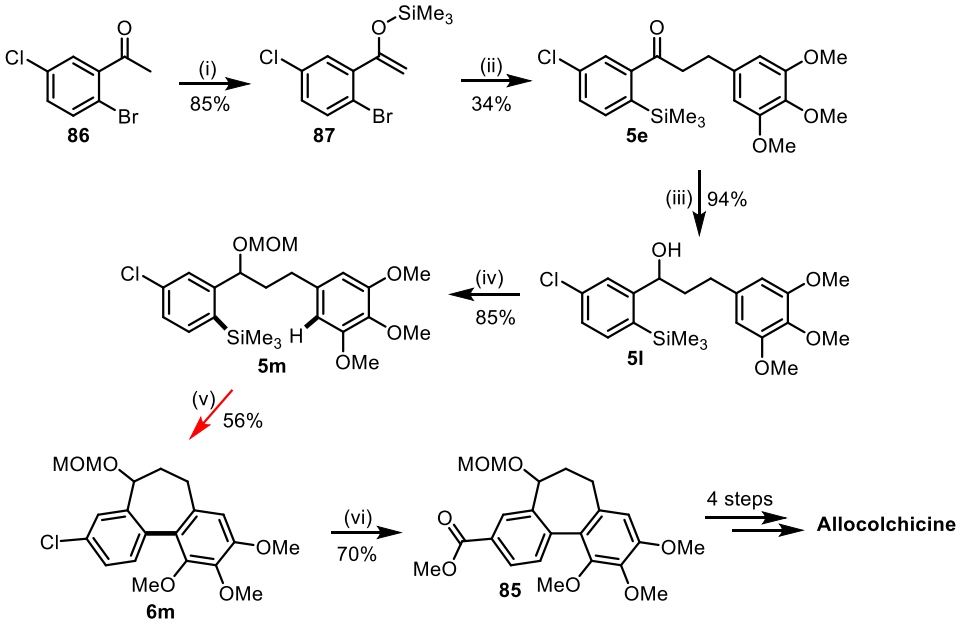

Scheme 2.40. Formal synthesis of allocolchicine. (i) TMSCl, Et_3N, NaI, CH_3CN, rt; (ii) 1. ^{n}BuLi, THF, −78 °C; 2. **88**, −78 °C – rt; (iii) $NaBH_4$, MeOH/THF, 0 °C – rt; (iv) MOMBr, DIPEA, DMAP, CH_2Cl_2, 0 °C – 70 °C; (v) thtAuBr$_3$ (5 mol%), $PhI(OCOCF_3)_2$, $CHCl_3$/MeOH (50:1); (vi) $Pd(OAc)_2$ (4 mol%), dcpp.2HBF$_4$ (8 mol%), K_2CO_3, 4 Å MS, CO, dmso, 120 °C.

Whilst the brevity of the route rivals that of Fagnou (10 steps to allocolchicine), the overall yield is particularly hampered by the poor isolated yield of **5e** from the retro-Brook alkylation reaction. Further developments to synthesise this scaffold *via* other higher yielding routes may make this synthesis more attractive. The completion of the formal synthesis of allocolchicine demonstrates both strengths and weaknesses in the gold-catalysed methodology. The tolerance of the highly rich trimethoxy-arene moiety represents a new benchmark in what can be achieved in terms of electronics in gold-catalysed direct arylation. It is made possible by rendering the reaction intramolecular; the use of PIFA, which is not competent in

intermolecular reactions, is key. The orthogonality of the methodology to palladium(0) cross-coupling is also demonstrated by the late stage methoxycarbonylation reaction, thus raising the possibility for facile diversification of this scaffold. The cyclisation step is also particularly mild, with half the catalyst loading required relative to the palladium needed, and significantly lower temperatures (room temperature *vs* 145 °C). However, the functional group tolerance is low and only methyl ethers were demonstrated to cyclise efficiently. In addition, the yield of the key cyclisation was lower than in the model study. The origin of these detrimental features is discussed in detail in Chapter 4.

2.4 Summary and Conclusions

The intramolecular gold-catalysed direct arylation of arenes by aryltrimethylsilanes has been developed. The reaction generates 5- to 9- membered rings in good to excellent yields, with the majority of examples requiring 1-2 mol% of catalyst and proceeding at room temperature. Of the 35 preparative examples, 10 form heterocycles. Deleterious diaryliodonium salt formation in the most electron-rich examples was circumvented with the use of PIFA as oxidant. With a reduced tendency for diaryliodonium salt formation, PIFA was implemented in the formal synthesis of allocolchicine, a natural product with a highly electron-rich trimethoxy-arene moiety. The broad substrate scope, as well as the mild reaction conditions, result in the gold-catalysed approach being a desirable alternative to state-of-the-art palladium-catalysed routes in the synthesis of a variety of cyclic biaryls. Although the scope presented herein encompasses a wide range of substrates, it is not exhaustive, and further investigations into the full substrate scope, in particular of larger ring sizes is still necessary. Whilst the investigation into the scope demonstrated the methodology to be synthetically useful, the major goal was to understand the mechanism of cyclisation, and use the intramolecular reaction as a vehicle to understand mechanistic processes which could not otherwise be investigated in the intermolecular system. A comprehensive investigation into the mechanism of cyclisation is the focus of the next chapter.

3. Mechanistic Study

ABSTRACT: Chapter 3

The mechanism of intramolecular gold-catalysed direct arylation is elucidated. Rendering the reaction intramolecular results in predominantly simple pseudo-zero order reaction profiles, perfect for kinetic study, and thus allows for a detailed investigation into linear free energy relationships and kinetic isotope effects. The resting state, and therefore the turnover-limiting step (TLS), of the reaction is highly dependent on tether length and the electronic properties of the aryl moiety, and shifts from reductive elimination when the tether is a single methylene unit, to π-complexation for longer tethers or when the arene bears strongly electron-withdrawing substituents ($\sigma > 0.43$). For the first time, the effect of aryl electronics on the rate of reductive elimination is demonstrated and is shown to be accelerated by electron-donating substituents ($\rho = -2.0$). Additionally, in contrast to previous reports into reductive elimination from diarylgold(III) complexes, reductive elimination is proposed to proceed *via* a rapidly reacting 3-coordinate species, *and*, a slower, methanol bound, 4-coordinate complex.

The results presented in this Chapter have been communicated: T. J. A. Corrie, L. T. Ball, G. C. Lloyd-Jones, C. A. Russell, *J. Am. Chem. Soc*. **2017**, *139*, 245.

3.1 Introduction

3.1.1 Mechanistic Background

In 2014, this research group reported the results of a mechanistic study into the intermolecular gold-catalysed direct arylation reaction.[83] The catalytic cycle (Scheme 3.1, bottom) was determined based on the examination of rate data, KIE experiments, linear free-energy relationships and competition studies. Most the studies were based on the coupling of **39a** with **96**, a well-behaved model system (Scheme 3.1, Top).

Transmetalation: The first step of the catalytic cycle is transmetalation of the aryltrimethylsilane. This is proposed to proceed via a reversible π-complexation, followed by irreversible Wheland intermediate (WI) formation. The origin of the selectivity for the silane over the arene at this step is the proposed stabilisation of the WI by silicon, due to silicon hyperconjugation.[122] In order for this selectivity to be achieved, π-complexation of the more electron-rich arene must be fully reversible, and therefore under Curtin-Hammett conditions, such that silane transmetalation outcompetes arene metalation ($k_{TMS} >> k_H$). After formation of the WI, re-aromatisation occurs through cleavage of the TMS group *via* attack from methanol.

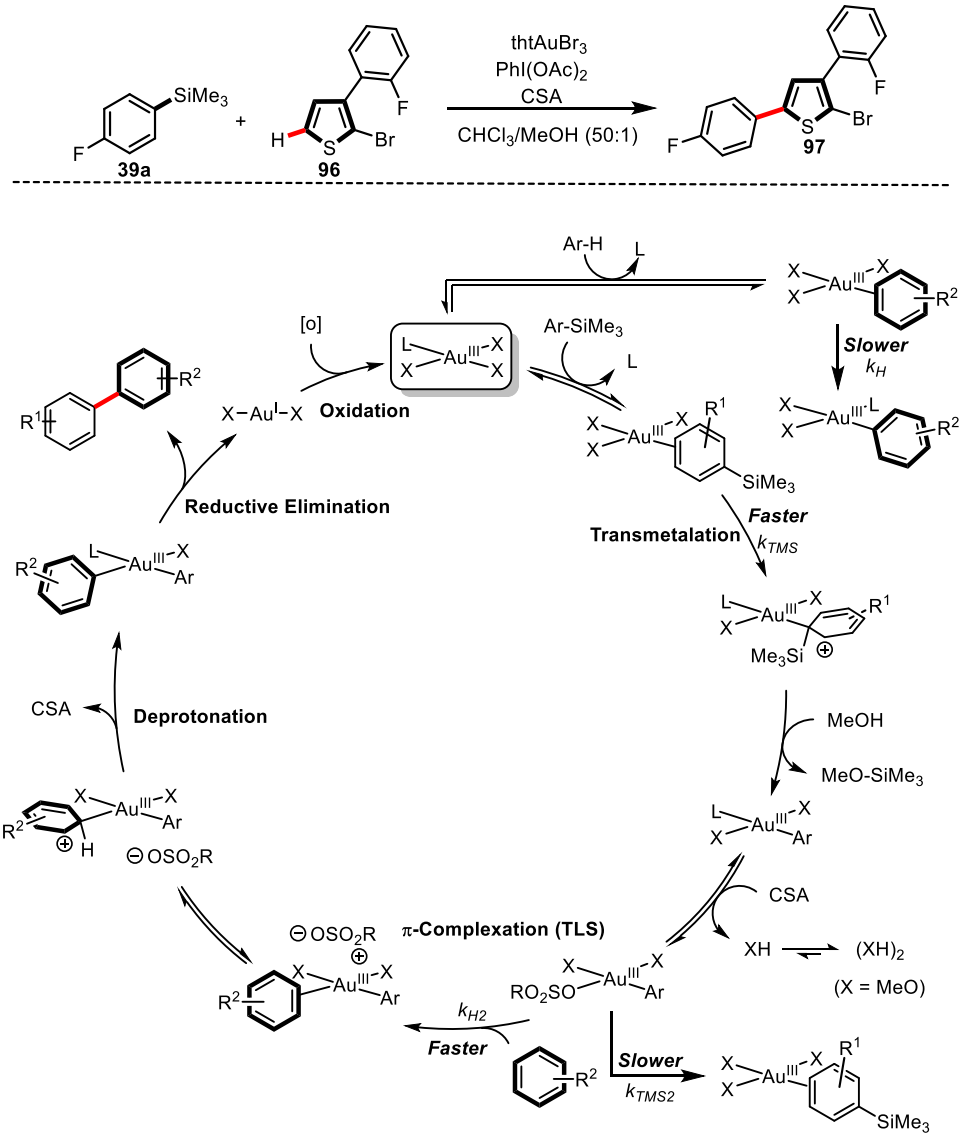

Scheme 3.1. Catalytic cycle (bottom) primarily based on kinetic data obtained from reaction of **39a** and **96** (Top).[83]

Competition experiments between different substituted silanes showed that transmetalation is accelerated by electron-donating groups ($\rho = -1.6$). In absolute rate terms, the electronic identity of the silane has little effect on the overall rate of the reaction ($\rho = -0.2$).

π-Complexation: The π-complexation of the incoming arene to the Au(III) centre was assigned as the TLS of the reaction, and therefore all rate data corresponded to this step in the cycle. For π-complexation to occur, CSA must displace methanol in a pre-equilibrium. This led to a first-order dependence on the concentration of CSA, and an inverse order in methanol. As methanol is known to exist as a dimer in chloroform, this was an inverse half relationship.[123] The π-complexation was proposed to be irreversible, as a reversible π-

complexation would lead to predominant silane homocoupling due to the stabilisation of the resultant WI by Si. However, an irreversible π-complexation results in the more electron-rich arene outcompeting an electronically neutral silane ($k_{H2} > k_{TMS2}$). When less activated arenes are coupled with electron-rich silanes, then competing silane homocoupling is observed.

Deprotonation: No KIEs were detected in independent rate measurements or intermolecular competition experiments, consistent with π-complexation as the TLS. An electrophilic metalation was proposed due to the observation of increasing rate with increasing arene electron-density.

Reductive Elimination: As π-complexation was found to be the TLS in this reaction, no information on reductive elimination was gained. However, Toste and co-workers propose that reductive elimination proceeds *via* a 4-coordinate complex (See Chapter 1, section 1.2.3).

Oxidation: The final step is the re-oxidation of Au(I) to Au(III). Only hypervalent iodine oxidants are competent, and the origin of this, and the mechanism of oxidation are unclear.

3.1.2 Chapter Aims

It was postulated that a mechanistic investigation into the intramolecular direct arylation reaction could lead to new mechanistic insights into the chemistry of gold(III) complexes. Although a thorough kinetic analysis into the intermolecular reaction had been performed, the conclusions were based on detailed study of a single, well-behaved, model system (Scheme 3.1, Top). Information on the other steps in the cycle were derived from competition experiments, literature precedent, or from model stoichiometric reactions rather than catalytic processes. In the intermolecular reaction, π-complexation of the arene to gold was found to be the turnover-limiting step, leading to pseudo first-order kinetic profiles. It was anticipated that the tethering of the arene to the aryl-silane, and thus in turn to the aryl-gold, would raise the effective molarity of the arene, and therefore potentially change the turnover limiting step to another point in the cycle.

As demonstrated in Chapter 2, the intramolecular process tolerates a large range of arene substituents. This is particularly notable in examples generating substituted fluorene products bearing highly electron withdrawing groups, such as CF_3. This is in contrast to intermolecular coupling where electron-rich arenes are required. The diverse electronic range, and minimal side product generation suggests that this could be a perfect system to study mechanistically. Indeed, the breadth of examples available alleviates the need for the use of a single model system, and afforded the opportunity to assess the effect of electronics, and tether length, on the mechanism of the reaction.

3.2 Mechanistic Investigation

3.2.1 Analysis of Reaction Kinetics

The mechanistic investigation began by monitoring the kinetics of cyclisation of **1b** by ^{1}H NMR spectroscopy under the standard reaction conditions (Figure 3.1, left). Doing so unveiled, after a short induction period, clean pseudo-zero order kinetics. The kinetic profile alone gave a wealth of information about the TLS of the reaction. Firstly, it must be a unimolecular process, as an intermolecular TLS, or an intermolecular pre-equilibrium would give pseudo-first order kinetics. This eliminated both the transmetalation of the silane and the Au(I)-Au(III) redox by the oxidant as the TLS. Also, no curvature toward the end of the reaction, which can be observed in pseudo-zero profiles, suggests that no change in the TLS to an intermolecular process occurs at the end of the reaction. This can happen as the rate of bimolecular reactions become very slow toward the end of the reaction due to the reduced probability of collision. This observation indicates that the bimolecular reactions in the catalytic cycle (transmetalation and oxidation) must be fast processes. Based on the catalytic cycle determined from the mechanistic study into the intermolecular reaction (Scheme 3.1), the TLS could be π-complexation of the arene, Wheland-intermediate formation, deprotonation, ligand loss or reductive elimination. To probe the mechanism further, the effect of temperature on the rate reaction of **1b** was measured. Eyring analysis over a temperature range of 10-35 °C gave activation parameters of $\Delta H^{\ddagger}$ = +26 kcal mol^{-1}and $\Delta S^{\ddagger}$ = +21 e.u. (Figure 3.1, right).

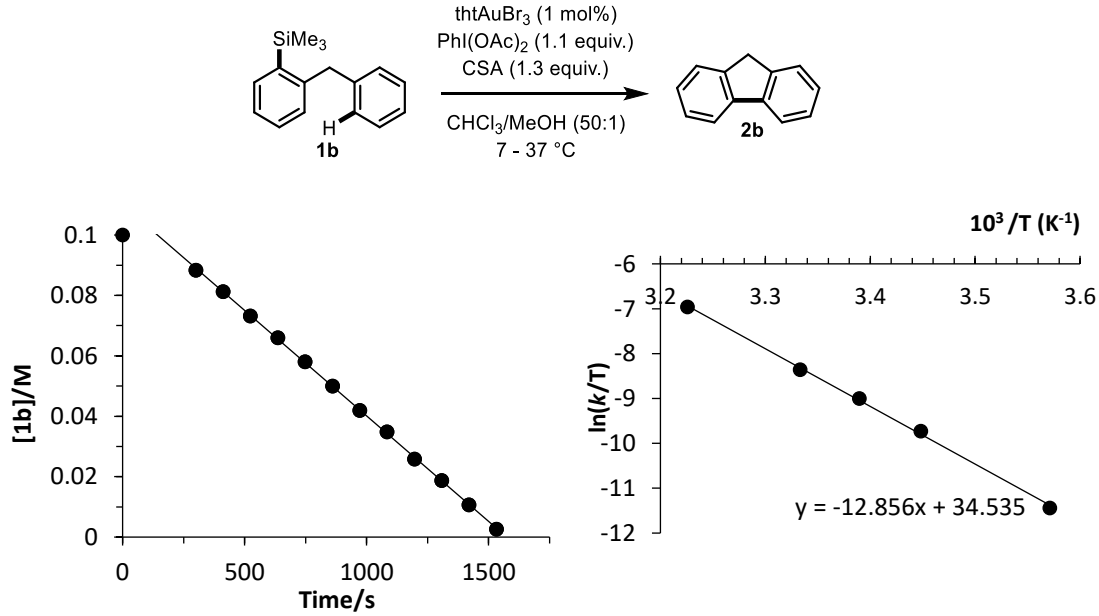

Figure 3.1. Left: Pseudo-zero-order kinetics for consumption of **1b** at 27 °C. Right: Eyring analysis for cyclisation of **1b** across a temperature range of 30 °C.

Although interpretation of these activation parameters must be taken with care, the results are markedly different from what would be expected if π-complexation of the arene to the gold were turnover-limiting (for intermolecular arylation, the activation entropy, $\Delta S^{\ddagger}$, is strongly negative).[83] The results suggest a turnover limiting step that occurs after π-complexation, and further experiments were performed to deduce whether it involves Wheland intermediate formation, deprotonation, reductive elimination from the resulting diarylgold species, or another process, prior to Au(I)-Au(III) redox.

3.2.2 Kinetic Isotope Effects

One of the simplest and widely-used strategies to investigate reaction mechanisms in C-H activation chemistry is the substitution of the reactive C-H bond with a C-D bond to measure the kinetic isotope effect (KIE). Despite the wide-spread use of this strategy, misinterpretations are rife in the literature, particularly when using competition experiments to comment on whether the deprotonation is turnover-limiting or not. In an attempt to clarify what insights can be drawn from KIE experiments, an essay by Hartwig outlines the three most common types of KIE experiments and the merits of each.[124]

The gold-standard approach to investigate whether C-H cleavage is involved in the TLS is through independent rate measurements of the protonated and deuterated substrates. The ratio of the rate constants obtained from these independent rate measurements gives the KIE for the reaction. Although the observation of a large and positive KIE is excellent evidence that C-H cleavage occurs at the TLS, the measurement of small KIEs resulting from equilibria or change in hybridisation relies on high accuracy measurements and may be undetectable. In the context of the intramolecular gold-catalysed direct arylation, the absolute rates of turnover of **1b** *versus* d_5-**1b** in (Scheme 3.2, Top) were experimentally indistinguishable. Thus, the perdeuterated phenyl ring induces no significant kinetic isotope effect (KIE) on the overall rate of catalytic turnover. This eliminates C-H cleavage as the turnover-limiting step of the reaction. The second strategy to investigate the C-H cleavage event is through intramolecular competition experiments. Although the identity of the TLS cannot be assigned with such an experiment, the selectivity determining event leading to deprotonation can be explored. In such experiments the accuracy of measuring the KIE is typically very high as only the product ratios, and not rates, need to be measured at the end of the reaction. To probe the deprotonation further, substrate d_1-**1b** was prepared and a significant KIE (k_H/k_D = 2.5) was measured by ^{1}H NMR spectroscopy (Scheme 3.2, bottom).

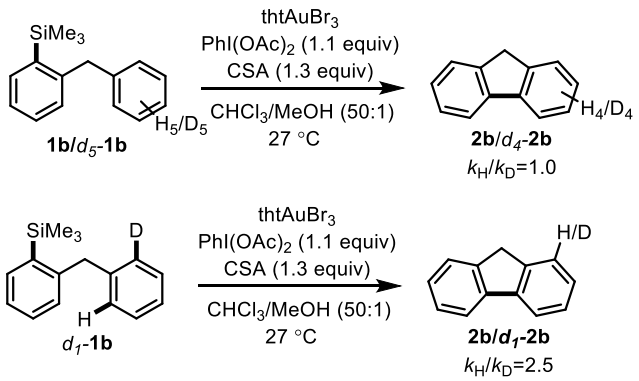

Scheme 3.2. KIE experiments. Top: Independent rate measurements; bottom: Intramolecular competition experiment.

This observation was important as, although deprotonation is not turnover-limiting, the deprotonation is clearly kinetically significant and selectivity determining in this competition experiment. The lack of an inverse secondary KIE also demonstrates that Wheland intermediate formation is not kinetically significant. For this KIE to be expressed, the isotopomeric precursor η^2 -complexes -**II**(**1b**) and **II'**(**1b**), Scheme 3.3- must be able to equilibrate prior to selectivity-determining C–H / C–D cleavage. Equilibration could occur in a non-dissociative manner, i.e. within discrete π-complexes (pathway **A**) or by reversible π-complexation (*via* **I**(**1b**), pathway **B**).

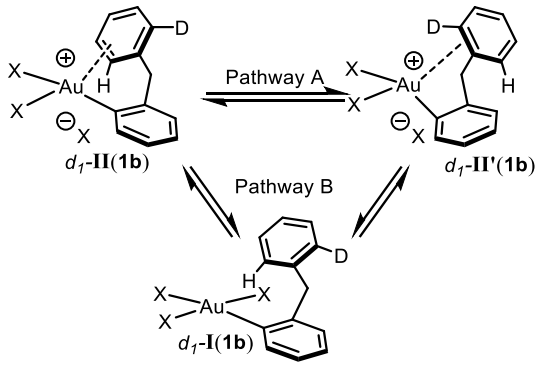

Scheme 3.3. Proposed η^2-Arene π-complexes.

To assess whether pathway B was operating and a reversible π-complexation was possible, a KIE experiment for bis-arene substrate *d*$_5$-**1x** was undertaken (Scheme 3.4). If π-complexation was irreversible, then no significant KIE would be expected as the product would be determined upon π-complexation, and therefore an approximate[1] 1:1 ratio would be obtained regardless of isotope incorporation. However, the same primary KIE (k_H/k_D = 2.5) was

[1] H and D have slightly different Hammett σ values[169]

measured with bis-arene substrate d_5-**1x** as d_5-**1b** confirming that π-complexation is indeed reversible under these conditions, with C–H / C–D cleavage being selectivity-determining, but not turnover-limiting. This is yet another mechanistic difference to the intermolecular protocol where π-complexation is irreversible and turnover-limiting.

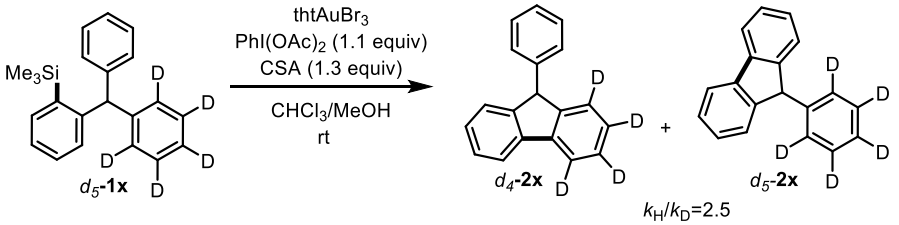

Scheme 3.4. Intramolecular KIE experiment.

3.2.3 Deprotonation Mechanism: S_EAr *vs* CMD

The observation of primary KIEs in direct arylation often leads to the conclusion that a concerted metalation deprotonation (CMD) type pathway is operative and not S_EAr. However, from a kinetic perspective, this is not necessarily correct, as an S_EAr pathway under Curtin-Hammett control whereby π-complexation, and subsequent Wheland intermediate formation, is fast and reversible but deprotonation is irreversible, the product distribution will reflect the relative rates of the irreversible deprotonation and therefore lead to a primary KIE. To explore the mechanism of deprotonation in more detail, a series of intramolecular competition experiments were designed so that the electronic demand of arylation could be measured (Figure 3.2). The aim of this experiment was to determine whether the acidity of the proton would be of importance, as expected in a CMD type process, or if the nucleophilicity of the arene would dominate, which is likely for an S_EAr type reaction. The results clearly show that reaction at the more electron-rich arene occurs, which is consistent with an S_EAr type process. All but one of the examples are *meta* substituted and hence electronic effects are primarily inductive and fit against σ, however the one *para* example **1y** fits the data significantly better when σ^+ is used instead of σ. While clearly more examples are required to verify this trend, this result could signify a selectivity determining Wheland intermediate formation, as the build-up of positive charge would be stabilised through resonance.

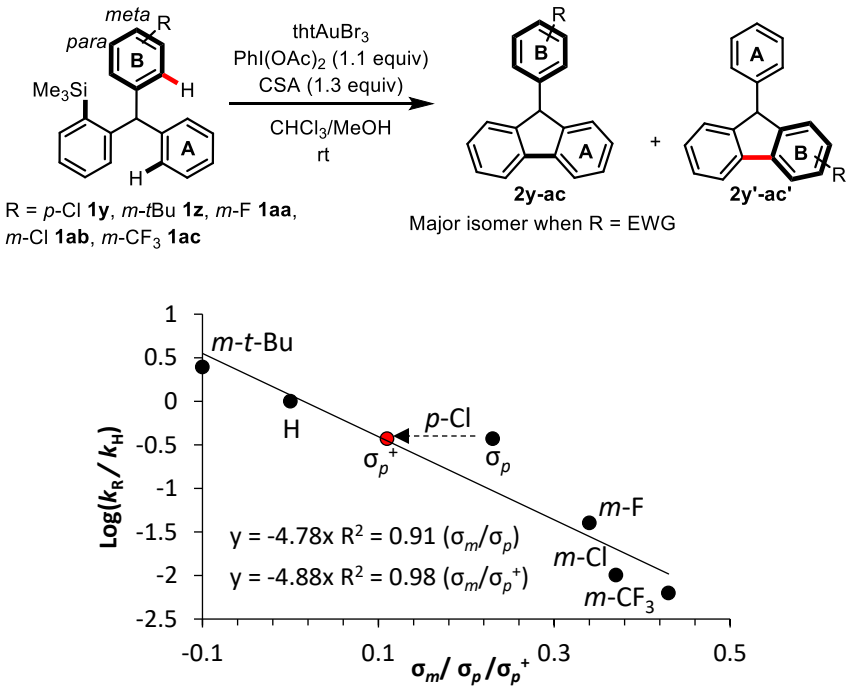

Figure 3.2. Substituent partitioning due to different arene electronics.

Therefore, the selectivity determining step may change from deprotonation when the electronic bias on the aromatic rings is negligible (d_5-**1x**) to WI formation upon electronic perturbation of the rings.

Although negative ρ values have been obtained in certain studies where a CMD type mechanism is proposed, the ranges observed (−0.4 - −1.6)[36] are significantly lower than what is obtained in this study. The reaction constant obtained from these competition experiments ($\rho/\rho^+ = -4.8/4.9$) is much more consistent with electrophilic metalation.

Further support for an S_EAr type pathway was obtained through the observed regioselectivity of substrates **1k** and **1ad (**Scheme 3.5, Top) and comparing these values to similar experiments under Pd-catalysis where CMD is the operative mechanism (Scheme 3.5, bottom). Firstly, preferential arylation *ortho*- to a fluorine substituent is characteristic of a CMD mechanism, as seen in the cyclisation of **19** where the *ortho*:*para* ratio of products is 19:81. This is not observed under gold-catalysis as the reaction is almost completely *para* selective with a ratio of isomers of >98:2 for the cyclisation of **1k**, and thus inconsistent with a CMD mechanism and entirely consistent with an electrophilic metalation. The naphthyl substrate **1ad** also reacts as expected for an S_EAr type reaction with the major isomer forming through reaction at the more nucleophilic 1-position. Whereas under Pd-catalysed direct arylation, the reaction of naphthyl substrate **22** is largely unselective.

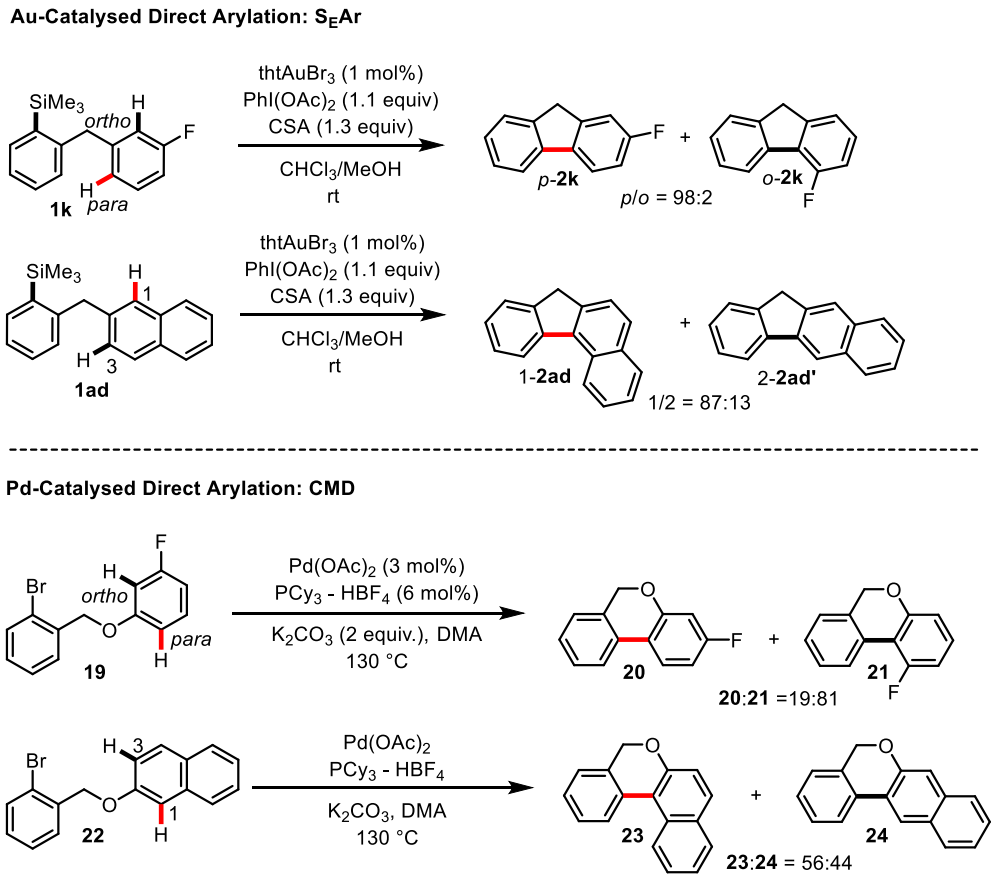

Scheme 3.5. Regioselectivity pattern arising from S_EAr (Top) and CMD (bottom) mechanisms.

Additional evidence supportive of Wheland intermediate formation along the reaction pathway is the attenuation of the KIE when the methylene bridge in d_1-**1b** is replaced with an O-linker d_1-**1v** (scheme 3.6). The presence of the oxygen linker next to the resulting carbocation could lead to its stabilisation relative to the methylene bridged example. This stabilisation may reduce reversibility to the π-complex and therefore Wheland intermediate would effectively become selectivity determining and a roughly equal proportion of H and D would react. At the limit of a fully irreversible Wheland intermediate formation, an inverse secondary KIE could be expected. As this is not the case and a small KIE is still measured, it is possible that the system is under non-Curtin-Hammett conditions and the product distribution could reflect the equilibrium population.

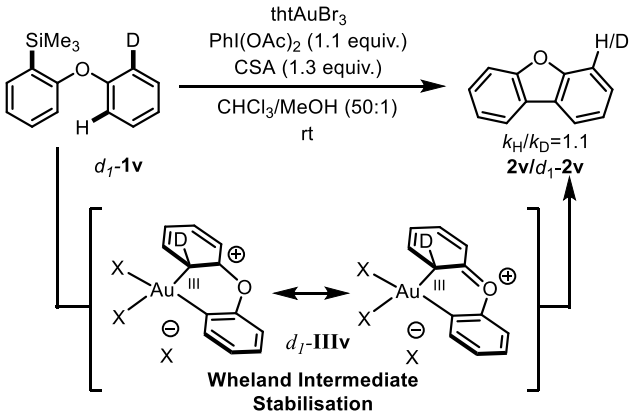

Scheme 3.6. Proposed origin of diminished KIE in presence of oxygen linker.

3.2.4 Hammett Linear Free Energy Relationships

The evidence obtained so far pointed towards reductive elimination as the TLS for substrate **1b**. Indeed, the pseudo-zero order kinetic profile ruled out transmetalation of the silane and oxidation of the metal, the large entropy of activation eliminated π-complexation and the results of the kinetic isotope effect experiments meant deprotonation or Wheland intermediate formation were not turnover-limiting. By process of elimination, it was therefore likely that reductive elimination, or a yet to be uncovered step in the catalytic cycle, was the TLS. To enforce this hypothesis the effect of aryl electronics on the rate of the reaction was measured. It was expected if reductive elimination was the TLS that, regardless of whether the substituent was initially on the arene (**1i-n**) or silane (*iso*-**1i-n**) ring, identical rates would be obtained. This is because each substrate would converge at common intermediate, **IV**(**1i-n**), prior to the TLS and therefore should react at equal rates (Scheme 3.7).

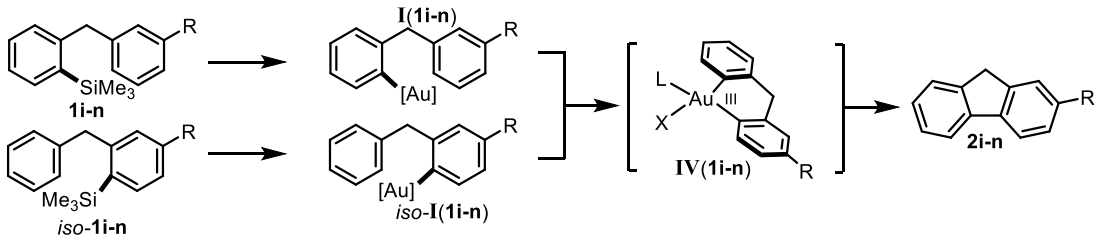

Scheme 3.7. Regioisomeric starting materials converging on common intermediate prior to reductive elimination.

The temporal kinetic profiles were obtained for a series of substituted arenes and silanes (Figure 3.3). When the arene is substituted (Figure 3.3, Top), pseudo-zero order profiles are maintained throughout the series, albeit with increased curvature with the most electron-withdrawing substituents. However, silane substitution (Figure 3.3, bottom) led to

significantly longer reaction times and complex kinetic profiles when electron-withdrawing groups were implemented.

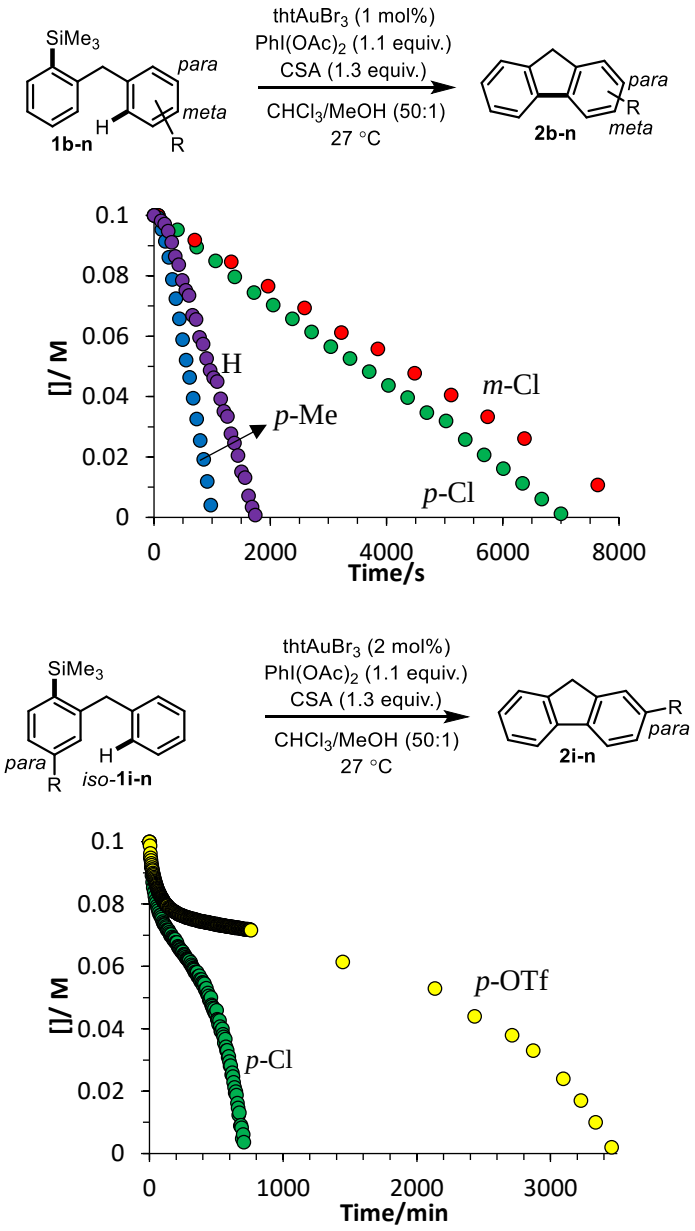

Figure 3.3. Select temporal kinetic profiles of substituted arenes (Top) and silanes (bottom).

By combining kinetic simulation with experimental observation, an off-cycle catalyst deactivation pathway was proposed and the exact nature of this deactivation is the focus of the next chapter. However, it was found that addition of electron-rich arenes to the reaction mixture could prevent the deactivation pathway and the on-cycle mechanism could be explored. The additive of choice was 2-bromothiophene, **98**, and its addition to examples bearing electron-withdrawing substituents on the aryltrimethylsilane led to pseudo-zero order profiles being observed once again (Figure 3.4).

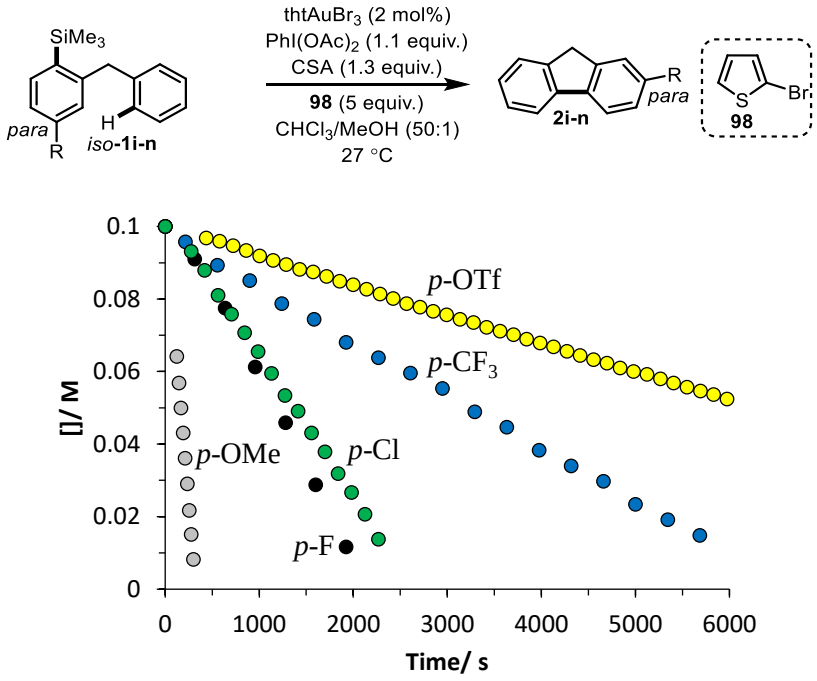

Figure 3.4. Temporal kinetic profiles of substituted silanes in the presence of 2-bromothiophene to eliminate catalyst deactivation.

Combining the data from arene and silane substitution into a single Hammett LFER plot (Figure 3.5) demonstrates that regardless of which ring the substituent is positioned on, identical rates are obtained up to $\sigma = 0.43$ with a reaction constant of $\rho = -2.0$. A break in the Hammett plot is observed for the most electron-withdrawing groups, where reduced rates and increased curvature is observed when the arene is substituted (*vide infra*). The effect of electronics on the TLS is therefore substantially different to what was earlier measured in competition between electronically biased pairs of arenes (Figure 3.2), therefore affirming the conclusion that the selectivity determining step leading to arylation is different to the TLS of the reaction.

To further explore the effect of aryl electronics on rate, the rate of cyclisation of disubstituted examples **1ae** and **1t**, were measured. The rates were predicted by the sum of their sigma values as shown on Figure 3.5, indicating that once again, regardless of provenance, the impact of a substituent on the rate of turnover is identical.

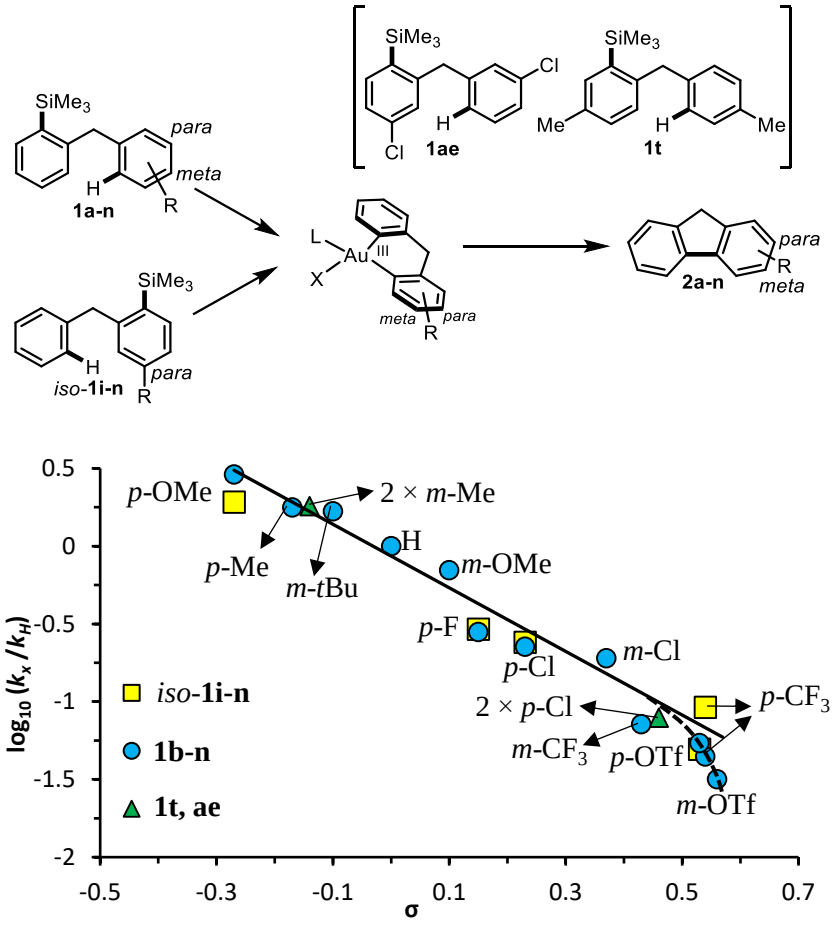

Figure 3.5. LFER analysis of rates of catalytic turnover during cyclisation of (di)substituted silanes and arenes; $\log_{10}(k_X/k_H) = -2.0\sigma - 0.06$; σ-values are additive for **1ae**/**1t**. Conditions: substrate (0.05 mmol), thtAuBr$_3$ (2 mol%), 2-bromothiophene (0.5 mmol), PhI(OAc)$_2$ (0.055 mmol), CSA (0.065 mmol), CDCl$_3$/CD$_3$OD (50:1, 0.1 M). Note: Dashed line for illustrative purposes only.

These results suggest convergence at a common intermediate at, or prior, to the TLS. This condition can be satisfied at any point after C−H cleavage to generate a diarylgold intermediate. Further evidence for convergence at a common intermediate arises from the identical rates of turnover of bis-TMS substrate **1af** and **1b** (R = H), both of which generate **2b**, via the same intermediate **IV**(**1b**) (Scheme 3.8). Reaction of bis-silane **1af** thus involves a *second* C-Si cleavage (pathway A), rather than C-H cleavage (Pathway B), at the stage of the

monoaryl-gold intermediate. This selective intramolecular C-Si *versus* C-H auration is consistent with the conclusions drawn previously from intermolecular examples: when π-complexation is reversible, generation of a TMS-stabilised Wheland intermediate is favoured. To ensure that the **2b** generated was not as a result of rapid protodesilylation of **2af**, the reaction was performed in deuterated solvent. As no deuterium incorporation was observed, **2b** must be formed exclusively *via* pathway A.

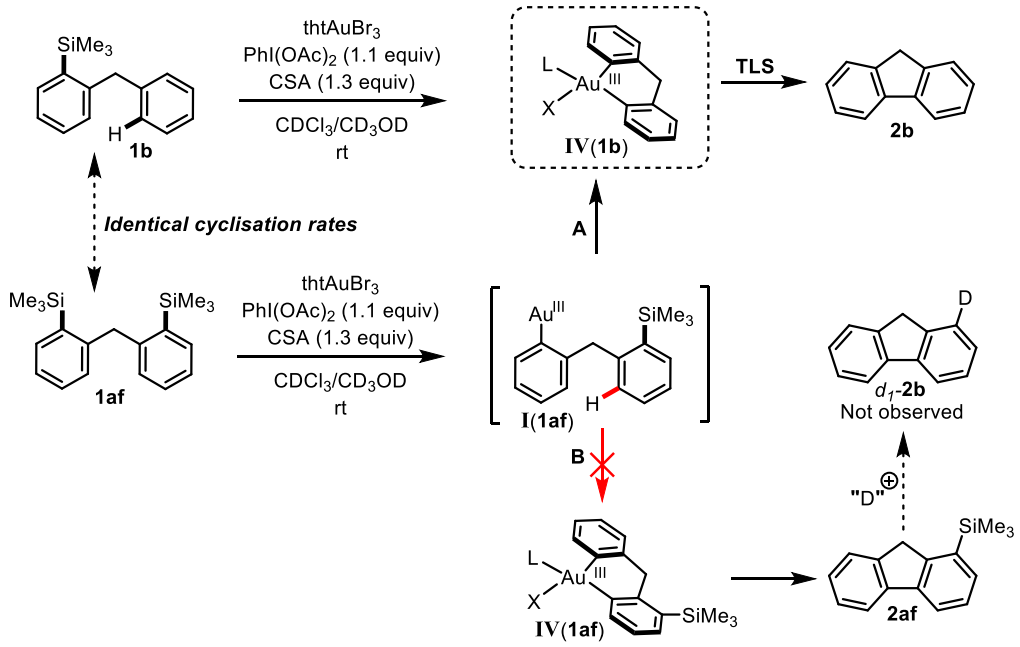

Scheme 3.8. Further evidence for reductive elimination as the TLS.

These results strongly indicate that reductive elimination is the TLS for the vast majority of examples measured.

3.2.5 Reductive Elimination

In Chapter 1, reductive elimination from gold(III) complexes was introduced, however the parameters that govern this process are not well understood. Two major studies have given some insights into the process. Kochi demonstrated that reductive elimination from dialkylgold(III) complexes requires the dissociation of a ligand to afford a three-coordinate gold species prior to reductive elimination, and that addition of phosphine retarded the reaction. Toste and co-workers came to the opposite conclusion for diarylgold(III) complexes,[77] and determined that reductive elimination can occur from the 4-coordinate species, and that addition of phosphine *increases* the rate of reaction by providing an ionic pathway. Despite determining the rate of reductive elimination from a particular gold complex ([$Ar_2Au(PPh_3)Cl$], where Ar = *p*-C_6H_4F (**41**)), there were no details on the effect of aryl

substituents on the rate of reductive elimination. However, comparing Toste's results with Nevado's study on [$Ar_2Au(PPh_3)Cl$] complex **40**, where Ar = C_6F_5, demonstrates that electron-withdrawing groups likely reduce the rate of reductive elimination as forcing conditions were required for reductive elimination to occur in this case (150 °C, 20 h).[74] The results presented herein confirm this, and quantify the electronic effect of aryl substituents through the Hammett LFER (Figure 3.5); reaction constant of $\rho = -2.0$. It was only by investigating the intramolecular reaction, and therefore changing the TLS from π-complexation to reductive elimination, that allowed for this elementary step to be studied without the reliance on stoichiometric studies, as is so often needed.[125–128] Indeed, it is relatively uncommon to find that reductive elimination as the turnover limiting step in any $C(sp^2)$-$C(sp^2)$ cross-coupling reaction.[129,130] In most examples, oxidative addition or transmetalation is turnover-limiting.

Despite determining that reductive elimination from these gold(III) complexes involves a large and positive $\Delta S^{\ddagger}$, indicating significant decrease in order at the transition state, and that the process is accelerated by electron-donating substituents ($\rho = -2.0$), there were still several key questions: 1) How does reductive elimination from diarylgold(III) complexes compare with other transition metals? 2) What is the ligand speciation, i.e. does reductive elimination occur from a 3- or 4-coordinate species? 3) Can the gold(III) intermediates be observed or characterised?

1) Comparison with Literature: The acceleration of reductive-elimination by electron-donating substituents ($\rho = -2.0$; Figure 3.5) is partially consistent with literature precedent for other $Ar_2[M]$ complexes (M = Pt, Pd), where electron-withdrawing substituents are found to strengthen the ground-state metal-carbon bonds, and therefore reduce the rate of reductive elimination ($\rho = -1.0$ - -1.5).[131,132] However, Hartwig showed from LFER analyses, that reductive elimination from $Ar_2[Pt]$ complexes "is faster from complexes with a larger difference between the electron-donating properties of the two aryl groups."[131,132] In other words, the electronic effects of substituent on reductive elimination rates are not simply additive. This is clearly not the case in the system measured herein, as disubstituted examples **1ae** and **1t** react at a rate predicted by the sum of their σ values, thus showing that within the electronic range analysed, electronic effects on reductive elimination from gold are indeed additive. This is in agreement with computational studies on reductive elimination from *cis*-[$AuPPh_3(Ar^1)(Ar^2)$] complexes which calculated that the electronic effect of aryl substitution should be additive.[133]

2) Ligand speciation: A much-discussed issue in the literature is whether reductive elimination from gold(III) complexes occurs from a three- or four- coordinate species. To

assess whether there was a pre-equilibrium prior to reductive elimination, and if any of the reaction components affected the rate, the order in each component was assessed. In the rate analysis of **1b**, it was found that the reaction had a zero-order dependence on all reaction components (oxidant, CSA, substrate) other than the catalyst itself and methanol. An inverse order was observed in methanol (Figure 3.6, Left). The inverse order suggests that methanol is behaving as an inhibitor, which was also found in the intermolecular study. However, in contrast to the intermolecular study, increasing the concentration of methanol does not lead to the rate of reaction becoming zero, instead, at high methanol concentrations the rate saturates. These results are consistent with two species being in equilibrium that can reductively eliminate. This can be interpreted as a fast reacting 3-coordinate species **V**(**1b**), and a slower reacting, methanol-bound 4-coordinate species **IV**(**1b**) (Figure 3.6, Left). Therefore, as the concentration of methanol increases, the equilibrium shifts to **IV**(**1b**), and the reaction slows until saturation occurs.

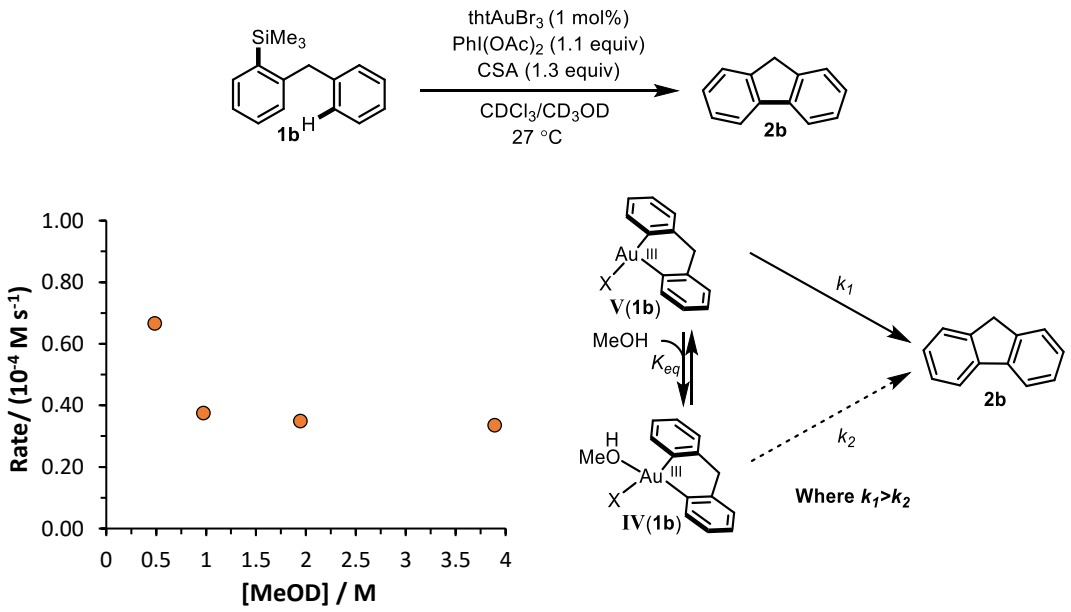

Figure 3.6. Left: Rate-dependence on [CD_3OD]. Right: Proposed pre-equilibrium to explain observed rate dependence.

Based on this hypothesis, the maximum rate of reductive elimination should occur when there is no methanol. Unfortunately, methanol is required in the reaction to solubilise the CSA, and therefore methanol was replaced with TFE to estimate the rate in its absence. As a significantly more acidic alcohol (pk_a 12.4 *vs* 15.5),[134] one would expect the equilibrium to shift significantly toward **V**(**1b**). Indeed, significantly greater rates were observed when methanol was replaced with TFE under comparable concentrations. Assuming that the k_{obs} obtained

when monitoring the reaction using TFE gives an approximation of k_1, and that the k_{obs} obtained when the reaction is saturated with methanol gives k_2, simulation software can be used to extract the equilibrium constant K_{eq} using the derived rate expression (equation 1). The aim of the simulation was to confirm that the observed rate dependence on methanol can be predicted by this hypothesis and the associated rate equation. However, a complication to the simulation is the fact that methanol is known to occur as a dimer in solution with chloroform, and the equilibrium constant K_{eq2} is not reported.[123] Whilst the presence of this dimerisation excludes the extraction of meaningful values of K_{eq} and K_{eq2} as various combinations can be used, good fits to the data can be obtained. This confirms that the observed kinetics can be explained by reductive elimination occurring *via* a fast reacting 3-coordindate species and a slower reacting, methanol-bound 4-coordinate species. Whilst this is at odds with the results from Toste and co-workers, the system demonstrated herein differs in that i) the two aryl groups are tethered and ii) there are no phosphine ligands present.

Alternatively, these results could be attributed to medium effects as Komiya and Kochi[135] demonstrated significant rate differences in reductive elimination from dialkylgold(III) complexes using different solvents. In their report, it was shown that increasing solvent polarity favoured reductive elimination. Whilst significant efforts would be required to eliminate the possibility of medium effects causing the changes in rate presented herein, the observation that increasing solvent polarity *reduces* the overall rates is at odds with Komiya and Kochi's[135] prior study.

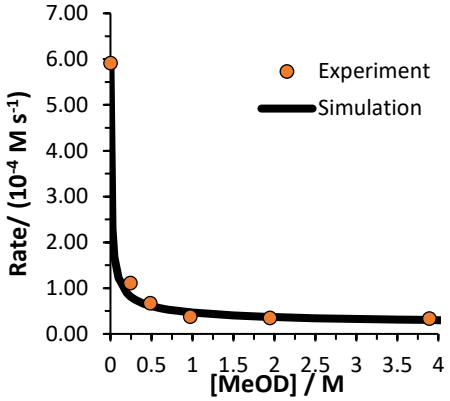

$$\frac{d[P]}{dt} = k_1[Au]_{tot} + \frac{(k_2 - k_1)K_{eq}[Au]_{tot}[MeOH]}{(K_{eq}[MeOH]+1)}$$

$$\text{where } [MeOH] = \frac{-1+\sqrt{1+8K_{eq2}[MeOH]_{tot}}}{4K_{eq2}}$$

Equation 1

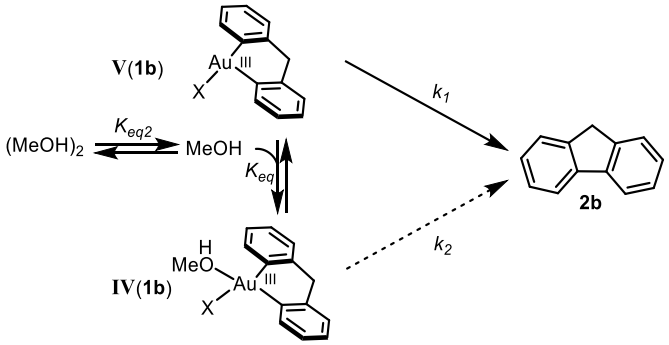

Figure 3.7. Overlay of simulated and experimental data (Top left) using the rate equation (Top right) derived from mechanistic hypothesis (Bottom).

3. Observation of Resting State. Although the purported resting states could not be independently isolated, a species consistent with being a catalytic intermediate, tentatively assigned as **IV**(**1b**), was observed by ^{1}H NMR spectroscopy. In the methylene region (*ca.* 4 ppm) of the ^{1}H NMR spectrum a peak was observed with an integral equating to approximately 1 mol% of the starting material, identical to the catalyst loading used in the experiment. The species is absent before initiation, grows to a steady state, and then disappears upon total consumption of the starting material. Additionally, repeating the reaction at increased catalyst loadings gave the expected increase in intermediate concentration, confirming the relationship between catalyst loading and intermediate concentration. A final confirmation of the connection between this intermediate and turnover is that the instantaneous rate of reaction of **1b** ($\frac{-d[\mathbf{1b}]}{dt}$ / M s^{-1}) can be directly related to the concentration of this intermediate.

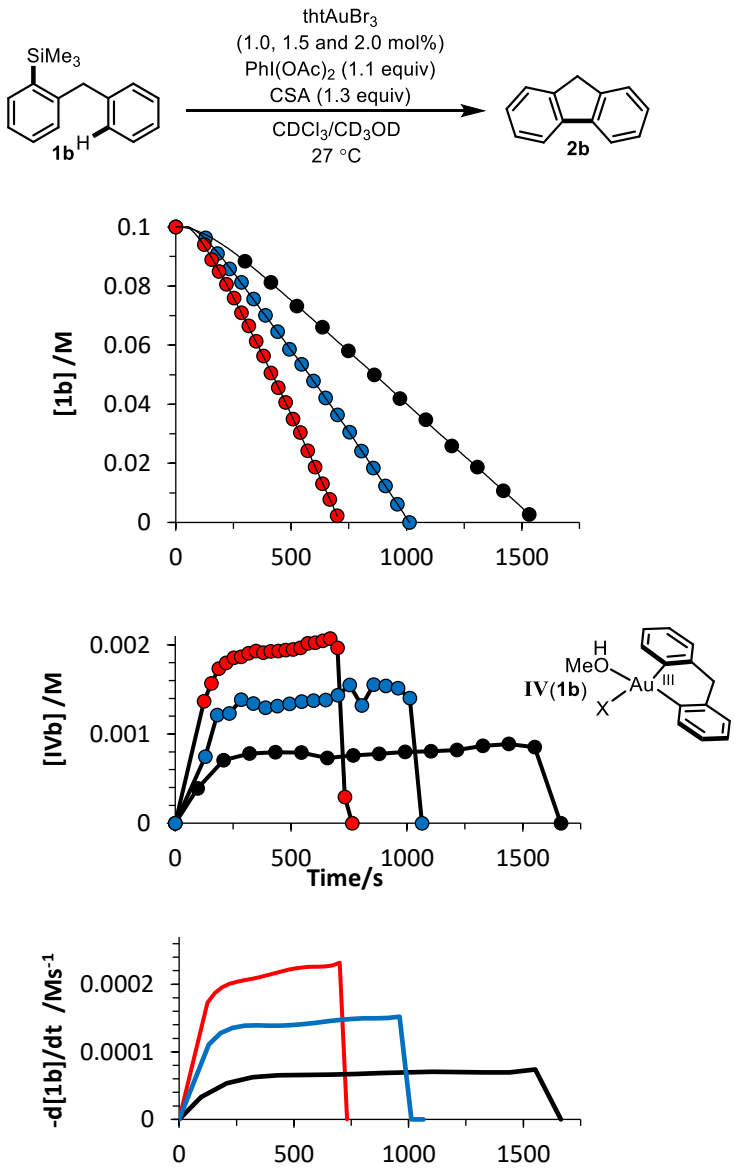

Figure 3.8. Top: Pseudo-zero-order kinetics (after induction period, ~300 s) for cyclisation of **1b** using 1.0, 1.5, and 2.0 mol% Au. Middle: temporal concentration of catalyst resting state, tentatively assigned as **IV**(**1b**). Bottom: temporal turnover rate of **1b**/M s^{-1}.

3.2.6 Change in TLS and Shifting Resting States

Reductive elimination is the TLS for the majority of cyclisations that lead to fluorenes. Strong evidence for this conclusion was the measurement of identical rates, regardless of whether substituents were located on the arene, or silane moiety. However, when substantially electron-withdrawing substituents are employed ($\sigma > 0.43$), this is no longer the case (Scheme 3.9).

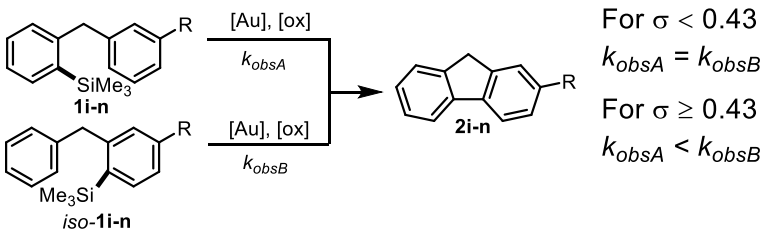

Scheme 3.9. Effect of aryl substituent on observed rate constant for cyclisation.

Whilst pseudo-zero order profiles are maintained when the substituent on the silane-bearing aromatic ring is varied, substitution of the arene with electron-withdrawing groups leads to slower cyclisation, with increased curvature in the kinetic profiles. This is particularly significant in the cyclisation of **1m**, where substantially different rates and kinetic profiles are observed when compared to its constitutional isomer *iso*-**1m** (Figure 3.9).

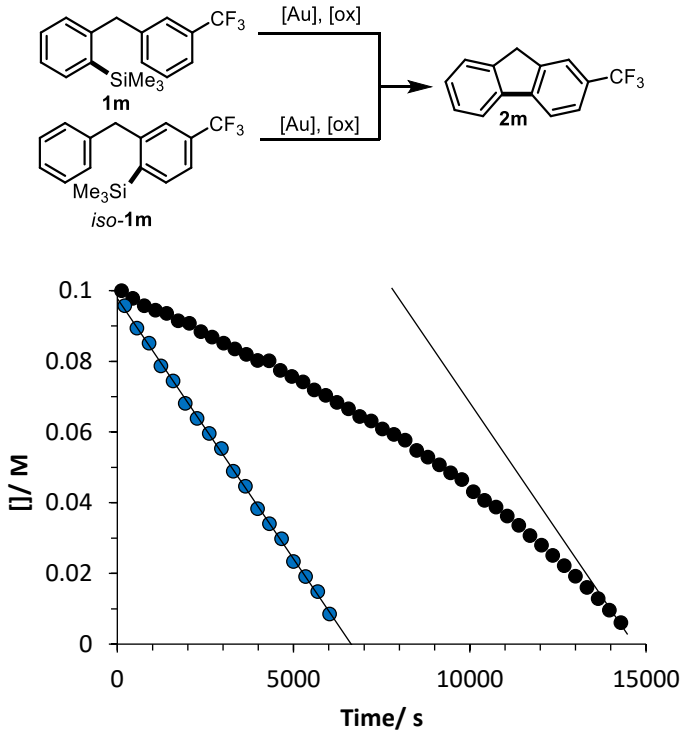

Figure 3.9. Comparison of rates of isomers **1m** and *iso*-**1m**. Conditions: substrate (0.05 mmol), thtAuBr$_3$ (2 mol%), 2-bromothiophene (0.5 mmol), PhI(OAc)$_2$ (0.055 mmol), CSA (0.065 mmol), CDCl$_3$/CD$_3$OD (50:1, 0.1 M).

These observations suggest a change in the TLS, and the curvature observed is the result of a rate dependence on CSA, which is not found in examples where reductive elimination is turnover-limiting. During the reaction, CSA is liberated as the oxidant is consumed, and therefore the rate of reaction continually increases in an autocatalytic fashion. This was

confirmed by deliberate addition of CSA to the reaction, and an observed increase in rate. These results are consistent with π-complexation as the TLS for **1m** as the dependence on CSA was also found in the intermolecular coupling where π-complexation is turnover limiting. This hypothesis was reinforced by interception of the proposed monoaryl resting state **I**(**1m**) with 2-bromothiophene **98**, resulting in co-generation of biaryl **99**. This interception is not observed with *iso*-**1m** due to the rapid rate of intramolecular C-H auration (Scheme 3.10).

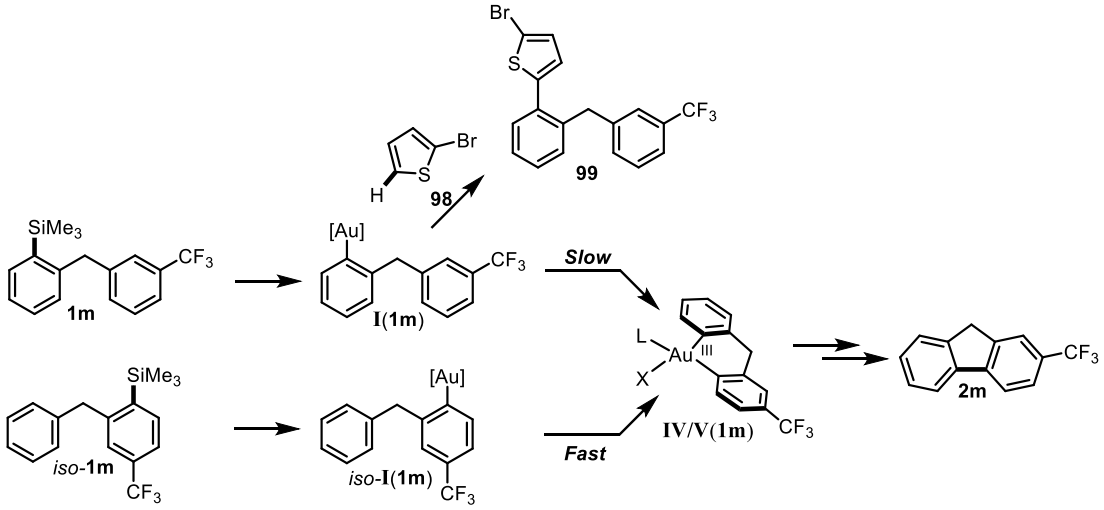

Scheme 3.10. Intermolecular interception of monoaryl resting state.

Intriguingly, the maximum rate observed in the cyclisation of **1m** approaches the rate observed for the cyclisation of *iso*-**1m**, where reductive elimination is the TLS (Figure 3.9). This suggests that the TLS may change during the reaction from π-complexation, when the concentration of CSA is low, to reductive elimination at high CSA concentrations. Analysis and kinetic simulation of the partitioning between **1m** and **99** as a function of conversion provided further evidence in support of a change in TLS (Figure 3.10).

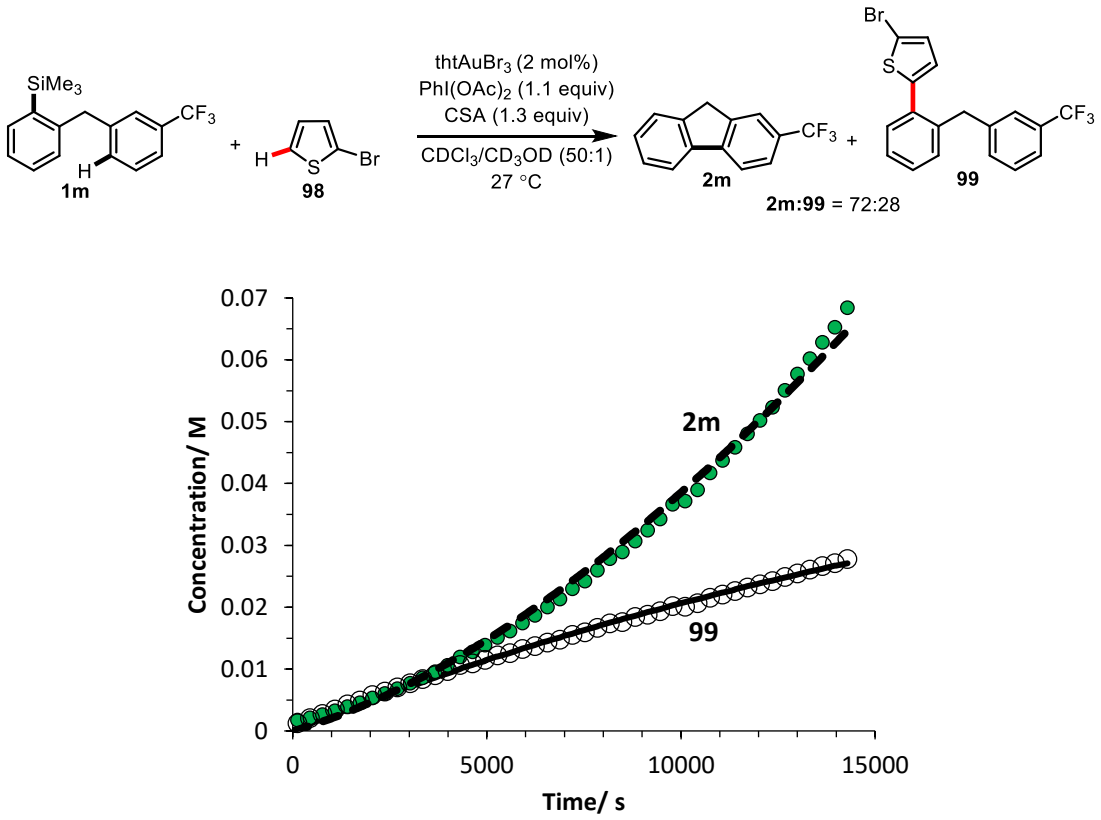

Figure 3.10. Interception of intramolecular cyclisation of **1m** by **98** with simulated data from model in Scheme 3.11.

It is clear from Figure 3.10 that the partition between **2m** and **99** is changing as the reaction progresses. Assuming π-complexation is the selectivity determining step, the observation suggests that the rate of π-complexation in the intramolecular coupling is affected by the free [CSA], which is increasing through the course of the reaction, whereas under the reaction conditions, the intermolecular coupling is not significantly affected and therefore $k_1 \approx k_2 < k_3$ (Scheme 3.11). The slight downward curve observed for the formation of **99** suggests a shift in TLS for the *intramolecular* cyclisation from π-complexation to reductive elimination and therefore reducing the concentration of the resting state, and therefore the rate of the *intermolecular* coupling.

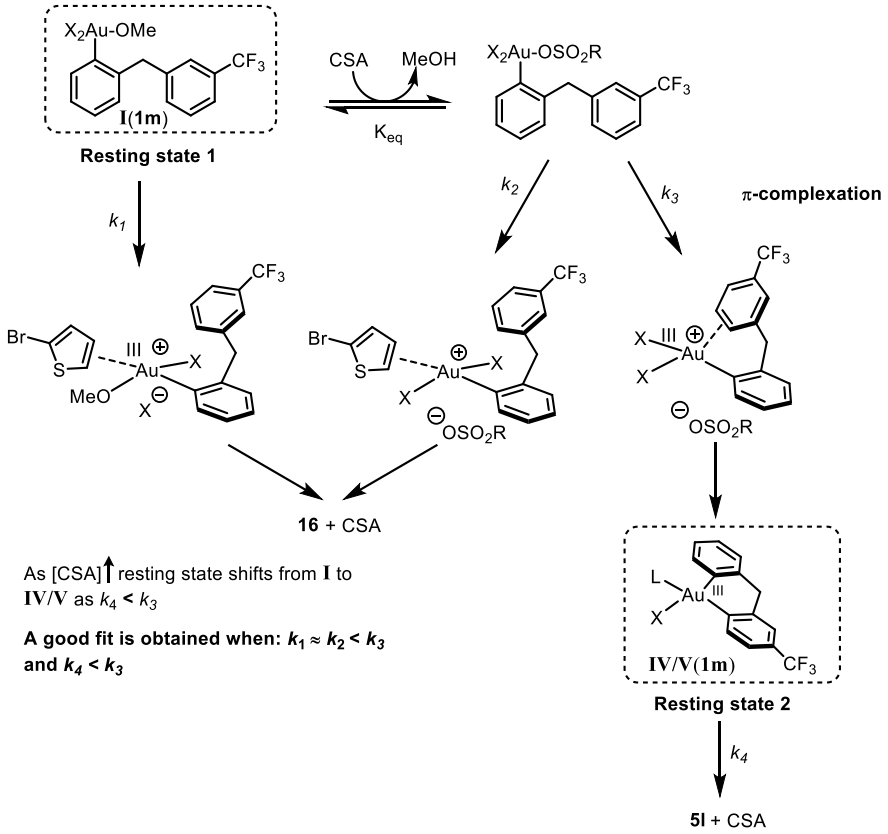

Scheme 3.11. Model to explain partition observed in Figure 3.10. X denotes anionic or neutral ligands

Kinetic modelling of the reaction based on Scheme 3.11 was performed based on the following rate and equilibrium constants: k_1 = 0.0027 $dm^3mol^{-1}s^{-1}$, k_2 = 0.0040 $dm^3mol^{-1}s^{-1}$, k_3 = 0.034 s^{-1}, k_4 = 0.0077 s^{-1} and K_{eq} = 1.85 (the values reported are for purely illustrative purposes only and no rate or equilibrium constant should be used in isolation). To investigate this further, the intermolecular coupling of **98** with **100** was monitored (Figure 3.12). As expected, the initial rate of formation of **99** and **101** are similar, however the rate of **101** is increasing slightly (as expected if k_2 is slightly greater than k_1) whereas the rate of **99** is decreasing with time, which is consistent with a shifting of resting state from **I**(**1m**) to **IV/V**(**1m**) in the competition experiment. In the absence of a shift in resting state, one would expect rate of formation of **99** and **101** to be nearly identical.

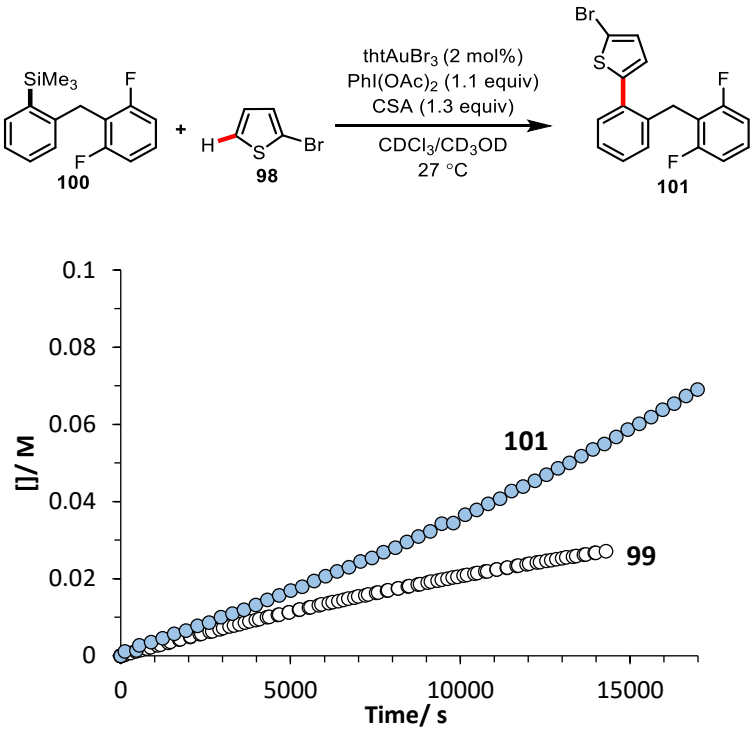

Figure 3.12. Combined concentration/time plots for the formation of **99** and **101**

3.2.7 Effect of Tether Length on Rate

Calculations on reductive elimination from unconstrained [$(Ar_1)(Ar_2)Au(PPh_3)Cl$] complexes show that the lowest energy transition state involves Au−Ar conformations in which the two aryl rings are oriented face-to-face.[133] The short tethers employed herein will likely make this conformation less accessible, and therefore reducing the rate of reductive elimination *versus* unconstrained examples. Longer, non-rigid tethers are therefore expected to allow greater Au−Ar conformational mobility and thus a lower energetic barrier to the attainment of the requisite face-to-face orientation of the two aryl rings. However, longer tethers will also reduce the effective molarity of the arene in the precursor C−H auration. The kinetics of cyclisation of **1b** (−CH_2− tether) are distinct from those of **3a** (−CH_2CH_2− tether), Figure 3.13. In the latter case, increase of the tether length by one methylene unit results in a curved kinetic profile, similar to that found for substrate **1m** (Figure 3.9) and therefore indicative of a monoaryl-gold(III) resting state and π-complexation as the TLS.

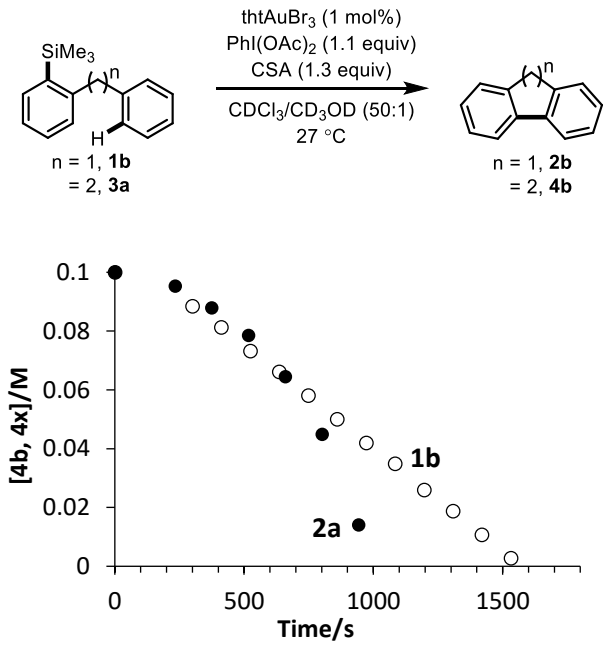

Figure 3.13. Turnover to generate 5- *versus* 6-membered rings. As the reaction proceeds, the turnover rate of **3a** accelerates, becoming faster than that of **1b**.

A key observation is that, as the reaction evolves, the rate of turnover of **3a** becomes faster than that of **1b**, for which reductive elimination is the TLS. In other words, the intrinsic rate of reductive elimination from the longer $-CH_2CH_2-$ tethered intermediate **IV**/**V**(**3a**) must be faster than that from the more constrained, $-CH_2-$ tethered intermediate **IV**/**V**(**1b**) (Scheme 3.12). However, the extent to which reductive elimination is accelerated cannot currently be quantified as the rate data obtained for **3a** does not result from reductive elimination as the TLS.

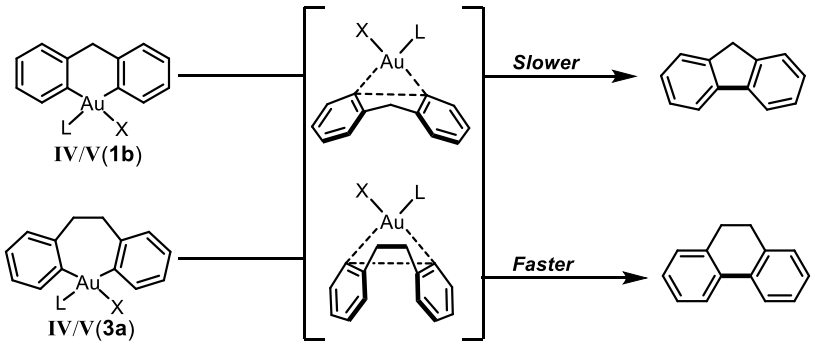

Scheme 3.12. Effect of tether length (n) and flexibility on rate of reductive elimination.

Whilst the relative rates of reductive elimination cannot be quantified in these examples, through competition experiments, the relative rates of C-H auration can be determined.

Although in absolute rate comparisons, **3a** cyclises faster than **1b**, in competition this is not the case. Using **102** to perform an intramolecular competition experiment, the 5-membered ring cyclisation outcompetes the 6-membered ring forming process by a factor of 13 (Scheme 3.13). This selectivity may arise from the differential developing strain in 6-membered versus 7-membered aurocycles generated from rings A / B respectively.

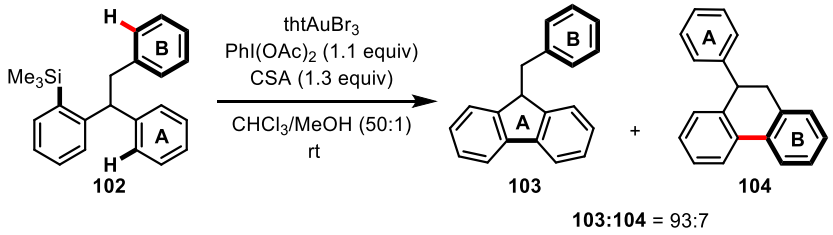

Scheme 3.13. Intramolecular competition (A *versus* B) to generate 5-membered (**103**) *versus* 6-membered (**104**) rings.

Further investigation into the formation of 6-membered ring systems revealed an intramolecular primary KIE of 1.9 for *d*$_1$-**3a**, indicative of partially reversible Wheland intermediate generation (Scheme 3.14). Once again, stabilisation of the Wheland intermediate by replacing the CH_2 linker with oxygen in *d*$_1$-**3d** eliminates the KIE.

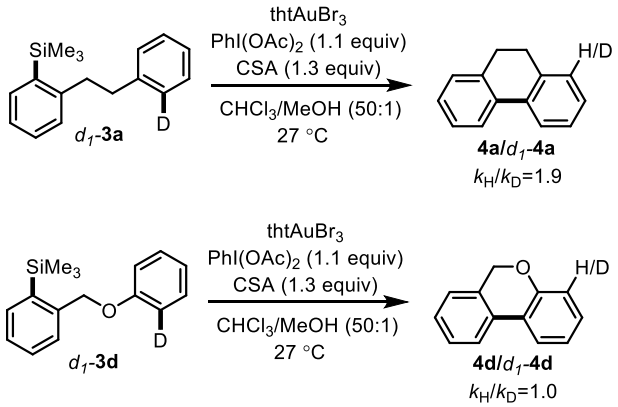

Scheme 3.14. KIEs for 6-membered ring cyclisation of *d*$_1$-**3a** and *d*$_1$-**3d**.

The final demonstration of the effect of tether length on the rate of cyclisation was through the monitoring of the cyclisation of **5a** to form 7-membered ring **6a** (Figure 3.14). The curvature that is seen in the cyclisation of **3a** is maintained, however a significantly slower rate is observed, approximately 30-fold slower than the 6-membered analogue **3a**. Despite the increased reaction times, this is still a significantly faster reaction than the coupling of toluene in the intermolecular reaction which took approximately 45 h. This demonstrates that even with longer tethers, the effect of rendering the reaction intramolecular is profound.

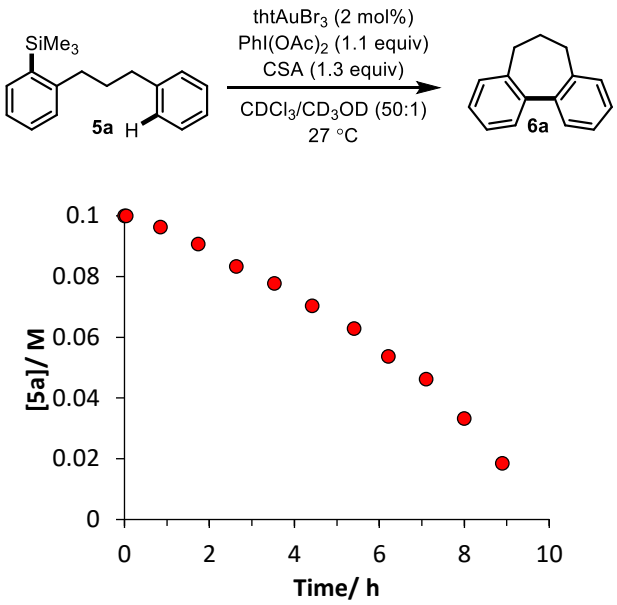

Figure 3.14. Turnover to generate 7-membered ring **6a**.

3.3 Summary

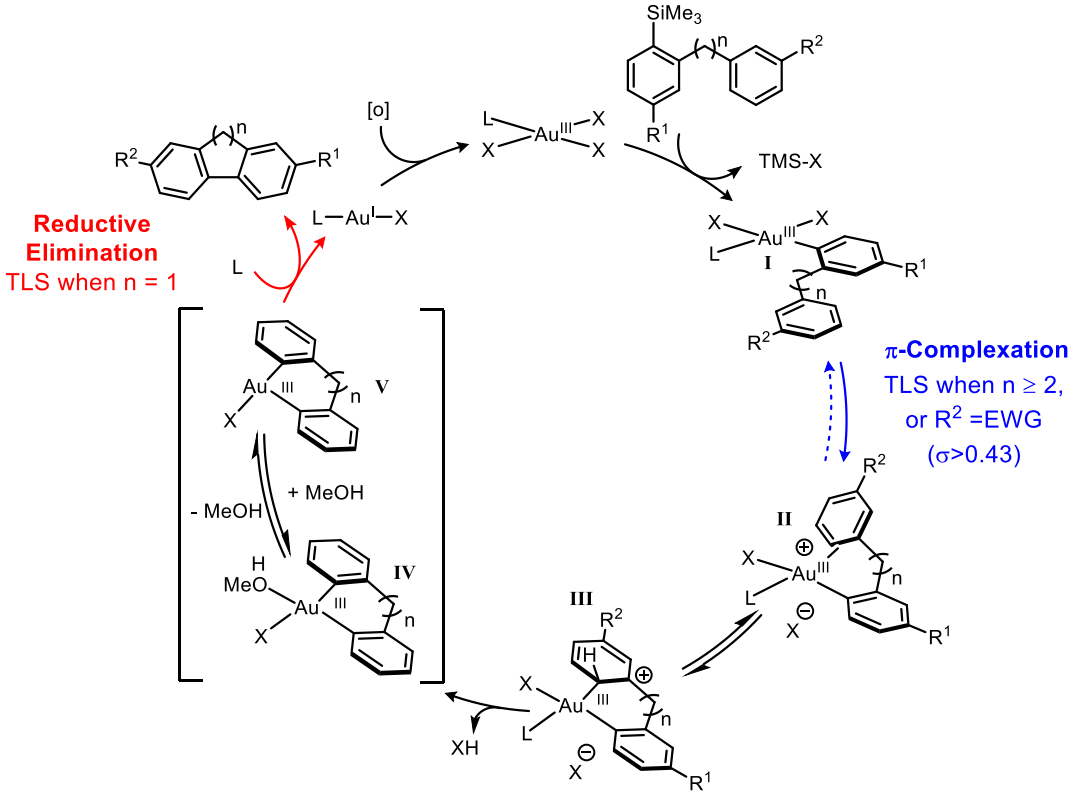

Scheme 3.15. Catalytic cycle of gold-catalysed intramolecular direct arylation.

In 2014, a mechanistic investigation into intermolecular gold-catalysed direct arylation resulted in the elucidation of the catalytic cycle. However, several features were unexplored due to the kinetic restrictions from π-complexation being the turnover-limiting step. This has led to the re-examination of the mechanistic features of the reaction through investigation of the intramolecular variant presented herein. The results of this study are in total agreement with the previous report, and through the exploitation of features not accessible to the intermolecular reaction, key new insights have been uncovered.

Rendering the arylation process intramolecular induces several changes that facilitate mechanistic investigation. First, unlike the intermolecular system, the vast majority of the intramolecular substrates undergo turnover with simple and reproducible kinetics, without complications from side reactions such as arene oxidation or arylsilane homocoupling. Second, only electron-rich arenes can be arylated intermolecularly, limiting the range of arene substituents that can be explored in linear free-energy relationships. In contrast, the intramolecular system tolerates a wide range of arene substituents, both electron-donating and electron-withdrawing, and the kinetics have been determined for substituents with σ- values ranging from −0.3 to +0.6. Third, relative to all of the other steps in the intermolecular catalytic cycle, reductive elimination from diarylgold(III) is fast. Consequently, it has not previously been possible to acquire kinetic data for this key C−C bonding-forming process. This is the case in many catalysed processes, and therefore kinetic data for reductive elimination under catalytically relevant conditions is sparse. The ability to monitor the reductive elimination from diarylgold(III) complexes **IV**/**V** in this study relies on the reaction being intramolecular. Not only does the short tether induce a high effective molarity which leads to rapid π-complexation, it also restricts the conformational freedom of the aromatic rings to attain the required face-to-face arrangement and thus reduces the rate of reductive elimination relative to the other steps in the cycle. The combination of these two processes is sufficient to cause reductive elimination to be the TLS in many cases. Therefore, for the first time, the effect of aryl electronics on the rate of reductive elimination has been demonstrated through Hammett LFER studies, with a reaction constant of $\rho = -2.0$.

Competition experiments exclusive to intramolecular coupling allowed for investigation into other steps in the catalytic cycle that are not turnover limiting. In particular, new insights into the mechanism of C-H auration were attained through KIE experiments and arene competition reactions. Strong evidence of an S_EAr metalation mechanism was attained through the measurement of the reaction constant for metalation ($\rho = -4.8$) and the attenuation of the observed KIE when resonance stabilisation of the WI (**III**) can occur.

However, the elucidation of this mechanism relied on the understanding of complex off-cycle processes. Indeed, electron-deficient silanes suffer from low reactivity under the standard conditions and examples of the unusual kinetic profiles obtained are shown in Figure 3.3. These effects were bypassed through the addition of a π-rich arene, 2-bromothiophene, and allowed for the on-cycle mechanism to be explored. The following chapter provides a detailed investigation into the cause of this reactivity, and through the combination of experimental studies and kinetic simulation, a novel, off-cycle mechanistic pathway resulting from catalyst deactivation is proposed.

4. Catalyst Deactivation Mechanisms

ABSTRACT: Chapter 4

A novel catalyst inhibition pathway is uncovered whereby initial catalyst deactivation is reversed by the product of the reaction. This auto-reactivation pathway results in unique kinetic profiles, and reactions with extreme sensitivity to both substrate and catalyst concentrations. Several mechanistic hypotheses are proposed to explain the observed data, and simulation software is employed to distinguish between models that cannot kinetically explain the results from those that can. Water is identified as the source of catalyst inhibition, and elimination of this results in significantly improved rates of reaction. Catalyst deactivation is also identified in the cyclisations of allocolchicine precursors. An entirely different catalyst deactivation pathway is proposed and results from the formation of a highly active inhibitor from the reaction of the starting material with the oxidant.

The results presented in section 4.5 of this Chapter have been communicated: T. J. A. Corrie, G. C. Lloyd-Jones, *Topics in Catalysis*, **2017**, *60*, 570.

4.1 Introduction

The aim of kinetic analysis is to uncover and detail the mechanism of a reaction, and by doing so, further optimisations, or inspirations for novel developments, may be possible. In catalysis, the turnover-limiting step is the key to understanding which components affect the rate of a reaction, and therefore the factors that govern this elementary step. The classical approach to uncovering the TLS is either through initial rate studies, or through pseudo first-order conditions, where the concentrations of other components are held artificially high whilst the rate dependence of a single component is measured. Whilst such methods do provide a route to determining the rate law and the TLS of a reaction, they do not provide a full picture of the whole reaction under synthetically relevant conditions.[136,137] The modernisation of analytical techniques has resulted in such approaches becoming redundant, as analysis of global kinetic profiles, through *in-situ* analysis or by sampling, is an attractive and viable alternative. Depending on the approach, the data obtained can be from differential methods, such as calorimetry, where rate is measured directly, or integral methods, such as NMR spectroscopy, where the change in concentration of a species can be monitored against time. If simple kinetics are observed, such as the pseudo-zero order profiles measured in this study, or clean pseudo-first order profiles, then trivial mathematical operations can be performed to extract rate constants. However, catalytic reactions can be complicated, indeed the dynamic nature of the solution resulting from changing concentrations of substrates can lead to varying importance of catalytic intermediates, and therefore the factors that govern the rate at the start of the reaction may be entirely different as the reaction comes to an end. It is only through the

monitoring of the entire reaction can such processes be identified. The presence of catalyst deactivation pathways and off-cycle processes can lead to significantly complex kinetic profiles, for which the cause can be difficult to untangle. Whilst hypotheses can be easily proposed, proving the exact mechanism of off-cycle processes is non-trivial. However, confidence in a mechanistic model can be attained through kinetic simulations, whereby agreement between computational and experimental results can serve to validate a model and indicate that a particular hypothesis is kinetically plausible.[136–138]

Catalyst deactivation is a deleterious and ultimately inevitable[139] process in any catalytic reaction whereby a catalyst loses its activity and productive turnover eventually ceases. The understanding of catalyst deactivation processes is vital, particularly in industrial cases where the efficiency of a process is key and even small amounts of catalyst deactivation can render a process inoperable. Catalyst deactivation can be caused by a number of different factors in both heterogeneous,[140–142] and homogeneous[139] catalysis, however the modes of catalyst deactivation in homogeneous catalysis are relatively under-studied. Factors that can cause catalyst deactivation in homogeneous catalysis include, amongst others, catalyst inhibition by a poison, ligand degradation and metal deposition.[139] The lack of research into modes of catalyst deactivation is likely due to such processes being overlooked. Indeed, in typical reaction screening techniques, several different catalysts or ligands at similar loadings will be left for an arbitrary amount of time and then product yields will subsequently be compared. Catalyst or ligands with poor conversions will often be discarded and those with good conversions further optimised. It is entirely possible, however, that the catalysts that lead to poor yields have a high activity and turnover frequency, but a low turnover-number due to deactivation. Only through analysis of temporal kinetic profiles can the cause of deactivation be identified, and the outcome of understanding deactivation can be a more active and stable catalyst.

4.2 Chapter Aims

In Chapter 3, the kinetic profiles associated with electron-deficient silanes were introduced. The kinetic profiles were highly complex, with three distinct regions, and significantly different to the pseudo-zero order profiles obtained when the silane was unsubstituted, indicating that catalyst inhibition was occurring. The aim of this chapter is to understand the cause of these unexpected profiles, and through kinetic simulation construct mechanisms that might explain the unusual behavior.

4.3 Initial studies

A common cause for catalyst deactivation is the presence of a poison or inhibitor, often introduced into the reaction due to impure starting materials, or generated during the reaction, that can react with the catalyst and prevent turnover. Depending on whether this reaction is reversible or irreversible, or where in the catalytic cycle the inhibition occurs, different kinetic profiles can be expected. This can be demonstrated with a basic simulation of a simple two step catalytic cycle where the first step is catalyst-substrate binding, and the second is product release (Figure 4.1). To reflect the conditions of intramolecular direct arylation, product release was assigned as the TLS. Two cycles were envisioned, with catalyst inhibition occurring at different stages in the cycle. Two simulations were run for each reaction, with inhibition being either reversible or irreversible.

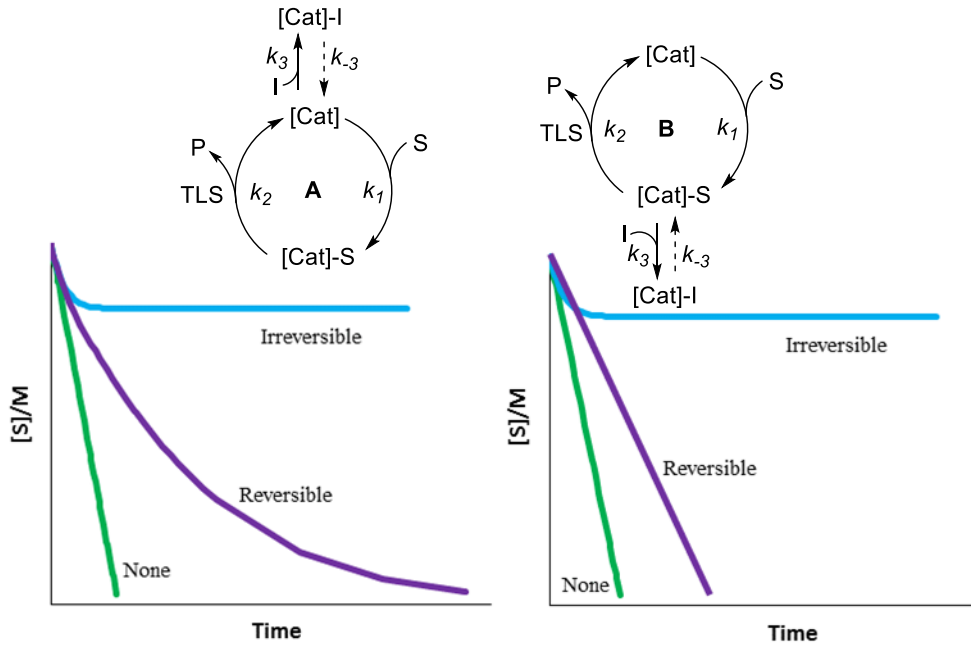

Figure 4.1. Hypothetical catalytic cycles **A** and **B** and expected kinetic profiles depending on presence and mode of catalyst inhibition.

The simulation was set with a constant concentration of inhibitor. In the absence of inhibition, pseudo-zero order profiles are obtained with rates dependent on k_2. When there is inhibition, and if it is reversible, curvature can be observed if cycle A is operating, with the extent of curvature dependent on the equilibrium constant (k_3/ k_{-3}) and the relative rate constants of inhibition and catalyst substrate binding (k_1 *vs* k_3). The origin of this curvature is due to the substrate concentration dependence in the inhibition pathway. As the reaction progresses, and the concentration of substrate decreases, the equilibrium position is affected, favouring the

catalyst-inhibitor species. In cycle B, this is not the case and instead pseudo-zero order profiles are maintained but the absolute rate of reaction is reduced. The rate is dependent on the equilibrium constant, and not the absolute values of k_3 and k_{-3} provided k_2 is not an order of magnitude greater than k_3. When deactivation is irreversible, both reactions will eventually stall. The conversion at which the reaction stalls will depend on the catalyst concentration, and, depending on inhibition location, the k_1:k_3 or k_2:k_3 partition respectively.

Whilst these kinetic profiles can give an appreciation of the impact that different modes of inhibition can have, real systems are often significantly more complex. Indeed, in this study, the kinetic profiles obtained when EWGs are positioned on the silane *vs* the simple pseudo-zero order profiles when the arene is substituted must be due to significantly more complicated processes (e.g. Figure 4.2).

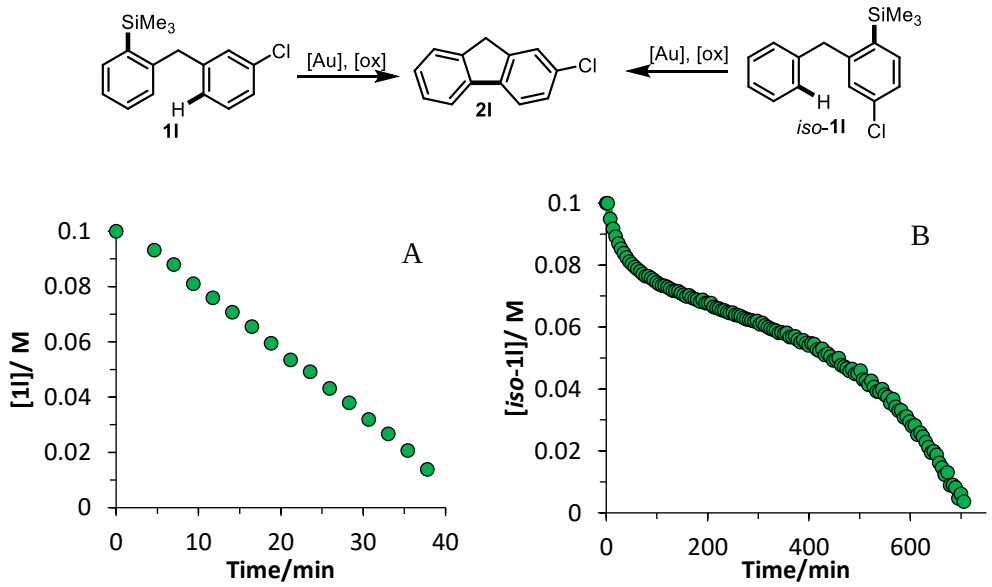

Figure 4.2. Comparison of kinetic profiles obtained when Cl is placed on: A) the arene and B) the silane. Conditions: Substrate (0.1 M), thtAuBr$_3$ (2 mol%), IBDA (0.11 M), CSA (0.13 M), $CDCl_3$/ CD_3OD (50:1).

It was of great interest to understand the cause of these unexpected profiles, and through kinetic simulation construct a mechanism to explain the unusual behavior. Prior to any simulation, an attempt to empirically rationalise the kinetic profiles was undertaken. In the first region of the kinetic profile, the initial rate is fast but rapidly decreases, consistent with catalyst deactivation. However, the reaction does not stall completely and, in the second distinct region of the curve, enters a pseudo-zero order regime for an extended time period. In the final part of the profile, the rate increases again, nearly reaching the initial rate. Based on

the reaction profile it was proposed that there is an initial, possibly irreversible, deactivation and that every catalyst turnover consumes a small percentage of the active species. If, however, the product that is generated is able to liberate the active catalyst from inhibition, this would allow for productive turnover to be restored once again. Based on this hypothesis, the addition of product at the beginning of the reaction should have a profound effect on the rate and kinetic profile and indeed that is what was found. The rate increased with increasing concentration of product with saturation at approximately 5 equivalents (Figure 4.3).

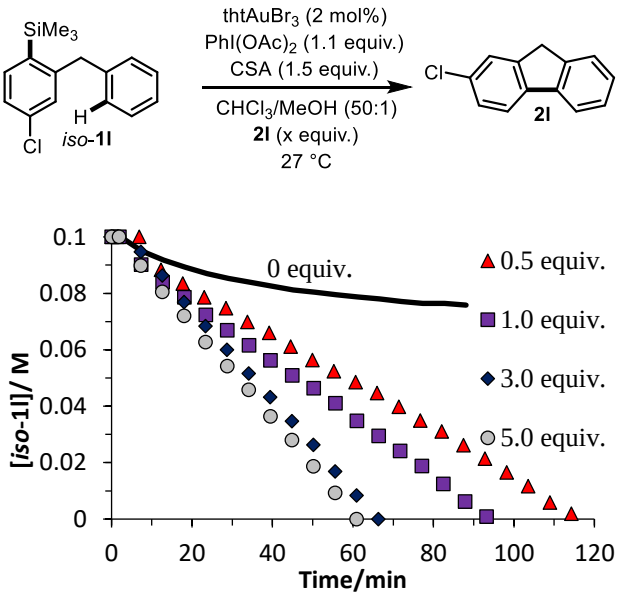

Figure 4.3. Effect of added product **2l** on the rate of turnover of *iso*-**1l**

At high product concentrations, pseudo-zero order kinetics were observed, with identical rates to the substituted arene example, consistent with reductive elimination as the TLS.

4.3.1 Source of Inhibition

Uncovering the source of the inhibition was vital for the construction of a successful model, because accurate concentrations for the inhibitor needed to be built into the simulation. Despite significant efforts, no impurity or side product could be identified to explain the observed kinetics. Trace impurities in the starting material silane were discounted as rigorous purification was undertaken, and the distinct kinetics were still observed across a range of substrates, and not one isolated case. In addition, careful analysis of the reaction mixture at the end of the reaction gave no indication of a side product that could explain the inhibition. It was eventually found that upon changing the batch of CSA, the extent of inhibition reduced significantly. The prior batch of CSA was found to be saturated with water, and placing this batch under a high vacuum for several hours, lessened the inhibition. Despite this observation,

attempts to prevent the inhibition by running the reaction under anhydrous conditions were unsuccessful, and this was found to be a result of water being generated as a co-product during the reaction. Under the standard reaction conditions IBDA and CSA are mixed to form the *in-situ* oxidants **62**/**63**, where presumably R=Me (**63**) under anhydrous conditions. However, it was found that the acetic acid that is generated from this reaction and the methanol co-solvent react to form methyl acetate and water in an acid-catalysed esterification (Scheme 4.1).

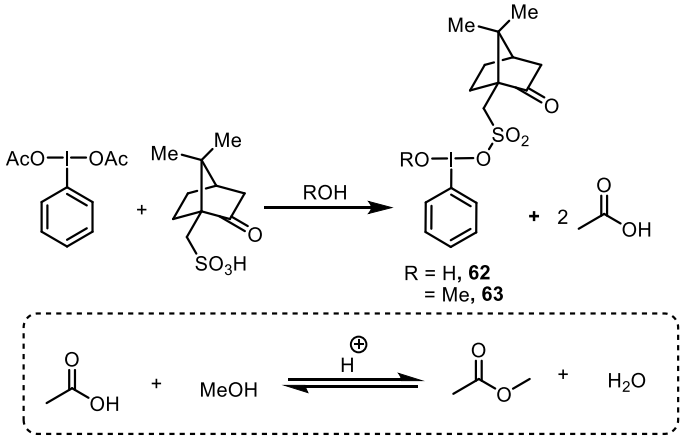

Scheme 4.1. Acid catalysed esterification leading to formation of water.

It was undesirable to include this equilibrium in subsequent simulations as it would be an additional source of error. Therefore, to simplify the system, IBDA and CSA were replaced with preformed oxidant, HCIB (R = H, **62**), to avoid the formation of acetic acid. Upon activation of the gold pre-catalyst, the oxidant will liberate an equivalent of water relative to the catalyst, and this could easily be built into any model. Deliberate addition of water at the start of the reaction led to a profound effect on the extent of deactivation, with more pronounced inhibition upon increasing water concentration (Figure 4.4).

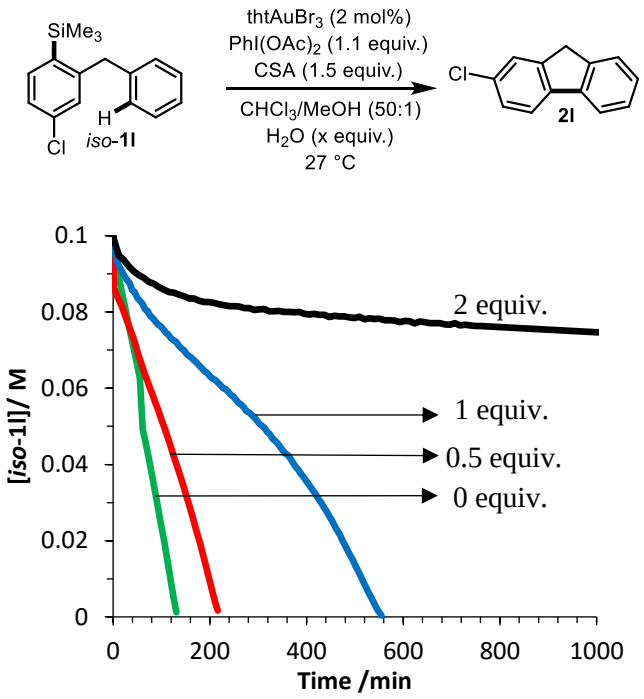

Figure 4.4. Effect of increasing H_2O concentration on inhibition of *iso*-**1l** to **2l**.

The deactivation was demonstrated to be reversible through the addition of 3 Å molecular sieves (MS) to the reaction. This is demonstrated in Figure 4.5 which displays the full kinetic profile when 2 equivalents of water are added to the reaction, and the effect of 3 Å MS, added after 15 h, to a repeat of this reaction.

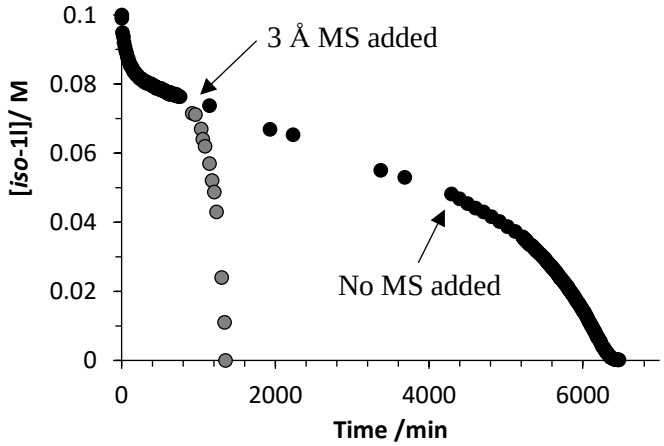

Figure 4.5. Full kinetic profile of addition of 2 equiv. of H_2O, and effect of addition of 3 Å MS to a repeat of this reaction.

In addition to water being an inhibitor, the oxidant was also found to be equally competent in inhibiting the reaction as water. Performing a Job-Plot type analysis, where the molar

concentration of HCIB and water is kept constant, but their mole fractions are varied, showed near identical kinetic profiles (Figure 4.6).

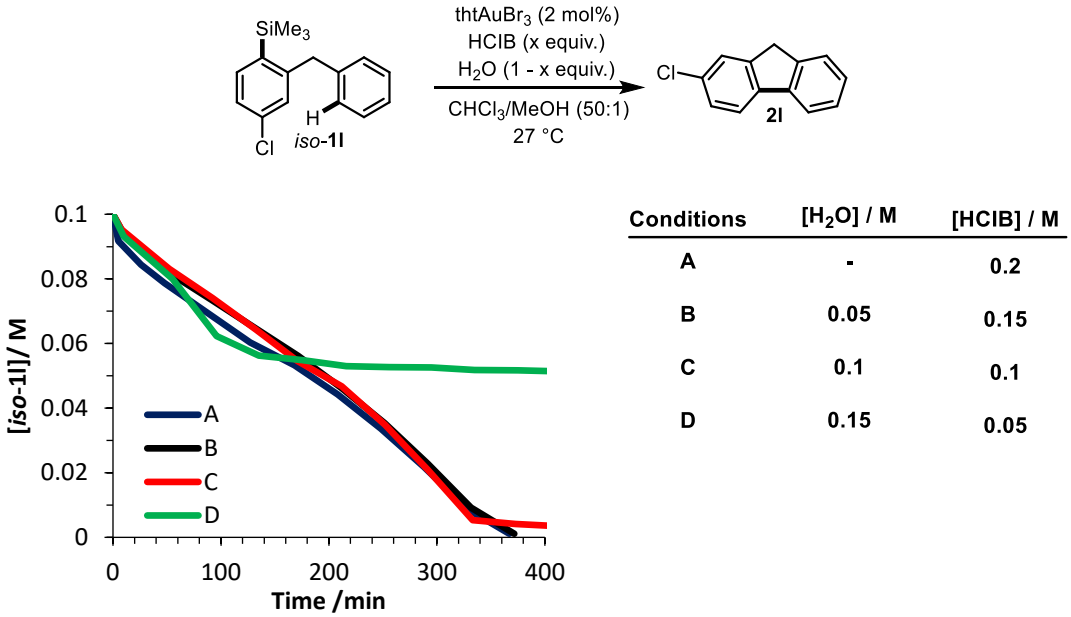

Figure 4.6. Effect of [H_2O] and [HCIB] on catalyst inhibition. Conditions: Substrate (0.1 M), thtAuBr$_3$ (2 mol%), $CDCl_3$/ CD_3OD (50:1).

Two plausible explanations for this observation are; 1) the oxidant behaves as an inhibitor with an identical ability to deactivate gold as water or; 2) The oxidant is in equilibrium with methanol, generating water, and therefore addition of HCIB leads to indirect addition of water. For the second hypothesis to be valid, the equilibrium must be biased towards the generation of water (Scheme 4.2).

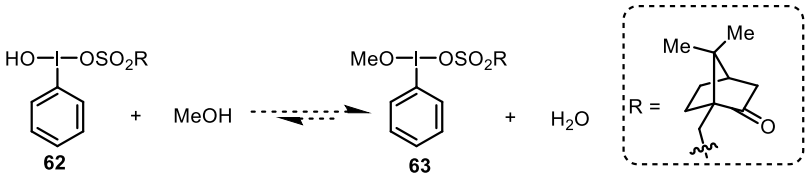

Scheme 4.2. Possible equilibrium to explain behaviour of **62** as an inhibitor.

4.4 Kinetic Simulations

With a reasonable hypothesis in hand, kinetic simulations[2] were then used to explore mechanisms for the proposed catalyst deactivation and off-cycle pathways. The catalytic cycle was simplified into a three-step process (Scheme 4.3). First, the gold(III) catalyst can react with the substrate (S), in the transmetalation step. This step must be set arbitrarily high, so as

[2] DynoChem 2011, version 4.1.0.0.

not to become fully or partially turnover-limiting. As reductive elimination is turnover-limiting, from a kinetic perspective it is unnecessary to include the steps in between transmetalation and reductive elimination. The second step, product release (reductive elimination), is the step that governs the rate of catalytic turnover in the absence of deactivation. The final step is re-oxidation of gold(I) to gold(III) to complete the cycle. Whilst the rate of this step is not kinetically significant, it is included in some cases (*vide infra*), the oxidant is the limiting reagent.

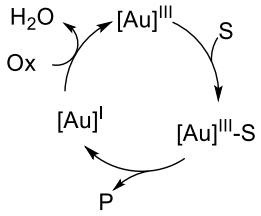

Scheme 4.3. Basic catalytic cycle to be simulated.

4.4.1 Model A

Model A was the first system tested to explain the observed kinetics (Scheme 4.4). The hypothesis was that at the beginning of the catalytic cycle the catalyst ($[Au]^{III}$) can partition between the substrate (S) (leading to productive catalysis) and an inhibitor (I), where I = H_2O, Oxidant (**62**). The catalyst-inhibitor complex ($[Au]^{III}$-I) is inactive but upon reaction with product (P) the active catalyst can be released. As no side product was isolated, a ligand displacement, rather than a chemical reaction, was preferred. The inhibition was placed at this point in the catalytic cycle to allow a competition between inhibition and transmetalation. The transmetalation rate of aryltrimethylsilanes is reduced when EWGs are in place,[83] and thus inhibition will be maximised when the silane is electron-deficient, consistent with the observation that only electron-deficient silanes exhibit these unusual processes.

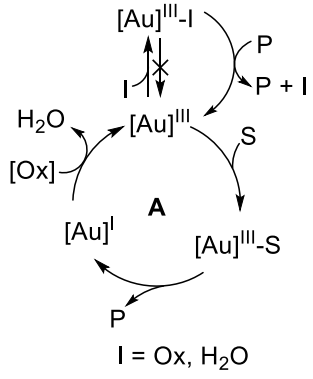

Scheme 4.4. Model A

The reaction used to test the model was the cyclisation of *iso*-**1l** to **2l**. In this reaction, one equivalent of water was deliberately added at the start of the reaction, with HCIB as the oxidant. However, the kinetic simulation was in poor agreement with experiment (Figure 4.7). Whilst the simulation was able to correlate with the experimental data initially, the end of the reaction gave a very poor fit and this is as a result of the expected dependence of the partition on substrate concentration. With decreasing concentration of substrate, partitioning to the catalyst-inhibitor complex would be maximized.

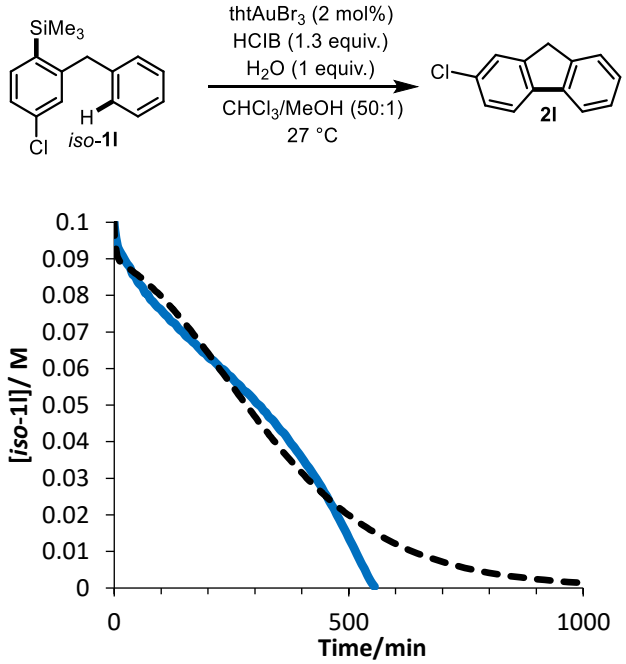

Figure 4.7. Simulated fit (dashed lines) to experimental data of conversion of *iso*-**1l** to **2l** using Model A.

4.4.2 Model B

To eliminate the dependence of the deactivation mechanism on the substrate concentration, Model B was generated. In Model B, the deactivation is moved to another point in the catalytic cycle, and by doing so removes dependence on the starting material in the deactivation mechanism. Although the fit was not perfect, it was a significant improvement to that obtained with Model A (Figure 4.8).

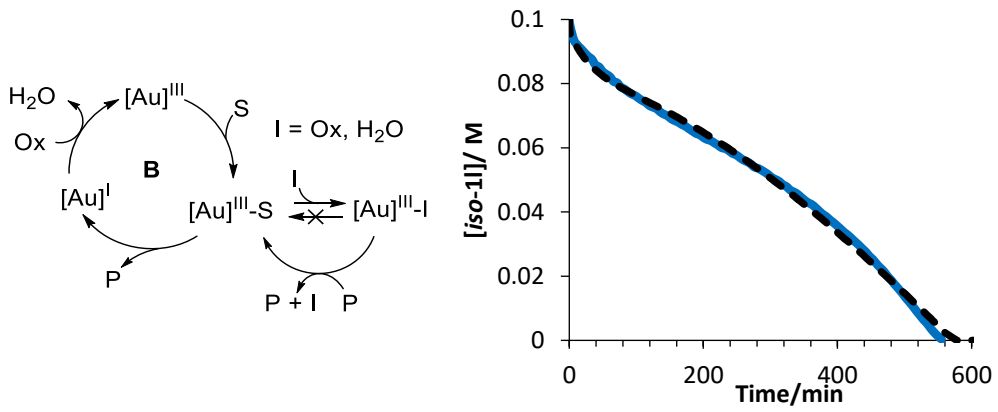

Figure 4.8. Simulated fit (dashed lines) to experimental data of conversion of *iso*-**1l** to **2l** using Model B.

To validate the model, further experiments were necessary. Indeed, a requirement of Model B is that a change in substrate concentration should not impact on the rate, or the overall appearance of the reaction profile. To test this hypothesis, the reaction was repeated under identical conditions apart from a 3-fold increase in substrate concentration. Model B predicts no change in the overall profile, however this was not observed and a significant rate increase was measured when higher substrate concentrations were employed (Figure 4.9). This observation cannot be explained using Model B, and is in fact more consistent with Model A, where an increase in starting material concentration will increase the rate of the partition favouring productive catalysis. In Model A, the deactivation is clearly in the correct part of the cycle, but the simulation demonstrates that there must be additional processes present.

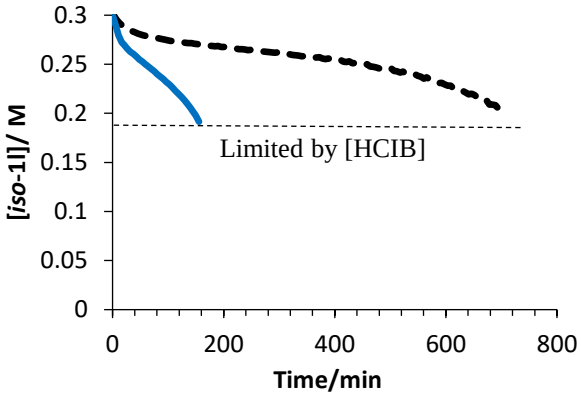

Figure 4.9. Simulated fit (dashed lines) to experimental data of conversion of *iso*-**1l** to **2l** at higher substrate concentrations using Model B. Limiting [oxidant] prevents further turnover.

4.4.3 Model C

Model A was augmented to provide the more complex Model C (Scheme 4.5). The hypothesis was that the product of the reaction had a dual role. Firstly, to displace the inhibitor from the catalyst and secondly to behave as a ligand to prevent further inhibition from occurring. Therefore, toward the end of the reaction when the substrate concentration is low, but product concentration is high, the inhibition pathway is effectively bypassed due to the stabilisation effect of the product on the catalyst. The simulation (Figure 4.10) gave an excellent fit to the experimental data based on the rate constants shown in Table 4.1, indicating that this model might be a better representation of the off-cycle pathways.

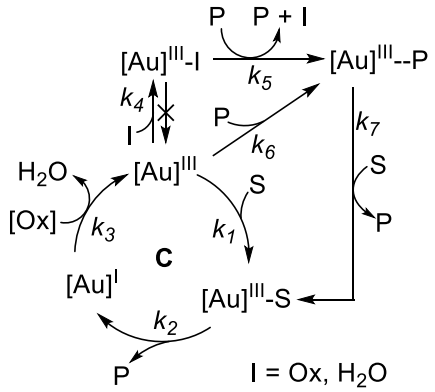

Scheme 4.5. Model C.

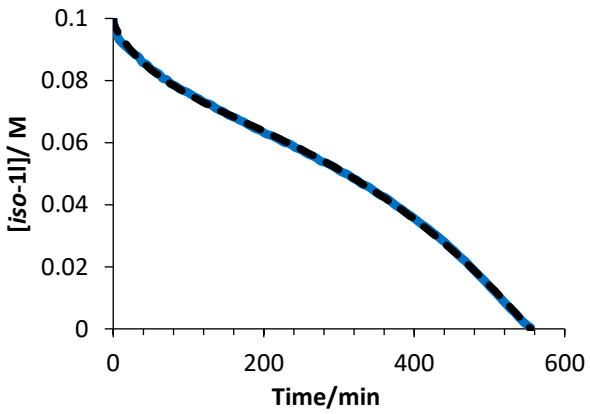

Figure 4.10. Simulated fit (dashed lines) to experimental data of conversion of *iso*-**1l** to **2l** using Model C.

Table 4.1. Rate constants for which the optimum fit to experimental data is obtained using Model C for conversion of *iso*-**1l** to **2l**.

Entry	Rate constant	Value	Standard Error
1	k_1	160 dm^3 mol^{-1} s^{-1}	30
2	k_2	0.0069 s^{-1}	7×10^{-4}
3	k_3	10000 dm^3 mol^{-1} s^{-1}	-
4	k_4	19 dm^3 mol^{-1} s^{-1}	1
5	k_5	4.7×10^{-4} dm^3 mol^{-1} s^{-1}	7×10^{-5}
6	k_6	8000 dm^3 mol^{-1} s^{-1}	1500
7	k_7	1000 dm^3 mol^{-1} s^{-1}	10000

4.4.4 Chemical Justification of Model

Whilst model C gives a plausible mechanistic pathway that explains the observed kinetics, it does not explain *why* such a deactivation process occurs. The inhibition kinetics observed in this study are unique, and there has been no other example of reactivation of a catalyst species by the product of said reaction reported in the literature to date. These kinetics are solely observed in the intramolecular reaction, and not detected in the intermolecular variant. A plausible explanation for this observation is the instability of the catalyst species in the absence of π-rich arenes. Due to the absence of strongly defined ligands, the ligand environment is possibly dynamic and changes depending on the electronic demand on each step of the cycle. π-Rich arenes possibly behave as L-type ligands in the form of π-complexes, and in their absence, it is likely that σ-donors such as water bind. If water bound as a ligand deactivates the catalyst, then the absence of π-rich arenes would be detrimental. In the intermolecular direct arylation, π-rich arenes are employed as substrates anyway, and therefore would prevent deactivation. However, by rendering the process intramolecular, due to the short tether length, and thus increased effective molarity of the arene moiety, substrates that otherwise would not react (i.e. non-π-rich arenes) are able to. Therefore, at the start of the reaction, there are no π-rich species and the gold species may be prone to deactivation. Fundamentally, the product of cyclisation, a substituted fluorene (e.g. **2l**), is π-rich, and therefore a stabilising ligand is

generated during the reaction, and able to recover any deactivated catalyst in an auto-reactivation process.

4.4.5 Validation of the Mechanistic Model

Although the simulation gave an excellent fit to the data for *iso*-**1l**, the model is quite complex, with several rate constants. Indeed, with enough freedom, any elaborate model will be able to fit a single set of data. This is emphasised in the large standard errors obtained from the simulation of data from the cyclisation of *iso*-**1l**. To validate the model, not only must it be chemically plausible, it must also fit over multiple data sets. The results from the simulation indicated that the reaction would have a large sensitivity to both catalyst and substrate concentration. Due to the length in which the reactions took with substrate *iso*-**1l** it was not convenient to systematically measure the effect of concentration with this substrate. Therefore, the reaction of substrate *iso*-**1k**, where turnover is faster, but similar kinetic profiles are obtained, was monitored. Using Model C, an excellent fit to across 6 different conditions using a single set of rate constants was obtained. This fit is excellent support that a mechanism resembling Model C is operating.

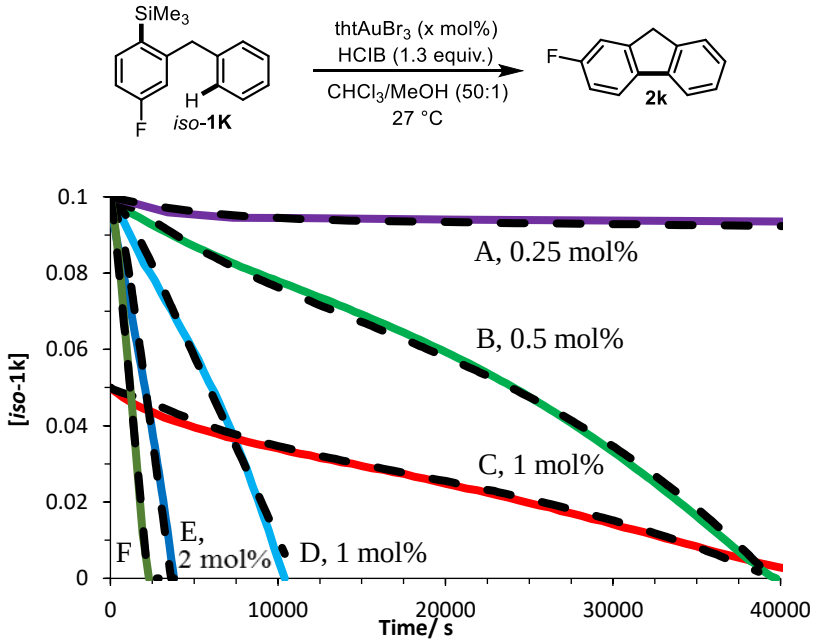

Figure 4.11. Simulated fit (dashed lines) to experimental data of conversion of *iso*-**1k** to **2k** using Model C. Conditions: HCIB (0.13 M), $CDCl_3$:CD_3OD (50:1) and; A: *iso*-**1k** (0.1 M), $thtAuBr_3$ (0.00025 M, 0.25 mol%); B: *iso*-**1k** (0.1 M), $thtAuBr_3$ (0.0005 M, 0.5 mol%); C: *iso*-**1k** (0.05 M), $thtAuBr_3$ (0.0005 M, 1 mol%); D: *iso*-**1k** (0.1 M), $thtAuBr_3$ (0.001 M, 1 mol%); E: *iso*-**1k** (0.1 M), $thtAuBr_3$ (0.002 M, 2 mol%); F: *iso*-**1k** (0.1 M), $thtAuBr_3$ (0.002 M, 2 mol%), 2-bromothiophene (0.5 M).

Table 4.2. Rate constants for which the optimum fit to experimental data is obtained using Model C for conversion of *iso*-**1k** to **2k**.

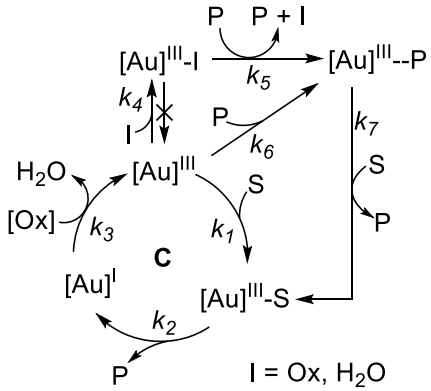

Entry	Rate constant	Value	Standard Error
1	k_1	0.032 dm^3 mol^{-1} s^{-1}	5×10^{-4}
2	k_2	0.024 s^{-1}	0.01
3	k_3	1000 dm^3 mol^{-1} s^{-1}	-
4	k_4	0.0031 dm^3 mol^{-1} s^{-1}	7×10^{-4}
5	k_5	4.7×10^{-4} dm^3 mol^{-1} s^{-1}	2×10^{-5}
6	k_6	3.22 dm^3 mol^{-1} s^{-1}	0.3
7	k_7	1000 dm^3 mol^{-1} s^{-1}	-

*Includes unimolecular precatalyst activation rate constant k_{precat} = 0.0042 s^{-1}

The most extreme effects are observed for the cyclisation of **1p** to **2p**, where the effect of changing both catalyst and substrate concentration is profound (Figure 4.12). Indeed, reaction times were increased by a factor of 40 when quartering the catalyst loading from 2 mol% to 0.5 mol%, 10 times more than what would be expected in the absence of deactivation. Perhaps more striking, and counterintuitive, is the effect of substrate concentration. Performing the reaction over 4 substrate concentrations, keeping the catalyst concentration constant, demonstrated that the reaction which had to do the most turnovers (0.2 M substrate, 0.001M catalyst = 0.5 mol%, >100 turnovers) was complete before the reaction which had to do the

fewest (0.01M substrate, 0.001 M catalyst = 10 mol%, 10 turnovers) had completed just a single turnover.

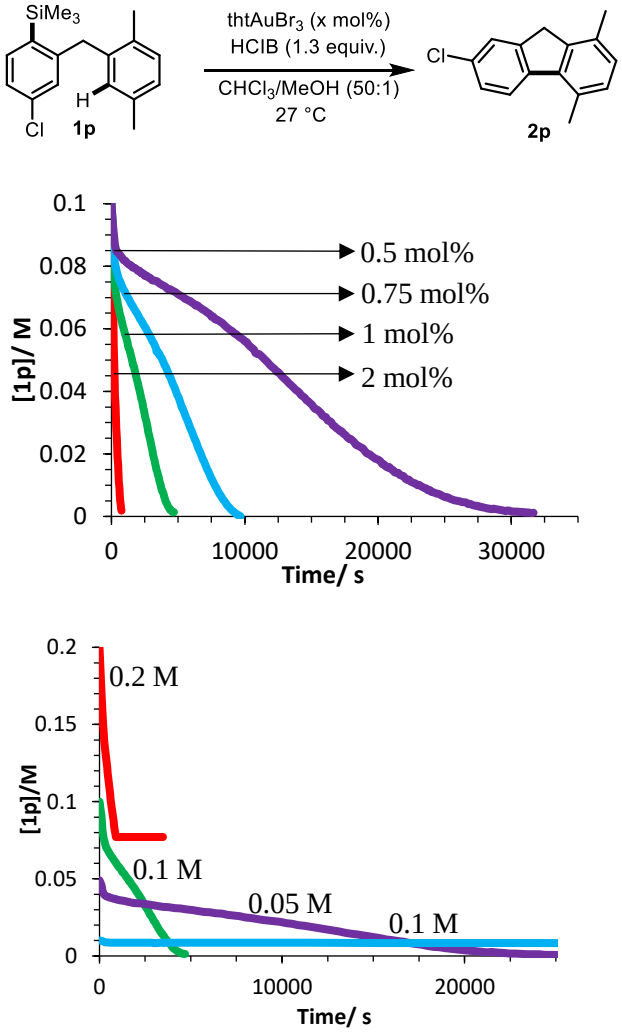

Figure 4.12. Top: Effect of varying catalyst concentration at a fixed [**1p**] (0.1 M)**.** Bottom: Effect of [**1p**] at a fixed [catalyst] (0.001 M).

These results emphasise the need for careful consideration of both catalyst and substrate concentration in screening of reaction conditions. If catalyst a deactivation mechanism similar to the process demonstrated herein occurs in other reactions, the difference between success and failure could be determined by a choice of catalyst loading, or initial substrate concentration, or both.

4.4.6 Re-optimisation of Reaction Conditions

With the knowledge that water was the source of inhibition, efforts were made to alter the system so that no catalyst deactivation occurred and maximum rates were achieved. Whilst the addition of product or a π-rich arene to the system removed deactivation, this was not a

sustainable solution. It was envisioned that replacing the methanol co-solvent with TFE could be a potential solution. As previously mentioned, the addition of IBDA and CSA in the presence of methanol leads to the production of water through an acid catalysed esterification of the resultant acetic acid. TFE is significantly more acidic than methanol, and therefore this esterification is unlikely to occur (Scheme 4.6).

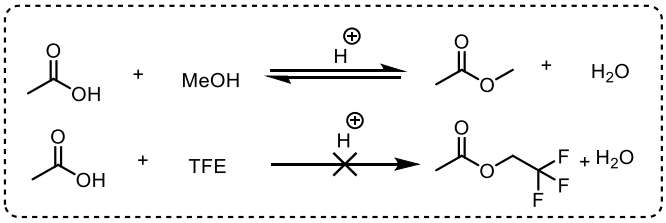

Scheme 4.6. Replacement of methanol with TFE should avoid production of water.

That is indeed the case, as the replacement of methanol with TFE eliminates the catalyst deactivation and restores rapid rates. This is emphasised in the synthesis of **2l** which takes approximately over 11 hours to go to completion under standard conditions due to catalyst deactivation, but when TFE is employed takes just 25 minutes (Figure 4.13).

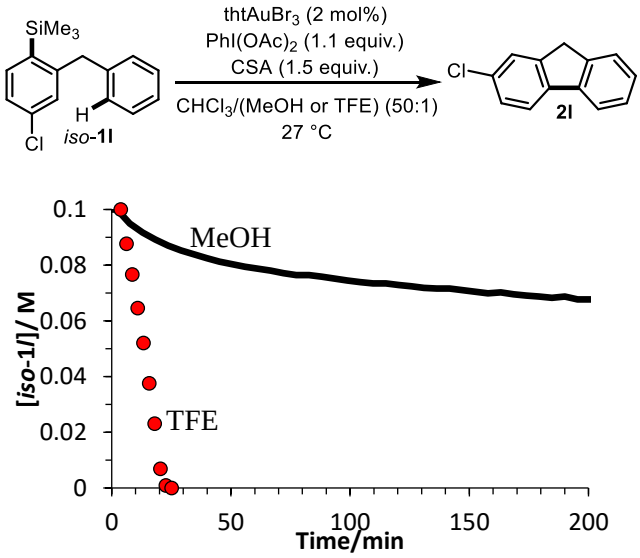

Figure 4.13. Comparison of rate when methanol is replaced with TFE as the co-solvent.

4.5 Catalyst Deactivation in Natural Product Synthesis

In Chapter 2, the formal synthesis of allocolchicine was presented. Despite good yields and short reaction times in the arylation step of model substrate **5k**, the inclusion of a chlorine *para* to the silane in the formal synthesis led to reduced yields and increased reaction times (Scheme 4.7).

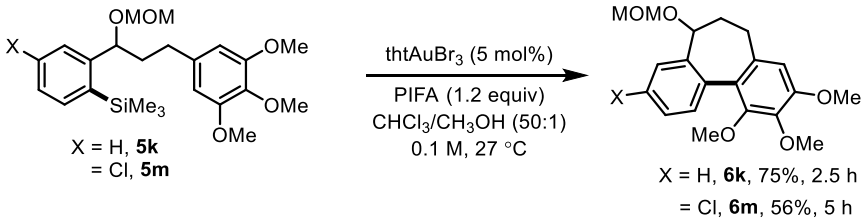

Scheme 4.7. Effect of electron-deficient silane on yield and reaction time in synthesis of allocolchicine skeleton.

As demonstrated in the first part of this chapter, electron-deficient silanes can cause catalyst inhibition. However, the strategies that eliminated the inhibition (i.e. addition of 2-bromothiophene or replacement of methanol with TFE) did not lead to improved yields in the synthesis of this scaffold. Therefore, another process must be causing the reduced efficiency. Indeed, a catalyst auto-reactivation mechanism would not be expected as electron-rich arenes were shown to prevent inhibition, and these substrates bear a highly electron-rich moiety. To probe the cause of the difference between **5k** and **5m**, and to gain an understanding of the implications of using these complex molecules in the direct arylation reaction, the kinetics of cyclisation were monitored (Figure 4.14). The observed kinetics are indicative of severe catalyst deactivation as both reactions stall with significant amounts of starting material remaining, with the reaction of **5m** stalling significantly earlier than **5k**, with only *ca.* 20% conversion.

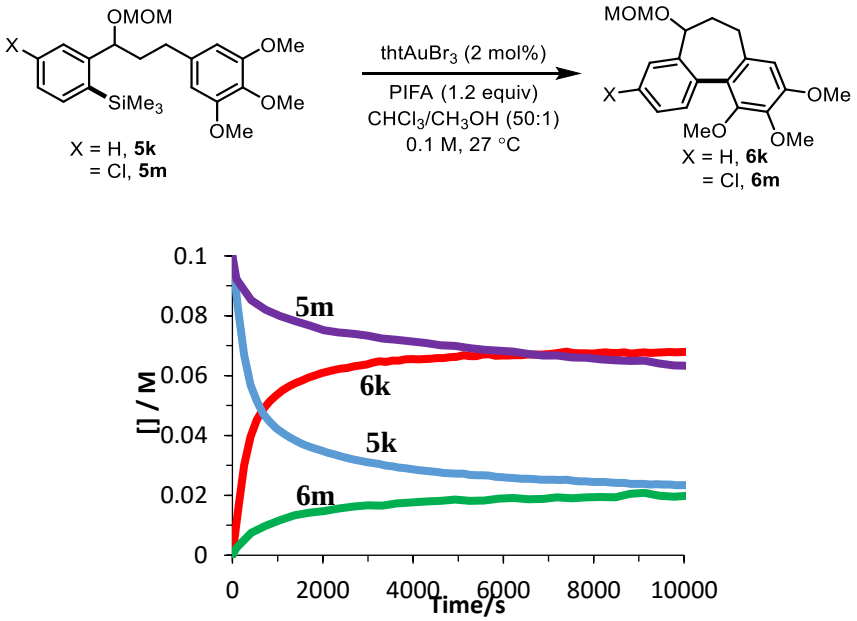

Figure 4.14. Comparison of kinetic profiles of the cyclisation of **3** and **11**.

In order to assess whether the deactivation is innate to the PIFA system, or as a result of the substrate, the kinetics of cyclisation of 'defunctionalised' **5a** were monitored (Figure 4.15). Although PIFA was used successfully in other substrates, reaction times were short and a full kinetic examination was not undertaken. Therefore, there could be a deactivation process unique to PIFA. The rate of cyclisation of **5a** is very slow compared to the initial rate of **5k** and **5m**, emphasising the impact of the highly reactive arene in **5k**, **5m**. However, the kinetic profile appears broadly *pseudo*-zero order and there is no indication of severe catalyst deactivation.

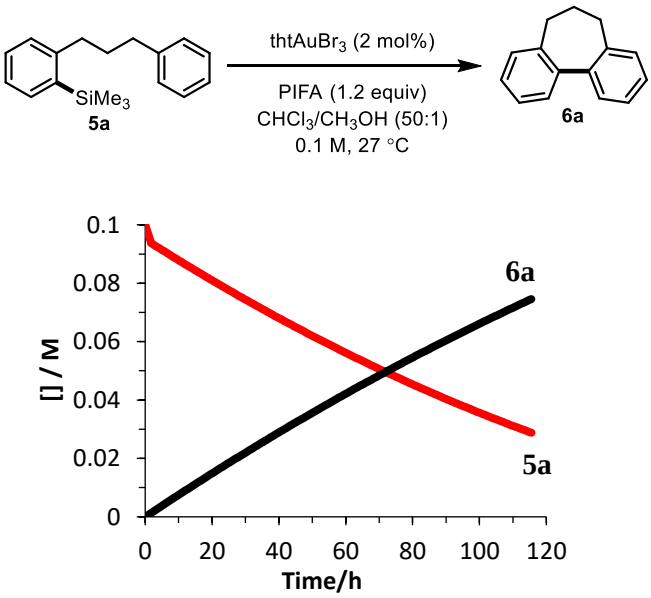

Figure 4.15. Kinetic profile of the cyclisation of **5a** to **6a**.

The difference in substrate structure between **5k** / **5m** and **5a**, is the absence of both the MOM ether and a highly electron-rich arene in **5a**, suggesting that the cause of deactivation is due to the presence of one or both of these functional groups. A generic catalyst deactivation mechanism was considered (Scheme 4.8). Here, a side-reaction, involving the sidechain ('Z') functionality, converts substrate (**5k** or **5m**) into an inhibitor (**105**), which then undergoes competitive transmetalation with the gold to generate an off-cycle complex **106**. If this species is unable to cyclise to **107**, or to reductively eliminate the biaryl product, and thus unable to release gold back on-cycle, then progressive catalyst inhibition will occur. The impact of the inhibition process will depend on the relative rate of reaction of substrate (**5k** / **5m**) *versus* the inhibitor (**105**) with the Au(III).

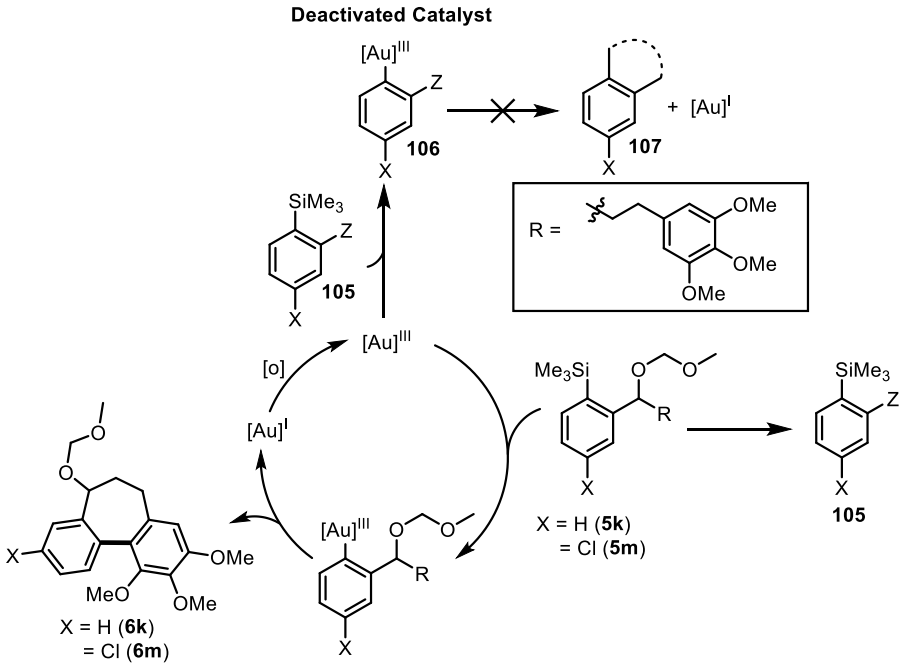

Scheme 4.8. General deactivation mechanism due to side product formation.

Initial concerns related to the lability of the MOM protecting group. Due to the acidic nature of the reaction medium, an *in-situ* deprotection of the MOM group back to **5g** or **5l** could occur (Scheme 4.9).

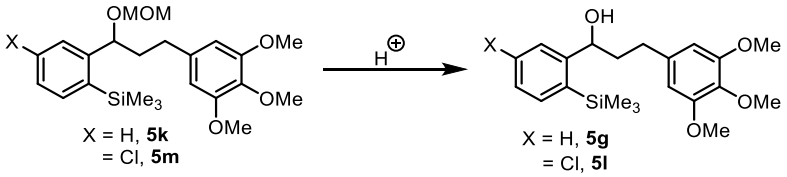

Scheme 4.9. Possible *in-situ* deprotection of MOM protecting group under the reaction conditions

As noted in Chapter 2, neither **5g** nor **5l** undergo cyclisation. Moreover, inclusion of a sub-stoichiometric amount of alcohol **5l** in the reaction of **5k** resulted in an even earlier onset of catalyst inhibition (Figure 4.16).

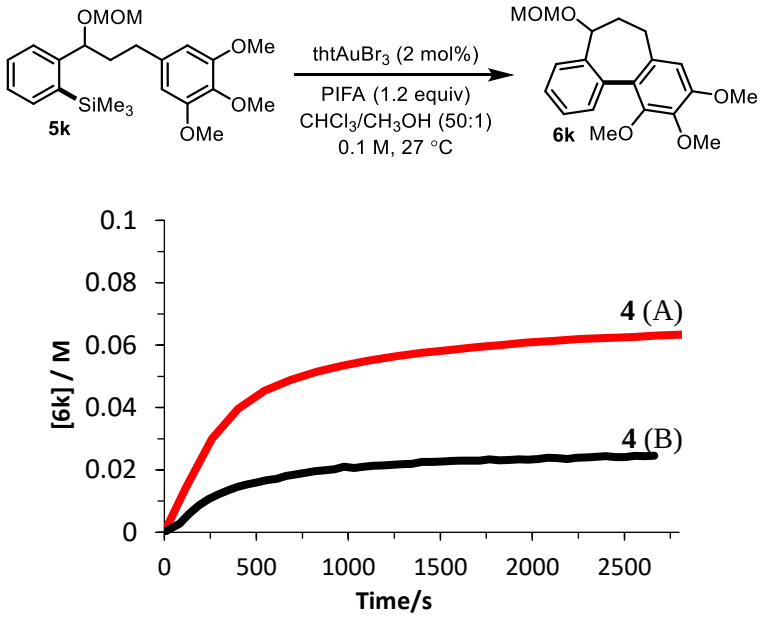

Figure 4.16. Cyclisation of **5k** under: A) standard conditions; B) with 10 mol% **5g** added at the start of the reaction.

Whilst this confirms that alcohol **5g** can act as a catalyst poison, possibly by competition with **5k** for the catalyst, and then strong off-cycle Au-chelation (**108**, Scheme 4.10), **5g** could not be isolated from the reaction, or detected *in-situ*. Consequently, the kinetics of cyclisation of the acid stable methyl ether **5h** were monitored, with the expectation that no catalyst deactivation would occur if MOM deprotection is required for inhibition. However, **5h** was found to undergo the same potent inhibition; indeed the initial rate and overall conversion (Figure 4.17) was even lower than with the MOM ether substrate, **5k**.

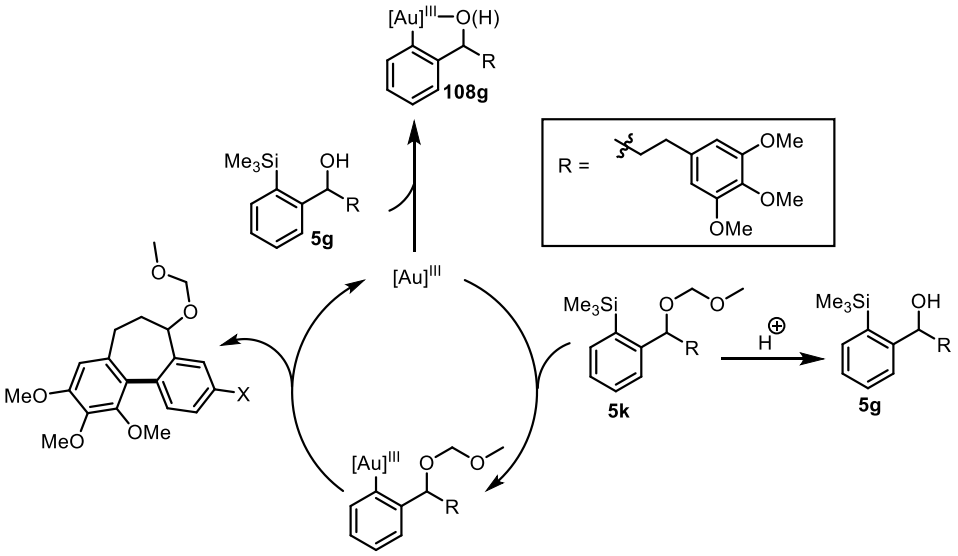

Scheme 4.10. Possible mechanism for deactivation by alcohol **5g**.

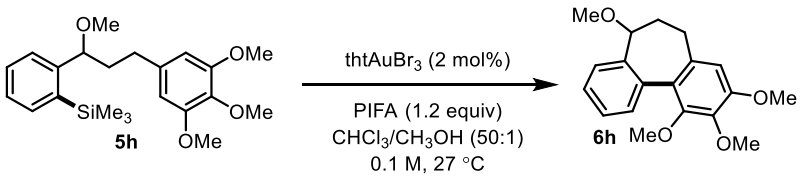

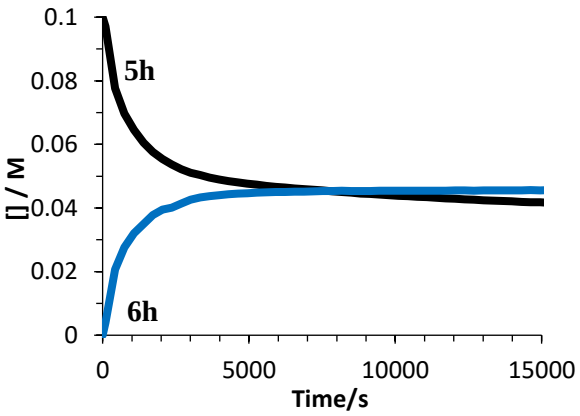

Figure 4.17. Kinetic profile for cyclisation of **5h** showing deactivation is still present without MOM protecting group.

Product inhibition of the catalyst was excluded by addition of the product to the reaction, which resulted in no detrimental effect to the rate. Therefore, efforts were made to identify side products in the reaction mixture that might behave as inhibitors. Whilst the reactions afforded satisfactory material balance, small quantities of side-products (**109a-c**) were identified by NMR spectroscopy. The rate of formation of these side products was largely independent of the substrate (Figure 4.18). Careful *in-situ* analysis of the reactions of **5h**, **5k**

and **5m** by ^{1}H NMR indicated that **109a-c** are diaryliodonium salts; this was subsequently confirmed by mass spectrometry.

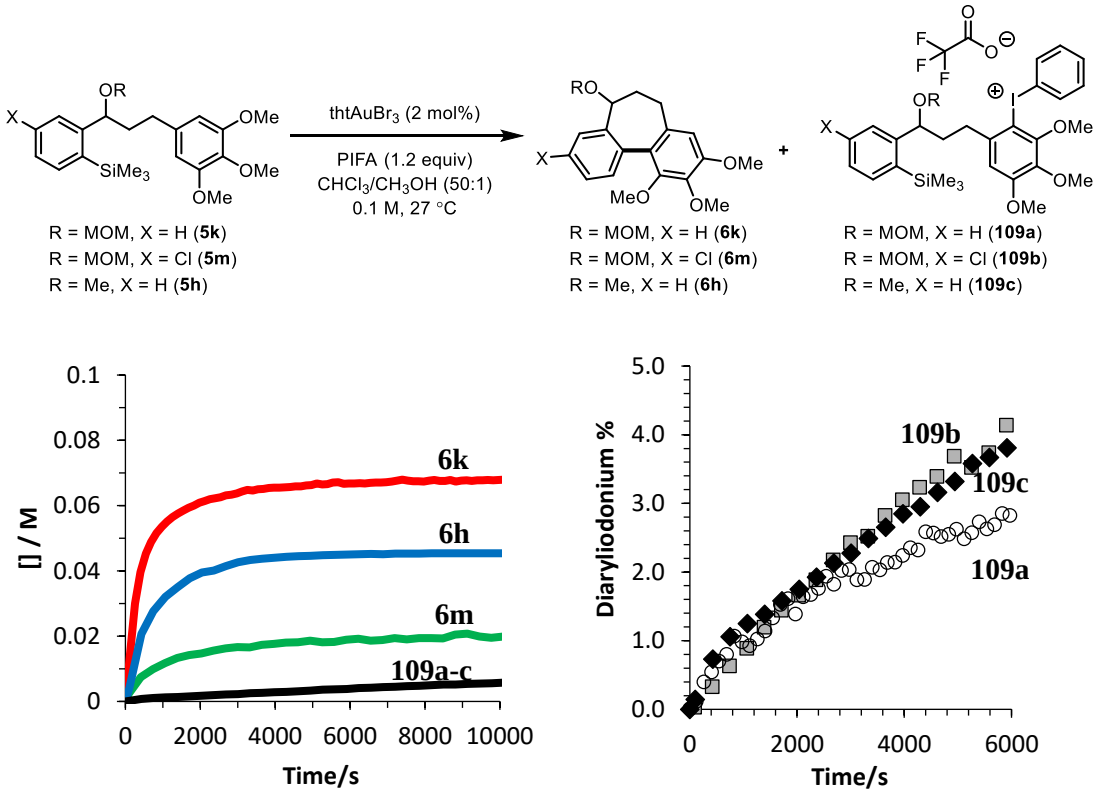

Figure 4.18. Formation of side products **109a-c** under the reaction conditions.

To assess whether the formation of these side products are connected to the deactivation, substrate **5k** was exposed to PIFA prior to addition of catalyst to allow for a build-up of **109a**. Significantly greater catalyst deactivation was observed when **109a** is present from the outset, thus strongly linking the reaction of the starting material with PIFA to the catalyst deactivation process (Figure 4.19).

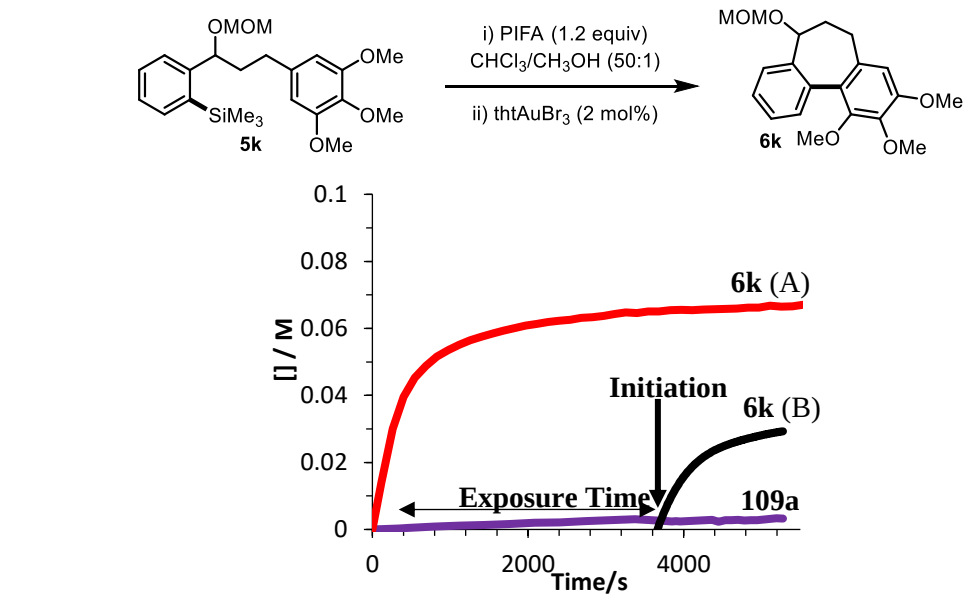

Figure 4.19. Cyclisation of **5k** under: A) standard conditions; B) with premixing of substrate **5k** and PIFA before initiating reaction.

On the basis of steric hindrance and reduced electron density on the arene ring, diaryliodonium generation would be expected to deactivate the trimethoxy-arene ring in aurated intermediates to aromatic electrophilic substitution (**110a-c** to **111a-c**), and thus prevent release of gold (Scheme 4.11). Therefore, it would not be the diaryliodonium salt generation *per se* that is poisoning the catalyst, but the result of tethering this salt to an arylsilane that can still undergo reaction with the gold catalyst (**109a-c** → **110a-c**).

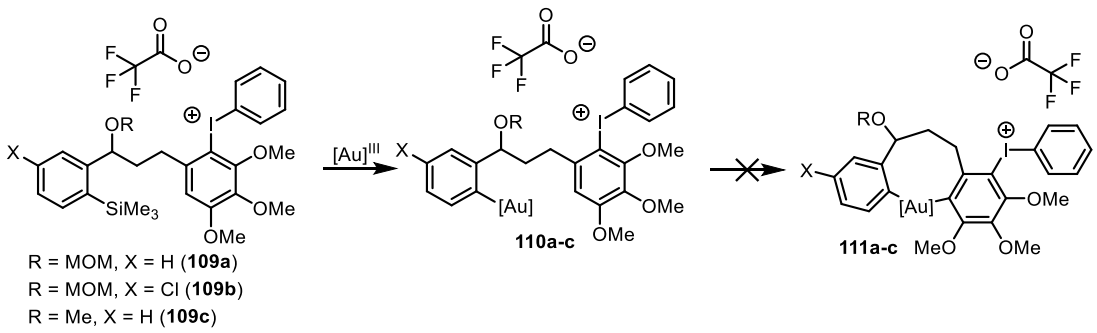

Scheme 4.11. Tentative assignment of catalyst inhibitor, and associated deactivation pathway.

To verify that the tethering of the silane to the diaryliodonium salt was instrumental to the deactivation and not an effect of diaryliodonium salts in general, trimethoxytoluene, **89**, was allowed to react with PIFA to form the diaryliodonium, **90** (Scheme 4.12). Addition of this to the reaction of **5k** did not have any additional adverse effect on the reaction, demonstrating

that the tethering of the silane is crucial in the proposed deactivation mechanism (Scheme 4.13).

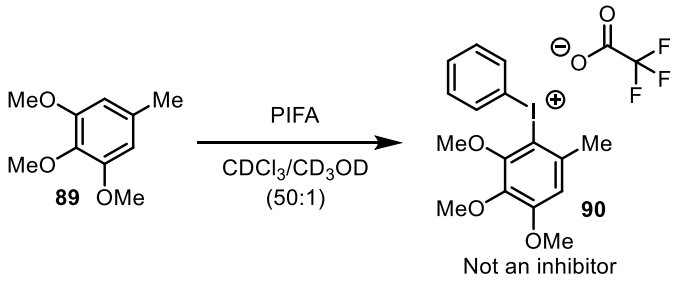

Scheme 4.12. Control experiment for diaryliodonium salts as general catalyst poisons.

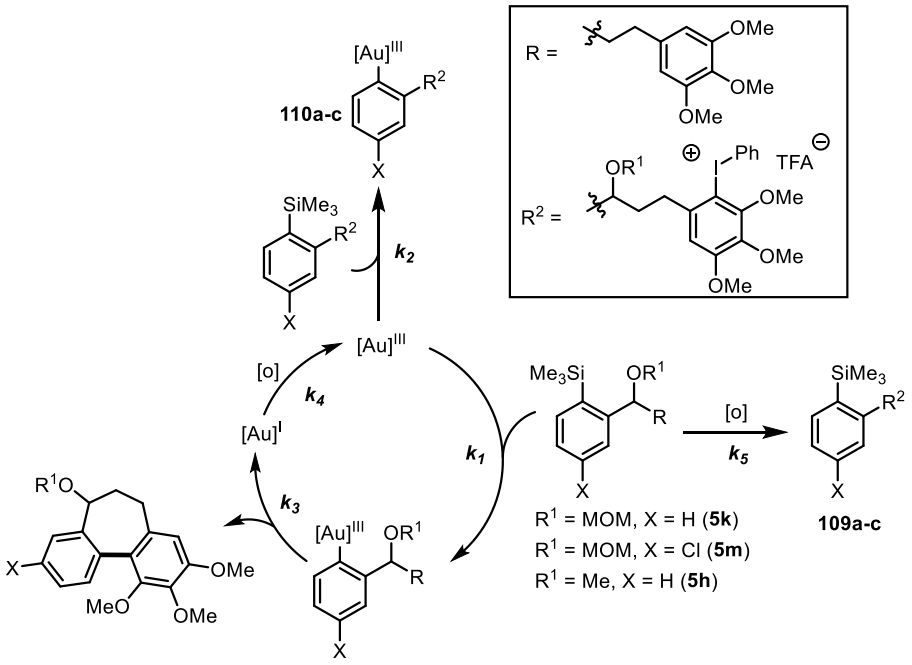

Scheme 4.13. Proposed deactivation mechanism.

This deactivation mechanism is consistent with the experimental observation that absolute rate of cyclisation is an important factor in dictating the final conversion (Figure 4.18); a feature that is not general in catalyst deactivation. As shown in Figure 4.18, the initial rate of inhibitor formation is independent of the identity of the substrate, as would be expected if there is no significant influence of the aryl silane at the end of the tether on the rate of reaction of the trimethoxybenzene ring with the oxidant. The impact of this is that the cyclisations that proceed with the fastest absolute rate will have the lowest percentage of inhibitor at a given time, and therefore will suffer least inhibition and attain greatest conversion before stalling (Scheme 4.14).

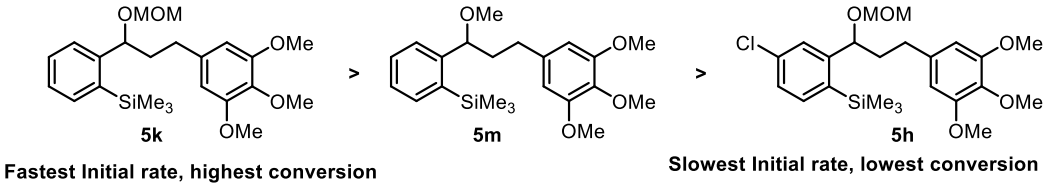

Scheme 4.14. Reactivity and conversion trend.

The difference in turnover rate between MOM-protected **5k**, methyl ether **5m**, and alcohol **5g**, can be tentatively attributed to the coordinating ability of the oxygen *ortho*- to the silane. If the oxygen can coordinate to the catalyst after the transmetalation (Scheme 4.15), this could serve to slow π-complexation of the arene to the gold, and thus the rate of cyclisation.

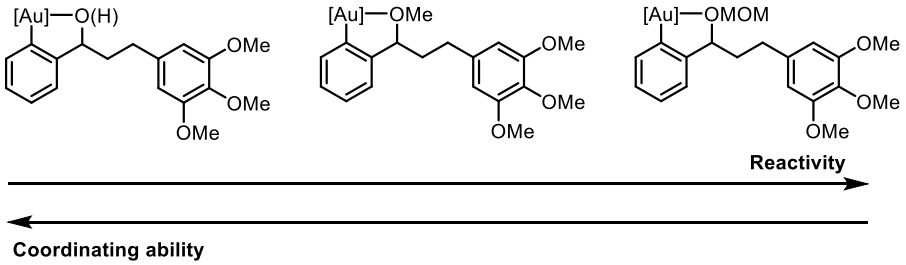

Scheme 4.15. Possible origin of decreased cyclisation rate with more-coordinating oxygen functionality.

Due to the ability to monitor the formation of the proposed inhibitor, kinetic modelling software can be used to calculate the partitioning between the productive cycle and the deactivation pathway (k_1 and k_2, Scheme 4.13). A good fit for the deactivation of **5k** can be obtained at both 1 and 2 mol% catalyst (Figure 4.19) using the deactivation mechanism shown in Scheme 4.13. The model indicates that the *in-situ* generated diaryliodonium salt (**106**) is a powerful inhibitor, as $k_2 \approx 5 \times k_1$. It is surprising that a distal diaryliodonium salt would have the effect of accelerating the rate of transmetalation at the silane. Whilst efforts are ongoing to understand this process, an accelerated transmetalation of the catalyst-inhibiting silane-tethered diaryliodonium salts may possibly involve localisation of a counter-anion for C-Si cleavage.

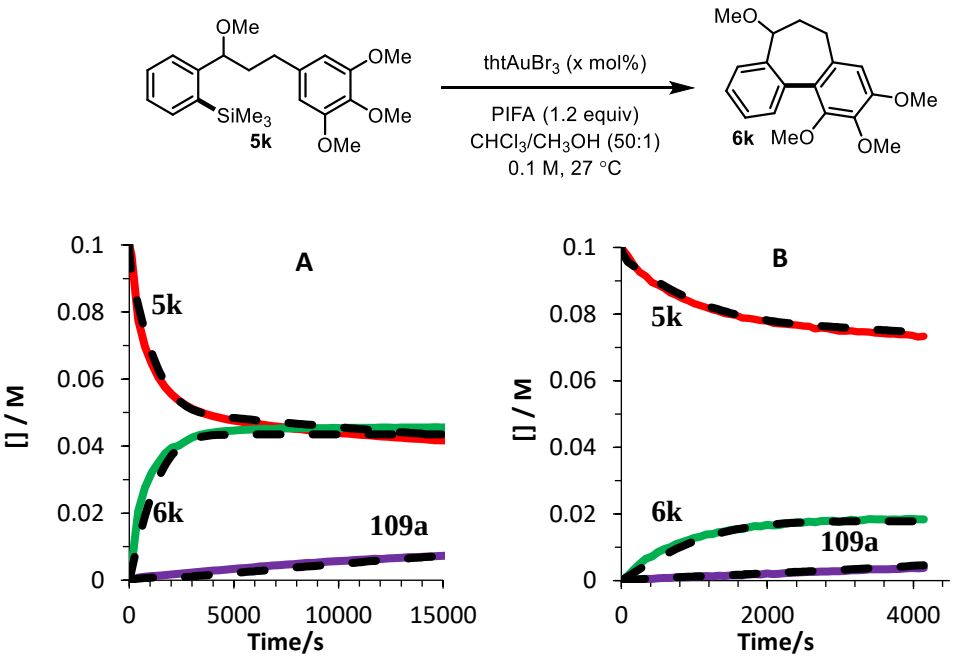

Figure 4.20. Kinetics of cyclisation of **5k** at: A) 2 mol% and B) 1 mol%. Dashed lines are simulated data using the model outlined in Scheme 4.13, simulation agrees with experimental when: k_1:k_2 = 1:5 (where k_1, k_2 >> k_3), k_3 = 0.014 s^{-1} (TLS) and k_5 = 1.63×10^{-4} dm^3 mol^{-1} s^{-1}. k_4 was set to an arbitrary value of > 100 dm^3 mol^{-1} s^{-1}.

4.6 Summary

Two mechanisms of catalyst deactivation have been unveiled. Whilst the mechanism of each deactivation process is different, the origin is the same. Both catalyst deactivation pathways occur as a result of the hypervalent iodine oxidant, and are unique to the intramolecular coupling. In the first case, the oxidant leads to production of water which was shown to be a potent, but reversible inhibitor when π-rich arenes are present. This is only arises in the intramolecular examples due to the significant differences in arene electronics in the starting material and product. In the second case, the oxidant can react with the tethered arene to form a diaryliodonium salt. This reaction serves to deactivate the arene to S_EAr, and therefore prevent release of the catalyst once transmetalation to this species occurs. Thus, the tethering of arene and silane is crucial to this deactivation mechanism. These two studies demonstrate the need to venture away from hypervalent iodine oxidants, a point which is addressed in Chapter 6.

5. Domino Arylation

ABSTRACT: Chapter 5

Through theoretical kinetic analysis, the general principles which govern the rate and selectivity of catalytic domino arylations combining intramolecular and intermolecular couplings, are described. Kinetic simulations reveal that the order of events, and whether intramolecular cyclisation precedes intermolecular coupling, or *vice versa*, has a large impact on the expected kinetic profiles. The potential for catalyst inhibition is uncovered, and the cause and possible solutions are discussed. The selectivity for one mechanistic pathway over the other is found to be key for high regioselectivity, as a combination of both routes leads to a mixture of products under the simulated conditions. The process is confirmed experimentally through the combination of intra- and intermolecular gold-catalysed direct arylation. The reaction proceeds predominantly *via* an intramolecular-intermolecular ordering of events, and gives good agreement to the theoretical data. Electronic perturbation of the system results in competing intermolecular-intramolecular coupling and the formation of a second regioisomer, as predicted in the theoretical kinetic analysis.

This project was performed in collaboration with Dr. L. Ball and Dr A. Cresswell. Preliminary results were collected by Dr. L. Ball, and authentic samples were synthesised and characterised by Dr. A. Cresswell (compounds specifically referenced in the text).

5.1 Introduction

One of the key requisites in the design of synthetic routes to complex molecules is efficiency. Within the term efficiency come a number of factors, including, but not limited to, step-economy, purification, waste and time. These factors are fundamental in reducing environmental impact as well as maximising profits. One strategy to improve efficiency which has gained significant attention is the performance of multiple transformations in 'one-pot.' The use of a single reactor to transform simple reagents into complex targets, which would otherwise take multiple steps, is the ultimate efficiency strategy. By performing reactions in one-pot, only one optimisation is needed, wasteful workups and purification steps are avoided, and therefore, significant energy and time is saved. In catalysis, depending on the nature of the transformations, several one-pot reaction types exist, however two of the main categories are domino (cascade) and tandem catalysis.[143–146]

5.1.1 Taxonomy

Tietze originally defined 'domino' reactions as those involving "two or more bond-forming transformations which take place under the same reaction conditions, without adding additional reagents or catalysts, and in which the subsequent reactions result as a consequence of the functionality formed in the previous step".[147] Subsequently, Fogg and dos Santos

stipulated that, in addition to Tietze's earlier definition for domino reactions, "multiple transformations are effected via a *single* catalytic mechanism". Conversely, 'tandem' catalysis denotes "coupled catalyses in which sequential transformation of the substrate occurs via two (or more) mechanistically distinct processes".[148] These definitions distinguish domino and tandem catalysis from other one-pot procedures where a second catalyst is added after the first catalytic transformation is complete, which are known as one-pot (multicatalytic) reactions.[148] Tandem catalysis can be subcategorised into orthogonal catalysis,[143] assisted-tandem catalysis and auto-tandem catalysis[149] depending on the number of catalyst species present and if the user intervenes in the reaction or not (Figure 5.1).

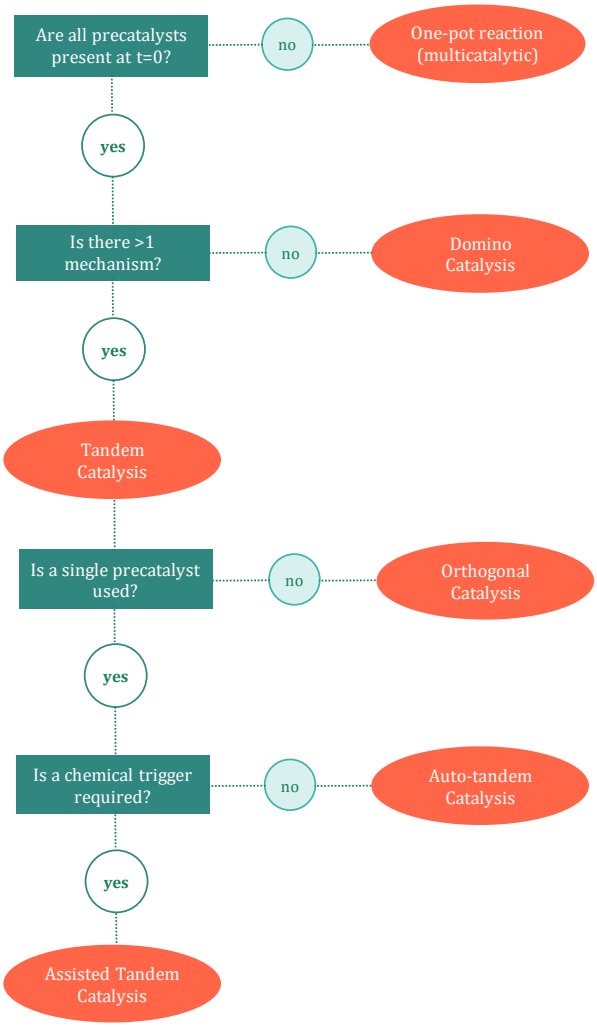

Figure 5.1. Flowchart guide to nomenclature of one-pot catalytic processes.

In orthogonal catalysis, two or more catalyst species are present in the reaction from the outset, each with a different mechanistic role. Each catalyst is, in theory, independent of one another, and the product of one catalytic cycle becomes the substrate for the other. Auto-tandem

catalysis is similar to orthogonal tandem catalysis as two (or more) mechanistically different catalytic cycles are operating, however in auto-tandem catalysis there is only a single catalyst species which can perform two or more functions. In assisted-tandem catalysis, there is a single multifunctional catalyst, but a chemical trigger is required to access new functionality.

5.1.2 Domino and Tandem Catalysis

Domino catalysis can either be intermolecular, where release of intermediates from the catalytic cycle occurs, or, more commonly, intramolecular where several elaborations occur within a single cycle. The term "cascade" catalysis is often used as an alternative to domino, particularly when there are ≥ 3 elaborations.[148] In 2009, Lautens and Candito reported an intramolecular palladium-catalysed domino direct arylation/N-Arylation procedure for the synthesis of phenanthridine **114** (Scheme 5.1, Top).[150] The proposed catalytic cycle is based on the Catellani reaction,[151–153] and the independent mechanistic studies by Hartwig *et al.*[154] and Barluenga *et al.*[155] into Pd-catalysed C-N bond forming reactions (Scheme 5.1, bottom).

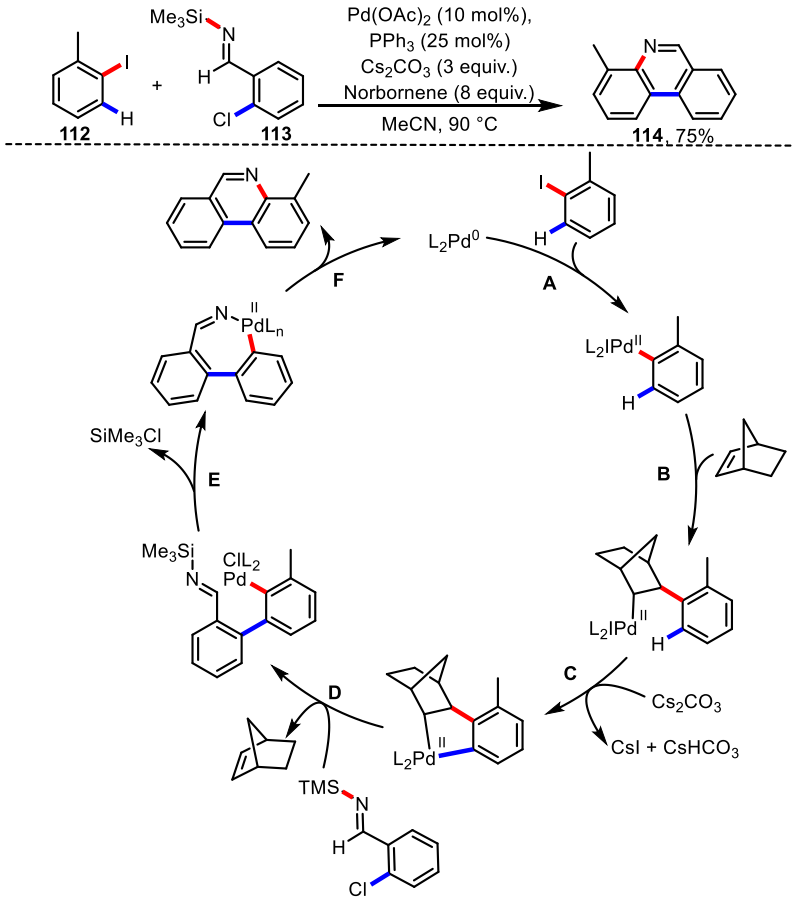

Scheme 5.1. Representative example (Top) and proposed mechanism of domino direct arylation/N-Arylation.

The proposed mechanism involves; **A**, oxidative addition of aryl iodide **112**; **B**, carbopalladation with norbornene; **C**, C-H activation; **D**, biaryl formation through a proposed oxidative addition to **113** (Pd^{II} – Pd^{IV}), reductive elimination, decarbopalladation sequence; **E**, N-Si bond cleavage and; **F**, product releasing reductive elimination.

A recent development of orthogonal tandem catalysis was demonstrated by, Lautens *et al* once again,[156,157] where rhodium-catalysed alkyne arylation of **115** precedes palladium-catalysed C-N coupling of intermediate **116**. Despite the potential for multiple reaction pathways, a single product was isolated (Scheme 5.2).

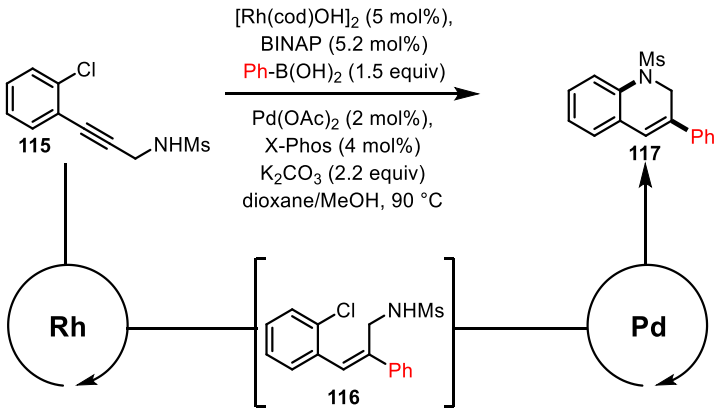

Scheme 5.2. Orthogonal catalysis employing Rh and Pd catalysts.

The reaction conditions were compatible for both metals and no interference between the catalysts on the individual steps were found. However, the choice of ligand was vital to the success of the reaction. In control experiments swapping the ligands on the metals, i.e. Rh/X-Phos and Pd/BINAP shut down each respective reaction in isolation. Whilst with rhodium this was because no binding to X-Phos was observed, and the phosphine-free rhodium led to decomposition of the starting material, with palladium the presence of BINAP reduced the reactivity of the metal altogether. Therefore, the presence of excess BINAP in the tandem reaction led to competitive binding with palladium *versus* X-Phos and reduced reactivity. To achieve optimum conditions the precatalysts and ligands were mixed in the desired ratio prior to addition to the reaction. An overall 69% yield was obtained for the domino reaction, compared with the 71% obtained for the two-step combined yield. The key issue here, which is a general problem with many one-pot procedures, is that one set of reaction conditions may not be the optimal reaction conditions for both catalytic processes. Although each step can be optimised in isolation, the combination may lead to unexpected interactions and reduced yields.[148]

Palladium displays a rich array of reactivity which has been exploited in catalysis for several coupling reactions including C-C, C-N and C-O bond forming processes.[3] It is therefore unsurprising that palladium is a popular choice for the development of auto-tandem reactions. A seminal contribution for the use of direct arylation in auto-tandem catalysis originated from the Bedford research group in the synthesis of carbazoles from 2-chloro-*N*-alkylated anilines and aryl bromides (Scheme 5.3).[158] The reaction combines a Buchwald-Hartwig coupling of an aryl halide **118** with an aniline **119**, yielding intermediate **120** which can undergo a direct arylation reaction.

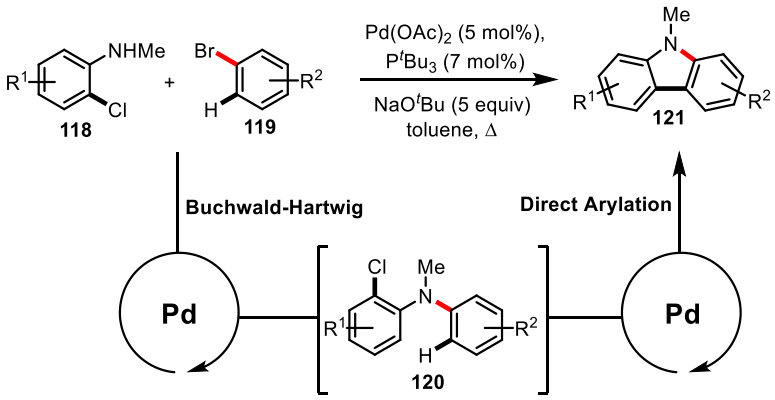

Scheme 5.3. Auto-tandem catalysis.

Utilising different halides allowed for discrimination between the two starting materials for the initial oxidative addition. The presence of the more reactive bromine on **119** allowed for the desired Buchwald-Hartwig reaction to occur before any oxidative addition into the **118** occurs. In auto-tandem reactions in general, excellent selectivity is often required as the substrates used are often activated for multiple transformations, but the order in which they occur can be vital for the success of the tandem protocol.

The necessity to control the order of reactions through excellent selectivity is emphasised in a palladium-catalysed auto-tandem Heck, direct arylation protocol advanced by Fagnou *et al.* to form functionalised cyclic biaryls (Scheme 5.4).[159]

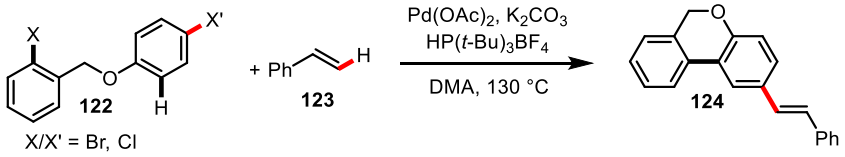

Scheme 5.4. Pd-catalysed auto-tandem Heck, direct arylation.

In theory, the order of events and whether the intramolecular direct arylation occurs first, followed by the intermolecular Heck in an intramolecular-intermolecular 'intra-inter' pathway or *vice-versa* in an 'inter-intra' pathway should lead to the same product (Scheme 5.5).

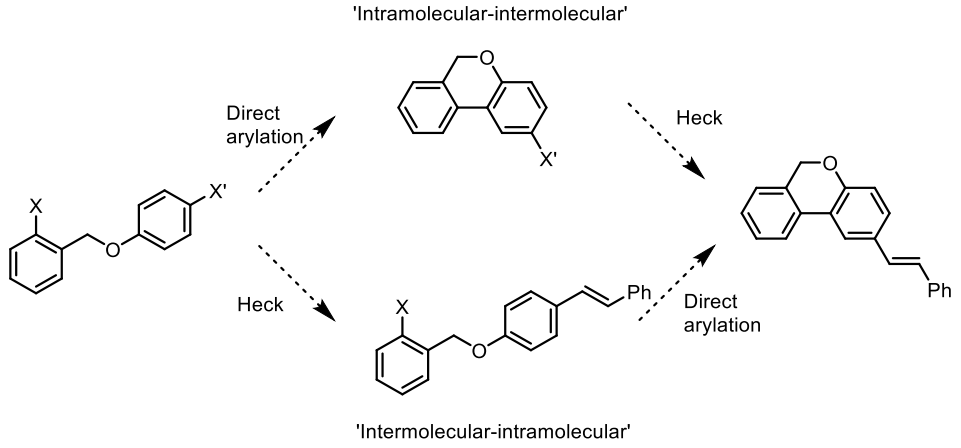

Scheme 5.5. "Intra-inter" *vs* "inter-intra" pathway.

However, the order in which the reaction events occurred proved to be vital. Once again, the utilisation of aryl chlorides and bromides to direct the order of oxidative addition led to the success or failure of the reaction depending on where they are situated. If the aryl bromide is placed on the substrate geared toward direct arylation **122a**, then the desired product is not isolated, instead the Heck product **125** forms competitively. The origin of this is intermolecular trapping of the palladium intermediate **I**(**122**) that would otherwise undergo the direct arylation (Scheme 5.6). In palladium catalysis, the direct arylation, or 'C-H activation' step can be turnover-limiting,[160] or at least kinetically significant enough to be sufficiently long lived that an intermolecular coupling can outcompete the intramolecular process. This observation led to the authors swapping the position of the halides such that the desired intermolecular reaction occurs first, followed by direct arylation. By doing so, good yields were obtained for the desired product (Scheme 5.7).

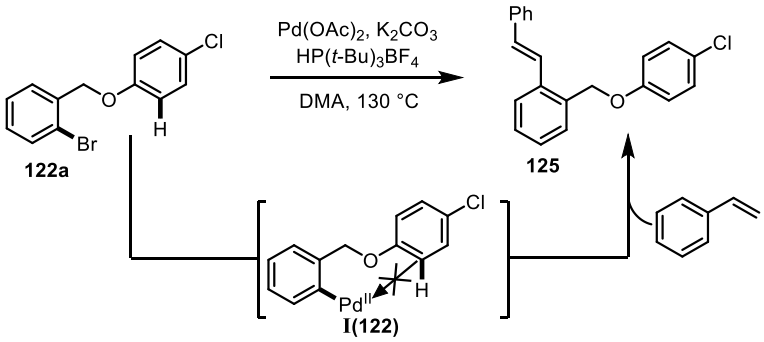

Scheme 5.6. Interception of catalyst intermediate in proposed "intra-inter" pathway.

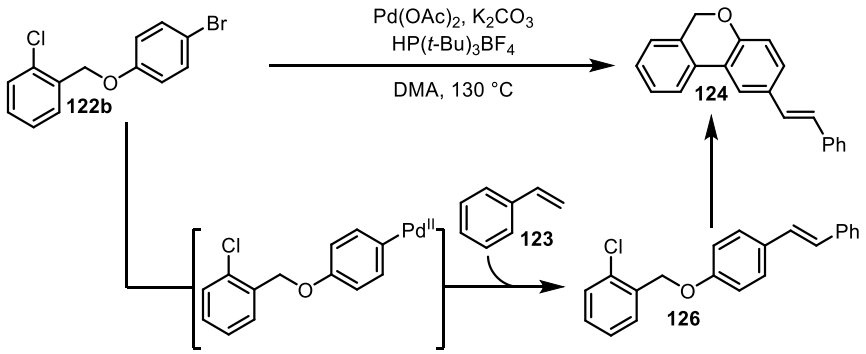

Scheme 5.7. Tandem "inter-intra" Heck, direct arylation reaction.

An assisted tandem step was also demonstrated through a final hydrogenation of the auto-tandem product **124**. In assisted tandem catalysis, a chemical trigger can transform the catalyst so that is has an additional function. The addition of hydrogen gas to the reaction after the auto-tandem reaction was complete allowed for a palladium-catalysed hydrogenation of **124** to occur (Scheme 5.8). This demonstrates the potential multifunctional catalysts like palladium have in generating molecular complexity in a single pot.

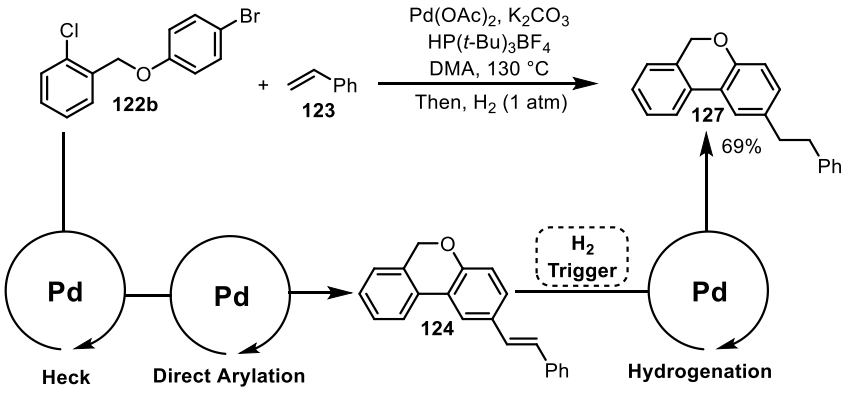

Scheme 5.8. Auto-tandem Heck, direct arylation and assisted-tandem hydrogenation.

5.1.3 Chapter Aims

Despite significant developments in domino and tandem catalysis, there are no examples of domino or tandem arylations combining intra- and intermolecular coupling. With the new mechanistic insights into the intramolecular cyclisation in-hand, and the prior knowledge into the kinetics of the intermolecular direct arylation, it was anticipated that these reactions could be combined into a one-pot arylation protocol. As inter- and intramolecular arylations with gold proceed *via* the same mechanism, this would be, by definition, a domino reaction. It was proposed that an *a priori* rationalisation of such a procedure with the aid of kinetic simulation would lead to insights that would guide the design of such a procedure. The aim of this was to outline a set of principles that would be required for this class of reaction to be successful in

general, and then use the gold-catalysed direct arylation as a case-study. Therefore, a general reaction sequence was envisioned where 'intra' and 'inter' substrates **128** and **129** could couple *via* intermediates **130**/**131b** (*vide infra*) to form domino arylation product **132** (Scheme 5.9). This is the general reaction for which a theoretical kinetic analysis would be performed on. This general reaction could apply to a variety of catalysts, and kinetic analysis would be performed under the important assumption that C-X functionalisation (transmetalation, oxidative addition) is the first selectivity determining step, followed by C-H metalation.

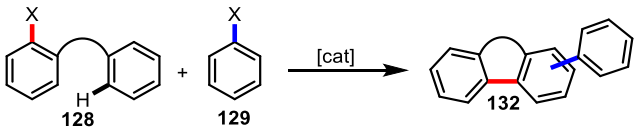

X = $SiMe_3$, Cl, Br, I, $B(OR)_2$...etc.

Scheme 5.9. General domino direct arylation reaction.

5.2 Kinetic Analysis of Domino Arylation

When considering a domino reaction combining an intramolecular and intermolecular direct arylation, two competing pathways can be envisioned. One pathway could involve the cyclisation preceding intermolecular coupling, in an intramolecular-intermolecular pathway "intra-inter," and *vice-versa* where intermolecular coupling occurs first, followed by intramolecular direct arylation, in an "inter-intra" pathway (Scheme 5.10). Whilst both routes can lead to a product of domino arylation, there is significant potential for each route to form a different isomer **130a/b**. Whilst the regioselectivity of intramolecular cyclisation is pre-defined due to the conformational bias enforced by the tether, the regioselectivity of the intermolecular coupling is dictated by the innate reactivity of the C-H bonds. The mechanism of metalation will control which C-H bond will react, with acidity being a factor in a CMD mechanism and nucleophilicity with S_EAr. As the reacting arenes **128** and **130** in the intermolecular coupling in the "inter-intra" and "intra-inter" routes are not identical, with differing steric and electronic properties, it is likely that that (at least) two regioisomeric products will form.

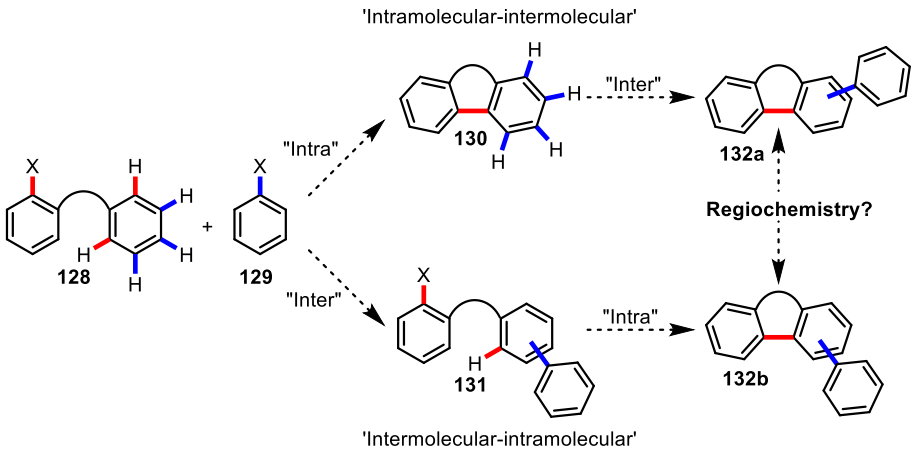

Scheme 5.10. "Inter-intra"- and "intra-inter" pathways to domino arylation products.

Therefore, it was envisioned that for a regioselective domino arylation procedure, one of these routes must be dominant, as a mixture could lead to poor selectivity. Using kinetic simulation software and constructing a mechanistic model based on the catalytic sequence depicted in Scheme 5.11, the kinetic parameters that impact on the success or failure of a "inter-intra" or "intra-inter" domino arylation protocol were assessed.

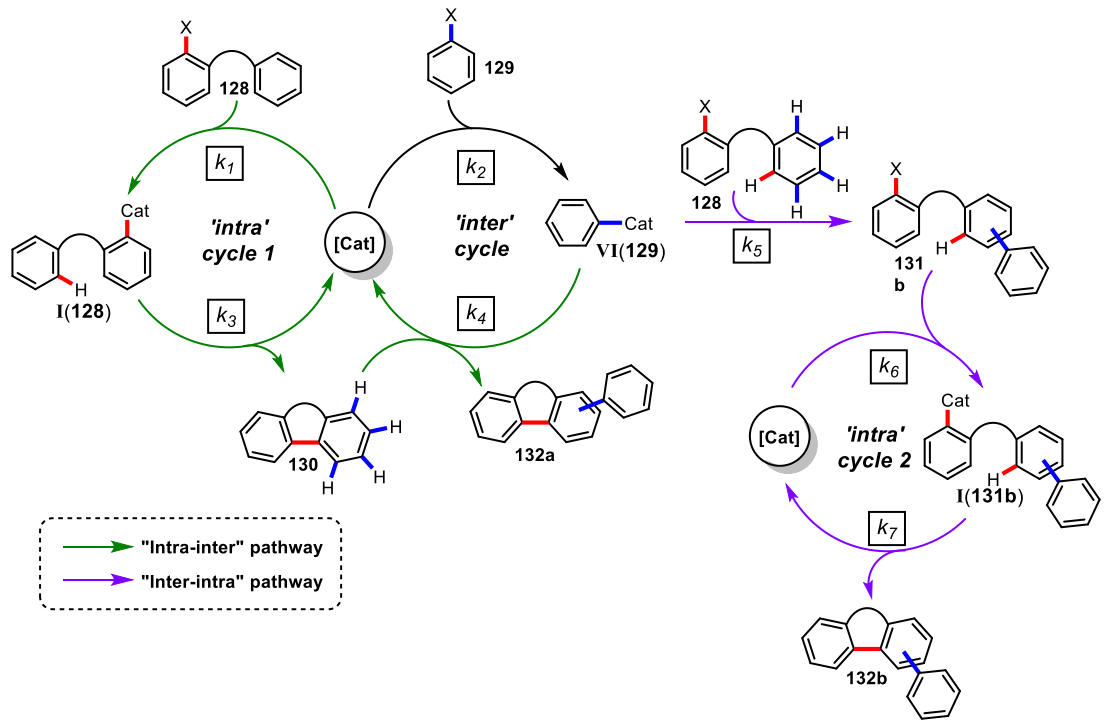

Scheme 5.11. General catalytic cycle for "intra-inter" and "inter-intra" domino arylation.

5.2.1 "Inter-Intra" Domino Reaction

First, the kinetic parameters that would allow for an "inter-intra" sequence were assessed using kinetic modelling. There are two key partitions in the catalytic cycle that were identified to influence product distribution: 1) The competition between substrate **128** and **129** for the catalyst, dictated by the k_1:k_2 ratio and, 2) The relative rates of intermolecular arylation (**130** → **132a**, and **128** → **131b**), which is determined by the k_4:k_5 ratio. To reflect the conditions found in the gold-catalysed direct arylation, the rate of the intramolecular reaction is controlled by k_3/k_7 and the rate of the intermolecular reaction controlled by k_4/k_5. The absolute values of k_1 and k_2 were set arbitrarily high so that they do not become turnover, or partially turnover-limiting. Due to the similarity of **128** and **131b**, it was assumed that $k_1 = k_6$, and $k_3 = k_7$. The effect of the partitioning between **128** and **129** (k_1:k_2) was initially assessed independently by enforcing the condition $k_4 = 0$ in the kinetic simulation (Table 5.1, entries 1-8), and then the effect of the k_4:k_5 ratio was analysed (Table 5.1, entries 9-11). Table 5.1 shows the effect these kinetic parameters have on product distribution, and Figures 5.1 and 5.2 (numbered according to entry number of Table 5.1) show the associated expected kinetic profiles for select examples. The *absolute* values of k_1, k_2 and k_6 do not affect the overall appearance of the kinetic profiles, providing they are much greater than the other rate constants. The absolute values of k_3, k_4, k_5 and k_7 will affect the overall reaction time, but providing the absolute values are within

one order of magnitude, the overall shape of the profile and expected conversion will not change significantly.

Table 5.1. Simulated product distribution of "inter-intra" domino arylation.

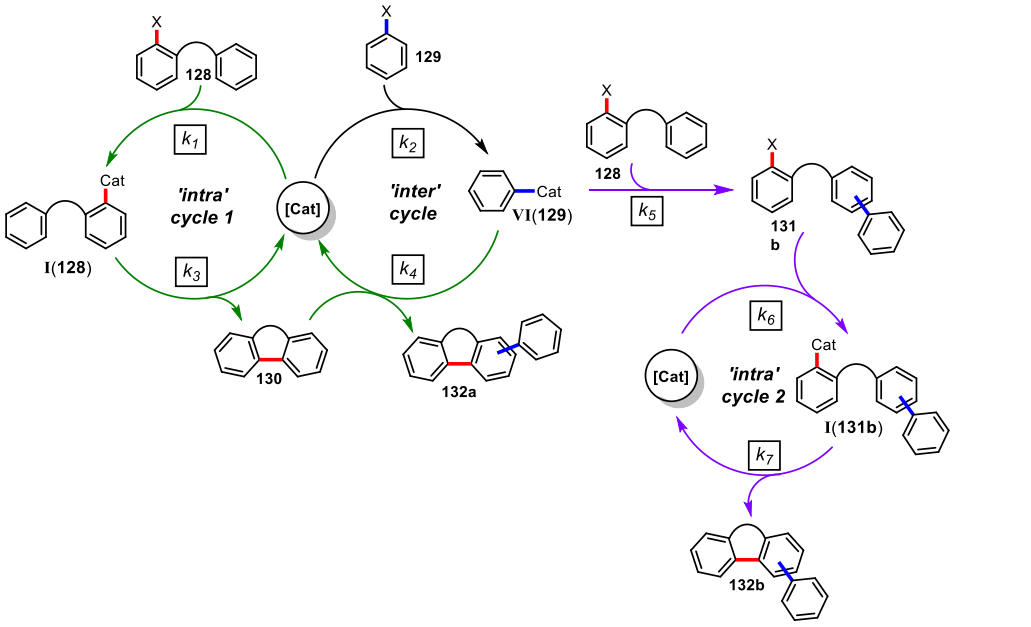

Entry	k_2:k_1	k_4:k_5	Cat/ mol%	130 (%)	132a (%)	131b (%)	132b (%)
1	1:1	0:1	2	37	-	38	25
2	5:1	0:1	2	14	-	65	21
3	10:1	0:1	2	8	-	76	16
4	50:1	0:1	2	2	-	85	13
5	**60:1**	0:1	**2**	**<2**	**-**	**0**	**>98**
6	10:1	0:1	5	9	-	72	19
7	10:1	0:1	10	11	-	59	30
8	**10:1**	0:1	**12**	**12**	**-**	**0**	**88**
9	10:1	0.1:1	2	0	8	0	92
10	10:1	0.5:1	2	1	9	0	90
11	10:1	10:1	2	0	13	0	87
12*	10:1	0:1	2	<2	-		>98

Fixed simulated conditions: **128** (0.05 M), **129** (0.05 M), k_1 and k_6 = 100 dm^3 mol^{-1} s^{-1} k_3 and k_7 = 0.027 s^{-1}, k_5 = 0.1 dm^3 mol^{-1} s^{-1}. * **128** (0.055 M), **129** (0.05 M).

The simulation gave vital insights into the kinetic parameters that govern an "inter-intra" direct arylation procedure. The effect of varying the k_2:k_1 ratio is striking, as low yields of the domino arylated product (**132b**) are predicted, even when high ratios in favour of the inter cycle are

employed (50:1), but at a critical ratio (60:1, Table 5.1, entry 5) the yield is predicted to become nearly quantitative. Counterintuitively, at ratios below 60:1, the yields are predicted to improve as this partition becomes less selective. For example, a 13% yield of **132b** is predicted with a ratio of 50:1 (Table 5.1, entry 4), whereas when the reaction is completely unselective (Table 5.1, entry 1), a 25% yield is predicted. However, significantly more of the pre-cyclised intermediate **131b** is predicted at higher ratios. These unusual observations, and the associated kinetic profiles (Figure 5.1), are a result of the k_2:k_6 ratio, and the presence of "intra cycle 1". The simulation was programmed with a 1:1 stoichiometry of **128** and **129**, however due to the competing "intra cycle 1," the total amount of **128** consumed per turnover is greater than the amount that is converted to **132b**, even when the k_2:k_1 ratio is high, as some is lost as **130**. The consequence of this is that the 1:1 stoichiometry is not maintained throughout the reaction, and at some point **128** is totally consumed when some **129** remains. With a high k_2:k_1 ratio, and therefore high k_2:k_6 ratio (as $k_1 \approx k_6$ under the simulated conditions), the catalyst will quickly partition to catalyst intermediate **VI**(**129**), and with no **128** to react with the reaction will stall. As the k_2/k_6:k_1 ratio is lowered, more catalyst can partition to **I**(**131b**) *via* "intra-cycle 2," and consequently form a higher yield of **132b**. At a critical ratio, which was observed to be *ca.* 60:1 under these conditions, the partition to "intra-cycle 1" is so insignificant that the loss of concentration of **128** by conversion to **130** is no longer important. However, achieving such selectivity under real conditions could be a significant challenge as discrimination between identical "X" functional groups is required.

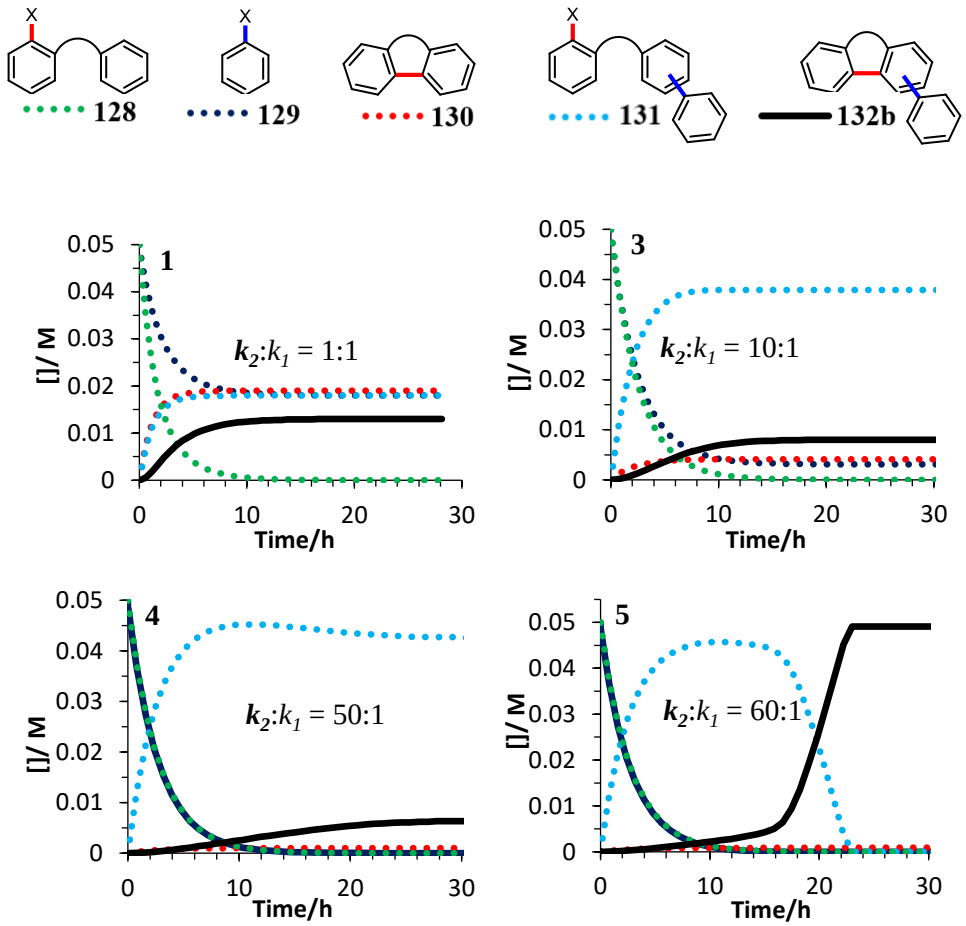

Figure 5.1. Simulated kinetic profiles of "inter-intra" domino arylation showing effect of k_2:k_1 ratio when k_4 = 0.

Three strategies were proposed to improve the yield of **132b** without the need for extremely high k_2:k_1 ratios (strategies assessed at k_2:k_1 = 10:1). The first strategy was to increase the **128**:**129** ratio so that there is always an excess of **128** to release the catalyst. This was indeed the case, and increasing the ratio to 1.1:1 was sufficient, and a 98% yield of **132b** was predicted (Table 5.1, entry 12) compared with a 16% yield under identical conditions with a 1:1 stoichiometry (Table 5.1, entry 3). The second strategy was to simply increase the catalyst loading. If the following conditions are satisfied $[Cat]_0 > [S2]$ when [S1] = 0, then although a significant proportion of the catalyst will rest at **VI**(**129**) once all **128** has been consumed, there will still be an excess concentration of catalyst that can continue to turnover. This is demonstrated in Table 5.1, entries 3,6-8 where an increase in loading from 2 mol% to 12 mol% catalyst is required for the reaction to go to completion, and a predicted 88% yield (See Figure 5.2 for associated kinetic profile). The final strategy was to allows the competing "inter-intra"

cycle to operate by varying the value of k_4. The cause of the reaction stalling is that **130** cannot react to release the catalyst once **128** has run out, and therefore by allowing **130** to react with **VI**(**129**), there is another route for the catalyst to be released. Using k_2:k_1 = 10:1 as the standard conditions to assess the effect of increasing k_4 values demonstrated that allowing this "undesired" pathway to occur is in fact beneficial for the reaction. Whilst reduced regioisomeric ratios would be obtained, the predicted effect on yield and reaction profile is profound. At a ratio of k_2:k_1 = 10:1, the absolute value of k_4 did not impact greatly on the overall regioselectivity. However, the overall rate of reaction was increased with increasing k_4 values as this rate constant controls the release of active catalyst from intermediate **VI**(**129**). The result of these simulations show that the factors which control a potential "inter-intra" domino arylation are complicated, particularly if complete regioselectivity is desired. Either extremely high selectivity (k_2:k_1) for one coupling partner is required, or careful consideration of stoichiometry and catalyst concentration is needed to prevent the reaction from stalling. In order for perfect selectivity, the product from the undesired, but unavoidable "intra cycle 1" must be unreactive to arylation (k_4 = 0), however, this requirement leads to the detrimental stalling of the reaction as without it, catalyst inhibition can occur.

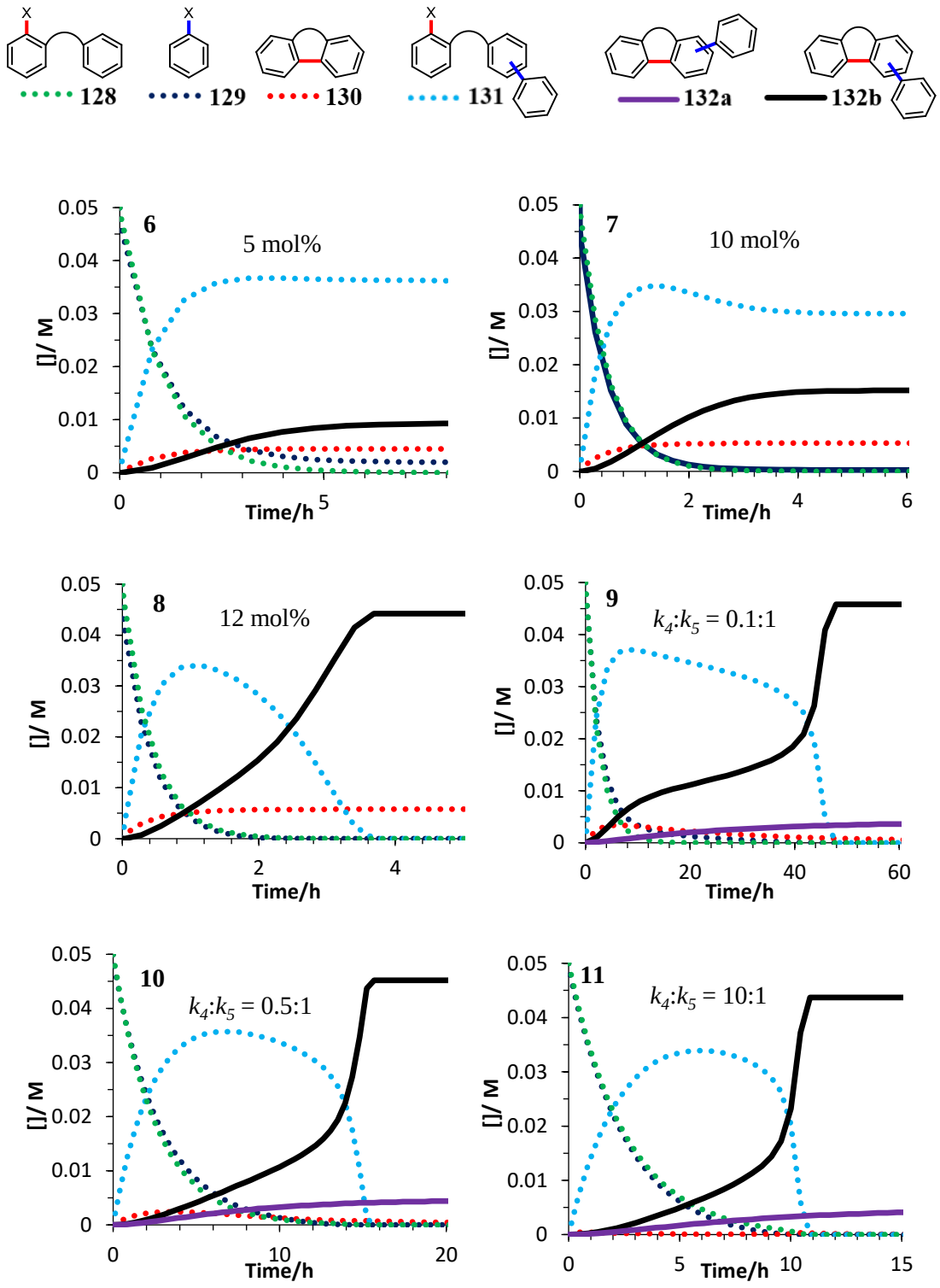

Figure 5.2. Effect of catalyst loading or k_4:k_5 ratio on kinetic profile at k_2:k_1 = 10:1.

5.2.2 "Intra-Inter" Domino Reaction

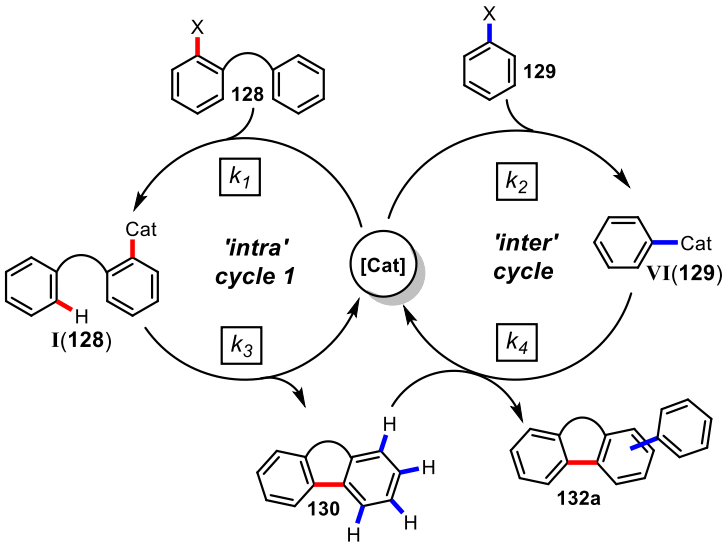

Scheme 5.12. General catalytic cycle for domino "intra-inter" direct arylation.

The same kinetic analysis for the "inter-intra" sequence was performed on a proposed "intra-inter" protocol, with the simulations performed under the initial assumption that $k_5 = 0$, so that once again the effect of the k_1:k_2 partition could be monitored in isolation. Once again, the rate of the intramolecular reaction is controlled by k_3 and the rate of the intermolecular reaction controlled by k_4 and the absolute values of k_1 and k_2 were set arbitrarily high. The same absolute k values were employed for direct comparison with the "inter-intra" system. In contrast to the results from the "inter-intra" system, the factors which affected the potential success of this reaction were significantly more intuitive. Under the conditions $k_1 > k_2$, the reaction is predicted to go to completion, with the extent of the build-up of intermediate **130** depending on how high the k_1:k_2 ratio is. Intriguingly, when $k_1 = k_2$ and therefore the partitioning is totally unselective, the reaction is still predicted to be successful. This is because, in theory, the 50% of catalyst that partitions to the intramolecular substrate will form cyclised product in perfect stoichiometry to react with the other 50% of catalyst that is resting as intermediate **VI**(**129**). However, this relies on an exact 1:1 stoichiometry of the two starting materials. Even a small discrepancy in favour of the intermolecular substrate **129**, will shift the partition slightly in favour of intermediate **VI**(**129**) and ultimately lead to deactivation of the catalyst. In addition, the lack of selectivity results in the prediction of significantly longer reaction times due to a steady state concentration of **130**. When $k_2 > k_1$, there is significant potential for deactivation to occur, as the catalyst will partition to **VI**(**129**) and will be unable to release. Even when the partition is only slightly biased (k_1:k_2 = 1:1.1), the reaction at the catalyst loading used in the simulation, is predicted to stall at 22% conversion (Figure 5.3).

The conversion is highly dependent on catalyst concentration, as the higher the catalyst loading employed, the greater the number of turnovers before it is all sequestered as **VI**(**129**).

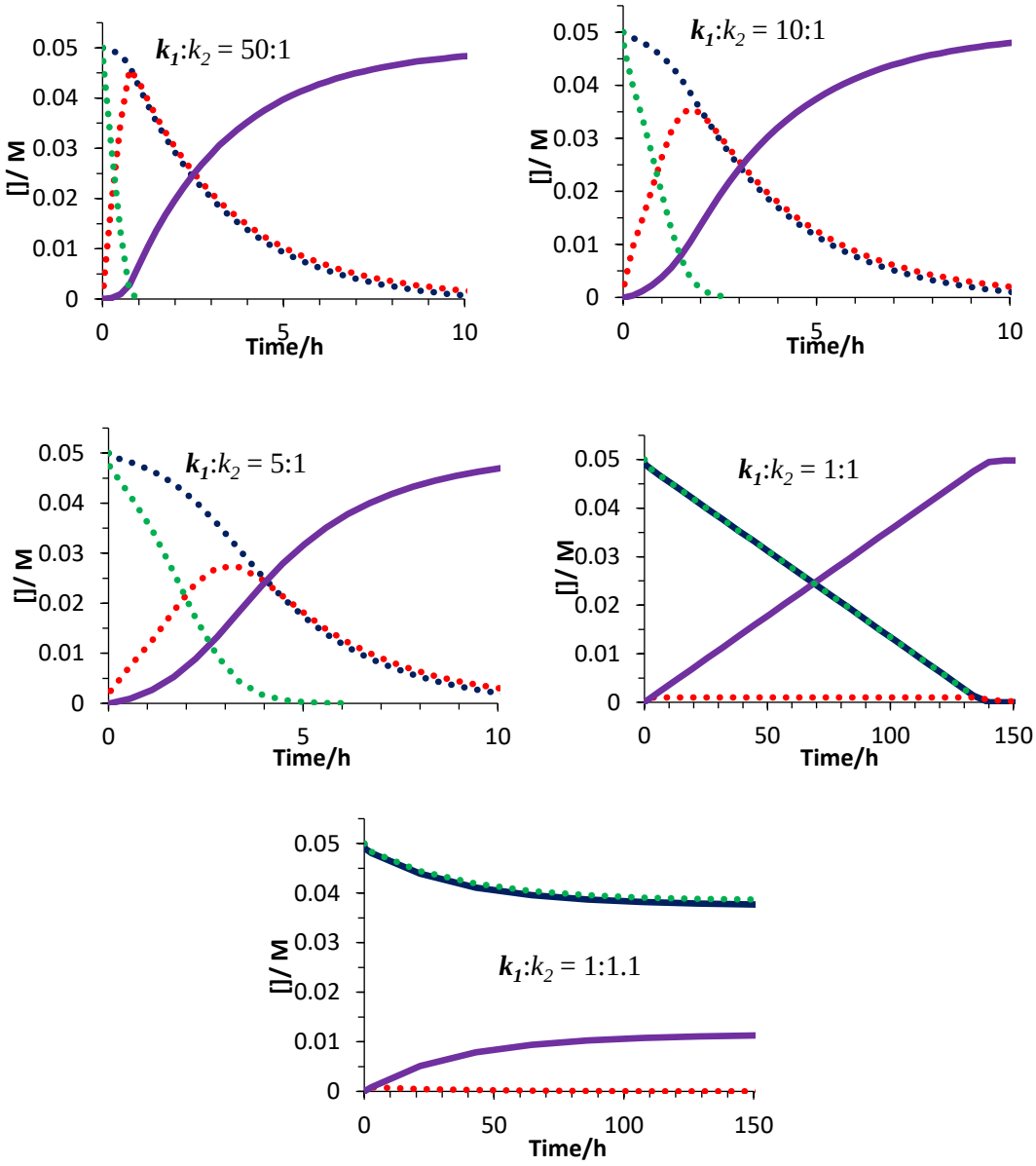

Figure 5.3. Effect of k_1:k_2 partition on "intra-inter" domino arylation.

Once again, if the competing cycle is allowed to operate and $k_5 \neq 0$, then stalling will not occur, but a mixture of isomers will be obtained, with the regioselectivity dependent on both k_1:k_2 and k_4:k_5. When k_1:k_2 significantly favours one pathway (e.g. k_1:k_2 = 10:1 or 1:10), then the effect of k_4:k_5 is not substantial, however when the k_1:k_2 partition is less selective, the ratio of k_4:k_5 can have a significant effect on selectivity (Table 5.2).

Table 5.2. Simulated effect of k_4:k_5 ratio at different k_1:k_2 ratios on regioisomeric ratio.

Entry	k_1:k_2	k_4:k_5	132a (%)	132b (%)
1	1:1	1:1	51	49
2	1:1	10:1	72	28
3	1:1	1:10	39	61
4	10:1	1:1	91	9
5	10:1	1:10	78	22
6	10:1	1:100	77	23
7	10:1	10:1	97	3
8	1:10	1:1	10	90
9	1:10	1:10	8	92
10	1:10	1:100	8	92
11	1:10	10:1	12	88

5.2.3 Additional Considerations

The results and kinetic profiles presented herein provide a guide to the requisite kinetic parameters that will guide a domino "intra-inter" or "inter-intra" reaction. The overriding message is that for good selectivity and yields, a high ratio for one "X" functional group over the other is required ($k_1 > k_2$ for "intra-inter" and $k_2 >> k_1$ for "inter-intra"). A perfectly regioselective "inter-intra" sequence provides a significantly greater challenge due to the potential for the reaction stalling if this selectivity if not extremely high, however strategies involving altering the stoichiometry of the starting materials or increasing catalyst loading are predicted to aid the process. Whilst this guide may provide a framework to which domino arylations could be designed, for simplicity some important assumptions were enforced upon the simulations. Firstly, the innate regioselectivity of intermolecular arylation was not discussed (Scheme 5.13). The simulation was set so that **130** formed a single regioisomer of **132a** in the "intra-inter" coupling and **128** formed **131b**, and therefore **132b** exclusively in the "inter-intra" coupling. However, considering the number of C-H bonds available, 4 possible isomers could form in either case, resulting from 7 possible intermediates in the "inter-intra" reaction. In addition to this, over-arylation of **132a** might be possible due to the electronic similarity between **130** and **132**. Therefore, perfect selectivity will be required to obtain a single regioisomer.

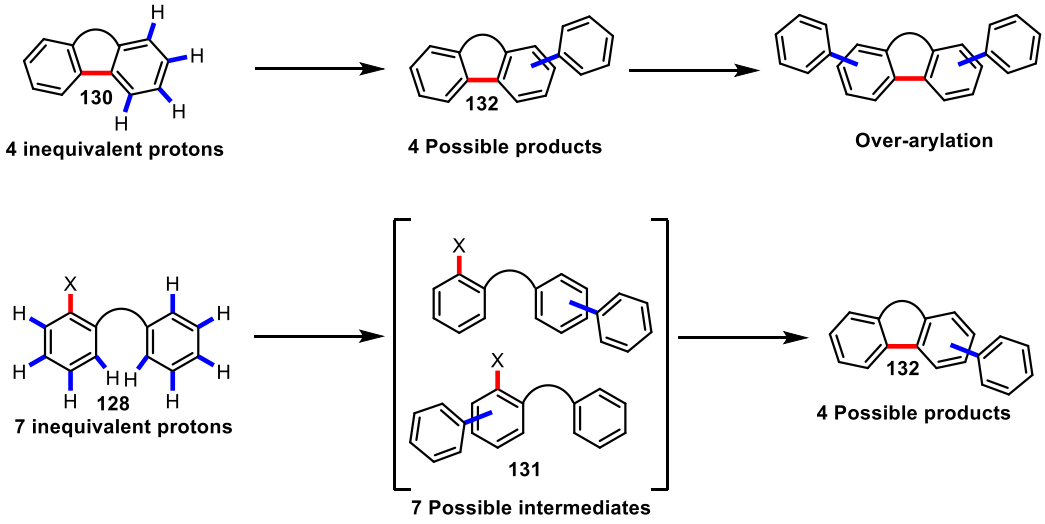

Scheme 5.13. Possible regioselectivity issues in domino arylation.

Another deleterious process could be the formation of side products from intermediate **I**(**128**). As seen in the auto-tandem Heck, direct arylation study by Fagnou *et al.*,[159] intermediates of type **I** can be prone to intermolecular trapping if they are sufficiently long lived (Scheme 5.14). If the rate of this is significant, then the overall tandem process could become inoperable.

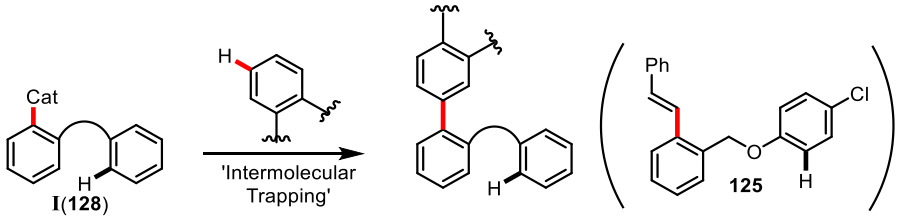

Scheme 5.14. Intermolecular interception of catalyst intermediate **I**(**128**).

5.3 Gold-Catalysed "Intra-inter" Domino Arylation

5.3.1 Identification of Model System

With these kinetic principles in-hand, it was anticipated that a gold-catalysed "intra-inter" domino sequence could be developed (Scheme 5.15). This prediction was based on a thorough mechanistic understanding of both the intramolecular (Chapter 3) and intermolecular direct arylation reaction,[83] with the key mechanistic details which should allow such a process outlined below.

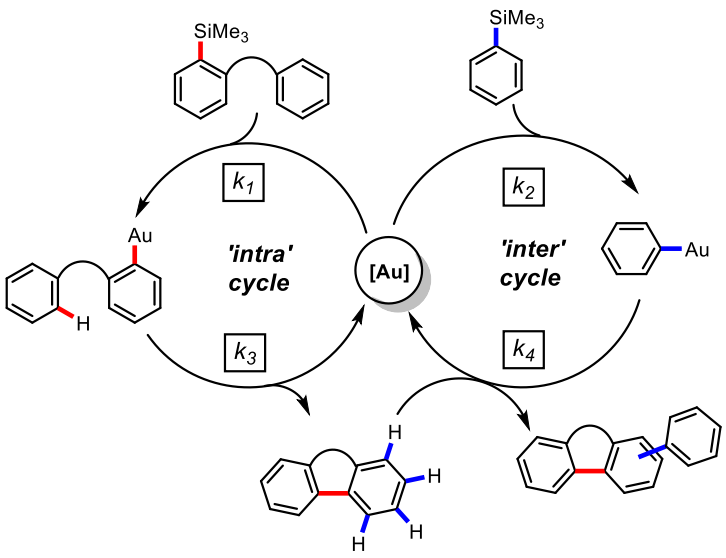

Scheme 5.15. General gold-catalysed "intra-inter" domino arylation.

It is clear from the simulations that for a successful reaction, k_1 must be greater than k_2 otherwise stalling of the reaction, or an 'inter-intra' pathway, will occur. This selectivity requirement is possibly the largest obstacle to a successful domino arylation protocol, as significant discrimination between identical functional groups may be difficult. Previous studies into the intermolecular direct arylation demonstrated that *ortho*-substituted aryltrimethylsilanes (e.g., **12b**, Scheme 5.16) transmetalate to Au(III) ~20 times faster than their non-*ortho*- substituted counterparts (e.g., **12c**), a phenomenon attributed to steric decompression upon Wheland intermediate formation. As all of the intramolecular substrates examined thus far are *ortho*-substituted, it was expected that a predominantly 'intra-inter' pathway should operate.

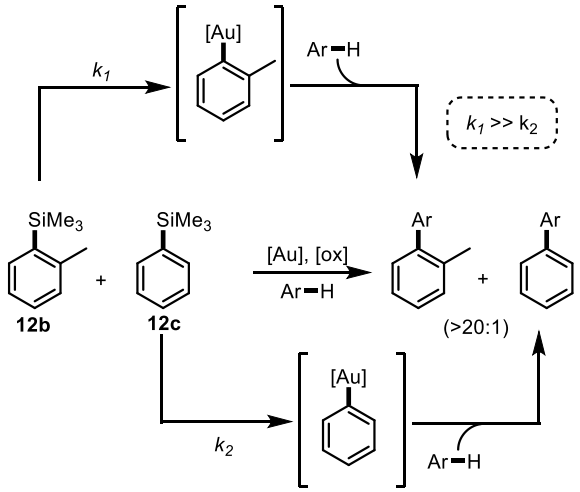

Scheme 5.16. Effect of *ortho*-substitution on rate of transmetalation.

It was clear that judicious choice of intramolecular substrate was going to be key to the success of the reaction. As shown in Chapter 2, the scope of the intramolecular direct arylation is large, spanning 5 – 9 membered rings. However, as the tether length increases, the lifetime of intermediate **I** increases substantially, to the point that varying the tether can alter the resting state of the catalyst (Scheme 5.17). In the domino arylation, if **I** is long lived then there is potential for intermolecular trapping of this intermediate.

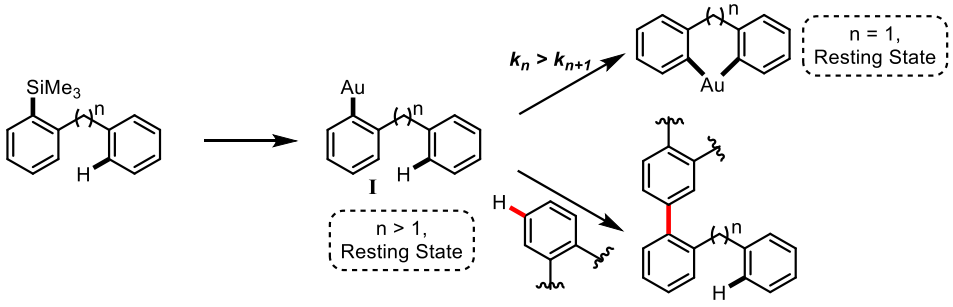

Scheme 5.17. Effect of tether-length on likelihood for intermolecular trapping of catalyst intermediate **I**.

Another consideration is the relative reactivity of the intramolecular substrate, and its cyclised product, toward S_EAr, and therefore k_4 *vs* k_5. Although these parameters were found to be less important than the k_1:k_2 ratio, for perfect regioselectivity, ideally k_5 would be close to zero. These factors led to the nomination of substrates leading to fluorenes to be the intramolecular coupling partners (Scheme 5.18).

This system was chosen for investigation for the following reasons: 1) The kinetics are well understood and the rate constant for cyclisation can easily extracted from the pseudo-zero order reaction profiles (k_3) ; 2) the turnover-limiting step is reductive elimination (k_3) and therefore intermolecular interception of short lived **I** (Scheme 5.17) is unlikely; 3) the fluorene product **2a-u** is sufficiently electron-rich to undergo effective intermolecular coupling but, 4) the starting material **1a-u** should not be significantly activated for intermolecular S_EAr and therefore k_4 is expected to be much greater than k_5. This will reduce the potential for an 'inter-intra' arylation; 5) the R group can be used modulate the sterics and electronics to prevent over-arylation; 6) control of regiochemistry should be achieved as fluorenes react preferentially at the 2-position in electrophilic aromatic substitution reactions.[161]

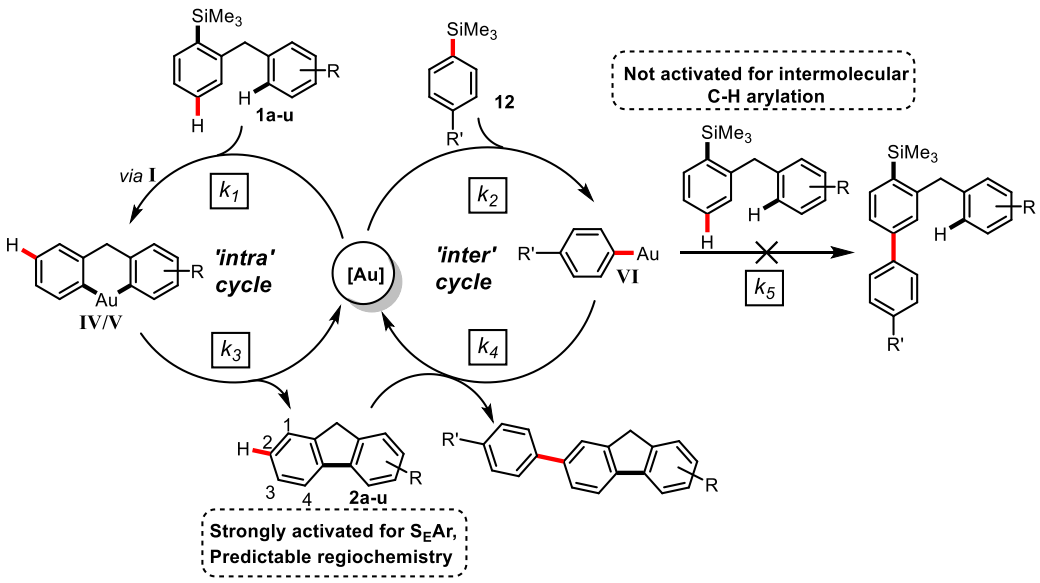

Scheme 5.18. Proposed "intra-inter" domino arylation cycle leading to arylated fluorenes.

5.3.2 Initial Studies

The domino arylation procedure was attempted with **1l** and **12a**. The reaction was monitored by both ^{19}F and ^{1}H NMR spectroscopy. The reaction conditions were modified from the standard conditions outlined in chapter 2 to minimise the effect of diaryliodonium salt formation, which is more significant due to the requirement of 2 equivalents of oxidant. Therefore, the concentration with respect to the substrates was reduced from 0.1 M to 0.05 M, but the overall concentration of oxidant was approximately the same (0.12 M) as previously reported (0.11 – 0.13 M).

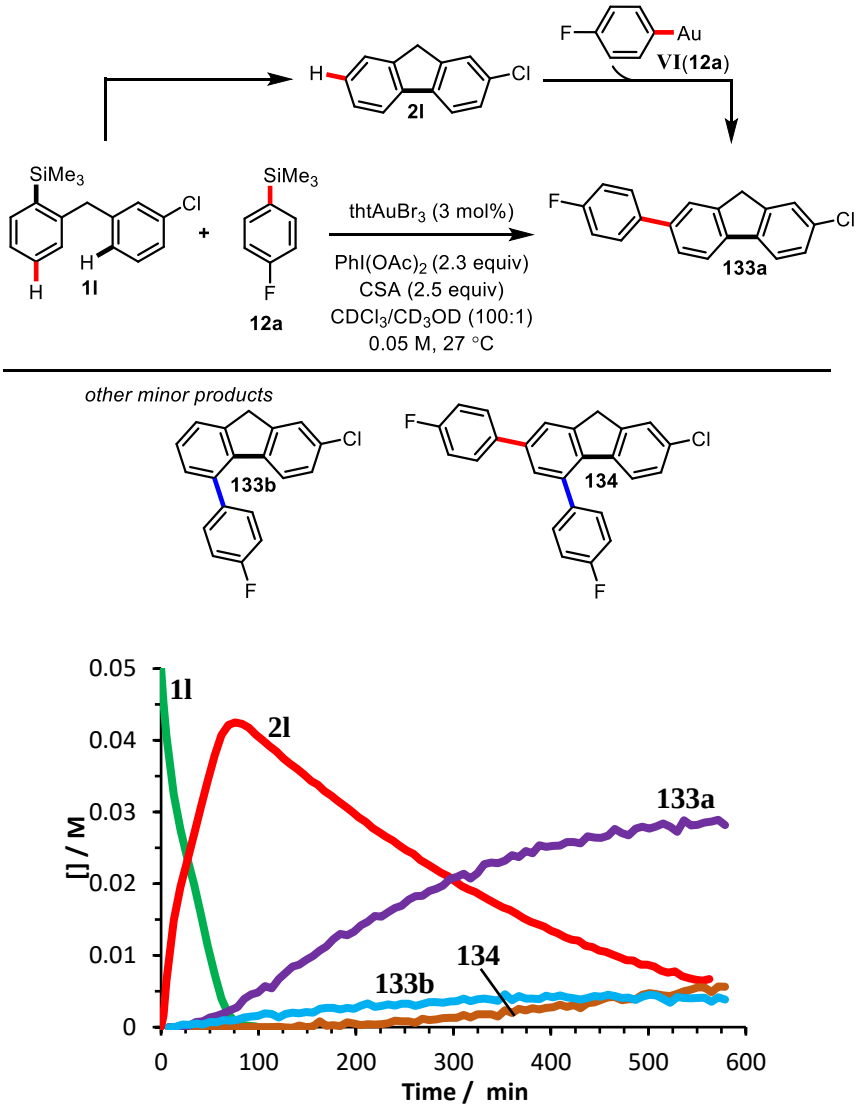

Figure 5.4. Domino arylation of **1l** and **12a**.

Pleasingly, the success of the "intra-inter" domino reaction was experimentally confirmed, with similar kinetic profiles to those predicted in the simulations for high k_1:k_2 ratios (Figure 5.3). As expected, a significant build-up of **2l** was observed, which then decayed to the desired product **133a**. Two other products were observed in the coupling reaction, and careful analysis by 1D and 2D NMR methods unveiled the structures as regioisomer **133b**, and over-arylation product **134**. It was anticipated that these products were a result of imperfect post-cyclisation regioselectivity as the second most reactive position for S_EAr is the 4-position in fluorenes.[161] However, to ensure this was not a result of a pre-cyclisation "inter-intra" pathway, the intermolecular reaction was monitored in isolation.

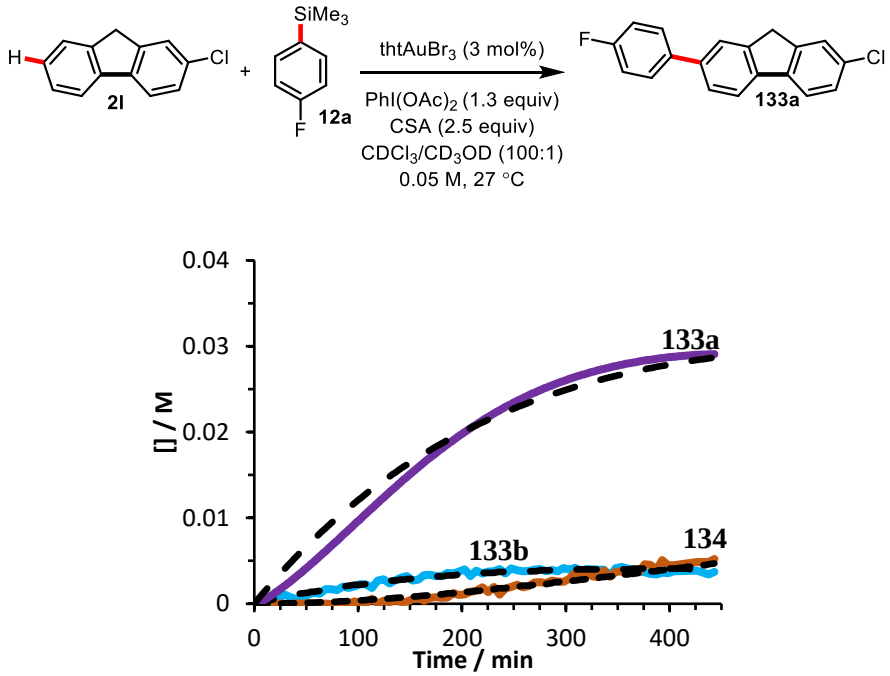

Figure 5.5. Intermolecular arylation of **2l** and **12a** (dashed lines indicate simulated data).

The same side products were observed when the intermolecular reaction was monitored in isolation (Figure 5.5), confirming the imperfect selectivity is inherent in the reaction, rather than being a result of a competing pathway. Through kinetic simulation of this reaction profile, the rate constant for intermolecular arylation (controlled by turnover-limiting π-complexation[83]) and over-arylation could be extracted. The extracted rate constants were k_4= 0.033 dm^3 mol^{-1} s^{-1} for the formation of major isomer **133a**, k_4'= 0.006 dm^3 mol^{-1} s^{-1} for the formation of minor isomer **133b**, and k_8= 0.020 dm^3 mol^{-1} s^{-1} for over-arylation to **134** from **133b** (Scheme 5.19).[iii] Interestingly, the simulation predicted that the over-arylation is solely from minor isomer **133b**. These results demonstrate that the 2-position of **2l** is 5.5× more reactive than the 4-position (k_4 *vs* k_4'), this is in excellent agreement for the rate difference of molecular chlorination of fluorene (**2b**), where the 2-position is measured to be 7.7-fold more reactive than the 4-position.[162]

[iii] For the best fit, a rate constant of k = 2.8×10^{-5} dm^3 mol^{-1} s^{-1} for diaryliodonium formation from **133a** was required.

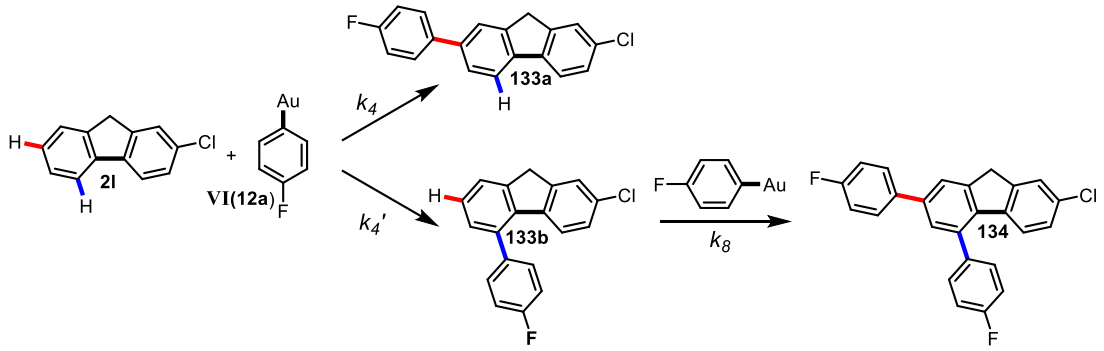

Scheme 5.19. Origin of regioselectivity and double arylation.

The next goal was to extract the k_1:k_2 ratio through simulation of the kinetic profile for the domino reaction. To do so, the individual rate constant for intramolecular coupling was also required. Monitoring the intramolecular reaction in isolation gave a rate constant of k_3 = 0.027 s^{-1} for the turnover-limiting reductive elimination. Employing the rate constants k_3, k_4 and k_4' extracted from the individual rate measurements, and allowing for flexibility in k_1 and k_2, an excellent fit to the experimental data was obtained when the ratio of the transmetalation partition (k_1/k_2) was 28:1. This k_1/k_2 ratio is pleasingly consistent with the previous investigation into relative transmetalation rates of *ortho*- and non-*ortho*-substituted aryltrimethylsilanes.[83]

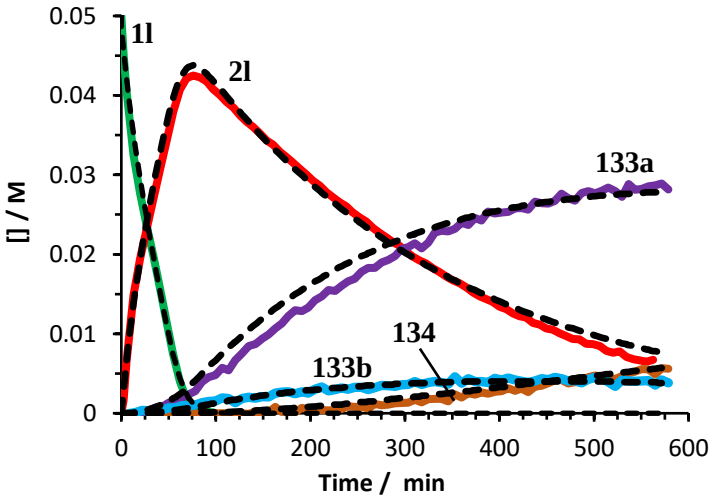

Figure 5.6. Overlay of simulated (dashed) and experimental data for domino arylation of **1l** and **12a** when k_1:k_2 = 28:1.

Although two regioisomers are obtained, the selective nature of the over-arylation means that after extended reaction times the only two products are isomer **133a** and over-arylation product **134**. However, on a preparative scale, the two compounds were not separable by column chromatography. The compounds could be separated by recrystallisation, yielding 30% of **133a**.

5.3.3 Substrate Scope and "Inter-Intra" pathways.

The successful domino arylation of **1l** and **12a** proves the concept of an "intra-inter" reaction, meeting the requirements outlined in the kinetic simulation study. Whilst the reaction was entirely selective for an "intra-inter" pathway, with no product observed from a competing "inter-intra" reaction, imperfect post cyclisation regioselectivity led to minor isomer **133b** and over-arylation product **134**. These side products ultimately led to poor isolated yields, and therefore reduced the synthetic utility of process. Therefore, efforts to uncover a different class of substrate where post cyclisation regiochemistry is perfect and over-arylation does not occur.

Fluorene **2o** (derived from arylsilane **1o**), where the 4-position is blocked, was found to undergo gold-catalysed arylation with **12a** to give **135-F-F** in 76% yield by NMR spectroscopy as a single regioisomer (>99:1 rr), and without any overarylation (Scheme 5.20). Therefore, this class of substrate was chosen to investigate the domino-arylation further.

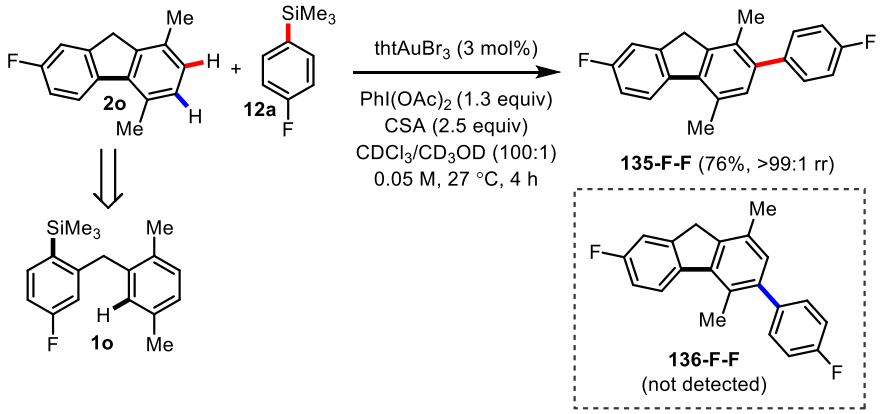

Scheme 5.20. Arylation of fluorene **2o** cleanly affords **135-F-F** as a single regioisomer (no **136-F-F**, or other isomer detected).

Following on from this result, the effect of electronic perturbation through varying the *para* substituent on **12** was measured. First, **1o** and **12b** were subjected to the standard domino arylation conditions and, again, the reaction was monitored by ^{1}H and ^{19}F NMR spectroscopy (Figure 5.7).

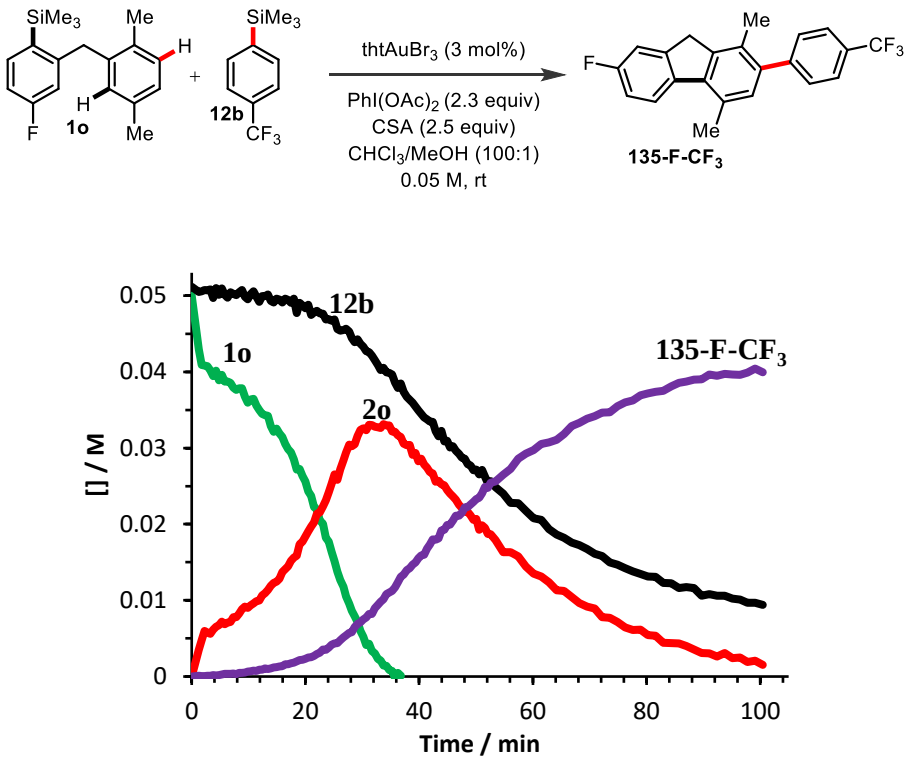

Figure 5.7. Regioselective Domino Arylation of **2o** and **12b**.

Pleasingly, a similar kinetic profile to the reaction of **1l** and **12a** was obtained, with a large build-up of **2o** and a subsequent decay to domino product **136a**. The product was formed as a single regioisomer, with an 80% yield by NMR in under 2 hours. The high yield was maintained on a preparative scale, as 78% could be isolated. A small substrate scope for a series of differently substituted intermolecular silane substrates were then studied (Scheme 5.21).

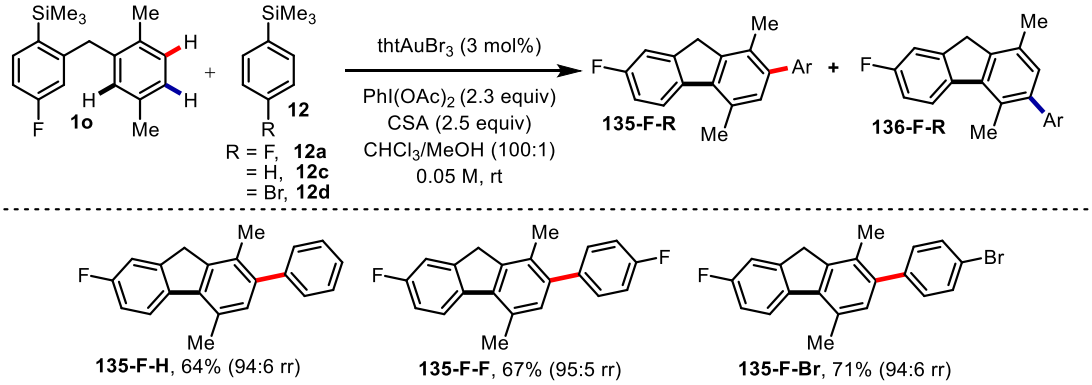

Scheme 5.21. Effect of varying "inter" silane on domino arylation.[iv]

[iv] Authentic sample of **136-F-F** prepared and characterised by Dr. A. Cresswell. Compounds **12a-d** prepared by Dr. A. Cresswell/ Dr. L. Ball.

Intriguingly, when less electron-deficient 'inter' silanes are employed, approximately 5% of a second regioisomer **136** is obtained. As perfect regioselectivity is obtained when the intermolecular arylation is performed in isolation, this result suggests that the intramolecular substrate **2o** is now sufficiently activated, and that a competing "inter-intra" pathway is operating (Scheme 5.22). The reactivity of **2o** toward arylation was confirmed through the control reaction of **138** and **12a**, in which isomer **139** was obtained.[v]

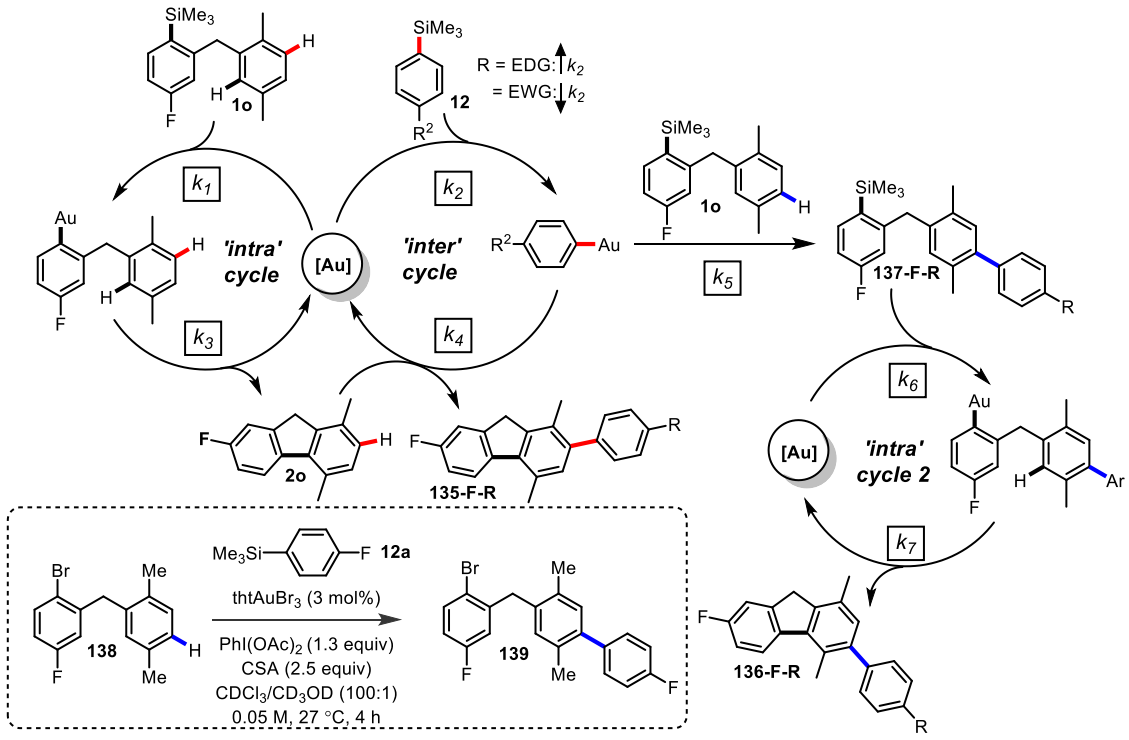

Scheme 5.22. Proposed mechanistic pathway for production of isomers **135** and **136**.

In the mechanistic study into intermolecular direct arylation, competition experiments confirmed that C–Si auration is accelerated by electron-releasing substituents ($\rho = -1.6$).[83] Therefore, more electron-rich 'inter' silanes will increase k_2 and more electron-rich 'intra' silanes will increase k_1. Therefore, more electron-deficient 'inter' silanes should lead to more product from the "intra-inter" pathway. This was observed as **135-F-CF$_3$**, which is formed from the most electron-deficient 'inter' silane **12b** (and therefore the lowest k_2), gave the highest regioselectivity, however a noticeable trend was not observed with the other examples. This is likely due to the transmetalation selectivity (k_1/k_2) being so high already that, within experimental error, a trend cannot be measured within this small electronic range (σ = 0 - 0.23).

[v] Reaction performed and analysed by Dr. A. Cresswell.

The effect of altering the electronics on the 'intra' silane on yield and product distribution was then studied (Scheme 5.23). Regioselectivity was mostly unaffected by the substituent on the 'intra' silane, apart from **1ag** which bears a strongly deactivating *para* CF_3 group. The identity of the substituent did have a large effect on yield, however. When R = H, significant quantities of diarylated product are observed, stressing the importance of having a substituent to prevent additional arylation either through electronic or steric effects. Longer reaction times, or more forcing conditions are required when the silane is deactivated due to the catalyst inhibition processes outlined in Chapter 4. This results in a poorer yield for **135-Cl-F**, and the necessity to heat the reaction of **1ag** and **12a** to form **135-CF_3-F**.

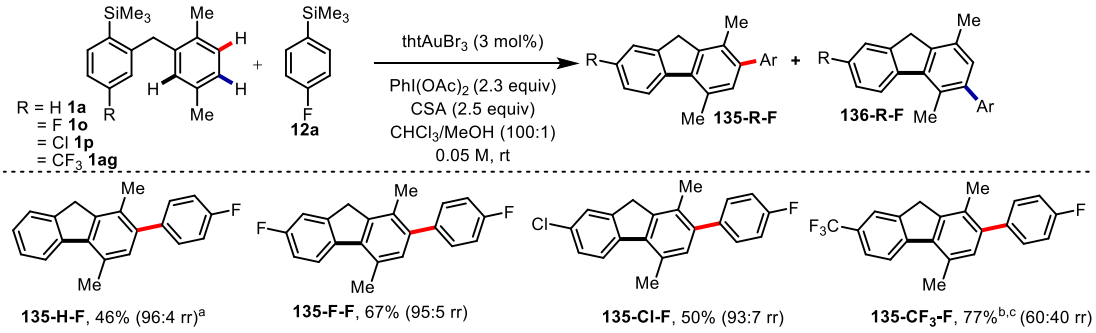

Scheme 5.23. Effect of varying "intra" silane on domino arylation. [a]17% of the diarylated product was also isolated. [b]Reaction was run at 50 °C. [c]Combined yield as measured by ^{19}F NMR spectroscopy against an internal standard.

The poor regioselectivity obtained in the coupling of **1ag** and **12a** (60:40 rr) indicated that a significant amount of product was being generated *via* an "inter-intra" pathway. To ensure this was the case, the intermolecular coupling was monitored in isolation (Scheme 5.24).

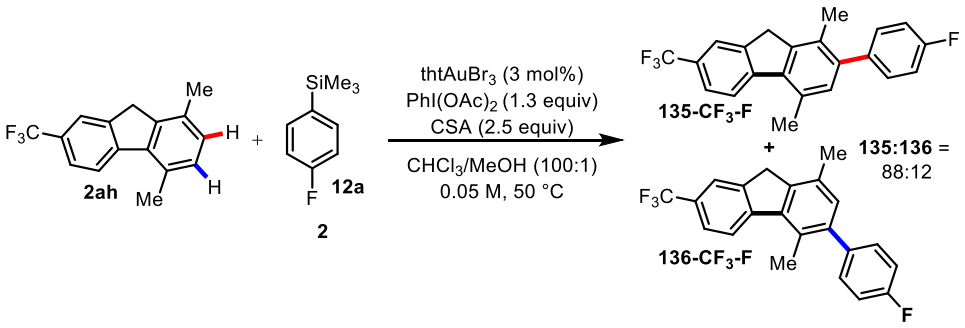

Scheme 5.24. Innate regioselectivity of arylation of **2ah** and **12a**.[vi]

[vi] Authentic sample of **136-CF_3-F** prepared and characterised by Dr. A. Cresswell.

Unlike the coupling of **2o** and **12a** (Scheme 5.20), the regioselectivity was not perfect in this case (88:12 rr), suggesting that the remote CF_3 substituent exerts a significant influence on innate regioselectivity. However, the regioselectivity obtained is significantly higher than that observed in the domino arylation, indicating a significant proportion of **135-F-CF$_3$** is formed from "inter-intra" coupling. Monitoring of the reaction confirmed this as a significant build-up of the products from both the "intra-inter" and "inter-intra" mechanistic pathways.

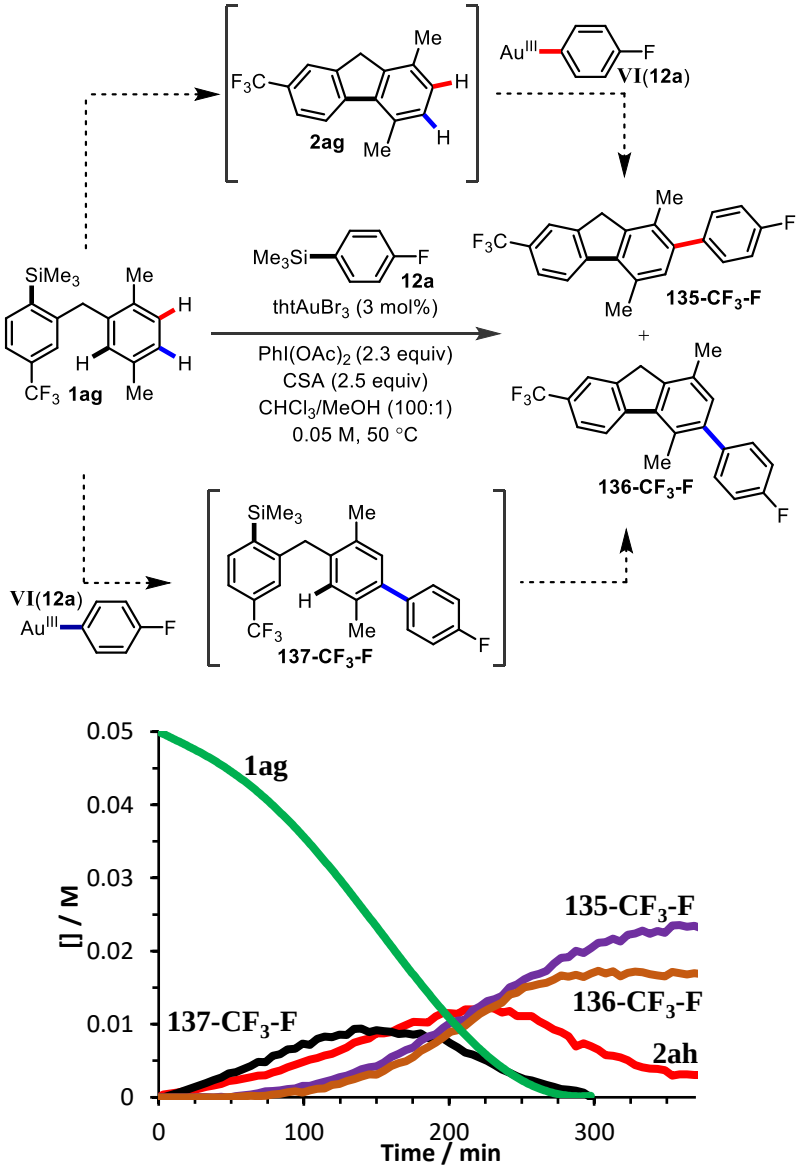

Figure 5.8. Domino arylation with intermediates and products from both "intra-inter" and "inter-intra" pathways.

The presence of two regioisomers which result from different mechanistic pathways raised the prospect of designing a system whereby either isomer could be obtained selectively. To do so,

a new class of coupling partner "T" would need to be designed as a replacement for the TMS group, which displays a greater selectivity for the gold catalyst, so that greater discrimination between the 'inter' and 'intra' substrates can be obtained. By doing so, depending on the position of "T", the reaction could proceed via an 'inter-intra' pathway yielding one regioisomer, or an 'inter-intra' to give the other (Scheme 5.25).

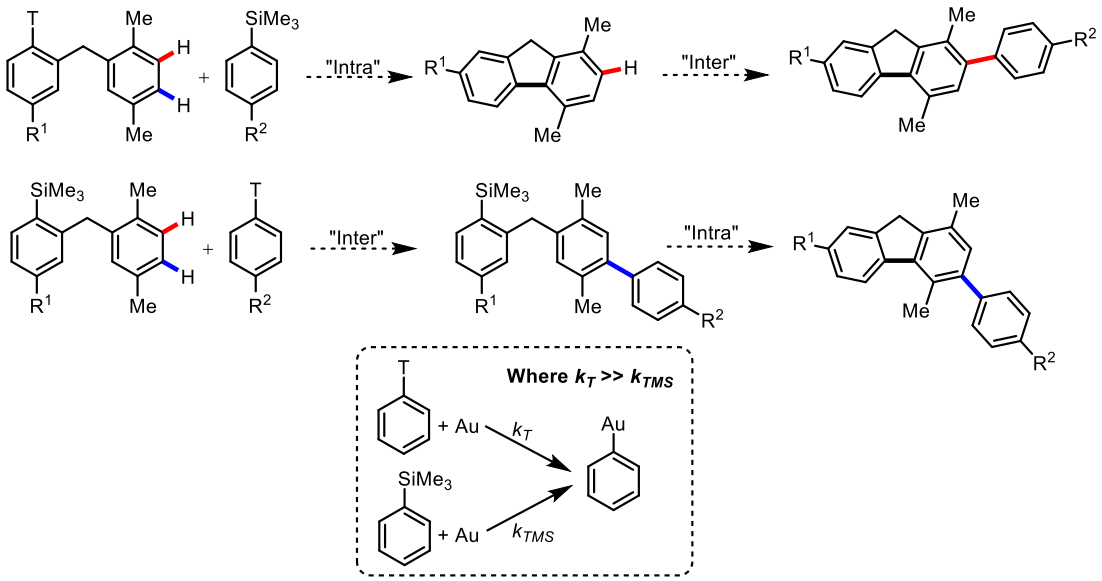

Scheme 5.25. Design of new transmetalating reagent could lead to increased regioselectivity.

Recent developments in the group have shown that replacing the TMS group with 3-hydroxypropyldimethylsilyl (HPDMS)[82] leads to increased transmetalation rates. Whilst the exact mechanism that leads to this rate acceleration is undetermined, a plausible explanation is through an intramolecular delivery of the gold after binding to the alcohol (Scheme 5.26).

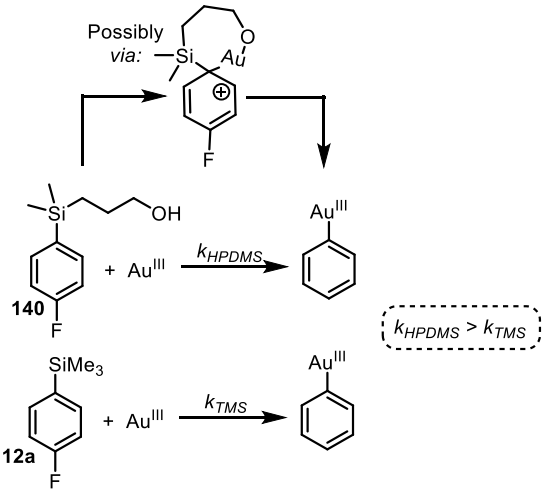

Scheme 5.26. HPDMS as an alternative transmetalating reagent.

It was hoped that replacing **12a** with **140**[vii] in the domino arylation with **1ag** could lead to a selectivity switch. Unfortunately, no change in selectivity was obtained when employing HPDMS (Scheme 5.27). Studies into quantifying the rate acceleration by HPDMS, and the exact mechanism of transmetalation are ongoing, however a possible explanation for this lack of improvement could be that at high temperatures the impact of intramolecular delivery by the alkoxy group is reduced.

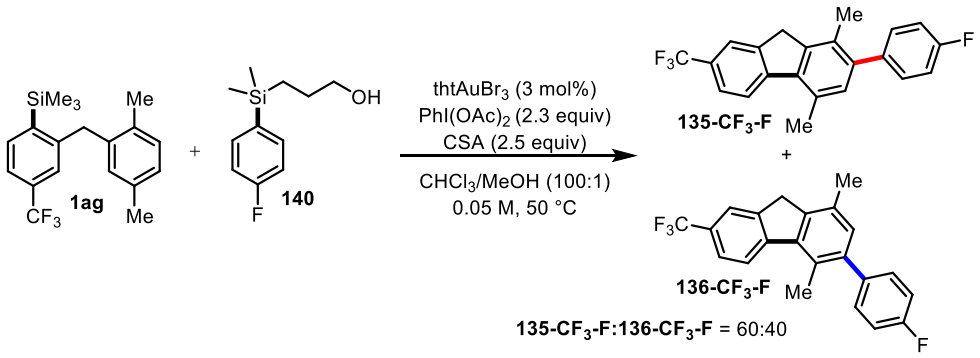

Scheme 5.27. Use of HPDMS on 'inter' silane for domino arylation.

5.4 Summary

Through kinetic simulation, the guiding principles for the development of domino reactions combining intra- and intermolecular direct arylation are presented. Two distinct mechanistic pathways are shown, where the ordering of events, either "intra-inter" or "inter-intra", can have a great impact on kinetic profile, yield and regioselectivity. The crucial kinetic parameter which largely determines these three factors is the partition between the "C-X" functional groups on the 'inter' and 'intra' substrate (k_1 *vs* k_2). For a successful reaction, one of these pathways must dominate (i.e. $k_1 > k_2$ or $k_2 > k_1$), as a mixture of both pathways could either lead to catalyst deactivation, or a mixture of isomers, depending on the innate reactivity of the substrates.

This theoretical analysis, in combination with prior mechanistic understanding into intra- and intermolecular gold-catalysed direct arylation, led to the proposal that an "intra-inter" arylation protocol could be developed. This is confirmed experimentally, with excellent agreement to the simulated data. The success of this reaction underpins how mechanistic understanding, in combination with computational rationale, can be key in the development of novel methodologies. Under certain circumstances the reaction displays impressive levels of both chemo- and regioselectivity, however, deliberate electronic perturbation of the system can

[vii] Prepared by Dr. A. Cresswell.

trigger an alternative “inter-intra” pathway and lead to a mixture of isomers, as predicted by the kinetic simulation. Attempts to exploit this competing process using novel transmetalating reagents failed, however further exploration into reagents that transmetalate at vastly different rates that could lead to complete discrimination between two mechanistic pathways is an enticing prospect for the future. Whilst only a select number of substrates were attempted as a proof of concept, considering the breadth of substrates available through intramolecular direct arylation, the full scope is likely to be diverse and synthetically valuable.

6. Conclusions and Future Work

6.1 Conclusions

The intramolecular direct arylation of aryltrimethylsilanes and arenes has been investigated from both preparative and mechanistic aspects. The reaction generates 5- to 9-membered rings, with the majority of reactions requiring only 1 – 2 mol% of catalyst at room temperature. The breadth of scope and mild reaction conditions employed establishes this methodology as a viable alternative to typical palladium-catalysed routes.

Intramolecular arylation, particularly the examples generating substituted fluorene products proved ideal for mechanistic study. The large electronic range tolerated allowed for a holistic investigation of the reaction mechanism, as opposed to the reliance on a single well-behaved model system. Investigation across numerous substrates avoided erroneous extrapolation of conclusions, as small structural changes resulted in significant kinetic consequences. Indeed, depending on tether length and arene electronics, the catalyst resting state moved from a monoaryl gold(III) complex **I**, to a diarylgold(III) complex **IV**/**V**, with turnover-limiting π-complexation or reductive elimination, respectively.

Monitoring of the entire kinetic profile, as opposed to initial rate studies, unveiled a complex off-cycle pathway when electron-deficient silanes are used. In combination with kinetic modelling, a novel catalyst inhibition pathway was unveiled. The importance of identifying catalyst inhibition pathways was stressed, as understanding and avoiding these processes can lead to highly active catalyst species.

Finally, the mechanistic understanding of both the intra- and intermolecular protocols led to the advance of a domino-arylation reaction. Kinetic simulation was key in outlining the general principles for such a reaction to be successful, with the conclusions applicable to any domino arylation protocol.

6.2 Additional Experiments and Future Work

6.2.1 Au(I)/Au(III) redox

In combination with prior studies into intermolecular arylation, the catalytic cycle and the factors that govern each step are now well-understood. It is only the final step in the catalytic cycle, the Au(I)/Au(III) redox, for which minimal mechanistic information is known. However, understanding this process could lead to significant synthetic advances. As demonstrated throughout this project, the oxidant is the source of several deleterious processes; it forms diaryliodonium salts from electron-rich arenes, limiting substrate scope and causing catalyst deactivation in the synthesis of allocolchicine, it releases water, which results in catalyst inhibition pathways, and relative to other oxidants, it is expensive. However,

it is necessary, as only hypervalent iodine oxidants have been shown to be competent. If it could be understood why hypervalent oxidants are needed, and if this information leads to the use of inorganic oxidants, the process would be transformed by the tolerance of new, highly electron-rich functionality, which could include a broader range of heterocycles, many of which are not currently tolerated.

6.2.1.1 Speciation of Hypervalent Iodine Oxidants

Studies into hypervalent iodine oxidant species by Koser *et al* demonstrated that that the speciation of hypervalent iodine oxidants in solution is complicated.[163] This is a significant hurdle to understanding the oxidation process as identifying the active species is non-trivial. When HCIB is employed under the reaction conditions, a single species is observed by ^{1}H NMR, suggesting that all species present are in rapid equilibrium. However, when PIFA was used it was noted that the speciation was different depending on whether methanol was a co-solvent or not.

In dry chloroform, PIFA can be observed as a single species in solution by ^{1}H NMR. However, upon addition of methanol, a new distinct species is observed immediately. The observation of two distinct by ^{1}H NMR suggests a relatively slow equilibrium, however the time between mixing and running the experiment is sufficient for the equilibrium to be reached. The peak of the new species broadens and slowly shifts upfield with time, consistent with a fast equilibrium with another species in solution (Figure 6.1). As PIFA was found to not be a competent oxidant in the absence of methanol, it was of interest to identify the different species as one of these is likely the active oxidant. In addition, PIFA is a commercially available oxidant, and has been used in combination with alcohols synthetically,[164–167] so identifying speciation would be of interest to the general chemical community.

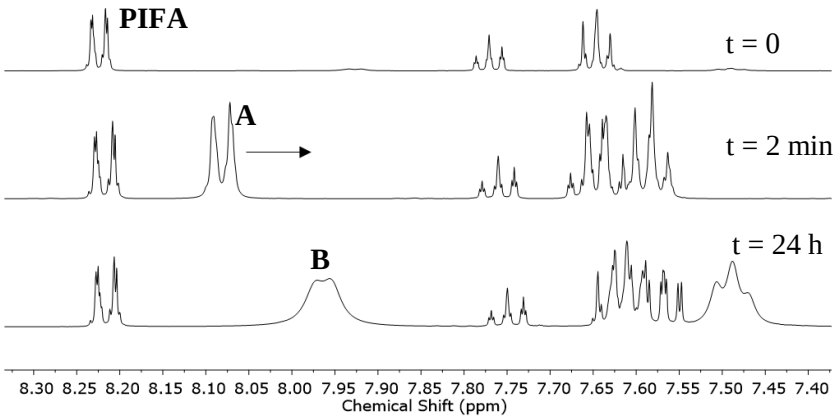

Figure 6.1. ^{1}H NMR spectra of PIFA, before and after addition of methanol.

X-ray crystallographic analysis on the final species, **C**, confirmed that the anhydride of PIFA had formed **141**. With the final species identified, the mechanism of its formation, and the identity of the intermediate species, was investigated.

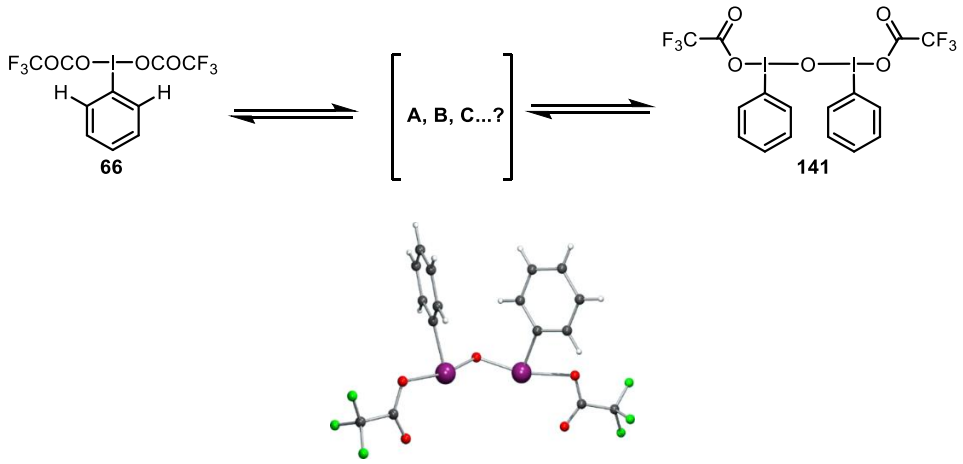

Scheme 6.1. Top: Formation of **141** *via* unknown intermediates. Bottom X-ray crystal structure of **141**.

Alcock and Varvoglis[168] previously reported the synthesis of **141** by treating PIFA with a strong base, such as NaOMe. Alongside **141**, trifluoromethyl acetate **142** was formed leading to the mechanistic conclusion that attack at the carbonyl occurred over attack at iodine to form **143**, which could then subsequently attack another molecule of PIFA, but at iodine. In the study presented herein, close inspection of the reaction mixture revealed trifluoromethyl acetate had formed, therefore it was of interest to assess whether the same type of mechanism was operating under non-basic conditions (Scheme 6.2).

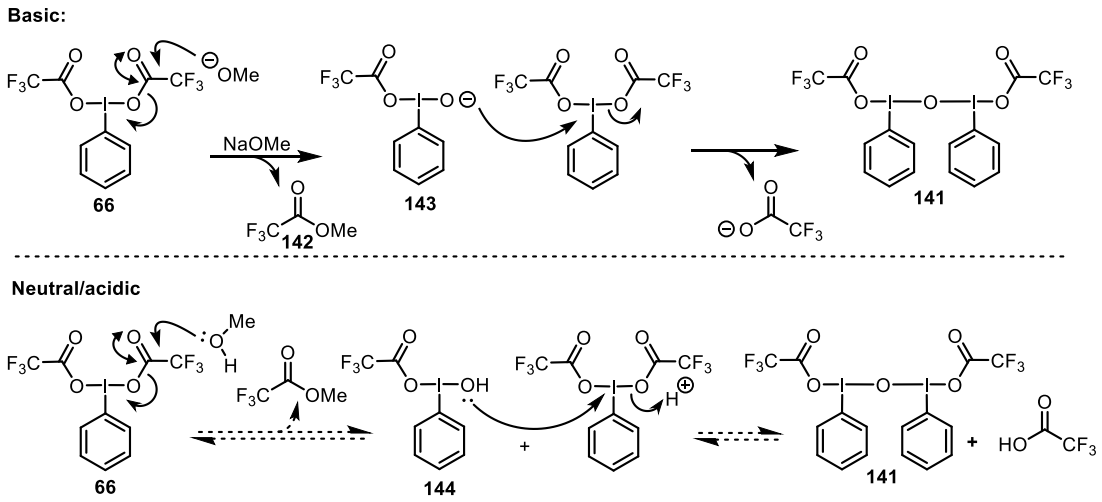

Scheme 6.2. Proposed mechanism of anhydride formation under basic conditions, and possible mechanism under neutral or acidic conditions

To assess whether a similar mechanism occurred in the non-basic system investigated herein, the temporal profile of the equilibration was measured (Figure 6.2). The formation of the anhydride was monitored by the change in chemical shift in the ^{1}H NMR spectra observed on conversion of **66** to **141**. The concentration of trifluoromethyl acetate was monitored by ^{19}F NMR spectroscopy.

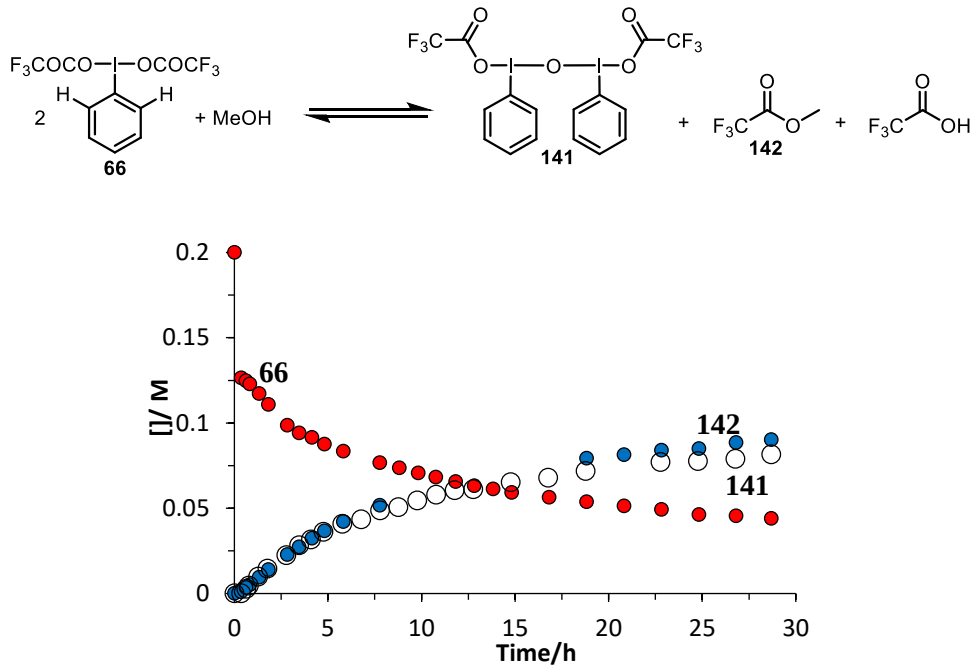

Figure 6.2. Formation of **141** and trifluoromethyl acetate from **66** and MeOH.

These results are inconsistent with the mechanism proposed by Alcock and Varvoglis for the base-mediated process.[168] PIFA reaches equilibrium with '**A**' rapidly, but without associated production of **142**, which would be expected if the identity of **A** was **144**. In fact, the rate of formation of **142** mirrors that of the anhydride **141**. Therefore, another mechanism must be controlling the conversion of PIFA to **141**. An alternative mechanism was proposed (Scheme 6.3), where methanol attacks PIFA at iodine first, liberating TFA and forming **145a**. The methanol co-solvent then reacts with TFA, forming an equilibrium with trifluoromethyl acetate and water. The water then displaces methanol, forming the hydroxy species **144,** which then rapidly reacts with another molecule of PIFA to form **141**. Since the generation of anhydride **141** mirrors the formation of **142**, the equilibrium from **144** to **141** must be fast. Control experiments confirmed that methanol and TFA do indeed form **142**. If methanol is replaced with water, then **144** can form directly from PIFA, and thus form **141**. Therefore, if dry solvents are not employed with PIFA, it is likely a significant proportion of the oxidant species is **141**.

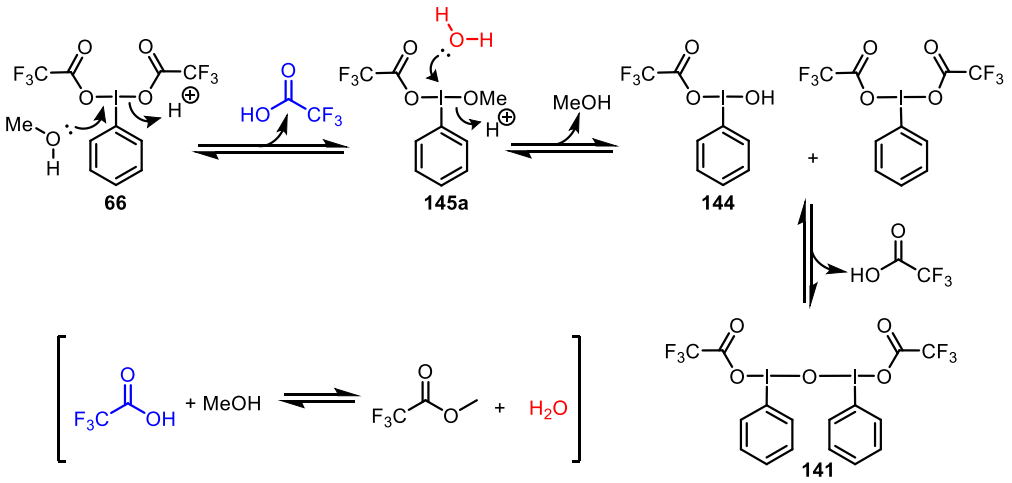

Scheme 6.3. Proposed mechanism and speciation of PIFA in $CHCl_3$/MeOH.

To investigate this equilibration in more detail, the effect of other alcohols on the equilibrium was measured. A Hammett LFER plot was generated from a series of *para* substituted benzyl alcohols. These alcohols were significantly less reactive towards esterification, and therefore the initial equilibrium of PIFA with **145** could be measured accurately by ^{1}H NMR spectroscopy.

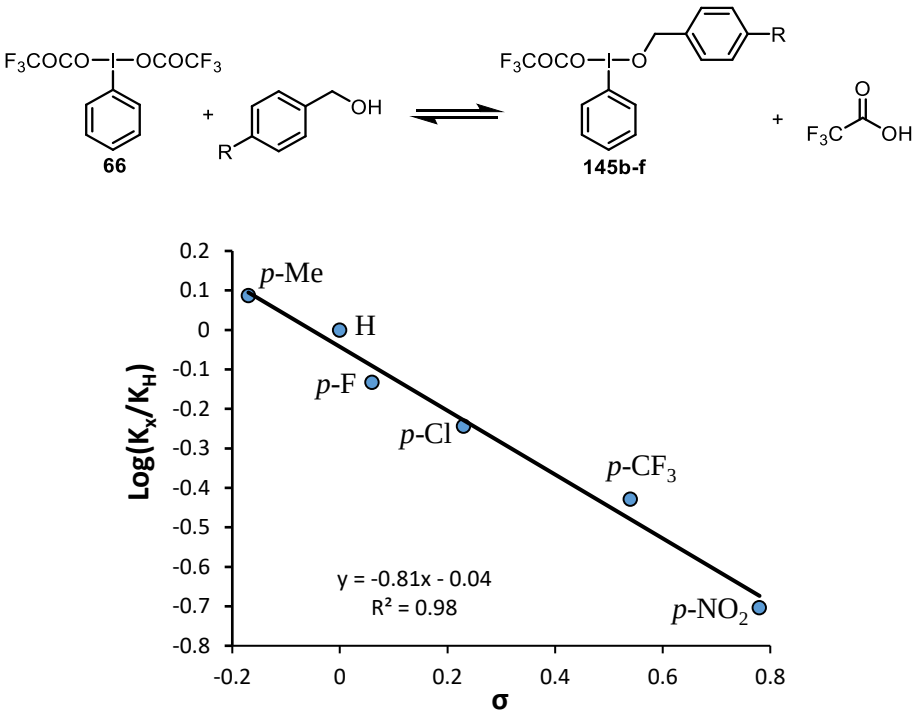

Figure 6.3. Hammett LFER for series of substituted benzyl alcohols.

The equilibrium is favoured by electron-donating substituents ($\rho = -0.8$), due to stabilisation of the electron-deficient iodine centre with a more electron-rich alcohol. The effect of different

alcohols on this equilibrium constant was then measured (Table 6.1). Surprisingly, even with very acidic alcohols such as TFE (entry 4) and hexafluoroisopropanol (HFIP, entry 5), this equilibrium still occurs, albeit with low equilibrium constants.

Table 6.1. Equilibrium constants for series of alcohols.

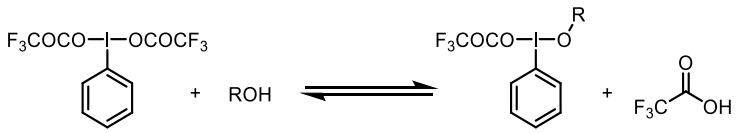

Entry	Alcohol	K_{eq}
1	MeOH	0.92
2	Isopropanol	1.03
3	*Tert*-butanol	0.59
4	Trifluoroethanol	0.005
5	HFIP	0.001

From a synthetic perspective, the presence of this equilibrium is important in the reduction of diaryliodonium salt formation. It was noted during the synthesis of allocolchicine that the absence of methanol, or the use of more acidic alcohols such as TFE, led to increased rates of diaryliodonium salt formation. This suggests that **145a** is less susceptible to diaryliodonium salt formation than PIFA. Additionally, the fact that the direct arylation procedure does not turnover in the absence of methanol suggests that the active oxidant is one of the species formed during this equilibration. A reasonable hypothesis is that the hydroxy species **144** is the active oxidant, as pre-coordination of this species to gold(I) may be required to facilitate oxidation.

Finally, the effect of addition of methanol to IBDA, which is widely used in organic synthesis was determined. The initial displacement of acetic acid with methanol to **146** was observed, but there was no further equilibration to the anhydride. Crucially, in control experiments, acetic acid did not react with methanol to form methyl acetate. In the absence of this equilibrium, no water is liberated, and therefore no route to the anhydride is available as **147** is not formed. A Job plot was constructed, and this confirmed the proposed 1:1 ratio between methanol and IBDA in the equilibrium.

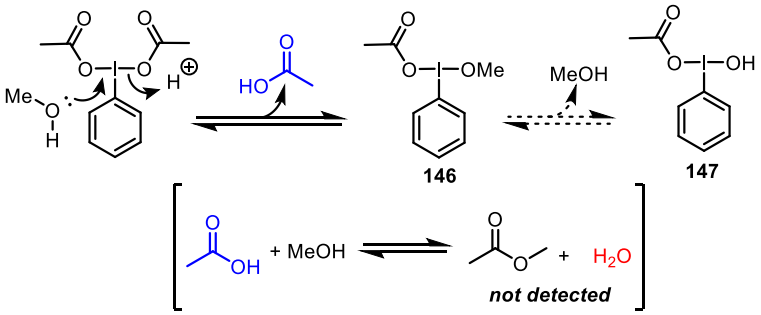

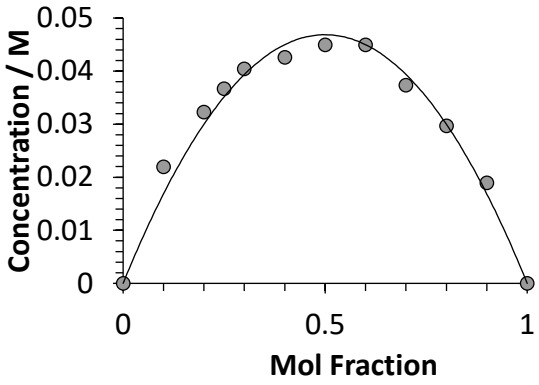

$$K = \frac{[\mathbf{146}][AcOH]}{[IBDA][MeOH]} = 0.07 \pm 0.01$$

Figure 6.4. Job plot of equilibrium of IBDA and MeOH and equilibrium constant.

The fact that IBDA is not a competent oxidant, even in the presence of methanol, gives further evidence of the importance of the hydroxy species **144**/**147**. Further experiments are needed to assess this hypothesis, possibly through deliberate addition of water to IBDA in catalysis to observe whether this induces turnover through the formation of the hydroxy species **147**.

6.2.1.2 *m*CPBA as an Alternative Oxidant

It was proposed that catalytically generating the active hypervalent iodine species through *in-situ* oxidation of an aryl iodide by *m*CPBA would limit the negative impacts of the hypervalent iodine oxidant by maintaining a constant low concentration (Scheme 6.4). The use of sub-stoichiometric levels of 4-fluoroiodobenzene **148** in the presence of a stoichiometric amounts of *m*CPBA was attempted in the cyclisation of **1a**. The use of 4-fluorobenzene was to track the oxidation process to F-HCIB (**149**) by ^{19}F NMR spectroscopy No turnover was observed under the standard conditions with 20 mol% **148** and *m*CPBA (Scheme 6.5).

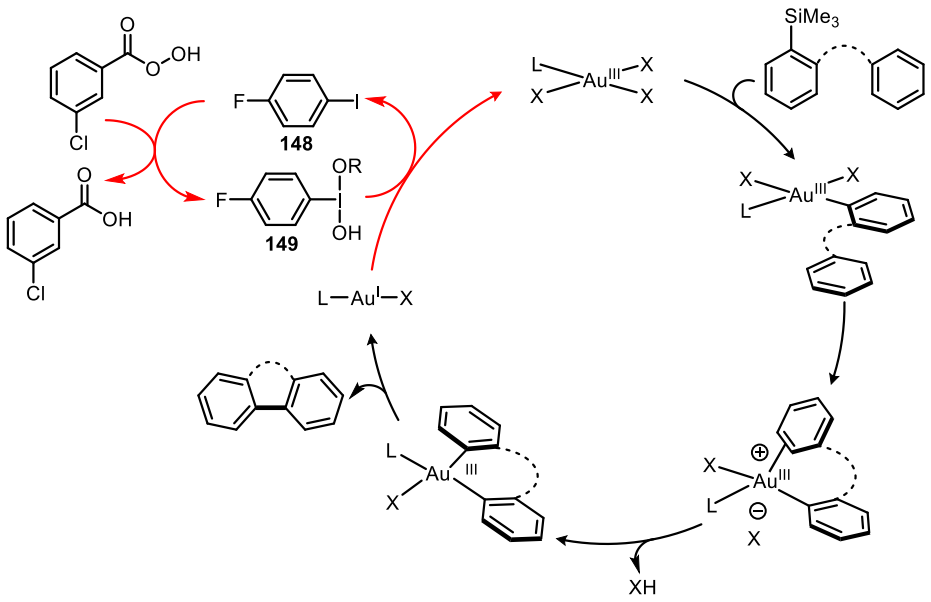

Scheme 6.4. Proposal for *in-situ* formation of active oxidant by *m*CPBA.

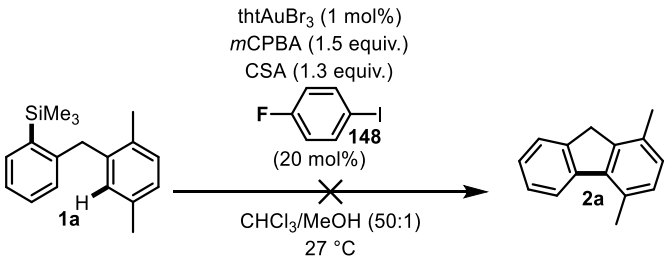

Scheme 6.5. Attempted synthesis of **2a** using aryl iodide **148** and *m*CPBA.

It was anticipated that this redox process could be dependent on solvent, and therefore chloroform and methanol were replaced with MeCN. Turnover was observed when MeCN was used as a solvent, however upon inspection of the ^{19}F NMR spectrum, there was no indication that **149** had formed. Control experiments revealed that the addition of **148** was not needed, and *m*CPBA was facilitating the Au(I)/Au(III) redox.

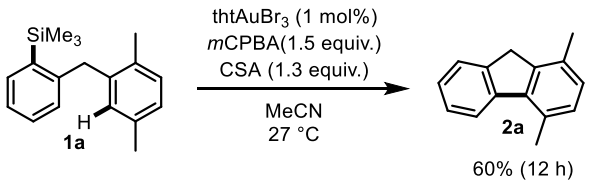

Scheme 6.6. Synthesis of **2a** using *m*CPBA as the oxidant.

However, the reaction was slow, as **1a**, which under the standard conditions forms **2a** quantitatively within a few minutes, took several hours to reach 60% yield by ^{1}H NMR

spectroscopy. Additionally, 1.5 equivalents of *m*CPBA was not sufficient due to an apparent background degradation of the by-product methoxytrimethylsilane by *m*CPBA (Figure 6.5).

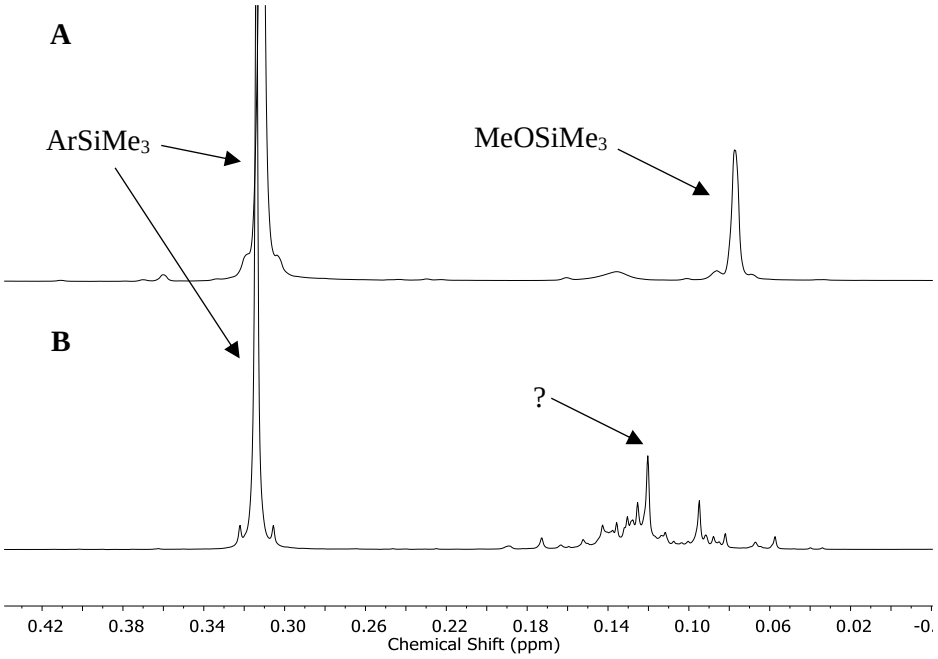

Figure 6.5. Fate of TMS group under **A**, the standard reaction conditions and **B**, with *m*CPBA.

Nevertheless, this is mechanistically interesting as it is the first example of a non-hypervalent iodine oxidant facilitating turnover. Additionally, qualitatively the identity of the substrate does not seem to affect the rate of turnover, as both **1a** and **1b**, which have vastly different reaction times under standard conditions (See Table 2.4, Chapter 2), form roughly the same amount of their respective products in equal times. This could be due to a turnover-limiting oxidation.

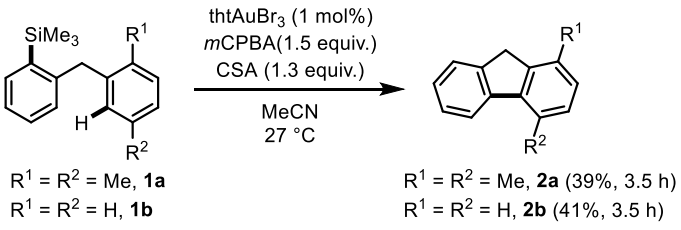

Scheme 6.7. Effect of substrate on conversion at identical time point using *m*CPBA as the oxidant. Yield by ^{1}H NMR.

If chloroform is used instead of MeCN, Au particulates form rapidly, and therefore the presence of MeCN may serve to stabilise Au(I) prior to slow oxidation. The overall structure of *m*CPBA is also not dissimilar to HCIB: as both contain a hydroxy group to which Au(I) can

bind, and an aromatic group, which could lead to stabilisation through π-complexation. These results warrant further investigation, and emphasise the point that solvent choice could be key in the identification of an alternative oxidant system.

6.2.2 Ligand Development

Preliminary results from Dr. L. Ball identified a rate increase in the coupling of **98** and **12a** upon addition of catalytic quantities of a sulfoxide (e.g. DMSO). It was not conclusively determined whether this increase was due to a ligand or solvent effect. The realisation that intra- and intermolecular direct arylation proceed with different turnover-limiting steps raised the prospect of investigating the effect of sulfoxides on different steps in the catalytic cycle. Repetition of the studies confirmed the effect of the addition of DMSO. The rate increase continued with increasing concentrations of DMSO, however, evidence of catalyst deactivation occurred when 5 equivalents of DMSO are added.

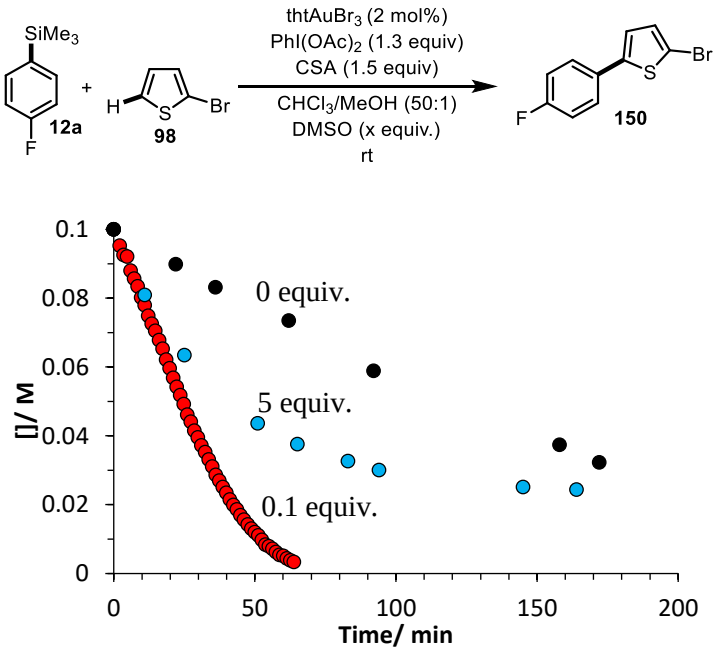

Figure 6.6. Effect of DMSO on rate of consumption of **12a**.

However, no effect was observed on the rate of intramolecular coupling (Scheme 6.8).

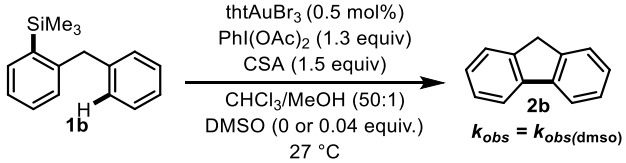

Scheme 6.8. Intramolecular cyclisation of **1b** proceeds at the same rate with and without DMSO.

As two different TLSs are operative, this suggested that sulfoxides exclusively increase the rate of π-complexation. To verify this hypothesis, the effect of DMSO on the rate of coupling of **12a** and **151** was investigated. Once again, no rate increase was observed. In fact, reduced rates are observed with added DMSO (Figure 6.7).

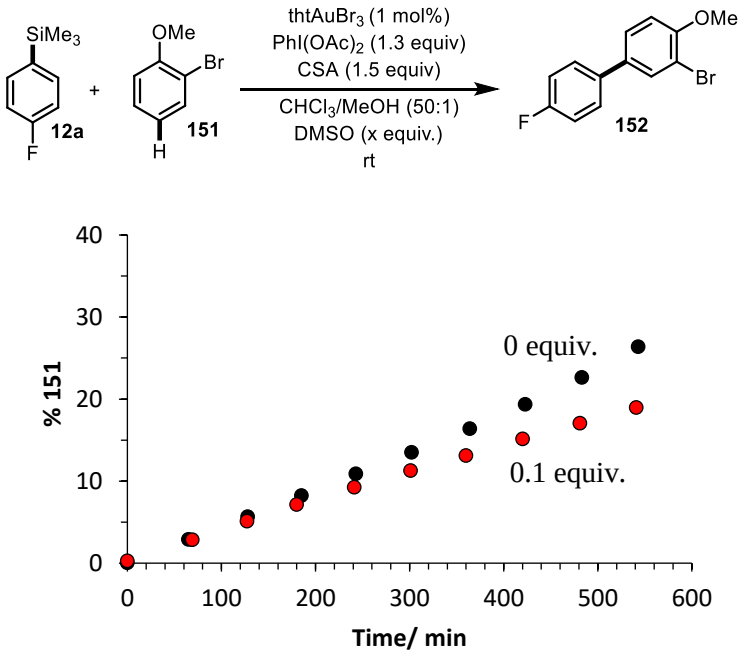

Figure 6.7. Effect of DMSO on rate of coupling of **12a** and **151**.

This seemingly selective rate enhancement for coupling of **98** is further demonstrated through the addition of DMSO to the competition experiment introduced in Chapter 3, where **98** can compete with the intramolecular cyclisation of **2m**. If π-complexation of the respective intra- and intermolecular arene moieties to the resulting monoaryl gold(III) resting state **I**(**2m**) is the selectivity determining step, then one would expect DMSO, if ligated to the gold, to accelerate each step equally. This should lead to no selectivity difference whether DMSO is present or not. However, this is not observed (Figure 6.8) and a complete selectivity switch occurs from **2m** as the major product in the absence of DMSO, to **99** when 20 mol% DMSO is added. Whilst these effects are not fully understood, it could suggest that the kinetically significant step of C-H metalation in substrates such as **2m** and **151** is not π-complexation, with WI formation being a viable alternative.

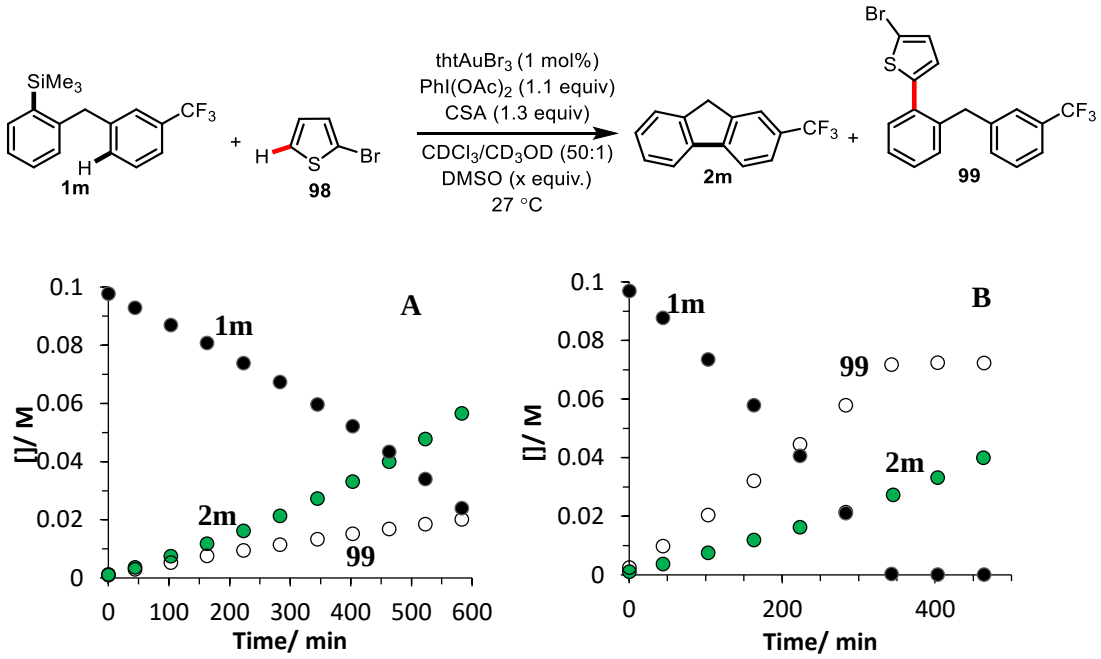

Figure 6.8. Partition between intramolecular cyclisation, and intermolecular coupling under standard conditions (**A**) and with 20 mol% DMSO (**B**)

Further investigation into the effect of DMSO is needed, as conclusive evidence of sulfoxide binding to gold could pave the way for chiral ligand development.

7. References

[1] M. Baumann, I. R. Baxendale, *Beilstein J. Org. Chem.* **2013**, *9*, 2265–2319.

[2] D. J. C. Constable, P. J. Dunn, J. D. Hayler, G. R. Humphrey, J. Leazer Johnnie L., R. J. Linderman, K. Lorenz, J. Manley, B. A. Pearlman, A. Wells, A. Zaks, T. Y. Zhang, *Green Chem.* **2007**, *9*, 411–420.

[3] C. C. C. Johansson Seechurn, M. O. Kitching, T. J. Colacot, V. Snieckus, *Angew. Chem. Int. Ed.* **2012**, *51*, 5062–5085.

[4] M. Tamura, J. Kochi, *Synthesis* **1971**, *1971*, 303–305.

[5] E. Negishi, D. E. Van Horn, *J. Am. Chem. Soc.* **1977**, *99*, 3168–3170.

[6] S. Baba, E. Negishi, *J. Am. Chem. Soc.* **1976**, *98*, 6729–6731.

[7] E. Negishi, S. Baba, *J. Chem. Soc. Chem. Commun.* **1976**, 596b–597b.

[8] K. Tamao, *J. Organomet. Chem.* **2002**, *653*, 23–26.

[9] K. Tamao, K. Sumitani, M. Kumada, *J. Am. Chem. Soc.* **1972**, *94*, 4374–4376.

[10] R. J. P. Corriu, J. P. Masse, *J. Chem. Soc. Chem. Commun.* **1972**, 144a–144a.

[11] M. Tamura, J. K. Kochi, *J. Am. Chem. Soc.* **1971**, *93*, 1487–1489.

[12] G. A. Molander, B. J. Rahn, D. C. Shubert, S. E. Bonde, *Tetrahedron Lett.* **1983**, *24*, 5449–5452.

[13] G. Cahiez, H. Avedissian, *Synthesis* **1998**, *1998*, 1199–1205.

[14] A. Fürstner, A. Leitner, M. Méndez, H. Krause, *J. Am. Chem. Soc.* **2002**, *124*, 13856–13863.

[15] E. Negishi, *Angew. Chem. Int. Ed.* **2011**, *50*, 6738–6764.

[16] J. H. Ahn, C. Wang, I. F. Perepichka, M. R. Bryce, M. C. Petty, *J. Mater. Chem.* **2007**, *17*, 2996–3001.

[17] J. K. Stille, *Angew. Chem. Int. Ed.* **1986**, *25*, 508–524.

[18] N. Miyaura, T. Yanagi, A. Suzuki, *Synth. Commun.* **1981**, *11*, 513–519.

[19] D. Alberico, M. E. Scott, M. Lautens, *Chem. Rev.* **2007**, *107*, 174–238.

[20] G. P. McGlacken, L. M. Bateman, *Chem. Soc. Rev.* **2009**, *38*, 2447–2464.

[21] I. Hussain, T. Singh, *Adv. Synth. Catal.* **2014**, *356*, 1661–1696.

[22] Y. Yang, J. Lan, J. You, *Chem. Rev.* **2017**, DOI 10.1021/acs.chemrev.6b00567.

[23] M. Lafrance, C. N. Rowley, T. K. Woo, K. Fagnou, *J. Am. Chem. Soc.* **2006**, *128*, 8754–8756.

[24] N. Kuhl, M. N. Hopkinson, J. Wencel-Delord, F. Glorius, *Angew. Chem. Int. Ed.* **2012**, *51*, 10236–10254.

[25] L. Ackermann, *Chem. Rev.* **2011**, *111*, 1315–1345.

[26] J. A. Labinger, J. E. Bercaw, *Nature* **2002**, *417*, 507–514.

[27] W. D. Jones, F. J. Feher, *J. Am. Chem. Soc.* **1982**, *104*, 4240–4242.

[28] W. D. Jones, F. J. Feher, *J. Am. Chem. Soc.* **1984**, *106*, 1650–1663.

[29] R. A. Periana, R. G. Bergman, *J. Am. Chem. Soc.* **1984**, *106*, 7272–7273.

[30] W. D. Jones, F. J. Feher, *J. Am. Chem. Soc.* **1986**, *108*, 4814–4819.

[31] S. T. Belt, S. B. Duckett, M. Helliwell, R. N. Perutz, *J. Chem. Soc. Chem. Commun.* **1989**, 928–930.

[32] S. T. Belt, L. Dong, S. B. Duckett, W. D. Jones, M. G. Partridge, R. N. Perutz, *J. Chem. Soc. Chem. Commun.* **1991**, 266–269.

[33] R. M. Chin, L. Dong, S. B. Duckett, M. G. Partridge, W. D. Jones, R. N. Perutz, *J. Am. Chem. Soc.* **1993**, *115*, 7685–7695.

[34] Y. Aoyama, T. Yoshida, K. Sakurai, H. Ogoshi, *Organometallics* **1986**, *5*, 168–173.

[35] I. V Seregin, V. Gevorgyan, *Chem. Soc. Rev.* **2007**, *36*, 1173–1193.

[36] D. Lapointe, K. Fagnou, *Chem. Lett.* **2010**, *39*, 1118–1126.

[37] L.-C. Campeau, M. Parisien, A. Jean, K. Fagnou, *J. Am. Chem. Soc.* **2006**, *128*, 581–590.

[38] L.-C. Campeau, M. Parisien, M. Leblanc, K. Fagnou, *J. Am. Chem. Soc.* **2004**, *126*, 9186–9187.

[39] D. García-Cuadrado, P. de Mendoza, A. A. C. Braga, F. Maseras, A. M. Echavarren, *J. Am. Chem. Soc.* **2007**, *129*, 6880–6886.

[40] G. A. Olah, S. C. Narang, J. A. Olah, *Proc. Natl. Acad. Sci. USA.* **1981**, *78*, 3298–3300.

[41] S. I. Gorelsky, D. Lapointe, K. Fagnou, *J. Am. Chem. Soc.* **2008**, *130*, 10848–10849.

[42] S. R. Neufeldt, M. S. Sanford, *Acc. Chem. Res.* **2012**, *45*, 936–946.

[43] F. Kakiuchi, S. Kan, K. Igi, N. Chatani, S. Murai, *J. Am. Chem. Soc.* **2003**, *125*, 1698–1699.

[44] F. Kakiuchi, Y. Matsuura, S. Kan, N. Chatani, *J. Am. Chem. Soc.* **2005**, *127*, 5936–5945.

[45] D. Leow, G. Li, T.-S. Mei, J.-Q. Yu, *Nature* **2012**, *486*, 518–522.

[46] N. Hofmann, L. Ackermann, *J. Am. Chem. Soc.* **2013**, *135*, 5877–5884.

[47] J. Luo, S. Preciado, I. Larrosa, *J. Am. Chem. Soc.* **2014**, *136*, 4109–4112.

[48] A. J. Paterson, S. St John-Campbell, M. F. Mahon, N. J. Press, C. G. Frost, *Chem. Commun.* **2015**, *51*, 12807–12810.

[49] C. J. Teskey, A. Y. W. Lui, M. F. Greaney, *Angew. Chem. Int. Ed.* **2015**, *54*, 11677–11680.

[50] L. Wan, N. Dastbaravardeh, G. Li, J.-Q. Yu, *J. Am. Chem. Soc.* **2013**, *135*, 18056–18059.

[51] Y.-X. Luan, T. Zhang, W.-W. Yao, K. Lu, L.-Y. Kong, Y.-T. Lin, M. Ye, *J. Am. Chem. Soc.* **2017**, *139*, 1786–1789.

[52] B. Hammer, J. K. Norskov, *Nature* **1995**, *376*, 238–240.

[53] A. S. K. Hashmi, *Chem. Rev.* **2007**, *107*, 3180–3211.

[54] H. Knosp, R. J. Holliday, C. W. Corti, *Gold Bull.* **2003**, *36*, 93–102.

[55] D. J. Gorin, B. D. Sherry, F. D. Toste, *Chem. Rev.* **2008**, *108*, 3351–3378.

[56] E. Jiménez-Núñez, A. M. Echavarren, *Chem. Rev.* **2008**, *108*, 3326–3350.

[57] A. Arcadi, *Chem. Rev.* **2008**, *108*, 3266–3325.

[58] A. M. Asiri, A. S. K. Hashmi, *Chem. Soc. Rev.* **2016**, *45*, 4471–4503.

[59] D. Pflasterer, A. S. K. Hashmi, *Chem. Soc. Rev.* **2016**, *45*, 1331–1367.

[60] A. Fürstner, *Chem. Soc. Rev.* **2009**, *38*, 3208–3221.

[61] M. R. Luzung, J. P. Markham, F. D. Toste, *J. Am. Chem. Soc.* **2004**, *126*, 10858–10859.

[62] D. J. Gorin, F. D. Toste, *Nature* **2007**, *446*, 395–403.

[63] T. Lauterbach, M. Livendahl, A. Rosellón, P. Espinet, A. M. Echavarren, *Org. Lett.* **2010**, *12*, 3006–3009.

[64] J. Guenther, S. Mallet-Ladeira, L. Estevez, K. Miqueu, A. Amgoune, D. Bourissou, *J. Am. Chem. Soc.* **2014**, *136*, 1778–1781.

[65] A. Sladek, S. Hofreiter, M. Paul, H. Schmidbaur, *J. Organomet. Chem.* **1995**, *501*, 47–51.

[66] M. Joost, A. Amgoune, D. Bourissou, *Angew. Chem. Int. Ed.* **2015**, *54*, 15022–15045.

[67] F. Rekhroukh, R. Brousses, A. Amgoune, D. Bourissou, *Angew. Chem. Int. Ed.* **2015**, *54*, 1266–1269.

[68] S. Dupuy, A. M. Z. Slawin, S. P. Nolan, *Chem. Eur. J.* **2012**, *18*, 14923–14928.

[69] L. T. Ball, M. Green, G. C. Lloyd-Jones, C. A. Russell, *Org. Lett.* **2010**, *12*, 4724–4727.

[70] Y. Chen, M. Chen, Y. Liu, *Angew. Chem. Int. Ed.* **2012**, *51*, 6181–6186.

[71] R. Usón, A. Laguna, *Coord. Chem. Rev.* **1986**, *70*, 1–50.

[72] S. Dupuy, L. Crawford, M. Bühl, A. M. Z. Slawin, S. P. Nolan, *Adv. Synth. Catal.* **2012**, *354*, 2380–2386.

[73] D.-A. Rosca, D. A. Smith, M. Bochmann, *Chem. Commun.* **2012**, *48*, 7247–7249.

[74] M. Hofer, E. Gomez-Bengoa, C. Nevado, *Organometallics* **2014**, *33*, 1328–1332.

[75] A. Tamaki, S. A. Magennis, J. K. Kochi, *J. Am. Chem. Soc.* **1974**, *96*, 6140–6148.

[76] J. Vicente, M. Dolores Bermudez, J. Escribano, *Organometallics* **1991**, *10*, 3380–3384.

[77] W. J. Wolf, M. S. Winston, F. D. Toste, *Nat. Chem* **2014**, *6*, 159–164.

[78] M. N. Hopkinson, A. D. Gee, V. Gouverneur, *Chem. Eur. J.* **2011**, *17*, 8248–8262.

[79] M. S. Kharasch, H. S. Isbell, *J. Am. Chem. Soc.* **1931**, *53*, 3053–3059.

[80] A. Kar, N. Mangu, H. M. Kaiser, M. Beller, M. K. Tse, *Chem. Commun.* **2008**, 386–388.

[81] L. T. Ball, G. C. Lloyd-Jones, C. A. Russell, *Science* **2012**, *337*, 1644–1648.

[82] A. J. Cresswell, G. C. Lloyd-Jones, *Chem. Eur. J.* **2016**, *22*, 12641–12645.

[83] L. T. Ball, G. C. Lloyd-Jones, C. A. Russell, *J. Am. Chem. Soc.* **2014**, *136*, 254–264.

[84] M. Hofer, A. Genoux, R. Kumar, C. Nevado, *Angew. Chem. Int. Ed.* **2016**, 1021–1025.

[85] P. Lu, T. C. Boorman, A. M. Z. Slawin, I. Larrosa, *J. Am. Chem. Soc.* **2010**, *132*, 5580–5581.

[86] X. C. Cambeiro, N. Ahlsten, I. Larrosa, *J. Am. Chem. Soc.* **2015**, *137*, 15636–15639.

[87] V. Gauchot, D. R. Sutherland, A.-L. Lee, *Chem. Sci.* **2017**, DOI 10.1039/C6SC05469B.

[88] World Health Organization Model List of Essential Medicines can be found under http://www.who.int/medicines/publications/essentialmedicines/en. Website visited Feb 2017.

[89] A.-H. Zhou, F. Pan, C. Zhu, L.-W. Ye, *Chem. Eur. J.* **2015**, *21*, 10278–10288.

[90] S. J. Hwang, H. J. Kim, S. Chang, *Org. Lett.* **2009**, *11*, 4588–4591.

[91] C.-G. Dong, Q.-S. Hu, *Angew. Chem. Int. Ed.* **2006**, *45*, 2289–2292.

[92] K. Fuchibe, T. Akiyama, *J. Am. Chem. Soc.* **2006**, *128*, 1434–1435.

[93] C.-C. Hsiao, Y.-K. Lin, C.-J. Liu, T.-C. Wu, Y.-T. Wu, *Adv. Synth. Catal.* **2010**, *352*, 3267–3274.

[94] K. Morimoto, M. Itoh, K. Hirano, T. Satoh, Y. Shibata, K. Tanaka, M. Miura, *Angew. Chem. Int. Ed.* **2012**, *51*, 5359–5362.

[95] T. P. Liu, C. H. Xing, Q. S. Hu, *Angew. Chem. Int. Ed.* **2010**, *49*, 2909–2912.

[96] G. Shi, D. Chen, H. Jiang, Y. Zhang, Y. Zhang, *Org. Lett.* **2016**, DOI 10.1021/acs.orglett.6b01300.

[97] D. E. Ames, A. Opalko, *Synthesis* **1983**, 234–235.

[98] L. Yet, *Chem. Rev.* **2000**, *100*, 2963–3008.

[99] G. Illuminati, L. Mandolini, *Acc. Chem. Res.* **1981**, *14*, 95–102.

[100] L.-C. Campeau, M. Parisien, M. Leblanc, K. Fagnou, *J. Am. Chem. Soc.* **2004**, *126*, 9186–9187.

[101] T. Saget, N. Cramer, *Angew. Chem. Int. Ed.* **2013**, *52*, 7865–7868.

[102] D. G. Pintori, M. F. Greaney, *J. Am. Chem. Soc.* **2011**, *133*, 1209–1211.

[103] E. M. Beccalli, G. Broggini, M. Martinelli, G. Paladino, E. Rossi, *Synthesis* **2006**, 2404–2412.

[104] J. Yamaguchi, A. D. Yamaguchi, K. Itami, *Angew. Chem. Int. Ed.* **2012**, *51*, 8960–9009.

[105] G. Bringmann, J. R. Jansen, H.-P. Rink, *Angew. Chem. Int. Ed.* **1986**, *25*, 913–915.

[106] G. Bringmann, T. Gulder, T. A. M. Gulder, M. Breuning, *Chem. Rev.* **2011**, *111*, 563–639.

[107] T. Matsumoto, T. Hosoya, K. Suzuki, *J. Am. Chem. Soc.* **1992**, *114*, 3568–3570.

[108] T. Harayama, H. Yasuda, *Heterocycles* **1997**, *46*, 61–64.

[109] H. Abe, T. Fukumoto, Y. Horino, T. Harayama, Y. Takeuchi, *Heterocycles* **2010**, *82*, 851–855.

[110] S. Takeda, H. Abe, Y. Takeuchi, T. Harayama, *Tetrahedron* **2007**, *63*, 396–408.

[111] M. Uemura, A. Daimon, Y. Hayashi, *J. Chem. Soc. Chem. Commun.* **1995**, 1943–1944.

[112] A. I. Meyers, J. R. Flisak, R. A. Aitken, *J. Am. Chem. Soc.* **1987**, *109*, 5446–5452.

[113] M. Leblanc, K. Fagnou, *Org. Lett.* **2005**, *7*, 2849–2852.

[114] A. L. Bowie, C. C. Hughes, D. Trauner, *Org. Lett.* **2005**, *7*, 5207–5209.

[115] E. A. Merritt, B. Olofsson, *Angew. Chem. Int. Ed.* **2009**, *48*, 9052–9070.

[116] W. Graham, J. B. Roberts, *Ann. Rheum. Dis.* **1953**, *12*, 16–19.

[117] O. Baudoin, F. Guéritte, in *Studies in Natural Products Chemistry, Vol. 29 (Part J)* (Ed.: A. Rahman), Elsevier, Amsterdam, **2003**, pp. 355–417.

[118] A. V Vorogushin, A. V Predeus, W. D. Wulff, H.-J. Hansen, *J. Org. Chem.* **2003**, *68*, 5826–5831.

[119] J. T. Suri, T. Vu, A. Hernandez, J. Congdon, B. Singaram, *Tetrahedron Lett.* **2002**, *43*, 3649–3652.

[120] G. Besong, K. Jarowicki, P. J. Kocienski, E. Sliwinski, F. T. Boyle, *Org. Biomol. Chem.* **2006**, *4*, 2193–2207.

[121] D. A. Watson, X. Fan, S. L. Buchwald, *J. Org. Chem.* **2008**, *73*, 7096–7101.

[122] S. G. Wierschke, J. Chandrasekhar, W. L. Jorgensen, *J. Am. Chem. Soc.* **1985**, *107*, 1496–1500.

[123] L. J. Bellamy, K. J. Morgan, R. J. Pace, *Spectrochim. Acta* **1966**, *22*, 535–545.

[124] E. M. Simmons, J. F. Hartwig, *Angew. Chem. Int. Ed.* **2012**, *51*, 3066–3072.

[125] K. Osakada, H. Onodera, Y. Nishihara, *Organometallics* **2005**, *24*, 190–192.

[126] S. Shekhar, J. F. Hartwig, *J. Am. Chem. Soc.* **2004**, *126*, 13016.

[127] W. J. Wolf, M. S. Winston, F. D. Toste, *Nat. Chem.* **2014**, *6*, 159–64.

[128] R. K. Merwin, R. C. Schnabel, J. D. Koola, D. M. Roddick, *Organometallics* **1992**, *11*, 2972–2978.

[129] L. Jin, H. Zhang, P. Li, J. R. Sowa, A. Lei, *J. Am. Chem. Soc.* **2009**, *131*, 9892–9893.

[130] C. Amatore, A. Jutand, *Organometallics* **1988**, *7*, 2203–2214.

[131] S. Shekhar, J. F. Hartwig, *J. Am. Chem. Soc.* **2004**, *126*, 13016–13027.

[132] J. F. Hartwig, *Inorg. Chem.* **2007**, *46*, 1936–1947.

[133] A. Nijamudheen, S. Karmakar, A. Datta, *Chem. Eur. J.* **2014**, *20*, 14650–14658.

[134] P. Ballinger, F. A. Long, *J. Am. Chem. Soc.* **1960**, *82*, 795–798.

[135] S. Komiya, J. K. Kochi, *J. Am. Chem. Soc.* **1976**, *98*, 7599–7607.

[136] D. G. Blackmond, *J. Am. Chem. Soc.* **2015**, *137*, 10852–10866.

[137] D. G. Blackmond, *Angew. Chem. Int. Ed.* **2005**, *44*, 4302–4320.

[138] J. E. Hein, A. Armstrong, D. G. Blackmond, *Org. Lett.* **2011**, *13*, 4300–4303.

[139] R. H. Crabtree, *Chem. Rev.* **2015**, *115*, 127–150.

[140] P. Forzatti, L. Lietti, *Catal. Today* **1999**, *52*, 165–181.

[141] J. A. Moulijn, A. E. van Diepen, F. Kapteijn, *Appl. Catal. A Gen.* **2001**, *212*, 3–16.

[142] C. H. Bartholomew, *Appl. Catal. A Gen.* **2001**, *212*, 17–60.

[143] T. L. Lohr, T. J. Marks, *Nat. Chem* **2015**, *7*, 477–482.

[144] X. Zeng, *Chem. Rev.* **2013**, *113*, 6864–6900.

[145] P. J. Parsons, C. S. Penkett, A. J. Shell, *Chem. Rev.* **1996**, *96*, 195–206.

[146] K. C. Nicolaou, T. Montagnon, S. A. Snyder, *Chem. Commun.* **2003**, 551–564.

[147] L. F. Tietze, *Chem. Rev.* **1996**, *96*, 115–136.

[148] D. E. Fogg, E. N. dos Santos, *Coord. Chem. Rev.* **2004**, *248*, 2365–2379.

[149] N. Shindoh, Y. Takemoto, K. Takasu, *Chem. Eur. J.* **2009**, *15*, 12168–12179.

[150] D. A. Candito, M. Lautens, *Angew. Chem. Int. Ed.* **2009**, *48*, 6713–6716.

[151] M. Catellani, F. Frignani, A. Rangoni, *Angew. Chem. Int. Ed.* **1997**, *36*, 119–122.

[152] F. Faccini, E. Motti, M. Catellani, *J. Am. Chem. Soc.* **2004**, *126*, 78–79.

[153] M. Catellani, M. C. Fagnola, *Angew. Chem. Int. Ed.* **1994**, *106*, 2559–2561.

[154] G. Mann, J. F. Hartwig, M. S. Driver, C. Fernández-Rivas, *J. Am. Chem. Soc.* **1998**, *120*, 827–828.

[155] J. Barluenga, F. Aznar, C. Valdés, *Angew. Chem. Int. Ed.* **2004**, *43*, 343–345.

[156] J. Panteleev, L. Zhang, M. Lautens, *Angew. Chem. Int. Ed.* **2011**, *50*, 9089–9092.

[157] A. A. Friedman, J. Panteleev, J. Tsoung, V. Huynh, M. Lautens, *Angew. Chem. Int. Ed.* **2013**, *52*, 9755–9758.

[158] R. B. Bedford, C. S. J. Cazin, *Chem. Commun.* **2002**, 2310–2311.

[159] J.-P. Leclerc, M. André, K. Fagnou, *J. Org. Chem.* **2006**, *71*, 1711–1714.

[160] H.-Y. Sun, S. I. Gorelsky, D. R. Stuart, L.-C. Campeau, K. Fagnou, *J. Org. Chem.* **2010**, *75*, 8180–8189.

[161] R. Taylor, *J. Chem. Soc. B Phys. Org.* **1968**, 1559–1562.

[162] P. B. D. de la Mare, E. A. Johnson, J. S. Lomas, *J. Chem. Soc.* **1964**, 5317–5326.

[163] H. W. Richter, B. R. Cherry, T. D. Zook, G. F. Koser, *J. Am. Chem. Soc.* **1997**, *119*, 9614–9623.

[164] Z. Zheng, S. Ma, L. Tang, D. Zhang-Negrerie, Y. Du, K. Zhao, *J. Org. Chem.* **2014**, *79*, 4687–4693.

[165] I. Tellitu, S. Serna, M. T. Herrero, I. Moreno, E. Domínguez, R. SanMartin, *J. Org. Chem.* **2007**, *72*, 1526–1529.

[166] Q. Jiang, A. Zhao, B. Xu, J. Jia, X. Liu, C. Guo, *J. Org. Chem.* **2014**, *79*, 2709–2715.

[167] F. F. Fleming, L. Funk, R. Altundas, Y. Tu, *J. Org. Chem.* **2001**, *66*, 6502–6504.

[168] J. Gallos, A. Varvoglis, N. W. Alcock, *J. Chem. Soc. Perkin Trans. 1* **1985**, 757–763.

[169] C. L. Perrin, Y. Dong, *J. Am. Chem. Soc.* **2007**, *129*, 4490–4497.

8. Experimental

Experimental Contents

8.1 General Information

Procedures employing air or moisture-sensitive materials were performed with anhydrous solvents (*vide infra*) using standard Schlenk techniques, under an atmosphere of anhydrous nitrogen. Glassware necessary for these manipulations were previously oven dried (200 °C) or flame-dried and allowed to cool under vacuum (*ca* 0.5 Torr).

Analytical thin-layer chromatography was performed on precoated aluminium-backed plates (Silica Gel 60 F254; Merck), and visualised using a combination of UV light (254 nm) and ethanolic phosphomolybdic acid, aqueous basic potassium permanganate, iodine or vanillin stains. Preparative thin-layer chromatography (for less than *ca* 15 mg of sample) was performed on precoated, analytical aluminium-backed plates (Silica Gel 60 F254; Merck). Column chromatography was performed using Davisil® 60A silica gel (35-70 μm; Fisher Scientific) or Geduran® Silica Gel 60 (40-63 μm; Merck).

NMR spectra were recorded at 27 °C unless stated otherwise; ^{1}H, $^{13}C\{^{1}H\}$, and ^{19}F NMR spectra were recorded at 600/500/400 MHz, 125/100 MHz and 470/376/282 MHz, respectively, using Bruker Avance I 600, Bruker Avance I 400, Bruker Avance III 500 and Bruker Avance III+ 400 spectrometers. ^{1}H and $^{13}C\{^{1}H\}$ NMR spectra were referenced to residual solvent peaks ($CHCl_3$, δ_H 7.26 ppm; $CDCl_3$, δ_C 77.16 ppm); chemical shifts are reported in ppm relative to tetramethylsilane standard. ^{19}F NMR spectra are reported in ppm relative to a $BF_3{\cdot}OEt_2$ external standard. Coupling constants, *J*, were calculated using Mestrenova versions 6, 8 or 9, and are reported to the nearest 0.1 Hz. Coupling constants that did not match as a result of digitization are reported as rounded averages. The following abbreviations (and their combinations) are used to label the multiplicities: s (singlet), d (doublet), t (triplet), q (quartet), m (multiplet) and br (broad).

Dry solvents were obtained by passing solvent through a column of anhydrous alumina using an Anhydrous Engineering Grubbs-type system and stored under anhydrous nitrogen. Reaction solvents chloroform ($CHCl_3$) (amylene stabilised, HPLC grade, Sigma-Aldrich) and chloroform-d_3 ($CDCl_3$) (99.8 atom % D, Sigma-Aldrich) were passed through a plug of activated basic Al_2O_3 (Brockmann I), distilled and held over 3 Å molecular sieves in a Strauss flask under nitrogen in the dark. Triethylamine and trimethylsilyl chloride were distilled from CaH_2. Solvents employed for Pd-catalysed cross-couplings were degassed by repeated freeze-pump-thaw cycles. Unless stated otherwise, reagents were purchased from commercial sources (Sigma Aldrich, Alfa Aesar, VWR, Fluorochem or Apollo Scientific), and were used without purification.

The precatalyst, thtAuBr$_3$, was prepared *via* an improved procedure[1] to that originally reported.[2]

Infrared spectra of neat compounds were recorded over the range 4000-600 cm^{-1} using a Bruker Platinum ATR Quicksnap™ attachment (diamond cell) on a Bruker Alpha FT-IR Spectrometer. Melting points were measured using a SMP10 melting point apparatus in open capillaries and are uncorrected. Mass spectra were recorded on Bruker microTOF II or Finnigan MAT 900 XLP spectrometers.

X-ray measurements were made on crystals mounted on a MITIGEN holder in Paratone oil. Data were collected using a Rigaku Oxford Diffraction SuperNova diffractometer equipped with an Oxford Cryosystems Cryostream 700+ low-temperature apparatus operating at T = 120.0 K. Data were measured using ω scans of 1.0° per frame for 1.0 s using CuK$_\alpha$ radiation (sealed X-ray tube, 50 kV, 0.8 mA). The total number of runs and images was based on the strategy calculation from the program CrysAlisPro (Agilent, V1.171.37.35e, 2014). Cell parameters were retrieved, refined and data reduction was performed using the CrysAlisPro (Agilent, V1.171.37.35e, 2014) software which corrects for Lorentz polarisation. The structures were solved by Direct Methods using the ShelXS[3] structure solution program and refined by Least Squares using ShelXL.[3] All non-hydrogen atoms were refined anisotropically. Hydrogen atom positions were calculated geometrically and refined using the riding model.

8.2 Experimental Procedures and Characterisation Data

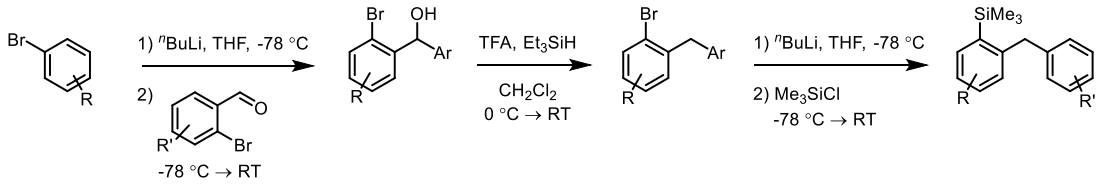

Scheme 8.1. General Procedures for Synthesis of (2-benzylphenyl)trimethylsilanes

General Procedure 1: *n*-Butyllithium (0.98 – 1.00 eq.) was added dropwise to a stirred solution of the requisite aryl bromide (1.00 – 1.03 equiv) in THF (0.4 M) at –78 °C. The reaction was stirred at this temperature for 1 h, then the requisite 2-bromobenzaldehyde (1.00 equiv) was added dropwise, and the mixture was allowed to warm to room temperature and was stirred for the time specified. The reaction was quenched with H_2O, then the aqueous phase was separated and extracted with Et_2O (3 ×), and the combined organic portions were dried ($MgSO_4$), filtered and concentrated *in vacuo* to give the crude product.

General Procedure 2A: A Schlenk flask containing the requisite diarylmethanol (1.00 equiv) was evacuated and back-filled with N_2 three times, then CH_2Cl_2 (0.3 M) was added. The solution was cooled to 0 °C, then TFA (4.00 equiv) was added dropwise. After 2 min, Et_3SiH (2.00 equiv) was added dropwise, and the reaction stirred at room temperature overnight. The volatiles were then evaporated under a stream of N_2 to give the crude product.

General Procedure 2B: A Schlenk flask containing the requisite diarylmethanol (1.00 equiv) was evacuated and back-filled with N_2 three times, then CH_2Cl_2 (1.6 M) was added. The solution was cooled to 0 °C, then TFA (8.00 equiv) was added dropwise. After 2 min, Et_3SiH (2.00 equiv) was added dropwise, and the reaction stirred at room temperature overnight. The volatiles were then evaporated under a stream of N_2 to give the crude product.

General Procedure 3: *n*-Butyllithium (1.10 equiv) was added dropwise to a stirred solution of the requisite aryl bromide (1.00 equiv) in THF (0.4 M) at –78 °C. The reaction was stirred at this temperature for the time specified, then Me_3SiCl (1.50 equiv) was added dropwise, and the mixture was allowed to warm to room temperature and was stirred overnight. The reaction was quenched with H_2O, then the aqueous phase was separated and extracted three times with Et_2O; the combined organic portions were dried ($MgSO_4$), filtered and concentrated *in vacuo* to give the crude product. Purification was achieved with flash column chromatography on silica gel using the eluent specified in individual entries.

(2-Benzylphenyl)trimethylsilane (1b)

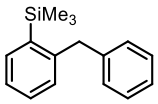

(2-Bromophenyl)phenylmethanol: Following **General Procedure** 1, *n*BuLi (1.6 M in hexanes, 3.13 mL, 5.00 mmol) was added dropwise to a stirred solution of bromobenzene (0.56 mL, 5.25 mmol) in THF (13 mL) at –78 °C. The reaction was stirred at this temperature for 1 h, then 2-bromobenzaldehyde (0.60 mL, 5.10 mmol) was added dropwise, and the mixture was allowed to warm to room temperature and was stirred for 2 h. Flash column chromatography (20% Et_2O in hexanes) afforded (2-bromophenyl)phenylmethanol as a viscous, colourless liquid (1.10 g, 4.18 mmol, 84%).

Characterisation data were consistent with literature values: ^{1}H and ^{13}C{H} NMR.[4]

^{1}H NMR (300 MHz, $CDCl_3$): δ 7.70 (dd, *J* = 7.8 Hz, 1.8 Hz, 1H), 7.55 (dd, *J* = 8.0 Hz, 1.3 Hz, 1H), 7.44-7.28 (m, 6H), 7.16 (ddd, *J* = 7.8 Hz, 7.4 Hz, 1.8 Hz, 1H), 6.21 (s, 1H), 2.39 (s, 1H). **^{13}C{^{1}H} NMR (125 MHz, $CDCl_3$):** δ 142.5, 142.1, 132.8, 129.1, 128.5, 127.8, 127.7, 127.0, 122.8, 74.8. *1 × C_{Ar} not observed*. **HRMS** calcd. for $C_{13}H_{11}BrO$: 261.9993 $[M]^+$; found (EI^+): 261.9986.

1-Benzyl-2-bromobenzene: Following **General Procedure 2A**, (2-bromophenyl)phenylmethanol (1.10 g, 4.18 mmol) in CH_2Cl_2 (14 mL) was reacted with TFA (1.23 mL, 16.0 mmol) and Et_3SiH (1.28 mL, 8.00 mmol). Purification *via* flash column chromatography (pentane) afforded 1-benzyl-2-bromobenzene as a colourless liquid (0.84 g, 3.38 mmol, 81%).

Characterisation data were consistent with literature values: ^{1}H and ^{13}C{^{1}H} NMR.[5]

^{1}H NMR (500 MHz, $CDCl_3$): δ 7.59 (app. d, *J* = 8.0 Hz, 1H), 7.32 (app. t, *J* = 7.6 Hz, 2H), 7.26-7.21 (m, 4H), 7.16 (dd, *J* = 7.7 Hz, 1.9 Hz, 1H), 7.10 (dd, *J* = 7.6 Hz, 2.1 Hz, 1H), 4.14 (s, 2H). **^{13}C{^{1}H} NMR (125 MHz, $CDCl_3$):** δ 140.4, 139.5, 132.8, 131.1, 129.0, 128.5, 127.9, 127.4, 126.2, 124.9, 41.7. **ν_{max}(neat)/cm^{-1}:** 3061, 2914, 1566, 1495, 1438, 1023, 742, 716. **HRMS** calcd. for $C_{13}H_{11}Br$: 246.0044 $[M]^+$; found (EI^+): 246.0045.

(2-Benzylphenyl)trimethylsilane: Following **General Procedure 3**, *n*BuLi (1.6 M in hexanes, 2.20 mL, 3.51 mmol) was added to 1-benzyl-2-bromobenzene (0.83 g, 3.34 mmol) in THF (8.5 mL) at –78 °C. The reaction was stirred at this temperature for 1 h, then Me_3SiCl (0.55 mL, 4.34 mmol) was added dropwise, and the mixture was stirred at room temperature

overnight. Purification *via* flash column chromatography (hexanes) afforded the title compound as a colourless liquid (0.70 g, 2.90 mmol, 87%).

^{1}H NMR (500 MHz, $CDCl_3$): δ 7.56 (dd, *J* = 7.3 Hz, 1.5 Hz, 1H), 7.32-7.27 (m, 3H), 7.24-7.21 (m, 2H), 7.12 (app. d, *J* = 7.3 Hz, 2H), 7.02 (app. d, *J* = 7.6 Hz, 1H), 4.18 (s, 2H), 0.33 (s, 9H). **^{13}C{^{1}H} NMR (125 MHz, $CDCl_3$):** δ 146.2, 141.4, 138.8, 134.5, 1298, 129.3, 129.1, 128.3, 125.9, 125.4, 41.6, 0.3. **ν_{max}(neat)/cm^{-1}:** 3059, 3027, 2953, 1495, 1451, 1248, 1121, 1074, 1030, 832, 723. **HRMS** calcd. for $C_{16}H_{20}Si$: 240.1334 $[M]^+$; found (EI^+): 240.1335.

[2-(4-Chlorobenzyl)phenyl]trimethylsilane (1f)

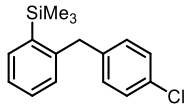

(2-Bromophenyl)(4-chlorophenyl)methanol: Following **General Procedure 1**, *n*BuLi (1.6 M in hexanes, 3.13 mL, 5.00 mmol) was added dropwise to a stirred solution of 1-bromo-4-chlorobenzene (1.01 mL, 5.25 mmol) in THF (13 mL) at –78 °C. The reaction was stirred at this temperature for 1 h, then 2-bromobenzaldehyde (0.60 mL, 5.10 mmol) was added dropwise, and the mixture was allowed to warm to room temperature and was stirred for 2 h. Column chromatography (20% Et_2O in hexanes) afforded (2-bromophenyl)(4-chlorophenyl)methanol as a viscous, colourless liquid (1.22 g, 4.09 mmol, 82%).

^{1}H NMR (300 MHz, $CDCl_3$): δ 7.57-7.53 (m, 2H), 7.39-7.30 (m, 5H), 7.17 (app. td, *J* = 7.9 Hz, 1.8 Hz, 1H), 6.18 (s, 1H), 1.25 (s, 1H). **^{13}C{^{1}H} NMR (125 MHz, $CDCl_3$):** δ 142.2, 140.6, 133.5, 132.9, 129.4, 128.6, 128.4, 127.9, 122.7, 74.1. *1 × C_{Ar} not observed.*

1-Bromo-2-(4-chlorobenzyl)benzene: Following **General Procedure 2A**, (2-bromophenyl)(4-chlorophenyl)methanol (1.20 g, 4.03 mmol) in CH_2Cl_2 (13 mL) was reacted with TFA (1.23 mL, 16.0 mmol) and Et_3SiH (1.28 mL, 8.0 mmol). Column chromatography (pentane) afforded 1-bromo-2-(4-chlorobenzyl)benzene as a colourless liquid (0.75 g, 2.65 mmol, 66%).

^{1}H NMR (500 MHz, $CDCl_3$): δ 7.59 (d, *J* = 7.9 Hz, 1H), 7.28-7.24 (m, 3H), 7.15-7.10 (m, 4H), 4.10 (s, 2H). **^{13}C{^{1}H} NMR (125 MHz, $CDCl_3$):** δ 139.8, 137.9, 133.0, 132.1, 131.0, 130.3, 128.9, 128.1, 127.6, 124.8, 41.1. **HRMS** calcd. for $C_{13}H_{10}ClBr$: 279.9654 $[M]^+$; found (EI^+): 279.9658.

[2-(4-Chlorobenzyl)phenyl]trimethylsilane: Following **General Procedure 3**, *n*BuLi (1.6 M in hexanes, 2.03 mL, 3.25 mmol) was added to 1-bromo-2-(4-chlorobenzyl)benzene (0.83 g,

2.96 mmol) in THF (7 mL) at –78 °C. The reaction was stirred at this temperature for 1 h, then Me_3SiCl (0.49 mL, 3.85 mmol) was added dropwise, and the mixture was stirred at room temperature overnight. Purification *via* flash column chromatography (pentane) afforded the title compound as a colourless liquid (0.64 g, 2.34 mmol, 79%).

^{1}H NMR (500 MHz, $CDCl_3$): δ 7.55 (dd, *J* = 7.4 Hz, 1.5 Hz, 1H), 7.30 (app. td, *J* = 7.4 Hz, 1.6 Hz, 1H), 7.26-7.22 (m, 3H), 7.02 (d, *J* = 8.6 Hz, 2H), 6.99 (app. d, *J* = 7.6 Hz, 1H), 4.13 (s, 2H), 0.31 (s, 9H).**^{13}C{^{1}H} NMR (125 MHz, $CDCl_3$):** δ 145.5, 139.9, 138.9, 134.6, 131.7, 130.4, 129.8, 128.4, 125.6, 40.9, 0.31. *1 × C_{Ar} not observed.* **ν_{max}(neat)/cm^{-1}:** 3056, 2953, 2897, 1489, 1431, 1406, 1262, 1248, 1123, 1091, 1015, 832, 793, 750. **HRMS** calcd. for $C_{16}H_{19}ClSi$: 274.0939 $[M]^+$; found (EI^+): 274.0926.

Trimethyl{2-[4-(trifluoromethyl)benzyl]phenyl}silane (1h)

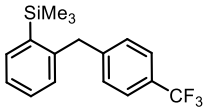

(2-Bromophenyl)[4-(trifluoromethyl)phenyl]methanol: Following **General Procedure 1**, *n*BuLi (2.38 M in hexanes, 3.81 mL, 9.06 mmol) was added dropwise to a stirred solution of 4-bromobenzotrifluoride (1.24 mL, 8.89 mmol) in THF (20 mL) at –78 °C. The reaction was stirred at this temperature for 20 min, then 2-bromobenzaldehyde (1.03 mL, 8.89 mmol) was added dropwise, and the mixture was allowed to warm to room temperature and was stirred for 2 h. Purification *via* flash column chromatography (20% EtOAc in hexanes) afforded (2-bromophenyl)[4-(trifluoromethyl)phenyl]methanol as a viscous, colourless liquid (2.40 g, 7.59 mmol, 85%).

Characterisation data were consistent with literature values: ^{1}H, ^{13}C{^{1}H} NMR and IR.[4]

^{1}H NMR (400 MHz, $CDCl_3$): δ 7.63 – 7.47 (m, 6H), 7.35 (app. t, *J* = 7.6 Hz, 1H), 7.18 (app. t, *J* = 7.6 Hz, 1H), 6.28 (s, 1H), 2.45 (br.s, 1H). **^{13}C{^{1}H} NMR (100 MHz, $CDCl_3$):** δ 146.1, 142.1, 133.2, 130.0 (q, *J* = 32 Hz), 129.7, 128.7, 128.1, 127.3, 125.6 (q, *J* = 3.9 Hz), 124.2 (q, *J* = 270 Hz), 122.9, 74.3. **^{19}F NMR (377 MHz, $CDCl_3$):** δ -62.5 (s). **ν_{max}(neat)/cm^{-1}:** 3330, 3067, 1619, 1467, 1321, 1161, 1108, 1065, 1014, 858, 838, 750.

1-Bromo-2-[4-(trifluoromethyl)benzyl]benzene: Following **General Procedure 2B**, (2-bromophenyl)[4-(trifluoromethyl)phenyl]methanol (2.38 g, 7.54 mmol) in CH_2Cl_2 (4.5 mL) was reacted with TFA (4.60 mL, 60.3 mmol) and Et_3SiH (2.41 mL, 15.1 mmol). Purification

via flash column chromatography (hexanes) afforded 1-bromo-2-[4-(trifluoromethyl)benzyl]benzene as a colourless liquid (1.90 g, 6.03 mmol, 80%).

^{1}H NMR (400 MHz, $CDCl_3$): δ 7.59 (dd, *J* = 7.9, 1.3 Hz, 1H), 7.55 (d, *J* = 7.7 Hz, 2H), 7.35 – 7.23 (m, 3H), 7.19 – 7.08 (m, 2H), 4.18 (s, 2H).**^{13}C{^{1}H} NMR (100 MHz, $CDCl_3$):** δ 143.8, 139.4, 133.2, 131.3, 129.3, 128.8 (q, *J* = 32 Hz), 128.5, 127.8, 125.5 (q, *J* = 3.8 Hz), 125.0, 124.4 (q, *J* = 270 Hz), 41.7. **^{19}F NMR (377 MHz, $CDCl_3$):** δ -62.4 (s). **ν_{max}(neat)/cm^{-1}:** 3063, 2929, 1618, 1469, 1417, 1321, 1160, 1116, 1065, 1018, 917, 839, 805, 743, 660. **HRMS** calcd. for $C_{14}H_{10}F_3Br$: 313.9913 $[M]^+$; found (EI^+): 313.9910.

Trimethyl{2-[4-(trifluoromethyl)benzyl]phenyl}silane: Following **General Procedure 3**, *n*BuLi (2.38 M in hexanes, 2.57 mL, 6.12 mmol) was added to 1-bromo-2-[4-(trifluoromethyl)benzyl]benzene (1.61 g, 5.10 mmol) in THF (15 mL) at –78 °C. The reaction was stirred at this temperature for 1 h, then Me_3SiCl (0.97 mL, 7.65 mmol) was added dropwise, and the mixture was stirred at room temperature overnight. Purification *via* flash column chromatography (hexanes) afforded the title compound as a colourless liquid (1.26 g, 4.07 mmol, 80%).

^{1}H NMR (400 MHz, $CDCl_3$): δ 7.57 (dd, *J* = 7.5, 1.7 Hz, 1H), 7.54 (d, *J* = 7.8 Hz, 2H), 7.30 (app. td, *J* = 7.5, 1.7 Hz, 1H), 7.24 (app. td, *J* = 7.5, 1.4 Hz, 1H), 7.20 (d, *J* = 7.8 Hz, 2H), 6.99 – 6.96 (m, 1H), 4.22 (s, 2H), 0.32 (s, 9H). **^{13}C{^{1}H} NMR (100 MHz, $CDCl_3$):** δ 145.8, 145.1, 139.2, 134.9, 130.1, 129.6, 129.5, 128.5 (q, *J* = 32 Hz), 126.0, 125.4 (q, *J* = 3.8 Hz), 124.5 (q, *J* = 270 Hz), 41.6, 0.48. **ν_{max}(neat)/cm^{-1}:** 2956, 1618, 1416, 1321, 1250, 1161, 1120, 1065, 1018, 833, 738. **HRMS** calcd. for $C_{17}H_{19}F_3Si$: 308.1203 $[M]^+$; found (EI^+): 308.1201

[2-(3-Methoxybenzyl)phenyl]trimethylsilane (1j)

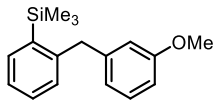

(2-Bromophenyl)(3-methoxyphenyl)methanol**:** Following **General Procedure 1**, *n*BuLi (1.6 M in hexanes, 3.13 mL, 5.00 mmol) was added dropwise to a stirred solution of 3-bromoanisole (0.66 mL, 5.25 mmol) in THF (13 mL) at –78 °C. The reaction was stirred at this temperature for 1 h, then 2-bromobenzaldehyde (0.60 mL, 5.10 mmol) was added dropwise, and the mixture was allowed to warm to room temperature and was stirred for 2 h. Column chromatography (15% EtOAc in hexanes) afforded (2-bromophenyl)(3-methoxyphenyl)methanol as a viscous, colourless liquid (1.23 g, 4.20 mmol, 84%).

Characterisation data were consistent with literature values: ^{1}H, ^{13}C{^{1}H} NMR and IR.[4]

^{1}H NMR (500 MHz, $CDCl_3$): δ 7.58 (dd, *J* = 8.0 Hz, 1.7 Hz, 1H), 7.55 (dd, *J* = 8.0 Hz, 1.1 Hz, 1H), 7.35 (app. td, *J* = 7.6 Hz, 1.2 Hz, 1H), 7.27 (app. t, *J* = 8.0 Hz, 1H), 7.16 (app. td, *J* = 7.6 Hz, 1.7 Hz, 1H), 7.00-6.19 (m, 2H), 6.84 (ddd, *J* = 8.3 Hz, 2.5 Hz, 1.2 Hz, 1H), 6.19 (s, 1H), 3.80 (s, 3H), 2.39 (s, 1H). **^{13}C{^{1}H} NMR (125 MHz, $CDCl_3$):** δ 159.6, 143.7, 142.3, 132.8, 129.5, 129.2, 128.5, 127.7, 122.8, 119.3, 113.0, 112.6, 74.6, 55.2. **ν_{max}(neat)/cm^{-1}:** 3376, 3060, 3000, 2834, 1585, 1487, 1465, 1454, 1435, 1254, 1014, 743.

1-Bromo-2-(3-methoxybenzyl)benzene: Following **General Procedure 2A**, (2-bromophenyl)(3-methoxyphenyl)methanol (1.20 g, 4.10 mmol) in CH_2Cl_2 (14 mL) was reacted with TFA (1.23 mL, 16.0 mmol) and Et_3SiH (1.28 mL, 8.0 mmol). Column chromatography (0% → 10% Et_2O in hexanes) afforded 1-bromo-2-(3-methoxybenzyl)benzene as a colourless liquid (0.64 g, 2.31 mmol, 56%).

Characterisation data were consistent with literature values: ^{1}H, ^{13}C{^{1}H} NMR and IR.[6]

^{1}H NMR (400 MHz, $CDCl_3$): δ 7.58 (dd, *J* = 8.0 Hz, 1.3 Hz, 1H), 7.24 (app. td, *J* = 7.3 Hz, 1.3 Hz, 1H), 7.23 (ddd, *J* = 8.0 Hz, 7.6 Hz, 0.6 Hz, 1H), 7.15 (dd, *J* = 7.7 Hz, 1.9 Hz, 1H), 7.09 (ddd, *J* = 8.0 Hz, 7.3 Hz, 1.8 Hz, 1H), 6.81-676 (m, 3H), 4.11 (s, 2H), 3.79 (s, 3H). **^{13}C{^{1}H} NMR (100 MHz, $CDCl_3$):** δ 159.7, 141.1, 140.2, 132.8, 131.1, 129.4, 127.9, 127.5, 124.9, 121.4, 114.9, 111.5, 55.1, 41.7. **ν_{max}(neat)/cm^{-1}:** 3054, 3000, 2833, 1598, 1567, 1488, 1454, 1436, 1253, 1146, 1044, 1023, 928, 874, 778, 738, 690, 660.

[2-(3-Methoxybenzyl)phenyl]trimethylsilane: Following **General Procedure 3**, *n*BuLi (1.6 M in hexanes, 1.59 mL, 2.54 mmol) was added to 1-bromo-2-(3-methoxybenzyl)benzene (0.64 g, 2.31 mmol) in THF (6 mL) at –78 °C. The reaction was stirred at this temperature for 1 h, then Me_3SiCl (0.38 mL, 3.00 mmol) was added dropwise, and the mixture was stirred at room temperature overnight. Purification *via* flash column chromatography (20% CH_2Cl_2 in hexanes) afforded the title compound as a colourless liquid (0.52 g, 1.91 mmol, 83%).

^{1}H NMR (400 MHz, $CDCl_3$): δ 7.54 (dd, *J* = 7.2 Hz, 1.7 Hz, 1H), 7.29 (dd, *J* = 7.4 Hz, 1.6 Hz, 1H), 7.22 (app. td, *J* = 7.4 Hz, 1.3 Hz, 1H), 7.21 (app. t, *J* = 7.9 Hz, 1H), 7.03 (ddd, *J* = 7.7 Hz, 1.9 Hz, 1.3 Hz, 1H), 6.76 (ddd, *J* = 8.2 Hz, 2.7 Hz, 0.8 Hz, 1H), 6.71 (dtd, *J* = 7.5 Hz, 1.6 Hz, 0.8 Hz, 1H), 6.66 (dd, *J* = 2.3 Hz, 1.8 Hz, 1H), 4.15 (s, 2H), 3.77 (s, 3H), 0.33 (s, 9H). **^{13}C{^{1}H} NMR (125 MHz, $CDCl_3$):** δ 159.7, 146.0, 143.1, 138.8, 134.5, 129.8, 129.30, 129.26, 125.5, 121.7, 115.1, 111.2, 55.1, 41.6, 0.34. **ν_{max}(neat)/cm^{-1}:** 3054, 2952, 2833, 1600, 1584, 1488, 1453, 1433, 1261, 1248, 1151, 1122, 1050, 832, 732. **HRMS** calcd. for $C_{17}H_{22}OSi$: 270.1440 $[M]^+$; found (EI^+): 270.1429.

3-(2-Trimethylsilylbenzyl)fluorobenzene (1k)

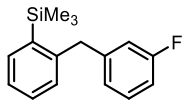

(2-Bromophenyl)(3-fluorophenyl)methanol: Following **General Procedure 1**, ^{n}BuLi (1.6 M in hexanes, 3.13 mL, 5.00 mmol) was added dropwise to a stirred solution of 3-bromofluorobenzene (0.59 mL, 5.25 mmol) in THF (10 mL) at –78 °C. The reaction was stirred at this temperature for 1 h, then 2-bromobenzaldehyde (0.60 mL, 5.10 mmol) was added dropwise, and the mixture was stirred at room temperature for 2 h. Purification *via* flash column chromatography (10% → 20% Et_2O in hexanes) afforded (2-bromophenyl)(3-fluorophenyl)methanol as a viscous, colourless liquid (1.31 g, 4.67 mmol, 93%).

^{1}H NMR (500 MHz, $CDCl_3$): δ 7.55 (app. td, *J* = 8.0 Hz, 1.4 Hz, 2H), 7.36 (app. td, *J* = 7.4 Hz, 1.4 Hz, 1H), 7.31 (app. td, *J* = 7.9 Hz, 5.9 Hz, 1H), 7.21-7.12 (m, 3H), 6.98 (m, 1H), 6.21 (s, 1H). **^{13}C{^{1}H} NMR (125 MHz, $CDCl_3$):** δ 162.9 (d, *J* = 246 Hz), 144.7 (d, *J* = 6.7 Hz), 142.1, 132.9, 129.9 (d, *J* = 7.6 Hz), 129.4, 128.5, 127.9, 122.7, 122.5 (d, *J* = 2.9 Hz), 114.6 (d, *J* = 21.0 Hz), 113.9 (d, *J* = 22.9 Hz), 74.1.**^{19}F NMR (470 MHz, $CDCl_3$):** δ –112.5 (ddd, *J* = 9.7 Hz, 8.7 Hz, 5.4 Hz). **ν_{max}(neat)/cm^{-1}:** 3329, 3066, 2251, 1589, 1438, 1246, 1016, 905. **HRMS** calcd. for $C_{13}H_{10}BrFO$: 279.9899 $[M]^+$; found (EI^+): 279.9896.

1-Bromo-2-(3-fluorobenzyl)benzene: Following **General Procedure 2A,** (2-bromophenyl)(3-fluorophenyl)methanol (1.29 g, 4.59 mmol) in CH_2Cl_2 (14 mL) was reacted with TFA (1.38 mL, 18.0 mmol) and Et_3SiH (1.44 mL, 9.0 mmol). Purification *via* flash column chromatography (pentane) afforded 1-bromo-2-(3-fluorobenzyl)benzene as a colourless liquid (0.85 g, 3.22 mmol, 70%).

^{1}H NMR (300 MHz, $CDCl_3$): δ 7.59 (dd, *J* = 7.9 Hz, 1.4 Hz, 1H), 7.30-7.23 (m, 2H), 7.18-7.09 (m, 2H), 6.99 (app. d, *J* = 7.6 Hz, 1H), 6.95-6.86 (m, 2H), 4.12 (s, 2H). **^{13}C{^{1}H} NMR (125 MHz, $CDCl_3$):** δ 162.9 (d, *J* = 245.1 Hz), 142.0 (d, *J* = 7.6 Hz), 139.5, 133.0, 131.1, 129.8 (d, *J* = 7.6 Hz), 128.2, 127.6, 124.8, 124.6 (d, *J* = 2.9 Hz), 115.8 (d, *J* = 21.0 Hz), 113.2 (d, *J* = 21.9 Hz), 41.4. **^{19}F NMR (282 MHz, $CDCl_3$):** δ –113.3 (ddd, *J* = 9.7 Hz, 8.7 Hz, 6.5 Hz). **ν_{max}(neat)/cm^{-1}:** 3059, 2924, 1589, 1486, 1440, 1248, 1025, 741. **HRMS** calcd. for $C_{13}H_{10}BrF$: 263.9950 $[M]^+$; found (EI^+): 263.9949.

3-(2-Trimethylsilylbenzyl)fluorobenzene: Following **General Procedure 3**, ^{n}BuLi (1.6 M in hexanes, 2.20 mL, 3.51 mmol) was added to 1-bromo-2-(3-fluorobenzyl)benzene (0.85 g, 3.19 mmol) in THF (6 mL) at –78 °C. The reaction was stirred at this temperature for 1 h, then

Me_3SiCl (0.53 mL, 4.15 mmol) was added dropwise, and the mixture was stirred at room temperature overnight. Purification *via* flash column chromatography (pentane) afforded the title compound as a colourless liquid (0.74 g, 2.87 mmol, 90%).

^{1}H NMR (500 MHz, $CDCl_3$): δ 7.56 (dd, *J* = 7.4 Hz, 1.5 Hz, 1H), 7.32 (app. td, *J* = 7.4 Hz, 1.5 Hz, 1H), 7.27-7.23 (m, 2H), 7.03 (app. d, *J* = 7.6 Hz, 1H), 6.93-6.89 (m, 2H), 6.78 (app. d, *J* = 10.1 Hz, 1H), 4.17 (s, 2H), 0.32 (s, 9H). **^{13}C{^{1}H} NMR (125 MHz, $CDCl_3$):** δ 162.9 (d, *J* = 245 Hz), 145.2, 144.1 (d, *J* = 7.6 Hz), 138.9, 134.7, 129.9, 129.7 (d, *J* = 8.6 Hz), 129.4, 125.7, 124.7 (d, *J* = 1.9 Hz), 115.9 (d, *J* = 21.0 Hz), 112.9 (d, *J* = 21.0 Hz), 41.3, 0.3. **^{19}F NMR (470 MHz, $CDCl_3$):** δ –113.6 (ddd, *J* = 9.3 Hz, 9.0 Hz, 6.2 Hz). **ν_{max}(neat)/cm^{-1}:** 2956, 2250, 1588, 1486, 1250, 1123, 906, 731. **HRMS** calcd. for $C_{16}H_{19}FSi$: 258.1240 $[M]^+$; found (EI^+): 258.1249.

[2-(3-Chlorobenzyl)phenyl]trimethylsilane (1l)

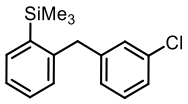

(2-Bromophenyl)(3-chlorophenyl)methanol: Following **General Procedure 1**, ^{n}BuLi (2.38 M in hexanes, 6.55 mL, 15.6 mmol) was added dropwise to a stirred solution of 3-chlorobromobenzene (1.84 mL, 15.6 mmol) in THF (39 mL) at –78 °C. The reaction was stirred at this temperature for 1 h, then 2-bromobenzaldehyde (1.82 mL, 15.6 mmol) was added dropwise, and the mixture was stirred at room temperature for 2 h. Purification *via* flash column chromatography (10% EtOAc in hexanes) afforded (2-bromophenyl)(3-chlorophenyl)methanol as a viscous, pale yellow liquid (3.89 g, 13.0 mmol, 84%).

^{1}H NMR (400 MHz, $CDCl_3$): δ 7.55 (dd, *J* = 8.0, 1.3 Hz, 1H), 7.52 (dd, *J* = 7.8, 1.7 Hz, 1H), 7.43 – 7.40 (m, 1H), 7.35 (app. td, *J* = 7.6, 1.3 Hz, 1H), 7.31 – 7.21 (m, 3H), 7.17 (app. td, *J* = 7.7, 1.7 Hz, 1H), 6.18 (s, 1H), 2.40 (br.s, 1H).**^{13}C{^{1}H} NMR (100 MHz, $CDCl_3$):** δ 144.3, 142.1, 134.5, 133.1, 129.9, 129.6, 128.7, 128.1, 128.0, 127.2, 125.3, 122.9, 74.3. **ν_{max}(neat)/cm^{-1}:** 3351, 3063, 1595, 1467, 1434, 1181, 1016, 887, 780, 755, 731, 701. **HRMS** calcd. for $C_{13}H_{10}OBrCl$: 295.9598 $[M]^+$; found (EI^+): 295.9590

1-Bromo-2-(3-chlorobenzyl)benzene: Following **General Procedure 2B,** (2-bromophenyl)(3-chlorophenyl)methanol (3.49 g, 11.7 mmol) in CH_2Cl_2 (7 mL) was reacted with TFA (10.0 mL, 93.6 mmol) and Et_3SiH (3.74 mL, 23.4 mmol). Purification *via* flash column chromatography (hexanes) afforded 1-bromo-2-(3-chlorobenzyl)benzene as a colourless liquid (3.29 g, 11.7 mmol, quant.).

^{1}H NMR (400 MHz, $CDCl_3$): δ 7.58 (dd, *J* = 7.9, 1.3 Hz, 1H), 7.31 – 7.05 (m, 7H), 4.10 (s, 2H). **$^{13}C\{^{1}H\}$ NMR (100 MHz, $CDCl_3$):** δ 141.7, 139.6, 134.4, 133.2, 131.3, 129.8, 129.2, 128.4, 127.8, 127.3, 126.6, 125.0, 41.5. **ν_{max}(neat)/cm^{-1}:** 2953, 2874, 1473, 1440, 1237, 1070, 1016, 869, 774, 739. **HRMS** calcd. for $C_{13}H_{10}BrCl$: 279.9649[M]$^+$; found (EI$^+$): 279.9645

[2-(3-Chlorobenzyl)phenyl]trimethylsilane: Following **General Procedure 3**, *n*BuLi (2.38 M in hexanes, 5.0 mL, 12.0 mmol) was added to 1-bromo-2-(3-chlorobenzyl)benzene (3.03 g, 10.8 mmol) in THF (25 mL) at –78 °C. The reaction was stirred at this temperature for 1 h, then Me_3SiCl (2.0 mL, 15.8 mmol) was added dropwise, and the mixture was stirred at room temperature overnight. Purification *via* flash column chromatography (hexanes) afforded the title compound as a colourless liquid (2.03 g, 7.38 mmol, 69%).

^{1}H NMR (400 MHz, $CDCl_3$): δ 7.62 (dd, *J* = 7.3, 1.4 Hz, 1H), 7.37 (app. td, *J* = 7.5, 1.6 Hz, 1H), 7.33 – 7.23 (m, 3H), 7.19 – 7.12 (m, 1H), 7.10 – 7.01 (m, 2H), 4.21 (s, 2H), 0.38 (s, 9H). **$^{13}C\{^{1}H\}$ NMR (100 MHz, $CDCl_3$):** δ 145.3, 143.7, 139.1, 134.8, 134.4, 130.1, 129.7, 129.6, 129.3, 127.4, 126.4, 125.9, 41.4, 0.49. **ν_{max}(neat)/cm^{-1}:** 3056, 2953, 1596, 1474, 1429, 1248, 1122, 832, 733, 753, 727. **HRMS** calcd. for $C_{16}H_{19}ClSi$: 274.0939 [M]$^+$; found (EI$^+$): 274.0943.

Trimethyl{2-[3-(trifluoromethyl)benzyl]phenyl}silane (1m)

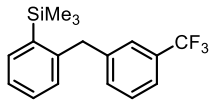

(2-Bromophenyl)[3-(trifluoromethyl)phenyl]methanol: Following **General Procedure 1**, *n*BuLi (2.38 M in hexanes, 3.55 mL, 8.46 mmol) was added dropwise to a stirred solution of 3-bromobenzotrifluoride (1.23 mL, 8.89 mmol) in THF (20 mL) at –78 °C. The reaction was stirred at this temperature for 1 h, then 2-bromobenzaldehyde (1.08 mL, 9.30 mmol) was added dropwise, and the mixture was allowed to warm to room temperature and was stirred for 2 h. Purification *via* flash column chromatography (5% → 10% EtOAc in hexanes) afforded (2-bromophenyl)[3-(trifluoromethyl)phenyl]methanol as a viscous, colourless liquid (2.34 g, 7.06 mmol, 79%).

Characterisation data were consistent with literature values: ^{1}H, $^{13}C\{^{1}H\}$ NMR and IR.[4]

^{1}H NMR (400 MHz, $CDCl_3$): δ 7.74 (s, 1H), 7.61 – 7.51 (m, 3H), 7.51 (dd, *J* = 7.8, 1.8 Hz, 1H), 7.45 (app. t, *J* = 7.7 Hz, 1H), 7.35 (app. td, *J* = 7.4, 1.0 Hz, 1H), 7.18 (app. td, *J* = 7.9, 1.8 Hz, 1H), 6.27 (s, 1H), 2.50 (br.s, 1H).**$^{13}C\{^{1}H\}$ NMR (100 MHz, $CDCl_3$):** δ 143.2, 142.1, 133.2, 131.0 (q, *J* = 32 Hz), 130.4, 129.7, 129.0, 128.7, 128.2, 124.7 (q, *J* = 3.7 Hz), 124.2 (q,

J = 270 Hz), 123.8 (q, *J* = 3.8 Hz), 122.9, 74.3. **^{19}F NMR (377 MHz, CDCl$_3$):** δ -62.5 (s). **ν_{max}(neat)/cm^{-1}:** 3375, 3068, 1592, 1569, 1468, 1439, 1376, 1161, 1119, 797, 748, 721, 701, 662.

1-Bromo-2-[3-(trifluoromethyl)benzyl]benzene: A Schlenk flask containing (2-bromophenyl)[3-(trifluoromethyl)phenyl]methanol (2.27 g, 7.20 mmol) was evacuated and back-filled with N_2 three times, then Et_3SiH (2.41 mL, 15.0 mmol) was added and the mixture was stirred and cooled to 0 °C. Cold TFA (10 mL, 130 mmol) was added dropwise and the reaction was allowed to warm to room temperature and was stirred overnight. The volatiles were then evaporated under a stream of N_2 to give the crude product which was purified *via* flash column chromatography (hexanes) to afford 1-bromo-2-[3-(trifluoromethyl)benzyl]benzene as a colourless liquid (1.91 g, 6.06 mmol, 84%).

Characterisation data were consistent with literature values: ^{19}F, ^{13}C{^{1}H} NMR and IR.[7]

^{1}H NMR (400 MHz, CDCl$_3$): δ 7.62 (dd, *J* = 7.9, 1.3 Hz, 1H), 7.54 – 7.48 (m, 2H), 7.46 – 7.34 (m, 2H), 7.29 (app. td, *J* = 7.5, 1.3 Hz, 1H), 7.21 – 7.11 (m, 2H), 4.20 (s, 2H). **^{13}C{^{1}H} NMR (100 MHz, CDCl$_3$):** δ 140.6, 139.5, 133.2, 132.4 (q, *J* = 1.6 Hz), 131.2, 130.9 (q, *J* = 32.0 Hz), 129.0, 128.5, 127.8, 125.8 (q, *J* = 3.9 Hz), 125.0, 124.3 (q, *J* = 270 Hz), 123.4 (q, *J* = 3.8 Hz), 41.7. **^{19}F NMR (377 MHz, CDCl$_3$):** δ -62.6 (s). **ν_{max}(neat)/cm^{-1}:** 3063, 2955, 2911, 2876, 1440, 1330, 1163, 1122, 1072, 1025, 741.

Trimethyl{2-[3-(trifluoromethyl)benzyl]phenyl}silane: Following **General Procedure 3**, *n*BuLi (2.38 M in hexanes, 2.23 mL, 5.32 mmol) was added to 1-bromo-2-[3-(trifluoromethyl)benzyl]benzene (1.40 g, 4.43 mmol) in THF (15 mL) at –78 °C. The reaction was stirred at this temperature for 1 h, then Me_3SiCl (0.84 mL, 6.65 mmol) was added dropwise, and the mixture was stirred at room temperature overnight. Purification *via* flash column chromatography (hexanes) afforded the title compound as a colourless liquid (1.05 g, 3.40 mmol, 76%).

^{1}H NMR (400 MHz, CDCl$_3$): δ 7.57 (dd, *J* = 7.3, 1.5 Hz, 1H), 7.50 – 7.46 (m, 1H), 7.42 – 7.36 (m, 2H), 7.30 (app. td, *J* = 7.4, 1.7 Hz, 1H), 7.28 – 7.21 (m, 2H), 6.98 (m, 1H), 4.22 (s, 2H), 0.32 (s, 9H). **^{13}C{^{1}H} NMR (100 MHz, CDCl$_3$):** δ 145.1, 142.6, 139.2, 134.9, 132.6, 130.8 (q, *J* = 32.1 Hz), 130.0, 129.7, 128.9, 126.0, 125.9 (q, *J* = 3.8 Hz), 124.4 (q, *J* = 272 Hz), 123.1 (q, *J* = 3.9 Hz), 41.5, 0.46. **^{19}F NMR (377 MHz, CDCl$_3$):** δ -62.6 (s). **ν_{max}(neat)/cm^{-1}:** 2956, 1466, 1330, 1251, 1161, 1120, 1073, 834, 739, 701. **HRMS** calcd. for $C_{17}H_{19}F_3Si$: 308.1203 $[M]^+$; found (EI^+): 308.1208

3-(2-Trimethylsilylbenzyl)phenol

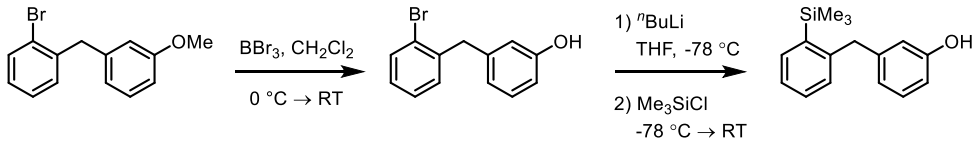

3-(2-Bromobenzyl)phenol: Boron tribromide (1.0 M in CH_2Cl_2; 6.10 mL, 6.10 mmol) was added dropwise to a stirred solution of 1-bromo-2-(3-methoxybenzyl)benzene (1.69 g, 6.10 mmol; prepared as for **1j** in CH_2Cl_2 (15 mL) at 0 °C. The reaction was allowed to warm to room temperature and was stirred overnight. H_2O (10 mL) was added, dropwise at first, and the biphasic mixture was stirred vigorously for 15 min. The aqueous phase was separated and extracted with CH_2Cl_2 (3 × 10 mL), and the combined organic portions were dried ($MgSO_4$), filtered and concentrated *in vacuo*. Purification *via* flash column chromatography (15% EtOAc in hexanes) afforded 3-(2-bromobenzyl)phenol as a brown oil (1.41 g, 5.36 mmol, 88%).

^{1}H NMR (400 MHz, $CDCl_3$): δ 7.57 (dd, *J* = 8.0, 1.3 Hz, 1H), 7.24 (app. td, *J* = 7.5, 1.4 Hz, 1H), 7.20 – 7.13 (m, 2H), 7.09 (app. td, *J* = 7.8, 1.8 Hz, 1H), 6.83 – 6.75 (m, 1H), 6.73 – 6.65 (m, 1H), 6.67 – 6.61 (m, 1H), 4.76 (br.s, 1H), 4.08 (s, 2H). **^{13}C{^{1}H} NMR (100 MHz, $CDCl_3$):** δ 155.7, 141.6, 140.2, 133.0, 131.3, 129.8, 128.1, 127.6, 125.0, 121.7, 116.0, 113.4, 41.7. **ν_{max}(neat)/cm^{-1}:** 3325, 3053, 1589, 1453, 1438, 1263, 1149, 1115, 1023, 952, 739. **HRMS** calcd. for $C_{13}H_{11}BrO$: 261.9988 $[M]^+$; found (EI^+): 262.0003

3-(2-Trimethylsilylbenzyl)phenol: *n*BuLi (2.38 M in hexanes, 2.70 mL, 6.40 mmol) was added dropwise to a stirred solution of 3-(2-bromobenzyl)phenol (0.77 g, 2.91 mmol) in THF (10 mL) at –78 °C. The reaction was stirred at this temperature for 1.5 h, then Me_3SiCl (1.29 mL, 10.2 mmol) was added dropwise, and the mixture was stirred at room temperature overnight. H_2O (5 mL), followed by glacial acetic acid (2 mL), was added, and the biphasic mixture was stirred vigorously for 1 h, then the aqueous phase was separated and extracted with Et_2O (3 × 10 mL), and the combined organic portions were dried ($MgSO_4$), filtered and concentrated *in vacuo*. Purification *via* flash column chromatography (10% EtOAc in hexanes) afforded the title compound as a yellow, viscous liquid (0.37 g, 1.44 mmol, 49%).

^{1}H NMR (400 MHz, $CDCl_3$): δ 7.54 (dd, *J* = 7.4, 1.4 Hz, 1H), 7.28 (app. td, J = 7.4, 1.7 Hz, 1H), 7.22 (app. td, *J* = 7.4, 1.4 Hz, 1H), 7.16 (app. t, *J* = 7.8 Hz, 1H), 7.07 – 7.00 (m, 1H), 6.74 – 6.63 (m, 2H), 6.55 – 6.48 (m, 1H), 4.61 (s, 1H), 4.11 (s, 2H), 0.31 (s, 9H).**^{13}C{^{1}H} NMR (100 MHz, $CDCl_3$):** δ 155.7, 146.0, 143.6, 139.0, 134.7, 130.1, 129.7, 129.5, 125.7, 121.9, 116.2, 113.1, 41.6, 0.48. **ν_{max}(neat)/cm^{-1}:** 3352, 2952, 1588, 1454, 1248, 1148, 1122, 833, 734. **HRMS** calcd. for $C_{16}H_{20}OSi$: 256.1278 $[M]^+$; found (EI^+): 256.1269

3-[2-(Trimethylsilyl)benzyl]phenyl trifluoromethanesulfonate (1n)

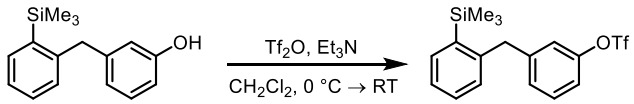

Triflic anhydride (0.28 mL, 1.62 mmol) was added dropwise to a stirred solution of 3-(2-trimethylsilylbenzyl)phenol (0.19 g, 0.74 mmol) and pyridine (0.78 mL, 9.70 mmol) in CH_2Cl_2 (10 mL) at 0 °C. The reaction was stirred overnight at room temperature, then H_2O (5 mL) was added, then the aqueous phase was separated and extracted with CH_2Cl_2 (3 × 10 mL), and the combined organic portions were dried ($MgSO_4$), filtered and concentrated *in vacuo*. Purification *via* flash column chromatography (10% EtOAc in hexanes) afforded the title compound as a colourless liquid (0.28 g, 0.72 mmol, 97%).

^{1}H NMR (400 MHz, $CDCl_3$): δ 7.57 (dd, *J* = 7.3, 1.4 Hz, 1H), 7.39 – 7.29 (m, 2H), 7.26 (app. td, *J* = 7.4 Hz, 1.4 Hz, 1H), 7.14 – 7.09 (m, 2H), 7.00 – 6.96 (m, 2H), 4.20 (s, 2H), 0.30 (s, 9H). **^{13}C{^{1}H} NMR (100 MHz, $CDCl_3$):** δ 149.9, 144.9, 144.6, 139.2, 135.0, 130.2, 130.1, 129.7, 129.1, 126.2, 122.0, 119.0, 118.9 (q, *J* = 321 Hz), 41.3, 0.43. **^{19}F NMR (377 MHz, $CDCl_3$):** δ -72.9 (s). **ν_{max}(neat)/cm^{-1}**: 2957, 1613, 1581, 1421, 1250, 1206, 1139, 1115, 941, 833, 756. **HRMS** calcd. for $C_{17}H_{19}O_3F_3NaSSi$: 411.0669 $[M+Na]^+$; found (ESI^+): 411.0647.

2-(2-Trimethylsilylbenzyl)-1,4-dimethylbenzene (1a)

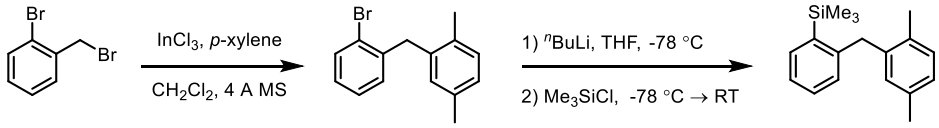

2-(2-Bromobenzyl)-1,4-dimethylbenzene:[8] Indium(III) chloride (106 mg, 0.50 mmol) was added to a stirred solution of 2-bromobenzyl bromide (1.25 g, 5.00 mmol) and *p*-xylene (3.10 mL, 25.0 mmol) in CH_2Cl_2 (10 mL) containing 4 Å molecular sieves (2.5 g). After 4 h, the reaction was filtered through a pad of Celite and concentrated *in vacuo*. Purification *via* flash column chromatography (hexanes) afforded 2-(2-bromobenzyl)-1,4-dimethylbenzene as a colourless liquid (1.07 g, 3.89 mmol, 78%).

Characterisation data were consistent with literature values: ^{1}H and ^{13}C{^{1}H} NMR.[9]

^{1}H NMR (400 MHz, $CDCl_3$): δ 7.60 (dd, *J* = 7.9 Hz, 1.5 Hz, 1H), 7.19 (app. td, *J* = 7.5 Hz, 1.3 Hz, 1H), 7.12-7.07 (m, 2H), 7.01 (dd, *J* = 7.7 Hz, 1.3 Hz, 1H), 6.88 (dd, *J* = 7.7 Hz, 1.5 Hz, 1H), 6.84 (br. s, 1H), 4.04 (s, 2H), 2.30 (s, 3H), 2.20 (s, 3H). **^{13}C{^{1}H} NMR (100 MHz,**

$CDCl_3$): δ 139.8, 137.3, 135.5, 133.1, 132.6, 130.5, 130.19, 130.15, 127.6, 127.4, 127.3, 125.0, 39.5, 21.0, 19.0. **ν_{max}(neat)/cm^{-1}:** 2920, 1566, 1503, 1465, 1439, 1024, 803, 745.

(2-Trimethylsilylbenzyl)-1,4-dimethylbenzene: Following **General Procedure 3**, *n*BuLi (1.6 M in hexanes, 2.80 mL, 4.50 mmol) was added to 2-(2-bromobenzyl)-1,4-dimethylbenzene (1.13 g, 4.09 mmol) in THF (10 mL) at –78 °C. The reaction was stirred at this temperature for 1 h, then Me_3SiCl (0.67 mL, 5.31 mmol) was added dropwise, and the mixture was stirred at room temperature overnight. Purification *via* flash column chromatography (hexanes) afforded the title compound as a colourless liquid (1.01 g, 3.76 mmol, 92%).

^{1}H NMR (400 MHz, $CDCl_3$): δ 7.57-7.55 (m, 1H), 7.25 (app. td, *J* = 7.4 Hz, 1.9 Hz, 1H), 7.21 (app. td, *J* = 7.4 Hz, 1.6 Hz, 1H), 7.10 (d, *J* = 7.6 Hz, 1H), 6.99 (dd, *J* = 7.6 Hz, 1.8 Hz, 1H), 6.83 (dd, *J* = 7.1 Hz, 2.1 Hz, 1H), 6.78 (s, 1H), 4.10 (s, 2H), 2.28 (s, 3H), 2.19 (s, 3H), 0.35 (s, 9H). **^{13}C{^{1}H} NMR (100 MHz, $CDCl_3$):** δ 146.0, 138.8, 138.6, 135.4, 134.5, 133.4, 130.8, 130.0, 129.3, 128.4, 127.0, 125.3, 39.7, 21.0, 19.2, 0.2. **ν_{max}(neat)/cm^{-1}:** 2953, 1503, 1431, 1261, 1249, 1123, 836, 805, 741. **HRMS** calcd. for $C_{18}H_{24}Si$: 268.1647 $[M]^+$; found (EI^+): 268.1652.

2-(2-Trimethylsilyl-4-fluorobenzyl)-1,4-dimethylbenzene (1o)

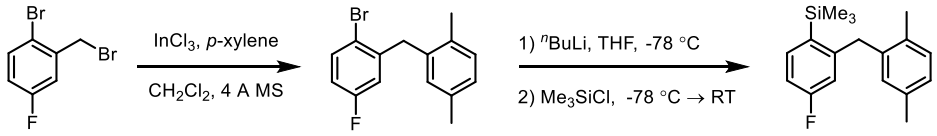

2-(2-Bromo-4-fluorobenzyl)-1,4-dimethylbenzene:[8] Indium(III) chloride (92.9 mg, 0.42 mmol) was added to a stirred solution of 2-bromo-4-fluorobenzyl bromide (1.11 g, 4.21 mmol) and *p*-xylene (2.65 mL, 20.7 mmol) in CH_2Cl_2 (8 mL) containing 4 Å molecular sieves (2 g). After 4 h, the reaction was filtered through a pad of Celite and concentrated *in vacuo*. Purification *via* flash column chromatography (hexanes) afforded 2-(2-bromo-4-fluorobenzyl)-1,4-dimethylbenzene as a colourless liquid (1.09 g, 3.71 mmol, 89%).

^{1}H NMR (300 MHz, $CDCl_3$): δ 7.54 (dd, *J* = 8.7 Hz, 5.4 Hz, 1H), 7.11 (d, *J* = 7.6 Hz, 1H), 7.03 (dd, *J* = 7.6 Hz, 1.4 Hz, 1H), 6.87-6.79 (m, 2H), 6.55 (dd, *J* = 9.8 Hz, 3.1 Hz, 1H), 3.98 (s, 2H), 2.31 (s, 3H), 2.17 (s, 3H). **^{13}C{^{1}H} NMR (125 MHz, $CDCl_3$):** δ 162.1 (d, *J* = 246 Hz), 142.3 (d, *J* = 7.6 Hz), 136.4, 135.7, 133.6, 133.5 (d, *J* = 7.6 Hz), 130.7, 130.4, 127.7, 118.8, 117.1 (d, *J* = 22.9 Hz), 114.8 (d, *J* = 22.9 Hz), 39.6, 21.0, 19.0. **^{19}F NMR (470 MHz, $CDCl_3$):** δ –114.9 (m). **ν_{max}(neat)/cm^{-1}:** 2921, 1603, 1579, 1463, 1265, 1147, 1028, 904. **HRMS** calcd. for $C_{15}H_{14}BrF$: 292.0263 $[M]^+$; found (EI^+): 292.0263.

2-(2-Trimethylsilyl-4-fluorobenzyl)-1,4-dimethylbenzene: Following **General Procedure 3**, ^{n}BuLi (1.6 M in hexanes, 2.54 mL, 4.06 mmol) was added to 2-(2-bromo-4-fluorobenzyl)-1,4-dimethylbenzene (1.08 g, 3.69 mmol) in THF (7 mL) at –78 °C. The reaction was stirred at this temperature for 1 h, then Me_3SiCl (0.61 mL, 4.81 mmol) was added dropwise, and the mixture was stirred at room temperature overnight. Purification *via* flash column chromatography (hexanes) afforded the title compound as a colourless liquid (0.83 g, 2.90 mmol, 79%).

^{1}H NMR (400 MHz, $CDCl_3$): δ 7.51 (dd, *J* = 8.2, 6.8 Hz, 1H), 7.11 (d, *J* = 7.6 Hz, 1H), 7.01 (d, *J* = 7.6 Hz, 1H), 6.89 (app. td, *J* = 8.5, 2.6 Hz, 1H), 6.81 (s, 1H), 6.51 (dd, *J* = 11.0, 2.5 Hz, 1H), 4.08 (s, 2H), 2.30 (s, 3H), 2.17 (s, 3H), 0.36 (s, 9H). **^{13}C{^{1}H} NMR (100 MHz, $CDCl_3$):** δ 164.3 (d, *J* = 248 Hz), 149.4 (d, *J* = 6.6 Hz), 138.1, 136.4 (d, *J* = 7.6 Hz), 135.7, 134.1 (d, *J* = 3.6 Hz), 133.5, 131.1, 130.4, 127.5, 115.5 (d, *J* = 20.0 Hz), 112.3 (d, *J* = 19.0 Hz), 39.8, 21.1, 19.3, 0.36. **^{19}F NMR (470 MHz, $CDCl_3$):** δ –112.5 (ddd, *J* = 11.0 Hz, 8.3 Hz, 7.0 Hz). **ν_{max}(neat)/cm^{-1}:** 2954, 1594, 1578, 1473, 1250, 1208, 1060, 908. **HRMS** calcd. for $C_{18}H_{23}FSi$: 286.1553 $[M]^+$; found (EI^+): 286.1561.

2-(2-Trimethylsilyl-4-chlorobenzyl)-1,4-dimethylbenzene (1p)

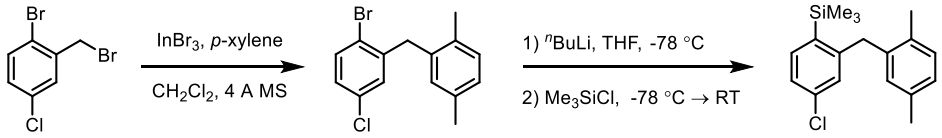

2-(2-Bromo-4-chlorobenzyl)-1,4-dimethylbenzene:[8] Indium(III) bromide (0.62 g, 1.76 mmol) was added to a stirred solution of 2-bromo-5-chlorobenzyl bromide (5.55 g, 19.5 mmol) and *p*-xylene (10.85 mL, 88.0 mmol) in CH_2Cl_2 (35 mL) containing 4 Å molecular sieves (8 g). After 6 h, the reaction was filtered through a pad of silica gel (eluent: Et_2O) and concentrated *in vacuo*. Purification *via* flash column chromatography (hexanes) afforded 2-(2-bromo-4-chlorobenzyl)-1,4-dimethylbenzene as a colourless liquid that solidified on standing (6.03 g, 19.5 mmol, quant.).

^{1}H NMR (400 MHz, $CDCl_3$): δ 7.51 (d, *J* = 8.4 Hz, 1H), 7.15 – 6.98 (m, 3H), 6.82 (m, 2H), 3.98 (s, 2H), 2.30 (s, 3H), 2.17 (s, 3H). **^{13}C{^{1}H} NMR (100 MHz, $CDCl_3$):** 142.0, 136.5, 135.9, 133.7, 133.7, 133.7, 130.7, 130.5, 130.2, 127.9, 127.8, 122.9, 39.6, 21.2, 19.2. **ν_{max}(neat)/cm^{-1}:** 2996, 2905, 1583, 1500, 1451, 1426, 1387, 1091, 1024, 865, 807. **HRMS** calcd. for $C_{15}H_{14}BrCl$: 307.9962 $[M]^+$; found (EI^+): 307.9960. **m.p. /°C:** 45-47.

2-(2-Trimethylsilyl-4-chlorobenzyl)-1,4-dimethylbenzene: Following **General Procedure 3**, *n*BuLi (2.50 M in hexanes, 6.9 mL, 17.2 mmol) was added to 2-(2-bromo-4-chlorobenzyl)-1,4-dimethylbenzene (4.83 g, 15.6 mmol) in THF (39 mL) at –78 °C. The reaction was stirred at this temperature for 1 h, then Me_3SiCl (3.0 mL, 23.4 mmol) was added dropwise, and the mixture was stirred at room temperature overnight. Purification *via* flash column chromatography (hexanes) afforded the title compound as a colourless liquid (4.16 g, 13.7 mmol, 88%).

^{1}H NMR (400 MHz, $CDCl_3$): δ 7.47 (d, *J* = 8.0 Hz, 1H), 7.19 (dd, *J* = 8.0, 2.0 Hz, 1H), 7.10 (d, *J* = 7.6 Hz, 1H), 7.01 (dd, *J* = 7.6, 2.0 Hz, 1H), 6.80 (d, *J* = 2.0 Hz, 1H), 6.77 (app. s, 1H), 4.06 (s, 2H), 2.29 (s, 3H), 2.18 (s, 3H), 0.35 (s, 9H).**^{13}C{^{1}H} NMR (100 MHz, $CDCl_3$):** δ 148.4, 138.0, 137.1, 136.0, 135.8, 135.7, 133.4, 131.0, 130.4, 128.5, 127.5, 125.6, 39.7, 21.2, 19.4, 0.27. **ν_{max}(neat)/cm^{-1}:** 2953, 1575, 1548, 1460, 1249, 1108, 835, 809, 756. **HRMS** calcd. for $C_{18}H_{23}ClSi$: 302.1252 $[M]^+$; found (EI^+): 302.1257.

Trimethyl[5-methyl-2-(4-methylbenzyl)phenyl]silane (1t)

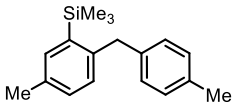

(2-Bromo-4-methylphenyl)(4-methylphenyl)methanol: Following **General Procedure 1**, *n*BuLi (2.38 M in hexanes, 2.10 mL, 5.00 mmol) was added dropwise to a stirred solution of 4-bromotoluene (0.86 g, 5.00 mmol) in THF (13 mL) at –78 °C. The reaction was stirred at this temperature for 1 h, then 2-bromo-4-methylbenzaldehyde (1.09 g, 5.50 mmol) was added portionwise, and the mixture was allowed to warm to room temperature and was stirred overnight. Purification *via* flash column chromatography (10% EtOAc in hexanes) afforded (2-bromo-4-methylphenyl)(4-methylphenyl)methanol as a viscous, colourless liquid (1.02 g, 3.51 mmol, 70%).

^{1}H NMR (400 MHz, $CDCl_3$): δ 7.44 (d, *J* = 7.9 Hz, 1H), 7.36 (d, *J* = 0.9 Hz, 1H), 7.28 (d, *J* = 8.1 Hz, 2H), 7.17 – 7.11 (m, 3H), 6.13 (s, 1H), 2.33 (s, 3H), 2.31 (s, 3H), 2.26 (br.s, 1H).**^{13}C{^{1}H} NMR (100 MHz, $CDCl_3$):** δ 139.8, 139.6, 139.3, 137.5, 133.4, 129.3, 128.6, 128.3, 127.0, 122.7, 74.7, 21.3, 20.8. **ν_{max}(neat)/cm^{-1}:** 3300, 3025, 2980, 2919, 2863, 1562, 1512, 1486, 1446, 1378, 1308, 1175, 1044, 1025, 871, 816, 768. **HRMS** calcd. for $C_{15}H_{15}OBr$: 290.0301 $[M]^+$; found (EI^+): 290.0309.

2-Bromo-4-methyl-1-(4-methylbenzyl)benzene: Following **General Procedure 2A**, (2-bromo-4-methylphenyl)(4-methylphenyl)methanol (0.97 g, 3.34 mmol) in CH_2Cl_2 (10 mL)

was reacted with TFA (1.00 mL, 13.4 mmol) and Et_3SiH (1.10 mL, 6.68 mmol). Purification *via* flash column chromatography (hexanes) afforded 2-bromo-4-methyl-1-(4-methylbenzyl)benzene as a colourless liquid (0.82 g, 2.99 mmol, 90%).

^{1}H NMR (400 MHz, $CDCl_3$): δ 7.41 (s, 1H), 7.14 – 7.00 (m, 6H), 4.05 (s, 2H), 2.33 (s, 3H), 2.31 (s, 3H). **^{13}C{^{1}H} NMR (100 MHz, $CDCl_3$):** δ 137.8, 137.5, 136.8, 135.7, 133.2, 130.7, 129.2, 128.8, 128.3, 124.6, 40.9, 21.1, 20.6. **ν_{max}(neat)/cm^{-1}:** 3046, 3020, 2977, 2919, 2860, 1513, 1489, 1437, 1381, 1211, 1038, 911, 861, 846, 821, 806, 763. **HRMS** calcd. for $C_{15}H_{15}Br$: 274.0352[M]$^+$; found (EI$^+$): 274.0349.

Trimethyl[5-methyl-2-(4-methylbenzyl)phenyl]silane: Following **General Procedure 3**, ^{n}BuLi (2.38 M in hexanes, 1.30 mL, 3.08 mmol) was added to 2-bromo-4-methyl-1-(4-methylbenzyl)benzene (0.71 g, 2.57 mmol) in THF (8 mL) at –78 °C. The reaction was stirred at this temperature for 1 h, then Me_3SiCl (0.49 mL, 3.86 mmol) was added dropwise, and the mixture was stirred at room temperature overnight. Purification *via* flash column chromatography (hexanes) afforded the title compound as a colourless liquid (0.60 g, 2.23 mmol, 87%).

^{1}H NMR (400 MHz, $CDCl_3$): δ 7.36 (d, *J* = 2.0 Hz, 1H), 7.14 – 7.08 (m, 3H), 7.01 (d, *J* = 8.0 Hz, 2H), 6.93 (d, *J* = 7.8 Hz, 1H), 4.11 (s, 2H), 2.35 (s, 3H), 2.36 (s, 3H), 0.34 (s, 9H). **^{13}C{^{1}H} NMR (100 MHz, $CDCl_3$):** δ 143.6, 138.73, 138.66, 135.5, 135.3, 134.6, 130.2, 129.9, 129.16, 129.15, 40.9, 21.3, 21.2, 0.54. **ν_{max}(neat)/cm^{-1}:** 3045, 3005, 2952, 2920, 2863, 1513, 1481, 1442, 1409, 1381, 1248, 1142, 1072, 1022, 993, 886, 833, 750. **HRMS** calcd. for $C_{18}H_{24}Si$: 268.1642 [M]$^+$; found (EI$^+$): 268.1645

Trimethyl(2-phenoxyphenyl)silane (1v)[10]

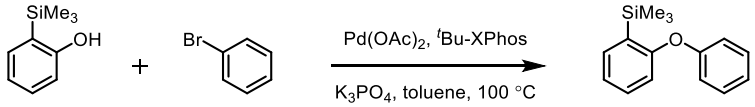

A Schlenk flask containing $Pd(OAc)_2$ (4.50 mg, 0.02 mmol), ^{t}Bu-XPhos (12.7 mg, 0.03 mmol) and potassium phosphate (0.42 g, 2.00 mmol) was evacuated and back-filled with N_2 three times, then 2-(trimethylsilyl)phenol[11] (0.20 g, 1.20 mmol) and bromobenzene (105 µL, 1.00 mmol) in toluene (2 mL) was added, and the flask was sealed and heated at 100 °C overnight. The reaction mixture was filtered through a pad of Celite (eluent: hexanes) and concentrated *in vacuo*. Purification *via* flash column chromatography (hexanes) afforded the title compound as a colourless liquid (0.16 g, 0.64 mmol, 64%).

^{1}H NMR (400 MHz, $CDCl_3$): δ 7.50 (dd, *J* = 7.3, 1.6 Hz, 1H), 7.36 – 7.27 (m, 3H), 7.15 – 7.04 (m, 2H), 7.00 – 6.92 (m, 2H), 6.80 (dd, *J* = 8.2, 1.0 Hz, 1H), 0.28 (s, 9H). **^{13}C{^{1}H} NMR (100 MHz, $CDCl_3$):** δ 162.1, 157.7, 135.5, 130.8, 130.83, 129.80, 123.1, 123.0, 118.9, 117.6, -0.76. **ν_{max}(neat)/cm^{-1}:** 3064, 2954, 2897, 1587, 1566, 1489, 1466, 1433, 1219, 1076, 834, 748, 720. **HRMS** calcd. for $C_{15}H_{18}OSi$: 242.1122 $[M]^+$; found (EI^+): 242.1115.

[4-Chloro-2-(2-phenylethyl)phenyl]trimethylsilane (3b)

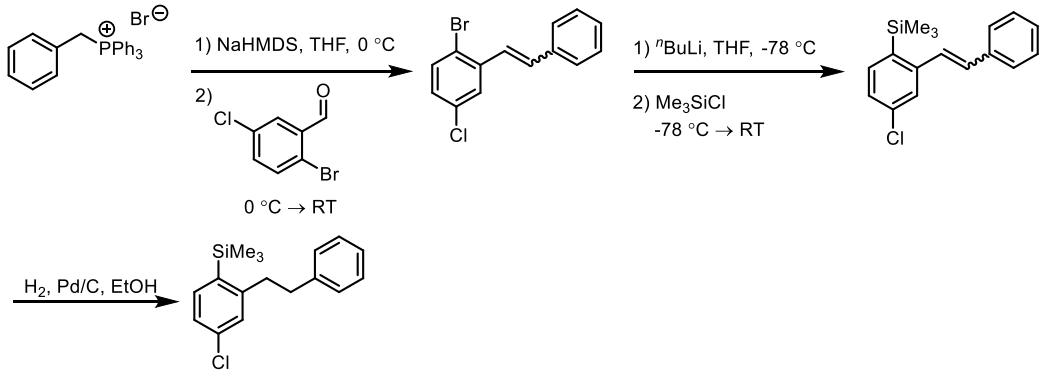

1-Bromo-4-chloro-2-(2-phenylethenyl)benzene: Sodium bis(trimethylsilyl)amide (2.0 M in hexanes, 1.25 mL, 2.50 mmol) was added dropwise to a stirred suspension of benzyltriphenylphosphonium bromide (1.08 g, 2.50 mmol) in THF (7 mL) at 0 °C. The reaction was stirred at this temperature for 1 h, then a solution of 2-bromo-5-chlorobenzaldehyde (0.55 g, 2.50 mmol) in THF (7 mL) was added dropwise, and the mixture was allowed to warm to room temperature and was stirred for 3 h. The reaction was quenched with H_2O (10 mL), then the aqueous phase was separated and extracted with Et_2O (3 × 15 mL), and the combined organic portions were dried ($MgSO_4$), filtered and concentrated *in vacuo*. Purification *via* flash column chromatography (hexanes) afforded a 6.4:1 mixture of (*E*)- to (*Z*)-1-bromo-4-chloro-2-(2-phenylethenyl)benzene as a colourless oil (0.67 g, 2.28 mmol, 91%). The identity of the major (*E*) isomer was confirmed by ^{1}H NMR ($^3J_{HH}$ analysis) and the mixture was used without further purification.

Data for (*E*)-isomer: **^{1}H NMR (400 MHz, $CDCl_3$)**: δ 7.52 (d, *J* = 8.5 Hz, 1H), 7.24 – 7.19 (m, 3H), 7.17 – 7.11 (m, 3H), 7.07 (ddd, *J* = 8.5, 2.6, 0.6 Hz, 1H), 6.73 (d, *J* = 12.1 Hz, 1H), 6.59 – 6.50 (m, 1H). **HRMS** calcd. for $C_{14}H_{10}BrCl$: 291.9649 $[M]^+$; found (EI^+): 291.9658.

[4-Chloro-2-(2-phenylethenyl)phenyl](trimethyl)silane: *n*BuLi (2.38 M in hexanes, 0.83 mL, 1.97 mmol) was added dropwise to a stirred solution of (*E*)/(*Z*)-1-bromo-4-chloro-2-(2-phenylethenyl)benzene (0.48 g, 1.63 mmol) in THF (4 mL) at –78 °C. The reaction was stirred

at this temperature for 1 h, then Me_3SiCl (0.31 mL, 2.46 mmol) was added dropwise, and the mixture was allowed to warm to room temperature and was stirred overnight. The reaction was quenched with H_2O (5 mL), then the aqueous phase was separated and extracted with Et_2O (3 × 10 mL), and the combined organic portions were dried ($MgSO_4$), filtered and concentrated *in vacuo*. Purification *via* flash column chromatography (hexanes) afforded a 6.4:1 mixture of (*E*)- to (*Z*)- [4-chloro-2-(2-phenylethenyl)phenyl](trimethyl)silane as a colourless oil (0.41 g, 1.43 mmol, 88%). The identity of the major (*E*)-isomer was confirmed by ^{1}H NMR ($^3J_{HH}$) analysis and the mixture was used without further purification.

Data for (*E*)-isomer: **^{1}H NMR (400 MHz, $CDCl_3$)**: δ 7.52 (d, *J* = 8.0 Hz, 1H), 7.27 – 7.18 (m, 3H), 7.15 (d, *J* = 2.0 Hz, 2H), 7.12 – 7.07 (m, 2H), 6.80 (d, *J* = 12.2 Hz, 1H), 6.65 (d, *J* = 12.2 Hz, 1H), 0.34 (s, 9H). **HRMS** calcd. for $C_{17}H_{19}ClSi$: 286.0939 $[M]^+$; found (EI^+): 286.0946.

[4-Chloro-2-(2-phenylethyl)phenyl]trimethylsilane: The mixture of (*E*)/(*Z*)-4-chloro-2-(2-phenylethenyl)phenyl](trimethyl)silane (0.20 g, 0.70 mmol) was dissolved in EtOH (5 mL) and nitrogen was bubbled through the solution for 10 min. Pd/C (10 wt%; 30 mg) was added and a balloon of H_2 was fitted and H_2 was bubbled through the solution. Another balloon of H_2 was fitted and the reaction was stirred under a static H_2 atmosphere for 5 h. The suspension was filtered through a pad of Celite (eluent: CH_2Cl_2) and the filtrate was concentrated *in vacuo*. Purification *via* flash column chromatography (hexanes) afforded the title compound as a colourless liquid (0.12 g, 0.41 mmol, 59%).

^{1}H NMR (400 MHz, $CDCl_3$): δ 7.42 (d, *J* = 8.0 Hz, 1H), 7.36 – 7.31 (m, 2H), 7.27 – 7.23 (m, 4H), 7.19 (dd, *J* = 8.0, 2.1 Hz, 1H), 3.05 – 2.97 (m, 2H), 2.96 – 2.88 (m, 2H), 0.34 (s, 9H). **^{13}C{^{1}H} NMR (100 MHz, $CDCl_3$):** δ 149.6, 141.5, 136.6, 136.1, 135.6, 128.9, 128.7, 128.5, 126.3, 125.6, 38.6, 38.0, 0.57. **ν_{max}(neat)/cm^{-1}:** 3062, 2954, 1576, 1549, 1496, 1470, 1454, 1408, 1382, 1249, 1190, 1076, 1061, 1030, 891, 874, 834, 813, 752, 723. **HRMS** calcd. for $C_{17}H_{21}ClSi$: 288.1096 $[M]^+$; found (EI^+): 288.1100

Trimethyl[2-(2-phenylethyl)-4-(trifluoromethyl)phenyl]silane (3c)

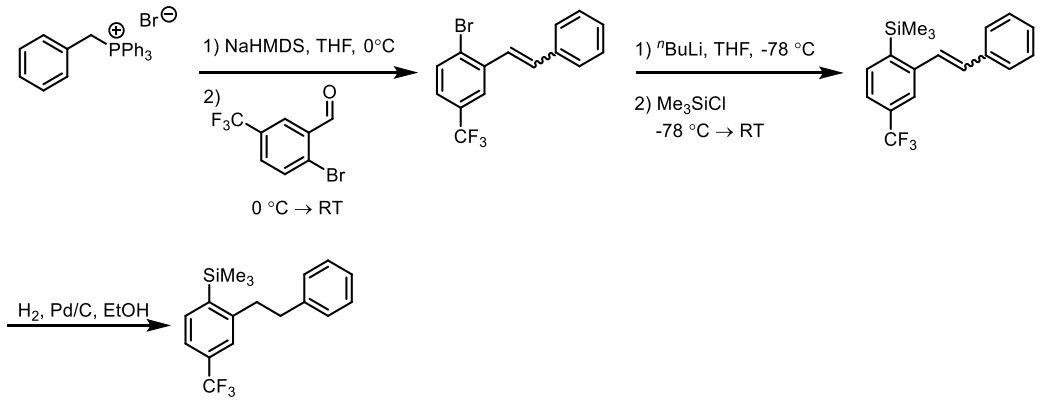

1-Bromo-2-(2-phenylethenyl)-4-(trifluoromethyl)benzene: Sodium bis(trimethylsilyl)amide (2.0 M in hexanes, 1.25 mL, 2.50 mmol) was added dropwise to a stirred suspension of benzyltriphenylphosphonium bromide (1.08 g, 2.50 mmol) in THF (7 mL) at 0 °C. The reaction was stirred at this temperature for 1 h, then a solution of 2-bromo-5-(trifluoromethyl)benzaldehyde (0.63 g, 2.50 mmol) in THF (7 mL) was added dropwise, and the mixture was stirred for 4 h at room temperature. The reaction was quenched with H_2O (15 mL), then the aqueous phase was separated and extracted with Et_2O (3 × 15 mL), and the combined organic portions were dried ($MgSO_4$), filtered and concentrated *in vacuo*. Purification *via* flash column chromatography (hexanes) afforded a 9:1 mixture of (*E*)- to (*Z*)-1-bromo-2-(2-phenylethenyl)-4-(trifluoromethyl)benzene as a colourless oil (0.59 g, 1.80 mmol, 72%). The identity of the major (*E*)-isomer was confirmed by ^{1}H NMR ($^3J_{HH}$ analysis) and the mixture was used without further purification.

Data for (*E*)-isomer: **^{1}H NMR (400 MHz, $CDCl_3$)**: δ 7.72 (d, *J* = 8.4 Hz, 1H), 7.41 (m, 1H), 7.35 – 7.29 (m, 1H), 7.24 – 7.17 (m, 3H), 7.15 – 7.08 (m, 2H), 6.80 (d, *J* = 12.1 Hz, 1H), 6.61 (d, *J* = 12.1 Hz, 1H). **^{19}F NMR (377 MHz, CD_2Cl_2):** δ – 63.0 (s, major), -62.7 (s, minor). **HRMS** calcd. for $C_{15}H_{10}BrF_3$: 325.9913 $[M]^+$; found (EI^+): 325.9912.

Trimethyl[2-(2-phenylethenyl)-4-(trifluoromethyl)phenyl]silane: ^{n}BuLi (2.38 M in hexanes, 0.58 mL, 1.39 mmol) was added dropwise to a stirred solution of (*E*)/(*Z*)-1-bromo-2-(2-phenylethenyl)-4-(trifluoromethyl)benzene (0.41 g, 1.26 mmol) in THF (3 mL) at –78 °C. The reaction was stirred at this temperature for 1 h, then Me_3SiCl (0.24 mL, 1.89 mmol) was added dropwise, and the mixture was allowed to warm to room temperature and was stirred overnight. The reaction was quenched with H_2O (5 mL), then the aqueous phase was separated and extracted with Et_2O (3 × 10 mL), and the combined organic portions were dried ($MgSO_4$), filtered and concentrated *in vacuo*. Purification *via* flash column chromatography (hexanes)

afforded a 9:1 mixture of (*E*)- to (*Z*)-trimethyl[2-(2-phenylethenyl)-4-(trifluoromethyl)phenyl]silane (0.27 g, 0.85 mmol, 67%). The identity of the major (*E*)- isomer was confirmed by ^{1}H NMR ($^{3}J_{HH}$ analysis) and the mixture was used without further purification.

Data for (*E*)-isomer: **^{1}H NMR (400 MHz, $CDCl_3$)**: δ 7.71 (d, *J* = 7.8 Hz, 1H), 7.50 – 7.46 (m, 1H), 7.39 (s, 1H), 7.21 – 7.15 (m, 3H), 7.10 – 7.03 (m, 2H), 6.86 (d, *J* = 12.2 Hz, 1H), 6.71 (d, *J* = 12.2 Hz, 1H), 0.38 (s, 9H). **^{13}C{^{1}H} NMR (100 MHz, $CDCl_3$):** δ 144.8, 143.7, 136.2, 135.2, 131.8, 131.1 (q, *J* = 32 Hz), 130.7, 129.3, 128.3, 127.6, 125.9 (q, *J* = 3.7 Hz), 122.7 (q, *J* = 3.7 Hz), -0.41. *1 × C_{Ar} not observed.* **^{19}F NMR (377 MHz, CD_2Cl_2):** δ – 63.2 (s), – 62.9 (s, minor). **HRMS** calcd. for $C_{18}H_{19}F_3Si$: 320.1203 $[M]^+$; found (EI^+): 320.1196.

Trimethyl[2-(2-phenylethyl)-4-(trifluoromethyl)phenyl]silane: The mixture of (*E*)/(*Z*)-trimethyl[2-(2-phenylethenyl)-4-(trifluoromethyl)phenyl]silane (0.22 g, 0.69 mmol) was dissolved in EtOH (5 mL) and N_2 was bubbled through the solution for 10 min. Pd/C (10 wt%; 22 mg) was added and a balloon of H_2 was fitted and H_2 was bubbled through the solution. Another balloon of H_2 was fitted and the reaction was stirred under a static H_2 atmosphere overnight. The suspension was filtered through a pad of Celite (eluent: CH_2Cl_2) and the filtrate was concentrated *in vacuo*. Purification *via* flash column chromatography (hexanes) afforded the title compound as a colourless liquid (0.20 g, 0.61 mmol, 88%).

^{1}H NMR (400 MHz, $CDCl_3$): δ 7.61 (app. d, *J* = 7.7 Hz, 1H), 7.48 – 7.41 (m, 2H), 7.38 – 7.31 (m, 2H), 7.29 – 7.22 (m, 3H), 3.17 – 3.06 (m, 2H), 3.03 – 2.88 (m, 2H), 0.38 (s, 9H). **^{13}C{^{1}H} NMR (100 MHz, $CDCl_3$):** δ 148.4, 143.2, 141.3, 135.2, 131.4 (q, *J* = 32 Hz), 128.7, 128.5, 126.4, 125.2 (q, *J* = 3.7 Hz), 124.4 (q, *J* = 270 Hz), 121.9 (q, *J* = 3.8 Hz), 38.6, 38.1, 0.46. **^{19}F NMR (377 MHz, $CDCl_3$):** δ -62.9 (s). **ν_{max}(neat)/cm^{-1}:** 3065, 3028, 2957, 1603, 1400, 1329, 1263, 1251, 1163, 1121, 1096, 828, 754, 726. **HRMS** calcd. for $C_{18}H_{21}F_3Si$: 322.1359 $[M]^+$; found (EI^+): 322.1369.

Trimethyl[2-(phenoxymethyl)phenyl]silane (3d)

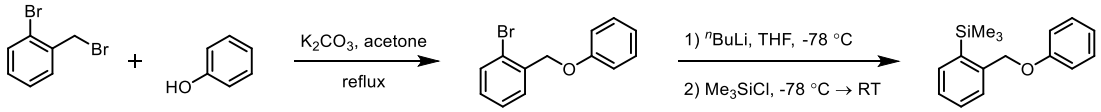

1-Bromo-2-(phenoxymethyl)benzene: A suspension of K_2CO_3 (0.62 g, 4.50 mmol), 2-bromobenzyl bromide (0.75 g, 3.00 mmol) and phenol (0.31 g, 3.30 mmol) in acetone (12 mL) was heated at reflux for 14 h. The reaction mixture was cooled to room temperature, filtered and concentrated *in vacuo*. The crude material was passed through a pad of silica gel (eluent:

Et_2O); concentration of the filtrate *in vacuo* afforded 1-bromo-2-(phenoxymethyl)benzene as a colourless liquid (0.79 g, 2.99 mmol, >99%).

Characterisation data were consistent with literature values: ^1H and $^{13}C\{^1H\}$ NMR.[12]

^1H NMR (400 MHz, $CDCl_3$): δ 7.67 – 7.54 (m, 2H), 7.35 (app. td, *J* = 7.5, 1.3 Hz, 1H), 7.32 (dd, *J* = 8.9, 7.9 Hz, 2H), 7.20 (app. td, *J* = 7.4, 1.8 Hz, 1H), 7.02-6.98 (m, 3H), 5.16 (s, 2H). **$^{13}C\{^1H\}$ NMR (125 MHz, $CDCl_3$):** δ 158.4, 136.4, 132.6, 129.5, 129.2, 128.9, 127.5, 122.2, 121.2, 114.9, 69.3. **HRMS** calcd. for $C_{13}H_{11}OBr$: 261.9993 $[M]^+$; found (EI^+): 261.9985.

Trimethyl[2-(phenoxymethyl)phenyl]silane: Following **General Procedure 3**, *n*BuLi (1.6 M in hexanes, 2.06 mL, 3.30 mmol) was added to 1-bromo-2-(phenoxymethyl)benzene (0.79 g, 2.99 mmol) in THF (6 mL) at –78 °C. The reaction was stirred at this temperature for 1 h, then Me_3SiCl (0.49 mL, 3.90 mmol) was added dropwise, and the mixture was stirred at room temperature overnight. Purification *via* flash column chromatography (10% toluene in hexanes) afforded the title compound as a viscous, colourless liquid (0.71 g, 2.78 mmol, 93%).

^1H NMR (500 MHz, $CDCl_3$): δ 7.62 (app. d, *J* = 7.3 Hz, 1H), 7.51 (app. d, *J* = 7.6 Hz, 1H), 7.42 (app. t, *J* = 7.5 Hz, 1H), 7.37-7.31 (m, 3H), 7.01-6.98 (m, 3H), 5.11 (s, 2H), 0.36 (s, 9H). **$^{13}C\{^1H\}$ NMR (125 MHz, $CDCl_3$):** δ 158.7, 142.0, 138.8, 134.8, 129.5, 129.4, 128.7, 127.4, 120.9, 114.7, 70.2, 0.3. **ν_{max}(neat)/cm^{-1}:** 3058, 2953, 2896, 1598, 1586, 1495, 1235, 1171, 1127, 1078, 1031, 1012, 833, 747, 724. **HRMS** calcd. for $C_{16}H_{20}OSi$: 256.1283 $[M]^+$; found (EI^+): 256.1281.

Trimethyl{2-[(2-phenylethoxy)methyl]phenyl}silane (7)

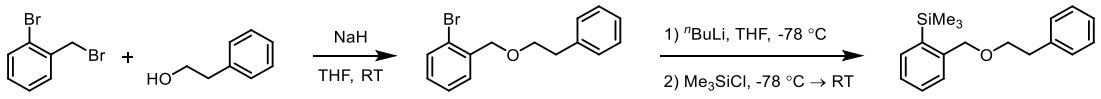

2-Bromobenzyl 2-phenylethyl ether: 2-Phenylethanol (0.60 mL, 5.50 mmol) was added slowly to NaH (99%; 0.14 g, 6.00 mmol) and 2-bromobenzyl bromide (1.25 g, 5.00 mmol) in THF (10 mL) at room temperature. The reaction was stirred overnight at room temperature, then quenched with HCl (10% aqueous, 0.5 mL) and diluted with Et_2O (20 mL). The mixture was dried by addition of $MgSO_4$, filtered and concentrated *in vacuo*. Purification *via* flash column chromatography (10% Et_2O in hexanes) afforded 2-bromobenzyl 2-phenylethyl ether as a viscous, colourless liquid (1.39 g, 4.77 mmol, 95%).

^1H NMR (400 MHz, $CDCl_3$): δ 7.54 (dd, *J* = 8.0, 1.3 Hz, 1H), 7.42 (ddt, *J* = 7.7, 1.8, 0.9 Hz, 1H), 7.34-7.21 (m, 6H), 7.14 (dddt, *J* = 8.0, 7.4, 1.8, 0.6 Hz, 1H), 4.61 (s, 2H), 3.80 (t, *J* = 7.1

Hz, 2H), 2.99 (t, *J* = 7.1 Hz, 2H). **^{13}C{^{1}H} NMR (100 MHz, CDCl$_3$):** δ 138.9, 137.8, 132.4, 128.9, 128.8, 128.7, 128.3, 127.4, 126.2, 122.5, 72.1, 71.2, 36.3.

Trimethyl{2-[(2-phenylethoxy)methyl]phenyl}silane: Following **General Procedure 3**, *n*BuLi (1.6 M in hexanes, 3.60 mL, 5.75 mmol) was added to 2-bromobenzyl 2-phenylethyl ether (1.36 g, 4.79 mmol) in THF (5 mL) at –78 °C. The reaction was stirred at this temperature for 1 h, then Me_3SiCl (0.91 mL, 7.19 mmol) was added dropwise, and the mixture was stirred at room temperature overnight. Purification by filtration through a pad of silica gel (eluent: hexanes) afforded the title compound as a colourless liquid (0.93 g, 3.28 mmol, 66%).

^{1}H NMR (400 MHz, CDCl$_3$): δ. 7.54 (dd, *J* = 7.3, 1.1 Hz, 1H), 7.44 – 7.36 (m, 1H), 7.35 (app. td, *J* = 7.4, 1.5 Hz, 1H), 7.33 – 7.20 (m, 6H), 4.61 (s, 2H), 3.73 (t, *J* = 7.3 Hz, 2H), 2.97 (t, *J* = 7.3 Hz, 2H), 0.33 (s, 9H). **^{13}C{^{1}H} NMR (100 MHz, CDCl$_3$):** δ. 143.8, 139.1, 138.4, 134.7, 129.3, 129.1, 128.5, 128.3, 127.0, 126.4, 73.3, 71.7, 36.6, 0.42. **ν_{max}(neat)/cm^{-1}:** 3058, 3028, 2951, 1496, 1453, 1358, 1247, 1203, 1127, 1094, 833, 744, 726. **HRMS** calcd. for $C_{18}H_{24}OSi$: 284.1591 $[M]^+$; found (EI^+): 284.1601.

Trimethyl[2-(3-phenylpropoxy)methyl]phenylsilane (9)

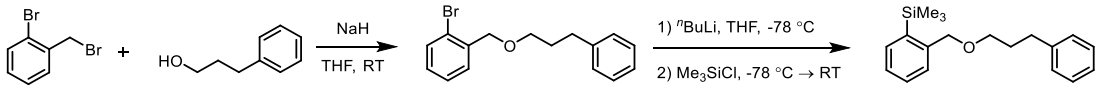

1-Bromo-2-[(3-phenylpropoxy)methyl]benzene: 3-Phenyl-1-propanol (0.68 mL, 5.00 mmol) was added slowly to NaH (60%; 0.24 g, 6.00 mmol) in THF (10 mL) at 0 °C and was stirred for 30 min. 2-Bromobenzyl bromide (1.25 g, 5.00 mmol) was added portionwise and the reaction was allowed to warm to room temperature and stirred for 4 h. The reaction was quenched with H_2O (10 mL) and diluted with Et_2O (20 mL). The aqueous phase was separated and extracted with Et_2O (3 × 20 mL), and the combined organic portions were dried ($MgSO_4$), filtered and concentrated *in vacuo*. Purification *via* flash column chromatography (2% EtOAc in hexanes) afforded 1-bromo-2-[(3-phenylpropoxy)methyl]benzene as a viscous, colourless liquid (1.25 g, 4.10 mmol, 82%).

^{1}H NMR (400 MHz, CDCl$_3$): δ 7.55 (dd, *J* = 8.0, 1.2 Hz, 1H), 7.51 – 7.48 (m, 1H), 7.36 – 7.26 (m, 3H), 7.23 – 7.12 (m, 4H), 4.57 (s, 2H), 3.58 (t, *J* = 6.3 Hz, 2H), 2.79 – 2.72 (m, 2H), 2.06 – 1.82 (m, 2H). **^{13}C{^{1}H} NMR (100 MHz, CDCl$_3$):** δ 142.1, 138.1, 132.6, 129.1, 128.9, 128.6, 128.5, 127.5, 125.9, 122.8, 72.3, 70.2, 32.6, 31.5. **ν_{max}(neat)/cm^{-1}:** 3061, 2857, 2791, 1439, 1360, 1124, 1102, 1025, 745, 697. **HRMS** calcd. for $C_{16}H_{17}OBr$: 304.0457 $[M]^+$; found (EI^+): 304.0454.

Trimethyl[2-(3-phenylpropoxy)methyl]phenylsilane**:** Following **General Procedure 3**, *n*BuLi (2.38 M in hexanes, 1.20 mL, 2.84 mmol) was added to 1-bromo-2-[(3-phenylpropoxy)methyl]benzene (0.79 g, 2.59 mmol) in THF (7 mL) at –78 °C. The reaction was stirred at this temperature for 1 h, then Me_3SiCl (0.49 mL, 3.82 mmol) was added dropwise, and the mixture was stirred at room temperature overnight. Purification *via* flash column chromatography (2% EtOAc in hexanes) afforded the title compound as a colourless liquid (0.63 g, 2.11 mmol, 82%).

^{1}H NMR (400 MHz, $CDCl_3$): δ 7.54 (dd, *J* = 7.4, 1.2 Hz, 1H), 7.50 – 7.43 (m, 1H), 7.38 (app. td, *J* = 7.5, 1.5 Hz, 1H), 7.33 – 7.26 (m, 3H), 7.23 – 7.16 (m, 3H), 4.58 (s, 2H), 3.54 (t, *J* = 6.4 Hz, 2H), 2.79 – 2.68 (m, 2H), 2.04 – 1.87 (m, 2H), 0.35 (s, 9H). **^{13}C{^{1}H} NMR (100 MHz, $CDCl_3$):** δ 144.0, 142.2, 138.4, 134.7, 129.3, 128.6, 128.5, 128.4, 127.0, 125.9, 73.3, 70.0, 32.7, 31.6, 0.47. **ν_{max}(neat)/cm^{-1}:** 3058, 2949, 2858, 1436, 1247, 1099, 833, 742, 697. **HRMS** calcd. for $C_{19}H_{26}OSi$: 298.1748 $[M]^+$; found (EI^+): 298.1759.

(2-Benzyl-4-methoxyphenyl)trimethylsilane (*iso*-1j)

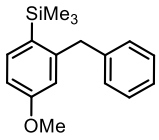

(2-Bromo-5-methoxyphenyl)(phenyl)methanol: Following **General Procedure 1**, *n*BuLi (2.38 M in hexanes, 2.41 mL, 5.73 mmol) was added dropwise to a stirred solution of bromobenzene (0.60 mL, 5.73 mmol) in THF (15 mL) at –78 °C. The reaction was stirred at this temperature for 1 h, then 2-bromo-5-methoxybenzaldehyde (1.36 g, 6.30 mmol) was added portionwise, and the mixture was allowed to warm to room temperature and was stirred for 2 h. Purification *via* flash column chromatography (15% EtOAc in hexanes) afforded (2-bromo-5-methoxyphenyl)(phenyl)methanol as a viscous, pale yellow liquid (1.30 g, 4.43 mmol, 77%).

Characterisation data were consistent with literature values: ^{1}H and ^{13}C{^{1}H} NMR:[13]

^{1}H NMR (400 MHz, $CDCl_3$): δ 7.46 – 7.38 (m, 3H), 7.37 – 7.27 (m, 3H), 7.17 (d, *J* = 3.1 Hz, 1H), 6.72 (dd, *J* = 8.8, 3.1 Hz, 1H), 6.14 (s, 1H), 3.79 (s, 3H), 2.31 (br.s, 1H). **^{13}C{^{1}H} NMR (100 MHz, $CDCl_3$):** δ 159.4, 143.6, 142.1, 133.6, 128.6, 128.0, 127.2, 115.2, 114.1, 113.1, 74.9, 55.6. **ν_{max}(neat)/cm^{-1}:** 3382 (br), 3062, 3029, 3001, 2961, 2936, 2905, 2835, 1592, 1572, 1466, 1416, 1290, 1271, 1233, 1157, 1130, 1117, 1079, 1044, 1024, 827, 805, 729.

2-Benzyl-1-bromo-4-methoxybenzene: Following **General Procedure 2A**, (2-bromo-5-methoxyphenyl)(phenyl)methanol (1.26 g, 4.29 mmol) in CH_2Cl_2 (13 mL) was reacted with TFA (1.31 mL, 17.2 mmol) and Et_3SiH (1.37 mL, 8.59 mmol). Purification *via* flash column chromatography (5% EtOAc in hexanes) afforded 2-benzyl-1-bromo-4-methoxybenzene as a colourless liquid (0.87 g, 3.12 mmol, 72%).

Characterisation data were consistent with literature values: ^{1}H and $^{13}C\{^{1}H\}$ NMR:[14]

^{1}H NMR (400 MHz, $CDCl_3$): δ 7.46 (d, *J* = 8.6 Hz, 1H), 7.35 – 7.28 (m, 2H), 7.25 – 7.18 (m, 3H), 6.73 – 6.64 (m, 2H), 4.08 (s, 2H), 3.73 (s, 3H). **$^{13}C\{^{1}H\}$ NMR (100 MHz, $CDCl_3$):** δ 159.1, 141.5, 139.5, 133.5, 129.1, 128.6, 126.4, 117.1, 115.5, 113.5, 55.5, 42.0. **ν_{max}(neat)/cm^{-1}:** 3084, 3061, 3027, 3001, 2958, 2935, 2906, 2834, 1594, 1570, 1473, 1453, 1430, 1291, 1276, 1237, 1157, 1054, 1015, 859, 801, 721.

(2-Benzyl-4-methoxyphenyl)trimethylsilane: Following **General Procedure 3**, *n*BuLi (2.38 M in hexanes, 1.24 mL, 2.94 mmol) was added to 2-benzyl-1-bromo-4-methoxybenzene (0.68 g, 2.45 mmol) in THF (7 mL) at –78 °C. The reaction was stirred at this temperature for 1 h, then Me_3SiCl (0.47 mL, 3.67 mmol) was added dropwise, and the mixture was stirred at room temperature overnight. Purification *via* flash column chromatography (5% EtOAc in hexanes) afforded the title compound as a colourless liquid (0.53 g, 1.94 mmol, 79%).

^{1}H NMR (400 MHz, $CDCl_3$): δ 7.48 (d, *J* = 8.3 Hz, 1H), 7.35 – 7.27 (m, 2H), 7.24 – 7.18 (m, 1H), 7.15 – 7.10 (m, 2H), 6.79 (dd, *J* = 8.3, 2.5 Hz, 1H), 6.59 (d, *J* = 2.5 Hz, 1H), 4.16 (s, 2H), 3.73 (s, 3H), 0.31 (s, 9H). **$^{13}C\{^{1}H\}$ NMR (100 MHz, $CDCl_3$):** δ 160.8, 148.3, 141.2, 136.1, 130.1, 129.3, 128.5, 126.2, 116.2, 110.8, 55.0, 41.9, 0.62. **ν_{max}(neat)/cm^{-1}:** 3062, 3026, 2953, 2898, 2835, 1592, 1561, 1453, 1292, 1248, 1225, 1159, 1121, 1077, 1033, 833, 754, 723. **HRMS** calcd. for $C_{17}H_{22}OSi$: 270.1435 $[M]^+$; found (EI^+): 270.1434

(2-Benzyl-4-fluorophenyl)trimethylsilane (*iso*-1k)

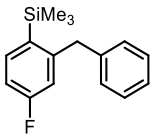

(2-Bromo-5-fluorophenyl)(phenyl)methanol**:** Following **General Procedure 1**, *n*BuLi (2.38 M in hexanes, 2.41 mL, 5.73 mmol) was added dropwise to a stirred solution of bromobenzene (0.60 mL, 5.73 mmol) in THF (15 mL) at –78 °C. The reaction was stirred at this temperature for 1 h, then 2-bromo-5-fluorobenzaldehyde (1.28 g, 6.30 mmol) was added portionwise, and the mixture was allowed to warm to room temperature and was stirred for 2 h. Purification *via*

flash column chromatography (10% EtOAc in hexanes) afforded (2-bromo-5-fluorophenyl)(phenyl)methanol as a viscous, pale yellow liquid (1.06 g, 4.00 mmol, 70%).

^{1}H NMR (400 MHz, $CDCl_3$): δ 7.48 (dd, *J* = 8.7, 5.2 Hz, 1H), 7.44 – 7.27 (m, 6H), 6.89 (ddd, *J* = 8.7, 7.7, 3.1 Hz, 1H), 6.12 (d, *J* = 3.5 Hz, 1H), 2.37 (d, *J* = 3.5 Hz, 1H). **^{13}C{^{1}H} NMR (100 MHz, $CDCl_3$):** δ 162.5 (d, *J* = 247 Hz), 144.9 (d, *J* = 6.8 Hz), 141.6, 134.2 (d, *J* = 7.9 Hz), 128.8, 128.3, 127.3, 116.6 (d, *J* = 3.2 Hz), 116.4 (d, *J* = 22.9 Hz), 115.8 (d, *J* = 23.9 Hz), 74.8. **^{19}F NMR (377 MHz, $CDCl_3$):** δ –113.6 (m). **ν_{max}(neat)/cm^{-1}:** 3310, 3065, 3031, 1464, 1408, 1143, 1105, 1014, 960, 881, 829, 809, 733. **HRMS** calcd. for $C_{13}H_{10}OBrF$: 279.9894 $[M]^+$; found (EI^+): 279.9894.

2-Benzyl-1-bromo-4-fluorobenzene: A Schlenk flask containing (2-bromo-5-fluorophenyl)(phenyl)methanol (1.01 g, 3.81 mmol) was evacuated and back-filled with N_2 three times, then Et_3SiH (1.22 mL, 15.2 mmol) was added and the mixture was stirred and cooled to 0 °C. Cold TFA (5 mL, 65 mmol) was added dropwise and the reaction was allowed to warm to room temperature and was stirred overnight. The volatiles were then evaporated under a stream of N_2 to give the crude product which was purified *via* flash column chromatography (hexanes) to afford 2-benzyl-1-bromo-4-fluorobenzene as a colourless liquid (0.87 g, 3.49 mmol, 90%).

^{1}H NMR (400 MHz, $CDCl_3$): δ 7.52 (dd, *J* = 9.6, 5.3 Hz, 1H), 7.37 – 7.28 (m, 2H), 7.28 – 7.15 (m, 3H), 6.87 – 6.76 (m, 2H), 4.09 (s, 2H). **^{13}C{^{1}H} NMR (100 MHz, $CDCl_3$):** δ 162.2 (d, *J* = 247 Hz), 142.8 (d, *J* = 7.2 Hz), 138.8, 134.0 (d, *J* = 8.0 Hz), 129.2, 128.8, 126.7, 118.9 (d, *J* = 3.1 Hz), 118.0 (d, *J* = 23 Hz), 115.2 (d, *J* = 23 Hz), 42.0 (d, *J* = 1.4 Hz).**^{19}F NMR (377 MHz, $CDCl_3$):** δ –114.8 (m). **ν_{max}(neat)/cm^{-1}:** 3063, 3028, 2980, 2915, 1601, 1578, 1494, 1465, 1431, 1405, 1269, 1233, 1148, 1102, 1074, 1028, 957, 872, 807, 721. **HRMS** calcd. for $C_{13}H_{10}BrF$: 263.9944 $[M]^+$; found (EI^+): 263.9936.

(2-Benzyl-4-fluorophenyl)trimethylsilane: Following **General Procedure 3**, *n*BuLi (2.38 M in hexanes, 1.50 mL, 3.57 mmol) was added to 2-benzyl-1-bromo-4-fluorobenzene (0.75 g, 3.00 mmol) in THF (9 mL) at –78 °C. The reaction was stirred at this temperature for 1 h, then Me_3SiCl (0.57 mL, 4.50 mmol) was added dropwise, and the mixture was stirred at room temperature overnight. Purification *via* flash column chromatography (hexanes) afforded the title compound as a colourless liquid (0.63 g, 2.45 mmol, 82%).

^{1}H NMR (400 MHz, $CDCl_3$): δ 7.51 (dd, *J* = 8.3, 6.8 Hz, 1H), 7.35 – 7.30 (m, 2H), 7.28 – 7.21 (m, 1H), 7.12 (m, 2H), 6.91 (app. td, *J* = 8.4, 2.5 Hz, 1H), 6.71 (dd, *J* = 10.7, 2.5 Hz, 1H), 4.16 (s, 2H), 0.34 (s, 9H)**. ^{13}C{^{1}H} NMR (100 MHz, $CDCl_3$):** δ 164.1 (d, *J* = 250 Hz), 149.4

(d, *J* = 6.5 Hz), 140.7, 136.4 (d, *J* = 7.6 Hz), 134.4 (d, *J* = 3.6 Hz), 129.3, 128.7, 126.4, 116.8 (d, *J* = 20 Hz), 112.6 (d, *J* = 19 Hz), 41.6 (d, *J* = 1.9 Hz), 0.49. **^{19}F NMR (377 MHz, $CDCl_3$):** δ –112.5 (ddd, *J* = 10.7, 8.7, 6.8 Hz). **ν_{max}(neat)/cm^{-1}:** 3063, 3028, 2954, 2898, 2854, 1594, 1576, 1495, 1476, 1453, 1397, 1274, 1249, 1212, 964, 834, 814, 755, 723. **HRMS** calcd. for $C_{16}H_{19}FSi$: 258.1235 $[M]^+$; found (EI^+): 258.1237.

(2-Benzyl-4-chlorophenyl)trimethylsilane (*iso*-1l)

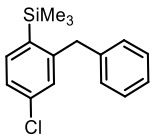

(2-Bromo-5-chlorophenyl)(phenyl)methanol: Following **General Procedure 1**, *n*BuLi (2.38 M in hexanes, 1.45 mL, 3.45 mmol) was added dropwise to a stirred solution of bromobenzene (0.36 mL, 3.45 mmol) in THF (9 mL) at –78 °C. The reaction was stirred at this temperature for 1 h, then 2-bromo-5-chlorobenzaldehyde (0.83 g, 3.80 mmol) was added portionwise, and the mixture was allowed to warm to room temperature and was stirred overnight. Purification *via* flash column chromatography (10% EtOAc in hexanes) afforded (2-bromo-5-chlorophenyl)(phenyl)methanol as a viscous, yellow liquid (0.69 g, 2.31 mmol, 67%).

Characterisation data were consistent with literature values: ^{1}H NMR and IR:[15]

^{1}H NMR (400 MHz, $CDCl_3$): δ 7.66 (d, *J* = 2.6 Hz, 1H), 7.45 (d, *J* = 8.5 Hz, 1H), 7.42 – 7.27 (m, 5H), 7.14 (dd, *J* = 8.5, 2.6 Hz, 1H), 6.12 (s, 1H), 2.32 (s, 1H). **^{13}C{^{1}H} NMR (100 MHz, $CDCl_3$):** δ 144.3, 141.6, 134.1, 134.0, 129.3, 128.8, 128.6, 128.3, 127.3, 120.5, 74.8. **ν_{max}(neat)/cm^{-1}:** 3335, 3086, 3063, 1452, 1391, 1374, 1038, 1014, 891, 809.

2-Benzyl-1-bromo-4-chlorobenzene: Following **General Procedure 2B**, (2-bromo-5-chlorophenyl)(phenyl)methanol (0.69 g, 2.31 mmol) in CH_2Cl_2 (1.4 mL) was reacted with TFA (1.40 mL, 18.5 mmol) and Et_3SiH (0.74 mL, 4.62 mmol). Purification *via* flash column chromatography (hexanes) afforded 2-benzyl-1-bromo-4-chlorobenzene as a colourless liquid (0.50 g, 1.78 mmol, 77%). **^{1}H NMR (400 MHz, $CDCl_3$)**: δ 7.49 (d, *J* = 8.4 Hz, 1H), 7.37 – 7.29 (m, 2H), 7.28 – 7.22 (m, 1H), 7.23 – 7.16 (m, 2H), 7.13 – 7.06 (m, 2H), 4.08 (s, 2H). **^{13}C{^{1}H} NMR (100 MHz, $CDCl_3$):** δ 142.2, 138.6, 133.9, 133.4, 130.9, 129.0, 128.7, 128.0, 126.6, 122.7, 41.7. **ν_{max}(neat)/cm^{-1}:** 3085, 3061, 3027, 2914, 1494, 1460, 1451, 1427, 1390, 1182, 1096, 1073, 1025, 876, 808, 755, 714, 703. **HRMS** calcd. for $C_{13}H_{10}BrCl$: 279.9649 $[M]^+$; found (EI^+): 279.9655.

(2-Benzyl-4-chlorophenyl)trimethylsilane: Following **General Procedure 3**, *n*BuLi (2.38 M in hexanes, 0.80 mL, 1.92 mmol) was added to 2-benzyl-1-bromo-4-chlorobenzene (0.45 g, 1.60 mmol) in THF (5 mL) at –78 °C. The reaction was stirred at this temperature for 1 h, then Me_3SiCl (0.30 mL, 2.40 mmol) was added dropwise, and the mixture was stirred at room temperature overnight. Purification *via* flash column chromatography (hexanes) afforded the title compound as a colourless liquid (0.31 g, 1.13 mmol, 71%).

^{1}H NMR (400 MHz, $CDCl_3$): δ 7.45 (d, *J* = 8.0 Hz, 1H), 7.35 – 7.28 (m, 2H), 7.26 – 7.20 (m, 1H), 7.19 (dd, *J* = 8.0, 2.0 Hz, 1H), 7.13 – 7.05 (m, 2H), 6.98 (d, *J* = 2.0 Hz, 1H), 4.13 (s, 2H), 0.32 (s, 9H). **^{13}C{^{1}H} NMR (100 MHz, $CDCl_3$):** δ 148.4, 140.6, 137.3, 136.0, 135.7, 129.9, 129.3, 128.7, 126.4, 125.8, 41.5, 0.39. **ν_{max}(neat)/cm^{-1}:** 3085, 3061, 3027, 2914, 1460, 1096, 1025, 808, 714, 703, 693. **HRMS** calcd. for $C_{16}H_{19}ClSi$: 274.0939 $[M]^+$; found (EI^+): 274.0946.

[2-Benzyl-4-(trifluoromethyl)phenyl]trimethylsilane (*iso*-1m)

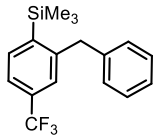

Following **General Procedure 1**, *n*BuLi (2.38 M in hexanes, 2.10 mL, 5.00 mmol) was added dropwise to a stirred solution of bromobenzene (0.53 mL, 5.00 mmol) in THF (13 mL) at –78 °C. The reaction was stirred at this temperature for 1 h, then 2-bromo-5-(trifluoromethyl)benzaldehyde (1.39 g, 5.50 mmol) was added, and the mixture was allowed to warm to room temperature and was stirred overnight. Flash column chromatography (5% EtOAc in hexanes) afforded [2-bromo-5-(trifluoromethyl)phenyl](phenyl)methanol (0.33 g) contaminated with *ca.* 30% of a number of unidentified impurities. TFA (1.3 mL, 17.0 mmol) was added directly to the impure [2-bromo-5-(trifluoromethyl)phenyl](phenyl)methanol (0.33 g) at 0 °C. After 2 min, Et_3SiH (0.32 mL, 2.02 mmol) was added dropwise, and the reaction stirred at room temperature for 1 h. The volatiles were then evaporated under a stream of N_2 to give the crude product. Flash column chromatography (hexanes) afforded 2-benzyl-1-bromo-4-(trifluoromethyl)benzene (0.15 g) contaminated with *ca.* 20% of a number of unidentified impurities. Following **General Procedure 3**, *n*BuLi (2.38 M in hexanes, 0.21 mL, 0.49 mmol) was added to the impure 2-benzyl-1-bromo-4-(trifluoromethyl)benzene (0.15 g) in THF (1.2 mL) at –78 °C. The reaction was stirred at this temperature for 1 h, then Me_3SiCl (79 μL, 0.62 mmol) was added dropwise, and the mixture was stirred at room temperature

overnight. Purification *via* flash column chromatography (hexanes) afforded the title compound as a colourless liquid (98 mg, 0.32 mmol, 6%).

^{1}H NMR (400 MHz, $CDCl_3$): δ 7.66 (app. d, *J* = 7.8 Hz, 1H), 7.45 (app. d, *J* = 7.8 Hz, 1H), 7.33 – 7.28 (m, 2H), 7.27 – 7.20 (m, 2H), 7.11 – 7.03 (m, 2H), 4.21 (s, 2H), 0.34 (s, 9H). **^{13}C{^{1}H} NMR (100 MHz, $CDCl_3$):** δ 147.0, 143.0, 140.4, 135.0, 131.3 (q, *J* = 32.0 Hz), 129.0, 128.6, 126.4, 126.2 (q, *J* = 3.7 Hz), 124.2 (q, *J* = 270 Hz), 122.0 (q, *J* = 3.7 Hz), 41.5, 0.13. **^{19}F NMR (377 MHz, $CDCl_3$):** δ -62.9 (s). **ν_{max}(neat)/cm^{-1}:** 3065, 3029, 2980, 2900, 1329, 1264, 1252, 1162, 1121, 1095, 1075, 1056, 829, 755, 725. **HRMS** calcd. for $C_{17}H_{19}F_3Si$: 308.1203 $[M]^+$; found (EI^+): 308.1196

3-Benzyl-4-(trimethylsilyl)phenol

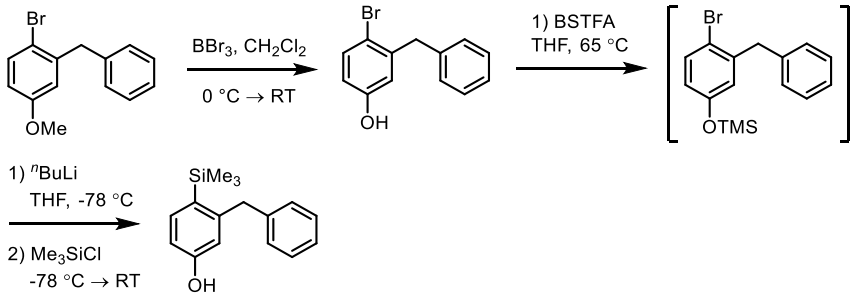

3-Benzyl-4-bromophenol: Boron tribromide (1.0 M in CH_2Cl_2; 3.90 mL, 3.90 mmol) was added dropwise to a stirred solution of 2-benzyl-1-bromo-4-methoxybenzene (0.99 g, 3.55 mmol; prepared as for *iso*-**1j**), in CH_2Cl_2 (8 mL) at 0 °C. The reaction was allowed to warm to room temperature and was stirred overnight. H_2O (10 mL) was added, dropwise at first, and the biphasic mixture was stirred vigorously for 15 min. The aqueous phase was separated and extracted with CH_2Cl_2 (3 × 10 mL), and the combined organic portions were dried ($MgSO_4$), filtered and concentrated *in vacuo*. Purification *via* flash column chromatography (20% EtOAc in hexanes) afforded 3-benzyl-4-bromophenol as a viscous brown oil (0.80 g, 3.02 mmol, 85%).

^{1}H NMR (400 MHz, $CDCl_3$): δ 7.41 (d, *J* = 8.1 Hz, 1H), 7.36 – 7.29 (m, 2H), 7.27 – 7.18 (m, 3H), 6.64 – 6.54 (m, 2H), 4.82 (s, 1H), 4.05 (s, 2H). **^{13}C{^{1}H} NMR (100 MHz, $CDCl_3$):** δ 154.9, 141.9, 139.3, 133.7, 129.2, 128.7, 126.5, 118.0, 115.5, 115.3, 41.8. **ν_{max}(neat)/cm^{-1}:** 3331 (br), 3063, 3028, 2913, 1572, 1466, 1449, 1426, 1344, 1279, 1265, 1241, 1189, 1157, 1121, 1072, 1025, 956, 930, 891, 876, 843, 811, 763, 725, 705. **HRMS** calcd. for $C_{13}H_{11}BrO$: 261.9988 $[M]^+$; found (EI^+): 261.9991.

3-Benzyl-4-(trimethylsilyl)phenol: To a Schlenk flask containing a solution of 3-benzyl-4-bromophenol (0.44 g, 1.67 mmol) in THF (3.3 mL) was added *N,O*-bis(trimethylsilyl)trifluoroacetamide (BSTFA). The flask was sealed and heated to 65 °C for 1 h. The reaction was cooled to 0 °C and the solvent was removed *in vacuo* directly from the Schlenk flask. Removal of an aliquot showed quantitative formation of the trimethylsilyl ether (as determined by ^{1}H NMR spectroscopy). The silyl ether was re-dissolved in THF (4 mL) and cooled to –78 °C. *n*BuLi (2.17 M in hexanes, 0.85 mL, 1.84 mmol) was added dropwise to the solution and it was stirred at –78 °C for 1 h, then Me_3SiCl (0.32 mL, 2.51 mmol) was added dropwise, and the mixture was stirred for 6 h at room temperature. HCl (10% aqueous, 10 mL) was added and the biphasic mixture was stirred vigorously for 1 h. The aqueous phase was separated and extracted with Et_2O (3 × 15 mL), and the combined organic portions were dried ($MgSO_4$), filtered and concentrated *in vacuo*. ^{1}H NMR spectroscopy of the crude material showed a significant amount of the des-silyl product, presumably the result of protodesilylation during the acidic work up. Purification *via* flash column chromatography (10% EtOAc in hexanes) afforded the title compound as pale yellow liquid (52 mg, 0.20 mmol, 12%).

^{1}H NMR (400 MHz, $CDCl_3$): δ 7.41 (d, *J* = 8.1 Hz, 1H), 7.33 – 7.27 (m, 2H), 7.24 – 7.18 (m, 1H), 7.16 – 7.06 (m, 2H), 6.69 (dd, *J* = 8.1, 2.5 Hz, 1H), 6.44 (d, *J* = 2.5 Hz, 1H), 4.64 (s, 1H), 4.11 (s, 2H), 0.30 (s, 9H).**^{13}C{^{1}H} NMR (100 MHz, $CDCl_3$):** δ 156.7, 148.8, 141.1, 136.4, 130.2, 129.4, 128.6, 126.3, 116.9, 112.7, 41.7, 0.61. **ν_{max}(neat)/cm^{-1}:** 3320, 2952, 1595, 1572, 1494, 1452, 1248, 1059, 968, 833, 725. **HRMS** calcd. for $C_{16}H_{20}OSi$: 256.1278 $[M]^+$; found (EI^+): 256.1282

3-Benzyl-4-(trimethylsilyl)phenyl trifluoromethanesulfonate (*iso*-1n)

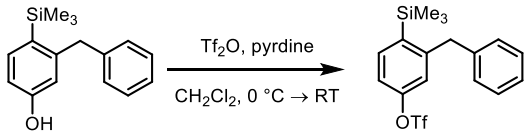

Triflic anhydride (0.37 mL, 2.20 mmol) was added dropwise to a stirred solution of 3-benzyl-4-(trimethylsilyl)phenol (0.28 g, 1.10 mmol) and pyridine (1.16 mL, 14.4 mmol) in CH_2Cl_2 (10 mL) at 0 °C. The reaction was stirred overnight at room temperature, then H_2O (10 mL) was added, then the aqueous phase was separated and extracted with CH_2Cl_2 (3 × 10 mL), and the combined organic portions were dried ($MgSO_4$), filtered and concentrated *in vacuo*. Purification *via* flash column chromatography (5% EtOAc in hexanes) afforded the title compound as a colourless liquid (0.39 g, 1.02 mmol, 93%).

^{1}H NMR (400 MHz, $CDCl_3$): δ 7.60 (d, *J* = 8.3 Hz, 1H), 7.36 – 7.30 (m, 2H), 7.28 – 7.22 (m, 1H), 7.12 (dd, *J* = 8.3, 2.5 Hz, 1H), 7.11 – 7.03 (m, 2H), 6.86 (d, *J* = 2.5 Hz, 1H), 4.19 (s, 2H), 0.34 (s, 9H). **^{13}C{^{1}H} NMR (100 MHz, $CDCl_3$):** δ 150.9, 149.6, 140.1, 140.0, 136.5, 129.2, 128.8, 126.7, 122.3, 118.8 (q, *J* = 320 Hz), 118.2, 41.5, 0.26. **^{19}F NMR (377 MHz, $CDCl_3$):** δ -73.0 (s). **ν_{max}(neat)/cm^{-1}:** 3029, 2957, 1588, 1571, 1422, 1246, 1205, 1137, 1064, 954, 833, 758, 724. **HRMS** calcd. for $C_{17}H_{19}F_3O_3SSi$: 388.0771 $[M]^+$; found (EI^+): 338.0760.

[4-Chloro-2-(3-chlorobenzyl)phenyl](trimethyl)silane (1ae)

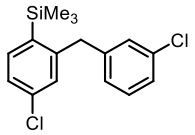

(2-Bromo-5-chlorophenyl)(3-chlorophenyl)methanol: Following **General Procedure 1**, *n*BuLi (2.38 M in hexanes, 2.59 mL, 6.17 mmol) was added dropwise to a stirred solution of 1-bromo-3-chlorobenzene (0.72 mL, 6.17 mmol) in THF (15 mL) at –78 °C. The reaction was stirred at this temperature for 1 h, then 2-bromo-5-chlorobenzaldehyde (1.30 g, 6.79 mmol) was added portionwise, and the mixture was allowed to warm to room temperature and was stirred overnight. Purification *via* flash column chromatography (10% EtOAc in hexanes) afforded (2-bromo-5-chlorophenyl)(3-chlorophenyl)methanol as a viscous, colourless liquid (1.45 g, 4.37 mmol, 71%).

^{1}H NMR (400 MHz, $CDCl_3$): δ 7.58 (d, *J* = 2.6 Hz, 1H), 7.47 (d, *J* = 8.5 Hz, 1H), 7.43 – 7.36 (m, 1H), 7.31 – 7.24 (m, 3H), 7.16 (dd, *J* = 8.5, 2.6 Hz, 1H), 6.10 (s, 1H), 2.43 (br.s, 1H). **^{13}C{^{1}H} NMR (100 MHz, $CDCl_3$):** δ 143.8, 143.6, 134.7, 134.3, 134.1, 130.0, 129.7, 128.7, 128.4, 127.3, 125.4, 120.4, 74.1. **ν_{max}(neat)/cm^{-1}:** 3064 (br), 2980, 1595, 1575, 1456, 1431, 1391, 1375, 1254, 1180, 1095, 1080, 1040, 1019, 899, 880, 810, 787, 735, 708, 700. **HRMS** calcd. for $C_{13}H_9OBrCl_2$: 329.9208 $[M]^+$; found (EI^+): 329.9208.

1-Bromo-4-chloro-2-(3-chlorobenzyl)benzene: Following **General Procedure 2B**, (2-bromo-5-chlorophenyl)(3-chlorophenyl)methanol (1.38 g, 4.16 mmol) in CH_2Cl_2 (2.5 mL) was reacted with TFA (2.6 mL, 33.5 mmol) and Et_3SiH (1.33 mL, 8.32 mmol). Purification *via* flash column chromatography (hexanes) afforded 1-bromo-4-chloro-2-(3-chlorobenzyl)benzene as a colourless liquid (0.75 g, 2.38 mmol, 57%).

^{1}H NMR (400 MHz, $CDCl_3$): δ 7.52 – 7.48 (m, 1H), 7.28 – 7.20 (m, 2H), 7.20 – 7.14 (m, 1H), 7.13 – 7.03 (m, 3H), 4.05 (s, 2H). **^{13}C{^{1}H} NMR (100 MHz, $CDCl_3$):** δ 141.3, 140.6, 134.5, 134.0, 133.6, 130.9, 129.9, 129.0, 128.4, 127.1, 126.9, 122.6, 41.3. **ν_{max}(neat)/cm^{-1}:**

3061, 2980, 2912, 1597, 1574, 1475, 1461, 1428, 1390, 1078, 1025, 930, 888, 809, 777, 734. **HRMS** calcd. for $C_{13}H_9BrCl_2$: 313.9259 $[M]^+$; found (EI^+): 313.9265.

[4-Chloro-2-(3-chlorobenzyl)phenyl](trimethyl)silane: Following **General Procedure 3**, *n*BuLi (2.38 M in hexanes, 0.92 mL, 2.18 mmol) was added to 1-bromo-4-chloro-2-(3-chlorobenzyl)benzene (0.58 g, 1.82 mmol) in THF (5.5 mL) at –78 °C. The reaction was stirred at this temperature for 1 h, then Me_3SiCl (0.35 mL, 2.73 mmol) was added dropwise, and the mixture was stirred at room temperature overnight. Purification *via* flash column chromatography (hexanes) afforded the title compound as a colourless liquid (0.46 g, 1.49 mmol, 82%).

^{1}H NMR (400 MHz, $CDCl_3$): δ 7.46 (d, *J* = 8.0 Hz, 1H), 7.30 – 7.17 (m, 3H), 7.11 – 7.04 (m, 1H), 6.99 – 6.90 (m, 2H), 4.10 (s, 2H), 0.31 (s, 9H). **^{13}C{^{1}H} NMR (100 MHz, $CDCl_3$):** δ 147.3, 142.7, 137.2, 136.2, 135.8, 134.6, 129.9, 129.3, 127.4, 126.7, 126.1, 41.1, 0.38. *1 × C_{Ar} not observed.* **ν_{max}(neat)/cm^{-1}:** 3062, 2954, 2898, 1596, 1574, 1548, 1474, 1428, 1250, 1184, 1109, 1078, 1059, 890, 834, 758, 731. **HRMS** calcd. for $C_{16}H_{18}Cl_2Si$: 308.0549 $[M]^+$; found (EI^+): 308.0536.

2-*d*$_1$-Bromobenzene

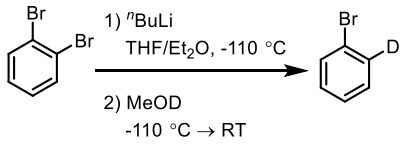

*n*BuLi (2.38 M in hexanes, 3.91 mL, 9.33 mmol) was added dropwise to a stirred solution of 1,2-dibromobenzene (1.00 mL, 8.48 mmol) in THF/Et_2O (24 mL, 1:1) over 15 min, maintaining the reaction temperature below –110 °C. The reaction was stirred at this temperature for 30 min, then methanol-*d*$_1$ (1.03 mL, 25.4 mmol) was added dropwise slowly, and the mixture was left in the cooling bath and allowed to warm to room temperature overnight. The reaction was quenched with H_2O (15 mL), then the aqueous phase was separated and extracted with Et_2O (3 × 20 mL), and the combined organic portions were dried ($MgSO_4$), filtered and concentrated *in vacuo*. Purification by distillation afforded the title compound as a colourless liquid (0.46 g, 2.93 mmol, 35%).

Characterisation data were consistent with literature values: ^{1}H and ^{13}C{^{1}H} NMR:[16]

^{1}H NMR (400 MHz, $CDCl_3$): δ 7.55 – 7.49 (m, 1H), 7.35 – 7.22 (m, 3H). **^{13}C{^{1}H} NMR (100 MHz, $CDCl_3$):** δ 131.7, 131.4 (t, *J* = 25.4 Hz), 130.2, 130.0, 127.0, 122.5.

Trimethyl{2-[(2-d_1)phenylmethyl]phenyl}silane (d_1-1b)

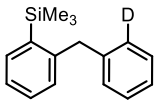

(2-Bromophenyl)[(2-d_1)phenyl]methanol: Following **General Procedure 1**, ^{n}BuLi (2.38 M in hexanes, 1.14 mL, 2.72 mmol) was added dropwise to a stirred solution of 2-d_1-bromobenzene (0.43 g, 2.72 mmol) in THF (6 mL) at –78 °C. The reaction was stirred at this temperature for 30 min, then 2-bromobenzaldehyde (0.32 mL, 2.72 mmol) was added dropwise, and the mixture was allowed to warm to room temperature and was stirred for 2 h. Purification *via* flash column chromatography (10% EtOAc in hexanes) afforded (2-bromophenyl)[(2-d_1)phenyl]methanol as a viscous, yellow liquid (0.50 g, 1.88 mmol, 69%).

Characterisation data were consistent with literature values: ^{1}H, ^{13}C{^{1}H} NMR and IR.[17]

^{1}H NMR (400 MHz, $CDCl_3$): δ 7.59 (dd, *J* = 7.8, 1.7 Hz, 1H), 7.55 (dd, *J* = 8.0, 1.3 Hz, 1H), 7.43 – 7.38 (m, 1H), 7.37 – 7.31 (m, 3H), 7.32 – 7.25 (m, 1H), 7.15 (app. td, *J* = 7.7, 1.7 Hz, 1H), 6.20 (s, 1H), 2.38 (br.s, 1H). **^{13}C{^{1}H} NMR (100 MHz, $CDCl_3$):** δ 142.7, 142.2, 133.0, 129.3, 128.63, 128.61, 128.5, 127.90, 127.86, 127.2, 126.9 (t, *J* = 24 Hz), 122.9, 74.9. **ν_{max}(neat)/cm^{-1}:** 3327 (br), 3061, 3019, 1567, 1468, 1438, 1333, 1302, 1228, 1183, 1159, 1119, 1011, 949, 869, 846, 820, 775, 747.

1-Bromo-2-[(2-d_1)phenylmethyl]benzene: Following **General Procedure 2A**, (2-bromophenyl)[(2-d_1)phenyl]methanol (0.46 g, 1.86 mmol) in CH_2Cl_2 (6 mL) was reacted with TFA (0.57 mL, 7.45 mmol) and Et_3SiH (0.59 mL, 3.72 mmol). Purification *via* flash column chromatography (hexanes) afforded 1-bromo-2-[(2-d_1)phenylmethyl]benzene as a colourless liquid (0.37 g, 1.47 mmol, 79%).

^{1}H NMR (500 MHz, $CDCl_3$): δ 7.58 (dd, *J* = 8.0, 1.3 Hz, 1H), 7.35 – 7.28 (m, 2H), 7.26 – 7.17 (m, 3H), 7.14 (dd, *J* = 7.7, 1.8 Hz, 1H), 7.09 (app. td, *J* = 7.6, 1.8 Hz, 1H), 4.13 (s, 2H). **^{13}C{^{1}H} NMR (125 MHz, $CDCl_3$):** δ 140.5, 139.6, 133.0, 131.2, 129.1, 128.8 (t, *J* = 24.0 Hz), 128.6, 128.5, 128.0, 127.6, 126.4, 125.1, 41.8. **ν_{max}(neat)/cm^{-1}:** 3062, 3015, 2980, 2912, 1593, 1566, 1474, 1438, 1258, 1158, 1114, 1045, 1024, 950, 917, 868, 806, 774, 744, 714. **HRMS** calcd. for $C_{13}H_{10}DBr$: 247.0101 $[M]^+$; found (EI^+): 247.0108.

Trimethyl{2-[(2-d_1)phenylmethyl]phenyl}silane: Following **General Procedure 3**, ^{n}BuLi (2.38 M in hexanes, 0.73 mL, 1.74 mmol) was added to 1-bromo-2-[(2-d_1)phenylmethyl]benzene (0.36 g, 1.45 mmol) in THF (4 mL) at –78 °C. The reaction was stirred at this temperature for 1 h, then Me_3SiCl (0.28 mL, 2.18 mmol) was added dropwise,

and the mixture was stirred at room temperature overnight. Purification *via* flash column chromatography (hexanes) afforded the title compound as a colourless liquid (0.23 g, 0.94 mmol, 65%). The deuterium content was observed to be >98% by ^{1}H NMR spectroscopy.

^{1}H NMR (400 MHz, $CDCl_3$): δ 7.56 (dd, *J* = 7.3, 1.4 Hz, 1H), 7.34 – 7.26 (m, 3H), 7.25 – 7.17 (m, 2H), 7.14 – 7.07 (m, 1.02H), 7.02 (app. dd, *J* = 7.6 0.6 Hz, 1H), 4.18 (s, 2H), 0.33 (s, 9H). **^{13}C{^{1}H} NMR (100 MHz, $CDCl_3$):** δ 146.4, 141.5, 139.0, 134.7, 130.0, 129.5, 129.3, 129.0 (t, *J* = 24.4 Hz), 128.5, 128.4, 126.1, 125.6, 41.8, 0.49. **ν_{max}(neat)/cm^{-1}:** 3057, 2952, 1474, 1435, 1248, 1122, 833, 773, 743. **HRMS** calcd. for $C_{16}H_{19}DSi$: 241.0139 $[M]^+$; found (EI^+): 241.0139.

Trimethyl{2-[(*d_5*)phenylmethyl]phenyl}silane (*d_5*-1b)

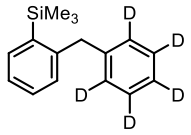

(2-Bromophenyl)[(*d_5*)phenyl]methanol: Following **General Procedure 1**, *n*BuLi (2.38 M in hexanes, 2.60 mL, 6.17 mmol) was added dropwise to a stirred solution of *d_5*-bromobenzene (0.65 mL, 6.17 mmol) in THF (13 mL) at –78 °C. The reaction was stirred at this temperature for 1 h, then 2-bromobenzaldehyde (0.72 mL, 6.17 mmol) was added dropwise, and the mixture was allowed to warm to room temperature and was stirred for 2 h. Purification *via* flash column chromatography (15% EtOAc in hexanes) afforded (2-bromophenyl)[(*d_5*)phenyl]methanol as a viscous, yellow liquid (0.77 g, 2.87 mmol, 47%).

^{1}H NMR (400 MHz, $CDCl_3$): δ 7.59 (dd, *J* = 7.8, 1.8 Hz, 1H), 7.54 (dd, *J* = 8.0, 1.3 Hz, 1H), 7.35 (m, 1H), 7.15 (app. td, *J* = 7.7, 1.7 Hz, 1H), 6.21 (s, 1H), 2.31 (br.s, 1H).**^{13}C{^{1}H} NMR (100 MHz, $CDCl_3$):** δ 142.7, 142.1, 133.0, 129.3, 128.6, 128.1 (t, *J* = 24 Hz), 127.9, 127.4 (t, *J* = 24 Hz), 126.7 (t, *J* = 24 Hz), 122.9, 74.87. **ν_{max}(neat)/cm^{-1}:** 3334, 3061, 2274, 1628, 1467, 1437, 1131, 1051, 1010, 853, 746, 700. **HRMS** calcd. for $C_{13}H_6D_5OBr$: 267.0302 $[M]^+$; found (EI^+): 267.0295.

1-Bromo-2-[(2-*d_5*)phenylmethyl]benzene: Following **General Procedure 2A**, (2-bromophenyl)[(*d_5*)phenyl]methanol (0.77 g, 2.87 mmol) in CH_2Cl_2 (9 mL) was reacted with TFA (0.88 mL, 11.49 mmol) and Et_3SiH (0.92 mL, 5.74 mmol). Purification *via* flash column chromatography (pentane) afforded 1-bromo-2-[(2-*d_5*)phenylmethyl]benzene as a colourless liquid (0.62 g, 2.47 mmol, 86%).

^{1}H NMR (400 MHz, $CDCl_3$): δ 7.59 (dd, *J* = 8.0, 1.3 Hz, 1H), 7.24 (app. td, *J* = 7.5, 1.3 Hz, 1H), 7.15 (dd, *J* = 7.7, 1.8 Hz, 1H), 7.10 (app. td, *J* = 7.8, 1.8 Hz, 1H), 4.14 (s, 2H). **^{13}C{^{1}H} NMR (100 MHz, $CDCl_3$):** δ 140.5, 139.4, 133.0, 131.2, 128.7 (t, *J* = 24 Hz), 128.1 (t, *J* = 24 Hz), 128.0, 127.6, 125.9 (t, *J* = 25 Hz), 125.0, 41.8. **ν_{max}(neat)/cm^{-1}:** 3057, 2911, 2273, 1567, 1473, 1438, 1377, 1348, 1315, 1275, 1258, 1115, 1038, 1022, 944, 908, 848, 821, 774, 744. **HRMS** calcd. for $C_{13}H_6D_5Br$: 251.0353 $[M]^+$; found (EI^+): 251.0353.

Trimethyl{2-[(*d_5*)phenylmethyl]phenyl}silane: Following **General Procedure 3**, *n*BuLi (2.38 M in hexanes, 1.04 mL, 2.47 mmol) was added to 1-bromo-2-[(2-*d_5*)phenylmethyl]benzene (0.52 g, 2.06 mmol) in THF (6 mL) at –78 °C. The reaction was stirred at this temperature for 1 h, then Me_3SiCl (0.39 mL, 3.09 mmol) was added dropwise, and the mixture was stirred at room temperature overnight. Purification *via* flash column chromatography (hexanes) afforded the title compound as a colourless liquid (0.47 g, 1.93 mmol, 93%). The deuterium content was observed to be > 98% by ^{1}H-NMR.

^{1}H NMR (400 MHz, $CDCl_3$): δ 7.58 (dd, *J* = 7.3, 1.5 Hz, 1H), 7.31 (app. td, *J* = 7.5, 1.7 Hz, 1H), 7.23 (app. td, *J* = 7.3, 1.3 Hz, 1H), 7.04 (app. d, *J* = 7.5 Hz, 1H), 4.20 (s, 2H), 0.35 (s, 9H). **^{13}C{^{1}H} NMR (100 MHz, $CDCl_3$):** δ 146.3, 141.3, 138.9, 134.6, 129.9, 129.4, 128.8 (t, *J* = 24 Hz), 127.9 (t, *J* = 24 Hz), 125.5 (t, *J* = 24 Hz), 125.5, 41.6, 0.39. **ν_{max}(neat)/cm^{-1}:** 3054, 2953, 2274, 1435, 1248, 1071, 833, 735. **HRMS** calcd. for $C_{16}H_{15}D_5NaSi$: 268.1540 $[M+Na]^+$; found (ESI^+): 268.1526.

Trimethyl{2-[(2-*d_1*)phenyloxy]phenyl}silane (*d_1*-1v)[10]

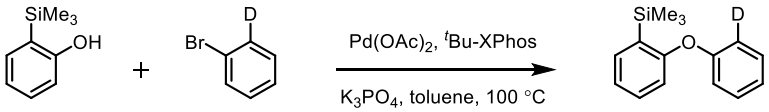

A Schlenk flask containing $Pd(OAc)_2$ (4.50 mg, 0.02 mmol), ^{t}Bu-XPhos (12.7 mg, 0.03 mmol) and potassium phosphate (0.42 g, 2.00 mmol) was evacuated and back-filled with N_2 three times, then 2-(trimethylsilyl)phenol[11] (0.20 g, 1.20 mmol) and 2-*d_1*-bromobenzene (105 μL, 1.00 mmol; prepared as above) in toluene (2 mL) was added, and the flask was sealed and heated at 100 °C overnight. The reaction mixture was filtered through a pad of Celite (eluent: hexanes) and concentrated *in vacuo*. Purification *via* flash column chromatography (hexanes) afforded the title compound as a colourless liquid (0.21 g, 0.85 mmol, 85%).

^{1}H NMR (400 MHz, $CDCl_3$): δ 7.51 (ddd, *J* = 7.4, 1.8, 0.5 Hz, 1H), 7.37 – 7.27 (m, 3H), 7.10 (app. qd, *J* = 7.4, 1.1 Hz, 2H), 6.99 (dd, *J* = 8.6, 1.1 Hz, 1H), 6.81 (dd, *J* = 8.2, 0.7 Hz, 1H), 0.29 (s, 9H). **^{13}C{^{1}H} NMR (100 MHz, $CDCl_3$):** δ 162.1, 157.6, 135.5, 130.8, 130.8, 129.8,

129.7, 123.1, 123.0, 118.9, 118.6 (t, *J* = 25 Hz), 117.6, -0.76. **ν_{max}(neat)/cm^{-1}:** 3065, 2954, 1590, 1566, 1464, 1433, 1246, 1124, 1076, 834, 752, 720. **HRMS** calcd. for $C_{15}H_{17}DONaSi$: 266.1082 $[M+Na]^+$; found (ESI^+): 266.1083.

Trimethyl(2-{[(2-^{2}H)phenyloxy]methyl}phenyl)silane (*d_1*-3d)

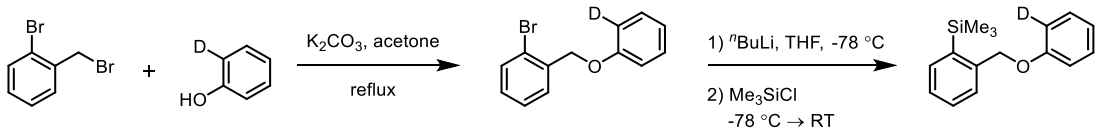

2-Bromobenzyl-(2-*d_1*)phenylether: A suspension of K_2CO_3 (0.52 g, 3.76 mmol), 2-bromobenzyl bromide (0.62 g, 2.50 mmol) and 2-*d_1*-phenol[18] (0.24 g, 2.50 mmol) in acetone (4.5 mL) was heated at reflux for 8 h. The reaction mixture was cooled to room temperature, filtered and concentrated *in vacuo*. Purification *via* column chromatography (hexanes) afforded 2-bromobenzyl-(2-*d_1*)phenylether as a colourless liquid (0.52 g, 1.98 mmol, 79%).

^{1}H NMR (400 MHz, $CDCl_3$): δ 7.64 – 7.55 (m, 2H), 7.39 – 7.30 (m, 3H), 7.20 (app. td, *J* = 7.7, 1.8 Hz, 1H), 7.05 – 6.97 (m, 2H), 5.16 (s, 2H). **^{13}C{^{1}H} NMR (100 MHz, $CDCl_3$):** δ 158.5, 136.5, 132.7, 129.7, 129.6, 129.3, 129.0, 127.7, 122.4, 121.3, 115.0, 114.7 (t, *J* = 24 Hz), 69.5. **ν_{max}(neat)/cm^{-1}:** 3064, 2903, 1589, 1474, 1437, 1378, 1308, 1232, 1217, 1118, 1045, 1023, 743. **HRMS** calcd. for $C_{13}H_{10}DOBr$: 263.0051 $[M]^+$; found (EI^+): 263.0051.

Trimethyl(2-{[(2-*d_1*)phenyloxy]methyl}phenyl)silane: Following **General Procedure 3**, *n*BuLi (2.17 M in hexanes, 0.91 mL, 1.98 mmol) was added to 2-bromobenzyl-(2-*d_1*)phenylether (0.48 g, 1.80 mmol) in THF (4.5 mL) at –78 °C. The reaction was stirred at this temperature for 1 h, then Me_3SiCl (0.34 mL, 2.70 mmol) was added dropwise, and the mixture was stirred at room temperature overnight. Purification *via* flash column chromatography (hexanes) afforded the title compound as a colourless liquid (0.36 g, 1.30 mmol, 72%).

^{1}H NMR (400 MHz, $CDCl_3$): δ 7.62 (dd, *J* = 7.3, 1.3 Hz, 1H), 7.55 – 7.48 (m, 1H), 7.42 (app. td, *J* = 7.5, 1.6 Hz, 1H), 7.38 – 7.29 (m, 3H), 7.03 – 6.96 (m, 2H), 5.12 (s, 2H), 0.36 (s, 9H). **^{13}C{^{1}H} NMR (100 MHz, $CDCl_3$):** δ 158.8, 142.1, 138.9, 135.0, 129.7, 129.6, 129.5, 128.9, 127.6, 121.0, 114.9, 114.5 (t, *J* = 24 Hz), 70.4, 0.42. **ν_{max}(neat)/cm^{-1}:** 3059, 2952, 2896, 1589, 1465, 1307, 1248, 1227, 1121, 1048, 1010, 833, 744, 724. **HRMS** calcd. for $C_{16}H_{19}DOSi$: 257.1341 $[M]^+$; found (EI^+): 257.1337.

Trimethyl(2-{2-[(2-*d*$_1$)phenyl]ethyl}phenyl)silane (*d*$_1$-3a)[19]

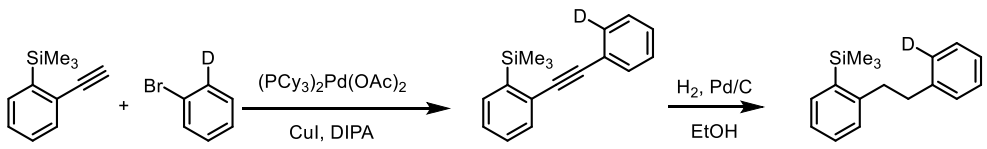

Trimethyl{2-[(2-*d*$_1$)phenylethynyl]phenyl}silane: A Schlenk flask containing $(PCy_3)_2Pd(OAc)_2$ (12.4 mg, 0.02 mmol) and copper(I) iodide (2.89 mg, 0.015 mmol) was evacuated and back-filled N_2 three times, then di*iso*propylamine (5.00 mL) and 2-*d*$_1$-bromobenzene (105 μL, 1.00 mmol; prepared as above) were added. The flask was heated to 80 °C, then (2-(phenylethynyl)phenyl)trimethylsilane (0.18 g, 1.05 mmol) was added and the reaction was stirred at this temperature for 6 h. The reaction mixture was allowed to cool to room temperature and was filtered through a pad of Celite (eluent: hexanes) and concentrated *in vacuo*. Column chromatography (hexanes) afforded trimethyl{2-[(2-*d*$_1$)phenylethynyl]phenyl}silane as a colourless liquid (0.13 g, 0.53 mmol, 53%).

^{1}H NMR (400 MHz, $CDCl_3$): δ 7.64 – 7.47 (m, 3H), 7.43 – 7.28 (m, 5H), 0.44 (s, 9H). **^{13}C{^{1}H} NMR (100 MHz, $CDCl_3$):** δ 142.5, 134.1, 132.6, 131.4, 131.1 (t, *J* = 25.0 Hz), 128.9, 128.6, 128.57, 128.55, 128.4, 127.6, 123.6, 92.1, 91.3, –0.8. **ν_{max}(neat)/cm^{-1}:** 3051, 3006, 2953, 2896, 1474, 1244, 1125, 833, 756, 718**. HRMS** calcd. for $C_{17}H_{17}DSi$: 251.1235 $[M]^+$; found (EI^+): 251.1236.

Trimethyl(2-{2-[(2-*d*$_1$)phenyl]ethyl}phenyl)silane: Trimethyl{2-[(2-*d*$_1$)phenylethynyl]phenyl}silane (121 mg, 0.48 mmol) was dissolved in EtOH (3.5 mL) and N_2 was bubbled through the solution for 10 min. Pd/C (10 wt%; 10 mg) was added and a balloon of H_2 was fitted and H_2 was bubbled through the solution. Another balloon of H_2 was fitted and the reaction was stirred under a static H_2 atmosphere overnight. The suspension was filtered through a pad of Celite (eluent: CH_2Cl_2) and the filtrate was concentrated *in vacuo.* Purification *via* flash column chromatography (hexanes) afforded the title compound as a colourless liquid (62.0 mg, 0.24 mmol, 50%).

^{1}H NMR (400 MHz, $CDCl_3$): δ 7.52 (dd, *J* = 7.4, 1.2 Hz, 1H), 7.40 – 7.20 (m, 7H), 3.09 – 3.01 (m, 2H), 2.98 – 2.91 (m, 2H), 0.37 (s, 9H). **^{13}C{^{1}H} NMR (100 MHz, $CDCl_3$):** δ 147.7, 142.0, 138.2, 134.8, 129.4, 128.9, 128.6, 128.52, 128.48, 128.2 (t, *J* = 24.1 Hz), 126.2, 125.5, 38.9, 38.2, 0.69. **ν_{max}(neat)/cm^{-1}:** 3057, 3014, 2954, 2865, 1589, 1563, 1475, 1437, 1248, 1108, 832, 772, 751, 725. **HRMS** calcd. for $C_{17}H_{21}DSi$: 255.1548 $[M]^+$; found (EI^+): 255.1552.

Trimethyl(2-{phenyl[(*d*$_5$)phenyl]methyl}phenyl)silane (*d*$_5$-1x)

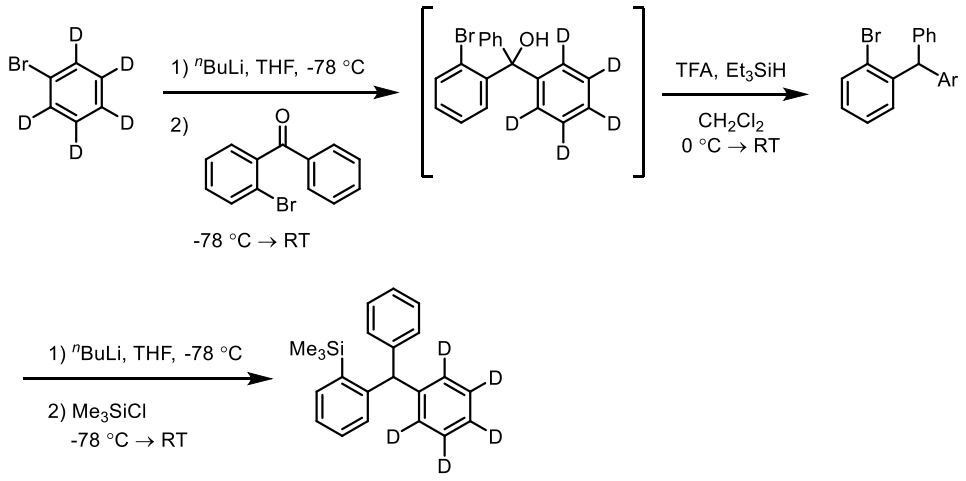

1-Bromo-2-{phenyl[(*d*$_5$)phenyl]methyl}benzene: ^{n}BuLi (2.38 M in hexanes, 0.88 mL, 2.10 mmol) was added dropwise to a stirred solution of *d*$_5$-bromobenzene (201 µL, 1.91 mmol) in THF (5 mL) at –78 °C. The reaction was stirred at this temperature for 1 h, then 2-bromobenzophenone (0.35 mL, 1.91 mmol) was added dropwise, and the mixture was stirred at room temperature overnight. The reaction was quenched with H_2O (5 mL), then the aqueous phase was separated and extracted with Et_2O (3 × 10 mL), and the combined organic portions were dried ($MgSO_4$), filtered and concentrated *in vacuo*. The crude reaction mixture was transferred to a Schlenk flask which was evacuated and back-filled with N_2 three times, then CH_2Cl_2 (5.5 mL) was added. The solution was cooled to 0 °C, then TFA (0.59 mL, 7.71 mmol) was added dropwise. After 5 min, Et_3SiH (0.61 mL, 3.86 mmol) was added dropwise, and the reaction mixture was allowed to warm to room temperature and was stirred for 3 h. The volatiles were then evaporated under a stream of N_2 and then dried under vacuum to give the product as an off-white solid. Recrystallization (methanol) afforded 1-bromo-2-{phenyl[(*d*$_5$)phenyl]methyl}benzene as a white solid (0.34 g, 1.05 mmol, 55%).

^{1}H NMR (400 MHz, CDCl$_3$): δ 7.59 (dd, *J* = 8.0, 1.4 Hz, 1H), 7.33 – 7.18 (m, 4H), 7.14 – 7.06 (m, 3H), 6.96 (dd, *J* = 7.7, 1.8 Hz, 1H), 5.97 (s, 1H). **^{13}C{^{1}H} NMR (100 MHz, CDCl$_3$):** δ 143.4, 142.8, 142.6, 133.2, 131.5, 129.8, 129.3 (t, *J* = 24 Hz), 128.5, 128.2, 128.0 (t, *J* = 24 Hz), 127.3, 126.6, 126.1 (t, *J* = 24 Hz), 125.7, 56.0. **ν_{max}(neat)/cm^{-1}:** 3084, 3057, 3025, 2886, 2275, 1600, 1584, 1563, 1493, 1463, 1450, 1436, 1372, 1345, 1325, 1301, 1274, 1238, 1181, 1159, 1113, 1077, 1047, 1024, 1011, 960, 949, 919, 878, 858, 845, 825, 806, 752, 735, 719. **HRMS** calcd. for $C_{19}H_{10}D_5Br$: 327.0666 $[M]^+$; found (EI^+): 327.0661. **m.p. /°C:** 80-81.

Trimethyl(2-{phenyl[(*d*$_5$)phenyl]methyl}phenyl)silane: Following **General Procedure 3**, ^{n}BuLi (2.38 M in hexanes, 0.35 mL, 0.84 mmol) was added to 1-bromo-2-{phenyl[(*d*$_5$)phenyl]methyl}benzene (0.25 g, 0.76 mmol) in THF (2.5 mL) at –78 °C. The reaction was stirred at this temperature for 5 min, then Me_3SiCl (0.14 mL, 1.14 mmol) was added dropwise, and the mixture was stirred at room temperature overnight. Purification *via* flash column chromatography (hexanes) afforded the title compound as a viscous, colourless liquid that solidified on standing (0.12 g, 0.36 mmol, 48%).

^{1}H NMR (400 MHz, $CDCl_3$): δ 7.59 (dd, *J* = 7.4, 1.3 Hz, 1H), 7.34 – 7.16 (m, 5H), 7.09 – 6.93 (m, 3H), 5.91 (s, 1H), 0.26 (s, 9H). **^{13}C{^{1}H} NMR (100 MHz, $CDCl_3$):** δ 148.9, 144.8, 144.6, 139.3, 135.1, 130.7, 129.8, 129.3 (t, *J* = 24 Hz), 129.2, 128.3, 127.8 (t, *J* = 24 Hz), 126.3, 125.8, 55.7, 0.78. *1 × C_{Ar} not observed.* **ν_{max}(neat)/cm^{-1}:** 3062, 3023, 3007, 2952, 2895, 2276, 1598, 1587, 1561, 1493, 1467, 1447, 1430, 1371, 1343, 1309, 1262, 1250, 1244, 1192, 1120, 1067, 1033, 833, 754, 726. **HRMS** calcd. for $C_{22}H_{19}D_5Si$: 321.1956 $[M]^+$; found (EI^+): 321.1948. **m.p. /°C:** 81-83.

[2-(1,2-Diphenylethyl)phenyl]trimethylsilane (102)

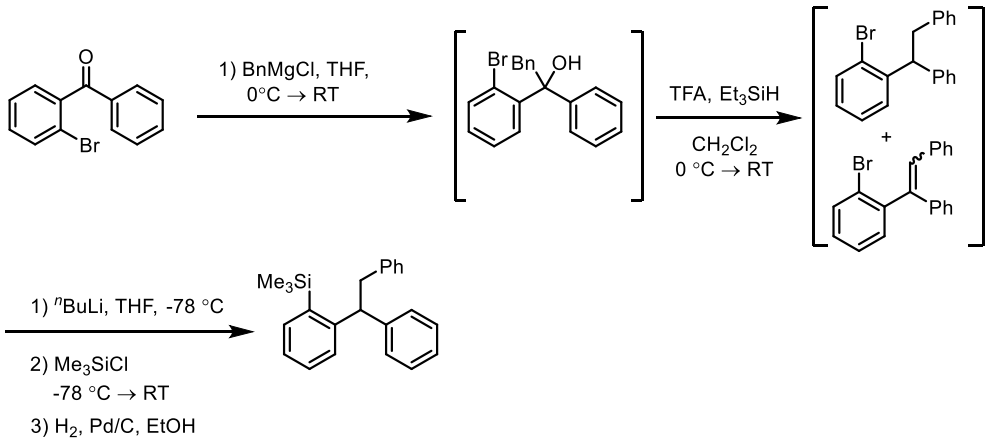

Benzylmagnesium chloride (1.40 M in THF; 4.10 mL, 5.74 mmol) was added dropwise to a stirred solution of 2-bromobenzophenone (0.70 mL, 3.83 mmol) in THF (21 mL) at 0° C. The mixture was allowed to warm to room temperature and was stirred for 3h. The reaction was quenched with H_2O (20 mL), then the aqueous phase was separated and extracted with Et_2O (3 × 30 mL), and the combined organic portions were dried ($MgSO_4$), filtered and concentrated *in vacuo*. The crude reaction mixture was transferred to a Schlenk flask which was evacuated and back-filled with N_2 three times, then CH_2Cl_2 (10 mL) was added. The solution was cooled to 0 °C, then TFA (1.20 mL, 15.3 mmol) was added dropwise. After 5 min, Et_3SiH (1.22 mL, 7.66 mmol) was added dropwise, and the reaction was allowed to warm to room temperature

and was stirred for 3 h. The volatiles were then evaporated under a stream of N_2 and column chromatography (hexanes) afforded 0.42 g of an inseparable, 14:1 mixture of 1-bromo-2-(1,2-diphenylethenyl)benzene and 1-bromo-2-(1,2-diphenylethyl)benzene. ^{n}BuLi (2.38 M in hexanes, 0.48 mL, 1.15 mmol) was added dropwise to a stirred solution of this mixture (0.39 g, 1.15 mmol) in THF (3 mL) at –78 °C. The reaction was stirred at this temperature for 1h, then Me_3SiCl (0.22 mL, 1.73 mmol) was added dropwise, and the mixture was stirred at room temperature overnight. The reaction was quenched with H_2O (5 mL), then the aqueous phase was separated and extracted with Et_2O (3 × 10 mL), and the combined organic portions were dried ($MgSO_4$), filtered and concentrated *in vacuo.* Column chromatography (2% EtOAc in hexanes) afforded 0.31 g of a 14:1 mixture of [2-(1,2-diphenylethenyl)phenyl](trimethyl)silane and the title compound. The mixture was transferred to a round bottom flask and EtOH (5 mL) and THF (2.5 mL) were added and N_2 was bubbled through this solution for 10 min. Pd/C (10 wt%; 16 mg) was added and a balloon of H_2 was fitted and H_2 was bubbled through the solution. Another balloon of H_2 was fitted and the reaction was stirred rapidly under a static H_2 atmosphere for 12 h. The suspension was filtered through a pad of Celite (eluent: CH_2Cl_2) and the filtrate was concentrated *in vacuo.* Purification *via* flash column chromatography (hexanes) afforded the title compound as a viscous, colourless liquid that solidified on standing (0.20 g, 0.60 mmol, 10%).

^{1}H NMR (400 MHz, $CDCl_3$): δ 7.51 (app. dd, J = 7.5, 0.9 Hz, 1H), 7.46 – 7.35 (m, 2H), 7.25 – 7.11 (m, 9H), 7.10 – 7.04 (m, 2H), 4.68 (app. t, *J* = 7.6 Hz, 1H), 3.45 – 3.32 (m, 2H), 0.23 (s, 9H). **^{13}C{^{1}H} NMR (100 MHz, $CDCl_3$):** δ 150.1, 144.3, 140.3, 138.9, 135.1, 129.4, 129.2, 128.6, 128.5, 128.3, 128.2, 126.1, 125.8, 50.6, 43.7, 0.96. **ν_{max}(neat)/cm^{-1}:** 3083, 3023, 2953, 2847, 1562, 1494, 1448, 1252, 1122, 1072, 833, 750, 723. **HRMS** calcd. for $C_{23}H_{26}Si$: 330.1798 $[M]^+$; found (EI^+): 330.1799. **m.p. /°C:** 68-69 (MeOH).

{2-[(3-Chlorophenyl)(phenyl)methyl]phenyl}trimethylsilane (1y)

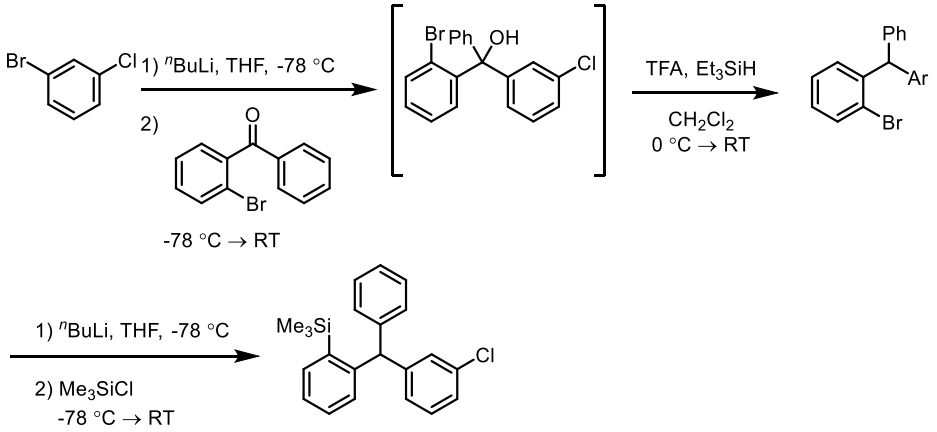

1-Bromo-2-[(3-chlorophenyl)(phenyl)methyl]benzene: ^{n}BuLi (2.38 M in hexanes, 0.88 mL, 2.10 mmol) was added dropwise to a stirred solution of 1-bromo-3-chlorobenzene (224 µL, 1.91 mmol) in THF (5 mL) at –78 °C. The reaction was stirred at this temperature for 1 h, then 2-bromobenzophenone (0.35 mL, 1.91 mmol) was added dropwise, and the mixture was stirred at room temperature overnight. The reaction was quenched with H_2O (5 mL), then the aqueous phase was separated and extracted with Et_2O (3 × 10 mL), and the combined organic portions were dried ($MgSO_4$), filtered and concentrated *in vacuo*. The crude reaction mixture was transferred to a Schlenk flask which was evacuated and back-filled with N_2 three times, then CH_2Cl_2 (5.5 mL) was added. The solution was cooled to 0 °C, then TFA (0.59 mL, 7.71 mmol) was added dropwise. After 5 min, Et_3SiH (0.61 mL, 3.86 mmol) was added dropwise, and the reaction mixture was allowed to warm to room temperature and was stirred for 3 h. The volatiles were then evaporated under a stream of N_2 and purification *via* flash column chromatography (hexanes) afforded 1-bromo-2-[(3-chlorophenyl)(phenyl)-methyl]benzene as a colourless liquid (0.35 g, 0.98 mmol, 51%).

^{1}H NMR (400 MHz, $CDCl_3$): δ 7.59 (dd, *J* = 8.0, 1.3 Hz, 1H), 7.36 – 7.29 (m, 2H), 7.28 – 7.20 (m, 4H), 7.12 (app. td, *J* = 7.7, 1.7 Hz, 1H), 7.08 – 7.03 (m, 3H), 6.99 – 6.95 (m, 1H), 6.93 (dd, *J* = 7.8, 1.7 Hz, 1H), 5.93 (s, 1H). **^{13}C{^{1}H} NMR (100 MHz, $CDCl_3$):** δ 144.9, 142.6, 142.0, 134.5, 133.4, 131.4, 129.79, 129.72, 129.69, 128.7, 128.5, 128.0, 127.5, 126.93, 126.91, 125.6, 55.8. **ν_{max}(neat)/cm^{-1}:** 3060, 1592, 1570, 1494, 1438, 1424, 1025, 780, 747, 699. **HRMS** calcd. for $C_{19}H_{14}BrCl$: 355.9962 $[M]^+$; found (EI^+): 355.9946.

{2-[(3-Chlorophenyl)(phenyl)methyl]phenyl}trimethylsilane: Following **General Procedure 3**, ^{n}BuLi (2.38 M in hexanes, 0.40 mL, 0.96 mmol) was added to 1-bromo-2-[(3-

chlorophenyl)(phenyl)methyl]benzene (0.31 g, 0.88 mmol) in THF (2.6 mL) at –78 °C. The reaction was stirred at this temperature for 5 min, then Me_3SiCl (0.17 mL, 1.31 mmol) was added dropwise, and the mixture was stirred at room temperature overnight. Purification *via* flash column chromatography (hexanes) afforded the title compound as a viscous, colourless liquid that solidified on standing (0.22 g, 0.63 mmol, 72%).

^{1}H NMR (400 MHz, $CDCl_3$): δ 7.59 (dd, *J* = 7.4, 1.4 Hz, 1H), 7.35 – 7.15 (m, 7H), 7.07 – 6.98 (m, 3H), 6.98 (dd, *J* = 7.7, 1.1 Hz, 1H), 6.95 – 6.91 (m, 1H), 5.86 (s, 1H), 0.25 (s, 9H). **^{13}C{^{1}H} NMR (100 MHz, $CDCl_3$):** δ 148.0, 147.0, 144.0, 139.4, 135.3, 134.3, 130.6, 129.8, 129.7, 129.5, 129.4, 128.5, 128.1, 126.60, 126.57, 126.1, 55.5, 0.79. **ν_{max}(neat)/cm^{-1}:** 3057, 3026, 2953, 2896, 1592, 1570, 1493, 1473, 1449, 1425, 1249, 1122, 1095, 1079, 833, 780, 746, 729, 716. **HRMS** calcd. for $C_{22}H_{23}ClSi$: 350.1252 $[M]^+$; found (EI^+): 350.1247. **m.p. /°C:** 62-64.

{2-[(4-*tert*-Butylphenyl)(phenyl)methyl]phenyl}trimethylsilane (1z)

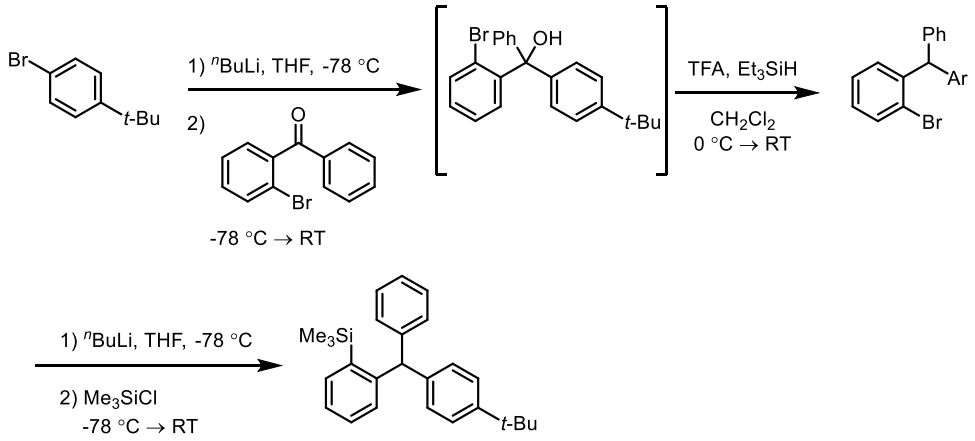

1-Bromo-2-[(4-*tert*-butylphenyl)(phenyl)methyl]benzene: *n*BuLi (2.38 M in hexanes, 0.88 mL, 2.10 mmol) was added dropwise to a stirred solution of 1-bromo-4-*tert*-butylbenzene (0.33 mL, 1.91 mmol) in THF (5 mL) at –78 °C. The reaction was stirred at this temperature for 1 h, then 2-bromobenzophenone (0.35 mL, 1.91 mmol) was added dropwise, and the mixture was allowed to warm to room temperature and was stirred overnight. The reaction was quenched with H_2O (5 mL), then the aqueous phase was separated and extracted with Et_2O (3 × 10 mL), and the combined organic portions were dried ($MgSO_4$), filtered and concentrated *in vacuo*. The crude reaction mixture was transferred to a Schlenk flask which was evacuated and back-filled with N_2 three times, then CH_2Cl_2 (5.5 mL) was added. The solution was cooled to 0 °C, then TFA (0.59 mL, 7.71 mmol) was added dropwise. After 5 min, Et_3SiH (0.61 mL, 3.86 mmol) was added dropwise, and the reaction was allowed to stir at room temperature for

3 h. The volatiles were then evaporated under a stream of N_2 and purification *via* flash column chromatography (twice 5% toluene in hexanes) afforded 1-bromo-2-[(4-*tert*-butylphenyl)(phenyl)methyl]benzene as a colourless liquid (0.11 g, 0.29 mmol, 15%) alongside trace amounts of an unidentified, highly UV active impurity. The identity of the desired product was confirmed by NMR spectroscopy and used without further purification.

^{1}H NMR (400 MHz, $CDCl_3$): δ 7.57 (dd, *J* = 7.9, 1.4 Hz, 1H), 7.34 – 7.17 (m, 6H), 7.12 – 7.06 (m, 3H), 7.03 – 6.96 (m, 3H), 5.93 (s, 1H), 1.31 (s, 9H). **^{13}C{^{1}H} NMR (100 MHz, $CDCl_3$):** δ 149.4, 143.6, 143.0, 139.6, 133.2, 131.5, 129.7, 129.3, 128.4, 128.1, 127.3, 126.5, 125.7, 125.4, 55.6, 34.6, 31.5.

2-[(4-*tert*-Butylphenyl)(phenyl)methyl]phenyl}(trimethyl)silane: Following **General Procedure 3**, ^{n}BuLi (2.38 M in hexanes, 0.12 mL, 0.30 mmol) was added to 1-bromo-2-[(4-*tert*-butylphenyl)(phenyl)methyl]benzene (100 mg, 0.27 mmol) in THF (1 mL) at –78 °C. The reaction was stirred at this temperature for 5 min, then Me_3SiCl (51 μL, 0.40 mmol) was added dropwise, and the mixture was stirred at room temperature overnight. Purification *via* flash column chromatography (hexanes) afforded the title compound as a viscous, colourless liquid (37 mg, 0.10 mmol, 37%).

^{1}H NMR (400 MHz, $CDCl_3$): δ 7.57 (dd, *J* = 7.4, 1.6 Hz, 1H), 7.35 – 7.16 (m, 7H), 7.10 – 7.01 (m, 3H), 6.95 (d, *J* = 8.4 Hz, 2H), 5.85 (s, 1H), 1.3 (s, 9H), 0.24 (s, 9H). **^{13}C{^{1}H} NMR (100 MHz, $CDCl_3$):** δ 149.3, 149.0, 144.8, 141.8, 139.3, 135.0, 130.7, 129.8, 129.3, 129.2, 128.2, 126.2, 125.7, 125.1, 55.4, 34.5, 31.5, 0.79. **ν_{max}(neat)/cm^{-1}:** 3056, 3025, 2959, 2902, 2868, 1513, 1493, 1465, 1449, 1429, 1410, 1363, 1307, 1262, 1249, 1122, 1019, 833, 806, 757, 728, 701. **HRMS** calcd. for $C_{26}H_{32}Si$: 372.2268 $[M]^+$; found (EI^+): 372.2279.

{2-[(4-Fluorophenyl)(phenyl)methyl]phenyl}trimethylsilane (1aa)

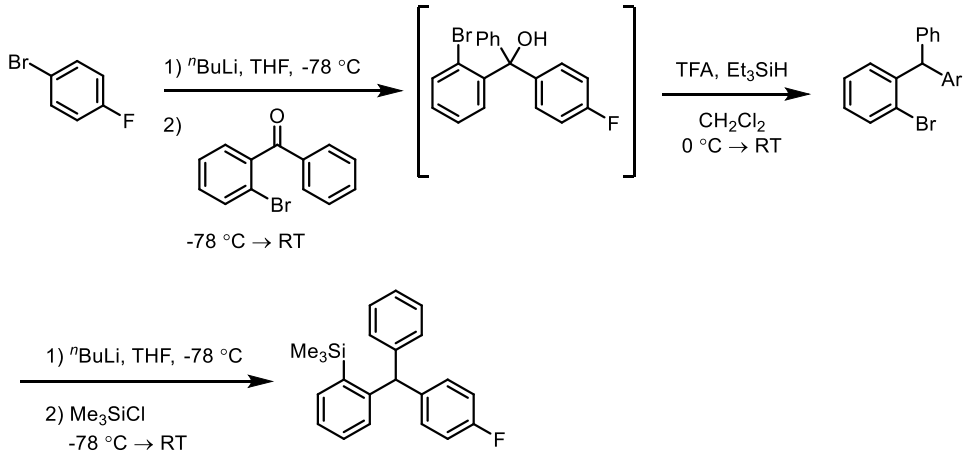

1-Bromo-2-[(4-fluorophenyl)(phenyl)methyl]benzene: *n*BuLi (2.17 M in hexanes, 0.90 mL, 1.96 mmol) was added dropwise to a stirred solution of 1-bromo-4-fluorobenzene (0.23 mL, 2.06 mmol) in THF (5 mL) at –78 °C. The reaction was stirred at this temperature for 1 h, then 2-bromobenzophenone (0.37 mL, 2.00 mmol) was added dropwise, and the mixture was stirred at room temperature overnight. The reaction was quenched with H_2O (10 mL), then the aqueous phase was separated and extracted with Et_2O (3 × 15 mL), and the combined organic portions were dried ($MgSO_4$), filtered and concentrated *in vacuo*. The crude reaction mixture was transferred to a Schlenk flask which was evacuated and back-filled with N_2 three times, then CH_2Cl_2 (5.5 mL) was added. The solution was cooled to 0 °C, then TFA (0.61 mL, 8.00 mmol) was added dropwise. After 5 min, Et_3SiH (0.64 mL, 4.00 mmol) was added dropwise, and the reaction mixture was allowed to warm to room temperature and was stirred for 2 h. The volatiles were then evaporated under a stream of N_2 and purification *via* flash column chromatography (hexanes) afforded 1-bromo-2-[(4-fluorophenyl)(phenyl)methyl]-benzene as a colourless liquid (0.45 g, 1.33 mmol, 67%).

^{1}H NMR (400 MHz, $CDCl_3$): δ 7.59 (dd, *J* = 7.9, 1.3 Hz, 1H), 7.36 – 7.19 (m, 4H), 7.11 (app. td, *J* = 7.7, 1.7 Hz, 1H), 7.08 – 6.95 (m, 6H), 6.92 (dd, *J* = 7.7, 1.8 Hz, 1H), 5.93 (s, 1H). **^{13}C{^{1}H} NMR (100 MHz, $CDCl_3$):** δ 161.6 (d, *J* = 245 Hz), 143.2, 142.6, 138.4 (d, *J* = 3.4 Hz), 133.3, 131.4, 131.2 (d, *J* = 7.9 Hz), 129.7, 128.6, 128.3, 127.4, 126.8, 125.6, 115.3 (d, *J* = 21 Hz), 55.4. **^{19}F NMR (377 MHz, $CDCl_3$):** –116.5 (m). **ν_{max}(neat)/cm^{-1}:** 3056, 3026, 1600, 1505, 1437, 1222, 1157, 1022, 792, 744. **HRMS** calcd. for $C_{19}H_{14}BrF$: 340.0257 $[M]^+$; found (EI^+): 340.0262.

{2-[(4-Fluorophenyl)(phenyl)methyl]phenyl}trimethylsilane: Following **General Procedure 3**, *n*BuLi (2.17 M in hexanes, 0.61 mL, 1.32 mmol) was added to 1-bromo-2-[(4-

fluorophenyl)(phenyl)methyl]benzene (0.41 g, 1.20 mmol) in THF (3 mL) at –78 °C. The reaction was stirred at this temperature for 5 min, then Me_3SiCl (0.23 mL, 1.79 mmol) was added dropwise, and the mixture was stirred at room temperature overnight. Purification *via* flash column chromatography (hexanes) afforded the title compound as a viscous, colourless liquid that solidified on standing (0.32 g, 0.96 mmol, 80%).

^{1}H NMR (400 MHz, $CDCl_3$): δ 7.58 (dd, *J* = 7.4, 1.7 Hz, 1H), 7.38 – 7.17 (m, 5H), 7.07 – 6.90 (m, 7H), 5.86 (s, 1H), 0.24 (s, 9H). **^{13}C{^{1}H} NMR (100 MHz, $CDCl_3$):** δ 161.5 (d, *J* = 245 Hz), 148.7, 144.7, 140.5 (d, *J* = 3.3 Hz), 139.3, 135.2, 131.2 (d, *J* = 7.9 Hz), 130.6, 129.7, 129.3, 128.4, 126.4, 126.0, 115.1 (d, *J* = 21 Hz), 55.0, 0.78. **^{19}F NMR (377 MHz, $CDCl_3$):** –117.0 (m). **ν_{max}(neat)/cm^{-1}:** 3054, 2955, 1599, 1505, 1427, 1248, 1223, 1159, 1120, 1032, 833, 794, 755, 739. **HRMS** calcd. for $C_{22}H_{23}FSi$: 334.1548 $[M]^+$; found (EI^+): 334.1547. **m.p. /°C:** 70.

{2-[(4-Chlorophenyl)(phenyl)methyl]phenyl}trimethylsilane (1ab)

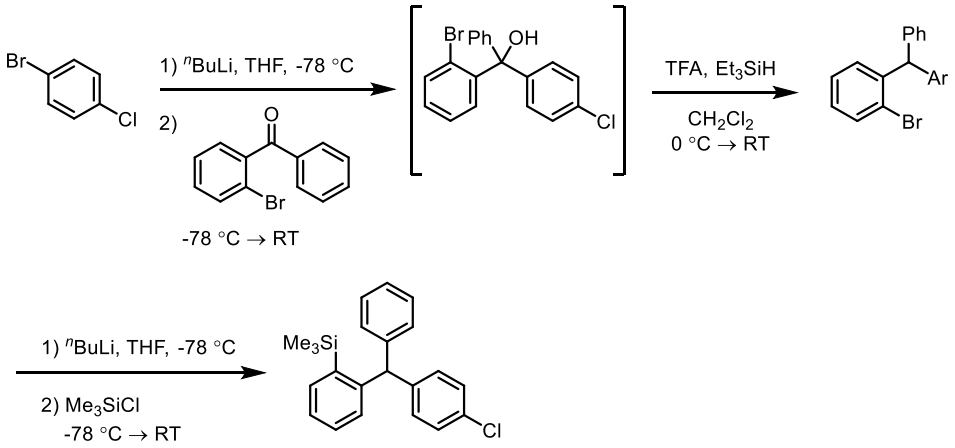

1-Bromo-2-[(4-chlorophenyl)(phenyl)methyl]benzene: *n*BuLi (2.38 M in hexanes, 0.88 mL, 2.10 mmol) was added dropwise to a stirred solution of 1-bromo-4-chlorobenzene (0.37 g, 1.91 mmol) in THF (5 mL) at –78 °C. The reaction was stirred at this temperature for 1 h, then 2-bromobenzophenone (0.35 mL, 1.91 mmol) was added dropwise, and the mixture was stirred at room temperature overnight. The reaction was quenched with H_2O (5 mL), then the aqueous phase was separated and extracted with Et_2O (3 × 10 mL), and the combined organic portions were dried ($MgSO_4$), filtered and concentrated *in vacuo*. The crude reaction mixture was transferred to a Schlenk flask which was evacuated and back-filled with N_2 three times, then CH_2Cl_2 (5.5 mL) was added. The solution was cooled to 0 °C, then TFA (0.59 mL, 7.71 mmol) was added dropwise. After 5 min, Et_3SiH (0.61 mL, 3.86 mmol) was added dropwise, and the reaction mixture was allowed to warm to room temperature and was stirred for 3 h.

The volatiles were then evaporated under a stream of N_2 and purification *via* flash column chromatography (hexanes) afforded 1-bromo-2-[(4-chlorophenyl)(phenyl)methyl]benzene as a colourless liquid (0.46 g, 1.28 mmol, 67%).

^{1}H NMR (400 MHz, $CDCl_3$): δ 7.59 (dd, *J* = 7.9, 1.3 Hz, 1H), 7.36 – 7.19 (m, 6H), 7.11 (app. td, *J* = 7.6, 1.8 Hz, 1H), 7.07 – 6.98 (m, 4H), 6.91 (dd, *J* = 7.8, 1.8 Hz, 1H), 5.92 (s, 1H).**^{13}C{^{1}H} NMR (100 MHz, $CDCl_3$):** δ 142.9, 142.3, 141.3, 133.3, 132.5, 131.4, 131.1, 129.7, 128.66, 128.62, 128.4, 127.5, 126.8, 125.6, 55.5. **ν_{max}(neat)/cm^{-1}:** 3059, 3025, 2980, 2890, 1599, 1566, 1488, 1464, 1450, 1438, 1405, 1089, 1014, 799, 745, 699. **HRMS** calcd. for $C_{19}H_{14}BrCl$: 355.9962 $[M]^+$; found (EI^+): 355.9962.

{2-[(4-Chlorophenyl)(phenyl)methyl]phenyl}(trimethyl)silane: Following **General Procedure 3**, *n*BuLi (2.38 M in hexanes, 0.55 mL, 1.31 mmol) was added to 1-bromo-2-[(4-chlorophenyl)(phenyl)methyl]benzene (0.43 g, 1.19 mmol) in THF (3.5 mL) at –78 °C. The reaction was stirred at this temperature for 5 min, then Me_3SiCl (0.23 mL, 1.79 mmol) was added dropwise, and the mixture was stirred at room temperature overnight. Purification *via* flash column chromatography (hexanes) afforded the title compound as a viscous, colourless liquid that solidified on standing (0.31 g, 0.88 mmol, 74%).

^{1}H NMR (400 MHz, $CDCl_3$): δ 7.58 (dd, *J* = 7.4, 1.3 Hz, 1H), 7.35 – 7.17 (m, 7H), 7.04 – 6.99 (m, 2H), 6.99 – 6.94 (m, 3H), 5.85 (s, 1H), 0.24 (s, 9H). **^{13}C{^{1}H} NMR (100 MHz, $CDCl_3$):** δ 148.4, 144.4, 143.4, 139.4, 135.2, 132.1, 131.1, 130.6, 129.7, 129.3, 128.44, 128.42, 126.5, 126.0, 55.2, 0.79. **ν_{max}(neat)/cm^{-1}:** 3056, 3026, 2955, 2895, 1489, 1470, 1449, 1431, 1404, 1249, 1122, 1090, 1014, 832, 798, 757, 744, 729, 700. **HRMS** calcd. for $C_{22}H_{23}ClSi$: 350.1252 $[M]^+$; found (EI^+): 350.1237. **m.p. /°C:** 57-59 °C.

Trimethyl(2-{phenyl[4-(trifluoromethyl)phenyl]methyl}phenyl)silane (1ac)

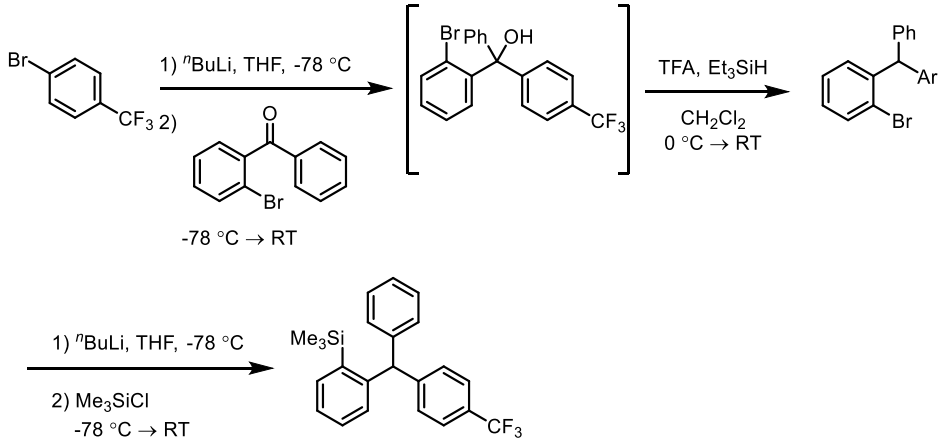

1-Bromo-2-{phenyl[4-(trifluoromethyl)phenyl]methyl}benzene: *n*BuLi (2.38 M in hexanes, 0.88 mL, 2.10 mmol) was added dropwise to a stirred solution of 4-bromobenzotrifluoride (0.27 mL, 1.91 mmol) in THF (5 mL) at –78 °C. The reaction was stirred at this temperature for 1 h, then 2-bromobenzophenone (0.35 mL, 1.91 mmol) was added dropwise, and the mixture was allowed to warm to room temperature and was stirred overnight. The reaction was quenched with H_2O (5 mL), then the aqueous phase was separated and extracted with Et_2O (3 × 10 mL), and the combined organic portions were dried ($MgSO_4$), filtered and concentrated *in vacuo*. The crude reaction mixture was transferred to a Schlenk flask which was evacuated and back-filled with N_2 three times, then CH_2Cl_2 (5.5 mL) was added. The solution was cooled to 0 °C, then TFA (0.59 mL, 7.71 mmol) was added dropwise. After 5 min, Et_3SiH (0.61 mL, 3.86 mmol) was added dropwise, and the reaction was allowed to warm to room temperature and was stirred for 3 h. The volatiles were then evaporated under a stream of N_2 and purification *via* flash column chromatography (hexanes) afforded 1-bromo-2-{phenyl[4-(trifluoromethyl)phenyl]methyl}benzene as a colourless liquid (0.41 g, 1.04 mmol, 54%).

^{1}H NMR (400 MHz, CD_2Cl_2): δ 7.62 (dd, *J* = 7.9, 1.4 Hz, 1H), 7.57 (d, *J* = 8.1 Hz, 2H), 7.36 – 7.20 (m, 6H), 7.15 (app. td, *J* = 7.6, 1.7 Hz, 1H), 7.10 – 7.05 (m, 2H), 6.93 (dd, *J* = 7.7, 1.7 Hz, 1H), 6.02 (s, 1H). **^{13}C{^{1}H} NMR (100 MHz, CD_2Cl_2):** δ 147.5, 142.9, 142.3, 133.8, 131.8, 130.6, 130.1, 129.12, 129.05, 128.0, 127.4, 125.9, 125.8 (q, *J* = 3.7 Hz), 124.9 (q, *J* = 270 Hz), 56.4. *1 × C_{Ar} not observed*. **^{19}F NMR (377 MHz, CD_2Cl_2):** δ -62.7 (s). **ν_{max}(neat)/cm^{-1}:** 3062, 3028, 1618, 1601, 1585, 1494, 1465, 1438, 1415, 1322, 1162, 1120, 1066, 1018, 874, 837, 806, 749, 719, 699. **HRMS** calcd. for $C_{20}H_{14}BrF_3$: 390.0223 $[M]^+$; found (EI^+): 390.0233.

Trimethyl(2-{phenyl[4-(trifluoromethyl)phenyl]methyl}phenyl)silane: Following **General Procedure 3**, *n*BuLi (2.38 M in hexanes, 0.55 mL, 1.31 mmol) was added to 1-bromo-2-

{phenyl[4-(trifluoromethyl)phenyl]methyl}benzene (0.38 g, 0.98 mmol) in THF (3 mL) at – 78 °C. The reaction was stirred at this temperature for 5 min, then Me_3SiCl (0.19 mL, 1.47 mmol) was added dropwise, and the mixture was stirred at room temperature overnight. Purification *via* flash column chromatography (hexanes) afforded the title compound as a viscous, colourless liquid (0.23 g, 0.59 mmol, 60%).

^{1}H NMR (400 MHz, $CDCl_3$): δ 7.60 (dd, *J* = 7.4, 1.5 Hz, 1H), 7.52 (d, *J* = 8.0 Hz, 2H), 7.36 – 7.19 (m, 5H), 7.16 (d, *J* = 8.0 Hz, 2H), 7.05 – 6.99 (m, 2H), 6.97 (dd, *J* = 7.7, 1.1 Hz, 1H), 5.93 (s, 1H), 0.25 (s, 9H). **^{13}C{^{1}H} NMR (100 MHz, $CDCl_3$):** δ 149.0, 147.9, 143.9, 139.5, 135.3, 130.6, 130.1, 129.7, 129.4, 128.6 (q, *J* = 32 Hz), 128.5, 126.7, 126.2, 125.2 (q, *J* = 3.7 Hz), 124.4 (q, *J* = 270 Hz), 55.6, 0.79. **^{19}F NMR (377 MHz, $CDCl_3$):** δ -62.3 (s). **ν_{max}(neat)/cm^{-1}:** 3059, 3027, 2958, 2897, 1618, 1414, 1323, 1251, 1162, 1121, 1111, 1067, 1018, 834, 753, 728, 701. **HRMS** calcd. for $C_{23}H_{23}F_3Si$: 384.1516 $[M]^+$; found (EI^+): 384.1517**.**

Bis-[2-trimethyl(phenyl)silyl]-methane (1af)

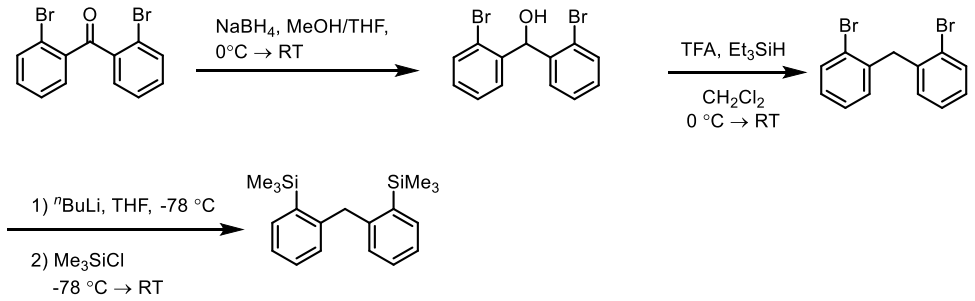

Bis(2-bromophenyl)methanol: Sodium borohydride (58 mg, 1.52 mmol) was added portionwise over 5 min to a solution of 2,2′-dibromobenzophenone (0.52 g, 1.52 mmol) in methanol (12 mL) and THF (3 mL) at 0 °C. The reaction was stirred at room temperature for 2 h, then diluted with a saturated solution of NH_4Cl (20 mL). The aqueous phase was separated and extracted with EtOAc (3 × 20 mL), and the combined organic portions were dried ($MgSO_4$), filtered and concentrated *in vacuo*. Purification *via* flash column chromatography (10% EtOAc in hexanes) afforded bis(2-bromophenyl)methanol as a viscous oil that solidified on standing (0.49 g, 1.42 mmol, 92%).

Characterisation data were consistent with literature values: ^{1}H and ^{13}C{^{1}H} NMR:[20]

^{1}H NMR (400 MHz, $CDCl_3$): 7.58 (dd, *J* = 7.7, 1.0 Hz, 2H), 7.36 – 7.28 (m, 4H), 7.21 – 7.15 (m, 2H), 6.41 (d, *J* = 4.0 Hz, 1H). **^{13}C{^{1}H} NMR (100 MHz, $CDCl_3$):** 141.0, 133.1, 129.5, 128.8, 127.7, 124.0, 74.3.

2,2'-Dibromodiphenylmethane: Following **General Procedure 2B**, bis(2-bromophenyl)methanol (0.71 g, 2.06 mmol) in CH_2Cl_2 (1.3 mL) was reacted with TFA (1.8 mL, 16.5 mmol) and Et_3SiH (0.65 mL, 4.12 mmol). Purification *via* flash column chromatography (hexanes) afforded 2,2'-dibromodiphenylmethane (0.54 g, 1.65 mmol, 80%) as a colourless liquid.

^{1}H NMR (400 MHz, $CDCl_3$): δ 7.61 (dd, *J* = 7.9, 1.3 Hz, 2H), 7.23 (app. td, *J* = 7.5, 1.3 Hz, 2H), 7.12 (app. td, *J* = 7.7, 1.8 Hz, 2H), 6.99 (dd, *J* = 7.6, 1.6 Hz, 2H), 4.21 (s, 2H). **^{13}C{^{1}H} NMR (100 MHz, $CDCl_3$):** δ 139.0, 133.0, 130.8, 128.2, 127.7, 125.2, 42.2. **ν_{max}(neat)/cm^{-1}:** 3056, 1566, 1466, 1438, 1045, 1022, 945, 740. **HRMS** calcd. for $C_{13}H_{10}Br_2$: 323.9144[M]$^+$; found (EI$^+$): 323.9142.

Bis-[2-trimethyl(phenyl)silyl]-methane: *n*BuLi (2.38 M in hexanes, 1.28 mL, 3.05 mmol) was added dropwise to a stirred solution of 2,2'-dibromodiphenylmethane (0.40 g, 1.22 mmol) in THF (6 mL) at –78 °C. The reaction was stirred at this temperature for 1.5 h, then Me_3SiCl (0.46 mL, 3.66 mmol) was added dropwise, and the mixture was allowed to warm to room temperature and was stirred overnight. The reaction was quenched with H_2O (10 mL), then the aqueous phase was separated and extracted with Et_2O (3 × 15 mL), and the combined organic portions were dried ($MgSO_4$), filtered and concentrated *in vacuo*. Purification *via* flash column chromatography (hexanes) afforded the title compound as a colourless liquid that solidified on standing (0.25 g, 0.81 mmol, 66%).

^{1}H NMR (400 MHz, $CDCl_3$): δ 7.56 (dd, *J* = 7.1, 1.7 Hz, 2H), 7.34 – 7.14 (m, 4H), 6.85 (app. d, *J* = 8.4 Hz, 2H), 4.32 (s, 2H), 0.35 (s, 18H). **^{13}C{^{1}H} NMR (100 MHz, $CDCl_3$):** δ 147.0, 139.0, 134.5, 129.8, 129.5, 125.5, 42.1, 0.43. **ν_{max}(neat)/cm^{-1}:** 3068, 2959, 2896, 1587, 1560, 1467, 1422, 1248, 1191, 1121, 833, 755, 745, 729. **HRMS** calcd. for $C_{19}H_{28}Si_2$: 312.1724[M]$^+$; found (EI$^+$): 312.1729. **m.p. /°C:** 60-62 (MeOH).

8.3 Intramolecular Direct Arylation: Scope

8.3.1 General Procedure and Considerations

thtAuBr$_3$ (1-4 mol%, as specified for individual compounds) was added to a 25 mL vial containing the requisite aryltrimethylsilane (0.50 mmol) in $CHCl_3$ (5 mL) and MeOH (100 μL). Camphorsulfonic acid (151 mg, 0.65 mmol) and iodobenzene diacetate (177 mg, 0.55 mmol) were added, and the reaction was stirred at 27 °C (reaction time as specified for individual compounds). After analysis of the composition by ^{1}H NMR spectroscopy, the reaction mixture was concentrated *in vacuo* and purified by flash column chromatography (dry-loaded onto silica gel, eluent as specified for individual compounds).

Notes:

- For reproducibility, reactions were performed in an oil bath set to 27 °C due to variations in room temperature throughout the year.
- The $CHCl_3$ used was CHROMASOLVRTM Plus, for HPLC, =99.9%, containing amylenes as stabilizers, bought from Sigma Aldrich. Ethanol stabilized $CHCl_3$ led to longer reaction times and reduced yields in certain examples (e.g. **1m** to **2m**, yield changes from 40% to 88%). The $CHCl_3$ was passed through a plug of activated basic Al_2O_3 (Brockmann I), distilled and held over 3 Å MS.
- Methanol was held over 3 Å MS.
- Camphorsulfonic acid was held in a desiccator and weighed out immediately before use.
- A useful indication that the reaction is complete is the change of colour from pale yellow to black. This occurs when all the oxidant is consumed and, presumably, deposition of gold nanoparticles occurs. This is most obvious in the faster reactions.

8.3.2 Experimental Procedures and Characterisation Data

9*H*-Fluorene (2b)

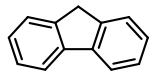

Subjecting **1b** (120 mg, 0.50 mmol) to the **general coupling procedure** (thtAuBr$_3$: 2.62 mg, 0.005 mmol, 1 mol%, 1 h) afforded, after flash column chromatography (hexanes), the title compound as a white solid (78 mg, 0.47 mmol, 94%).

Characterisation data were consistent with literature values: ^{1}H, $^{13}C\{^{1}H\}$ NMR and IR:[21]

^{1}H NMR (400 MHz, $CDCl_3$): δ 7.81 (app. d, *J* = 7.6 Hz, 2H), 7.56 (app. d, *J* = 7.4 Hz, 2H), 7.44 – 7.34 (m, 2H), 7.31 (app. td, *J* = 7.4, 1.2 Hz, 2H), 3.92 (s, 2H). **$^{13}C\{^{1}H\}$ NMR (100 MHz, $CDCl_3$):** δ 143.4, 141.8, 126.85, 126.83, 125.2, 120.0, 37.1. **ν_{max}(neat)/cm^{-1}:** 3059, 3037, 2919, 1477, 1446, 1384, 1187, 953, 732. **m.p. /°C:** 114 (Lit.[22] 113-114)**.**

3-Methoxyl-9*H*-fluorene (2c)

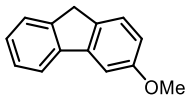

thtAuBr$_3$ (2.62 mg, 0.005 mmol, 1 mol%) was added to a 7 mL vial containing **1c** (135 mg, 0.50 mmol) in $CHCl_3$ (5 mL) and MeOH (100 μL). PIFA (237 mg, 0.55 mmol) was added, and the reaction was stirred at 27 °C for 1.5 h. The reaction mixture was concentrated *in vacuo* and purification by flash column chromatography (dry-loaded onto silica gel, 2% EtOAc) afforded the title compound as a white solid (87 mg, 0.44 mmol, 88%).

Characterisation data were consistent with literature values: ^{1}H, $^{13}C\{^{1}H\}$ NMR and IR:[22,23]

^{1}H NMR (600 MHz, $CDCl_3$): δ 7.76 (d, *J* = 7.6 Hz, 1H), 7.54 (d, *J* = 7.4 Hz, 1H), 7.44 (d, *J* = 8.3 Hz, 1H), 7.38 (app. t, *J* = 7.5 Hz, 1H), 7.33 – 7.29 (m, 2H), 6.89 (dd, *J* = 8.2, 2.4 Hz, 1H), 3.91 (s, 3H), 3.84 (s, 2H). **$^{13}C\{^{1}H\}$ NMR (100 MHz, $CDCl_3$):** δ 159.4, 144.4, 143.1, 141.8, 135.5, 126.9, 126.8, 125.7, 125.2, 119.9, 113.4, 105.1, 55.7, 36.3. **ν_{max}(neat)/cm^{-1}:** 3047, 2932, 1607, 1576, 1453, 1436, 1305, 1243, 1215, 1169, 1034, 848, 766, 734.

3-*tert*-Butyl-9*H*-fluorene (2e)

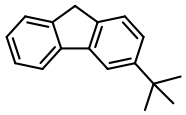

Subjecting **1e** (148 mg, 0.50 mmol) to the **general coupling procedure** (thtAuBr$_3$: 2.62 mg, 0.005 mmol, 1 mol%, 1 h) afforded, after flash column chromatography (hexanes), the title compound as a white solid (90 mg, 0.40 mmol, 81%).

Characterisation data were consistent with literature values: ^{1}H and $^{13}C\{^{1}H\}$ NMR.[22]

^{1}H NMR (600 MHz, $CDCl_3$): δ 7.85 (d, *J*=1.7 Hz, 1H), 7.83 (d, *J*=7.6 Hz, 1H), 7.54 (app. d, *J*=7.5 Hz, 1H), 7.50 (app. d, *J*= 7.9 Hz, 1H), 7.41 – 7.37 (m, 2H), 7.32 (app. td, *J* = 7.4, 1.1 Hz, 1H), 3.88 (s, 2H), 1.43 (s, 9H). **$^{13}C\{^{1}H\}$ NMR (100 MHz, $CDCl_3$):** δ 150.1, 143.8, 142.1, 141.7, 140.5, 126.8, 126.6, 125.1, 124.7, 124.2, 119.8, 116.7, 36.6, 35.0, 31.8. **ν_{max}(neat)/cm^{-}**

[1]: 3042, 2967, 2955, 2863, 1613, 1469, 1452, 1397, 1359, 1312, 1254, 1202, 1105, 1034, 820, 765, 735, 704. **m.p. /°C:** 56-57 (Lit.[22] 55-56).

3-Chloro-9*H*-fluorene (2f)

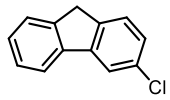

Subjecting **1f** (137 mg, 0.50 mmol) to the **general coupling procedure** (thtAuBr$_3$: 2.62 mg, 0.005 mmol, 1 mol%, 4 h) afforded, after flash column chromatography (hexanes), the title compound as a white solid (90 mg, 0.45 mmol, 90%).

Characterisation data were consistent with literature values: ^{1}H, ^{13}C{^{1}H} NMR and IR:[23]

^{1}H NMR (400 MHz, CDCl$_3$): δ 7.77 – 7.72 (m, 2H), 7.55 (app. d, *J* = 7.4 Hz, 1H), 7.45 (d, *J* = 8.0 Hz, 1H), 7.42 – 7.37 (m, 1H), 7.34 (app. td, *J* = 7.4, 1.3 Hz, 1H), 7.27 (dd, *J* = 8.1, 1.8 Hz, 1H), 3.86 (s, 2H). **^{13}C{^{1}H} NMR (100 MHz, CDCl$_3$):** δ 143.8, 143.6, 141.5, 140.7, 132.9, 127.5, 127.1, 126.8, 126.1, 125.3, 120.3, 36.7. *1 × C_{Ar} not observed, in agreement with literature.* **ν_{max}(neat)/cm^{-1}:** 3050, 2926, 1597, 1473, 1441, 1386, 1069, 879, 856, 806, 766, 733. **m.p. /°C:** 89-90 (Lit.[23] 90-92).

9*H*-Fluoren-3-yl 2,2-dimethylpropanoate (2g)

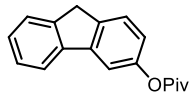

Subjecting **1g** (175 mg, 0.50 mmol) to the **general coupling procedure** (thtAuBr$_3$: 2.62 mg, 0.005 mmol, 1 mol%, 6 h) afforded, after flash column chromatography (hexanes), the title compound as a white solid (108 mg, 0.41 mmol, 81%).

^{1}H NMR (400 MHz, CDCl$_3$): δ 7.75 (app. d, *J* = 7.5 Hz, 1H), 7.55 (app. d, *J* = 7.4 Hz, 1H), 7.52 (d, *J* = 8.2 Hz, 1H), 7.47 (d, *J* = 2.1 Hz, 1H), 7.38 (app. td, *J* = 7.4, 1.1 Hz, 1H), 7.33 (app. td, *J* = 7.4, 1.1 Hz , 1H), 6.99 (dd, *J* = 8.2, 2.2 Hz, 1H), 3.88 (s, 2H), 1.42 (s, 9H). **^{13}C{^{1}H} NMR (100 MHz, CDCl$_3$):** δ 177.5, 150.6, 144.1, 143.2, 141.2, 140.4, 127.2, 126.9, 125.6, 125.2, 120.3, 119.9, 113.3, 39.3, 36.6, 27.4. **ν_{max}(neat)/cm^{-1}:** 2961, 2929, 2870, 1741, 1615, 1477, 1449, 1395, 1267, 1175, 1157, 1119, 916, 761, 728. **HRMS** calcd. for $C_{18}H_{18}O_2$: 266.1301 [M]$^+$; found (EI$^+$): 266.1294. **m.p. /°C:** 66-69 (EtOH).

3-(Trifluoromethyl)-9*H*-fluorene (2h)

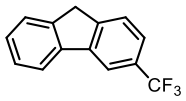

Subjecting **1h** (154 mg, 0.50 mmol) to the **general coupling procedure** (thtAuBr$_3$: 2.62 mg, 0.005 mmol, 1 mol%, 14.5 h) afforded, after flash column chromatography (hexanes), the title compound as a white solid (94 mg, 0.40 mmol, 80%).

Characterisation data were consistent with literature values: ^{1}H, ^{13}C{^{1}H} NMR and IR:[23]

^{1}H NMR (400 MHz, CDCl$_3$): δ 8.02 (s, 1H), 7.83 (d, *J* = 7.4 Hz, 1H), 7.64 (app. d, *J* = 7.9 Hz, 1H), 7.62 – 7.55 (m, 2H), 7.45 – 7.40 (m, 1H), 7.37 (app. td, *J* = 7.4, 1.3 Hz, 1H), 3.95 (s, 2H). **^{13}C{^{1}H} NMR (100 MHz, CDCl$_3$):** δ 146.9, 143.4, 142.5, 140.6, 129.5 (q, *J* = 32.0 Hz), 127.8, 127.2, 125.4, 125.3, 124.8 (q, *J* = 270 Hz), 123.6 (q, *J* = 3.7 Hz), 120.4, 116.9 (q, *J* = 3.9 Hz), 37.1. **^{19}F NMR (377 MHz, CDCl$_3$):** δ -61.9 (s). **ν_{max}(neat)/cm^{-1}:** 3054, 2930, 1789, 1611, 1404, 1321, 1265, 1233, 1160, 1098, 1056, 896, 827, 769, 736. **m.p. /°C:** 69-70 (MeOH) (Lit.[23] 65-67).

9*H*-Fluoren-3-yl trifluoromethanesulfonate (2n)

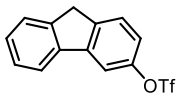

Subjecting **1n** (194 mg, 0.50 mmol) to the **general coupling procedure** (thtAuBr$_3$: 5.24 mg, 0.01 mmol, 2 mol%, 16 h) afforded, after flash column chromatography (2% EtOAc in hexanes), the title compound as a colourless oil (145 mg, 0.46 mmol, 92%).

^{1}H NMR (400 MHz, CDCl$_3$): δ 7.78 (app. d, *J* = 6.7 Hz, 1H), 7.64 (d, *J* = 2.3 Hz, 1H), 7.60 – 7.53 (m, 2H), 7.45 – 7.34 (m, 2H), 7.19 (dd, *J* = 8.2, 2.4 Hz, 1H), 3.92 (s, 2H). **^{13}C{^{1}H} NMR (100 MHz, CDCl$_3$):** δ 149.2, 144.2, 144.0, 143.2, 140.2, 128.1, 127.3, 126.4, 125.4, 120.6, 119.3, 119.0 (q, *J* = 320 Hz), 113.0, 36.7. **^{19}F NMR (377 MHz, CDCl$_3$):** δ –72.8 (s). **ν_{max}(neat)/cm^{-1}:** 3066, 2899, 1482, 1418, 1244, 1202, 1137, 1118, 903, 850, 811, 765, 727. **HRMS** calcd. for $C_{14}H_9F_3O_3S$: 314.0219 [M]$^+$; found (EI$^+$): 314.0218.

3-Methyl-9*H*-fluorene / 4-Methyl-9*H*-fluorene (2i)

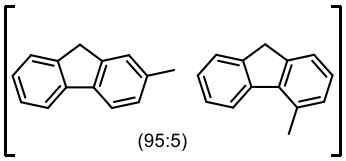

thtAuBr$_3$ (2.62 mg, 0.005 mmol, 1 mol%) was added to a 7 mL vial containing **1i** (127 mg, 0.50 mmol) in $CHCl_3$ (5 mL) and MeOH (100 μL). PIFA (237 mg, 0.55 mmol) was added, and the reaction was stirred at 27 °C for 1 h. The reaction mixture was concentrated *in vacuo* and purification by flash column chromatography (dry-loaded onto silica gel, hexanes) afforded the title compounds as a white solid (95:5 mixture of isomers; 87 mg, 0.47 mmol, 95%).

Characterisation data were consistent with literature values: ^{1}H and ^{13}C{^{1}H} NMR:[42, 45]

Data for major regioisomer: **^{1}H NMR (400 MHz, $CDCl_3$)**: δ 7.77 (app. d, *J* = 7.6 Hz, 1H), 7.69 (d, *J* = 7.7 Hz, 1H), 7.58 – 7.50 (m, 1H), 7.41 – 7.35 (m, 2H), 7.29 (app. td, *J* = 7.4, 1.2 Hz, 1H), 7.23 – 7.19 (m, 1H), 3.88 (s, 2H), 2.46 (s, 3H). **^{13}C{^{1}H} NMR (100 MHz, $CDCl_3$):** δ 143.5, 143.1, 141.8, 139.1, 136.6, 127.6, 126.7, 126.2, 125.8, 125.0, 119.60, 119.56, 36.8, 21.7. Select data for minor regioisomer: **^{1}H NMR (400 MHz, $CDCl_3$)**: δ 7.96 (d, *J* = 7.8 Hz, 1H), 3.96 (s, 2H), 2.76 (s, 3H). **ν_{max}(neat)/cm^{-1}:** 3020, 2910, 2853, 1453, 1400, 1393, 1298, 1177, 953, 821, 760, 728. **LRMS** (EI$^+$): 180 ([M]$^+$, 90%), 165 ([M - CH_3]$^+$, 100%).

2-Methoxy-9*H*-fluorene (2j)

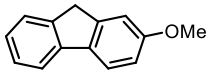

thtAuBr$_3$ (2.62 mg, 0.005 mmol, 1 mol%) was added to a 7 mL vial containing **1j** (135 mg, 0.50 mmol) in $CHCl_3$ (5 mL) and MeOH (100 μL). PIFA (237 mg, 0.55 mmol) was added, and the reaction was stirred at 27 °C for 1 h. Analysis of the composition by ^{1}H NMR spectroscopy showed a mixture of 2/4-methoxy-9*H*-fluorene (88:12). The reaction mixture was concentrated *in vacuo* and purification by flash column chromatography (dry-loaded onto silica gel, 4% EtOAc) afforded the title compound as a white solid (79 mg, 0.40 mmol, 80%; 91% conversion based on both isomers).

Characterisation data were consistent with literature values: ^{1}H and ^{13}C{^{1}H} NMR:[24]

^{1}H NMR (400 MHz, $CDCl_3$): 7.74 – 7.66 (m, 2H), 7.51 (app. d, *J* = 7.4 Hz, 1H), 7.35 (app. t, *J* = 7.5 Hz, 1H), 7.25 (app. td, J = 7.4, 1.1 Hz, 1H), 7.13 – 7.10 (m, 1H), 6.95 (dd, *J* = 8.4, 2.4

Hz, 1H), 3.88 (s, 5H).**^{13}C{^{1}H} NMR (100 MHz, $CDCl_3$):** 159.4, 145.2, 142.8, 141.8, 134.9, 126.9, 125.7, 125.0, 120.6, 119.2, 113.1, 110.7, 55.7, 37.2. **ν_{max}(neat)/cm^{-1}:** 3039, 2827, 1603, 1488, 1420, 1309, 1266, 1139, 1038, 829, 764, 733. **m.p. /°C:** 109-110 (Lit.[25] 109-110).

2-Fluoro-9*H*-fluorene (2k)

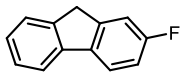

Subjecting **1k** (129 mg, 0.50 mmol) to the **general coupling procedure** (thtAuBr$_3$: 2.62 mg, 0.005 mmol, 1 mol%, 2 h) afforded, after flash column chromatography (hexanes), the title compound as a white solid (78 mg, 0.42 mmol, 85%).

Characterisation data were consistent with literature values: ^{1}H, ^{13}C{^{1}H} ^{19}F NMR and IR:[26,27]

^{1}H NMR (600 MHz, $CDCl_3$): δ 7.74 (app. d, *J* = 7.6 Hz, 1H), 7.71 (dd, *J* = 8.3, 5.2 Hz, 1H), 7.55 – 7.53 (m, 1H), 7.39 (app. t, *J* = 7.5 Hz, 1H), 7.30 (app. td, *J* = 7.5, 1.2 Hz, 1H), 7.27 – 7.24 (m, 1H), 7.09 (app. td, *J* = 8.7, 2.4 Hz, 1H), 3.89 (s, 2H). **^{13}C{^{1}H} NMR (150 MHz, $CDCl_3$):** δ 162.5 (d, *J* = 240 Hz), 145.4 (d, *J* = 8.6 Hz), 143.1 (d, *J* = 1.8 Hz), 141.0, 137.9 (d, *J* = 2.5 Hz), 127.0, 126.5, 125.1, 120.8 (d, *J* = 8.9 Hz), 119.7, 114.1 (d, *J* = 23 Hz), 112.4 (d, *J* = 23 Hz), 37.1 (d, *J* = 2.4 Hz). **^{19}F NMR (377 MHz, $CDCl_3$):** –115.8 (app. td, *J* = 9.1, 5.1 Hz). **ν_{max}(neat)/cm^{-1}:** 3051, 2923, 2906, 2854, 1589, 1469, 1423, 1399, 1249, 1120, 926, 821, 761, 728. **m.p. /°C:** 99-100 (Lit.[28] 99-100).

2-Chloro-9*H*-fluorene (2l)

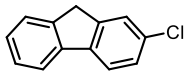

thtAuBr$_3$ (10.5 mg, 0.002 mmol, 1 mol%) was added to a 50 mL round bottom flask containing **1l** (549 mg, 2.00 mmol) in $CHCl_3$ (20 mL) and MeOH (400 μL). Camphorsulfonic acid (603 mg, 2.60 mmol) and iodobenzene diacetate (709 mg, 2.20 mmol) were added, and the reaction was stirred at 27 °C for 3 h. After analysis of the composition by ^{1}H NMR spectroscopy, the reaction mixture was concentrated *in vacuo* and purification by flash column chromatography (dry-loaded onto silica gel, hexanes) afforded the title compound as a white solid (362 mg, 1.80 mmol, 90%).

Characterisation data were consistent with literature values: ^{1}H, ^{13}C{^{1}H} NMR and IR:[23]

^{1}H NMR (400 MHz, $CDCl_3$): δ 7.75 (d, *J* = 7.5 Hz, 1H), 7.69 (d, *J* = 8.1 Hz, 1H), 7.57 – 7.52 (m, 2H), 7.43 – 7.28 (m, 3H), 3.89 (s, 2H). **^{13}C{^{1}H} NMR (100 MHz, $CDCl_3$):** δ 145.0, 143.1,

140.8, 140.4, 132.5, 127.18, 127.12, 127.07, 125.5, 125.2, 120.9, 120.0, 36.9. **ν_{max}(neat)/cm^{-1}:** 3062, 2924, 1808, 1468, 1447, 1414, 1394, 1071, 872, 821, 762, 729. **m.p. /°C:** 97-98 (Lit[29] 96.5).

2-(Trifluoromethyl)-9*H*-fluorene (2m)

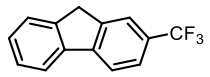

Subjecting **1m** (154 mg, 0.50 mmol) to a modified general coupling procedure (thtAuBr$_3$: 2.62 mg, 0.005 mmol, 1 mol%, 16 h) and CSA (232 mg, 0.20 mmol) afforded, after flash column chromatography (hexanes), the title compound as a pale yellow solid (103 mg, 0.44 mmol, 88%).

Characterisation data were consistent with literature values: ^{1}H, ^{13}C{^{1}H} and IR:[23]

^{1}H NMR (400 MHz, CDCl$_3$): δ 7.85 (app. t, *J* = 7.3 Hz, 2H), 7.80 (s, 1H), 7.68 – 7.55 (m, 2H), 7.46 – 7.35 (m, 2H), 3.96 (s, 2H). **^{13}C{^{1}H} NMR (100 MHz, CDCl$_3$):** δ 145.2, 143.9, 143.6, 140.4, 128.7 (q, *J* = 32 Hz), 128.1, 127.8, 127.2, 125.4, 124.8 (q, *J* = 270 Hz), 124.2 (q, *J* = 3.9 Hz), 122.1 (q, *J* = 3.9 Hz), 120.0, 37.1. **^{19}F NMR (377 MHz, CDCl$_3$):** δ -61.7 (s). **ν_{max}(neat)/cm^{-1}:** 3051, 2858, 1619, 1427, 1325, 1284, 1159, 1099, 1061, 882, 839, 772, 738.

9*H*-Fluoren-2-yl-trifluoromethanesulfonate (2n)

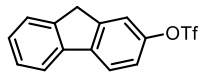

thtAuBr$_3$ (2.26 mg, 0.0043 mmol, 1 mol%) was added to a 7 mL vial containing **1n** (166 mg, 0.43 mmol) in CHCl$_3$ (4.3 mL) and MeOH (86 µL). Camphorsulfonic acid (130 mg, 0.56 mmol) and iodobenzene diacetate (152 mg, 0.47 mmol) were added, and the reaction was stirred at 27 °C for 15 h. The reaction mixture was concentrated *in vacuo* and purification by flash column chromatography (dry-loaded onto silica gel, 3% EtOAc in hexanes) afforded the title compound as a white solid (105 mg, 0.34 mmol, 78%).

^{1}H NMR (400 MHz, CDCl$_3$): δ 7.84 – 7.76 (m, 2H), 7.57 (app. d, *J* = 7.4 Hz, 1H), 7.48 – 7.45 (m, 1H), 7.44 – 7.38 (m, 1H), 7.36 (app. td, *J* = 7.4, 1.3 Hz, 1H), 7.29 (dd, *J* = 8.3, 2.3 Hz, 1H), 3.95 (s, 2H). **^{13}C{^{1}H} NMR (100 MHz, CDCl$_3$):** δ 148.6, 145.4, 143.5, 142.1, 140.1, 127.7, 127.3, 125.3, 121.0, 120.4, 120.1, 119.0 (q, *J* = 320 Hz), 118.4, 37.2. **^{19}F NMR (377 MHz, CDCl$_3$):** δ -72.8 (s). **ν_{max}(neat)/cm^{-1}:** 3062, 3022, 2919, 1418, 1207, 1130, 1094, 933, 866, 849, 833, 818, 769, 752, 735, 710. **HRMS** calcd. for $C_{14}H_9F_3O_3S$: 314.0219 $[M]^+$; found (EI^+): 314.0220. **m.p. /°C:** 84-85 (MeOH).

1,4-Dimethylfluorene (2a)

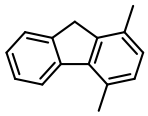

Subjecting **1a** (134 mg, 0.50 mmol) to the **general coupling procedure** (thtAuBr$_3$: 2.62 mg, 0.005 mmol, 1 mol%, 10 min) afforded, after flash column chromatography (hexanes), the title compound as a white solid (94 mg, 0.48 mmol, 95%).

Characterisation data were consistent with literature values: ^{1}H, ^{13}C{^{1}H} NMR and IR. [2]

^{1}H NMR (400 MHz, CDCl$_3$): δ 7.96 (d, *J* = 7.6 Hz, 1H), 7.60 (d, *J* = 7.4 Hz, 1H), 7.41 (m, 1H), 7.34 (app. td, *J* = 7.4 Hz, 1.0 Hz, 1H), 7.10 (d, J = 7.6 Hz, 1H), 7.05 (d, J = 7.6 Hz, 1H), 3.80 (s, 2H), 2.73 (s, 3H), 2.41 (s, 3H). **^{13}C{^{1}H} NMR (100 MHz, CDCl$_3$):** δ 143.6, 143.2, 142.4, 139.4, 131.4, 130.6, 129.4, 127.5, 126.7, 126.0, 125.0, 123.2, 36.2, 20.9, 18.8. **ν_{max}(neat)/cm^{-1}:** 3037, 2955, 1455, 1379, 1027, 804, 732.

7-Fluoro-1,4-dimethylfluorene (2o)

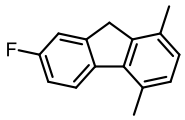

Subjecting **1o** (143 mg, 0.50 mmol) to the **general coupling procedure** (thtAuBr$_3$: 2.62 mg, 0.005 mmol, 1 mol%, 15 min) afforded, after flash column chromatography (hexanes), the title compound as a white solid (94 mg, 0.44 mmol, 89%).

^{1}H NMR (400 MHz, CDCl$_3$): δ 7.86-7.82 (dd, *J* = 8.5, 5.2 Hz, 1H), 7.31 – 7.23 (m, 1H), 7.12 – 7.06 (m, 2H), 7.03 (d, J = 7.6 Hz, 1H), 3.74 (s, 2H), 2.68 (s, 3H), 2.39 (s, 3H). **^{13}C{^{1}H} NMR (100 MHz, CDCl$_3$):** δ 161.8 (d, *J* = 244 Hz), 145.9 (d, *J* = 8.6 Hz), 142.2 (d, *J* = 2.1 Hz), 139.2 (d, *J* = 2.3 Hz), 138.6, 131.5, 130.0 (d, *J* = 0.9 Hz), 129.5, 127.3, 123.9 (d, *J* = 8.7 Hz), 113.7 (d, *J* = 22.3 Hz), 112.3 (d, *J* = 22.5 Hz), 36.2 (d, *J* = 2.4 Hz), 20.7, 18.7. **^{19}F NMR (377 MHz, CDCl$_3$):** –116.9 (app. td, *J* = 9.0, 5.1 Hz). **ν_{max}(neat)/cm^{-1}:** 3050, 3023, 2976, 2946, 2918, 2888, 2863, 1592, 1466, 1384, 1222, 925, 855, 807. **HRMS** calcd. for $C_{15}H_{13}F$: 212.0996 $[M]^+$; found (EI^+): 212.0987. **m.p. /°C:** 67-68.

7-Chloro-1,4-dimethylfluorene (2p)

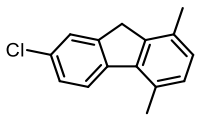

thtAuBr$_3$ (15.8 mg, 0.03 mmol, 2 mol%) was added to a 50 mL round bottom flask containing **1p** (454 mg, 1.50 mmol) in $CHCl_3$ (15 mL) and MeOH (300 μL). Camphorsulfonic acid (453 mg, 1.95 mmol) and iodobenzene diacetate (531 mg, 1.65 mmol) were added, and the reaction was stirred at 27 °C for 1 h. After analysis of the composition by ^{1}H NMR spectroscopy, the reaction mixture was concentrated *in vacuo* and purification by flash column chromatography (dry-loaded onto silica gel, hexanes) afforded the title compound as a white solid (311 mg, 1.36 mmol, 91%).

^{1}H NMR (400 MHz, $CDCl_3$): δ 7.82 (d, *J* = 8.3 Hz, 1H), 7.54 (s, 1H), 7.35 (dd, *J* = 8.3, 2.1 Hz, 1H), 7.12 – 7.02 (m, 2H), 3.75 (s, 2H), 2.67 (s, 3H), 2.38 (s, 3H). **^{13}C{^{1}H} NMR (100 MHz, $CDCl_3$):** δ 145.4, 142.2, 141.7, 138.5, 131.8, 131.6, 130.5, 129.6, 127.9, 127.0, 125.3, 123.9, 36.0, 20.8, 18.7. **ν_{max}(neat)/cm^{-1}:** 3042, 2971, 2944, 2916, 2889, 1500, 1452, 1442, 1376, 1188, 1076, 891, 852, 805,753, 735. **HRMS** calcd. for $C_{15}H_{13}Cl$: 228.0700 $[M]^+$; found (EI^+): 228.0691. **m.p. /°C:** 98-100 (EtOH).

1-Fluoro-9*H*-fluorene (2q)

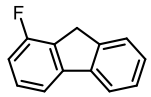

Subjecting **1q** (129 mg, 0.50 mmol) to the **general coupling procedure** (thtAuBr$_3$: 2.62 mg, 0.005 mmol, 1 mol%, 16 h) afforded, after flash column chromatography (hexanes), the title compound as a white solid (80 mg, 0.44 mmol, 87%).

Characterisation data were consistent with literature values: ^{1}H, ^{13}C{^{1}H} NMR and IR:[30]

^{1}H NMR (600 MHz, $CDCl_3$): δ 7.79 (app. d, *J* = 7.3 Hz, 1H), 7.58 (app. d, *J* = 8.1 Hz, 2H), 7.40 (app. t, *J* = 7.4 Hz, 1H), 7.38 – 7.34 (m, 2H), 7.01 (app. t, *J* = 8.7 Hz, 1H), 3.94 (s, 2H). **^{13}C{^{1}H} NMR (150 MHz, $CDCl_3$):** δ 159.9 (d, *J* = 250 Hz), 145.2 (d, *J* = 6.6 Hz), 143.0, 141.1 (d, *J* = 2.5 Hz), 129.0 (d, *J* = 7.1 Hz), 128.7 (d, *J* = 18.0 Hz), 127.5, 127.1, 125.4, 120.4, 115.9 (d, *J* = 3.1 Hz), 113.5 (d, *J* = 21 Hz), 33.6. **^{19}F NMR (377 MHz, $CDCl_3$):** –118.3 (dd, *J* = 9.2, 5.1 Hz). **ν_{max}(neat)/cm^{-1}:** 3052, 3035, 1622, 1579, 1490, 1453, 1277, 1235, 1206, 1071, 907, 791, 750, 725. **m.p. /°C:** 81 (Lit[30] 79.6-80).

2-Fluoro-6-methyl-9*H*-fluorene (2r)

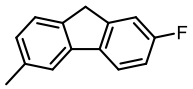

Subjecting **1r** (136 mg, 0.50 mmol) to the **general coupling procedure** (thtAuBr$_3$: 2.62 mg, 0.005 mmol, 1 mol%, 5 h) afforded, after flash column chromatography (hexanes), the title compound as a white solid (88 mg, 0.44 mmol, 89%).

^{1}H NMR (400 MHz, CDCl$_3$): δ 7.68 (dd, *J* = 8.3, 5.2 Hz, 1H), 7.55 (s, 1H), 7.41 (d, *J* = 7.6 Hz, 1H), 7.25 – 7.21 (m, 1H), 7.13 – 7.03 (m, 2H), 3.84 (s, 2H), 2.46 (s, 3H). **^{13}C{^{1}H} NMR (100 MHz, CDCl$_3$):** δ 162.4 (d, *J* = 240 Hz), 145.8 (d, *J* = 8.6 Hz), 141.1, 140.2 (d, *J* = 2.0 Hz), 137.9 (d, *J* = 2.4 Hz), 136.7, 127.5, 124.8, 120.6 (d, *J* = 9.0 Hz), 120.3, 114.0 (d, *J* = 23 Hz), 112.4 (d, *J* = 23 Hz), 36.8 (d, *J* = 2.5 Hz), 21.7. **ν_{max}(neat)/cm^{-1}:** 3008, 2919, 2858, 2733, 2711, 1613, 1585, 1480, 1432, 1381, 1250, 1213, 1123, 1091, 925, 854, 831, 806, 736, 715. **^{19}F NMR (377 MHz, CDCl$_3$):** –116.1 (app. td, *J* = 9.0, 5.1 Hz). **HRMS** calcd. for $C_{14}H_{11}F$: 198.0839 $[M]^+$; found (EI^+): 198.0841. **m.p. /°C:** 79-80 (MeOH).

11*H*-Benzo[*a*]fluorene (2s)

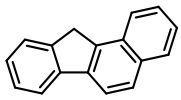

thtAuBr$_3$ (2.62 mg, 0.005 mmol, 1 mol%) was added to a 7 mL vial containing **1s** (145 mg, 0.50 mmol) in $CHCl_3$ (5 mL) and MeOH (100 μL). PIFA (237 mg, 0.55 mmol) was added, and the reaction was stirred at 27 °C for 1 h. The reaction mixture was concentrated *in vacuo* and purification by flash column chromatography (dry-loaded onto silica gel, hexanes) afforded the title compound as a white solid (90 mg, 0.40 mmol, 80%).

Characterisation data were consistent with literature values: ^{1}H and ^{13}C{^{1}H} NMR.[22]

^{1}H NMR (400 MHz, CDCl$_3$): δ 8.03 (d, *J* = 8.2 Hz, 1H), 7.96 – 7.82 (m, 4H), 7.64 (app. d, *J* = 7.4 Hz, 1H), 7.59 – 7.51 (m, 1H), 7.51 – 7.43 (m, 1H), 7.42 (app. t, *J* = 7.4 Hz, 1H), 7.33 (app. td, *J* = 7.4, 1.2 Hz, 1H), 4.20 (s, 2H). **^{13}C{^{1}H} NMR (100 MHz, CDCl$_3$):** δ 143.4, 142.8, 139.9, 139.1, 133.0, 130.9, 129.1, 127.9, 126.9, 126.6, 126.5, 125.4, 125.0, 124.2, 119.8, 118.9, 35.8. **ν_{max}(neat)/cm^{-1}:** 3051, 1467, 1407, 1393, 1370, 1327, 1260, 1167, 1015, 943, 861, 823, 779, 750, 715. **m.p. /°C:** 184-185 °C (Lit.[22] 183-184 °C).

3,6-Dimethyl-9*H*-fluorene (2t)

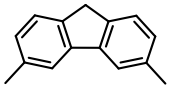

Subjecting **1t** (134 mg, 0.50 mmol) to the **general coupling procedure** (thtAuBr$_3$: 2.62 mg, 0.005 mmol, 1 mol%, 1 h) afforded, after flash column chromatography (hexanes), the title compound as a white solid (74 mg, 0.38 mmol, 76%).

Characterisation data were consistent with literature values: ^{1}H, ^{13}C{^{1}H} NMR and IR:[31]

^{1}H NMR (400 MHz, CDCl$_3$): δ 7.62 (br. s, 2H), 7.44 (d, *J* = 7.6 Hz, 2H), 7.14 (app. d, *J* = 8.2 Hz, 2H), 3.84 (s, 2H), 2.49 (s, 6H). **^{13}C{^{1}H} NMR (100 MHz, CDCl$_3$):** δ 142.0, 140.9, 136.3, 127.6, 124.8, 120.5, 36.3, 21.7. **ν_{max}(neat)/cm^{-1}:** 3006, 2915, 2857, 1613, 1496, 1454, 1399, 1307, 1281, 1194, 1147, 1035, 884, 801, 752. **m.p. /°C:** 129-130 °C (Lit.[32] 130-131 °C).

2,9-Dimethyl-9*H*-fluorene/ 4,9-dimethyl-9*H*-fluorene (2u)

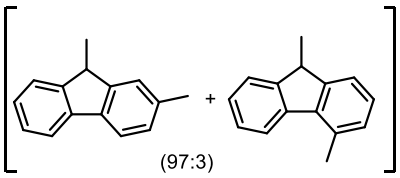

thtAuBr$_3$ (5.24 mg, 0.05 mmol, 2 mol%) was added to a 7 mL vial containing **1u** (134 mg, 0.50 mmol) in CHCl$_3$ (5 mL) and MeOH (100 μL). PIFA (237 mg, 0.55 mmol) was added, and the reaction was stirred at 27 °C for 1 h. The reaction mixture was concentrated *in vacuo* and purification by flash column chromatography (dry-loaded onto silica gel, hexanes) afforded the title compound as a yellow oil (97:3 mixture of isomers, 77 mg, 0.40 mmol, 79%).

Characterisation data were consistent with literature values: ^{1}H and ^{13}C{^{1}H} NMR.[33,34]

Major: **^{1}H NMR (400 MHz, CDCl$_3$)**: δ 7.74 (app. d, *J* = 7.5 Hz, 1H), 7.67 (d, *J* = 7.7 Hz, 1H), 7.54 – 7.49 (m, 1H), 7.39 – 7.36 (m, 1H), 7.35 (s, 1H), 7.31 (app. td, *J* = 7.4, 1.2 Hz, 1H), 7.23 – 7.19 (m, 1H), 3.93 (q, *J* = 7.5 Hz, 1H), 2.47 (s, 3H), 1.54 (d, *J* = 7.5 Hz, 3H). **^{13}C{^{1}H} NMR (100 MHz, CDCl$_3$):** 149.4, 149.0, 140.8, 138.0, 136.9, 127.9, 127.0, 126.6, 124.9, 124.1, 119.72, 119.65, 42.4, 21.8, 18.4. Select minor peaks: **^{1}H NMR (400 MHz, CDCl$_3$)**: 7.92 (d, *J* = 7.7 Hz, 1H), 2.75 (s, 3H), 1.54 (d, *J* = 7.5 Hz, 3H). **ν_{max}(neat)/cm^{-1}:** 2924, 1454, 1089, 821, 774, 736, 702. **LRMS** (EI$^+$): 194 ([M]$^+$, 50%), 179 ([M - Me]$^+$, 100%).

2,7-Dichloro-9*H*-fluorene (2ae)

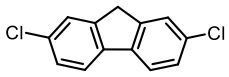

To a 2 mL screw-cap borosilicate vial containing **1ae** (15.5 mg, 0.05 mmol) was added $CDCl_3$ (436 μL), CD_3OD (10 μL) and $thtAuBr_3$ (0.001 mmol, 64 μL of a 0.0155 M stock solution in $CDCl_3$). CSA (0.065 mmol, 15.1 mg) followed immediately by IBDA (0.055 mmol, 17.7 mg) were added. The vial was sealed and shaken vigorously until all the contents had dissolved. The solution was stirred for 48 h and then filtered through a plug of silica gel. The product was isolated by preparative TLC as a white solid (eluent: hexanes).

Characterisation data were consistent with literature values: ^{1}H NMR.[35]

^{1}H NMR (400 MHz, $CDCl_3$): 7.65 (d, *J* = 8.2 Hz, 2H), 7.51 (br. s, 2H), 7.35 (dd, *J* = 8.2, 1.9 Hz, 2H), 3.87 (s, 2H). **^{13}C{^{1}H} NMR (100 MHz, $CDCl_3$):** 144.7, 139.4, 132.9, 127.5, 125.6, 120.9, 36.8. **LRMS** (EI^+): 234 ($[M]^+$, 100%).

Dibenzo[*b,d*]furan (2v)

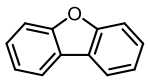

Subjecting **1v** (121 mg, 0.50 mmol) to the **general coupling procedure** ($thtAuBr_3$: 2.62 mg, 0.005 mmol, 1 mol%, 30 min) afforded, after flash column chromatography (hexanes), the title compound as a white solid (79 mg, 0.44 mmol, 87%).

Characterisation data were consistent with literature values: ^{1}H, ^{13}C{^{1}H} NMR and IR.[36]

^{1}H NMR (400 MHz, $CDCl_3$): δ 7.98 (app. d, *J* = 7.7 Hz, 2H), 7.60 (app. d, *J* = 8.2 Hz, 2H), 7.48 (app. t, *J* = 7.7 Hz, 2H), 7.37 (app. t, *J* = 7.5 Hz, 2H). **^{13}C{^{1}H} NMR (100 MHz, $CDCl_3$):** δ 156.3, 127.2, 124.4, 122.8, 120.8, 111.8. **ν_{max}(neat)/cm^{-1}:** 3046, 1595, 1469, 1443, 1193, 1100, 927, 849, 839, 742, 719. **m.p. /°C:** 82-83 (Lit.[36] 83-84).

2-(Dibenzo[*b,d*]furan-2-ylmethyl)-1*H*-isoindole-1,3(2*H*)-dione (2w)

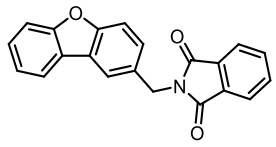

Subjecting **1w** (201 mg, 0.50 mmol) to the general coupling procedure (thtAuBr$_3$: 2.62 mg, 0.005 mmol, 1 mol%, 45 min) afforded, after flash column chromatography (20% EtOAc in hexanes), the title compound as a white solid (153 mg, 0.47 mmol, 94%).

^{1}H NMR (400 MHz, CDCl$_3$): δ 8.05 (d, *J* = 1.7 Hz, 1H), 7.97 – 7.93 (m, 1H), 7.85 (dd, *J* = 5.5, 3.0 Hz, 2H), 7.69 (dd, *J* = 5.5, 3.0 Hz, 2H), 7.58 (dd, *J* = 8.5, 1.8 Hz, 1H), 7.55 – 7.48 (m, 2H), 7.48 – 7.39 (m, 1H), 7.33 (app. td, *J* = 7.5, 1.0 Hz, 1H), 5.00 (s, 2H). **^{13}C{^{1}H} NMR (100 MHz, CDCl$_3$):** δ 168.2, 156.7, 155.9, 134.1, 132.3, 131.2, 128.3, 127.4, 124.7, 124.1, 123.5, 122.9, 121.4, 121.0, 111.9, 111.8, 41.8. **ν_{max}(neat)/cm^{-1}:** 3042, 3027, 2962, 1770, 1702, 1481, 1393, 1327, 1198, 1106, 952, 797, 745, 720. **HRMS** calcd. for $C_{21}H_{13}NO_3$: 327.0890 $[M]^+$; found (EI^+): 327.0880. **m.p. /°C:** 154-156 (EtOH).

9,10-dihydrophenanthrene (4a)

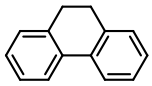

Subjecting **3a** (127 mg, 0.50 mmol) to the **general coupling procedure** (thtAuBr$_3$: 2.62 mg, 0.005 mmol, 1 mol%, 1 h) afforded, after flash column chromatography (hexanes), the title compound as a colourless oil (75 mg, 0.36 mmol, 72%).

Characterisation data were consistent with literature values: ^{1}H, ^{13}C{H} NMR and IR.[37]

^{1}H NMR (400 MHz, CDCl$_3$): 7.78 (app. d, *J* = 7.7 Hz, 2H), 7.37 – 7.17 (m, 6H), 2.90 (s, 4H). **^{13}C{^{1}H} NMR (100 MHz, CDCl$_3$):** 137.5, 134.6, 128.3, 127.5, 127.1, 123.8, 29.2. **ν_{max}(neat)/cm^{-1}:** 3064, 3015, 2932, 2890, 2833, 1484, 1453, 1442, 771, 741, 724.

2-chloro-9,10-dihydrophenanthrene (4b)

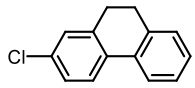

Subjecting **3b** (144 mg, 0.50 mmol) to the **general coupling procedure** (thtAuBr$_3$: 5.25 mg, 0.01 mmol, 2 mol%, 1 h) afforded, after flash column chromatography (hexanes), the title compound as a yellow oil (97 mg, 0.46 mmol, 91%).

^{1}H NMR (400 MHz, $CDCl_3$): 7.71 (app. d, *J* = 7.5 Hz, 1H), 7.67 (d, *J* = 8.3 Hz, 1H), 7.36 – 7.21 (m, 5H), 3.04 – 2.65 (m, 4H). **^{13}C{^{1}H} NMR (100 MHz, $CDCl_3$):** 139.3, 137.2, 133.7, 133.2, 133.0, 128.4, 128.2, 127.8, 127.24, 127.15, 125.2, 123.7, 29.1, 28.9. **ν_{max}(neat)/cm^{-1}:** 3063, 3027, 2936, 2892, 2834, 1597, 1476, 1451, 1408, 1188, 1105, 1088, 1005, 875, 846, 820, 762, 723. **HRMS** calcd. for $C_{14}H_{11}Cl$: 214.0544 $[M]^+$; found (EI^+): 214.0535

2-(Trifluoromethyl)-9,10-dihydrophenanthrene (4c)

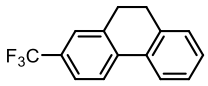

thtAuBr$_3$ (4.04 mg, 0.0078 mmol, 2 mol%) was added to a 7 mL vial containing **3c** (124 mg, 0.39 mmol) in $CHCl_3$ (3.9 mL) and MeOH (77 μL). Camphorsulfonic acid (116 mg, 0.50 mmol) and iodobenzene diacetate (135 mg, 0.42 mmol) were added, and the reaction was stirred at 27 °C for 15 h. The reaction mixture was concentrated *in vacuo* and purification by flash column chromatography (dry-loaded onto silica gel, hexanes) afforded the title compound as a yellow oil (79 mg, 0.32 mmol, 82%).

^{1}H NMR (400 MHz, $CDCl_3$): δ 7.84 (d, *J* = 8.1 Hz, 1H), 7.78 (dd, *J* = 7.4, 1.4 Hz, 1H), 7.55 (app. d, *J* = 8.2 Hz, 1H), 7.50 (s, 1H), 7.38 – 7.26 (m, 3H), 2.99 – 2.86 (m, 4H). **^{13}C{^{1}H} NMR (100 MHz, $CDCl_3$):** δ 138.1, 138.0, 137.8, 133.4, 129.2 (q, *J* = 32 Hz), 128.6, 128.5, 127.4, 125.1 (q, *J* = 3.8 Hz), 124.5 (q, *J* = 270 Hz), 124.3, 124.1, 124.0 (q, *J* = 4.0 Hz), 29.1, 28.8. **^{19}F NMR (377 MHz, $CDCl_3$):** δ -62.4 (s). **ν_{max}(neat)/cm^{-1}:** 2942, 2897, 2839, 1620, 1421, 1334, 1318, 1259, 1158, 1113, 1100, 1075, 895, 861, 833, 771, 734, 711. **HRMS** calcd. for $C_{15}H_{11}F_3$: 248.0807 $[M]^+$; found (EI^+): 248.0810

6*H*-Benzo[c]chromene (4d)

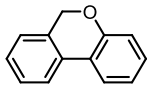

thtAuBr$_3$ (5.25 mg, 0.01 mmol, 2 mol%) was added to a 20 mL round bottom flask containing **3c** (128 mg, 0.50 mmol) in $CHCl_3$ (10 mL) and MeOH (200 μL). Camphorsulfonic acid (151 mg, 0.65 mmol) and iodobenzene diacetate (177 mg, 0.55 mmol) were added, and the reaction was stirred at 27 °C for 2 h. The reaction mixture was concentrated *in vacuo* and purification by flash column chromatography (dry-loaded onto silica gel, 5% toluene in hexanes) afforded the title compound as a colourless oil (78 mg, 0.43 mmol, 86%).

Characterisation data were consistent with literature values: ^{1}H NMR and IR.[38]

^{1}H NMR (400 MHz, $CDCl_3$): δ 7.75 (dd, *J* = 7.8, 1.6 Hz, 1H), 7.71 (app. d, *J* = 7.7 Hz, 1H), 7.42 – 7.36 (m, 1H), 7.30 (dd, *J* = 7.5, 1.2 Hz, 1H), 7.28 – 7.23 (m, 1H), 7.18 – 7.14 (m, 1H), 7.07 (app. td, *J* = 7.6, 1.2 Hz, 1H), 7.01 (dd, *J* = 8.1, 1.2 Hz, 1H), 5.14 (s, 2H). **^{13}C{^{1}H} NMR (100 MHz, $CDCl_3$):** δ 154.9, 131.6, 130.3, 129.6, 128.6, 127.8, 124.8, 123.4, 123.1, 122.3, 122.1, 117.5, 68.6. **ν_{max}(neat)/cm^{-1}:** 3069, 3035, 2964, 2839, 1605, 1592, 1485, 1438, 1242, 1195, 1015, 937, 810, 750, 722. **LRMS** (EI$^+$): 182.0 ([M]$^+$, 100%).

2-*tert*-Butyl-6*H*-benzo[*c*]chromene (4e)[12]

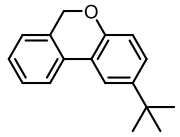

3e (156 mg, 0.50 mmol) was added to a 20 mL round bottom flask containing thtAuBr$_3$ (5.24 mg, 0.01 mmol, 2 mol%) in $CHCl_3$ (10 mL) and MeOH (200 μL). Camphorsulfonic acid (151 mg, 0.65 mmol) and iodobenzene diacetate (177 mg, 0.55 mmol) were added, and the reaction was stirred at 27 °C for 1 h. The reaction mixture was concentrated *in vacuo* and purification by flash column chromatography (dry-loaded onto silica gel, 10% toluene in hexanes) afforded the title compound as a colourless oil (71 mg, 0.30 mmol, 60%).

Characterisation data were consistent with literature values: ^{1}H and ^{13}C{^{1}H} NMR.[12]

^{1}H NMR (400 MHz, $CDCl_3$): δ 7.77 (d, *J* = 2.4 Hz, 1H), 7.75 (app. d, *J* = 7.7 Hz, 1H), 7.42 – 7.36 (m, 1H), 7.31 – 7.26 (m, 2H), 7.20 – 7.12 (m, 1H), 6.95 (d, *J* = 8.5 Hz, 1H), 5.11 (s, 2H), 1.39 (s, 9H). **^{13}C{^{1}H} NMR (100 MHz, $CDCl_3$):** δ 152.7, 144.9, 131.8, 130.7, 128.5, 127.6, 126.7, 124.8, 122.3, 122.0, 120.0, 116.2, 68.7, 34.6, 31.7. **ν_{max}(neat)/cm^{-1}:** 3035, 2960, 2866, 2838, 1496, 1447, 1362, 1246, 1214, 1198, 1016, 821, 767, 728. **LRMS** (EI$^+$): 238 ([M]$^+$, 40%), 223 ([M - Me]$^+$, 100%).

3-Methyl-6*H*-benzo[*c*]chromene; 1-Methyl-6*H*-benzo[*c*]chromene (4f)

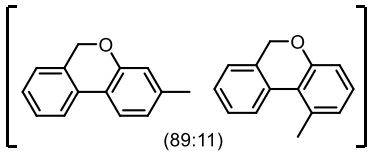

thtAuBr$_3$ (5.25 mg, 0.01 mmol, 2 mol%) was added to a 20 mL round bottom flask containing **3f** (135 mg, 0.50 mmol) in $CHCl_3$ (10 mL) and MeOH (200 μL). Camphorsulfonic acid (151 mg, 0.65 mmol) and iodobenzene diacetate (177 mg, 0.55 mmol) were added, and the reaction was stirred at 27 °C for 1 h. The reaction mixture was concentrated *in vacuo* and purification

by flash column chromatography (dry-loaded onto silica gel, 10% toluene in hexanes) afforded the title compounds as a colourless oil (89:11 mixture of isomers, 78 mg, 0.43 mmol, 86%).

Characterisation data were consistent with literature values: ^{1}H, ^{13}C{^{1}H} NMR, and IR:[39]

Major Isomer: **^{1}H NMR (400 MHz, $CDCl_3$)**: δ 7.67 (app. d, *J* = 7.7 Hz, 1H), 7.62 (d, *J* = 7.9 Hz, 1H), 7.41 – 7.32 (m, 1H), 7.29 – 7.22 (m, 1H), 7.17 – 7.11 (m, 1H), 6.92 – 6.84 (m, 1H), 6.82 (s, 1H), 5.11 (s, 2H), 2.35 (s, 3H). Select minor peaks: δ 7.77 (app. d, *J* = 7.9 Hz, 1H), 6.97 – 6.90 (m, 1H), 4.95 (s, 2H), 2.70 (s, 3H). **^{13}C{^{1}H} NMR (100 MHz, $CDCl_3$):** δ 154.8, 140.0, 131.2, 130.4, 128.5, 127.3, 124.7, 123.23, 123.19, 121.8, 120.3, 117.9, 68.7, 21.5. Select minor peaks: δ 127.9, 127.0, 126.4, 125.8, 125.0, 115.2, 69.2, 22.9. **ν_{max}(neat)/cm^{-1}:** 3030, 2962, 2841, 1618, 1484, 1448, 1206, 1150, 1030, 763, 741, 726, 701.

6,7-Dihydro-5*H*-dibenzo<*a*,*c*>cycloheptene (6a)

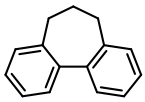

Subjecting **5a** (134 mg, 0.50 mmol) to the **general coupling procedure** (thtAuBr$_3$: 5.24 mg, 0.01 mmol, 2 mol%, 15 h) afforded, after flash column chromatography (hexanes), the title compound as a colourless oil (82 mg, 0.43 mmol, 85%).

Characterisation data were consistent with literature values: ^{1}H NMR.[40]

^{1}H NMR (500 MHz, $CDCl_3$): δ 7.43 (dd, *J* = 7.5, 1.6 Hz, 2H), 7.38 (app. td, *J* = 7.3, 1.5 Hz, 2H), 7.33 (app. td, *J* = 7.3, 1.6 Hz, 2H), 7.28 (dd, *J* = 7.4, 1.5 Hz, 2H), 2.55 (t, *J* = 7.1 Hz, 4H), 2.24 (p, *J* = 7.1 Hz, 2H). **^{13}C{^{1}H} NMR (125 MHz, $CDCl_3$):** δ 141.2, 139.7, 128.5, 128.4, 127.6, 126.8, 33.6, 31.5. **ν_{max}(neat)/cm^{-1}:** 3062, 3014, 2928, 2854, 1481, 1451, 1441, 1307, 1195, 1099, 1006, 939, 746. **LRMS** (EI^{+}): 194.1 ([M]$^{+}$, 100%).

6-(Methylsulfonyl)-6,7-dihydro-5*H*-dibenzo[*c*,*e*]azepine (6b)

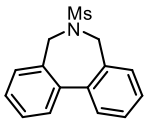

Subjecting **5b** (174 mg, 0.50 mmol) to the **general coupling procedure** (thtAuBr$_3$: 5.24 mg, 0.005 mmol, 2 mol%, 16 h) afforded, after flash column chromatography (20% EtOAc in hexanes), the title compound as an off-white solid (100 mg, 0.36 mmol, 73%).

^{1}H NMR (400 MHz, $CDCl_3$): δ 7.56 – 7.49 (m, 4H), 7.47 – 7.41 (m, 4H), 4.18 (s, 4H), 2.81 (s, 3H). **^{13}C{^{1}H} NMR (100 MHz, $CDCl_3$):** δ 140.7, 132.2, 129.9, 129.4, 128.7, 128.5, 49.2,

37.2. **ν_{max}(neat)/cm^{-1}:** 3016, 2921, 1481, 1459, 1449, 1322, 1304, 1152, 1134, 1117, 1025, 947, 754, 712. **HRMS** calcd. for $C_{15}H_{15}NO_2S$: 273.0818 $[M]^+$; found (EI^+): 273.0821. **m.p. /°C:** 149-150 (MeOH).

5,7-Dihydrodibenzo[*c,e*]oxepine (6c)

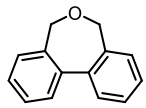

Subjecting **5c** (135 mg, 0.50 mmol) to a modified general coupling procedure (thtAuBr$_3$: 5.24 mg, 0.01 mmol, 2 mol%, 14 h) and CSA (232 mg, 0.20 mmol) afforded, after flash column chromatography (5% EtOAc in hexanes), the title compound as a colourless oil that solidified on standing (74 mg, 0.38 mmol, 76%).

Characterisation data were consistent with literature values: ^{1}H and ^{13}C{^{1}H} NMR.[41]

^{1}H NMR (400 MHz, CDCl$_3$): δ 7.59 – 7.55 (m, 2H), 7.54 – 7.49 (m, 2H), 7.47 – 7.40 (m, 4H), 4.37 (s, 4H). **^{13}C{^{1}H} NMR (100 MHz, CDCl$_3$):** δ 141.3, 135.3, 129.8, 129.1, 128.4, 127.6, 67.7. **ν_{max}(neat)/cm^{-1}:** 3064, 3017, 2852, 1450, 1196, 1073, 1043, 994, 901, 886, 748.

3-Fluoro-8-methyl-5,7-dihydrodibenzo[*c,e*]oxepine (6d)

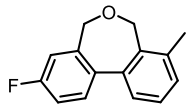

Subjecting **5d** (151 mg, 0.50 mmol) to the **general coupling procedure** (thtAuBr$_3$: 5.24 mg, 0.01 mmol, 2 mol%, 14.5 h) afforded, after flash column chromatography (5% EtOAc in hexanes), the title compound as a white solid (94 mg, 0.41 mmol, 82%).

^{1}H NMR (400 MHz, CDCl$_3$): δ 7.52 (dd, *J* = 8.4, 5.5 Hz, 1H), 7.40 – 7.25 (m, 3H), 7.22 – 7.11 (m, 2H), 4.39 (s, 2H), 4.29 (s, 2H), 2.52 (s, 3H). **^{13}C{^{1}H} NMR (100 MHz, CDCl$_3$):** δ 162.6 (d, *J* = 250 Hz), 141.1, 137.9 (d, *J* = 3.2 Hz), 137.0, 136.9, 133.2, 130.3, 129.2 (d, *J* = 8.1 Hz), 128.5, 125.6, 116.4 (d, *J* = 21 Hz), 115.8 (d, *J* = 21 Hz), 67.4 (d, *J* = 1.7 Hz), 62.8, 19.8. **^{19}F NMR (377 MHz, CDCl$_3$):** δ –114.3 (td, *J* = 8.6, 5.4 Hz). **ν_{max}(neat)/cm^{-1}:** 2996, 2857, 1593, 1493, 1461, 1229, 1064, 874, 839, 791, 773, 723. **HRMS** calcd. for $C_{15}H_{13}FO$: 228.0945 $[M]^+$; found (EI^+): 228.0952. **m.p. /°C:** 115-116 (MeOH).

7,8-Dihydro-5*H*-dibenzo[*c*,*e*]oxocine (8)

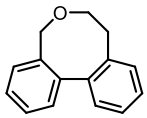

Subjecting **7** (142 mg, 0.50 mmol) to the **general coupling procedure** (thtAuBr$_3$: 10.48 mg, 0.020 mmol, 4 mol%, 14 h) afforded, after flash column chromatography (3% EtOAc in hexanes), the title compound as a white solid (79 mg, 0.38 mmol, 75%).

^{1}H NMR (400 MHz, CDCl$_3$): δ 7.53 – 7.20 (m, 8H), 4.66 (d, *J* = 12.5 Hz, 1H), 4.21 (ddd, *J* = 11.7, 5.9, 1.7 Hz, 1H), 3.87 (d, *J* = 12.5 Hz, 1H), 3.61 (app. t, *J* = 10.9 Hz, 1H), 2.80 (dd, *J* = 14.5, 5.9 Hz, 1H), 2.54 (ddd, *J* = 14.5, 10.3, 1.7 Hz, 1H). **^{13}C{^{1}H} NMR (125 MHz, CDCl$_3$):** δ 140.7, 140.5, 140.2, 137.7, 130.8, 129.8, 129.61, 129.59, 128.4, 128.31, 128.29, 126.5, 71.1, 70.5, 37.3. **ν_{max}(neat)/cm^{-1}:** 3051, 3019, 2956, 2931, 2911, 2858, 1481, 1438, 1238, 1105, 1083, 1030, 929, 754. **HRMS** calcd. for $C_{15}H_{14}O$: 210.1033 $[M]^+$; found (EI^+): 210.1032. **m.p. /°C:** 99-100 (MeOH).

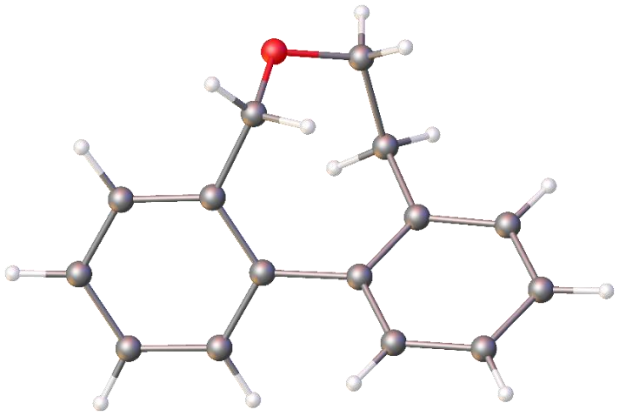

Figure 8.1. The molecular structure of **8**, with displacement ellipsoids at the 50% probability level.

Table 8.1: Crystal data and structure refinement for **8**.

Formula	$C_{15}H_{14}O$
$D_{calc.}$/ g cm^{-3}	1.280
μ/mm^{-1}	0.609
Formula Weight	210.26
Colour	colourless
Shape	block
Max Size/mm	0.39
Mid Size/mm	0.31
Min Size/mm	0.07
T/K	120.0
Crystal System	orthorhombic
Space Group	Pbca
a/Å	7.69025(7)
b/Å	13.54657(17)
c/Å	20.9417(2)
α/°	90
β/°	90
γ/°	90
V/Å^3	2181.63(4)
Z	8
Z'	1
Θ_{min}/°	4.222
Θ_{max}/°	76.161
Measured Refl.	17154
Independent Refl.	2265
Reflections Used	2132
R_{int}	0.0678
Parameters	202
Restraints	0
Largest Peak	0.331
Deepest Hole	-0.232
GooF	1.054
wR_2 (all data)	0.1390
wR_2	0.1370
R_1 (all data)	0.0515
R_1	0.0499

5,7,8,9-Tetrahydrodibenzo[*c*,*e*]oxonine (10)

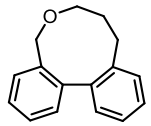

thtAuBr$_3$ (10.5 mg, 0.02 mmol, 4 mol%) was added to a 7.5 mL vial containing **9** (149 mg, 0.50 mmol) in CHCl$_3$ (5 mL) and MeOH (100 μL). Camphorsulfonic acid (232 mg, 1.00 mmol) and iodobenzene diacetate (177 mg, 0.55 mmol) were added, and the reaction was stirred at 50 °C for 15 h. The reaction mixture was concentrated *in vacuo* and purification by

flash column chromatography (dry-loaded onto silica gel, 5% EtOAc in hexanes) afforded the title compound as a white solid (58 mg, 0.26 mmol, 52%).

^{1}H NMR (400 MHz, $CDCl_3$): δ 7.41 – 7.29 (m, 4H), 7.28 – 7.18 (m, 3H), 7.11 (dd, *J* = 7.5, 1.5 Hz, 1H), 4.52 (d, *J* = 12.5 Hz, 1H), 4.13 (d, *J* = 12.5 Hz, 1H), 3.78 (ddd, *J* = 11.4, 5.9, 4.1 Hz, 1H), 3.38 (ddd, *J* = 11.5, 7.9, 3.8 Hz, 1H), 2.61 (dt, *J* = 13.5, 4.0 Hz, 1H), 2.34 (ddd, *J* = 13.5, 11.9, 4.5 Hz, 1H), 1.89 – 1.67 (m, 2H). **^{13}C{^{1}H} NMR (100 MHz, $CDCl_3$):** 142.8, 141.7, 141.5, 137.9, 130.2, 130.1, 128.6, 128.4, 128.1, 127.9, 127.5, 125.5, 75.2, 71.4, 32.2, 30.5. **ν_{max}(neat)/cm^{-1}:** 3054, 2938, 2858, 1475, 1438, 1367, 1197, 1091, 977, 778, 750. **HRMS** calcd. for $C_{16}H_{16}O$: 224.1198[M]$^{+}$; found (EI^{+}): 224.1192. **m.p. /°C:** 99-100 (MeOH).

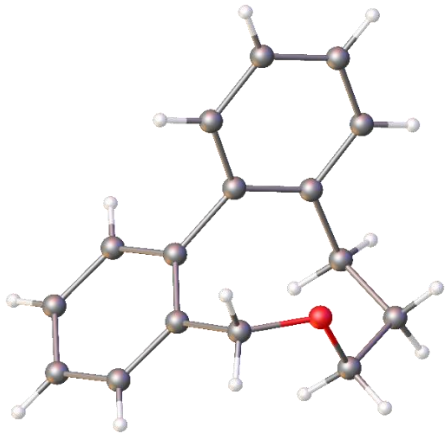

Figure 8.2. The molecular structure of **10** (one of two independent molecules in the unit cell), with displacement ellipsoids at the 50% probability level.

Table 8.2: Crystal data and structure refinement for **10**.

Formula	$C_{16}H_{16}O$
$D_{calc.}$/ g cm^{-3}	1.252
μ/mm^{-1}	0.589
Formula Weight	224.29
Colour	colourless
Shape	plate
Max Size/mm	0.21
Mid Size/mm	0.12
Min Size/mm	0.07
T/K	120.0
Crystal System	monoclinic
Flack Parameter	-0.02(16)
Hooft Parameter	0.01(6)
Space Group	Cc
a/Å	13.92506(15)
b/Å	7.62053(8)
c/Å	22.4351(2)
α/°	90
β/°	90.4854(9)
γ/°	90
V/Å^3	2380.65(4)
Z	8
Z'	2
Θ_{min}/°	3.941
Θ_{max}/°	76.555
Measured Refl.	55336
Independent Refl.	4857
Reflections Used	4802
R_{int}	0.0683
Parameters	307
Restraints	2
Largest Peak	0.197
Deepest Hole	-0.140
GooF	1.042
wR_2 (all data)	0.0932
wR_2	0.0930
R_1 (all data)	0.0360
R_1	0.0356

8.4 Allocolchinoid Syntheses

{[1-(2-Bromo-5-chlorophenyl)ethenyl]oxy}(trimethyl)silane, 5e

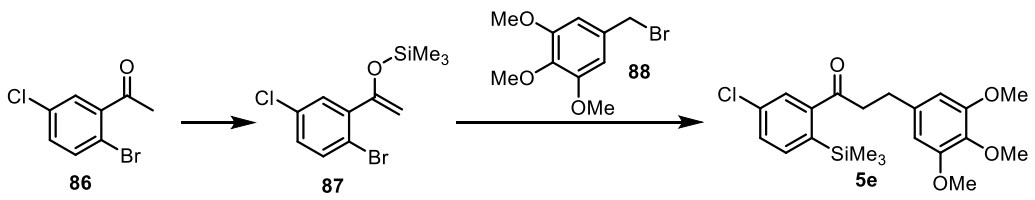

To a solution of **86** (5.57 g, 23.9 mmol), TMSCl (3.33 mL, 26.2 mmol) and Et_3N (3.66 mL, 26.2 mmol) was added NaI (3.93 g, 26.2 mmol) in CH_3CN (25 mL) over 10 min at room temperature. After stirring for 2 h the reaction mixture was diluted with cold hexane (20 mL). The hexane layer was removed *via* syringe into a separating funnel under an inert atmosphere (repeated 3 ×). The organic layer was washed rapidly with H_2O (1 × 30 mL), dried ($MgSO_4$) and concentrated *in vacuo* to afford **87** as a pale yellow oil (5.40 g, 17.6 mmol, 74%).[42] Repetition of this procedure gave yields in the range 74 – 85%. The identity of **87** was confirmed by ^{1}H NMR and used without further purification. **^{1}H NMR (400 MHz, $CDCl_3$):** δ 7.48 (d, *J* = 8.5 Hz, 1H), 7.38 (d, *J* = 2.6 Hz, 1H), 7.12 (dd, *J* = 8.5, 2.6 Hz, 1H), 4.61 (d, *J* = 1.7 Hz, 1H), 4.55 (d, *J* = 1.7 Hz, 1H), 0.24 (s, 9H). ^{n}BuLi (2.17 M in hexanes, 8.1 mL, 17.6 mmol) was added dropwise to a solution of **87** (5.40 g, 17.6 mmol) in THF (50 mL) at -78 °C. The reaction was stirred at this temperature for 1 h, then **88** (3.82 g, 14.6 mmol) was added portionwise over 5 min. The reaction was allowed to warm to room temperature and was stirred for 16 h. The reaction was quenched with water (50 mL). The aqueous phase was separated and extracted with Et_2O (3 × 50 mL), and the combined organic portions were dried ($MgSO_4$), filtered and concentrated *in vacuo*. Purification *via* flash column chromatography (10 - 15% EtOAc in hexanes) afforded the title compound as a white solid (2.03 g, 4.98 mmol, 34%).

^{1}H NMR (400 MHz, $CDCl_3$): δ 7.78 (d, *J* = 2.0 Hz, 1H), 7.65 (d, *J* = 8.0 Hz, 1H), 7.47 (dd, *J* = 8.0, 2.0 Hz, 1H), 6.46 (s, 2H), 3.85 (s, 6H), 3.82 (s, 3H), 3.26 (t, *J* = 7.5 Hz, 2H), 3.01 (t, *J* = 7.5 Hz, 2H), 0.27 (s, 9H). **^{13}C {^{1}H} NMR (100 MHz, $CDCl_3$):** δ 200.6, 153.4, 144.3, 140.4, 137.5, 136.8, 136.6, 135.3, 131.4, 129.0, 105.6, 61.0, 56.3, 41.5, 30.8, 0.41. **ν_{max}(neat)/cm^{-1}:** 3005, 2940, 2836, 1685, 1590, 1455, 1352, 1133, 1073, 983, 833, 821, 746. **HRMS** calcd. for $C_{21}H_{27}O_4ClSi$**:** 406.1362 $[M]^+$; found (EI^+): 406.1353. **m.p. /°C:** 95-96

3-(3,4,5-Trimethoxyphenyl)-1-[2-(trimethylsilyl)phenyl]propan-1-one, 5f

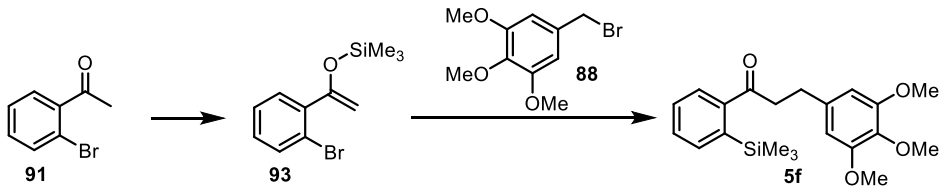

To a solution of 2′-bromoacetophenone **91** (10.4 g, 7.0 mL, 52 mmol), TMSCl (7.9 mL, 62 mmol) and Et_3N (8.6 mL, 62 mmol) was added NaI (9.3 g, 62 mmol) in CH_3CN (60 mL) over 15 min at room temperature. After stirring for 1 h the reaction mixture was diluted with cold hexane (30 mL). The hexane layer was removed *via* syringe into a separating funnel under an

inert atmosphere (repeated 3 ×). The organic layer was washed rapidly with H_2O (1 × 50 mL), dried ($MgSO_4$) and concentrated *in vacuo* to afford **93** as a colourless oil (11.6 g, 43 mmol, 82%). Characterisation data were consistent with literature values: ^{1}H NMR and $^{13}C\{^1H\}$ NMR.[42,43] **^{1}H NMR (400 MHz, $CDCl_3$):** δ 7.56 (dd, *J* = 8.0, 1.2 Hz, 1H), 7.40 (dd, *J* = 7.5, 1.8 Hz, 1H), 7.26 (app. td, *J* = 7.5, 1.2 Hz, 1H), 7.14 (app. td, *J* = 8.0, 1.8 Hz, 1H), 4.61 (d, *J* = 1.4 Hz, 1H), 4.53 (d, *J* = 1.4 Hz, 1H), 0.23 (s, 9H). **$^{13}C\{^1H\}$ NMR (100 MHz, $CDCl_3$):** δ 156.1, 140.3, 133.4, 130.7, 129.5, 127.1, 121.7, 96.2, 0.25. ^{n}BuLi (2.27 M in hexanes, 19 mL, 43 mmol) was added dropwise to a solution **93** (11.6 g, 43 mmol) in THF (110 mL) at -78 °C. The reaction was stirred at this temperature for 1 h, then **88** (8.05 g, 30.8 mmol) was added portionwise over 5 min. The reaction was allowed to warm to room temperature and was stirred for 5 h. The reaction was quenched with water (70 mL). The aqueous phase was separated and extracted with Et_2O (3 × 50 mL), and the combined organic portions were dried ($MgSO_4$), filtered and concentrated *in vacuo*. Purification *via* flash column chromatography (20% EtOAc in hexanes) afforded the title compound as a white solid (4.59 g, 12.32 mmol, 40%).

*Note: **5f** and **88** have very close R_f values, with the product having a slightly lower value. For TLC visualisation a freshly prepared vanillin stain was used to distinguish between the two, as the product appears bright blue, whereas the starting material stains black.*

^{1}H NMR (400 MHz, $CDCl_3$): δ 7.86 (dd, *J* = 7.5, 0.7 Hz, 1H), 7.75 (dd, *J* = 7.5, 1.0 Hz, 1H), 7.51 (app. td, *J* = 7.5, 1.3 Hz, 1H), 7.44 (app.td, *J* = 7.5, 1.4 Hz, 1H), 6.47 (s, 2H), 3.84 (s, 6H), 3.82 (s, 3H), 3.30 (t, *J* = 7.6 Hz, 2H), 3.02 (t, *J* = 7.6 Hz, 2H), 0.29 (s, 9H). **^{13}C {^1H} NMR (100 MHz, $CDCl_3$):** δ 201.7, 153.4, 142.7, 142.2, 137.2, 136.5, 136.2, 131.7, 128.9, 105.6, 61.0, 56.2, 41.4, 31.0, 0.51. *1 × C_{Ar} not observed.* **ν_{max}(neat)/cm^{-1}:** 2938, 2838, 1680, 1587, 1459, 1282, 1129, 1007, 835, 748. **HRMS** calcd. for $C_{21}H_{28}O_4Si$**:** 372.1751 [M]$^+$; found (EI$^+$): 372.1738. **m.p. /°C:** 61-62

1-[5-Chloro-2-(trimethylsilyl)phenyl]-3-(3,4,5-trimethoxyphenyl)propan-1-ol, 5l

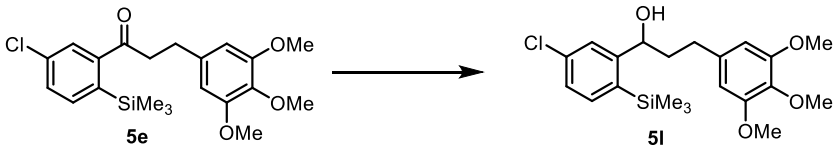

$NaBH_4$ (56 mg, 1.47 mmol) was added portionwise to a solution of **5e** (199 mg, 0.49 mmol) in methanol and THF (9:1, 10 mL) at 0 °C. The reaction was stirred at this temperature for 10 min then allowed to warm to room temperature and stirred for 4 h. The reaction was quenched with a saturated aqueous solution of NH_4Cl (10 mL) and then extracted with Et_2O (3 × 20 mL).

The combined organic portions were dried ($MgSO_4$), filtered, concentrated *in vacuo*. Purification via flash column chromatography (20% EtOAc in hexanes) afforded the title compound as a white solid (190 mg, 0.46 mmol, 94%). Repetition of this reaction on a 5 mmol scale afforded **5l** in a 74% yield.

^{1}H NMR (400 MHz, $CDCl_3$): δ 7.56 (d, *J* = 2.1 Hz, 1H), 7.37 (d, *J* = 8.0 Hz, 1H), 7.22 (dd, *J* = 8.0, 2.1 Hz, 1H), 6.45 (s, 2H), 4.86 (dd, *J* = 9.9, 3.1 Hz, 1H), 3.84 (s, 6H), 3.82 (s, 3H), 2.88 (ddd, *J* = 13.6, 8.9, 4.8 Hz, 1H), 2.73 (app. dt, *J* = 13.6, 8.2 Hz, 1H), 2.21 – 2.07 (m, 1H), 1.94 – 1.73 (m, 2H), 0.21 (s, 9H). **^{13}C {^{1}H} NMR (100 MHz, $CDCl_3$):** δ 153.4, 152.5, 137.4, 136.5, 136.3, 136.0, 135.7, 127.4, 126.2, 105.8, 72.0, 61.0, 56.2, 40.7, 33.0, 0.51. **ν_{max}(neat)/cm^{-1}:** 3501, 2940, 2824, 1593, 1422, 1244, 1123, 1060, 1006, 961, 839, 803, 720. **HRMS** calcd. for $C_{21}H_{29}O_4ClSi$: 408.1518 $[M]^+$; found (EI^+): 408.1512. **m.p. /°C:** 137-139

3-(3,4,5-Trimethoxyphenyl)-1-[2-(trimethylsilyl)phenyl]propan-1-ol, 5g

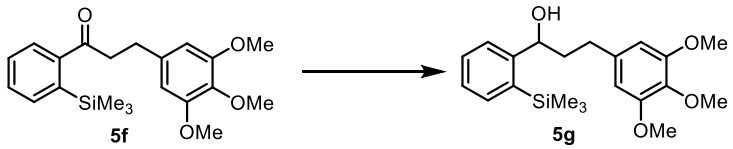

$NaBH_4$ (0.17 g, 4.45 mmol) was added portionwise to a solution of **5f** (0.83 g, 2.22 mmol) in methanol (30 mL) at 0 °C. The reaction was stirred at this temperature for 10 min then allowed to warm to room temperature and stirred for 5 h. The reaction was quenched with a saturated aqueous solution of NH_4Cl (30 mL) and then extracted with Et_2O (3 × 50 mL). The combined organic portions were dried ($MgSO_4$), filtered and concentrated *in vacuo*. Purification *via* flash column chromatography (20% EtOAc in hexanes) afforded the title compound as a white solid (0.73 g, 1.96 mmol, 88%).

^{1}H NMR (400 MHz, $CDCl_3$): δ 7.57 (app. d, *J* = 7.8, 1H), 7.46 (dd, *J* = 7.5, 1.3 Hz, 1H), 7.40 (app. td, *J* = 7.5, 1.3 Hz, 1H), 7.25 (app. td, *J* = 7.5, 1.0 Hz, 1H), 6.45 (s, 2H), 4.88 (dd, *J* = 9.8, 3.2 Hz, 1H), 3.83 (s, 6H), 3.81 (s, 3H), 2.87 (ddd, *J* = 13.7, 9.1, 4.7 Hz, 1H), 2.72 (app. dt, *J* = 13.7, 8.3 Hz, 1H), 2.22 – 2.12 (m, 1H), 1.88 (dddd, *J* = 14.0, 9.1, 8.0, 3.2 Hz, 1H), 1.74 (s, 1H), 0.23 (s, 9H). **^{13}C {^{1}H} NMR (100 MHz, $CDCl_3$):** δ 153.3, 150.5, 137.7, 137.6, 136.4, 134.6, 130.0, 127.3, 125.8, 105.7, 72.4, 61.0, 56.2, 40.6, 33.1, 0.62. **ν_{max}(neat)/cm^{-1}:** 3506, 2932, 2834, 1590, 1508, 1419, 1239, 1127, 1059, 998, 826, 760, 730. **HRMS** calcd. for $C_{21}H_{30}O_4Si$: 374.1908 $[M]^+$; found (EI^+): 374.1890. **m.p. /°C:** 82-85

{4-Chloro-2-[1-(methoxymethoxy)-3-(3,4,5-trimethoxyphenyl)propyl]phenyl}(trimethyl)silane, 5m

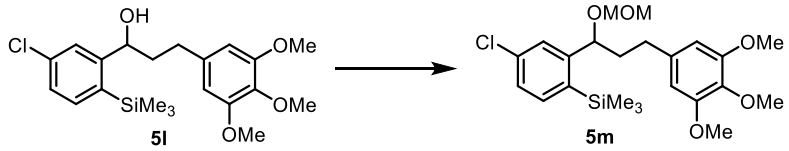

MOMBr (132 µL, 1.63 mmol) was added to a solution of **5l** (167 mg, 0.41 mmol), DIPEA (1.2 mL, 6.89 mmol) and DMAP (12.2 mg, 0.10 mmol) in CH_2Cl_2 (4.7 mL) at 0 °C. The reaction was heated to reflux (70 °C) and was stirred overnight. The reaction was allowed to cool to room temperature then a saturated aqueous solution of $NaHCO_3$ (10 mL) was added slowly and the mixture was left to stir for 30 min. The aqueous phase was separated and extracted with CH_2Cl_2 (3 × 15 mL), and the combined organic portions were dried ($MgSO_4$), filtered and concentrated *in vacuo*. Purification *via* flash column chromatography (20% EtOAc in hexanes) afforded the title compound as a white solid (159 mg, 0.35 mmol, 85%).

^{1}H NMR (400 MHz, $CDCl_3$): δ 7.51 (d, *J* = 2.2 Hz, 1H), 7.37 (d, *J* = 8.0 Hz, 1H), 7.20 (dd, *J* = 8.0, 2.2 Hz, 1H), 6.44 (s, 2H), 4.86 (dd, *J* = 10.4, 2.3 Hz, 1H), 4.52 (app. q, *J* = 6.8 Hz, 2H), 3.84 (s, 6H), 3.81 (s, 3H), 3.45 (s, 3H), 3.02 – 2.89 (m, 1H), 2.73 (ddd, *J* = 13.5, 9.5, 6.7 Hz, 1H), 2.09 – 1.94 (m, 1H), 1.77 (dddd, *J* = 14.2, 9.5, 6.7, 2.3 Hz, 1H), 0.26 (s, 9H). **^{13}C {^{1}H} NMR (100 MHz, $CDCl_3$):** δ 153.4, 151.1, 137.7, 136.4, 136.1, 135.9, 135.8, 127.2, 126.4, 105.7, 94.4, 76.0, 61.0, 56.2, 55.9, 41.7, 33.4, 0.34. **ν_{max}(neat)/cm^{-1}:** 2924, 2839, 1589, 1420, 1241, 1130, 1079, 1016, 935, 836, 720. **HRMS** calcd. for $C_{23}H_{33}O_5ClSi$: 452.1780 $[M]^+$; found (EI^+): 452.1806. **m.p. /°C:** 72-73

{2-[1-(Methoxymethoxy)-3-(3,4,5-trimethoxyphenyl)propyl]phenyl}(trimethyl)silane, 5k

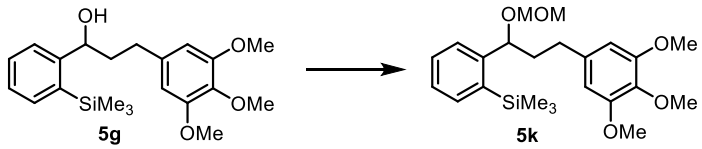

MOMBr (314 µL, 3.84 mmol) was added dropwise to a solution of **5g** (0.48 g, 1.28 mmol), DIPEA (1.9 ml, 10.91 mmol) and DMAP (39 mg, 0.32 mmol) in CH_2Cl_2 (6 mL). The reaction was heated to reflux (70 °C) and was stirred for 8 h. The reaction was allowed to cool to room temperature then a saturated aqueous solution of $NaHCO_3$ (10 mL) was added slowly and the mixture was left to stir for 30 min. The aqueous phase was separated and extracted with CH_2Cl_2 (3 × 15 mL), and the combined organic portions were dried ($MgSO_4$), filtered and concentrated

in vacuo. Purification *via* flash column chromatography (20% EtOAc in hexanes) afforded the title compound as a viscous oil that solidified on standing (0.36 g, 0.86 mmol, 67%).

^{1}H NMR (400 MHz, $CDCl_3$): δ 7.53 (dd, *J* = 7.8, 1.2 Hz, 1H), 7.46 (dd, *J* = 7.5, 1.2 Hz, 1H), 7.38 (app. td, *J* = 7.5, 1.2 Hz, 1H), 7.24 (app.td, *J* = 7.5, 1.2 Hz, 1H), 6.45 (s, 2H), 4.90 (dd, *J* = 10.4, 2.3 Hz, 1H), 4.54 – 4.51 (m, 2H), 3.84 (s, 6H), 3.81 (s, 3H), 3.46 (s, 3H), 2.96 (ddd, *J* = 13.6, 10.1, 4.9 Hz, 1H), 2.75 (ddd, *J* = 13.6, 9.7, 6.7 Hz, 1H), 2.12 – 2.00 (m, 1H), 1.81 (dddd, *J* = 14.2, 10.1, 6.7, 2.3 Hz, 1H), 0.27 (s, 9H). **^{13}C {^{1}H} NMR (100 MHz, $CDCl_3$):** δ 153.3, 148.8, 137.9, 137.7, 136.3, 134.4, 129.7, 127.0, 126.2, 105.7, 94.2, 76.5, 61.0, 56.2, 55.9, 41.7, 33.6, 0.47. **ν_{max}(neat)/cm^{-1}:** 2996, 2955, 2820, 1598, 1508, 1456, 1417, 1240, 1124, 1091, 1014, 837, 767, 731. **HRMS** calcd. for $C_{23}H_{34}O_5Si$: 418.2170 $[M]^+$; found (EI^+): 418.2165. **m.p. /°C:** 73-74.

2-[1-Methoxy-3-(3,4,5-trimethoxyphenyl)propyl]phenyltrimethylsilane, 5h

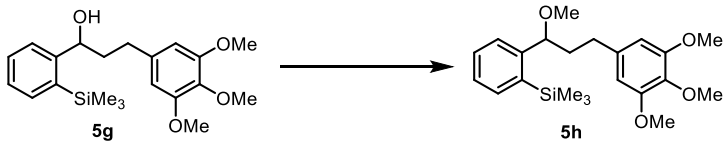

To a solution of **5g** (0.53 g, 1.41 mmol) and Proton-sponge® (0.91 g, 4.23 mmol) in CH_2Cl_2 (8 ml) was added trimethyloxonium tetrafluoroborate (0.63 g, 4.23 mmol) portionwise. The suspension was stirred rapidly at room temperature for 16 h. Water (10 ml) was added slowly and the aqueous phase was separated and extracted with CH_2Cl_2 (3 × 15 mL), and the combined organic portions were dried ($MgSO_4$), filtered and concentrated *in vacuo*. Purification *via* flash column chromatography (20% EtOAc in hexanes) afforded the title compound as a white solid (458 mg, 1.18 mmol, 84%).

^{1}H NMR (400 MHz, $CDCl_3$): δ 7.55 – 7.44 (m, 2H), 7.40 (app. td, *J* = 7.5, 1.5 Hz, 1H), 7.25 (app. td, *J* = 7.5, 1.3 Hz, 1H), 6.44 (s, 2H), 4.40 (dd, *J* = 10.2, 2.6 Hz, 1H), 3.84 (s, 6H), 3.82 (s, 3H), 3.22 (s, 3H), 2.92 – 2.85 (m, 1H), 2.82 – 2.73 (m, 1H), 2.04 – 1.94 (m, 1H), 1.85 – 1.70 (m, 1H), 0.24 (s, 9H). **^{13}C {^{1}H} NMR (100 MHz, $CDCl_3$):** δ 153.3, 148.8, 137.8, 137.7, 136.4, 134.4, 129.8, 126.9, 125.8, 105.8, 81.0, 61.0, 56.4, 56.2, 41.4, 33.2, 0.87. **ν_{max}(neat)/cm^{-1}:** 3059, 2932, 1587, 1494, 1460, 1417, 1335, 1249, 1235, 1120, 1101, 1004, 928, 828, 759, 728. **HRMS** calcd. for $C_{22}H_{32}O_4Si$: 388.2064 $[M]^+$; found (EI^+): 388.2078. **m.p. /°C:** 71-72.

1,2,3-Trimethoxy-7-methoxymethoxy-6,7-dihydro-5*H*-dibenzo[*a*,*c*]cycloheptene, 6k

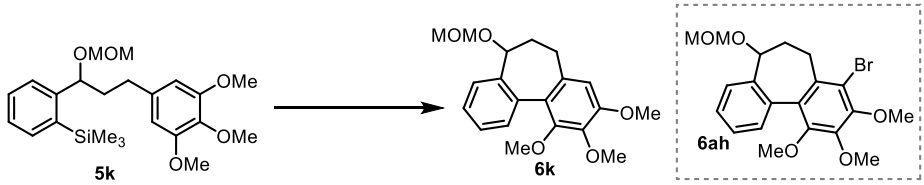

thtAuBr$_3$ (13.12 mg, 0.025 mmol, 5 mol%) was added to a 20 mL vial containing **5k** (209 mg, 0.50 mmol) in $CHCl_3$ (5 mL) and MeOH (100 μL). PIFA (258 mg, 0.60 mmol) was added, and the reaction was stirred at 27 °C for 2.5 h. The reaction mixture was concentrated *in vacuo* and purification by flash column chromatography (dry-loaded onto silica-gel, 5 – 15% EtOAc in hexanes) afforded, in order of elution, **6ah** (20 mg, 0.047 mmol, 9%, 14:1 mixture of atropisomers,[44] see section 8.5.7) and the title compound as a viscous liquid (129 mg, 0.38 mmol, 75%, 16.5:1 mixture of atropisomers).

Characterisation data were consistent with literature values: ^{1}H NMR, ^{13}C {^{1}H} NMR and IR.[45]

Data for **6k**: ^{1}H **NMR (400 MHz, $CDCl_3$)** (Major atropisomer): δ 7.63 – 7.55 (m, 1H), 7.48 – 7.43 (m, 1H), 7.39 – 7.30 (m, 2H), 6.58 (s, 1H), 4.67 (d, *J* = 6.6 Hz, 1H), 4.57 (d, *J* = 6.6 Hz, 1H), 4.50 (dd, *J* = 10.8, 7.2 Hz, 1H), 3.92 (s, 3H), 3.91 (s, 3H), 3.61 (s, 3H), 3.35 (s, 3H), 2.62 – 2.37 (m, 2H), 2.35 – 2.22 (m, 1H), 1.97 (dddd, *J* = 12.0, 10.8, 7.4, 1.3 Hz, 1H). Minor atropisomer (select peaks): 6.59 (s, 1H), 4.26 (d, *J* = 6.6 Hz, 1H), 4.12 (d, *J* = 6.6 Hz, 1H), 3.90 (s, 3H), 3.89 (s, 3H), 3.57 (s, 3H), 3.20 (s, 3H). **^{13}C {^{1}H} NMR (100 MHz, $CDCl_3$)** (Major atropisomer): δ 152.7, 150.9, 141.0, 139.4, 135.5, 133.7, 129.8, 127.1, 126.4, 124.6, 123.1, 107.6, 95.3, 74.4, 61.1, 60.9, 56.0, 55.5, 40.0, 30.4. Minor atropisomer (Select peaks): 152.1, 150.7, 140.8, 136.0, 132.0, 129.8, 127.6, 126.6, 107.4, 93.0, 61.0, 60.6, 55.8, 55.1, 40.4. **LRMS** (EI^+): 344.2 ([M^+], 100%). **ν_{max}(neat)/cm^{-1}:** 2934, 1598, 1482, 1236, 1032, 917, 764, 748.

Data for **6ah**: **^{1}H NMR (400 MHz, $CDCl_3$)** (Major atropisomer): δ 7.66 – 7.54 (m, 1H), 7.48 – 7.31 (m, 3H), 4.69 (d, *J* = 6.7 Hz, 1H), 4.58 (d, *J* = 6.7 Hz, 1H), 4.41 (dd, *J* = 10.7, 7.3 Hz, 1H), 3.97 (s, 3H), 3.96 (s, 3H), 3.56 (s, 3H), 3.36 (s, 3H), 3.19 – 3.09 (m, 1H), 2.52 (dddd, *J* = 13.4, 12.3, 7.4, 6.0 Hz, 1H), 2.10 (app. td, *J* = 13.4, 7.0 Hz, 1H), 1.89 (dddd, *J* = 12.3, 10.7, 7.0, 1.5 Hz, 1H). (Minor atropisomer, selected peaks): δ 4.26 (d, *J* = 6.6 Hz, 1H), 4.12 (d, *J* = 6.6 Hz, 1H), 3.52 (s, 3H), 3.19 (s, 3H). **^{13}C {^{1}H} NMR (100 MHz, $CDCl_3$)** (Major atropisomer)**:** δ 150.6, 150.3, 146.2, 139.6, 134.8, 133.2, 129.9, 129.2, 128.0, 126.6, 123.3, 113.8, 95.5, 74.4, 61.4, 61.1, 61.0, 55.7, 38.4, 29.6. **ν_{max}(neat)/cm^{-1}:** 2934, 1463, 1397, 1316,

1147, 1079, 1034, 995, 918, 756. **HRMS** calcd. for $C_{20}H_{23}O_5Br$: 422.0723 $[M]^+$; found (EI^+): 422.0730.

1,2,3,7-Tetramethoxy-5,6-dihydro-5*H*-dibenzo[*a,c*]cycloheptene, 6h

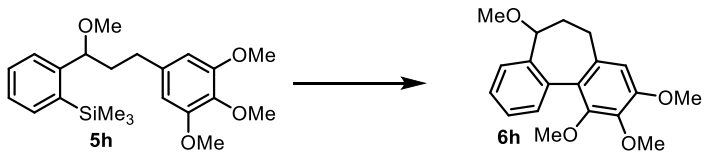

To a 7 mL screw-cap borosilicate vial containing **5h** (38.9 mg, 0.10 mmol) was added $CDCl_3$ (500 μL), CD_3OD (20 μL) and thtAuBr$_3$ (0.005 mmol, 500 μL of a 0.01 M stock solution in $CDCl_3$). Dichloromethane (9.3 mg, 7 μL, 0.11 mmol) was also added as an internal standard for ^{1}H NMR. PIFA was added to the vial, which was then sealed and shaken vigorously until all the contents had dissolved. After 1.5 h an NMR yield of 85% was determined by comparison to literature ^{1}H NMR values.[46] Isolation of the product by preparative TLC (20% EtOAc in hexanes) confirmed the identity of **6h** (13:1 mixture of atropisomers).

^{1}H NMR (400 MHz, $CDCl_3$) (Major atropisomer): δ 7.56 – 7.51 (m, 1H), 7.47 (dd, *J* = 7.3, 1.4 Hz, 1H), 7.42 – 7.31 (m, 2H), 6.59 (s, 1H), 4.04 (dd, *J* = 10.8, 7.1 Hz, 1H), 3.92 (s, 3H), 3.91 (s, 3H), 3.64 (s, 3H), 3.33 (s, 3H), 2.61 – 2.46 (m, 1H), 2.46 – 2.36 (m, 1H), 2.34 – 2.19 (m, 1H), 1.98 – 1.82 (m, 1H). (Minor atropisomer, selected peaks): δ 6.57 (s, 1H), 3.88 (s, 3H), 3.63 (s, 3H), 2.90 (s, 3H). **^{13}C {^{1}H} NMR (100 MHz, $CDCl_3$)** (Major atropisomer): δ 152.8, 150.9, 141.2, 139.2, 135.8, 134.1, 130.0, 127.3, 126.5, 124.8, 123.0, 107.7, 79.6, 61.3, 61.0, 57.8, 56.2, 39.7, 30.4. **LRMS** (EI^+): 314.1 ($[M^+]$, 100%)

9-Chloro-1,2,3-trimethoxy-7-(methoxymethoxy)-6,7-dihydro-5*H*-dibenzo[*a,c*]cyclo-heptene, 6m

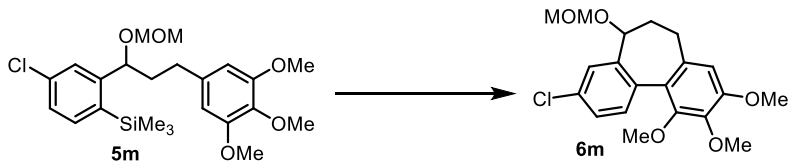

thtAuBr$_3$ (28.96 mg, 0.055 mmol, 5 mol%) was added to a 20 mL RBF containing **5m** (500 mg, 1.10 mmol) in $CHCl_3$ (11 mL) and MeOH (216 μL). PIFA (568 mg, 1.32 mmol) was added in a single portion, and the reaction was stirred at room temperature for 5 h. The reaction mixture was filtered through a plug of silica gel and concentrated *in vacuo*. Purification by flash column chromatography (dry-loaded onto silica-gel, 20% EtOAc in hexanes) gave, in order of elution, recovered starting material (120 mg, 0.26 mmol, 24%), and the title

compound as a viscous pale yellow liquid (233 mg, 0.62 mmol, 56%, 23:1 mixture of atropisomers).

^{1}H NMR (400 MHz, $CDCl_3$) (Major atropisomer): δ 7.58 (dd, *J* = 2.2, 0.7 Hz, 1H), 7.39 (d, *J* = 8.2 Hz, 1H), 7.34 – 7.26 (m, 1H), 6.57 (s, 1H), 4.67 (d, *J* = 6.7 Hz, 1H), 4.55 (d, *J* = 6.7 Hz, 1H), 4.44 (dd, *J* = 10.7, 7.2 Hz, 1H), 3.91 (s, 6H), 3.61 (s,3H), 3.34 (s, 3H), 2.60 – 2.38 (m, 2H), 2.34 – 2.20 (m, 1H), 2.03 – 1.89 (m, 1H). (Minor atropisomer, tentatively assigned, selected peaks): δ 7.50 (d, *J* = 8.2 Hz, 1H), 4.28 (d, *J* = 6.6 Hz, 1H), 3.86 (s, 3H), 3.60 (s, 3H), 3.22 (s, 3H). **^{13}C {^{1}H} NMR (100 MHz, $CDCl_3$)** (Major atropisomer): δ 153.1, 150.9, 141.7, 141.2, 135.5, 133.2, 132.2, 131.4, 126.7, 123.7, 123.7, 107.8, 95.5, 74.2, 61.2, 61.1, 56.2, 55.7, 39.9, 30.3. **HRMS** calcd. for $C_{20}H_{23}O_5Cl$: 378.1229 $[M]^+$; found (EI^+): 378.1220. **ν_{max}(neat)/cm^{-1}:** 2936, 1596, 1455, 1398, 1236, 1146, 1034, 997, 918, 833, 819, 730.

9,10,11-Trimethoxy-5-methoxymethoxy-6,7-dihydro-5*H*-dibenzo[*a,c*]cycloheptene-3-carboxylic acid methyl ester 85

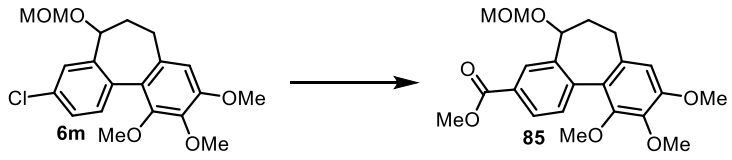

Caution: Carbon monoxide is a highly toxic gas and must be used within a well-ventilated fume hood and an alarm fitted for leak detection.

According to literature procedure,[47] potassium carbonate (54 mg, 0.39 mmol) and molecular sieves (4Å, 50 mg, powdered) were added to a Schlenk tube containing a stir bar. The tube was sealed with a septum, evacuated, and the contents were heated using a blow torch for 2 min. The tube was cooled to room temperature under vacuum and then refilled with nitrogen. The septum was briefly removed, and palladium acetate (2.37 mg, 0.011 mmol) and dcpp•2HBF_4 (12.7 mg, 0.021 mmol) were added to the tube, followed by **6m** (100 mg, 0.26 mmol) and the contents were evacuated and backfilled with nitrogen once more. DMSO (0.9 mL) was then added via syringe. A double-lined balloon of CO was fitted and bubbled through the solution, a second balloon was then fitted and the reaction mixture was lowered into an oil bath at 120 °C and stirred rapidly for 16 h. The balloon was removed and purged with nitrogen and the tube was removed from the oil bath and allowed to cooled to room temperature. The reaction mixture was filtered through a pad of Celite and washed with ethyl acetate. The solvent was removed *in vacuo*, then dissolved in CH_2Cl_2 and dry loaded onto Celite. Purification by flash column chromatography (20 – 40% EtOAc in hexanes) afforded the title

compound as a viscous pale yellow oil (73 mg, 0.18 mmol, 70%, 15:1 mixture of atropisomers).

Characterisation data were consistent with literature values for major and minor atropisomers.[45]

^{1}H NMR (400 MHz, $CDCl_3$) (Major atropisomer): 8.28 (d, *J* = 1.8 Hz, 1H), 8.00 (dd, *J* = 8.0, 1.8 Hz, 1H), 7.53 (d, *J* = 8.0 Hz, 1H). 6.58 (s, 1H), 4.70 (d, *J* = 6.7 Hz, 1H), 4.56 (d, *J* = 6.7 Hz, 1H), 4.50 (dd, *J* = 10.7, 7.2 Hz, 1H), 3.94 (s, 3H), 3.91 (s, 6H), 3.61 (s, 3H), 3.35 (s, 3H), 2.65 – 2.46 (m, 1H), 2.48 – 2.37 (m, 1H), 2.30 – 2.15 (m, 1H), 2.06 – 1.92 (m, 1H). (Minor atropisomer, selected peaks): 7.92 (d, *J* = 1.9 Hz, 1H), 7.61 (d, *J* = 8.0 Hz, 1H), 4.83 (d, *J* = 6.0 Hz, 1H), 3.57 (s, 3H), 3.19 (s, 3H). **^{13}C {^{1}H} NMR (100 MHz, $CDCl_3$)** (Major atropisomer)**:** 167.4, 153.4, 151.1, 141.2, 140.0, 138.9, 135.6, 130.2, 128.9, 127.8, 124.8, 123.8, 107.9, 95.6, 74.3, 61.2, 61.1, 56.2, 55.7, 52.2, 39.9, 30.4. **HRMS** calcd. for $C_{22}H_{26}O_7$: 402.1673[M]$^+$; found (EI$^+$): 402.1671. **ν_{max}(neat)/cm^{-1}:** 2938, 1717, 1595, 1484, 1400, 1229, 1146, 1100, 1035, 917, 734.

8.5 Domino Arylation

8.5.1 General Procedure for Domino C–H Arylation

A 50 mL, round-bottomed flask equipped with a stirrer bar was charged with arylsilane **1** (1.00 mmol), arylsilane **12** (1.00 mmol), thtAuBr$_3$ (15.8 mg, 0.03 mmol), MeOH (200 μL), and $CHCl_3$ (20 mL). PhI(OAc)$_2$ (741 mg, 2.30 mmol) and CSA (581 mg, 2.30 mmol) were added simultaneously in a single portion, and the flask was sealed with a glass stopper and stirred at rt (unless otherwise indicated) for the time specified. Following analysis of the crude product mixture by ^{19}F NMR, the reaction was concentrated *in vacuo* and then purified as specified.

2-Chloro-7-(4-fluorophenyl)-9*H*-fluorene, 133a

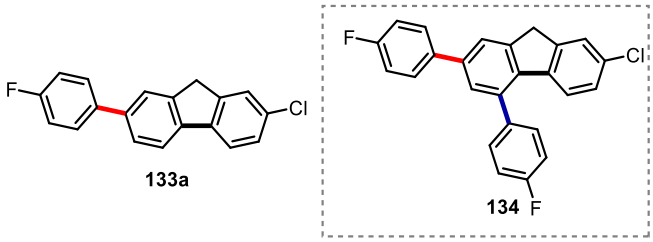

Following the **General Procedure for Domino C–H Arylation**, **2l** (275 mg, 1.00 mmol) and **12a** (168 mg, 1.00 mmol) were reacted for 15 h. Purification *via* flash column chromatography (SiO_2, 99:1 40–60 °C petrol/EtOAc) gave an 80:20 mixture of **133a**:**134** (186 mg). To effect further purification *via* recrystallisation, the mixture was taken up in boiling EtOH (8 mL) and

EtOAc (ca. 1 mL) was added dropwise until complete dissolution. The solution was allowed to cool to rt over 1 h, during which time colourless crystals formed. The crystals were collected by Buchner filtration and washed with cold EtOH, then dried *in vacuo* to give **133a** as a white crystalline solid (88 mg, 30%).

Data for **133a**: **^{1}H NMR (400 MHz, $CDCl_3$)**: δ 7.79 (d, *J* = 7.9 Hz, 1H), 7.73–7.68 (m, 2H), 7.63–7.51 (m, 4H), 7.37 (dd, *J* = 8.1, 2.1 Hz, 1H), 7.19–7.11 (m, 2H), 3.93 (s, 2H). **^{13}C {^{1}H} NMR (100 MHz, $CDCl_3$):** 162.6 (d, *J* = 246 Hz), 145.2, 143.9, 140.03, 140.01, 139.4, 137.6 (d, *J* = 3.4 Hz), 132.7, 128.8 (d, *J* = 8.0 Hz), 127.4, 126.2, 125.5, 123.9, 121.0, 120.4, 115.8 (d, *J* = 21.4 Hz), 37.0. **^{19}F NMR (376 MHz, $CDCl_3$):** –115.8 (tt, *J* = 8.6, 5.3 Hz). **ν_{max}(neat)/cm^{-1}:** 3066, 2928, 1599, 1514, 1457, 1400, 1239, 1224, 1159, 1102, 1071, 830, 811, 753. **HRMS** calcd. for $C_{19}H_{12}ClF$: 294.0606 $[M]^+$; found (EI^+): 294.0620. **m.p. /°C:** 173 – 175 (EtOH/EtOAc).

Data for **134** (Select Data; tentatively assigned): **^{1}H NMR (400 MHz, $CDCl_3$)**: δ 7.25 – 7.18 (m, 2H), 7.18 – 7.09 (m, 2H), 7.07 (dd, *J* = 8.4, 2.0 Hz, 1H), 6.85 (d, *J* = 8.4 Hz, 1H), 3.99 (s, 2H). **^{19}F NMR (376 MHz, $CDCl_3$):**–114.4 (tt, *J* = 8.7, 5.4 Hz), –115.4 (tt, *J* = 8.6, 5.3 Hz)

7-Fluoro-1,4-dimethyl-2-phenyl-9*H*-fluorene, 135-F-H

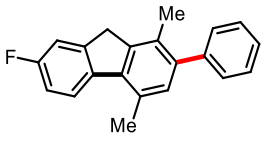

135-F-H

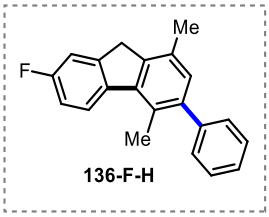

136-F-H

Following General Procedure 1, **1o** (286 mg, 1.00 mmol) and **12c** (150 mg, 1.00 mmol) were reacted for 15 h. Purification *via* flash column chromatography (SiO_2, 90:10 40–60 °C petrol/toluene) gave a 94:6 mixture of **135-F-H**:**136-F-H** as a white solid (185 mg, 64%).

Data for **135-F-H**: **^{1}H NMR (400 MHz, $CDCl_3$)**: δ 7.86 (dd, *J* = 8.5, 5.1 Hz, 1H), 7.50 – 7.42 (m, 2H), 7.41 – 7.34 (m, 3H), 7.34 – 7.25 (m, 1H), 7.15 – 7.08 (m, 2H), 3.83 (s, 2H), 2.71 (s, 3H), 2.32 (s, 3H). **^{13}C {^{1}H} NMR (100 MHz, $CDCl_3$):** δ 161.9 (d, *J* = 245 Hz), 146.1 (d, *J* = 8.5 Hz), 143.2 (d, *J* = 2.0 Hz), 142.0, 140.2, 139.1 (d, *J* = 2.4 Hz), 137.9, 131.5, 129.7, 129.6, 129.0, 128.2, 126.8, 123.8 (d, *J* = 8.6 Hz), 113.8 (d, *J* = 22.4 Hz), 112.3 (d, *J* = 22.6 Hz), 36.9 (d, *J* = 2.4 Hz), 20.6, 16.6. **^{19}F NMR (376 MHz, $CDCl_3$):** δ -116.78 (m). **ν_{max}(neat)/cm^{-1}:** 2914, 2862, 1592, 1464, 1439, 1227, 1127, 1106, 1013, 938, 852, 771, 703. **HRMS** calcd. for $C_{21}H_{17}F$: 288.1309 $[M]^+$; found (EI^+): 288.1297.

Selected data for **136-F-H**: **^{1}H NMR (400 MHz, $CDCl_3$)**: δ 7.94 (dd, *J* = 8.6, 5.1 Hz, 1H), 2.58 (s, 3H), 2.42 (s, 3H).

2-(4-Bromophenyl)-7-fluoro-1,4-dimethyl-9*H*-fluorene, 135-F-Br

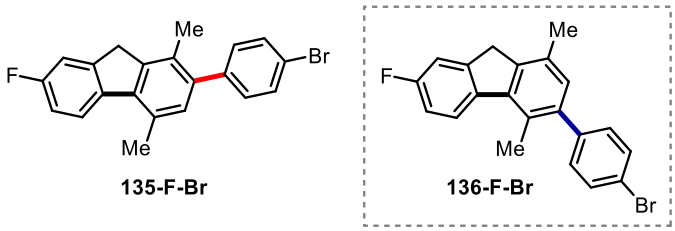

Following General Procedure 1, **1o** (286 mg, 1.00 mmol) and **12d** (229 mg, 1.00 mmol) were reacted for 15 h. Purification *via* flash column chromatography (SiO_2, 90:10 40–60 °C petrol/toluene) gave a 94:6 mixture of **135-F-Br**:**136-F-br** as a white solid (260 mg, 71%).

^{1}H NMR (400 MHz, $CDCl_3$): δ 7.86 (dd, *J* = 8.5, 5.1 Hz, 1H), 7.60 – 7.51 (m, 2H), 7.34 – 7.21 (m, 3H), 7.11 (app. td, *J* = 8.9, 2.6 Hz, 1H), 7.05 (s, 1H), 3.83 (s, 2H), 2.70 (s, 3H), 2.29 (s, 3H). **^{13}C {^{1}H} NMR (100 MHz, $CDCl_3$):** δ 162.0 (d, *J* = 245 Hz), 146.1 (d, *J* = 8.6 Hz), 143.3 (d, *J* = 2.1 Hz), 140.9, 139.0 (d, *J* = 2.4 Hz), 138.9, 138.2, 131.33, 131.31, 131.2, 129.9, 128.8, 123.9 (d, *J* = 8.7 Hz), 121.0, 113.9 (d, *J* = 22.5 Hz), 112.3 (d, *J* = 22.6 Hz), 36.9 (d, *J* = 2.4 Hz), 20.6, 16.6. **^{19}F NMR (377 MHz, $CDCl_3$):** δ -116.49 (m). **ν_{max}(neat)/cm^{-1}:** 2949, 2915, 2886, 2861, 1587, 1462, 1384, 1230, 1132, 1107, 1070, 1005, 938, 895, 857, 830, 818, 756, 723. **HRMS** calcd. for $C_{21}H_{16}BrF$: 366.0414 $[M]^+$; found (EI^+): 366.0434.

Selected data for **136-F-Br**: **^{1}H NMR (400 MHz, $CDCl_3$)**: δ 7.92 (dd, *J* = 8.6, 5.1 Hz, 1H), 2.55 (s, 3H), 2.41 (s, 3H). **^{19}F NMR (377 MHz, $CDCl_3$):** δ -116.5 (m).

7-Fluoro-1,4-dimethyl-2-[4-(trifluoromethyl)phenyl]-9*H*-fluorene, 135-F-CF_3

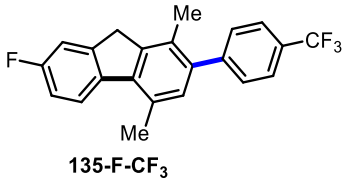

Following General Procedure 1, **1o** (286 mg, 1.00 mmol) and **12b** (218 mg, 1.00 mmol) were reacted for 3 h. Purification *via* flash column chromatography (SiO_2, 99:1 40–60 °C petrol/EtOAc) gave **135-F-CF_3** as a white solid (279 mg, 78%, >99:1 rr).

^{1}H NMR (400 MHz, $CDCl_3$): δ. 7.87 (dd, *J* = 8.6, 5.1 Hz, 1H), 7.70 (d, *J* = 8.0 Hz, 2H), 7.49 (d, *J* = 8.0 Hz, 2H), 7.34 – 7.26 (m, 1H), 7.12 (app. td, *J* = 8.9, 2.6 Hz, 1H), 7.07 (s, 1H), 3.85 (s, 2H), 2.71 (s, 3H), 2.30 (s, 3H). **^{13}C {^{1}H} NMR (100 MHz, $CDCl_3$):** δ 162.1 (d, *J* = 245 Hz), 146.12 (d, *J* = 8.7 Hz), 145.7, 143.4 (d, *J* = 2.0 Hz), 138.9 (d, *J* = 2.4 Hz), 138.7, 138.6, 131.2, 130.00, 129.97, 129.07 (q, *J* = 32.5 Hz), 128.9, 125.2 (q, *J* = 3.8 Hz), 124.5 (q, *J* = 272 Hz), 124.0 (d, *J* = 8.7 Hz), 113.9 (d, *J* = 22.5 Hz), 112.4 (d, *J* = 22.5 Hz), 36.9 (d, *J* = 2.4 Hz), 20.7, 16.6. **^{19}F NMR (377 MHz, $CDCl_3$):** δ – 62.34 (s, 3F), -116.30 (app. td, *J* = 8.9, 5.1 Hz). **ν_{max}(neat)/cm^{-1}:** 2895, 1614, 1466, 1320, 1065, 1013, 841, 819, 759. **HRMS** calcd. for $C_{22}H_{16}F_4$: 356.1183 [M]$^+$; found (EI$^+$): 366.1167. **m.p. /°C:** 189-190 (EtOH).

2-(4-Fluorophenyl)-1,4-dimethyl-9*H*-fluorene, 12-H-F and 2,7-bis(4-fluorophenyl)-1,4-dimethyl-9*H*-fluorene, 22

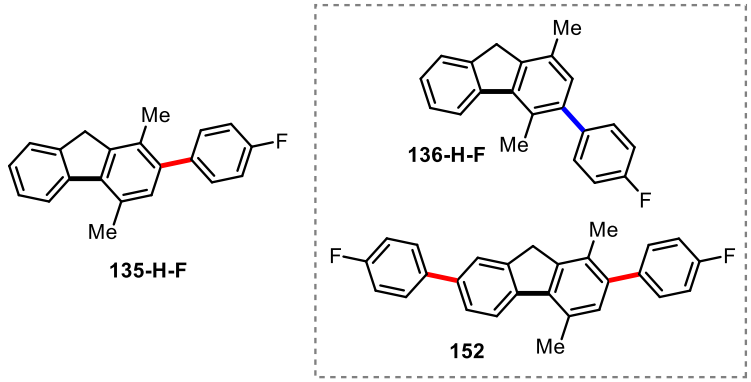

Following General Procedure 1, **1a** (268 mg, 1.00 mmol) and **12a** (168 mg, 1.00 mmol) were reacted for 1 h. Purification *via* flash column chromatography (SiO_2, 99:1 40–60 °C petrol/EtOAc) gave, in order of elution, a 96:4 mixture of **135-H-F**:**136-H-F** as a white solid (133 mg, 46%) and **152** as an off-white solid (73 mg, 17%).

Data for **135-H-F**: **^{1}H NMR (400 MHz, $CDCl_3$)**: δ 7.96 (app. d, *J* = 7.8 Hz, 1H), 7.61 (app. d, *J* = 7.3 Hz, 1H), 7.42 (app. t, *J* = 7.5 Hz, 1H), 7.38 – 7.30 (m, 3H), 7.18 – 7.10 (m, 2H), 7.08 (s, 1H), 3.86 (s, 2H), 2.74 (s, 3H), 2.31 (s, 3H). **^{13}C {^{1}H} NMR (100 MHz, CDCl3):** δ 162.0 (d, *J* = 245 Hz), 143.9, 143.5, 143.0, 139.3, 138.8, 138.0 (d, *J* = 3.5 Hz), 131.3, 131.1 (d, *J* = 7.9 Hz), 130.3, 128.9, 126.8, 126.1, 125.0, 123.1, 115.0 (d, *J* = 21 Hz), 36.9, 20.8, 16.6. **^{19}F NMR (376 MHz, CDCl3):** δ -116.33 (tt, J = 8.8, 5.5 Hz). **ν_{max}(neat)/cm^{-1}:** 3067, 3042, 2948, 2865, 1601, 1509, 1455, 1384, 1219, 1156, 1094, 1010, 838, 807, 774, 741, 707. **HRMS** calcd. for $C_{21}H_{17}F$: 288.1309 [M]$^+$; found (EI$^+$): 288.1307 **m.p. /°C:** 138-140 (EtOH).

Selected data for **136-H-F**: **^{1}H NMR (400 MHz, $CDCl_3$)**: δ 8.02 (d, J = 7.7 Hz, 1H), 2.60 (s, 3H), 2.43 (s, 3H).

Data for **152**: **^{1}H NMR (400 MHz, CDCl$_3$)**: δ 7.99 (d, *J* = 8.1 Hz, 1H), 7.79 (s, 1H), 7.70 – 7.56 (m, 3H), 7.40 – 7.32 (m, 2H), 7.22 – 7.10 (m, 4H), 7.09 (s, 1H), 3.90 (s, 2H), 2.75 (s, 3H), 2.32 (s, 3H). **^{13}C {^{1}H} NMR (100 MHz, CDCl3):** δ162.4 (d, *J* = 246.4 Hz), 161.9 (d, *J* = 245.6 Hz), 144.6, 143.7, 142.2, 139.4, 138.5, 138.1, 137.9 (d, *J* = 3.3 Hz), 137.6 (d, *J* = 3.2 Hz), 131.4, 131.1 (d, *J* = 7.8 Hz), 130.4, 129.0, 128.8 (d, *J* = 8.0 Hz), 125.8, 123.6, 123.3, 115.8 (d, *J* = 21.4 Hz), 115.1 (d, *J* = 21.2 Hz), 36.9, 20.7, 16.7. **^{19}F NMR (376 MHz, CDCl3):** δ -115.98 (tt, J = 8.6, 5.3 Hz, 1F), -116.25 (tt, J = 8.8, 5.4 Hz, 1F). **ν_{max}(neat)/cm^{-1}:** 2920, 1604, 1511, 1461, 1399, 1386, 1238, 1156, 1097, 1010, 890, 871, 838, 818, 732. **HRMS** calcd. for $C_{27}H_{20}F_2$: 382.1528 [M]$^+$; found (EI$^+$): 382.1508. **m.p. /°C:** 233-236 (EtOAc/EtOH 1:1).

7-Fluoro-2-(4-fluorophenyl)-1,4-dimethyl-9*H*-fluorene, 135-F-F

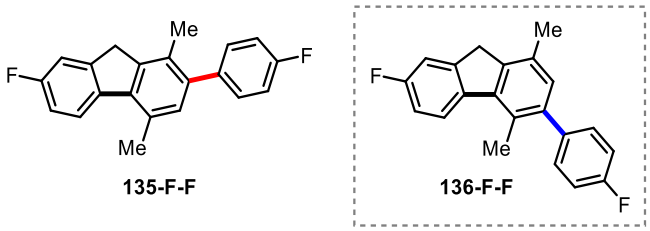

Following General Procedure 1, **1o** (286 mg, 1.00 mmol) and **12a** (168 mg, 1.00 mmol) were reacted for 14 h. Purification *via* flash column chromatography (SiO_2, 99:1 40–60 °C petrol/EtOAc) gave a 95:5 mixture of **135-F-F**:**136-F-F** as a white solid (205 mg, 67%).

Data for **135-F-F**: **^{1}H NMR (400 MHz, CDCl$_3$)**: δ 7.86 (dd, *J* = 8.5, 5.1 Hz, 1H), 7.41 – 7.28 (m, 3H), 7.20 – 7.09 (m, 3H), 7.07 (s, 1H), 3.83 (s, 2H), 2.70 (s, 3H), 2.29 (s, 3H). **^{13}C {^{1}H} NMR (100 MHz, CDCl3):** δ 162.1 (d, *J* = 245 Hz), 161.9 (d, *J* = 245 Hz), 146.1 (d, *J* = 8.4 Hz), 143.2 (d, *J* = 2.0 Hz), 139.1, 139.02 (d, *J* = 2.4 Hz), 138.0, 137.9 (d, *J* = 3.4 Hz), 131.4, 131.12 (d, *J* = 7.9 Hz), 129.8, 129.0, 123.87 (d, *J* = 8.7 Hz), 115.06 (d, *J* = 21.2 Hz), 113.83 (d, *J* = 22.3 Hz), 112.32 (d, *J* = 22.6 Hz), 36.9 (d, *J* = 2.4 Hz), 20.6, 16.6. **^{19}F NMR (376 MHz, CDCl3):** δ -116.22 (tt, J = 8.7, 5.4 Hz), -116.62 (app. td, *J* = 9.0, 5.2 Hz, 1F). **ν_{max}(neat)/cm^{-1}:** 2955, 2920, 2887, 2863, 1604, 1592, 1509, 1479, 1458, 1389, 1274, 1218, 1158, 1130, 1107, 1090, 1013, 936, 881, 841, 815, 776, 728, 708. **HRMS** calcd. for $C_{21}H_{16}F_2$: 306.1215 [M]$^+$; found (EI$^+$): 306.1219. **m.p. /°C:** 163-165 (3% EtOAc in EtOH)

Selected data for **136-F-F**: **^{1}H NMR (400 MHz, CDCl$_3$)**: δ 7.92 (dd, *J* = 8.6, 5.2 Hz, 1H), 2.56 (s, 3H), 2.41 (s, 3H).

7-Chloro-2-(4-fluorophenyl)-1,4-dimethyl-9*H*-fluorene, 135-Cl-F

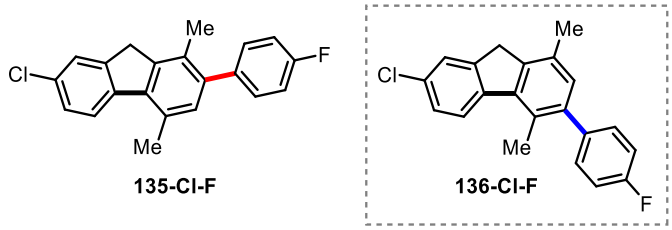

Following General Procedure 1, **1p** (303 mg, 1.00 mmol) and **12a** (168 mg, 1.00 mmol) were reacted for 15 h. Purification *via* flash column chromatography (SiO_2, 100:0→90:10 40–60 °C petrol/toluene) gave a 93:7 mixture of **135-Cl-F**:**136-Cl-F** as an off-white solid (162 mg, 50%).

Data for **135-Cl-F**: **^{1}H NMR (400 MHz, $CDCl_3$)**: δ 7.83 (d, *J* = 8.3 Hz, 1H), 7.57 – 7.54 (m, 1H), 7.37 (dd, *J* = 8.3, 2.0 Hz, 1H), 7.35 – 7.28 (m, 2H), 7.16 – 7.10 (m, 2H), 7.07 (s, 1H), 3.81 (s, 2H), 2.69 (s, 3H), 2.28 (s, 3H). **^{13}C {^{1}H} NMR (100 MHz, $CDCl_3$):** δ 162.0 (d, *J* = 245 Hz), 145.6, 143.3, 141.5, 139.7, 137.85, 137.80 (d, *J* = 3.2 Hz), 132.0, 131.5, 131.1 (d, *J* = 7.9 Hz), 130.3, 129.1, 127.1, 125.3, 123.8, 115.1 (d, *J* = 21.3 Hz), 36.7, 20.6, 16.6. **^{19}F NMR (376 MHz, $CDCl_3$):** δ -116.10 (tt, J = 8.8, 5.4 Hz). **ν_{max}(neat)/cm^{-1}:** 2948, 2918, 2864, 1600, 1510, 1452, 1384, 1223, 1071, 839, 816. **HRMS** calcd. for $C_{21}H_{16}ClF$: 322.0919 $[M]^+$; found (EI^+): 322.0925.

Selected data for **136-Cl-F**: **^{1}H NMR (400 MHz, $CDCl_3$)**: δ 7.89 (d, J = 8.4 Hz, 1H), 2.55 (s, 3H), 2.41 (s, 3H). **^{19}F NMR (376 MHz, $CDCl_3$):** δ -116.19 (tt, J = 8.8, 5.4 Hz)

2-(4-Fluorophenyl)-1,4-dimethyl-7-(trifluoromethyl)-9*H*-fluorene, 12-CF_3-F

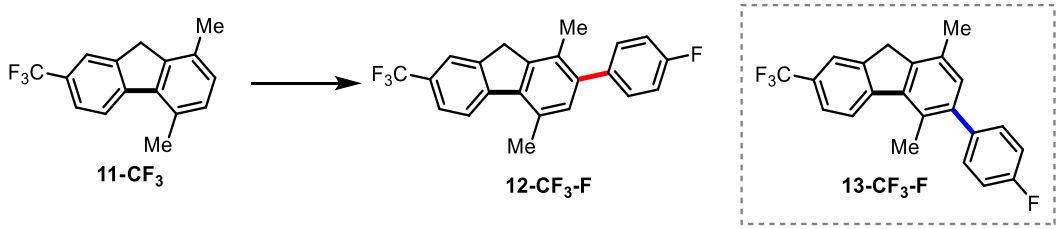

A 7 mL, screw-capped scintillation vial equipped with a stirrer bar was charged with **2ah** (26.2 mg, 0.10 mmol), **12a** (16.8 mg, 0.10 mmol), thtAuBr$_3$ (300 µL of a 0.01 M stock solution in $CDCl_3$, 0.003 mmol), CD_3OD (20 µL), and $CDCl_3$ (1.7 mL). Dibromomethane (18 mg, 7 µL, 0.10 mmol) and 1-bromo-2-fluorobenzene (18 mg, 11 µL, 0.10 mmol) were also added as internal standards for ^{1}H and ^{19}F NMR respectively. CSA (34.9 mg, 0.15 mmol) and $PhI(OAc)_2$ (41.9 mg, 0.13 mmol) were added sequentially, and the vial was sealed and shaken vigorously

until the contents were homogeneous. The mixture was stirred at 50 °C overnight. A combined 70% NMR yield was obtained (88:12 mixture of **135-CF_3-F**:**136-CF_3-F**) after analysis of the reaction mixture by ^{19}F NMR spectroscopy. The mixture was isolated by preparatory TLC (eluent: 99:1 40–60 °C petrol/EtOAc) to give a white solid.

Data for **135-CF_3-F: ^{1}H NMR (400 MHz, $CDCl_3$)**: δ 8.01 (d, *J* = 8.1 Hz, 1H), 7.83 (s, 1H), 7.71 – 7.63 (m, 1H) 7.37 – 7.28 (m, 2H), 7.17 – 7.08 (m, 3H), 3.89 (s, 2H), 2.74 (s, 3H), 2.31 (s, 3H). **^{13}C {^{1}H} NMR (100 MHz, $CDCl_3$):** δ 162.1 (d, *J* = 245 Hz), 146.3, 144.2 (d, *J* = 8.0 Hz), 140.5, 137.7 (d, *J* = 3.3 Hz), 137.5, 131.7, 131.13, 131.10 (d, *J* = 7.9 Hz), 131.05, 129.3, 127.9 (q, *J* = 32.0 Hz), 124.2 (q, *J* = 3.8 Hz), 123.5, 123.0, 121.8 (q, *J* = 4.0 Hz), 115.2 (d, *J* = 21.2 Hz), 36.9, 20.8, 16.7. *1 × C_{Ar} not observed (**CF_3**)*. **^{19}F NMR (377 MHz, $CDCl_3$):** δ –61.74 (s, 3F), –115.62 (tt, J = 8.7, 5.4 Hz, 1F). **HRMS** calcd. for $C_{22}H_{16}F_4$: 356.1183 $[M]^+$; found (EI^+): 356.1179

8.6 Kinetic data: Procedure and Analysis

8.6.1 Standard Kinetics Protocol

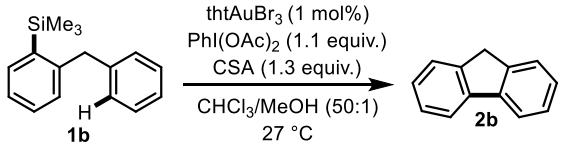

Representative experiment: To a 7 mL screw-cap borosilicate vial containing **1b** (24.0 mg, 0.10 mmol) was added $CDCl_3$ (900 μL), CD_3OD (20 μL) and thtAuBr$_3$ (0.001 mmol, 100 μL of a 0.01 M stock solution in $CDCl_3$). The solution was transferred into a NMR tube and loaded into a Bruker Avance III 400 MHz NMR spectrometer with a probe temperature of 27 °C. After tuning to ^{1}H, locking to $CDCl_3$ and performing a quick shimming experiment (topshim 1Dfast, Bruker software), the sample was ejected and poured back into the vial. CSA (0.13 mmol, 30.2 mg) followed immediately by IBDA (0.11 mmol, 35.4 mg) were added to the vial, which was then sealed and shaken vigorously until all the contents had dissolved. The solution was transferred by a 1 mL syringe back into the NMR tube and loaded into the NMR spectrometer. The kinetics experiment was initiated after locking to $CDCl_3$. The time between addition of IBDA/CSA and the first kinetics time-point was measured by stopwatch and was typically 90 – 120 sec.

General Considerations: $CDCl_3$ was filtered through a pad of basic Al_2O_3 (Brockmann I) and distilled prior to use and held under a nitrogen atmosphere, over 3 Å MS. CD_3OD was transferred from a new bottle into a J Young's tap sealed tube and held under N_2, over 3 Å MS. Stock solutions were prepared by weighing reagents directly into volumetric glassware,

and were stored in sealed vials at 0 °C thereafter. The necessary volume of a stock solution was measured with a gas-tight µL-syringe once the solution had warmed to ambient temperature. IBDA and CSA were weighed to the nearest 0.05 mg. Measured rates varied depending on how wet the CSA was. For reproducibility, the CSA was stored under an inert atmosphere and used within 10 minutes of weighing. Kinetics experiments were implemented using standard Bruker software. Typical experiment: 4 scans per spectrum (20 s), total delay between spectra varied from 10 – 600 s depending on experiment. NMR data were processed using standard *Mestrenova* software, version 6, 8 or 9.

8.6.2 Kinetic Data

Figures 8.3 – 8.8 show reaction profiles (A) and rate/concentration plots (B) for the cyclisation of **1b**. Reactions are performed as per the *standard kinetics procedure*. In each figure, variation of one variable is made from the 'standard' conditions of [thtAuBr$_3$] = 0.001 M, [**1b**] = 0.10 M, [IBDA] = 0.11 M, [CSA] = 0.13 M, [CD_3OD] = 0.49 M, 27 °C.

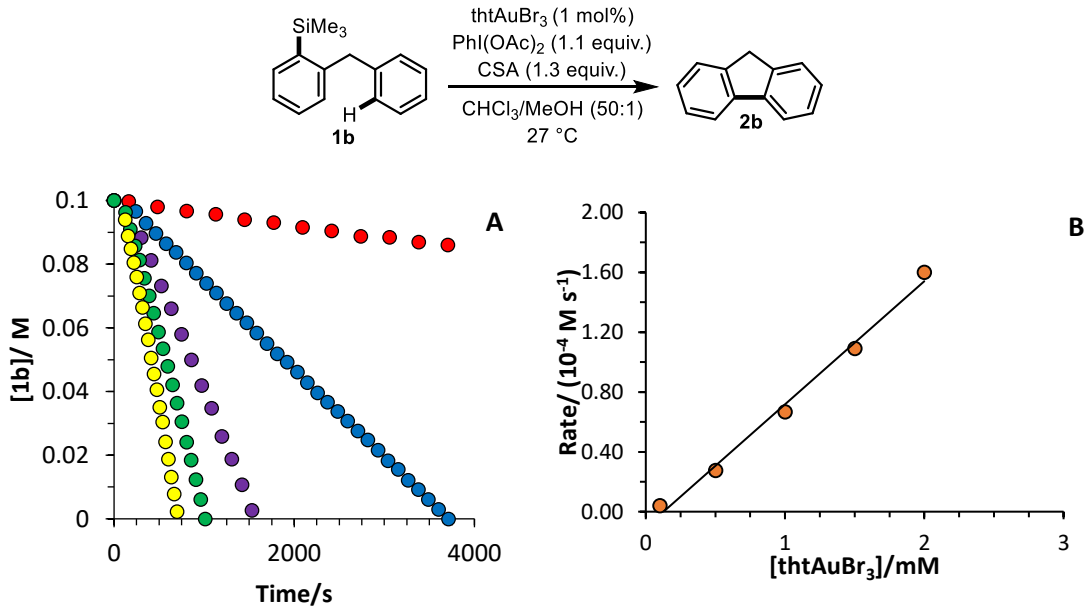

Figure 8.3. Rate-dependence on [thtAuBr$_3$]

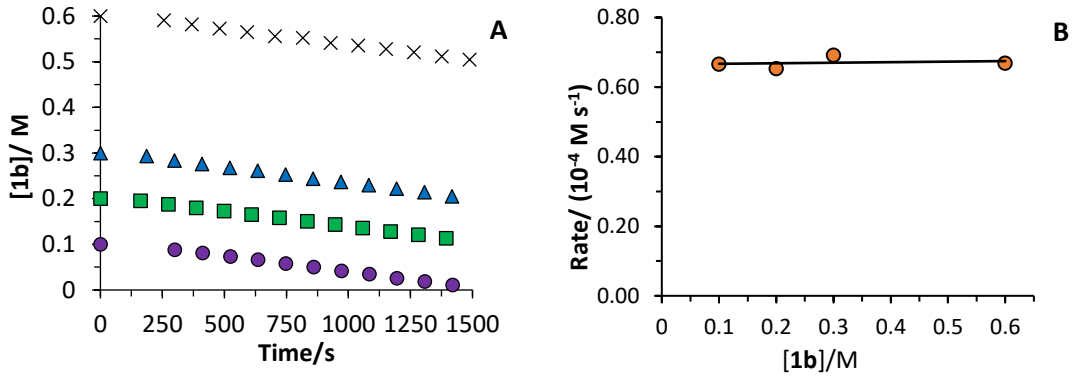

Figure 8.4. Rate-dependence on [**1b**]

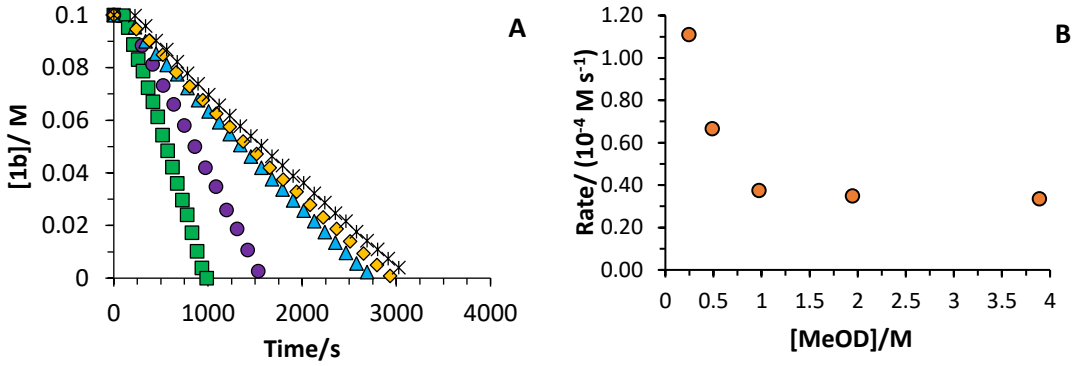

Figure 8.5. Rate-dependence on [CD_3OD]

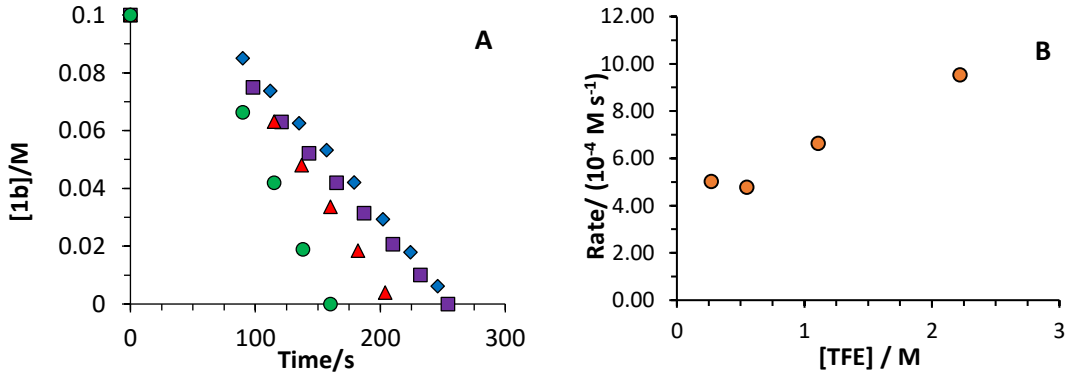

Figure 8.6. Rate-dependence on [2,2,2-trifluoroethanol]

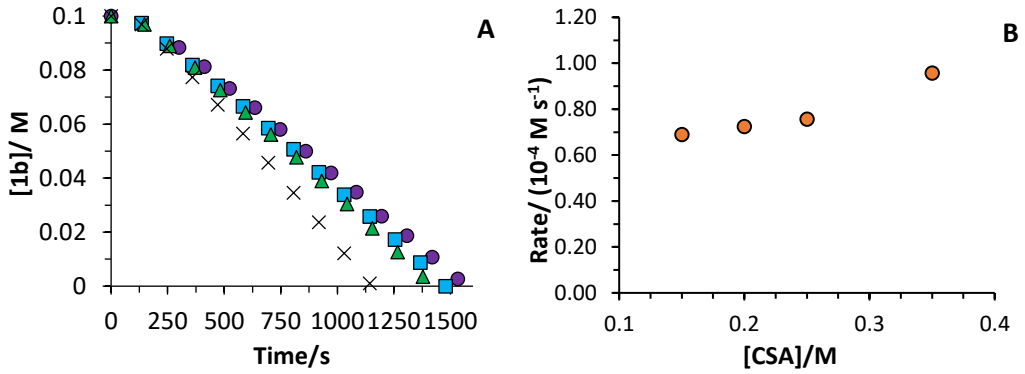

Figure 8.7. Rate-dependence on [CSA]

There is a negligible rate dependence on [CSA] in the concentration range that these reactions are performed, however a slight increase in rate is observed at very high concentrations.

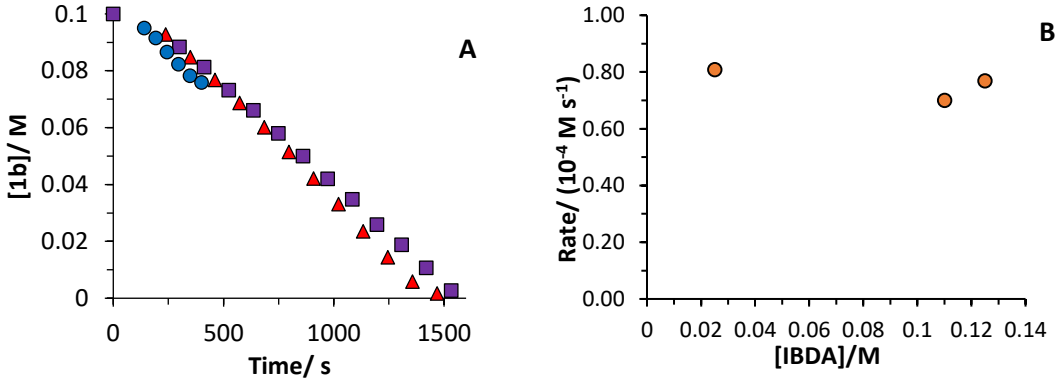

Figure 8.8. Rate-dependence [IBDA] (at [CSA] = 0.13 M, such that [CSA] > [IBDA])

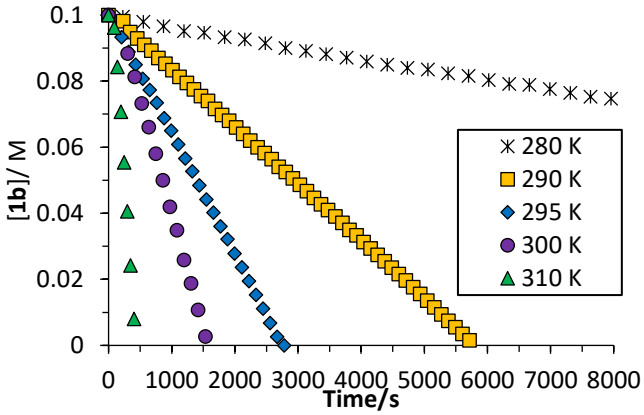

Figure 8.9. Rate-dependence on temperature

8.6.3 Rate Law Derivation

$$\frac{d[P]}{dt} = k_1[\mathbf{V}] + k_2[\mathbf{IV}]$$

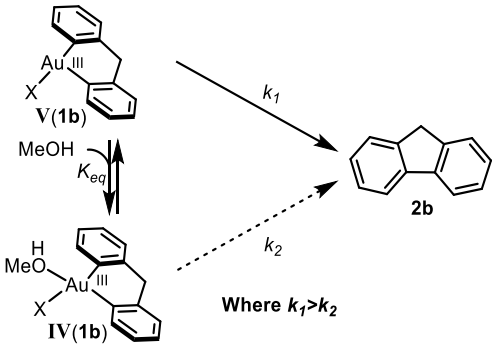

$$K_{eq} = \frac{[\mathbf{IV}]}{[\mathbf{V}][\text{MeOH}]}$$

Assuming:

$$[\text{Au}]_{tot} = [\mathbf{V}] + [\mathbf{IV}]$$

$$\frac{d[P]}{dt} = k_1([\text{Au}]_{tot} - [\mathbf{IV}]) + k_2[\mathbf{IV}]$$

$$= k_1[\text{Au}]_{tot} + (k_2 - k_1)[\mathbf{IV}]$$

$$[\mathbf{IV}] = K_{eq}[\mathbf{V}][\text{MeOH}]$$

$$[\mathbf{IV}] = K_{eq}([\text{Au}]_{tot} - [\mathbf{IV}])[\text{MeOH}]$$

$$[\mathbf{IV}] = K_{eq}[\text{Au}]_{tot}[\text{MeOH}] - K_{eq}[\mathbf{IV}][\text{MeOH}]$$

$$[\mathbf{IV}] + K_{eq}[\mathbf{IV}][\text{MeOH}] = K_{eq}[\text{Au}]_{tot}[\text{MeOH}]$$

$$[\mathbf{IV}](K_{eq}[\text{MeOH}] + 1) = K_{eq}[\text{Au}]_{tot}[\text{MeOH}]$$

$$\therefore [\mathbf{IV}] = \frac{K_{eq}[\text{Au}]_{tot}[\text{MeOH}]}{(K_{eq}[\text{MeOH}] + 1)}$$

$$\therefore \frac{d[P]}{dt} = k_1[\text{Au}]_{tot} + \frac{(k_2 - k_1)K_{eq}[\text{Au}]_{tot}[\text{MeOH}]}{(K_{eq}[\text{MeOH}] + 1)} \text{ where } [\text{MeOH}] = \frac{-1 + \sqrt{1 + 8K_{eq2}[\text{MeOH}]_{tot}}}{4K_{eq2}}$$

See below for derivation

$$K_{eq2} = \frac{[(\mathrm{MeOH})_2]}{[\mathrm{MeOH}]^2}$$

$$[(\mathrm{MeOH})_2] = K_{eq2}[\mathrm{MeOH}]^2$$

$$[\mathrm{MeOH}]_{tot} = 2\times\ [(\mathrm{MeOH})_2] + [\mathrm{MeOH}]$$

$$[\mathrm{MeOH}]_{tot} = 2\times\ K_{eq2}[\mathrm{MeOH}]^2 + [\mathrm{MeOH}]$$

$$\therefore 0 = 2\times\ K_{eq2}[\mathrm{MeOH}]^2 + [\mathrm{MeOH}] - [\mathrm{MeOH}]_{tot}$$

$$x = \frac{-b \pm \sqrt{b^2 - 4ac}}{2a} \text{ where } x = [\mathrm{MeOH}]\ a = 2K_{eq2}\ b = 1\ c = -[\mathrm{MeOH}]_{tot}$$

$$\therefore [\mathrm{MeOH}] = \frac{-1 \pm \sqrt{1^2 - 4\times 2K_{eq2}\times -[\mathrm{MeOH}]_{tot}}}{2\times 2K_{eq2}}$$

Solving for $[\mathrm{MeOH}] \geq 0$

$$[\mathrm{MeOH}] = \frac{-1 + \sqrt{1 + 8K_{eq2}[\mathrm{MeOH}]_{tot}}}{4K_{eq2}}$$

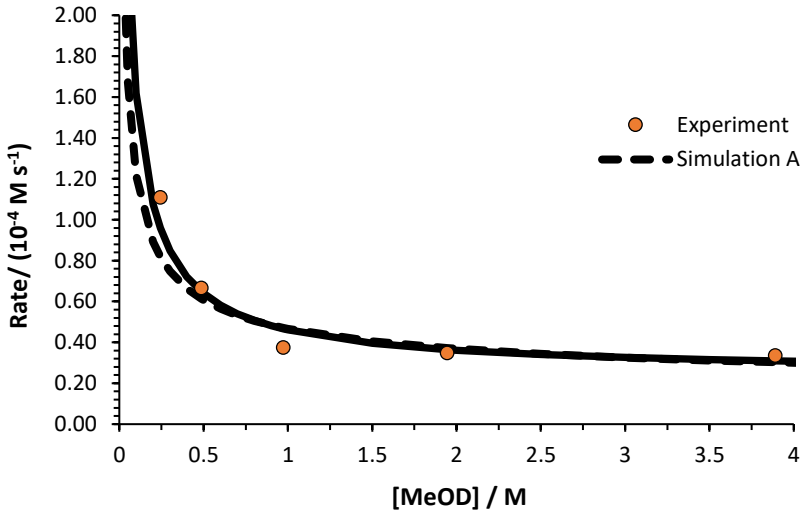

Figure 8.10. Simulated *vs* experimental data for cyclisation of **1b**. Simulation A: k_1 = 0.59 s^{-1}, k_2 = 0.014 s^{-1}, K_{eq} = 100 and K_{eq2} = 15. Simulation B (Where both MeOH and $(MeOH)_2$ can bind to gold): k_1 = 0.59 s^{-1}, k_2 = 0.025 s^{-1}, K_{eq} = 45 and K_{eq2} = 20. The values reported are for purely illustrative purposes only and no rate or equilibrium constant should be used in isolation

In support of the derived catalytic rate law, the experimental rate for different concentrations of MeOD can be predicted using the derived catalytic rate law and excel solver by changing the values of k_1, k_2, K_{eq} and K_{eq2}. A number of combinations of rate and equilibrium constants

give a good fit to the experimental data. Due to the insolubility of the oxidant and acid in the absence of MeOH, k_1 was estimated by performing the reaction with TFE (50:1 $CDCl_3$:TFE, 0.27 M). Good fits can still be obtained in the range $0.4 \leq k_1 \leq 1.5$ s^{-1}.

8.6.4 Kinetic Isotope Effects

Independent Rate Kinetic Isotope Effects:

The standard kinetics procedure was followed with d_0 and d_5-(2-benzylphenyl)trimethylsilane in two independent experiments. The experiments were performed on the same day, with the same stock solution of catalyst, solvents and batch of reagents.

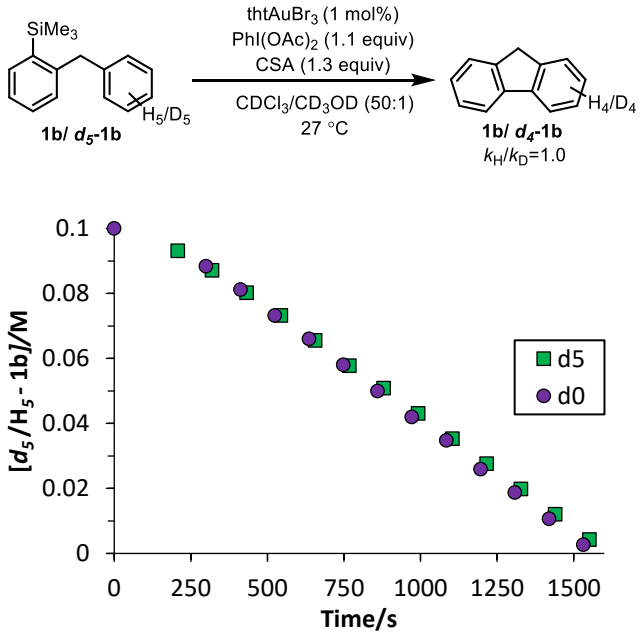

Figure 8.11. Combined plots of rate of cyclisation of d_0 and d_5-(2-benzylphenyl)trimethylsilane

Intramolecular Competition Kinetic Isotope Effects:

The reactions were performed by analogy to the standard kinetics procedure: To a 7 mL screw-cap borosilicate vial containing the requisite deuterated substrate was added $CDCl_3$ (900 μL), CD_3OD (20 μL) and $thtAuBr_3$ (0.001 mmol, 100 μL of a 0.01 M stock solution in $CDCl_3$). CSA (0.13 mmol, 30.2 mg) followed immediately by IBDA (0.11 mmol, 35.4 mg) were added to the vial, which was then sealed and shaken vigorously until all the contents had dissolved. Once the reaction had gone to completion (determined by ^{1}H NMR spectroscopy) the reaction was filtered through a plug of silica gel (eluent: hexane) and concentrated *in vacuo*. The isotopologues were isolated as a mixture by preparative TLC (eluent: hexanes), and the ratio

of isotopologues was determined by ^{1}H NMR spectroscopy ($CDCl_3$ or CD_2Cl_2). Assignments were made by comparison to authentic, non-deuterated samples or literature values.

Table 8.3: KIEs calculated from the ratio of isotopologues isolated

Entry	Substrate	Products	*k*(H/D)
1	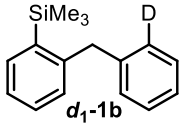 ***d*$_1$-1b**	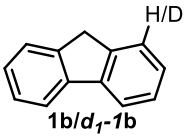 **1b/*d*$_1$-1b**	2.53±0.06
2	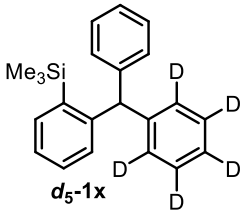 ***d*$_5$-1x**	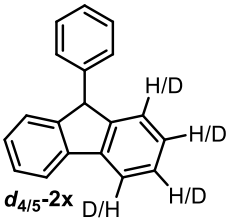 ***d*$_{4/5}$-2x**	2.50±0.30[34]
3			1.92±0.20
4	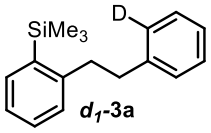 ***d*$_1$-3a**	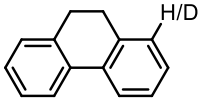 **4a/*d*$_1$-4a**	1.07±0.08
5			1.03±0.03
	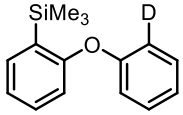 ***d*$_1$-1v**	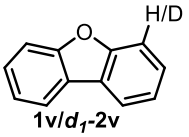 **1v/*d*$_1$-2v**	
	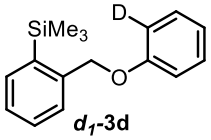 ***d*$_1$-3d**	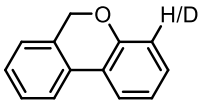 **4d/*d*$_1$-4d**	

8.6.5 Hammett LFER Analysis

The standard kinetics procedure was followed using the appropriate aryltrimethylsilane. For reactions that displayed *pseudo* zero-order profiles, rates were measured over the entire reaction; for reactions with non-*pseudo* zero-order profiles, both initial and maximum rate values were measured. In the Hammett plot, the best fit was against σ.

Arene:

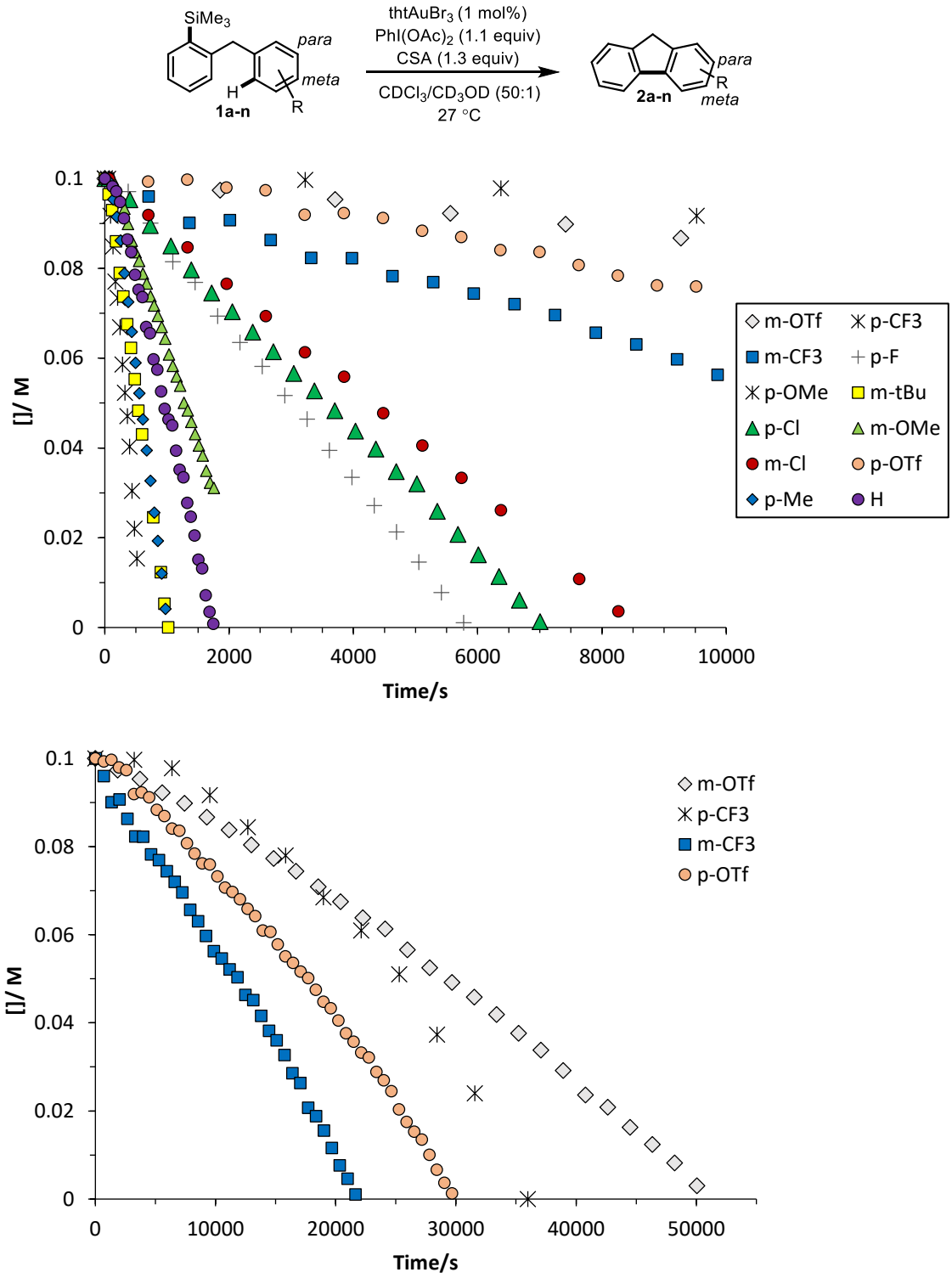

Figure 8.12. Combined concentration/time plot for rate analysis of substituted arenes (Top: Comparison of all data; Bottom: Full profile for slowest substrates)

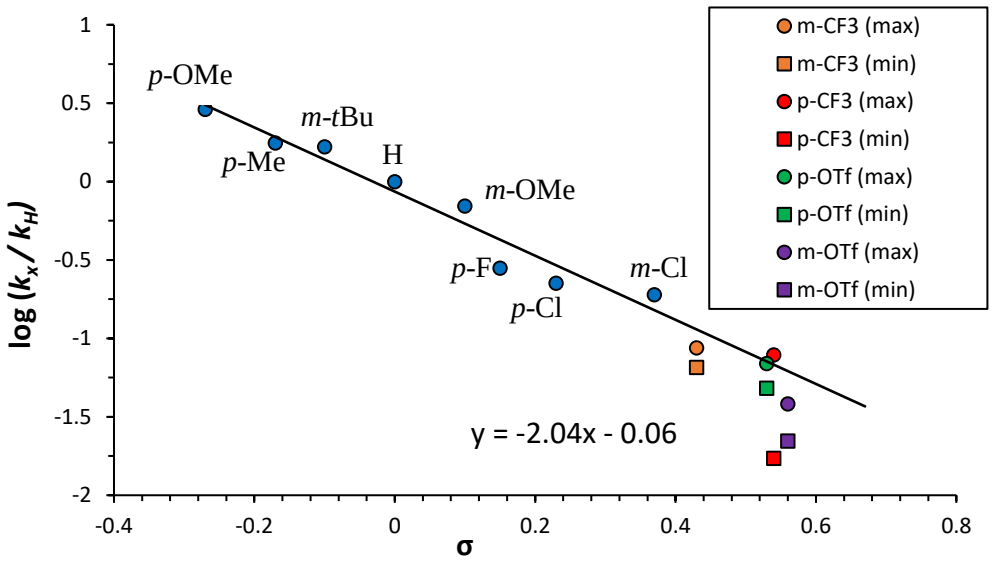

Figure 8.13. Arene Hammett Plot with minimum and maximum rates given for σ ≥ 0.43. Line of best fit shown for filled circles only

Silane:

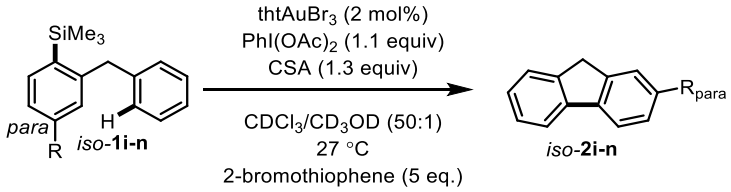

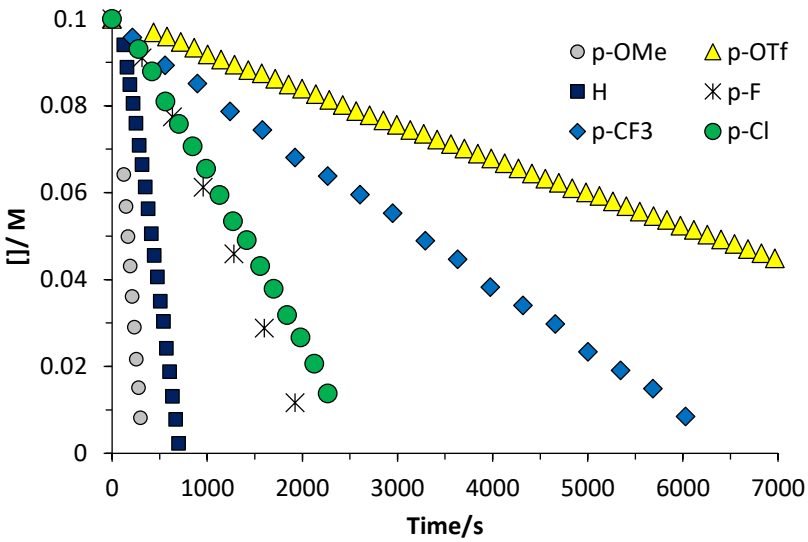

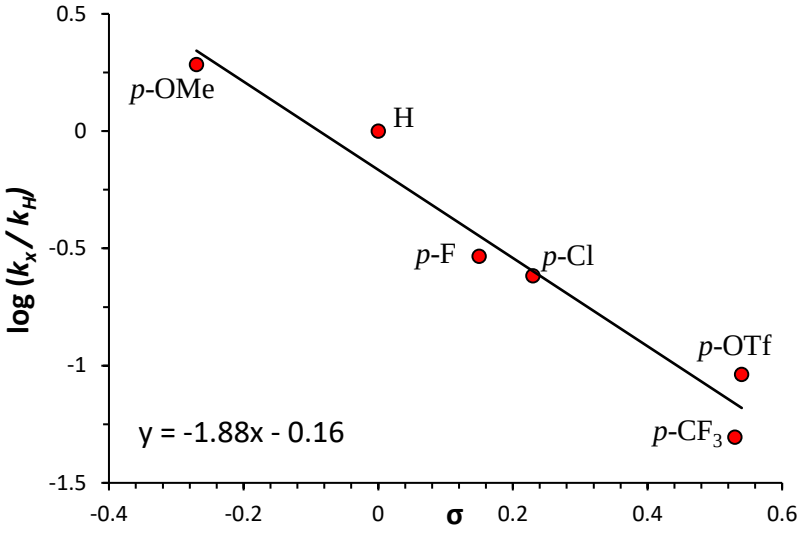

Figure 8.14. Combined concentration/time plot for rate analysis of substituted silanes and associated Hammett plot. In the absence of 2-bromothiophene unusual kinetic profiles were observed and this is currently under investigation

Disubstituted substrates:

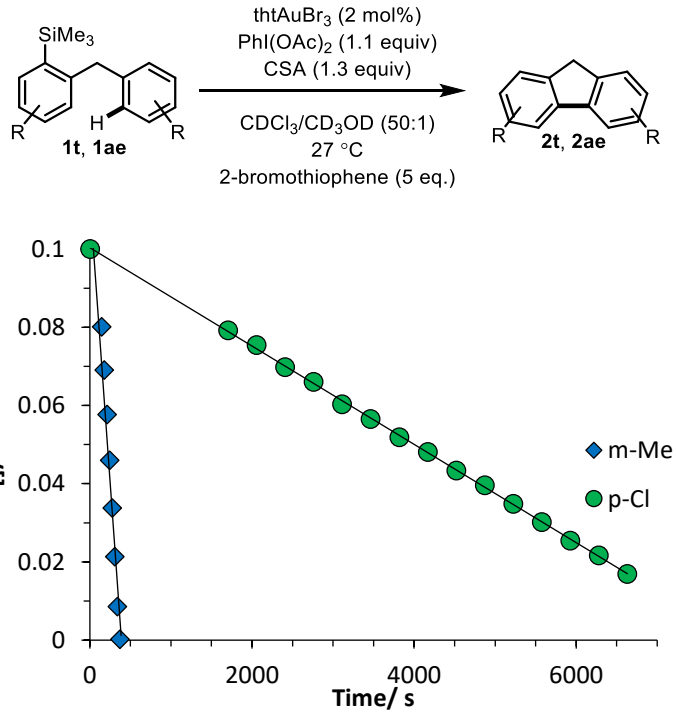

Figure 8.15. Combined concentration/time plot for rate analysis of disubstituted substrates

8.6.6 Competition Experiments

Intermolecular interception of cyclisation by 2-bromothiophene

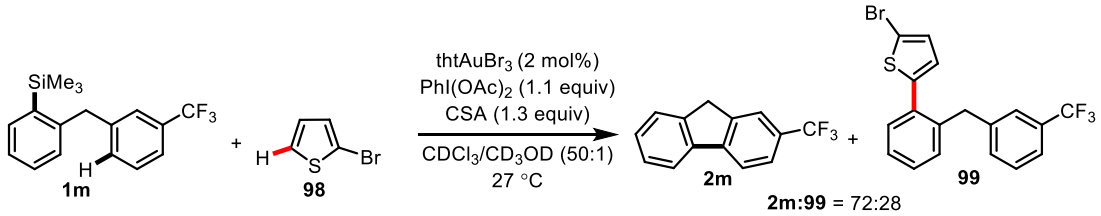

To a 7 mL screw-cap borosilicate vial containing trimethyl{2-[3-(trifluoromethyl)benzyl]phenyl}silane **1m** (0.05 mmol) and 2-bromothiophene (0.25 mmol) was added $CDCl_3$ (436 µL), CD_3OD (10 µL) and thtAuBr$_3$ (0.001 mmol, 64 µL of a 0.0155 M stock solution in $CDCl_3$). CSA (0.065 mmol, 15.1 mg) followed immediately by IBDA (0.055 mmol, 17.7 mg) were added. The vial was sealed and shaken vigorously until all the contents had dissolved. The solution was transferred by a 1 mL syringe into a NMR tube and loaded into a Bruker Avance III 400 MHz NMR spectrometer with a probe temperature of 27 °C, already tuned to ^{1}H. The kinetics experiment was initiated after locking to $CDCl_3$ and performing a quick shimming experiment (topshim 1Dfast, Bruker software). After the reaction had gone to completion, as determined by ^{1}H NMR, the solution was filtered through a plug of silica gel and concentrated *in vacuo*. Preparative TLC (eluent: hexanes) afforded **99** as a thin film: **^{1}H NMR (400 MHz, $CDCl_3$):** δ 7.44 (d, *J* = 7.8 Hz, 1H), 7.40 – 7.28 (m, 5H), 7.22 – 7.15 (m, 2H), 6.97 (d, *J* = 3.7 Hz, 1H), 6.61 (d, *J* = 3.7 Hz, 1H), 4.14 (s, 2H). **^{13}C{^{1}H} NMR (125 MHz, $CDCl_3$):** 144.0, 142.0, 138.4, 133.8, 132.2, 131.5, 130.84 (q, *J* = 32.0 Hz), 130.81, 130.1, 129.01, 128.95, 127.2, 127.0, 125.6 (q, *J* = 3.9 Hz), 123.1 (q, *J* = 3.9 Hz), 124.28 (app. d, *J* = 270 Hz), 112.1, 39.3. **^{19}F NMR (377 MHz, $CDCl_3$):** δ – 62.6 (s). **HRMS** calcd. for $C_{18}H_{12}BrF_3S$: 395.9790 [M]$^+$; found (EI$^+$): 395.9771.

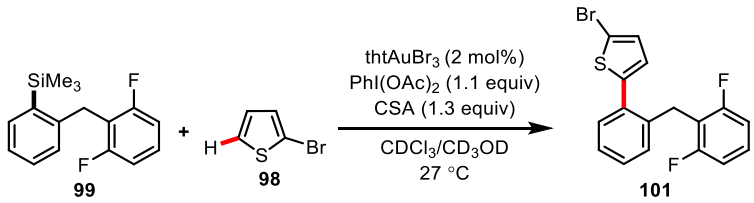

To a 2 mL screw-cap borosilicate vial containing **99** (0.05 mmol) and 2-bromothiophene (0.25 mmol) was added $CDCl_3$ (436 µL), CD_3OD (10 µL) and thtAuBr$_3$ (0.001 mmol, 64 µL of a 0.0155 M stock solution in $CDCl_3$). CSA (0.065 mmol, 15.1 mg) followed immediately by IBDA (0.055 mmol, 17.7 mg) were added. The vial was sealed and shaken vigorously until all the contents had dissolved. The solution was transferred by a 1 mL syringe into a NMR tube

and loaded into a Bruker Avance III 400 MHz NMR spectrometer with a probe temperature of 27 °C, already tuned to ^{1}H. The kinetics experiment was initiated after locking to $CDCl_3$ and performing a quick shimming experiment (topshim 1Dfast, Bruker software). After the reaction had gone to completion, as determined by ^{1}H NMR, the solution was filtered through a plug of silica gel and concentrated *in vacuo*. Preparative TLC (eluent: hexanes) afforded **99** as a thin film. **^{1}H NMR (400 MHz, $CDCl_3$):** δ 7.36 – 7.30 (m, 1H), 7.25 – 7.16 (m, 3H), 7.06 (d, *J* = 3.7 Hz, 1H), 7.02 – 6.97 (m, 1H), 6.90 – 6.82 (m, 3H), 4.12 (s, 2H). **^{13}C{^{1}H} NMR (100 MHz, $CDCl_3$):** 161.8 (dd, *J* = 250 Hz, 8.4 Hz), 144.1, 137.7,133.3, 131.2, 130.1, 128.9, 128.6, 128.3 (t, *J* = 10.2 Hz), 127.4, 126.4, 116.2 (t, *J* = 20.0 Hz), 112.0, 111.3 (dd, *J* = 20.0, 6.0 Hz), 26.0 (t, *J* = 3.0 Hz). **^{19}F NMR (377 MHz, $CDCl_3$):** δ – 114.3 (m). **HRMS** calcd. for $C_{17}H_{11}BrF_2S$: 363.9727 $[M]^+$; found (EI^+): 363.9736.

Intramolecular competition reactions

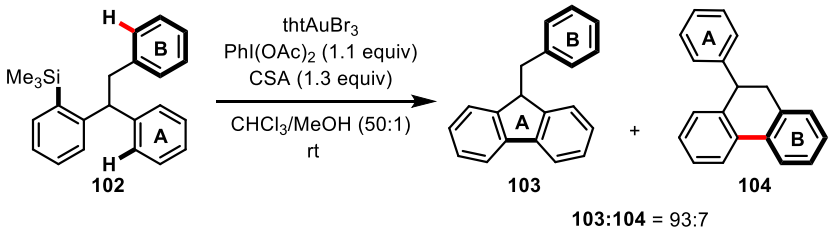

$thtAuBr_3$ (2 mol%, 0.001 mmol, 64 µL of a 0.0155 M stock solution in $CDCl_3$) was added to a 2 mL vial containing **102** (16.5 mg, 0.05 mmol) in $CDCl_3$ (0.5 mL) and MeOH (10 µL). CSA (15.1 mg, 0.065 mmol) and iodobenzene diacetate (17.7 mg, 0.055 mmol) were added, and the reaction was stirred at room temperature for 30 min. After analysis of the composition by ^{1}H NMR, the reaction mixture was filtered through a plug of silica gel to remove the CSA and unreacted oxidant, concentrated *in vacuo* and placed under high vacuum until no iodobenzene remained. The product ratios were determined by ^{1}H NMR and assigned based on literature values.[48,49]

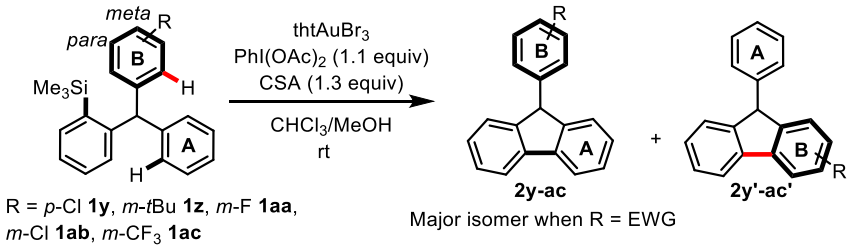

$thtAuBr_3$ (1 mol%, 0.0005 mmol, 32 µL of a 0.0155 M stock solution in $CDCl_3$) was added to a 2 mL vial containing the requisite aryltrimethylsilane (0.05 mmol) in $CDCl_3$ (0.5 mL) and MeOH (10 µL). CSA (15.1 mg, 0.065 mmol) and iodobenzene diacetate (17.7 mg, 0.055

mmol) were added, and the reaction was stirred at room temperature for 1 h. After analysis of the composition by ^{1}H NMR, the reaction mixture was filtered through a plug of silica gel to remove the CSA and unreacted oxidant, concentrated *in vacuo* and held under high vacuum until no iodobenzene remained. The product ratios were determined by either ^{1}H or ^{19}F NMR spectroscopy in $CDCl_3$ or CD_2Cl_2. Assignments were made by comparison to literature values or tentatively assigned *in situ* and product rations are shown in Table 8.4

Table 8.4: Intramolecular competition of arenes

Entry	R	X:X′	*k*(X/H)
1	***m*-*t*Bu**	**0.4:1**[50]	**2.46**
2	***m*-F**	**>25:1**[51]	**0.04**
3	***p*-Cl**	**2.7:1**[52]	**0.37**
4	***m*-Cl**	**>99:1**[52]	**0.01**
5	***m*-CF_3**	**>159:1**[53]	**0.006**

Silane homocoupling

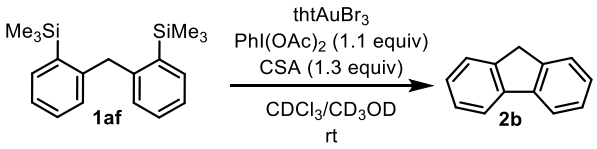

The standard kinetics procedure was followed with **1af** (31.3 mg, 0.10 mmol) using 1 mol% $thtAuBr_3$.

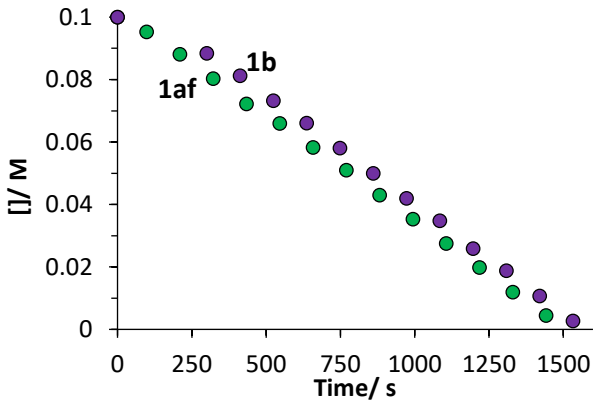

Figure 8.16. Combined concentration/time plots for the cyclisation of **1a** and **1af** to **2b**

8.6.7 Allocolchinoid Cyclisation Kinetics and Procedure

Representative Kinetics Protocol

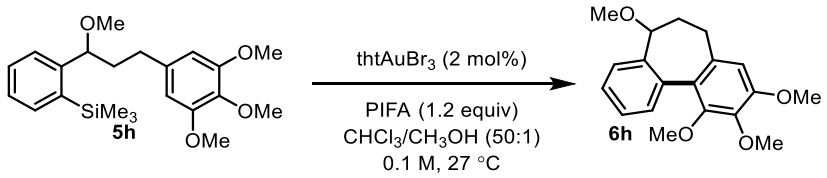

Representative experiment: To a 7 mL screw-cap borosilicate vial containing **5h** (38.9 mg, 0.10 mmol) was added $CDCl_3$ (800 µL), CD_3OD (20 µL) and thtAuBr$_3$ (0.002 mmol, 200 µL of a 0.01 M stock solution in $CDCl_3$). Dichloromethane (9.3 mg, 7 µL, 0.11 mmol) was also added as an internal standard for ^{1}H NMR. The solution was transferred into a NMR tube and loaded into a Bruker Avance III 400 MHz NMR spectrometer with a probe temperature of 27 °C. After tuning to ^{1}H, locking to $CDCl_3$, and shimming, the sample was ejected and poured back into the vial. PIFA (51.6 mg, 0.12 mmol) was added to the vial, which was then sealed and shaken vigorously until all the contents had dissolved. The solution was transferred by a 1 mL syringe back into the NMR tube and loaded into the NMR spectrometer. The kinetics experiment was initiated after locking to $CDCl_3$. The time between addition of PIFA and the first kinetics time-point was measured by stopwatch and was typically 90 – 120 sec.

Identification of Diaryliodonium Salt

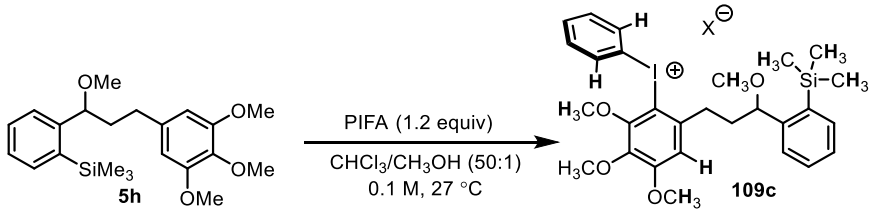

To a 7 mL screw-cap borosilicate vial containing **5k** (38.9 mg, 0.10 mmol) was added $CDCl_3$ (1 mL) and CD_3OD (20 µL). PIFA (51.6 mg, 0.12 mmol) was added to the vial, which was then sealed and shaken vigorously until all the contents had dissolved. *In situ* analysis of the resultant side product by ^{1}H NMR led to the assignment of structure **109c** (signals observed shown in bold, tentatively assigned). **^{1}H NMR (400 MHz, $CDCl_3$)**: δ 7.89 – 7.83 (m, 2H), 6.73 (s, 1H), 3.97 (s, 3H), 3.88 (s, 3H), 3.20 (s, 3H), 0.27 (s, 9H). Dilution of the reaction mixture in methanol to *ca.* 100 µM followed by direct injection into a microTOF focus II ESI mass spectrometer showed the molecular ion of the diaryliodonium salt (Figure 8.17). **LRMS** calcd. for $C_{28}H_{36}IO_4Si^+$: 591.14 $[M]^+$; found (ESI): 591.14 ($[M^+]$, 100%). Identical procedures were performed on **5k**, **5m** and **89** and the molecular ion was observed for each diaryliodonium salt: **109a** (621.15), **109b** (655.11) and **90** (385.04).

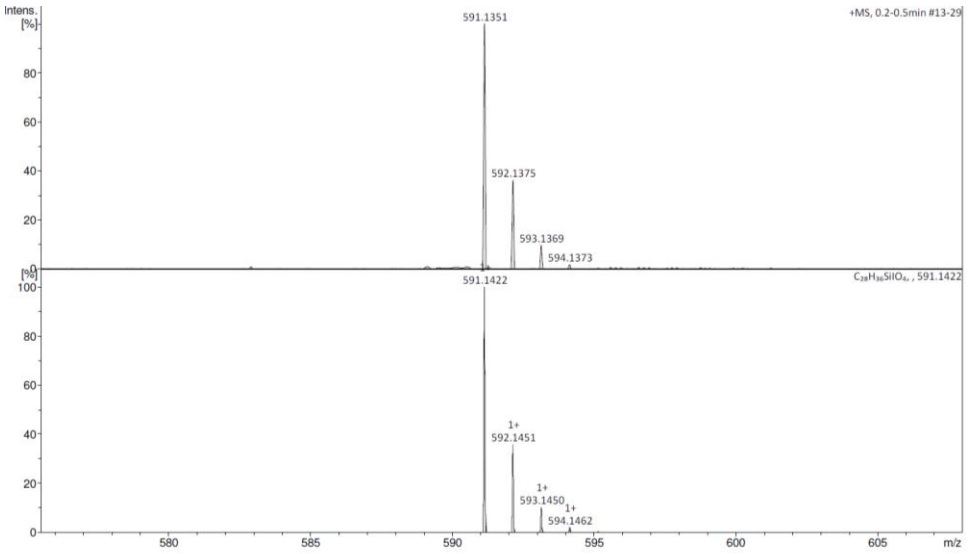

Figure 8.17: Measured (Top) and predicted (bottom) mass spectra of **109c**.

Kinetic Procedure for Pre-formation of Inhibitor

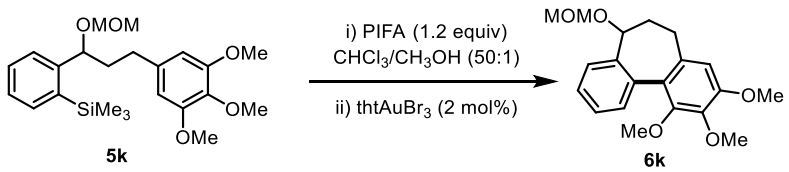

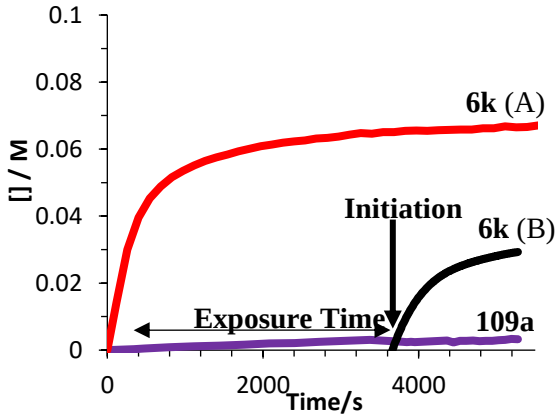

Figure 8.18: Kinetics of Cyclisation of **5k** under: A) standard conditions; B) with premixing of substrate and oxidant before initiating reaction.

To a 7 mL screw-cap borosilicate vial containing **5k** (20.93 mg, 0.05 mmol) was added $CDCl_3$ (500 µL) and CD_3OD (10 µL). Dichloromethane (9.3 mg, 7 µL, 0.11 mmol) was also added as an internal standard for ^1H NMR. The solution was transferred into a NMR tube and loaded into a Bruker Avance III 400 MHz NMR spectrometer with a probe temperature of 27 °C. After tuning to ^1H, locking to $CDCl_3$ and shimming, the sample was ejected and poured back

into the vial. PIFA (25.8 mg, 0.06 mmol) was added to the vial, which was then sealed and shaken vigorously until all the contents had dissolved. The solution was transferred by a 1 mL syringe back into the NMR tube and loaded into the NMR spectrometer. The kinetics experiment was initiated after locking to $CDCl_3$. After *ca.* 3700 s (during which time *ca*. 0.04 M of **109a** had formed) the NMR tube was ejected and poured into a new vial containing **3** (20.93 mg, 0.05 mmol), $CDCl_3$ (300 μL), CD_3OD (10 μL) and thtAuBr$_3$ (0.002 mmol, 200 μL of a 0.01 M stock solution in $CDCl_3$), followed immediately by addition of PIFA as a solid (25.8 mg, 0.06 mmol). The solution was transferred by a 1 mL syringe back into the NMR tube to continue monitoring the reaction. *Note*: *At the point of initiation, reactions A and B only differ by the presence of ca. 2% of* ***109a*** *and the resulting consumption of PIFA and* ***5k*** *(2% each).*

Simulation of Inhibition Kinetics

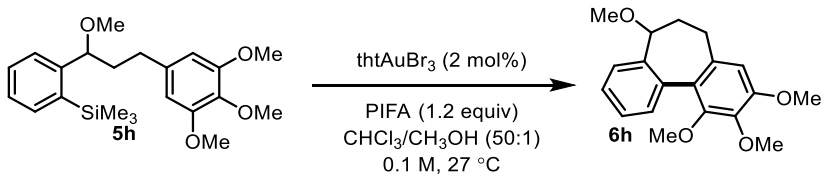

Kinetic simulations were performed using DynoChem 2011 software. The models were built using the processes shown in Scheme 8.2 and Figure 8.19. In order to obtain to obtain good fits, steps for pre-catalyst activation and bromination were added to the model (k_a and k_b). [Note: The mechanism of the pre-catalyst activation is not known and it is included here simply to account for loss of starting material to brominated product, see below for discussion of bromination products]. The model was optimised using a Levenberg-Marquardt fitting algorithm and Rosenbrock solver integration method. The simulation was allowed to solve against the concentration vs time plots for the cyclisation of **5h** to **6h** at both 1 and 2 mol% of catalyst. The rate constants obtained are shown in Table 8.5. The *absolute* values of k_1 and k_2 were both set at $\geq$ 1000 $dm^3\ mol^{-1}\ s^{-1}$ (as a turnover-limiting k_3 was assumed) and are not kinetically significant, but the relative values are important in obtaining a good fit.

a			PreCat	>	Cat	+	2Br
b	**5h**	+	Br	>	**5ag**		
1	**5h**	+	Cat	>	INT		
2	**109c**	+	Cat	>	**110c**		
3	INT	>	**6h**	+	Cat1		
4	Cat1	+	Oxidant	>	Cat		
5	**5h**	+	Oxidant	>	**109c**		

Scheme 8.2. Elementary steps for reaction in DynoChem format.

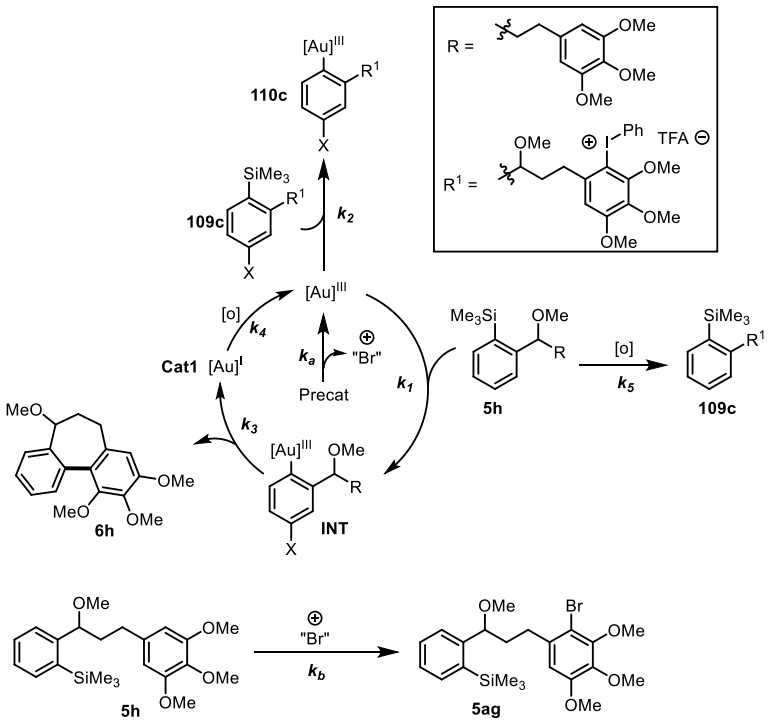

Figure 8.19: Graphical representation of DynoChem model shown in Scheme 8.2.

Table 8.5. Rate constants from DynoChem simulation for which a good fit can be obtained. k_1:k_2 ≈1:5 for a good fit. Arbitrary examples are fixed, fitted values are iteratively optimised.

Rate constant	Value		Standard Error
k_a	0.5 s^{-1}	Arbitrary	-
k_b	0.15 dm^3 mol^{-1} s^{-1}	Fitted	0.06
k_1	1000 dm^3 mol^{-1} s^{-1}	Arbitrary	-
k_2	4974 dm^3 mol^{-1} s^{-1}	Fitted	284
k_3	0.0142 s^{-1}	Fitted	0.0004
k_4	1000 dm^3 mol^{-1} s^{-1}	Arbitrary	-
k_5	1.63×10^{-4} dm^3 mol^{-1} s^{-1}	Fitted	1.7×10^{-6}

Bromination Products from Catalyst Activation

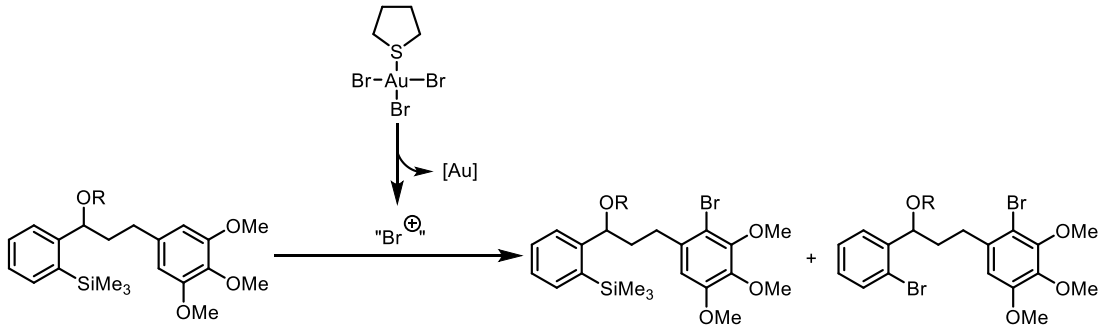

Scheme 8.3 Possible bromination products from catalyst activation.

In general, 2 equivalents (relative to the catalyst) of brominated products are observed after catalyst activation. Depending on the relative reactivity of the two aryl rings in the starting material, bromination can occur ipso to the silane group and/or on the arene (Scheme 8.3). A significant amount of cyclised brominated material **6ah** was isolated from the cyclisation of **5k** to **6k**, suggesting that a large proportion of the bromination occurs on the trimethoxy arene of **5k**, to give **5ah**, which can subsequently cyclise to **6ah** (Scheme 8.4).

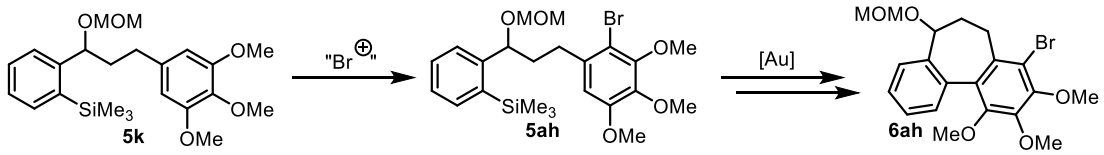

Scheme 8.4: Origin of bromination product, **6ah**.

8.7 Procedural References

[1] A. J. Cresswell, G. C. Lloyd-Jones, *Chem. Eur. J.* **2016**, *22*, 12641–12645.

[2] L. T. Ball, G. C. Lloyd-Jones, C. A. Russell, *J. Am. Chem. Soc.* **2014**, *136*, 254–264.

[3] G. M. Sheldrick, *Acta Crystallogr. Sect. A* **2008**, *64*, 112–122.

[4] Y.-Z. Sui, X.-C. Zhang, J.-W. Wu, S. Li, J.-N. Zhou, M. Li, W. Fang, A. S. C. Chan, J. Wu, *Chem. Eur. J.* **2012**, *18*, 7486–7492.

[5] J. Zhu, M. Pérez, C. B. Caputo, D. W. Stephan, *Angew. Chem. Int. Ed.* **2016**, *55*, 1417–1421.

[6] M. L. N. Rao, R. J. Dhanorkar, *RSC Adv.* **2014**, *4*, 13134–13144.

[7] G. Schäfer, J. W. Bode, *Angew. Chem. Int. Ed.* **2011**, *50*, 10913–10916.

[8] M. Kaneko, R. Hayashi, G. R. Cook, *Tetrahedron Lett.* **2007**, *48*, 7085–7087.

[9] X. K. Guo, D. Y. Zhao, J. H. Li, X. G. Zhang, C. L. Deng, R. Y. Tang, *Synlett* **2012**, 627–631.

[10] C. H. Burgos, T. E. Barder, X. Huang, S. L. Buchwald, *Angew. Chem. Int. Ed.* **2006**, *45*, 4321–4326.

[11] L. T. Ball, G. C. Lloyd-Jones, C. A. Russell, *Science* **2012**, *337*, 1644–1648.

[12] C.-L. Sun, Y.-F. Gu, W.-P. Huang, Z.-J. Shi, *Chem. Commun.* **2011**, *47*, 9813–9815.

[13] L. Mahendar, G. Satyanarayana, *J. Org. Chem.* **2014**, *79*, 2059–2074.

[14] A. B. Williams, R. N. Hanson, *Tetrahedron* **2012**, *68*, 5406–5414.

[15] K. Kobayashi, W. Miyatani, N. Matsumoto, *Helv. Chim. Acta* **2013**, *96*, 239–245.

[16] P. Gandeepan, C. H. Cheng, *J. Am. Chem. Soc.* **2012**, *134*, 5738–5741.

[17] K. Inamoto, T. Saito, K. Hiroya, T. Doi, *J. Org. Chem.* **2010**, *75*, 3900–3903.

[18] J. J. Talley, I. A. Evans, *J. Org. Chem.* **1984**, *49*, 5267–5269.

[19] M. Schilz, H. Plenio, *J. Org. Chem.* **2012**, *77*, 2798–2807.

[20] T. K. Wood, W. E. Piers, B. A. Keay, M. Parvez, *Angew. Chem. Int. Ed.* **2009**, *121*, 4069–4072.

[21] L. Xu, W. Yang, L. Zhang, M. Miao, Z. Yang, X. Xu, H. Ren, *J. Org. Chem.* **2014**, *79*, 9206–9221.

[22] M. Itoh, K. Hirano, T. Satoh, Y. Shibata, K. Tanaka, M. Miura, *J. Org. Chem.* **2013**, *78*, 1365–1370.

[23] S. J. Hwang, H. J. Kim, S. Chang, *Org. Lett.* **2009**, *11*, 4588–4591.

[24] Y. Wang, P. R. McGonigal, B. Herlé, M. Besora, A. M. Echavarren, *J. Am. Chem. Soc.* **2014**, *136*, 801–809.

[25] K. Bowden, A. F. Cockerill, *J. Chem. Soc. B Phys. Org.* **1970**, 173–179.

[26] J. Iskra, M. Zupan, S. Stavber, *Org. Biomol. Chem.* **2003**, *1*, 1528–1531.

[27] H. G. Lee, P. J. Milner, S. L. Buchwald, *J. Am. Chem. Soc.* **2014**, *136*, 3792–3795.

[28] J. H. Hammons, *J. Org. Chem.* **1968**, *33*, 1123–1127.

[29] G. H. Beaven, P. B. D. de la Mare, E. A. Johnson, N. V Klassen, *J. Chem. Soc.* **1962**, 988–993.

[30] C.-C. Hsiao, Y.-K. Lin, C.-J. Liu, T.-C. Wu, Y.-T. Wu, *Adv. Synth. Catal.* **2010**, *352*, 3267–3274.

[31] T. P. Liu, C. H. Xing, Q. S. Hu, *Angew. Chem. Int. Ed.* **2010**, *49*, 2909–2912.

[32] L. Chardonnens, A. Würmli, *Helv. Chim. Acta* **1946**, *29*, 922–928.

[33] B. Hatano, D. Kubo, H. Tagaya, *Chem. Pharm. Bull.* **2006**, *54*, 1304–1307.

[34] Z. Liu, H. Tan, L. Wang, T. Fu, Y. Xia, Y. Zhang, J. Wang, *Angew. Chem. Int. Ed.* **2015**, *54*, 3056–3060.

[35] H. Nakamura, Y. Tomonaga, K. Miyata, M. Uchida, Y. Terao, *Environ. Sci. Technol.* **2007**, *41*, 2190–2195.

[36] C. S. Nervig, P. J. Waller, D. Kalyani, *Org. Lett.* **2012**, *14*, 4838–4841.

[37] Y. Wang, A. Yepremyan, S. Ghorai, R. Todd, D. H. Aue, L. Zhang, *Angew. Chem. Int. Ed.* **2013**, *52*, 7795–7799.

[38] Z. Shen, Z. Ni, S. Mo, J. Wang, Y. Zhu, *Chem. Eur. J.* **2012**, *18*, 4859–4865.

[39] L.-C. Campeau, M. Parisien, A. Jean, K. Fagnou, *J. Am. Chem. Soc.* **2006**, *128*, 581–590.

[40] J. Rotzler, H. Gsellinger, A. Bihlmeier, M. Gantenbein, D. Vonlanthen, D. Häussinger, W. Klopper, M. Mayor, *Org. Biomol. Chem.* **2012**, 110–118.

[41] D. D. Hennings, T. Iwama, V. H. Rawal, *Org. Lett.* **1999**, *1*, 1205–1208.

[42] P. Cazeau, F. Duboudin, F. Moulines, O. Babot, J. Dunogue, *Tetrahedron* **1987**, *43*, 2075–2088.

[43] M. Yamashita, K. I. Yamada, K. Tomioka, *J. Am. Chem. Soc.* **2004**, *126*, 1954–1955.

[44] Q. Shi, K. Chen, X. Chen, A. Brossi, P. Verdier-Pinard, E. Hamel, A. T. McPhail, A. Tropsha, K.-H. Lee, *J. Org. Chem.* **1998**, *63*, 4018–4025.

[45] M. Leblanc, K. Fagnou, *Org. Lett.* **2005**, *7*, 2849–2852.

[46] A. V. Vorogushin, A. V. Predeus, W. D. Wulff, H.-J. Hansen, *J. Org. Chem.* **2003**, *68*, 5826–5831.

[47] D. A. Watson, X. Fan, S. L. Buchwald, *J. Org. Chem.* **2008**, *73*, 7096–7101.

[48] E. H. Licht, H. G. Alt, M. M. Karim, *J. Organomet. Chem.* **2000**, *599*, 275–287.

[49] S. S. Bhojgude, A. Bhunia, R. G. Gonnade, A. T. Biju, *Org. Lett.* **2014**, *16*, 676–679.

[50] P. D. Robinson, A. W. McLean, C. Y. Meyers, *Acta Crystallogr. Sect. C Cryst. Struct. Commun.* **2003**, *59*, 539–540.

[51] Y.-Y. Ji, L.-L. Lu, Y.-C. Shi, L.-X. Shao, *Org. Biomol. Chem.* **2014**, *12*, 8488–8498.

[52] G. Li, E. Wang, H. Chen, H. Li, Y. Liu, P. G. Wang, *Tetrahedron* **2008**, *64*, 9033–9043.

[53] J. J. Chen, S. Onogi, Y. C. Hsieh, C. C. Hsiao, S. Higashibayashi, H. Sakurai, Y. T. Wu, *Adv. Synth. Catal.* **2012**, *354*, 1551–1558.